

PUBLICATION NO. 50 2/2014

NORDIC CONCRETE RESEARCH

**EDITED BY
THE NORDIC CONCRETE FEDERATION**

**CONCRETE ASSOCIATIONS OF: DENMARK
FINLAND
ICELAND
NORWAY
SWEDEN**

**PUBLISHER: NORSK BETONGFORENING
POSTBOKS 2312, SOLLI
N - 0201 OSLO
NORWAY**

PROCEEDING

XXII NORDIC CONCRETE RESEARCH SYMPOSIA

REYKJAVIK, ICELAND 2014

VODSKOV, JULY 2014

Preface

In many ways the Nordic countries have been leading in concrete technology having some of the foremost pioneers in the world in for instance regarding fracture mechanic, rheology, chloride permeability, frost resistance, not forgetting application of silica fume and lignin bases dispersing admixture. We were among the pioneer in development high strength concrete and ultra high performance concrete and have from early on marked us greatly in precast industry.

This publication is a compilation of papers presented in the XXII Nordic Concrete Research symposium arranged in the Harpa Concert Hall in Reykjavik, Iceland. The Symposium took place 13th to 15th August 2014. It was arranged by Innovation Center Iceland on behalf of Icelandic Concrete Association in cooperation with the Research Council of the Nordic Concrete Federation.

Nordic Concrete Research Symposium has a long history and is organized after every three year. The event circulates between the member countries of the Nordic Concrete Federation, i.e. Iceland, Denmark, Norway, Sweden and Finland, in this order. The XXIII Nordic Concrete Research Symposium will be held in Denmark in 2017.

The aim of the symposium is to present and document the versatile concrete research conducted in Nordic research laboratories, universities and companies, in the field of concrete science and technology, construction and maintenance of concrete structures. Another as important intention is to bring people working with research together, to promote co-operation between researchers, research organizations as well as practicing engineers in the Nordic regime.

This year 119 papers are presented in 25 sessions. Major part, 105 papers, from the Nordic countries: 14 from Denmark, 10 from Finland, 9 from Iceland, 24 from Norway and 48 from Sweden. 14 papers came from other countries all over the world.

Having this occasion I would like to express my warm thanks to all the authors, speakers and chairpersons for their valuable contribution as well as to the symposium participants who together make the symposium fruitful. Warm thanks also to Dr. Dirch H. Bager, the editor of this publication. Thank to member of the Nordic Concrete Research Council and to coworker at the ICI Rheocenter at the Reykjavik University and Innovation center Iceland.

Reykjavik, July 2014

Olafur H. Wallevik
Chairman of the Nordic Concrete Research Council

Scientific Committee

Dr. Dirch H. Bager (DK)

Mr. Claus Pade, Danish Technological Institute, Concrete Centre (DK)

Mr. Juha Valjus, Concrete Association of Finland (FI)

Lic.Sc.Tech. Klaus Juvas, Consolis Technology Oy Ab (FI)

Prof. Dr. Olafur H. Wallevik, Innovation Centre Iceland (IS)

Dr. Jón E. Wallevik, Innovation Centre Iceland (IS)

Dr. Terje F. Rønning, Norcem R&D Department (NO)

Prof. Dr. Mette R. Geiker, NTNU, SINTEF (NO)

Tekn.Dr. Docent Mikael Hallgren, Tyréns AB (SE)

Tekn.Dr. Peter Utgenannt, CBI Swedish Cement and Concrete Research (SE)

Organizing Committee

Prof. Dr. Olafur H. Wallevik, Innovation Center Iceland and Reykjavik University (IS)

Erla Margret Gunnarsdottir, Innovation Center Iceland (IS)

Mr. Björn Hjartarson, Innovation Center Iceland (IS)

Dr. Jon E. Wallevik, Innovation Center Iceland (IS)

Dr. Kristjan F. Alexandersson, Innovation Center Iceland (IS)

Thordur I. Kristjansson, Innovation Center Iceland (IS)

CONTENTS

| | |
|--|----|
| OPENING SESSION | 1 |
| Tor Arne Martius-Hammer | 3 |
| COIN – Main Achievements | |
| 1 DURABILITY, MAINTENANCE, RENOVATION & FROST ACTION - PER FIDJESTØL MEMORIAL SESSION | 7 |
| R. Doug Hooton | 9 |
| Advantages of Silica Fume-Slag Ternary Binders for Production of Durable Concrete | |
| Olafur H. Wallevik, Indriði Níelsson & Björn Hjartarson | 13 |
| Self-compacting concrete without chemical admixture for Per Fidjestol | |
| Martin Kaasgaard, Claus Pade, Ulf Jönsson & Christian Munch-Petersen | 17 |
| Comparison of Durability Parameters of Self-Compacting Concrete and Conventional Slump Concrete Designed for Marine Environment | |
| Marianne Tange Hasholt | 21 |
| The Interplay Between Inner and Outer Frost Damage and its Implication for Accelerated Freeze-Thaw Testing | |
| Jonny Nilimaa, Jens Häggström, Niklas Bagge, Thomas Blanksvärd, Gabriel Sas, Ulf Ohlsson, Lars Bernspång, Björn Täljsten, Lennart Elfgren, Anders Carolin, Håkan Thun & Björn Paulsson | 25 |
| Maintenance and Renewal of Concrete Rail Bridges – Results from EC Project MAINLINE | |
| 2 STRUCTURAL BEHAVIOUR AND DESIGN | 29 |
| Tarek Edrees Saaed, George Nikolakopoulos & Jan-Erik Jonasson | 31 |
| Semi-Active Structural Control Strategies | |
| Linn Grepstad Nes & Jan Arve Øverli | 35 |
| Structural Behaviour of Beams with Fibre Reinforced LWAC and Normal Density Concrete | |
| Mario Plos, Costin Pacoste & Morgan Johansson | 39 |
| Recommendations for Finite Element Analysis for Design of RC Slabs | |
| Håvard Nedrelid & Terje Kanstad | 43 |
| Tests and Design of Fibre-Reinforced RC Beams with Dapped Ends | |
| Morten Engen, Max A. N. Hendriks, Jan Arve Øverli & Erik Åldstedt | 47 |
| Application of NLFEA in the Design of Large Concrete Structures | |

| | | |
|----------|--|----|
| 3 | DURABILITY, MAINTENANCE, RENOVATION & FROST ACTION - PER FIDJESTØL MEMORIAL SESSION - Cont. | 51 |
| | Martin Strand & Katja Fridh | 53 |
| | The Influence of SSMs on The Durability of Concrete Structures Exposed to Severe Conditions – Part I. Salt Frost Scaling | |
| | Vladimir Ronin , Jan-Erik Jonasson & Lennart Elfgren | 57 |
| | Self-Healing Concrete – Results with Energetically Modified Cements (EMC) | |
| | N. Williams Portal, M. Flansbjer, K. Tammo & K. Malaga | 61 |
| | Alkali Resistance of Textile Reinforcement for Concrete Façade Panels | |
| | Ricardo Antonio Barbosa, Kurt Kielsgaard Hansen, Linh Cao Hoang & Erik Stoklund Larsen | 65 |
| | Alkali-Silica Reaction in Reinforced Concrete Structures. Part I: Material Properties and Crack Orientation | |
| | Ricardo Antonio Barbosa, Kurt Kielsgaard Hansen, Linh Cao Hoang & Iben Maag | 69 |
| | Alkali-Silica Reaction in Reinforced Concrete Structures. Part II: Shear Strength of Severe ASR Damaged Concrete Beams | |
| 4 | STRUCTURAL BEHAVIOUR AND DESIGN, Cont | 73 |
| | Johan Silfwerbrand | 75 |
| | Safety Levels in Industrial Steel Fibre Concrete Floors | |
| | Daniel Ekström, Rasmus Rempling & Mario Plos | 79 |
| | Industrial Bridge Building - An Effective Bridge Construction Process Through an Integrated Design and Construction Process | |
| | Niklas Bagge, Thomas Blanksvärd, Gabriel Sas, Lars Bernspång, Björn Täl- jsten, Anders Carolin & Lennart Elfgren | 83 |
| | Full-Scale Test to Failure of a Prestressed Concrete Bridge in Kiruna | |
| | Per Goltermann | 87 |
| | Prefabricated Elements and Structures: Developments, Tests and Experiences. | |
| | Thorhallsson, E. R. & Birgisson, S. R. | 91 |
| | Experiment on Concrete Beams without Shear Reinforcement | |
| 5 | AGGREGATES AND ADDITIVES | 95 |
| | Börge Johannes Wigum | 97 |
| | RILEM Technical Committee (2014 – 2019) Avoiding Alkali Aggregate Reactions in Concrete Performance Based Concept. | |

| | | |
|----------|---|-----|
| | Bård Pedersen & Reidar Kompen | 101 |
| | Influence of Aggregates on Compressive Strength and E-Modulus of C45/55 Concrete | |
| | Björn Lagerblad, Jaume Cirera Riu & Hans-Erik Gram | 105 |
| | How to Evaluate Fillers from Crushed Rock Aggregate for Concrete Production | |
| | Yahya Ghasemi & Niklas Johansson | 109 |
| | Particle Packing of Aggregates for Concrete Mix Design: Models and Methods. | |
| | Hans-Erik Gram, Mikael Westerholm & Mats Emborg | 113 |
| | Crushed Fine Aggregate for Concrete Production | |
| 6 | LABORATORY AND FIELD TESTING | 117 |
| | Stefan Jacobsen | 119 |
| | A Norwegian Concrete-Ice Abrasion Laboratory | |
| | Ari Vepsä & Ilkka Hakola | 123 |
| | Impact Testing of Reinforced Concrete Slabs | |
| | Anja Klausen, Terje Kanstad, Øyvind Bjøntegaard & Gunrid Kjellmark | 127 |
| | Updated Temperature-Stress-Testing-Machine (TSTM): Introductory Tests, Calculations and Verification | |
| | Lars Elof Bryne & Anders Ansell | 131 |
| | Laboratory Testing of Early Age Shotcrete Bond Strength | |
| | Edgar Bohner, Janne Häkli & Timo Lehikoinen | 135 |
| | Demonstration of Wireless Monitoring in Rock Mass, Compacted Bentonite and Reinforced Concrete. | |
| 7 | STRUCTURAL BEHAVIOUR AND DESIGN, Cont | 139 |
| | Elena Vidal Sarmiento, Terje Kanstad, Mette R. Geiker & Max Hendriks | 141 |
| | Impact of the combined effect of fibre orientation and volume fraction on the mechanical properties of fibre reinforced concrete | |
| | Sveinbjörn Sveinbjörnsson, Þórdís Björnsdóttir, Guðbjartur Jón Einarsson & Eyþór Rafn Þórhallsson. | 145 |
| | Elastic Modulus of Concrete with Icelandic Basalt Aggregates | |
| | Thomas Juul Andersen | 149 |
| | Tailor-Made Concrete Structure with the use of Digital Fabrication | |
| | Andri Gunnarsson , Eythor Rafn Thorhallsson & Jonas Thor Snaebjornsson | 153 |
| | Simulation of Experimental Research of Concrete Beams Prestressed with BFRP Tendons | |
| | J. Ekström, R. Rempling & M. Plos | 157 |
| | Influence of Strain Softening on Spalling of Concrete due to Blast Load | |

| | | |
|-----------|---|-----|
| 8 | AGGREGATES AND ADDITIVES, Cont. | 161 |
| | Peter Billberg, Patrick Rogers & Katja Fridh | 163 |
| | Technique and Use of Crushed Concrete from Precast Elements as Aggregate in Concrete Production | |
| | Kayode Bamikole Olawuni & Özgür Eren | 167 |
| | Engineering Properties of Palm Kernel Shell Fiber Reinforced Concrete | |
| | Thorgeir S. Helgason, Vera Hofer & Holger Bach | 171 |
| | Pioneering Methods for Control of Aggregates Using Machine Vision, Spectroscopy and Statistical Modelling | |
| | Rolands Cepuritis, Stefan Jacobsen, Ernst Mørtzell, Sverre Smeplass & Børge J. Wigum | 175 |
| | Research Project on Manufactured Sand for Concrete | |
| | Johann A. Hardarson, Thordur I. Kristjansson, Olafur H. Wallevik | 179 |
| | Discrepancies in Measured and Modelled E-modulus due to Porous Aggregates. Some Experiences from tests on Icelandic Concrete | |
| 9 | BINDERS, ADMIXTURES, MIX DESIGN AND RHEOLOGY | 183 |
| | Jon E. Wallevik & Olafur H. Wallevik | 185 |
| | Analysis of Shear Rate Inside a Concrete Truck Mixer as a Function of Drum Charge Volume and Plastic Viscosity | |
| | S. Ng, & H. Justnes | 189 |
| | SCMs and Plasticizers: A Study on Their Effects on The Rheology and Early Age Hydration of Blended Cements | |
| | Ya Peng, Klaartje de Weerd, Bård Pedersen & Stefan Jacobsen | 193 |
| | Hydrostatic Pressure to Measure Sedimentation and Bleeding | |
| | Ahmad Ghadban, Mohammed Albahtiti, Kyle Riding, & David Lange | 197 |
| | Attenuation of Vibrations in Fresh Concrete | |
| | Niklas Johansson & Mats Emborg | 201 |
| | Methods to Optimize Aggregate Composition – Evaluation by Concrete Experiments | |
| 10 | FIBRES | 205 |
| | Katalin Orosz | 207 |
| | Strengthening of Concrete with Carbon Fibre Reinforced Polymer (CFRP) Grids Bonded by Cementitious Binders | |
| | Terje Kanstad & Steinar Trygstad | 211 |
| | Design, Testing and Evaluation of a Fullscale Post-Tensioned Steelfibre Reinforced Flat Slab | |

| | | |
|-----------|---|-----|
| | Gunrid Kjellmark, Tor Arne Martius-Hammer & Terje Kanstad | 215 |
| | COIN's 15 MPa Target Fibre Concrete: Materials Development Towards High Residual Flexural Strength | |
| | Ali Mohammadi Mohaghegh, Johan Silfwerbrand & Vemund Årskog | 219 |
| | An Initial Investigation of the Possibility to use Basalt Fibres for More Durable Concrete Structures in Norwegian Fish Farming | |
| | Carlos Gil Berrocal, Karin Lundgren & Ingemar Löfgren | 223 |
| | Experimental Investigation on Rebar Corrosion in Combination with Fibres | |
| 11 | SUSTAINABILITY AND AGEING | 227 |
| | Martin Nilsson | 229 |
| | Re-usage of Concrete Elements – To Determine Their New Possible Environment | |
| | Per Goltermann, Lisbeth Ottosen, Pernille Erland Jensen & Gunvor Marie Kirkelund | 233 |
| | ZeroWaste: Turning Waste into a New, Sustainable Resource for Concrete | |
| | Tobias Gasch & Richard Malm | 237 |
| | Effects of Aging Concrete in Support Structures for Hydroelectric Machinery | |
| | Mohamed Tabet & Abd El Hamid Guettala | 241 |
| | Numerical Modelling of Alkali Silica Gel in Mesoscopic Scale. | |
| | Gitte Normann Munch-Petersen & Christian Munch-Petersen | 245 |
| | Early Property Development in Concrete | |
| 12 | BINDERS, ADMIXTURES, MIX DESIGN AND RHEOLOGY, Cont. | 249 |
| | Tobias Danner, Harald Justnes, Mette R. Geiker & Alessia Colombo | 251 |
| | In-Situ XRD Studies of Phase Evolution During Hydration of Portland Cement Paste with Lignosulfonates | |
| | Helén Jansson & Tang Luping | 255 |
| | The Initial Setting Time of Ground Granulated Blastfurnace Slag GGBS and its Relation to the Modulus of The Alkali-Activating Solution | |
| | H. Justnes | 259 |
| | Properties of Gypsum-Free Portland Cement | |
| | Björn Lagerblad & Lars Elof Bryne | 263 |
| | Cement Hydration and Development of Texture and Bond at Interfacial Zone Between Hard Rock and Shotcrete. | |
| | Alessia Colombo, Tobias Alexander Danner, Klaartje De Weerd, Mette Rica Geiker & Harald Justnes | 267 |
| | Impact of mixing on early hydration of cement paste with lignosulphonate | |

| | | |
|-----------|--|-----|
| 13 | FIBRES, Cont. | 271 |
| | Oldrich Svec & Claus Pade | 273 |
| | Ultra High Performance Fibre Reinforced Concrete as a Waterproofing Solution for Concrete Bridge Deck Renovations | |
| | V. Tamužs | 277 |
| | Strengthening of Concrete by Fibres and Fibre Reinforced Plastics | |
| | Giedrius Žirgulis, Oldřich Švec, Terje Kanstad, Mette Rica Geiker & Andrzej Cwirzen | 281 |
| | Characterisation and Observation of Fibre Orientation in Flowable Steel Fibre Reinforced Concrete: Influence of Formwork and Reinforcement Layout | |
| | Cosmin Popescu, Gabriel Sas & Björn Täljsten | 285 |
| | Experimental Program for Axially Loaded RC Walls with Openings Strengthened by FRP | |
| | Björn Täljsten, Gabriel Sas & Thomas Blanksvärd | 289 |
| | Strengthening of concrete structures with FRP – a guideline | |
| 14 | SHRINKAGE AND DILATION | 293 |
| | Anders Ansell & Lars Elof Bryne | 295 |
| | Laboratory Evaluation of Shrinkage in Shotcrete Sprayed on Soft Drains | |
| | Katalin Orosz, Peter Fjellström, Jan-Erik Jonasson, Mats Emborg & Hans Hedlund | 299 |
| | Evaluation of Thermal Dilation and Autogenous Shrinkage at Sealed Conditions | |
| | Mia S. M. Lund & Kurt Kielsgaard Hansen | 303 |
| | Shrinkage Properties of Cement Stabilized Gravel | |
| | Valgeir O. Flosason, Olafur H. Wallevik & Eva L. Agustsdottir | 307 |
| | Long-term Shrinkage of Concrete using some Porous Icelandic Aggregates | |
| | Abdulaziz Alaskar & R Douglas Hooton | 311 |
| | Autogenous Deformation of High Performance Concrete - Pilot Study | |
| 15 | BINDERS, ADMIXTURES, MIX DESIGN AND RHEOLOGY, Cont. | 315 |
| | T.Østnor and H. Justnes | 317 |
| | Calcined Marl as Supplementary Cementing Material (SCM) | |
| | Erika Holt & Hannele Kuosa | 321 |
| | Developing Pervious Concretes for Urban Stormwater Management in Nordic Environments | |
| | Kalle Loimula | 325 |
| | Finnish Clay based Pozzolan and Dehydrated Cement Paste as Cement Replacement Materials | |

| | | |
|-----------|---|-----|
| | M. Fourmentin, P. Faure, U. Peter, D. Lesueur & P. Coussot NMR and Rheometrical Study of Lime-Cement Pastes | 329 |
| | Yared Assefa Abebe & Ludger Lohaus Effects of the Composition and Amount of Paste on the Pumpability and Pump-Stability of Flowable Concretes | 333 |
| 16 | CRACKING, CREEP AND REPAIR | 337 |
| | Mikael Hallgren Analyses of Minimum Reinforcement for Crack Control | 339 |
| | Jan Arve Øverli Slabs on Ground Subjected to Concentrated Loads | 343 |
| | Majid Al-Gburi , Jan Erik Jonasson & Martin Nilsson Effect of The Boundary Conditions on the Crack Distribution in Early Age Concrete | 347 |
| | Faez Sayahi, Mats Emborg & Hans Hedlund Plastic Shrinkage Cracking: Researches in Scandinavia | 351 |
| | Jonas Carlswård & Mats Emborg Shrinkage Cracking of Thin Concrete Overlays | 355 |
| 17 | CHLORIDES | 359 |
| | Dimitrios Boubitsas, Peter Utgenannt & Tang Luping Estimation of Chloride Threshold Values after 20 Years' Field Exposure in Swedish Marine Environment | 361 |
| | Søren L. Poulsen & Henrik E. Sørensen Experimental Determination of Chloride Threshold Values for Reinforcement Corrosion in Concrete: Experiences From the Lab | 365 |
| | Klaartje De Weerd, Silje Gystad Ytterdal & Mette R. Geiker On the Impact of Phase Changes on Chloride Profiles in Concrete | 369 |
| | Miguel Ferreira, Hannele Kuosa, Markku Leivo, Lasse Makkonen & David Lange The Effect of Freeze-Thaw Loading on Chloride Ingress. | 373 |
| | Tang Luping, Peter Utgenannt & Dimitrios Boubitsas Chloride Ingress in Concrete – Results from Over 20 Years' Field Exposure in Swedish Marine Environment | 377 |
| 18 | SELF-COMPACTING CONCRETE (SCC) | 381 |
| | Dimitri Feys & Kamal H. Khayat Analytical and Empirical Equations to Predict Pressure During Pumping of Self-Consolidating Concrete | 383 |

| | | |
|-----------|---|-----|
| | David A. Lange, Daniel I. Castaneda, Jeremy A. Koch, Randy H. Ewoldt & Kyle A. Riding | 387 |
| | Stability of Entrained Air in Self-Consolidating Concrete under Vibration | |
| | Þórður I. Kristjánsson & Olafur H. Wallevik | 391 |
| | Frost Resistance of Non Air Entrained Self Compacting Concrete | |
| | Abhay Bulsari & Klaus Juvas | 395 |
| | Nonlinear Modelling of Rheology of Self-Compacting Concrete with Two Rapid Cements | |
| | Farid Van Der Vurst, Ehsan Ghafari, Dimitri Feys, & Geert De Schutter | 399 |
| | Influence of Mixing Sequence on Rheological Properties of Self-Compacting Concrete | |
| 19 | CRACKING, CREEP AND REPAIR, Cont. | 403 |
| | Sara Korte, Veerle Boel, Wouter De Corte & Geert De Schutter | 405 |
| | Experimental Investigation of Concrete Fatigue Resistance | |
| | Jan-Erik Jonasson, Lars-Olof Nilsson, Mats Emborg & Hans Hedlund | 409 |
| | Moisture and Mechanical Properties Aimed for Crack Risk Analyses of Early Age Concrete | |
| | Markku Leivo | 413 |
| | Self-Healing Concrete HEALCON | |
| | Katalin Orosz, Peter Fjellström, Jan-Erik Jonasson, Mats Emborg & Hans Hedlund | 417 |
| | Evaluation of the Linear Logarithmic Creep Model | |
| | Edgar Bohner & Harald S. Müller | 421 |
| | Analytical Model for Predicting Time to Concrete Cover Cracking due to Corrosion of Reinforcement | |
| | Jonny Nilimaa | 425 |
| | Upgrading the Haparanda Bridge – Unbonded Posttensioning | |
| 20 | CARBONATION AND CORROSION | 429 |
| | Mahdi Kioumars, Max A.N. Hendriks & Mette Geiker | 431 |
| | Effect of Mesh Alignment on Simulated Interference of Localised Corrosion on Adjacent Reinforcement Rebars | |
| | Emma Qingnan Zhang & Tang Luping | 435 |
| | A Novel Anode Material for Cathodic Protection of Steel Reinforced Concrete Structures with Hybrid Functions | |
| | Carlos Gil Berrocal, Karin Lundgren & Ingemar Löfgren | 439 |
| | Experimental Investigation on Rebar Corrosion in Combination with Fibres | |
| | | 443 |

| | | |
|-----------|---|-----|
| | Katja Fridh, Ronny Andersson, Håkon Stripple, Martin Häglund, Lars-Olof Nilsson & Björn Lagerblad | |
| | A Model to Calculate the CO₂-Uptake in a Country's Concrete Structures During Service Life and After | |
| | M. Auroy, S. Poyet, P. Le Bescop, J-M. Torrenti, T. Charpentier, M. Moskura & X. Bourbon | 447 |
| | Representativeness of Accelerated Carbonation Testing of Cement Pastes | |
| 21 | MODELLING, ANALYSING AND TESTING | 451 |
| | Jiangpeng Shu, Mario Plos, Kamyab Zandi & Karin Lundgren | 453 |
| | Structural Assessment of Bridge Deck Slabs | |
| | Filippo Sangiorgio, Johan Silfwerbrand & Giuseppe Mancini | 457 |
| | Statistical Investigation on the Ultimate Load Behaviour of RC Continuous Beams Subjected to Multiple Failure Modes | |
| | Roghayeh Abbasiverki & Anders Ansell | 461 |
| | Analysis of Buried Reinforced Concrete Pipelines Subjected to Seismic Waves | |
| | Richard Malm & Tobias Gasch | 465 |
| | Finite Element Analyses of an Arch Dam Subjected to Seismic Loads and Hydrodynamic Forces | |
| | Niklas Johansson & Peter Johansson | 469 |
| | Water Absorption in Concrete – Experimental Studies and Modelling | |
| 22 | NUCLEAR, HYDRAULICS AND AGGRESSIVE ENVIRONMENTS | 473 |
| | M. Neji, B. Bary, N. Burlion & P. Le Bescop | 475 |
| | Modelling of The Chemo-Mechanical Behaviour of a Composite made of Ion Exchange Resins Incorporated into a Cement-Based Matrix | |
| | Mikael Oxfall, Peter Johansson & Manouchehr Hassanzadeh | 479 |
| | Moisture Profiles in Concrete Walls of a Nuclear Reactor Containment After 30 Years of Operation. | |
| | Martin Rosenqvist, Katja Fridh & Manouchehr Hassanzadeh | 483 |
| | Deterioration of Concrete in Hydraulic Structures due to Frost Action | |
| | Arezou Babaahmadi, Luping Tang & Zareen Abbas | 487 |
| | Chloride Penetration Resistance of Calcium Depleted Concrete Specimens | |
| | Markku Leivo, Tapio Vehmas & Erika Holt | 491 |
| | Developing Low pH Concrete for Tunnel Plugging Structures in Nuclear Waste Containment | |
| | Lise Juel-Hansen, Martin Kaasgaard | 495 |
| | Jack Anderson & Claus Pade | |
| | Development of Resistant Concrete Pipes to be Exposed in Aggressive Environments | |

| | | |
|-----------|--|-----|
| 23 | MODELLING, ANALYSING AND TESTING | 499 |
| | Jan-Erik Jonasson, Peter Fjellström, Mats Emborg & Hans Hedlund Measurement and Modelling of Strength and Heat of Hydration for Young Concrete | 501 |
| | Anders Hösthagen, Jan-Erik Jonasson, Mats Emborg & Hans Hedlund Equivalent Restraint Method Correlated to Empirical Measurements | 505 |
| | Martin Persson, Ulf Ohlsson & Mats Emborg Bridge Deck Concrete Overlays – Full Scale Studies and Theoretical Analysis | 509 |
| | Abhay Bulsari & Erik Nordenswan Nonlinear Modelling of the Dynamics of Accelerated Hardening of Concrete | 513 |
| | Lasse Frølich Engsig Using Isothermal Calorimetry to Predict Early Mortar Strengths | 517 |
| 24 | CONCRETE CAFÉ | 521 |
| | Per Goltermann Teaching Concrete Structures: Development and New Experiences | 523 |
| | AUTHORS LIST | 527 |

OPENING SESSION

COIN – Main Achievements



Tor Arne Martius-Hammer
 Centre Director, COIN – Concrete Innovation Centre (www.coinweb.no) at
 SINTEF Building and Infrastructure,
 Rich. Birkelands v3, N-7465 Trondheim, Norway,
tor.hammer@sintef.no

ABSTRACT

The present paper presents a glance of main achievements from COIN – Concrete Innovation Centre, which is a Norwegian centre for research based innovation, founded by the Research council of Norway. The centre has proven to be an effective tool for innovation and creation of added value, as well as to communicate concrete research results to the society and educate state-of-the-art engineers. The work is organised in three focus areas, as a result of the need of partners and society: Environmentally friendly concrete structures, economically competitive construction and technical performance. The work has created new products, some of them already taken to the market, e.g. binders and admixtures, new software soon on the market, guides, e.g. design guide for fibre reinforced concrete, material models and test methods, the latter for instance to allow more reliable service life prediction and more environmentally friendly or economical use of resources.

Key words: Innovation, Research centre, Environmental friendly concrete structures, economically competitive construction, technical performance

1. INTRODUCTION

In 2006 the Research Council of Norway (<http://www.forskningsradet.no>) established 14 Centres for Research-based Innovation, CRI, as a tool to stimulate the industry to further innovation. The purpose is to build up and strengthen Norwegian research groups that work in close collaboration with partners from innovative industry and innovative public enterprises, through long-term research. COIN – Concrete Innovation Centre is one of these 14 CRIs, and the only one within materials and structures. The paper presents a glance of main achievements from COIN, after 7 years of work. More information can be found on www.coinweb.no.

The consortium partners of COIN represent the value chain of the business sector, and they represent leading multinational companies in the cement and building industry. All partners are represented in the Board. The main measures to establishing links and integration between the partners, and to ensure competence transfer between the partners, are to have joint activities from project initiation and planning to report.

The research work is performed by the staff at SINTEF, NTNU including 16 PhDs, and by the industrial partners (in-kind). The technical activities in COIN are organized based on the social, environmental and industrial needs, as well as on the innovation strategies anchored in the corporate management of the industry partners. The work is organized in 3 focus areas:

- F1) Environmental friendly concrete structures
- F2) Economically competitive construction
- F3) Technical performance

COIN started in 2007 and the RCN grants terminate at the end of 2014. All CRI's were evaluated at mid-term; the fall 2010. A part of the evaluation was a self-evaluation made by

each partner. The industrial partners of COIN said that it is important to have a central research centre and that it contributes to: Increased and more active research as well as strengthened innovation strategy in the companies - Short communication lines and way to the competence - New liaisons and extended network - Easier recruiting - Improved basis for new markets, products and processes with better quality and sustainability - Safer structures with longer service life and lower maintenance cost - Results used directly in marketing - Increased sales and significantly reduced cost under run.

NTNU said: Increased research activity - "Excellent" collaboration and strengthened industry contact - Short way from industry relevant research to education – Many master thesis - Attracts highly qualified PhD-students (a total of 16 COIN PhDs) - Increased international cooperation.

COIN has become well known and the display window for concrete research in Norway. Hence, this centralisation, and the fact that most of the results are public, has made it considerably easier for the environment outside the COIN partners, public authorities included, to have access to concrete research results (e.g. via www.coinweb.no), and to see the importance of concrete. Also, the direct use of the results in the education at NTNU contributes to educate engineers with state of the art knowledge, to the benefit of the industry and society.

2. SUSTAINABLE BINDERS AND HARDENING ACCELERATOR

The easiest way of making concrete more sustainable is to either replace clinker in cement, or cement in concrete, with supplementary cementing materials, e.g. fly ash, that have a smaller "carbon footprint" than clinker or cement, respectively. A combination of 30% fly ash/5% limestone has proven to give higher strength than 35% fly ash only, meaning that limestone has higher efficiency factor than fly ash in terms of strength. A 35% calcined marl replacement showed much higher strength than any of the other replacements. Also, replacement with calcined marl up to 50% show really lowered intrusion of chlorides.

Using fly ash blended with higher replacement level of OPC is limited by the low rate of reaction at early age of fly ash, leading to low early compressive strength. Therefore, a hardening accelerator was developed and now patented. A combination of small dosages of a sodium thiocyanate, diethanolamine and glycerol ("3-component admixture") appeared to be effective in enhancing the early strength of OPC-FA. A synergistic effect on the acceleration of the hydration of OPC-FA was observed when applying the 3-component admixture, in that it lead to a higher rate of cement hydration compared to samples using the chemicals individually

3. ROBUSTNESS OF SCC

One obstacle for more extended use of SCC is the lack of understanding on concrete stability and simple tools for describing and control of stability both for lab and jobsite. The work revealed that commonly used stability test methods, static stability methods in particular, do not reflect the stability challenges occurring on site. Hence there is a need for better test methods. The fundamental stability principles of the matrix phase are investigated by the use of a proposed conceptual model for sedimentation and bleeding. A new sedimentation test method for fresh matrix was developed based on continuous recording of the pore water pressure at various heights.

4. DUCTILE HIGH TENSILE STRENGTH CONCRETE (FIBRE REINFORCED CONCRETE)

The objectives are formulated as; (1) To do R&D work which stimulates and makes use of fibres possible in load carrying concrete structures, and (2) Further develop an ordinary concrete

with high residual tensile strength, exemplified with target of 15MPa. The good agreement which is achieved between flow simulations, Computer tomography (CT-) scans, image analyses of sawn sections and mechanical testing clearly indicates that further research with these processes will lead to improved practice with safer and more economical use of fibres in general. The work shows that optimised proportioning and fibre types has allowed quite high amounts of fibres and still satisfactory workability. However, the high amount cannot be utilised fully to improve the tensile strength and ductility in normal strength concretes, because there is a strong tendency of collective pull out. Hence, it is necessary to increase the concrete strength to reach the goal.

5. IMPROVING THE QUALITY OF CRUSHED FINE AGGREGATES

One conclusion from the work is that the finest part of the crushed sand should get most of the further research attention. One of the main research directions, with a direct link to industry and society, would then be to develop a crushing and processing technique that would allow improving the quality of crushed fine aggregates. This was addressed by studying how the crushing process parameters, influence the fresh state properties (rheology) of concrete. The results revealed the principal differences between different types of crushers used, and it was mapped out some crushing parameters that can have crucial effect on the fresh concrete rheology.

6. CONCRETE SURFACE CLASSIFICATION

The goal is to develop a classification tool in order to describe smooth formed concrete surfaces objectively, in order to avoid subjective descriptions leading to misunderstandings and time-consuming and expensive conflicts for owners, architects and construction companies. In the suggested classification system, greyscale variations and pore size and distribution are the main parameters. The system is based on pictures. A prerequisite is then to find a procedure that always gives the same light conditions during photographing. This is solved by using a "soft box" (large umbrella). The pictures are then managed in a Matlab-based software, called "BetongGUI" (will commercially available) with two separate functions; pores and greyscale variations. Currently, work is undertaken to gain experience about the robustness of the method, and to generate a database to calibrate the picture-taking procedure in-situ and the software.

7. CRACK FREE CONCRETE STRUCTURES

The issue is risk of early age cracking (thermal cracking) in heavy structures where the hydration generated heat may cause large temperature differences. A new special purpose early age concrete calculation program, "Crack-TestCOIN", has been developed. The use of low-heat concrete is favourable for sustainability reasons. So far it seems like the optimum FA content, is around one third of the total binder content. When higher FA dosages are being used, the negative effect of the loss in tensile strength seems to be larger than the positive effect of reduced hydration heat.

8. CHLORIDE INGRESS AND ELECTRICAL RESISTIVITY

A thorough literature review has shown that the present state of the art does not allow improving current practice. Moreover, values for theoretical chloride contents commonly used are based on experience with Portland cement; critical chloride contents for modern binder types are in general unknown. Our experimental work indicated how measuring setups for the critical chloride content can be improved so that the results are more reliable and realistic. On the basis of theoretical, probabilistic considerations it is suggested how laboratory results might be transferred to practice. A correlation could be expected between the corrosion process of steel embedded in concrete and the electrical resistivity of concrete. A literature review shows

however, that the dependency varies between studies of different concretes, and one single relationship cannot be established between corrosion rate and conductivity.

9. ALKALI-SILICA-REACTIONS

COIN has aimed to evaluate whether concrete prism tests (CPTs) developed for assessment of alkali-silica reactivity of aggregates, might be suitable for general ASR performance testing of concrete. Focus has been on the internal moisture state in the test prisms and extent of alkalis leaching out from the prisms during the ASR exposure. Our work has continuously given important input to the work in RILEM TC-219 ACS-P (2007-2012), where the objective is to develop a reliable performance testing concept. Based on our preliminary results, the RILEM committee immediately withdrew two of the three RILEM methods.

10. LIGHTWEIGHT AGGREGATE CONCRETE (LWAC)

There is a general scepticism regarding the use of LWAC in heavy loaded structures because of the more brittle post-peak material behaviour and smoother crack surfaces. In our work, the main hypothesis is that the strength and especially the ductility of structural concrete members depend on local multiaxial stress conditions that develop within the compressive zone prior to failure. This was confirmed by multiaxial tests. It led to the hypotheses that fibre reinforcement could be a good solution. This was verified by a series of large beam tests, to study the passive confinement effect of different configurations in the compression zone in a structure. The experiments demonstrated that a reinforced LWAC structure, may satisfy requests for energy dissipation and controlled behaviour, and even a capacity increase, in the post-peak response when steel fibre reinforced.

Using LWAC in combination with normal weight concrete is another possibility of structural optimisation with respect to weight. The beams studied are composed by different layers of concrete either cast wet-on-wet or at different times, and with really promising results.

Development of high performance LWA is a parallel activity to further improve the competitiveness of LWAC. Different strategies to improve the mechanical properties of expanded clay aggregates have been tested with very good results. New understanding of the strength determining factors as well as the fracture behaviour of LWA was achieved.

11. ICE ABRASION

A purpose-built test rig was used to simulate the effect of ice sliding against concrete surfaces. The rig allows variation in different parameters such as ice-pressure, temperature, velocity and material qualities. By exposing new materials for the same test conditions as materials collected from structures with long-term field exposure, we can estimate the expected design lifetime for the new materials. The results have helped to design the exposed ice zone of arctic offshore concrete shafts without the expensive steel lining.

ACKNOWLEDGEMENTS

COIN has an annual budget of NOK 25 mill, and is financed by RCN (approx. 40 %), industrial partners (approx 45 % of which ¼ is cash) and by SINTEF and NTNU (in all approx 15 %). The Centre is directed by SINTEF, with NTNU as a research partners and with the present industrial partners: Kværner, Norcem, the Norwegian Public Roads Administration, Mapei, Skanska, Unicon, Veidekke and Weber Saint Gobain.

DURABILITY, MAINTENANCE, RENOVATION & FROST ACTION
PER FIDJESTØL MEMORIAL SESSION

Advantages of Silica fume-Slag Ternary Binders for Production of Durable Concrete



R. Doug Hooton
University of Toronto
Department of Civil Engineering
Toronto, Canada, M5S1A4
Email: hooton@civ.utoronto.ca

ABSTRACT

Regardless of exposure, durable concretes need to have high resistance to ingress of water and aggressive ions, such as chlorides and sulphates. When properly dispersed with high-range water reducers, silica fume has enabled the attainment of high fluid penetration resistance at early ages. However, long-term improvements in concrete economy and properties including fluid penetration resistance can also be obtained using locally available, supplementary cementitious materials such as slag. As a result, in Ontario, Canada, since 1986 almost all high-strength and high-durability concretes using silica fume also include slag. The physical and durability properties of concretes made using these ternary binder systems are discussed.

Key words: Durability, ternary cements.

1. INTRODUCTION

The introduction of silica fume in Ontario, Canada during the mid-1980s had an immediate positive impact on the ability of concrete suppliers to provide high early strength concrete for tall buildings /Bickley et al 1994/ and also in improving resistance to aggressive environments /Hooton 2000/. However, this also included challenges in controlling rheology, in concrete finishing, plastic shrinkage cracking and increased heats of hydration. Since ground-granulated blast-furnace slag was already in common use in Ontario (at a 20-35% level depending on the season), with the exception of a few early projects, silica fume has always been added together with slag. The slag reduced the high-range water reducer requirements, reduced “stickiness” during finishing, reduced early-age heat of hydration and also provided increased long-term strength gain. The plastic shrinkage cracking issue on bridge and parking decks (a problem not unique to silica fume concretes) was solved by introduction of fog misters and evaporation retarders. In addition, since about 1987-88, improved distribution of silica fume in the concrete ingredients has been handled by the introduction of silica fume blended cements containing 7-8% silica fume. Due to Canadian concrete industry interest in adopting the use of silica fume, the Canadian CSA standard for silica fume was adopted in 1983, which was the first national standard globally.

2. CHLORIDE RESISTANCE

El-Dieb and Hooton /1995/ showed that silica fume-slag ternary concretes had extremely low permeability to water. McGrath and Hooton /1997/ showed that these systems have high

resistance to chloride diffusion. Nokken and Hooton /2006/ found that electric conductivity of ternary blends were lower than with slag or silica fume alone. In addition, Titherington and Hooton /2004/ showed that when exposed to accelerated curing (held at 9h at 65°C), 18h strengths of over 40 MPa could be obtained and the ternary systems maintained low chloride diffusion coefficients better than Portland cement concretes as shown in Table 1.

Table 1 – 18 h Strength and 28 day chloride resistances of concrete exposed to either accelerated curing at 65°C, or ambient at 23°C, then cured in air unless noted until 28 days

Note: migration tests as described in McGrath and Hooton /1996/.

| Mixture w/cm = 0.30 | Curing | 18 hr Strength (MPa) | ASTM C1202 (Coulombs) | Non-steady state chloride migration (10^{-12} m^2/s) | Steady-state chloride migration (10^{-12} m^2/s) |
|------------------------|-----------------------------------|----------------------------|-----------------------------|---|---|
| 100% PC | ambient | 24.2 | 2280 | 4.4 | 4.0 |
| 100% PC | accelerated | 31.3 | 3120 | 20.1 | 18 |
| 4% SF | ambient | 25.6 | 520 | 1.1 | 0.92 |
| 4% SF | accelerated + 6d moist cure | 40.7 | 980 | 2.9 | 2.7 |
| 4% SF | accelerated | 40.9 | 1050 | 7.2 | 4.5 |
| 8% SF | ambient | 24 | 270 | 0.48 | 0.28 |
| 8% SF | accelerated | 45.4 | 230 | 1.0 | 0.95 |
| 4% SF, 25% Slag | ambient | 17.5 | 310 | 0.86 | 0.55 |
| Type 10SF, 25% Slag | ambient | 25.6 | 260 | 0.91 | 0.52 |
| 8% SF, 25% Slag | ambient | 12.7 | 175 | 0.41 | 0.18 |
| 8% SF, 25% Slag | accelerated | 40.5 | 125 | 0.57 | 0.54 |

3. SULPHATE RESISTANCE

When used independently, both silica fume /Hooton 1993/ and slag /Hooton 2000/ are effective in improving resistance to sulphate attack. Ternary systems are effective at much lower slag replacement levels (less than 50%). Figure 1 shows that 25% both slag plus 6% SF and 35% slag plus 5% SF were effective in keeping ASTM C1012 expansions with a 12% C₃A portland cement to less than 0.10% after 18 m exposure to 5% NaSO₄ solutions (the ACI 318 code limit for very severe exposures) /unpublished data from MASc thesis of A. Smith 2002/.

4. MITIGATION OF ALKALI-SILICA REACTION

In both laboratory ASTM C1567 mortar bar and ASTM C1293 concrete prism tests and in large field exposure specimens, silica fume plus slag ternary mixtures have shown excellent performance /Bleszynski et al 2002; Hooton et al 2012/. Concrete beams 0.6 x 0.6 x 2.0 m as well as pavement sections made with 3.8% silica fume and 25% slag have not shown any damage after 20 years outdoor exposure /Hooton et al 2012/. Without the silica fume, 50% slag was required to mitigate ASR damage, but 50% slag was higher than what the Ontario Ministry of Transportation wanted to use due to concerns regarding de-icer salt scaling. At another location but using the same Spratt reactive aggregate, 16 year old pavements made with 8% silica fume, 6% silica fume plus 25% slag; 4% silica fume plus 35% slag have all mitigated expansion. As shown by Bleszynski et al /2002/ and Hooton et al /2010/, sufficient mitigation to reduce 2-year ASTM C1293 concrete prism expansions to below 0.040% (the limits used in CSA A23.2-28A and ASTM C1293), resulted when the pore solution alkalinities were reduced to less than 320 to 365 mmol/l (measured either as OH⁻ or as the sum of K⁺ and Na⁺) as shown

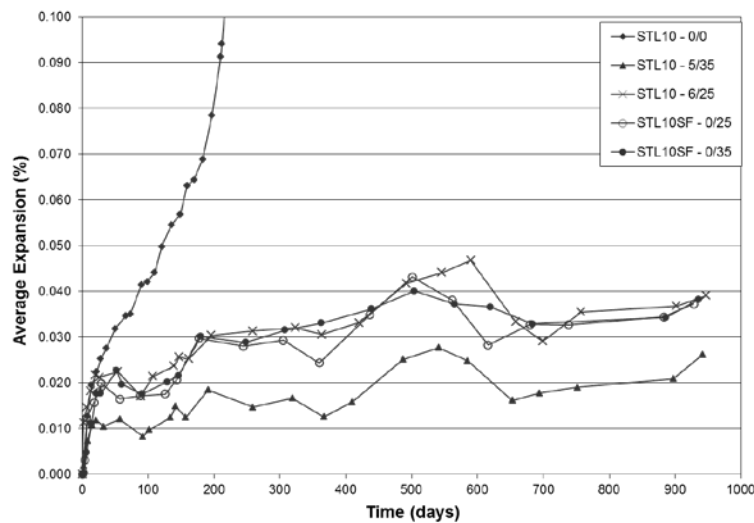


Figure 1 - ASTM C1012 sulphate expansions of 12% C3A cement and ternary mixtures containing silica fume and slag Notes: STL10 = Portland cement; STL10SF= blended cement with 8% SF; X/XX= % silica fume/ % slag replacements respectively.

in Figures 2 and 3. These pore solution alkalinities are higher than the 200 to 250 mmol/L values previously proposed by Diamond /1983/. On its own, the silica fume is effective at reducing the alkalinity at early ages but alkalinity rises slightly over time. This rise in alkalinity does not occur with alumina-bearing supplementary cementing materials such as slag, perhaps due to higher and more permanent alkali binding in alumina substituted C-A-S-H /Hong and Glasser 2002/. In ternary mixtures, due to its aluminate contribution and longer-term hydration, the slag helped maintain the low alkalinity over the long-term.

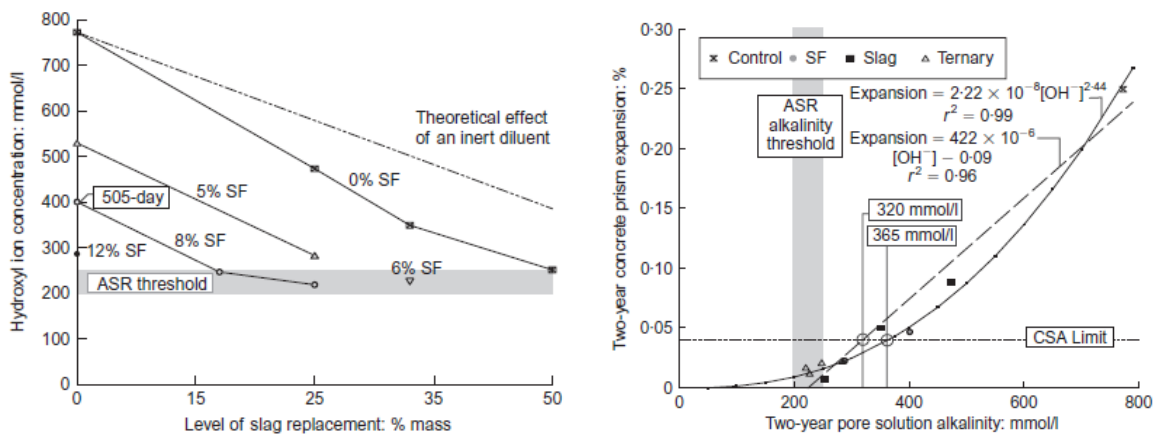


Figure 2a (left) – Pore solution alkalinity after 2 years with increasing slag and silica fume replacements of a high alkali cement.

Figure 2b(right) – 2-year ASTM C1293 expansion in relation to pore solution alkalinity.

5. SUMMARY

Silica fume plus slag ternary mixtures have been used successfully in both high strength and high durability applications for almost 30 years in Ontario in both ready mixed and precast concrete. The impact of using these cementitious combinations to improve both early-age and long-term physical properties and durability was significant. This paper is dedicated to Per Fidjestol of Elkem Materials who had an influence on the early adoption of silica fume

technology through his active participation in Canadian and US conferences and standards committees.

REFERENCES

- Bickley, J.A., Ryell, J., Rogers, C., Hooton, R.D., 1994.
 “Some Characteristics of High Strength Structural Concrete: Part 2”, Canadian Journal of Civil Engineering, Vol. 21, 1994, 1084-1087.
- Bleszynski, R.F., Hooton, R.D., Thomas, M.D.A., Rogers, C.A., 2002,
 “Durability of Ternary Blend Concretes with Silica Fume and Blastfurnace Slag: Laboratory and Outdoor Exposure Site Studies”, ACI Materials Journal, Vol. 99, No. 5, Sept-Oct 2002, pp. 499-508.
- Diamond, S., 1983.
 “Alkali Reactions in Concrete-Pore Solution Effects,” Proceedings, 6th International Conference on Alkalis in Concrete, Danish Concrete Association, Copenhagen, pp. 155-166.
- El-Dieb, A.S., Hooton, R.D., 1995.
 “Water Permeability Measurement of High Performance Concrete Using a High Pressure Triaxial Cell”, Cement and Concrete Research, Vol. 25, No. 6, 1995, pp. 1199-1208.
- Hong, S-U., Glasser, F.P., 2002.
 “Alkali sorption by C-S-H and C-A-S-H gels Part II. Role of alumina,” Cement and Concrete Research, Vol. 32, pp. 1101–1111.
- Hooton, R.D., 1993.
 “Influence of Silica Fume Replacement of Cement on Physical Properties and Resistance to Sulfate Attack, Freezing and Thawing, and Alkali-Silica Reactivity”, ACI Materials Journal, Vol. 90, No. 2, March/April 1993, pp. 143-151.
- Hooton, R.D., 2000.
 “Canadian Use of Ground Granulated Blast-Furnace Slag as a Supplementary Cementing Material for Enhanced Performance of Concrete”, Canadian Journal of Civil Engineering, Vol. 27, 2000, pp. 754-760.
- Hooton, R.D., Thomas, M.D.A., Ramlochan, T., 2010.
 “Use of Pore Solution Analysis in Design for Concrete Durability,” Advances in Cement Research, Vol. 22, No. 4, Oct. 2010, pp.203-210.
- Hooton, R.D., Rogers, C.A., MacDonald, C.A., Ramlochan, T., 2013.
 “20-Year Field Evaluation of Alkali-Silica Reaction Mitigation,” ACI Materials Journal, Vol. 110, No. 5, 2010, pp. 539-548.
- McGrath, P.F. and Hooton, R.D., 1996.
 “Influence of Voltage on Chloride Diffusion Coefficients from Chloride Migration Tests”, Cement and Concrete Research, Vol. 26, No. 8, pp. 1239-1244.
- McGrath, P.F., Hooton, R.D., 1997.
 “Effect of Binder Composition on Chloride Penetration Resistance of Concrete”, Proceedings of the Fourth International Conference on Durability of Concrete, Sydney, ACI SP-170, Vol. 1, Aug. 1997, pp. 331-347.
- Nokken, M.R., Hooton, R.D., 2006.
 “Electrical Conductivity as a Prequalification and Quality Control Tool”, Concrete International, Vol. 28, No. 10, pp. 61-66.
- Titherington, M.P., Hooton, R.D., 2004.
 “Chloride Resistance of High Performance Concretes Subjected to Accelerated Curing,” Cement and Concrete Research, Vol. 34, No. 9, 2004, pp.1561-1567.

Self-compacting concrete without chemical admixture for Per Fidjestol



Olafur H. Wallevik
 Dr.Ing., Prof.
 ICI Rheocenter, Reykjavik University & Innovation Center Iceland
 Arleynir 2-8
 IS-112 Reykjavik
 E-mail: wallevik@ru.is



Indridi Nielsson
 B.Sc., M.Phil.
 Verkis
 Ofanleiti 2
 IS-103 Reykjavik
 E-mail: in@verkis.is



Bjorn Hjartarson
 B.Sc., M.Sc.
 ICI Rheocenter, Reykjavik University & Innovation Center Iceland
 Arleynir 2-8
 IS-112 Reykjavik
 E-mail: bh@nmi.is

ABSTRACT

Research on self-compacting concrete (SCC) in a project named TOPIC showed that it is possible to cast SCC without chemical admixtures. This required relatively high addition of water to about 230 l/m^3 which is very high, but though not unknown in production of concrete in some countries at the time this research was conducted (between the year 1999 to 2002). Silica fume was used as a stabilisator as it reduces the mobility of water in the mix and thereby reduce particle segregation in the mix. The major goal in this research is to lower the water content. It is clear that the binder type and composition plays the largest role in the water demand of concrete and therefore has the focus been mainly on its rheological properties. Rheological measurements on fresh concrete and mortar was the key factor in the mix-design development. Several binder composition where evaluated in a coaxial cylinder viscometer before finding the solution. The final mix had very low plastic viscosity or about $10 \text{ Pa}\cdot\text{s}$ and slump flow 630 mm. The binder content (cement, FA and silica fume) was 375 Kg/m^3 resulting in cylinder compressive strength of 22 MPa. Several other mixes were conducted where for instance fly ash was replaced with lime stone filler and as expected resulted in lower strength but otherwise very acceptable as a SCC. The project work was initiated by Per Fidjestol from Elkem and is presented here in his honour.

Key words: Self compacting concrete, Silica fume, no chemical admixture, rheology.

Comparison of durability parameters of self-compacting concrete and conventional slump concrete designed for marine environment



Martin Kaasgaard
Consultant, M.Sc.
Danish Technological
Institute
Gregersensvej
DK-2630 Taastrup
E-mail: mkaa@dti.dk



Claus Pade
Team Manager, M.Sc.
Danish Technological
Institute
Gregersensvej
DK-2630 Taastrup
E-mail: cpa@dti.dk

Ulf Jönsson
Construction Manager, M.Sc.
Femern A/S
Vester Søgade 10
DK-1601 København V
E-mail: ujo@femern.dk

Christian Munch-Petersen
Concrete Expert, M.Sc.
Emcon A/S
Ordrupvej 60
DK-2920 Charlottenlund
E-mail: cmp@emcon.dk

ABSTRACT

In this study self-compacting and slump concretes of respectively fly ash concrete, 3-powder concrete (Portland cement, fly ash, silica fume) and concrete based on slag cement were investigated. The concretes were batched and mixed using an industrial scale concrete mixing station applying special procedures that ensured high batching accuracy and identical mixing sequence. The fresh concrete properties were measured and a suite of test specimens were cast comprising cylinders and cubes as well as larger size blocks for long term exposure testing. The strength development and accelerated durability parameters such as frost resistance and chloride migration coefficient were assessed. Chloride penetration profiles were obtained after 6 months of exposure to sea water. The results indicate that self-compacting concrete performs similar to the conventional slump concrete in all aspects of durability.

Key words: Self-compacting concrete, slump concrete, supplementary cementitious materials, durability.

1. INTRODUCTION

Self-compacting concrete (SCC) is widely used in DK. The majority of precast plastic concrete is SCC and close to 40 % of the ready-mixed concrete production is SCC. However, even if SCC in Danish regulations is fully allowed for any exposure, SCC is generally not used under severe exposure conditions such as marine environments, the purpose for which it was originally developed in Japan in the late 1980's [Okamura, 2003].

Even if SCC is allowed in any exposure class only limited documentation exists that SCC based on local materials and traditions will perform just as good in service in terms of durability as a conventional solution using slump concrete. This is obviously not an optimal situation for the promotion of SCC.

Consequently, in Denmark there is a need for documentation of durability properties of SCC mix designs having comparable materials cost to conventional concrete mix designs. This was among the reasons why Femern A/S as owner of the coming Femern Belt Fixed Link between Denmark and Germany initiated laboratory and field tests on the durability of a variety of concrete compositions - including SCC - all potentially suitable for marine structures.

2. EXPERIMENTAL WORK

The concrete compositions and the testing program were designed in a co-operation between Femern A/S and Danish Technological Institute. The experimental work comprised mixing, casting and testing of six types of concrete, three self-compacting and three conventional slump concretes of similar binder compositions; Portland cement (CEM I) + fly ash, Portland cement (CEM I) + fly ash + silica fume, blast furnace slag cement (CEM III/B). All concretes had w/c ratio 0.40 and a target air content of 4.5%. For each concrete type two concrete blocks with dimensions 2000 x 1000 x 200 mm and 1000 x 1000 x 200 mm respectively were produced and furthermore a number of cylinders and cubes were cast. The large blocks were exposed to the marine conditions at the Femern Belt exposure site at Rødbyhavn, while the smaller blocks, the cylinders and the cubes were used for initial characterization of the different concrete types.

Only selected important durability related parameters from the test program are presented in this article. More data on the 6 concrete types presented in this study can be found in the original article [Kaasgaard et.al., 2013] and data on all 15 concrete types can be found at www.concreteexpertcentre.dk.

3. RESULTS AND DISCUSSION

Results from testing of frost resistance and chloride ingress are presented in Table 1.

Table 1 – Durability parameters of frost resistance (m56 scaling) and chloride ingress (chloride migration coefficient (CMC), chloride diffusion coefficient (CDC), surface concentration (Cs) and K value.

| | Fly ash Slump | Fly ash SCC | 3-powder Slump | 3-powder SCC | Slag cem. Slump | Slag cem. SCC |
|-----------|------------------|----------------|-------------------|-----------------|--------------------|------------------|
| m56 | 0.02 | 0.04 | 0.03 | 0.05 | 0.39 | 0.41 |
| CMC, 28d | 27.5 | 23.3 | 9.7 | 9.9 | 2.5 | 2.3 |
| CMC, 180d | 2.3 | 2.9 | 2.8 | 3.1 | 1.3 | 1.0 |
| CDC | 2.93 | 3.11 | 2.76 | 1.68 | 0.61 | 0.33 |
| Cs | 0.35 | 0.40 | 0.44 | 0.46 | 0.29 | 0.31 |
| K | 19.9 | 21.6 | 20.9 | 16.6 | 8.5 | 6.4 |

The frost resistance of slump concrete and SCC is virtually identical. The fly ash and 3-powder concretes have “very good” frost resistance ($< 0.10 \text{ kg/m}^2$ scaling after 56 freeze/thaw cycles), while both the CEM III/B concretes have only what corresponds to “good” frost resistance according to the SS 13 72 44 test method. The finding that concrete containing blast furnace slag has a reduced salt scaling frost resistance is in agreement with previously reported results [Utgenannt, 2001], [Valenza, 2007].

In general the results seem to suggest that there is no difference in the frost resistance between slump concrete and SCC of comparable air void structure provided that both types of concrete have been cast properly. Although not supported by any referenced results this was also the conclusion by the recent RILEM TC 205-DSC [RILEM, 2008].

No difference between slump concrete and SCC could be recognized in the chloride ingress parameters recorded.

Quite similar chloride migration coefficients were obtained for the respective slump and SCC concretes with same binder systems at 28 maturity days as well as after 180 maturity days. The development in the migration coefficient over time is markedly different for the three binder systems investigated. At early stages (28 days) as expected the slag cement concretes have the lowest values, the 3-powder concretes have intermediate values, and the fly ash concretes the

higher values. After 180 days the slag concretes still exhibit the lowest migration coefficients, but the fly ash concretes have “caught up” with the 3-powder mixtures; both binder systems having migration coefficients in the range 2 to $3 \times 10^{-12} \text{ m}^2/\text{s}$ or about twice that of the slag cement concretes.

The chloride profiles of cores drilled below sea level from the larger blocks after six months of exposure are presented in Figure 1. As seen from the figure the ingress profiles of the SCC and slump concretes with similar binder systems are fairly similar. These similarities are also expressed in the diffusion coefficients, surface concentrations and K value parameters estimated from the best fit Fick’s second law solution to the profiles (Table 1). For the 3-powder and slag cement concretes, the SCCs generally have lower chloride contents at all depths than their slump counter parts, whereas the opposite is the case for the fly ash concretes. However, the differences are quite small and presumably within what can be expected between two profiles from the same level of the same concrete specimen.

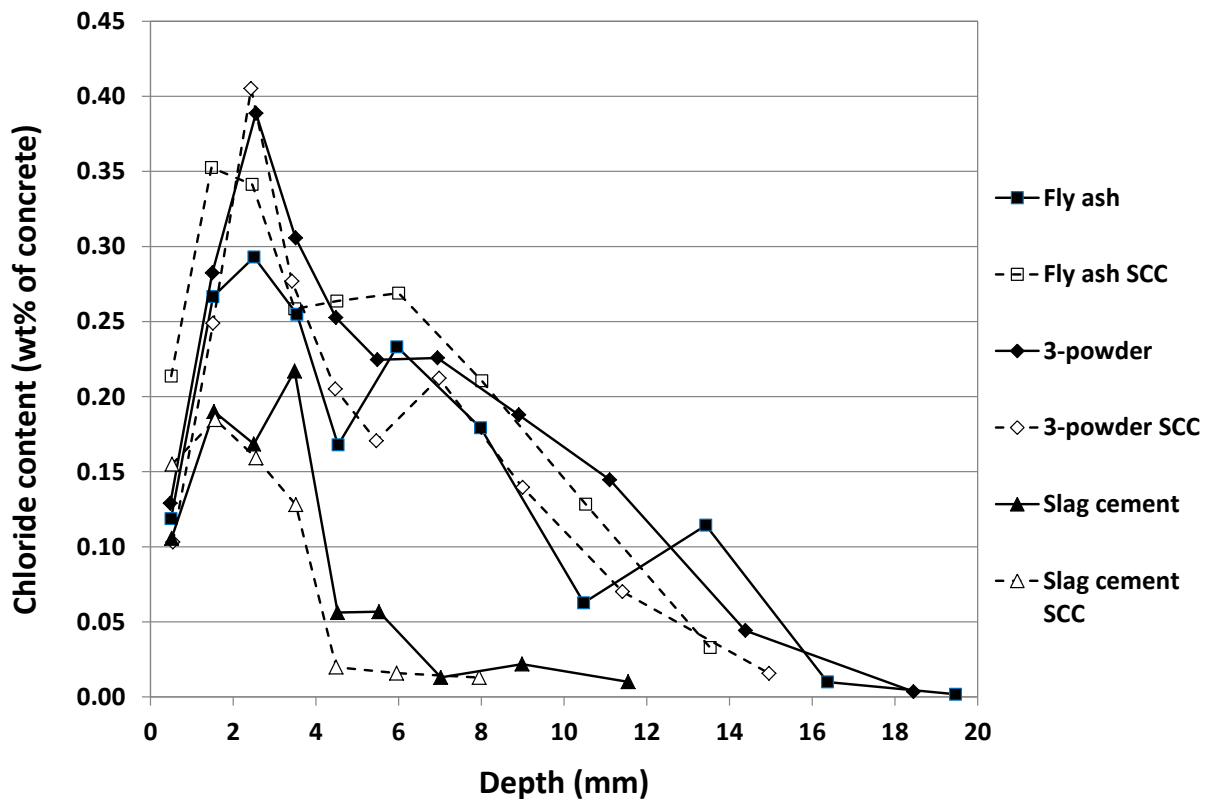


Figure 1 – Chloride profiles from 1m below the waterline after 6 months exposure of large blocks at the Femern Belt exposure site at Rødbyhavn.

Only limited information has until now been made available in the literature concerning chloride ingress in SCC [RILEM, 2008]. However, a recent Swiss study [6] investigating the chloride ingress into concrete by three different accelerated methods of four different binder systems at different water/powder ratios ranging from 0.35 to 0.60 supports the findings of the current study, i.e. that the chloride resistance of SCC is similar to that of slump concrete with corresponding binder.

Likewise, Zhu and Bartos [Zhu, 2003] found that the chloride migration coefficients of fly ash SCC and fly ash slump concrete with water to powder ratios of 0.35 and 0.36 respectively were almost identical, i.e. 6.3 and $6.6 \times 10^{-12} \text{ m}^2/\text{s}$.

A discussion of the reasons behind the observed differences between the chloride ingress parameters of the three investigated binder systems is beyond the scope of this paper.

4. CONCLUSIONS

For the three investigated binder systems Portland cement (CEM I) + fly ash, Portland cement (CEM I) + fly ash + silica fume and slag cement (CEM III/B) it may be concluded that self-compacting concrete performs similar to conventional slump concrete with respect to the durability parameters investigated.

5. ACKNOWLEDGEMENTS

The authors gratefully acknowledge Femern A/S and the Danish Expert Centre for Infrastructure Construction, without their support this paper would not have been possible.

REFERENCES

- Kaasgaard, M.; Pade, C.; Jönsson, U.; Munch-Petersen, C., 2013
 “Comparison of durability parameters of self-compacting concrete and conventional slump concrete designed for marine environment”, *Nordic Concrete Research*, No. 47, 2013
- Loser, R.; Lothenbach, B.; Leeman, A.; Tuchschnid, M., 2010
 “Chloride resistance of concrete and its binding capacity – Comparison between experimental results and thermodynamic modeling”, *Cement and Concrete Composites*, V. 32, 2010, pp. 34-42.
- Okamura, H.; Ouchi, M., 2003
 “Self-Compacting Concrete”, *Journal of Advanced Concrete Technology*, V. 1, No. 1, April 2003, pp. 5-15.
- RILEM Technical Committee 205-DSC, “Durability of self-compacting concrete”, 2008
Materials and Structures, V. 41, 2008, pp. 225-233.
- Utgenannt, P., 2001
 “Frost resistance of concrete – Experience from three field exposure sites”, *SP report 2001:30*, Swedish National Testing Institute, Borås, Sweden, 2001
- Valenza II, J.J.; and Scherer, G.W., 2007
 “A review of salt scaling: I. Phenomenology”, *Cement and Concrete Research*, V. 37, 2007, pp. 1007-1019
- Zhu, W.; Bartos, P.J.M., 2003
 “Permeation properties of self-compacting concrete”, *Cement and Concrete Research*, V. 33, 2003, pp. 921-926

The interplay between inner and outer frost damage and its implication for accelerated freeze-thaw testing



Marianne Tange Hasholt
Associate professor, M.Sc., Ph.D.
Department of Civil Engineering
Technical University of Denmark
E-mail: matah@byg.dtu.dk

ABSTRACT

In the present project salt frost scaling was registered during an accelerated freeze-thaw test (CEN/TS 12390-9). After the test, inner damage was evaluated by observing the crack patterns on fluorescence impregnated plane sections. The results indicate that the developments of inner and outer damage are linked processes. The link is related to the moisture transport in the concrete, as both inner cracking and scaling change if a moisture barrier is implemented parallel to the test surface, 25 mm below the test surface.

Key words: Frost action, salt frost scaling, inner frost damage, testing.

1. INTRODUCTION

In a cold climate, concrete that is not frost resistant can suffer from inner damage in the form of cracks and outer damage in the form of surface scaling /Pigeon & Pleau., 1995/. Concrete deterioration during frost action has been a subject of research for more than 60 years, but still the degradation mechanisms are not fully understood. One of the remaining questions is the interplay between development of inner and outer damage. It is not known if surface scaling is a consequence of inner damage or if surface scaling contributes to starting or accelerating development of inner damage – or if inner and outer damage are caused by two different mechanisms that act independent of each other, as supposed by /Valenza & Scherer, 2007/.

The development of both inner and outer frost damage depends on the availability of freezable water and therefore also on moisture transport in the concrete. In a BSc project, specimens with artificial barriers for moisture movement were prepared for freeze-thaw testing to see how it influenced the development of inner and outer frost damage /Hedegaard & Kleiter 2013/.

2. EXPERIMENTAL WORK

2.1 Materials

It was the intention to test a non-frost resistant type of concrete. It was decided to use concrete with $w/c = 0.45$ without air entrainment. The following constituents were used:

- *Cement:* CEM I 52.5 N (LA), 475 kg per m^3 concrete
- *Aggregate:* Sea sand and crushed granite (maximum size 11 mm), environmental class E (Extra aggressive), i.e. suitable for production of concrete exposed to frost action.

The air content of the fresh concrete was 1.4% measured by pressuremeter (natural air content).

2.2 Test methods

The air void structure of the hardened concrete was evaluated by the method described in EN

480-11: *Admixtures for concrete, mortar and grout - Test methods - Part 11: Determination of air void characteristics in hardened concrete* (2005).

The accelerated freeze-thaw test was carried out according to the reference method of CEN/TS 12390-9: *Testing hardened concrete – Part 9: Freeze-thaw resistance – Scaling* (2006). Two sets of Ø150 mm test specimens were prepared in parallel:

- *standard*: preparation followed exactly the preparation described in CEN/TS 12390-9, including a sample height of 50 mm
- *25+25 mm*: preparation followed CEN/TS 12390-9, except that the 50 mm specimen was cut in half to obtain two 25 mm discs. The discs were assembled by gluing a 3 mm rubber sheet in between (same type of rubber sheet as used on the external surfaces of the test specimen except the test surface). The position of the rubber sheet can be seen in figure 2 (right).

After the freeze-thaw test, one specimen from each series was epoxy impregnated with fluorescent dye to make cracks clearly visible on a plane section of the specimen.

3. RESULTS

3.1 Air void structure

The air void structure of the hardened concrete was examined according to EN 480-11. The results showed a total air content of 1.4% and a spacing factor of 0.74 mm.

3.2 Accelerated freeze-thaw testing

Figure 1 shows the development of scaling during the accelerated freeze-thaw test according to CEN/TS 12390-9. Due to electrical power cuts in the laboratory, there were less than 56 freeze-thaw cycles during the test period. Scaling was registered after 7, 13, 20, 27, 41, and 53 cycles:

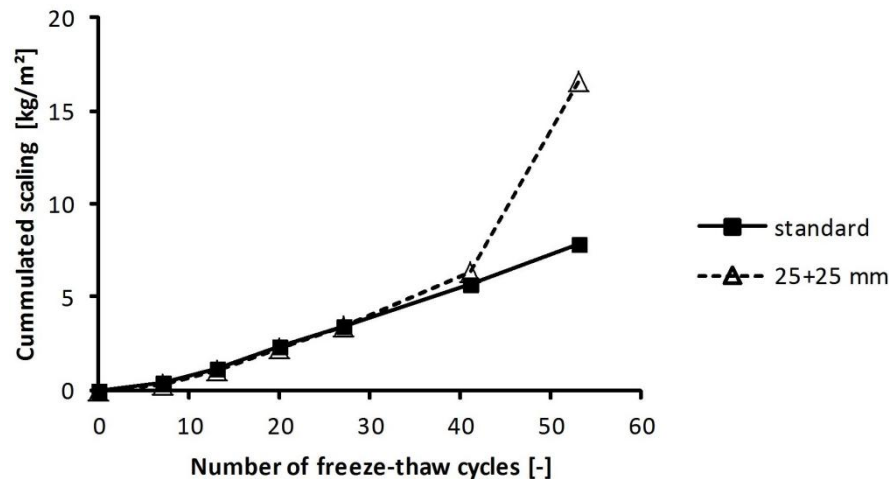


Figure 1 – Development of salt frost scaling.

3.3 Inner frost damage

Figure 2 shows fluorescence impregnated plane sections in UV light of “standard” and “25+25 mm”, respectively:

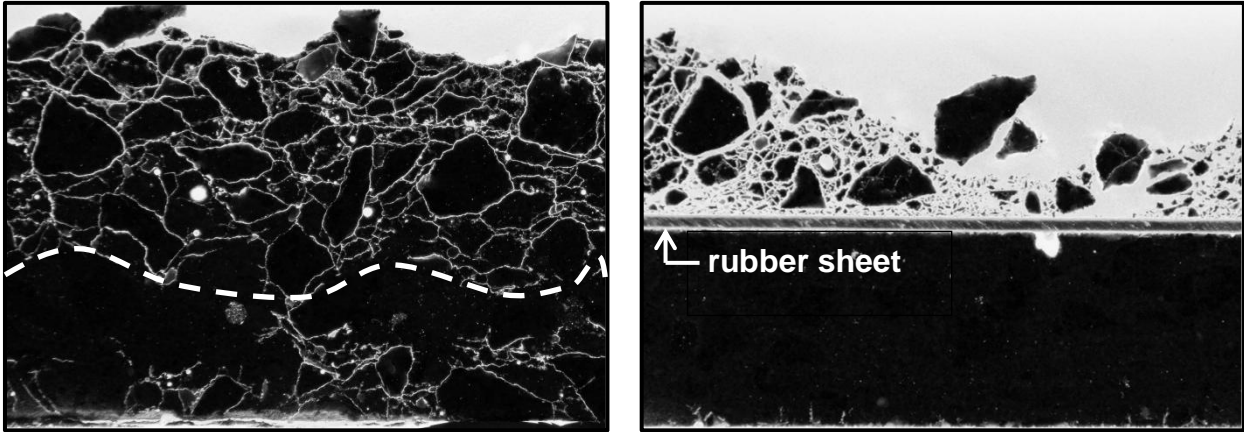


Figure 2 – Fluorescence impregnated specimens of samples after 53 freeze-thaw cycles. The upper edge of each photo corresponds to the original test surfaces before testing, and the height corresponds to the height of the specimen (50 mm) Left: “standard”. Right: “25+25 mm”.

4. DISCUSSION

The air void analysis reveals that the spacing factor is $0.74 \text{ mm} \gg 0.20 \text{ mm}$, so the concrete cannot be expected to be frost resistant. The results of the accelerated freeze-thaw test confirm this, as the amounts of scaling for both test series exceed the accept limits normally used.

The development of scaling for *standard* specimens and for *25+25mm* specimens is almost identical up to 41 freeze-thaw cycles, and the scaling rate seems to be constant. After 41 cycles, scaling for *standard* specimens continues with the same rate of scaling, whereas scaling accelerates for *25+25 mm* specimens.

The mapping of inner cracking shows somewhat different crack patterns for the two test series. For the *standard* specimen, fine cracks are homogeneously distributed in the upper 30 mm of the specimen (above the dotted line in figure 2, left), and there is a distinct front to an un-cracked zone. For the *25+25 mm* specimen, the cracking of the upper 25 mm is more severe than the cracking of the *standard* specimen; both crack density and crack width is higher. Below the moisture barrier (rubber sheet), there are no cracks.

If one imagines that the inner cracking of the *standard* specimen has developed as a front progressing through the specimen at constant rate, then the front has reached the depth of 25 mm after $53 \cdot 25/30 = \text{approx. } 44$ freeze-thaw cycles. This coincides with time where scaling in the *25+25 mm* specimen accelerates. This can be explained in the following way: Crack formation starts during the first freeze-thaw cycle at the top surface of the specimen. Between frost periods, moisture is transported via the cracks, so un-cracked concrete in the border zone between cracked and un-cracked becomes critically saturated, and it therefore cracks in the following cycle. Therefore, the front of the cracked zone propagates with almost constant rate. The cracked front also marks a moisture front. The moisture content of the cracked concrete is higher than the moisture content of the un-cracked concrete and the moisture content of cracked concrete remains constant as long as moisture can escape to the un-cracked zone. However, when the moisture front meets a barrier, the cracked zone becomes wetter, and therefore cracking in the paste phase aggravates. This weakens the concrete, and for this reason scaling increases. In fact, the amount of scaling measured at this point is to some extent arbitrary, as the crumbled concrete can almost be brushed off the specimen.

There is also some cracking at the bottom of the *standard* specimen. This may be because some of the sodium chloride solution from the reservoir on top of the specimen has leaked through the specimen and accumulated at the bottom, so a similar process can take place from beneath.

If this sequence of deterioration during testing is a correct interpretation, then it also ought to have implications for how we perform accelerated freeze-thaw tests and evaluate the results. Often, the observation of accelerated scaling (e.g. that the total amount of scaling after 56 cycles is more than twice the amount of scaling after 28 cycles) is included in the evaluation of frost resistance. On one hand, one may argue that the accelerated scaling is due to an artefact of the test method: The moisture front meets a barrier at the bottom of the specimen, which it would not meet in a thicker concrete structure. Therefore it is irrelevant to take acceleration into account during the evaluation of results. On the other hand, one may argue that if acceleration occurs, it is an indirect measure of how prone the concrete is to inner frost damage, as it shows that cracking has reached a depth of 50 mm, and this makes it a relevant evaluation criterion.

At the moment, there is no European test standard for testing susceptibility of hardened concrete to development of inner frost damage. It has been suggested to use measurements of ultrasonic pulse transmission time (UPTT) during the scaling test for this purpose /Setzer et al., 2004/. However, if inner damage is not homogeneously distributed in the specimen - in fact there are separate zones of cracked and un-cracked concrete - then it is difficult to differentiate the degree of damage by using UPTT measurements. For practical reasons, e.g. the size of the sender and receiver of the UPTT equipment, measuring heads have to be placed some distance from the test surface. If they are placed so their centres are 25 mm below the test surface, then the upper 25 mm of the concrete can be cracked, before a change in UPTT is registered, and this extent of cracking may be more than what is acceptable to categorise concrete as frost resistant.

ACKNOWLEDGEMENT

The experimental work presented in this paper was performed by Jens Hedegaard and Anton Kleiter. Their effort during the project is highly appreciated. Fluorescence impregnated plane sections are prepared by Pelcon A/S, and the project has been financially supported by the Larsen & Nielsen Foundation. This is greatly acknowledged.

REFERENCES

- Hedegaard, J., & Kleiter, A. 2013
 ”Undersøgelse af luftporestrukturens indvirkning på fryse/tø-mekanismer og isdannelse i cementpasta” (in Danish), BSc report, Technical University of Denmark, Lyngby, 2013.
- Pigeon, M., & Pleau, R., 1995
 “Durability of concrete in cold climates”, E & FN Spon, London, 1995.
- Setzer, M.J., et al., 2004
 ”Test methods of frost resistance of concrete: CIF-test: Capillary suction, internal damage and freeze thaw test – Reference method and alternative methods A and B”, *Materials and Structures*, vol. 37, 2004, pp. 743-753.
- Valenza, J.J., & Scherer, G.W., 2007
 “A review of salt frost scaling: II. Mechanisms”, *Cement and Concrete Research*, vol. 37, 2007, pp. 1022-1034.

Maintenance and Renewal of Concrete Railway Bridges – Results from EC Project MAINLINE



Jonny Nilimaa¹
PhD Student



Jens
Häggström¹
PhD Student



Niklas Bagge¹
PhD Student



Thomas
Blanksvärd¹
Ass. Professor



Gabriel Sas¹
Ass. Professor



Ulf Ohlsson¹
Ass. Professor



Lars Bernspång¹
Assoc. Professor



Börn. Täljsten¹
Professor



Lennart Elfgrén¹
Em. Professor



Anders Carolin²
Bridge Engr.



Björn Paulsson²
Sr Engineer

¹ Luleå Univ.
of Technol.
SE-971 87
Luleå
N.N@ltu.se
² Trafikverket
SE-781 89
Borlänge
N.N@trafik
verket.se

ABSTRACT

There is a need to extend the life and capacity of many existing railway bridges. One of the objects of the EC-FP7-Project MAINLINE, 2011-2014, is to facilitate this. Guidelines for assessment and strengthening methods are presented as well as case studies in which existing bridges are being studied in order to extend their life length. Case studies on bridges tested to failure in order to calibrate assessment methods are also presented. Fatigue is often a vital question. A Life Cycle Assessment Tool (LCAT) is being prepared to enable Infrastructure Managers to choose optimal maintenance strategies.

Key words: Aging, Knowledge and Teaching, Modelling, Repair, Structural Design, Sustainable, Testing, Railway bridges, extended life, assessment methods, concrete bridges, strengthening, calibrate model, loading to failure, fatigue.. Life Cycle Assessment

1. INTRODUCTION

1.1. Background

Growth in demand for rail transportation across Europe is predicted to continue. Much of this growth will have to be accommodated on existing lines that contain old infrastructure. This demand will increase both the rate of deterioration of these elderly assets and the need for shorter line closures for maintenance or renewal interventions. The impact of these interventions must be minimized and will also need to take into account the need for lower economic and environmental impacts. New interventions will need to be developed along with additional tools to inform decision makers about the economic and environmental consequences of different intervention options being considered.



Figure 1. A concrete trough bridge built in 1959 in Haparanda close to the border to Finland. In 2012 the bridge was strengthened with eight post-stressed bars installed in holes drilled through the slab (insert left). In this way it was possible to increase the bending and shear capacity of the slab to enable an upgrading of the line from an axle load of 25 to 30 ton (insert right shows traffic on the two tracks on the top of bridge), see further MAINLINE (2014).

1.2. MAINLINE – A project within EC-FP7 –

The project MAINLINE target a reduced environmental footprint in terms of embodied carbon and other environmental benefits. The project will:

- Apply new technologies to extend the life of elderly infrastructure (WP 1)
- Improve degradation and structural models to develop more realistic life cycle cost and safety models (WP 2)
- Investigate new construction methods for the replacement of obsolete infrastructure (WP 3)
- Investigate monitoring techniques to complement or replace existing examination techniques (WP4)
- Develop management tools to assess whole life environmental and economic impact (WP 5).

The project consortium includes leading railways, contractors, consultants and researchers from across Europe, including from both Eastern Europe and the emerging economies. Partners also bring experience on approaches used in other industry sectors which have relevance to the rail sector. Project benefits will come from keeping existing infrastructure in service through the application of technologies and interventions based on life cycle considerations. Although MAINLINE will focus on certain asset types, the management tools developed will be applicable across a broader asset base.

The project is led by UIC, France, with Björn Paulsson as coordinator. Luleå University of Technology, Sweden, acts as Scientific and Technical Coordinator. Other partners are: Network Rail Infrastructure Limited, United Kingdom; COWI, Denmark; SKM, United Kingdom; University of Surrey, United Kingdom; TWI, United Kingdom; University of Minho, Portugal; DB Netz AG, Germany; MÁV Magyar Államvasutak Zrt, Hungary; Universitat Politècnica de Catalunya, Spain; Graz University of Technology, Austria; TCDD, Turkey; Damill AB, Sweden; COMSA EMTE, Spain; Trafikverket, Sweden; SETRA, France; ARTTIC, France; and Skanska a.s., Czechia.



Figure 2. Near Surface Mounted Reinforcement, NSMR, can be placed in groves that are grinded in e.g. the bottom of a slab (left, middle). Carbon Fibre Reinforced Polymer (CFRP) bars (right) can then be glued into the groves, see e.g. *Sustainable Bridges* (2007), *Täljsten et al* (2011), *MAINLINE* (2014).

2. ASSESSMENT, STRENGTHENING AND RENEWAL

A Questionnaire on bridges has been prepared and eleven Infrastructure Managers have responded. If the results from this bridge sample are extrapolated from the about 125 000 km of network and the about 150 000 railway bridges that these Infrastructure Managers oversee to the full European network, which is about 230 000 km, a rough estimate may be obtained of the needs for the next years. Such an extrapolation suggests that in the next ten years we may expect to strengthen some 1 500 bridges, to replace some 4 500 bridges and to replace the deck of some 3 000 bridges. Some of the bridges that are planned to be replaced may instead be strengthened, if the new technologies presented in the project would be used

Methods for assessment of structures is a key activity that was investigated already in an earlier project, *Sustainable Bridges* (2007). It is now further developed and tested on case studies. Methods for strengthening with prestressing or using near surface mounted reinforcement is studied, see Figure 1 and 2.

3. LIFE CYCLE COSTS (LCC), LIFE CYCLE ANALYSIS (LCA) AND LIFE CYCLE ASSESSMENT TOOL (LCAT)

Many Infrastructure Managers currently do not yet use Life Cycle Costing (i.e. financial) and/or Life Cycle Assessment (i.e. environmental) in the planning of maintenance and repair of their rail infrastructure. There is a lack of data and methods and here the Mainline project is intending to give guidance. Some data on different types of bridges in northern Sweden are given in Ditrani (2009). There is also often a lack of economic resources for maintenance which may lead to a shorter life length and less sustainability than would otherwise be the case; results from the Mainline Project are also intended to give advice that may help to improve this situation. The aim is to develop a Life Cycle Assessment Tool (LCAT) which allow users to demonstrate optimum interventions and reduce capital expenditure, see Figure 3.

ACKNOWLEDGEMENT

The authors gratefully acknowledge financial support from the European Union, Trafikverket, LKAB/HLRC, SBUF and Luleå University of Technology (LTU). They also thank their colleagues in the project and especially in the Swedish Universities of the Built Environment (Oskar Larsson, LTH; Karin Lundgren and Mario Plos, Chalmers; and Raid Karoumi and Håkan Sundquist, KTH) for fruitful cooperation.

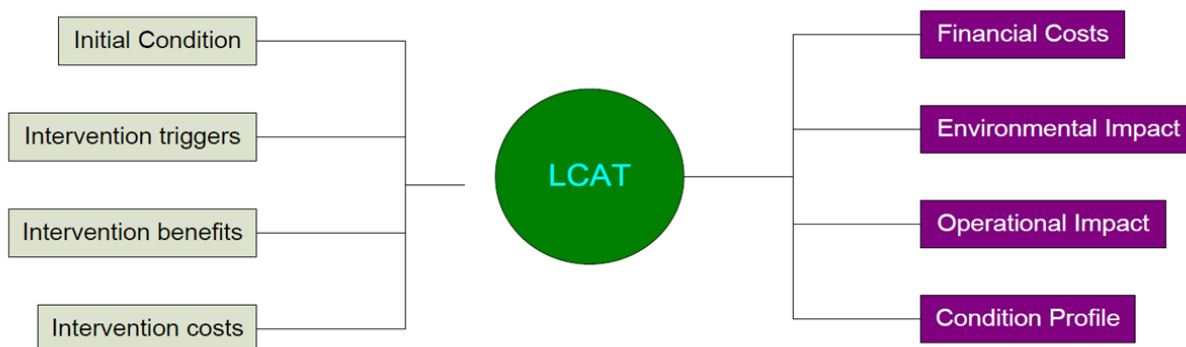


Figure 3. Life Cycle Assessment Tool (LCAT), MAINLINE (2014)

REFERENCES

Ditrani, Marco, 2009.

“Improving transportation investment decisions through life cycle cost analysis: Comparative LCCA of bridges” *M. Sc. Thesis 2009:189 CIV*, Luleå University of Technology, 201 pp, <http://pure.ltu.se/portal/files/31153583/LTU-EX-09189-SE.pdf>

MAINLINE, 2014.

“MAINLINE - MAINTenance, renewal and Improvement of rail transport Infrastructure to reduce Economic and environmental impacts”. A European FP7 Research Project during 2011-2014 with the aim to increase the life length of existing rail infrastructure. So far the following reports are available; while final guidelines and conclusions are still in preparation, see <http://www.mainline-project.eu/>

D1.1 *Benchmark of new technologies to extend the life of elderly rail infrastructure*, 77 pp.; D1.2 *Assessment methods for elderly rail infrastructure*, 112 pp.; D2.1 *Degradation and performance specifications for selected assets*, 113 pp.; D2.2 *Degradation and intervention modelling techniques*, 184 pp.; D2.3 *Time-variant Performance Profiles for Lif-Cycle Cost and Life-Cycle Analysis*, 67 pp.; D3.1 *Benchmark of production and replacement of railway infrastructure*, 59 pp.; D4.1 *Report on assessment of current monitoring and examination practices in relation to degradation models*, 84.; D4.2 *Solution in Gaps in Compatibility between Monitoring and Examination Systems and Degradation Models*, 106 pp.; D5.1 *Assessment of asset management tools*, 22 pp.; D5.2 *Assessment of environmental performance tools and methods*, 92 pp.; D5.3 *Recommendations for Format of a Life Cycle Assessment tool (LCAT)*, 58 pp.; D5.4 *Proposed methodology for a Life Cycle Assessment Tool (LCAT)*, 169 pp.

Sustainable Bridges, 2007. –

“Sustainable Bridges: Assessment for Future Traffic Demands and Longer Lives”, .A European FP 6 Integrated Research Project during 2003-2007. Four guidelines and 35 background documents are available at www.sustainablebridges.net: *Inspection and Condition Assessment*, 259 pp; *Load and Resistance Assessment of Railway Bridge*, 428 pp; *Guideline for Monitoring of Railway Bridges*, 83 pp; *Guide for use of Repair and Strengthening Methods for Railway Bridges*, 139 pp.

Täljsten, B., Blanksvärd, Th. And Sas, G., 2011.

”Handbok för dimensionering i samband med förstärkning av betongkonstruktioner med pålimmade fiberkompositer (Design Guideline for FRP Strengthening of Existing Concrete Structures. In Swedish)”. *Div. of Structural Engineering, Luleå University of Technology*. 2011, 184 pp. ISBN 978-91-7439-146-6,

STRUCTURAL BEHAVIOUR AND DESIGN

Semi-active structural control strategies



Tarek Edrees Saaed
M.Sc., Ph.D. Student
Department of Civil, Environmental and Natural
resources engineering. Division of Structural and
Construction Engineering.
Luleå University of Technology, Sweden.
tarek.edrees@ltu.se



George Nikolakopoulos
Professor.
Department of Computer Science, Electrical and Space
Engineering. Control Engineering Group.
Luleå University of Technology Sweden.
geonik@ltu.se



Jan-Erik Jonasson
Professor.
Department of Civil, Environmental and Natural
resources engineering. Division of Structural and
Construction Engineering.
Luleå University of Technology, Sweden.
jan-erik.jonasson@ltu.se

ABSTRACT

The utilization of structural control systems to alleviate the responses of civil engineering structures, under the effects of dynamics loadings, has become a standard technology, while still there are numerous of current research approaches for advancing the effectiveness of these methodologies. It is important for successful application of smart structure to provide an effective control algorithm to compute the control forces to be applied on the building in order to reduce the external disturbances. The aim of this article is to provide a review of the control strategies to control the performance of semi-active systems utilized in civil engineering structures.

Keywords: Structural Behaviour, Structural Design, Structural Control Systems, Control Strategies, Semi-Active Control Structures.

1. INTRODUCTION

It is very important for any successful application of smart structure technology is an effective control algorithm to compute the magnitude of control forces to be applied to the structure. Owing to the large size and complexity of civil engineering structures and the stochastic nature for the external dynamic excitations, an efficient control algorithm has to be robust and valid for various dynamic loading conditions and thus the selection of a proper control scheme based on the existing methodologies, and available actuators are of paramount importance. Existing control algorithms developed for other fields, for instance, aerospace engineering, were utilized in the first attempts on structural control. Recently, research has shifted to adjusting the existing

control algorithms or to evolve new algorithms to meet the needs of civil engineering structures /Fisco 2011/. Based on control strategy, According to Datta /Datta 2003/ control system can be classified as: 1) open loop control system where only measured excitations are used as feedback information to the control algorithm, b) closed-loop control system where only structural responses are measured and used as feedback information to the control algorithm, c) open-closed loop control system if both of excitations and structural responses are measured and used as feedback information to the control algorithm, d) adaptive control system, which is a variation of open-close loop control with a controller which can adjust parameters of the system. This system is frequently used to control structures whose parameters are unidentified, e) learning control system, which has the capability to learn and can convert from open loop control system to close loop control system according to the requirements. The target of this research effort is to present a review of the existing control strategies essential to control the performance of semi-active systems utilized in civil engineering structures. This article is structured as follows: In Section 2, a review of the current control strategies is given, and the conclusions are drawn in section 3.

2. SEMI-ACTIVE CONTROL THEORIES (STRATEGIES)

With a semi-active control device, energy can only be dissipated. Therefore, they cannot lead to an instable system, even in the worst case, because they are considered as passive dampers with changing characteristics to be adjusted on line /Marazzi 2002/. In general, the equation of motion for the semi-active of structure has the following form /Datta 2010/:

$$M\ddot{X} + (C + C_v)\dot{X} + (K + K_v)X = -M\ddot{x}_g \quad (1)$$

In which C_v and K_v are variables. These can take positive discrete values (within specified bounds), and depend on the state. In order to give general overview about structural semi-active control strategies without going into details, a very short summary of some of them is listed below. More details are available on references mentioned in the text:

2.1 Clipping control:

This strategy was proposed by Dyke /Dyke 1996/. The design of the controller in this type of control strategy can be divided into two parts. The first part involves designing an active control law assuming that an ideal active device is present. While the second part involves the design of a clipping controller allowing the semi-active damper to develop the force that the active device would have applied on the structure. This means that, for the first part, any type of control strategy can be selected (for instance; optimal control, generalized feed-back control, H_2 or H_∞) because the second step is independent of it. The following rule (depicted in Fig.1) is generally used to clip the active control law to a semi active one: “when the magnitude of the force F_d produced by the damper (that is the control force f in this case) is smaller than the required target force f_c and the two forces have the same sign, the voltage applied to the current driver is increased to the maximum level, so as to match the required control force; otherwise, the command voltage is set to zero”. This strategy is usually called “clipped on-off” and the formula is given in equation (2) below /Marazzi 2002/:

$$v = V_{max}H[(f_c - f)f] \quad (2)$$

here v is the command signal, $H[.]$ is the Heaviside function, V_{max} is the maximum voltage applicable on the semi active device to obtain the maximum damping and f and f_c are the measured and required control forces.

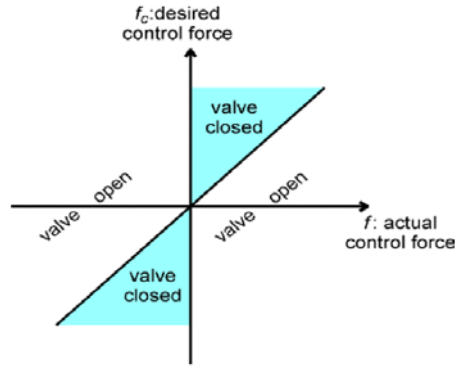


Fig.1: Clipping Control Strategy /Marazzi 2002/.

2.2 Direct Lyapunov control:

This strategy based on application of Lyapunov's direct method to stability analysis in the design of a feedback controller. Lyapunov function, denoted $V(z)$, is used. Assuming that the origin is a stable equilibrium point. According to this theory, if the rate of change of the Lyapunov function $\dot{V}(z)$, is negative semi-definite, the origin is stable. Thus, in developing the control law, the aim is to select control inputs for each device that will result in producing \dot{V} as negative as possible. A variety of control laws will result because there are unlimited numbers of Lyapunov functions may be selected. For instance, In 1994, Leitmann used the following control law to minimize \dot{V} :

$$v_i = V_{max} H((-z)^T P B_i f_i) \quad (3)$$

In which $H(\cdot)$ is the Heaviside step function, f_i is the measured force, P is a real symmetric positive definite matrix, and B_i is the i^{th} column of the B matrix. Kalman filter is necessary to estimate the states based on the available measurements and a well performance is likely when full response measurements of the structure are available /Jansen 2000/.

2.3 Bang-bang control:

In this strategy, the Lyapunov function was selected to represent the total vibratory energy in the structure. This method requires only measurements of the floor velocities and applied forces. To make \dot{V} as large and negative as possible, the following control law is used in this strategy /Jansen 2000/:

$$v_i = V_{max} H(-(\dot{x} + \Gamma \dot{x}_g)^T \Lambda_i f_i) \quad (4)$$

In which Λ_i is the i^{th} column of the Λ matrix. This strategy works like a brake depending on the relative displacement and the relative velocity of the two ends of the damping device, if they are in the same direction, bang-bang control act in the trend of increasing the friction forces into the device to a maximum value. In contrast, if they are in opposite direction, the control law decreases the friction forces to a minimum in order to make the device motion as easy as possible /Marazzi 2002/.

2.4 Fuzzy logic control:

Fuzzy logic is utilized in a number of controllers since it does not need a precise model of the system to be controlled. Its mechanism is based on implementation of rules that correlate the controller inputs with the required outputs. These rules are usually created through the perception or information of the designer concerning the process of the system being controlled. For any fuzzy logic controller, there are three common basic steps involves: the fuzzification of

the controller inputs, the execution of the rules of the controller, and the defuzzification of the output to a crisp value to be implemented by the controller /Marazzi 2002/.

2.5 Neural network:

The major advantage of the neural network concept is that identification of an unknown system and evaluation of responses can be accomplished without constructing a mathematical model of the system. They are simplified models of the biological structure found in human brains. These models comprise of elementary processing units (also called neurons). They have a strong capability for predicting and classification due to the huge amount of interconnections between these neurons and their ability to learn from data /Fisco 2011, Xu 2003/.

3. CONCLUSIONS

The control strategies were reviewed by briefly summarizing the general literatures review of control strategies utilized to control the performance of civil engineering structures.

REFERENCES

- Datta, T. 2003
A state-of-the-art review on active control of structures, ISET Journal of earthquake technology. 40 (2003) 1-17.
- TK Datta, T.K. 2010
Seismic analysis of structures, Wiley, Singapore, 2010.
- Dyke, S., Sain, M., J Carlson, J. 1996
Modeling and control of magnetorheological dampers for seismic response reduction, Smart Mater.Struct.5 (1996) 565
- Fisco, N., Adeli, H. 2011
Smart structures: part II—hybrid control systems and control strategies, ScientiaIranica—Transaction A: Civil Engineering. 18 (2011) 285-295.
- Jansen, L.M., Dyke, S.J. 2000
Semiaactive control strategies for MR dampers: comparative study, J.Eng.Mech. 126 (2000) 795-803
- Marazzi, F. 2002
Semi-active control of civil structures: implementation aspects. (2002) Dissertation / University of Pavia, Italy.
- Xu, Z.D., Shen, Y.P., Guo, Y.Q. 2003
Semi-active control of structures incorporated with magneto rheological dampers using neural networks, Smart Mater.Struct. 12 (2003) 80.

Structural Behaviour of Beams with Fibre Reinforced LWAC and Normal Density Concrete



Linn Grepstad Nes, Ph.D
 Department of Structural Engineering
 Norwegian University of Science and Technology
 7491 Trondheim, Norway
 E-mail: linn.g.nes@ntnu.no



Jan Arve Øverli
 Associate Professor, Ph.D
 Department of Structural Engineering
 Norwegian University of Science and Technology
 7491 Trondheim, Norway
 E-mail: jan.overli@ntnu.no

ABSTRACT

This experimental investigation consists of beams composed by layers of different types of concrete. Normal density concrete (NC) is used in the top layer combined with a layer of fibre reinforced lightweight concrete (FRLWC). Hence, the beams have low weight and the NC layer fulfils requirements for ductility in compression. The beams had 0.5% and 1.0% 60mm long steel fibres, and were subjected to the 4-point bending test in order to study the performance in terms of both shear and bending actions. The types of failure were as expected but the resemblance between test and analytical results were not were good. No problem with the bond between the layers of concrete was registered.

Key words: Testing, Fibres, Cracking, Structural design.

1. INTRODUCTION

The motivation for investigating the performance of concrete beams with different type of concrete was to design a structural element which utilises the most beneficial properties of different materials and combine them in one cross-section. The beams may represent one-way slab elements of which the bottom layer(s) constitutes a precast formwork, resulting in a cost-effective product with respect to manufacturing, transport/assembling of the element and load capacity. Use of LWAC minimizes the self-weight and the structural performance is taken care of by the conventional longitudinal tensile reinforcement and the top layer of normal density concrete. In order to improve the performance and mechanical properties of the lightweight concrete steel fibres, Dramix 65/60 was used, which is a cold drawn wire fibre of bright steel with hooked ends and a length of 60mm. To produce the concrete, a lightweight expanded clay aggregate was used to achieve the desired density of the LWAC off about 1250kg/m³.

2. EXPERIMENTAL PROGRAM AND RESULTS

The experimental program covered 16 beams subjected to the 4-point bending test in order to study the performance in terms of both shear and bending actions (Nes 2013) . The program and results are given in Table 1. The cross section width was 150mm and the height was divided in a top layer of 50mm with NC and a 200mm layer of FRLWC, see Figure 1.

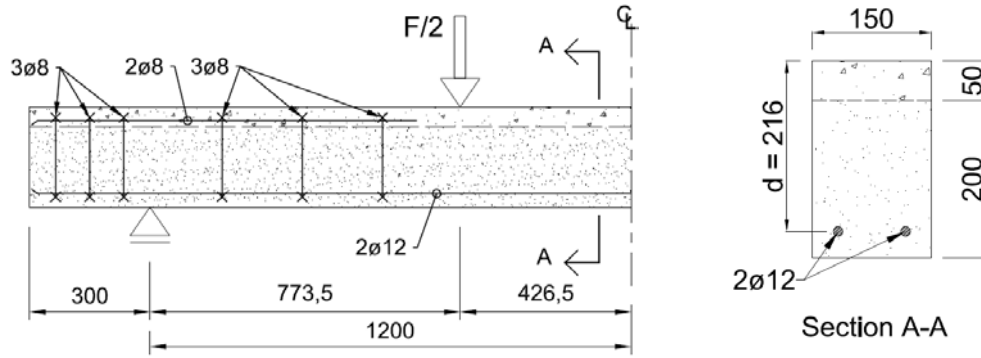


Figure 1 – Test setup (Beam 9-12) and cross-section (dimensions in mm).

3-point bending test (3PBT) tests were used for obtaining the residual tensile strength, $f_{tm,res2.5}$, of the FRLWC. Fibre counting was carried out to find the number of fibres, n_f , for calculating the fibre orientation factor α . The recommendations in Eurocode 2 (Standards Norway 2008) and the Norwegian Design Rule Proposal for Fibre Reinforced Concrete (Kanstad 2011) were employed to compare the test results with theoretical predictions of the capacities. As seen in Table 1 the beams failing in shear are difficult to analyse, mainly due to the great influence of fibre distribution and orientation, while beams experiencing bending failures can be calculate quite accurate.

Table 1 – Test results and calculated failure loads

| Beam | f_{ic} [MPa] | Fibre [%] | $f_{tm,res2.5}$ [MPa] | Shear links | n_f [pr. cm ²] | α | Failure type | P_{fail} [kN] | P_{calc} [kN] |
|------|-------------------|--------------|--------------------------|----------------|---------------------------------|----------|-----------------|--------------------|--------------------|
| 1 | 20.2 | 0 | - | - | - | - | shear | 43.4 | 41.4 |
| 2 | 20.2 | 0 | - | - | - | - | shear | 31.2 | 41.4 |
| 3 | 20.5 | 0.5 | 1.26 | - | 1.69 | 0.80 | shear | 70.6 | 57.4 |
| 4 | 20.5 | 0.5 | 1.26 | - | 1.29 | 0.61 | shear | 51.0 | 41.0 |
| 5 | 20.5 | 0.5 | 1.26 | - | 1.40 | 0.67 | shear | 64.1 | 70.4 |
| 6 | 19.4 | 1.0 | 1.4 | - | 2.98 | 0.71 | shear | 94.6 | 89.0 |
| 7 | 19.4 | 1.0 | 1.4 | - | 2.53 | 0.60 | shear | 87.4 | 73.0 |
| 8 | 19.4 | 1.0 | 1.4 | - | 2.64 | 0.63 | shear | 82.2 | 53.8 |
| 9 | 20.5 | 0.5 | 1.26 | ø8c190 | - | - | moment | 70.5 | 69.7 |
| 10 | 20.5 | 0.5 | 1.26 | ø8c190 | - | - | moment | 71.4 | 69.7 |
| 11 | 19.4 | 1.0 | 1.4 | ø8c190 | - | - | moment | 73.5 | 71.2 |
| 12 | 19.4 | 1.0 | 1.4 | ø8c190 | - | - | moment | 72.2 | 71.2 |
| 13 | 20.5 | 0.5 | 1.26 | - | 1.67 | 0.79 | shear | 41.2 | 46.6 |
| 14 | 20.5 | 0.5 | 1.26 | - | 1.74 | 0.83 | shear | 49.1 | 52.6 |
| 15 | 19.4 | 1.0 | 1.4 | - | 3.34 | 0.79 | shear | 70.4 | 74.8 |
| 16 | 19.4 | 1.0 | 1.4 | - | 2.05 | 0.49 | shear | 65.1 | 61.8 |

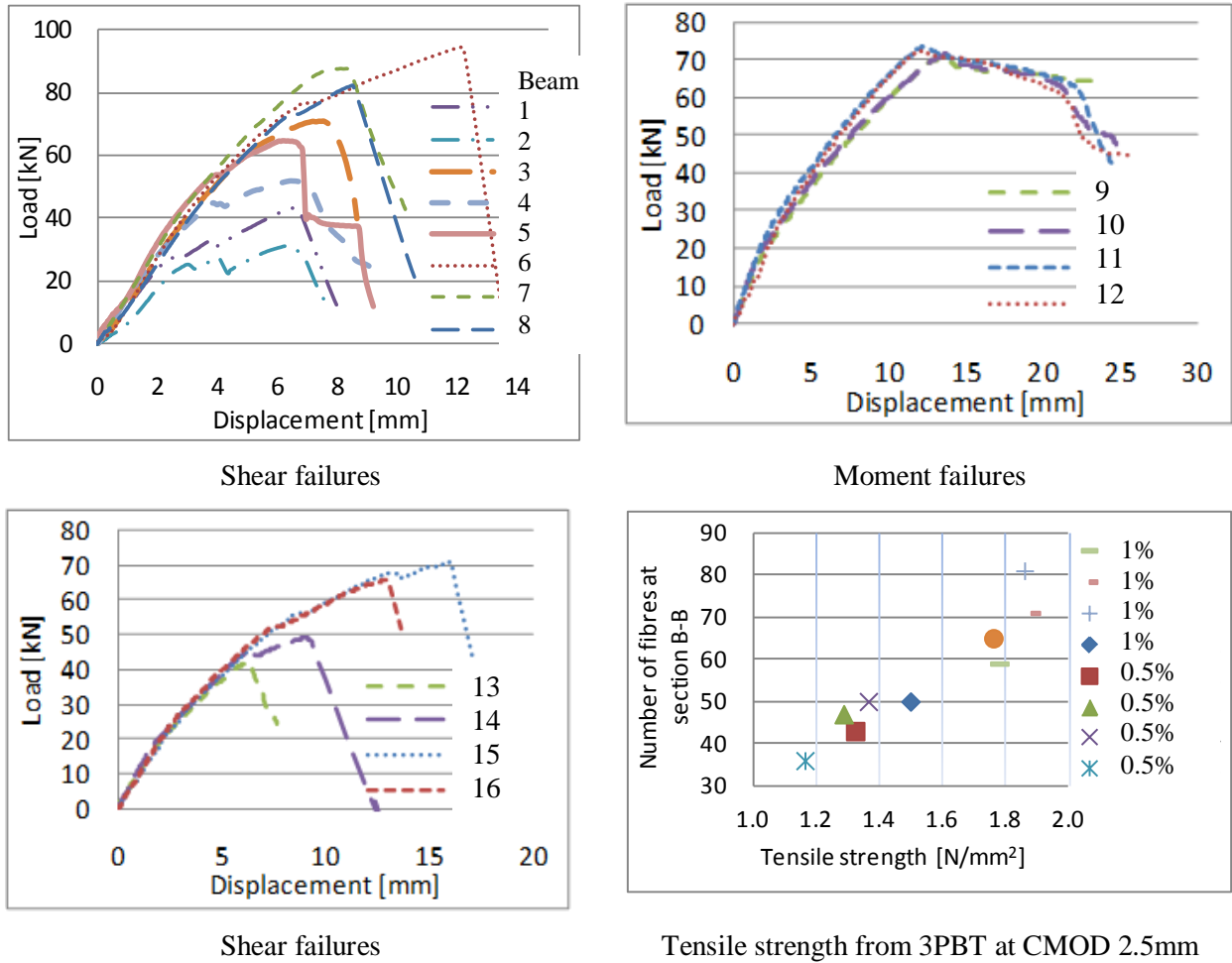


Figure 2 – Load displacement diagrams and fibre counting

Figure 2 presents the load displacement diagrams for all beams. As expected, the results show that the shear resistance increases with increasing fibre content. A possible explanation is the orientation of fibres. Result from fibre counting show that the number of fibres crossing a plane parallel to the diagonal crack is higher for beams with 1.0% fibre reinforcement than for beams with 0.5% fibres. For the beams failing in bending, 1.0% fibres achieved approximately the same load capacity as the beams with 0.5% fibre reinforcement. This can partly be explained by the results from fibre counting which indicate that beams with 1.0% fibre content have a more three dimensional orientation than beams with 0.5% fibres where they are more uni-directed in the longitudinal direction of the beams. This explanation is supported by the results from 3PBT which showed the same tendency, see Figure 2

The crack patterns at for beams failing in bending with 0.5% fibre reinforcement (top beam) and with 1.0% fibre reinforcement (lowest) is shown in Figure 3. The picture shows that the cracks in the beam containing 0.5% fibres tend to split when developing. For the beam with 1% fibre, the fibres seem to limit the crack development leading to a somewhat stiffer behaviour.

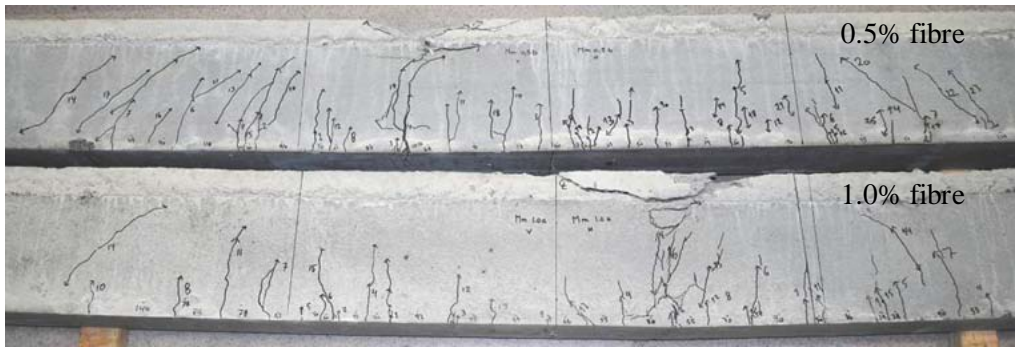


Figure 2 - Crack pattern at failure for beams with 0.5% and 1% fibre

3. CONCLUSIONS

This study shows that the concept of combining NC and FRLWC in one cross-section is working well. No problem with the bond between the layers of concrete was registered. Steel fibre reinforcement of the lightweight concrete increased the ductility in tension and the amount of conventional shear reinforcement might be reduced. The shear capacity increases with increasing number of fibres. However, the results are strongly dependent on the distribution and orientation of the fibres. Results from fibre counting indicate that 1% of fibres give a more 3-dimensional orientation of the fibres, while 0.5% of fibres tend to orientate in longitudinal direction of the beams. The concept provides low self-weight of the structure, practical solutions in the construction phase and good premises for more efficient building.

REFERENCES

- Kanstad, T. 2011. Proposal for norwegian guidelines for design, execution and control of fibre reinforced concrete. SINTEF Building and Infrastructure.
- Nes, L. G. 2013. *Experimental and numerical study of hybrid concrete structures: Optimised structural performance with fibre reinforced lightweight and normal concrete*. PhD thesis, Trondheim: Norwegian University of Science and Technology.
- Standards Norway. 2008. *NS-EN 1992-1-1:2004+NA:2008. Eurocode 2: Design of concrete structures - General rules and rules for buildings*. Norway: Standards Norway.

Recommendations for Finite Element Analysis for Design of RC Slabs



Mario Plos, Ph.D., Associate Professor
Chalmers University of Technology, Div. of, Structural Engineering,
Göteborg, Sweden
E-mail: mario.plos@chalmers.se



Costin Pacoste, Ph.D., Adjunct Professor
ELU Konsult AB / Royal Institute of Technology, Div. of Structural
Engineering and Bridges, Stockholm, Sweden
E-mail: Costin.Pacoste@elu.se



Morgan Johansson, Ph.D.
Reinertsen Sverige AB, Göteborg, Sweden
E-mail: morgan.johansson@reinertsen.com

ABSTRACT

The finite element method (FEM) is increasingly used for design of reinforced concrete structures. 3D FE analysis can provide more accurate structural analysis, but to use its full strength in daily design a number of critical issues have been addressed. Practical guidelines are provided for detailed design of reinforced concrete slabs. Recommendations are given on linear FE modelling, e.g. regarding geometry, support conditions and mesh density, as well as on the use of analysis results, e.g. regarding stress concentrations, choice of critical sections and redistribution widths for practical reinforcement design.

Key words: Structural Design, Modelling, Reinforced Concrete Slabs

1. INTRODUCTION

In design of reinforced concrete (RC) structures, the use of 3D linear elastic finite element (FE) analysis has increased substantially in the last few years. Such analyses provide the possibility for more accurate structural analysis than more traditional design tools. However, in order to use the full strength of the finite element method (FEM) in daily design practice a number of critical issues have to be addressed. These issues are related either to the FE-modelling itself (geometry, support conditions, mesh density, etc.) or to the post processing of the obtained results (stress concentrations, choice of critical sections, redistribution widths and so on). To address these problems for design of RC slabs, recommendations for engineering practice were developed by the authors in a project for the Swedish Transport Administration.

In daily design of RC slabs, linear FE analysis is used to determine the load effects in terms of sectional moments and forces. For this purpose, the use of structural finite elements like shell

elements can be recommended. The use of linear analysis can often be justified even though the slabs normally have a non-linear response due to concrete cracking and reinforcement yielding: for ultimate limit state (ULS) based on theory of plasticity and in serviceability limit state (SLS) based on the assumption that redistribution of moments and forces due to concrete cracking is limited.

2. A NEW GUIDE FOR PRACTISING ENGINEERS

The aim of the work was to provide practical guidelines on how to model RC slabs and interpret the results needed for detailed design. Three aspects of particular importance were addressed: modelling of support conditions; choice of result sections; and choice of redistribution widths to practically handle stress concentrations. The work is presented in a guide with recommendations for practicing structural engineers, Pacoste *et al.* (2012). The recommendations are based on relevant literature, e.g. CEB-FIP (2008), Rombach (2004) and Blaauwendraad (2010), combined with engineering judgement and considerations from engineering practice. The recommendations are believed to be conservative, implicating a potential for improvement based on increased knowledge.

3. MODELLING OF SUPPORT CONDITIONS

The support conditions in a finite element model of a structure often have a decisive influence on the analysis results. Consequently, the modelling of the supports needs to be paid special attention. For slabs, it is often sufficient to model supports or connections to other structural parts in single points or lines. For slabs supported in single points, this will result in singularities; the sectional forces and moments will tend to infinity upon mesh refinement. However, for reinforcement design, the peak values right at the connection are not of interest. Instead, design results are needed in critical sections adjacent to the supports, where potential failure mechanisms may occur. Consequently, if the slab has sufficiently dense FE mesh in the support region and the results are taken in the critical sections, the singularities at the connection may be disregarded.

Recommendations are given regarding how to model support conditions depending on the type of support, how the slab is connected, the support stiffness and support extension. For example, a slender interior column can generally be modelled in a simplified way by preventing vertical displacement at the centre point only. On the other hand, walls and edge or corner columns monolithically connected with the slab are recommended to be included in the model. Sometimes it is preferable to model supports in a way that describes the support pressure in order to avoid singularities; recommendations for this are also included.

Recommendations are further given regarding the mesh density in support regions. It is recommended to have at least one (quadrilateral) shell element, regardless of order, between a single support node and the critical section. This was found to be sufficient; increased mesh density was shown to have negligible influence on the resulting reinforcement amounts.

4. CHOICE OF RESULT SECTIONS

When the supports or connections to other structural parts are modelled in single points or lines, the results from the critical sections adjacent to the support are needed for reinforcement design; these are the sections where potential failure mechanisms may occur. In figure 1, recommended result sections for some different types of connections and failure modes are shown.

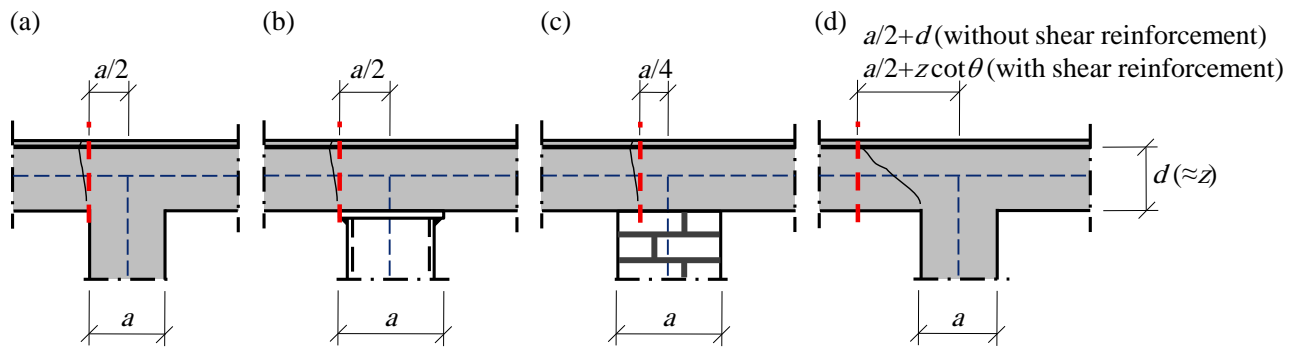


Fig. 1: Examples of result sections for (a) bending moments for monolithic connection, (b) bending moments for rigid simple support, (c) bending moments for weak simple support (conservative approximation) and (d) shear force (independent of design and stiffness of the slab-support connection).

5. REDISTRIBUTION OF SECTIONAL FORCES AND MOMENTS

The material simplification introduced through the assumption of linear elastic response will lead to higher cross-sectional moments than in reality, even when the stresses in the critical sections are used; in reality, cracking of concrete and yielding of reinforcement will lead to redistributions. A slab loaded normal to its plane should be designed to resist the reinforcement moments in the reinforcement directions, including the effect of torsional moment. The slab should also be able to resist the resultant shear force. Due to the non-linear response, the reinforcement moments and the shear force can be redistributed over a certain slab width, and the average value of the moment or shear force can be used to design necessary reinforcement within this width. The procedure for moment redistribution is illustrated on a column supported slab in figure 2. The varying reinforcement moment in the direction orthogonal to the moment's direction (i.e. orthogonal to the reinforcement bar direction) is replaced by its average value within the redistribution width, w (to the right in the figure). This results in slab strips with constant reinforcement bar spacing.

Conceptually, the redistribution width for moments in ULS is limited to the width over which yielding of the reinforcement can distribute without exceeding the rotational capacity of the slab. In SLS it is limited by the crack widths. In the literature, it was not possible to find scientifically based advices for redistribution widths. Recommendations for flat slabs have generous redistribution widths for moments, with concentration of reinforcement above point supports. For bridges in Sweden, more rigorous demands have been applied. On the other hand, a case study indicated that the choice of redistribution widths had minor influence on the plastic rotations in ULS and crack widths in SLS, Sustainable Bridges (2007).

The recommendations for redistribution widths in the guide are less rigorous than previous demands for bridges in Sweden, but are still believed to be conservative with potential for more liberal provision in the future based on improved knowledge. For moments in ULS, the recommended redistribution widths depend on the ductility of the slab, the slab thickness and a characteristic span length, determined differently for different categories of slabs; the recommendations distinguish between two-way, one-way, and predominantly one-way spanning slabs, and cantilever slabs. The redistribution widths in SLS and for the resultant shear force are based on the widths for moments, but with some limitations. For cantilever slabs it was possible to find models for load distribution based on tests in the literature; more specific and less conservative recommendations could therefore be given for these.

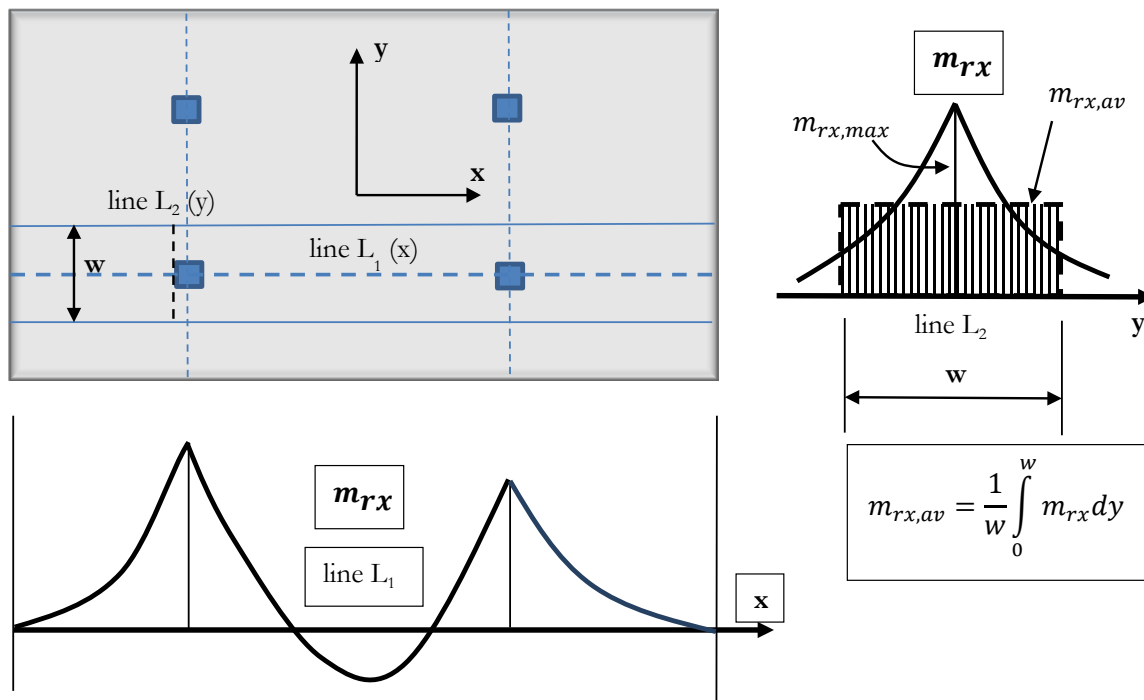


Fig. 2 Redistribution of the reinforcement moment m_{rx} over a width w .

6. CONCLUSIONS

A new guide provides practical recommendations for design of concrete slabs based on FE analysis. Guidelines are given on modelling and interpretation of analysis results needed for detailed design. Three aspects of particular importance are addressed in the recommendations: modelling of support conditions, choice of result sections and choice of redistribution widths. The recommendations are based on relevant literature combined with engineering judgement and considerations from engineering practice. They are believed to be conservative, implicating a potential for future improvement based on increased knowledge.

ACKNOWLEDGMENT

The financial support from Trafikverket and the authors' organisations is gratefully acknowledged. The authors also want to express their gratitude to the members of the reference group. Their comments and suggestions have been invaluable for developing the guide.

REFERENCES

- Blaauwendraad J. (2010)
Plates and FEM, Surprises and Pitfalls, Springer Science +Business Media B.V., 2010.
- CEB-FIP Bulletin 45, Task Group 4.4 (2008)
Practitioners' guide to finite element modelling of reinforced concrete structures, State of the art report.
- Pacoste C.; Plos M., Johansson M. (2012)
Recommendations for finite element analysis for the design of reinforced concrete slabs. Royal Institute of Technology, KTH/BKN/R-144-SE, Stockholm, 52 pp.
- Rombach G.A. (2004),
Finite Element Design of Concrete Structures, Thomas Telford, 2004.
- Sustainable Bridges (2007)
Assessment for Future Traffic Demands and Longer Lives, Background Document D4.5, Non-Linear Analysis and Remaining fatigue Life of Reinforced Concrete Bridges.

Tests and design of fibre-reinforced RC beams with dapped ends



Håvard Nedreid¹
PhD, Researcher
havard.nedreid@ntnu.no



Terje Kanstad¹
PhD, Professor
terje.kanstad@ntnu.no

¹Department of Structural Engineering, Norwegian University of Science and Technology, Trondheim, Norway

ABSTRACT

Although a lot of research exists on structural applications of RC beams with fibres, only a few tests have been conducted to study the performance of disturbed regions where beam theory does not apply. Hence, this paper reports tests on five RC beams with dapped ends and, further, seeks to establish a design model which account for the effect of fibres. The main test variables are the amount of steel fibres (0 or 1.0vol%) and the layout of the reinforcement in the region of the dapped ends.

Key words: Fibres, structural design, testing.

1. INTRODUCTION

Precast RC beams with dapped ends are often used as drop-in beams between corbels. This enables the building height to be reduced and makes the erection of the building easier. However, due to the disturbed flow caused by the sudden change in cross-section, as shown in Figure 1, a complex reinforcement layout is usually required to limit crack widths and prevent premature failure.

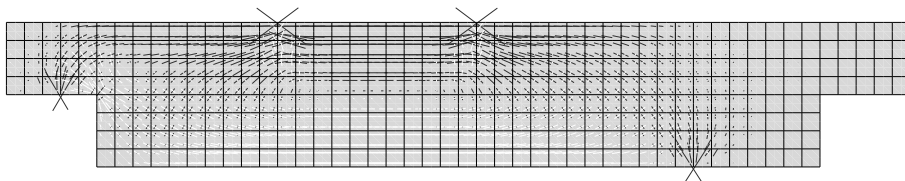


Figure 1 – Principal stress trajectories from an elastic finite-element analysis.

Although a lot of research exists on the structural applications of steel-fibre reinforced concrete (SFRC), only a few tests have been conducted to study the performance of dapped-end RC beams with fibres /Ajina 1986, Fu 2004, Mohamed 2008, Robinson 2012/. Moreover, SFRC for structural applications has yet to gain wide acceptance due to the lack of proper design rules. Hence, an experimental program was undertaken to study the possible role of fibres in dapped-end RC beams, and a simple design formula which accounts for the effect of fibres is proposed.

2. EXPERIMENTAL PROGRAM

Five dapped-end RC beams were tested as shown in Figure 2. The overall dimensions of the beams were $B \times H \times L = 250 \times 400 \times 2500$ mm. The beam flexural reinforcement consisted of 3 \varnothing 25 steel bars with 40 mm cover, whereas the main nib reinforcement consisted of 2 \varnothing 16 steel bars with 25 mm cover. The loading arrangement and the amount of beam reinforcement were chosen such that failure occurred in the region of the left dapped end. Hence, after failure, the beam could be reverted and the test repeated for the other end. Two beams were made of ordinary concrete, whereas the remaining three were made of SFRC with 1.0 vol% hooked-end steel fibres of the type Dramix 65/60. The yield strength of the steel bars was assumed to be 500 MPa.

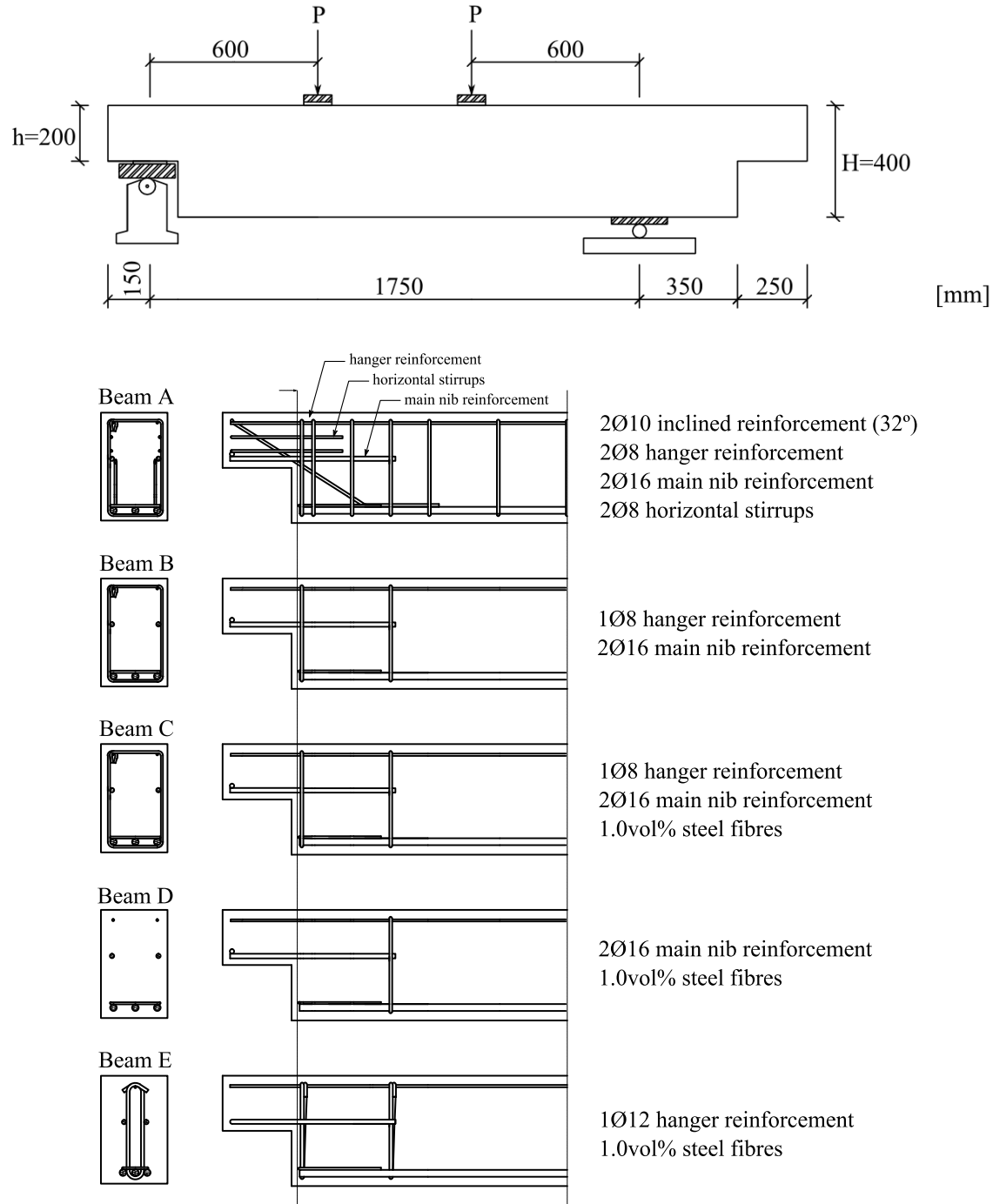


Figure 2 – Specimen geometry, loading arrangement and reinforcement layout.

3. SPECIMEN DESIGN AND BEHAVIOUR

Figure 3 and Table 1 summarises the main results from the experimental program.

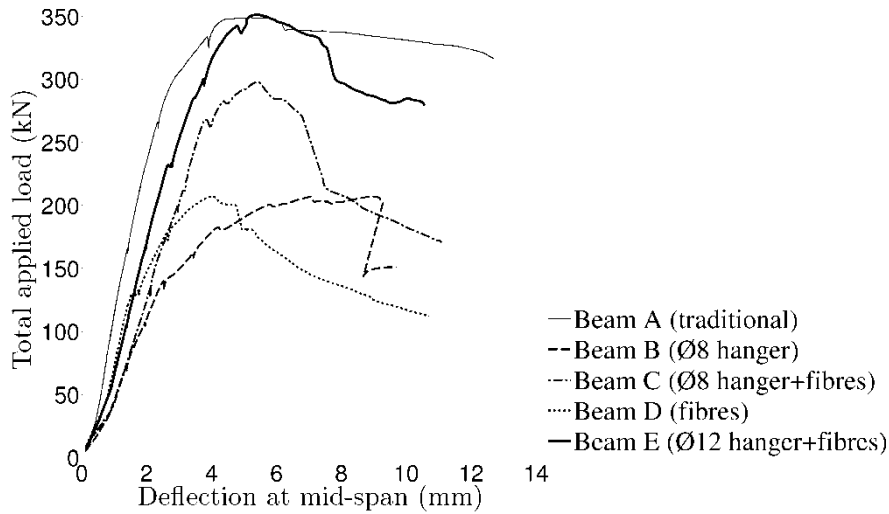


Figure 3 – Load-deflection behaviour of the tested beams.

Table 1 – Main test parameters together with the experimental and estimated shear resistance.

| Beam | f_c Mpa | $f_{ftres,2.5}$ Mpa | d_{nib} | A_s mm^2 | A_{vh} mm^2 | A_{vhq} mm^2 | V_{calc} kN | V_{test} kN | V_{test}/V_{calc} |
|------|--------------|------------------------|-----------|-----------------|--------------------|---------------------|------------------|------------------|---------------------|
| A | 43 | - | 167 | 402 | 201 | 157 | 142 | 175 | 1.23 |
| B | 43 | - | 167 | 402 | 100.5 | - | 50.3 | 96.7 | 1.92 |
| C | 64 | 4.0 | 167 | 402 | 100.5 | - | 121 | 149 | 1.23 |
| D | 64 | 4.0 | 167 | 402 | - | - | 70.7 | 105 | 1.49 |
| E | 64 | 2.8 | 167 | 402 | 226 | - | 163 | 173 | 1.06 |

Three types of failure must be catered for in the design of dapped end beams with $a/d < 1.0$: yield of the hanger reinforcement A_{vh} , yield of the main nib reinforcement A_s , and splitting of the concrete in the nib along the compressive diagonal /Mattock 1979/. Since the amount of hanger reinforcement was low compared to both the concrete cross-section and the amount of main nib reinforcement, the estimated resistance was limited by yielding of the hangers in all cases. Hence, if the strut-and-tie model in Figure 4 is used, the capacity is simply given by multiplying the area of hanger reinforcement with its yield strength. If inclined reinforcement is provided, its vertical component can be added to the resistance.

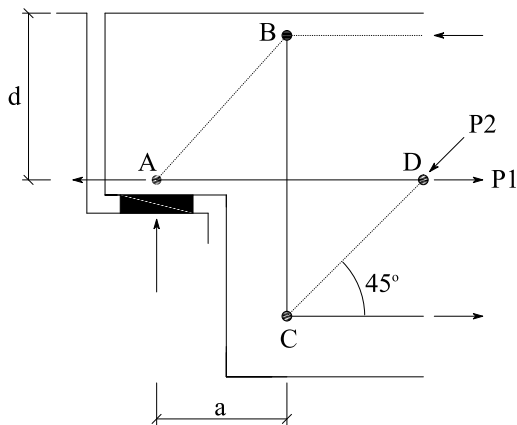


Figure 4 – Simplified strut-and-tie model. The external tensile restraint P_1 is provided by the development length extension of Tie AD /Mattock 2012/.

To account for the effect of fibres, it can be imagined that the fibres form a tensile band which has the same effect as inclined bars. It is proposed that strength of this band may be taken as

$$F_{\text{fib}} = f_{\text{ftres},2.5} b h/2$$

where $f_{\text{ftres},2.5}$ is the residual direct tensile strength at 2.5mm crack width, as derived from three-point bending tests on notched prisms according to EN 14651:2005 /CEN 2005/, and b is the width of the nib. The inclination of the band can be assumed to be 45 degree to the beam axis.

4. DISCUSSION

From Table 1 it can be seen that the estimated resistance is conservative for all specimens. This is not surprising, since after yielding of the hangers, the concrete can contribute through arching action until the main nib reinforcement yields. Moreover, the hangers will eventually start to strain harden. In fact, the final failure of all beams with hangers, except beam E, was triggered by snapping of the hangers. For beam E the final failure was triggered by splitting along the compressive diagonal, probably due to the load in this case became concentrated over a smaller area owing to the centred layout /Robinson 2012/, which probably explains the least conservative result for this member.

5. FINAL REMARKS

A simple design rule which account for the effect of fibres in RC beams with dapped ends have been proposed and compared to tests results. The only material parameter used to account for the effect of fibres is the residual direct tensile strength at 2.5mm crack width as derived from three-point bending tests on small notched prisms.

ACKNOWLEDGEMENTS

The research was financially supported by COIN – Concrete Innovation Centre.

REFERENCES

- Ajina, J.M., 1986,
 “Effect of steel fibers on precast dapped-end beam connections”. Master’s Thesis, South Dakota State University.
- CEN, 2005,
 “EN 14651:2005 - Test method for metallic fibre concrete”. CEN, European Committee for Standardization,.
- Fu, Z., 2004,
 “Use of fibres and headed bars in dapped end beams”. Master’s Thesis, McGill University.
- Mattock, A.H., 1979,
 “Design and behaviour of dapped-end beams”. PCI Journal, November-December, 28-44.
- Mattock, A.H, 2012,
 “Strut-and-tie models for dapped-end beams”, Concrete International, February, 35-40.
- Mohamed, R.N., Elliott, K.S., 2008,
 “Shear strength of short recess precast dapped end beams made of steel fibre self-compacting concrete.” 33rd Conference on our world in Concrete & Structures.
- Robinson, G.P., Palermi, A., Austin, S.A., 2012,
 “Influence of steel fibres used in conjunction with unconfined rebar configurations, on the structural performance of precast elements”, BEFIB2012.

Application of NLFEA in the Design of Large Concrete Structures



Morten Engen^{1,2}
M.Sc., Industrial PhD-candidate
morten.engen@ntnu.no

Max A. N. Hendriks^{1,3}
PhD, Professor
max.hendriks@ntnu.no

Jan Arve Øverli¹
PhD, Associate Professor
jan.overli@ntnu.no

Erik Åldstedt²
PhD, Senior Consultant
erik.aaldstedt@multiconsult.no

¹Norwegian University of Science and Technology, Department of Structural Engineering, Trondheim, Norway

²Multiconsult AS, Oslo, Norway

³Delft University of Technology, Delft, The Netherlands

ABSTRACT

A general description of the process of designing large concrete structures is outlined. Special focus is directed towards the application of non-linear Finite Element Analyses (NLFEA) in the design process. It is stated that there is need for a general, robust and stabile engineering solution strategy for NLFEA in addition to a method for applying safety formats to large and statically indeterminate concrete structures.

Key words: Large Concrete Structures, Modelling, Non-linear Finite Element Analysis, Safety Format, Structural Design.

1. INTRODUCTION

Since the 1970s large concrete structures have been designed and constructed for supporting topsides operating oil and gas fields worldwide (*fib* 2009). During their lifetime these structures go through different phases with different loading arrangements. The lower parts of the structures are normally constructed in a dry dock. When the construction approaches a certain height, the dock is water filled and the structure can be towed to a deep water site where the concrete works are finished on the floating structure. The topside is normally mated onto the concrete substructure which is lowered to a minimum freeboard resulting in maximum hydrostatic pressure. Finally, the complete structure is installed at site where the largest environmental loads are experienced during operation. As a result, the structure needs to be designed for a high number of load cases and load combinations. The Hebron platform, which is currently under construction at Newfoundland, is designed for approximately 700 load cases resulting in nearly 100 000 load combinations.

The high number of design load combinations calls for a robust and accurate design method. The method, which is currently used, is fully described elsewhere (Brekke, Åldstedt & Grosch

1994) and will only be briefly summarized here. In order to take advantage of the principle of linear superposition, the design is based on linear Finite Element Analyses (LFEA) of each load case, using relatively large solid elements. Partial safety factors (PSF) for load and material are used in order to obtain the intended level of safety. The results from the LFEAs are superpositioned to form load combinations using in-house developed post-processor software, and a local non-linear section design and capacity control is taking into account the non-linear material behaviour of reinforced concrete. Due to cracking of concrete and yielding of reinforcement a redistribution of internal forces occurs even at low load levels. Such effects cannot be revealed by the LFEA due to the lack of a realistic connection between load and material response during calculation of internal forces (Schlune 2011). Despite the inconsistency of this *two-step* procedure, it is considered safe when equilibrium is satisfied, the material strengths are not exceeded and sufficient ductility is provided. To compensate for the inconsistency a *one-step* procedure using non-linear Finite Element Analyses (NLFEA) where the non-linear material behaviour is directly taken into account, could be carried out to verify the reliability of the design. The present paper considers how such a one-step procedure could be utilized at the ultimate limit state (ULS).

2. APPLICATION OF NLFEA IN THE DESIGN OF LARGE CONCRETE STRUCTURES

Figure 1 shows schematically how the process of designing large concrete structures could be complemented using NLFEA. Note that the initial design based on LFEA is kept.

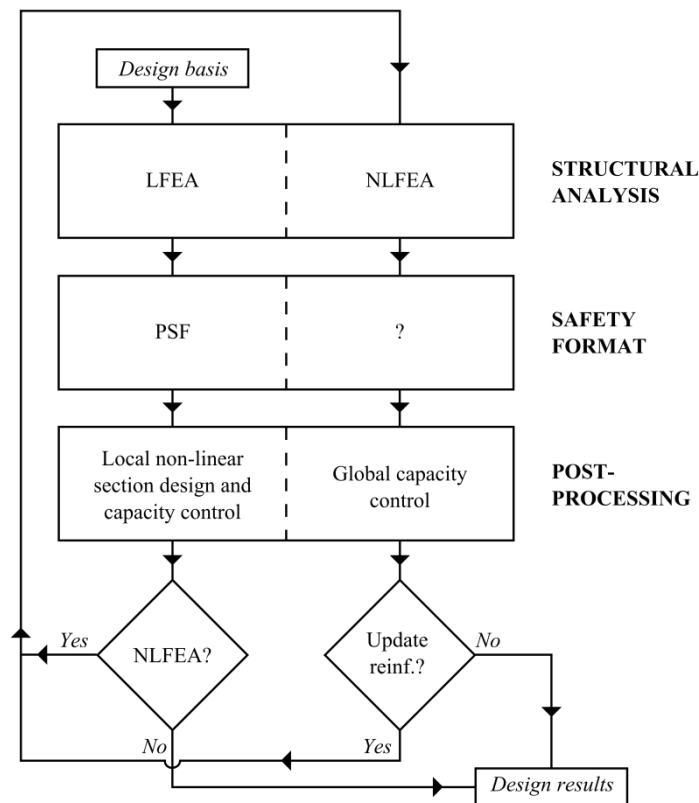


Figure 1 – Outline of the design process for large concrete structures (LFEA – linear Finite Element Analysis, NLFEA – non-linear Finite Element Analysis, PSF – Partial Safety Factors).

The process consists of three parts with distinct purposes, but possibly different approaches in the left and right path. The structural analysis transforms the applied loads to internal forces, while the safety format ensures the intended level of safety and the post-processor is used by the designer to review the results. The path to the left describes the design process summarized in Section 1. If the structure is sufficiently complex, there could be need for an assessment of the reliability using NLFEA, and the path to the right shows how this could be carried out. The use of design values for material parameters as input for NLFEA could lead to distorted failure modes and unrealistic load distributions (Cervenka 2013). PSFs are thus not recommended for NLFEA. In *fib Model Code 2010* (*fib* 2013) safety formats for NLFEA accounting for material, geometrical and modelling uncertainty are presented. Examples of application of such safety formats to relatively simple structures can be found in the work by Schlune (2011) and Cervenka (2013). It still remains unclear how safety formats could be applied to large statically indeterminate structures with a high number of load cases.

At present the path to the right in Figure 1 is a very time consuming process due to the lack of a sound safety format and the need for establishing new or additional finite element models. Note that there is no need for a further local capacity control as the NLFEA can be considered a virtual test revealing the *global* capacity of the structure to which all sections contribute (Cervenka 2013).

3. SOLUTION STRATEGY FOR NLFEA

In order to use NLFEA in practical design a general, robust and stable solution strategy should be selected (Vecchio 2001). This is of particular importance in design of offshore concrete structures due to the wide range of loading conditions encountered during their lifetime. A solution strategy for NLFEA comprises choices regarding equilibrium, kinematics and constitutive relations, i.e.: Iteration method and convergence criteria, finite element type and integration scheme, and material models and representation of cracking. A general *engineering* solution strategy was developed by Kotsovos and Pavlovic, fully described elsewhere for the case of static and sequential loading (Kotsovos & Pavlovic 1995). The solution strategy is based on a material model for concrete describing the full triaxial material behaviour obtained from experiments and recognizing the existence of a localized triaxial stress state close to ultimate stress levels due to dilation.

In the present study a collection of nearly 70 benchmark analyses (e.g. Kotsovos & Pavlovic 1995) revealed a mean ratio of analytical to experimental capacity of 1.0 with a coefficient of variation (COV) of 14%. This is considered adequate when the only material input is the concrete strength and the collection comprised a wide range of failure modes, concrete strengths and structural forms. In general a COV of 5-30% and 10-40% could be typical for problems involving beams in bending and shear respectively (Schlune 2011). Further development seems necessary for the solution strategy to be fully applicable to large concrete structures with simultaneous cracking in adjacent areas.

4. DISCUSSION

An engineering solution strategy including three-dimensional finite elements and a fully triaxial material model with few input parameters seem necessary for NLFEA of reinforced concrete to yield results with sufficient accuracy at ultimate load levels. Although a fully triaxial material model could seem complex, it seems more attractive compared to the extension to three dimensions of simplified *uniaxial* material models, which are presently being applied in many cases. More refined strategies allowing for more parameters to be adjusted seems more applicable for research purposes where local effects like e.g. crack propagation, bond-slip or

sliding along cracks are to be studied in detail. This also holds for analyses at service limit load levels where tightness and crack width estimates could call for a more refined approach.

To secure that all relevant load effects are accounted for during design, the left path in Figure 1 should be followed for all load combinations. Compared to running several NLFEA this is computationally inexpensive due to the efficiency of the post-processing software which incorporates special sorting routines to decide on the governing load combination for each design section. In order to secure efficiency in the assessment of the global reliability only a limited number of load combinations and sequences could be analysed following the path to the right in Figure 1. A method for selecting the governing global load combinations could therefore be an important part of the outlined design process.

5. CONCLUSION

It is shown schematically how the efficiency of the design process for large concrete structures could be considerably improved by utilizing NLFEA to complement the design based on LFEA. In order to obtain the improved efficiency, research needs to be focused on developing a general, robust and stable engineering solution strategy for NLFEA at ULS load levels and a method for applying a safety format to NLFEA of large statically indeterminate concrete structures. The solution strategy should require as few input parameters as possible in order to reduce time consumption, modelling uncertainty and possible sources of human error. These topics are the scope of this ongoing Industrial PhD-project initiated by Multiconsult AS.

ACKNOWLEDGEMENTS

The present Industrial PhD is funded by Multiconsult AS and The Research Council of Norway. The author thanks his supervisors and all colleagues in Multiconsult, department for Marine Structures, for valuable discussions and specially Per Horn, Senior Vice President of Multiconsult AS, for having the courage to initiate the research project.

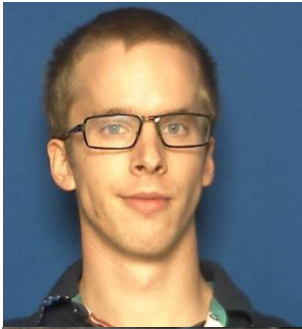
REFERENCES

- Brekke, D.-E., Åldstedt, E., Grosch, H., 1994
 “Design of Offshore Concrete Structures Based on Postprocessing of Results from Finite Element Analysis (FEA): Methods, Limitations and Accuracy”, Proceedings of the Fourth International Offshore and Polar Engineering Conference, Osaka, Japan, 318-328.
- Cervenka, V., 2013
 “Reliability-based non-linear analysis according to *fib* Model Code 2010”, Structural Concrete, 14(1), 19-28.
- fib*, 2009
 “Bulletin 50: Concrete structures for oil & gas fields”, International Federation for Structural Concrete (*fib*).
- fib*, 2013
 “*fib* Model Code for Concrete Structures 2010”, Ernst & Sohn.
- Kotsovos, M. D., Pavlovic, M. N., 1995
 “Structural Concrete: Finite-element analysis for limit-state design”, Thomas Telford.
- Schlune, H., 2011
 “Safety Evaluation of Concrete Structures with Nonlinear Analysis”, Chalmers University of Technology.
- Vecchio, F. J., 2001
 “Non-linear finite element analysis of reinforced concrete: at the crossroads?”, Structural Concrete, 2(4), 201-212.

DURABILITY, MAINTENANCE, RENOVATION & FROST ACTION
PER FIDJESTØL MEMORIAL SESSION

Cont.

The Influence from SCMs on Salt Frost Scaling of Concrete Structures - Minimum Required Air Content and effect from Carbonation



Martin Strand
M.Sc. PhD Student
Building Materials
Department of Building and Environmental Technology
Faculty of Engineering, LTH, Lund University
P O Box 188, SE-221 00 Lund, Sweden
Phone +46 46 222 4260
E-mail: martin.strand@byggtek.lth.se



Katja Fridh
M.Sc., PhD., Supervisor
Building Materials
Department of Building and Environmental Technology
Faculty of Engineering, LTH, Lund University
P O Box 188, SE-221 00 Lund, Sweden
Phone +46 46 222 3323
E-mail: katja.fridh@byggtek.lth.se

ABSTRACT

The goal for this PhD thesis is to evaluate the effect different additives has on the salt frost scaling resistance regarding air content required in well hydrated carbonated and non-carbonated concrete which contains admixtures. To evaluate this, freeze-thaw scaling tests, image analysis of the air void structure in hardened concrete, measurements with an air void analyser and a low-temperature calorimeter will be performed. The results should link the required air content, and air void system created, for each binder when using a working combination of superplasticizer and air entraining agent for the concrete to be considered salt frost scaling resistant.

Key words: Additives, Admixtures, Salt-frost Scaling, Freeze-thaw, Air void system

1. INTRODUCTION

The energy consumption and production of carbon dioxide (CO₂) emissions from producing cement could be reduced by replacing some of the cement with additives, e.g. fly ash, slag and lime filler. This will lower cement consumption which would lower both the net energy consumption and the CO₂ emissions from the production of cement. When adding SCMs, studies have shown that this effects the salt frost resistance of the concrete surface in different ways. This project will study the salt frost scaling resistance in concrete with 0.40 w/b-ratio and modern admixtures when fly ash, slag, or slag with lime filler are added in different amounts in comparison to a regular ordinary Portland cement (OPC). This will evaluate the viability of using these binders in bridges where concrete with a high salt frost resistance is needed.

The planned studies in the project will analyse air voids in fresh and hardened concrete. The studies on fresh concrete focus on the air void stability and how this can be effected by increased alkali content, and by mixing and vibration of the concrete. The two studies on hardened concrete will study the minimum required total air content for each binder to make the

concrete salt frost scaling resistant. One test will study well hydrated concrete and the other will study “aged” carbonated concrete, both with a combination of admixtures.

2. MATERIALS

The two different OPC used in the studies is CEM I 42,5 N - SR 3 MH/LA and CEM I 52,5 R from Sweden. These were selected for their alkali content, one with lower than 0.6 w-% alkali which is considered a low alkali content, and the other one contains more than 1.0 w-% alkali which is considered a high alkali content. The recipes with 20% additives are chosen to be studied since these are considered reliable and are allowed in the most exposed environments according to the Swedish standard. The binders with 35% and 70% additive will be studied to enable a comparison to the others and also give some information about how to make these salt frost scaling resistant.

Table 1 - Binders used in the studies.

| Cement | Swedish standard |
|-------------------------|---------------------------|
| OPC | CEM I 42,5 N - SR 3 MH/LA |
| OPC 20% FA | CEM II/A-V |
| OPC 35% FA | CEM II/B-V |
| OPC 20% ggbs | CEM II/A-S |
| OPC 35% ggbs | CEM II/B-S |
| OPC 35% ggbs+LF (25+10) | CEM II/B-M |
| OPC 70% ggbs | CEM III/B |
| OPC | CEM I 52,5 R |

3. STUDIES ON FRESH CONCRETE

In the first part of the PhD project different combinations of superplasticizers and air entraining agents will be evaluated in combination with each binder using a method to study the foam created when the paste is dissolved in water. This will allow a comparison between the foam created from each mix and how its stability is influenced by an increased amount of soluble alkali, which is done by adding Na(OH)₂. These tests are complemented with a literature study. The effect alkalis have on the air voids in concrete have been studied in /Mielenz 1958/, /Fagerlund 1982/, /Pistilli 1983/, /Pigeon 1992/, and /Smaoui 2005/. The research indicates that an increased amount of alkali content will result in a creation of larger air voids in the fresh and hardened concrete. The first study will investigate if an increased amount of alkali will have the same effect on the air voids on the binders used in this study while using different combinations of superplasticizer and air entraining agent. The purpose of this study is to see the effect, from an increased amount of alkali, on the air void stability for each binder. This study will also give input regarding which combinations of superplasticizers and air entraining agents that performs well and which combinations which perform poorly for all binders. The study comprises three air entraining agents and five superplasticizers. Two air entraining agents are synthetic detergents and one is based on Vinsol resin, wood resin. Four of the superplasticizers are modified polycarboxylates and one is based on sulphonated melamine-formaldehyde condensate. It is assumed that the foam-reduction varies in the superplasticizers.

The hypothesis is that an increased amount of alkali will result in the air voids merging and popping more in comparison to when no alkali is added. This effect could effect the creation of the air void system in the fresh concrete and reduce the salt frost scaling resistance in the hardened concrete.

Approximately 4 dm³ of mortar will be mixed per combination. The mortar/concrete-recipe will have a water/cement-ratio 0.40 and aggregate/cement ratio 3. The 0-8 mm quartzite aggregate are used to acquire some of the effect the aggregates has on the air voids in regular fresh concrete. First the cement, additive, and aggregates are homogenized, then water together with the air entraining agent are added and mixed, and when the mortar have been mixed for 2.5 min the superplasticizer will be added to obtain a workability which is visually considered good whilst avoiding water separation. When the fresh concrete is ready the workability and the air content is measured. Then, the foam stability is visually observed by taking a specified amount of mortar into a bucket of water. The paste is then separated and the air voids will end up at the surface of the water. If the bubbles merge with each other and pop, the combination of admixtures will be considered not working well. If the bubbles do not merge with each other or pops, the foam is considered stable and the combination is considered good. These results will then be compared to when the same recipes are mixed, but with an increased amount of soluble alkali by adding Na(OH)₂. These results will enable comparison for each recipe with and without an increased amount of alkali.

The purpose of the second study on fresh concrete is to evaluate the effect from prolonged mixing time and vibration of the fresh concrete on air void size distribution and total air content. This will be done by using an air void analyser and an 8 dm³ air content meter. The concrete will be mixed using the same method as in the first study. After the mixing is done and after each separate procedure of vibration and each cycle of mixing, the workability, total air content, and air void distribution will be measured. The same concrete recipes which are used in the first study will be used together with one combination of superplasticizer and air entraining agent that seems to perform well and one combination that seems to perform poorly according to the results from the first study.

4. STUDIES ON HARDENED CONCRETE

The purpose of the third study is to evaluate the minimum air contents and air void systems required in hardened concrete for each binder to be considered frost resistant. The combinations of superplasticizer and air entraining agent that performed well for each binder in the two studies of the fresh concrete will be used to get a good air void system.

To evaluate the air void systems the following studies will be done. Low-temperature Calorimetric measurements to investigate the ice formation in the different materials. These results will then be evaluated together with image analysis of the air void system regarding e.g. total air content, spacing factor and specific surface. The results from these two studies will be linked to freeze-thaw studies with 3 w-% sodium chloride solution. Each concrete will be cast with four different total air contents. The freeze-thaw test will be based on the German CDF method /Setzer 1996/. This is considered a robust test which is similar to the Swedish Borås-method, but the sodium chloride solution is placed in the bottom of the container instead of on top of the concrete surface. This is done to minimize the risk of leakage. The first freeze-thaw test will be done on concrete which has been cured with no drying for about 100 days. This will result in a well hydrated concrete regardless of binder when the freeze-thaw test begins. With consideration to delayed pozzolanic reactions this will make the comparison of results more comparable than when each concrete is tested earlier and the degree of hydration of each binder differs which makes the freeze-thaw test more favourable to certain binders.

The influence from carbonation on each binder will also be studied. This is done with a second freeze-thaw test where the concrete, from the same cast as previous freeze-thaw test, has been exposed to carbon dioxide, and therefore has a carbonated surface. Since the carbonation of the

cement paste is a slow process the carbonation will be accelerated using higher concentrations of carbon dioxide. The concrete will be stored approximately 4 years exposed to the carbon dioxide before the test is started. These results will be compared to the non-carbonated tests to determine the effect from carbonation on each type of additive.

The PhD project has a 60% rate and the described studies, excluding the freeze-thaw test on the carbonated concrete, is planned to finish in the autumn 2016.

REFERENCES

- Fagerlund G., 1982,
 "The influence of slag cement on the frost resistance of the hardened concrete", CBI research, Fo 1.
- Mielenz C. R., et al., 1958,
 "Origin, Evolution, and Effects of the Air Void System in Concrete. Part 1 - Entrained Air in Unhardened Concrete.", ACI 55, p. 95-121.
- Pigeon, M., et al., 1992,
 "Influence of soluble alkalis on the production and stability of the air-void system in superplasticized and nonsuperplasticized concrete.", ACI Materials Journal 89, p. 24-31.
- Pistilli, M. F., 1983,
 "Air-void parameters developed by air-entraining admixtures, as influenced by soluble alkalis from fly ash and Portland cement", Journal of the American Concrete Institute 80, p. 217-222.
- Setzer M. J., et al., 1996,
 "CDF TEST – Test method for the freeze-thaw resistance of concrete – tests with sodium chloride solution (CDF)", Materials and Structures 29, p. 523-528.
- Smaoui, N., et al., 2005,
 "Effects of alkali addition on the mechanical properties and durability of concrete", Cement and Concrete Research 35, p. 203-212.
- Vangi S. Ramachandran, et al., 1996,
 "Concrete Admixtures Handbook (2)".

Self-Healing Concrete – Results with Energetically Modified Cements (EMC)



Prof. Dr. Vladimir Ronin
EMC Cement B.V.,
Alvägen 33, SE-973 32 Luleå,
E-mail: emcdev@telia.com



Prof. Dr. Jan-Erik Jonasson
Division of Structural Engineering
Luleå University of Technology, SE-971 87 Luleå
E-mail: jan-erik.jonasson@ltu.se



Prof. em. Dr. Lennart Elfgren
Division of Structural Engineering
Luleå University of Technology, SE-971 87 Luleå
E-mail: lennart.elfgren@ltu.se

ABSTRACT

Energetically Modified cement (EMC) containing up to 70 % of pozzolans have been tested to have the ability to deliver long term pozzolanic reactions (silicon dioxide + calcium oxide + water) leading to the formation of additional amounts of C-H-S gel. This can fill voids and cracks of widths up to 200 μm , up to twice the crack width that usually can be healed. EMC is Portland cement mechanically activated in a process with a pozzolan, silica sand or blast furnace slag. The process was discovered 1992 at Luleå University of Technology and has been further developed since then.

Key words: Aging, Knowledge and Teaching, Modelling, Repair, Sustainable, Testing, Extended life, Concrete roads and bridges

1. INTRODUCTION

1.1 General

Energetically Modified Cement (EMC) is Portland Cement mechanically activated in a process with a pozzolan, silica sand or blast furnace slag. The process was discovered 1992 at Luleå University of Technology and has been further developed since then, Ronin et al (1994, 1997, 2005), Rao et al (1997), Johansson et al (1999) and Justnes et al (2005, 2007).

1.2 Particle modification of binder – the Energetically Modified Cement (EMC) process

Particle surface modification takes place by processing of inorganic materials in comminuting devices, where solids are subjected to high intensive mechanical and temperature impacts, see Figure 1.. These comminuting devices have been called “mechano-chemical reactors” instead of traditional mills. As a different physiochemical process (phase transition, melting and solidification), chemical reactions in solid state could be initiated. The EMC (Energetically Modified Cement) technique, Ronin et al (1994, 1997, 2005), is one most promising in the world. With it, it has been shown that the portion of Portland cement in concrete can be significantly reduced maintaining and sometimes even improving the properties of the concrete, Pike et al (2009), Justnes (2011). Both traditional powders (fly ash and blast furnace slag) as

well as new powders (fine quartz sand, recycled concrete) can be used. Such techniques have the potential to reduce the Portland cement content by at least 50 % compared with traditional usage of today. It is a real challenge to develop this method so that it can be applied world wide. There are both theoretical obstacles in understanding the complex concrete chemistry and societal hardships as new technologies may be a threat to present practice.

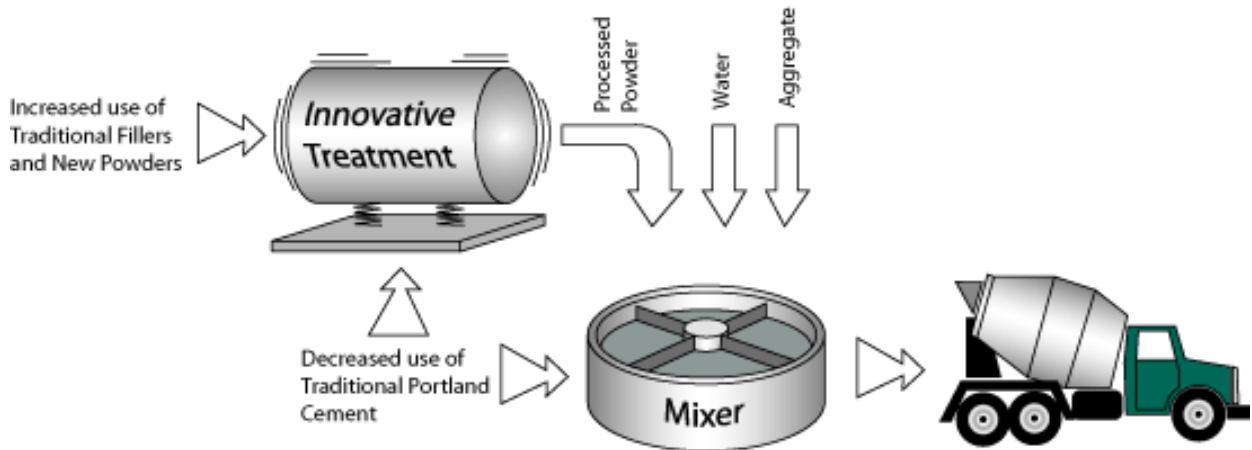


Figure 1. The principal components in creation of a durable and environmentally friendly concrete, produced with Energetically Modified Cement (EMC) materials.

2. TEST PROGRAM

In a pilot test carried out in 2012-2013 at Luleå University of Technology, a concrete beam made of Energetically Modified Cement, EMC, has been loaded using RILEM 3-point bending, RILEM (1985), see Figures 2-4. The loading induced cracks in order to test EMC's self-healing capabilities. A concrete (total amount of cement: 350 kg/m³) was used containing 40% Portland cement and 60% EMC made from fly ash. Cracks of an average width of 150-200 µm were induced after ~3 weeks of water curing, see Figure 3. Control cubes were tested for compressive strength at different ages.

2. TEST RESULTS

Without any intervention, the high volume pozzolan concrete gradually filled the cracks. The theoretical hypothesis is that this was done with newly-synthesized C-S-H gel (a product of the ongoing pozzolanic reaction). The cracks were completely filled-in after ~4.5 months, see Figure 4. The photograph shows that the former cracks have undergone a complete self-healing process without any intervention.

During the observation period, continuous strength-development was also recorded by virtue of the ongoing pozzolanic reaction. The strength development of the concrete was: 30d ca 85 MPa and 150d 94.5 MPa. This increase should have a positive impact on the concrete durability.

3. CONCLUSIONS AND FUTURE WORK

The method can fill voids and cracks of widths up to 200 µm, up to twice the crack width that usually can be healed. Future research is planned to focus on a validation of the hypothesis by further tests to determine boundary conditions and concrete mixtures that can be used in practice in e.g. road construction. The EMC Company, has performed similar tests in the United States and also performed a follow up of the self-healing of the drying shrinkage cracks on concrete paving. Here they obtained an even shorter time period for crack healing than in Sweden. This may be attributed to a lower FACaO content in the LTU test.

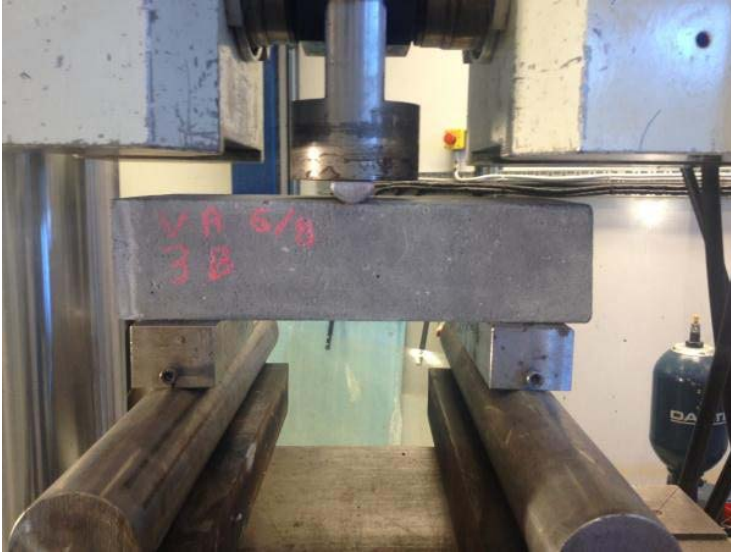


Figure 2. A concrete test-beam made of Energetically Modified Cement, EMC, undergoing RILEM 3-point bending at Luleå University of Technology in September 2012, see RILEM (1985). This treatment induced cracks in order to test EMC's self-healing capabilities. Concrete with total amount of cement of 350 kg/m³ was used, containing 40% Portland cement and 60% EMC made from fly ash. Cracks of average width 150-200 μm were induced after ~3 weeks of water curing see Figure 3.

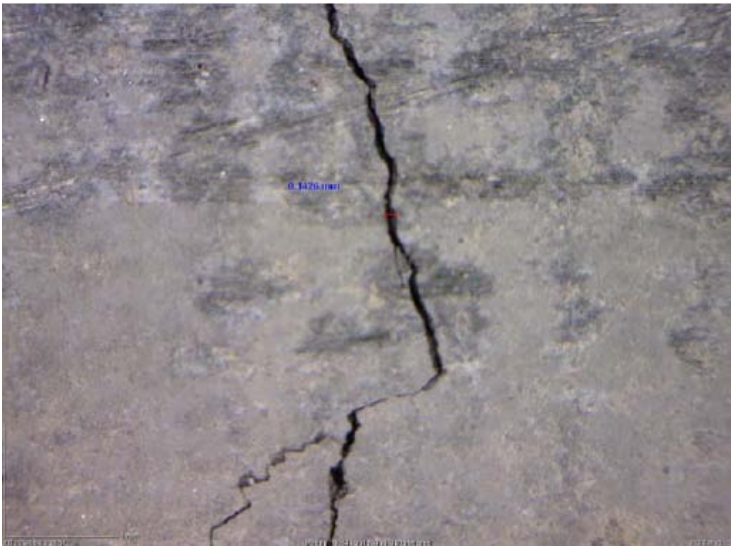


Figure 3. Cracks created as in Figure 2 of average width 150-200 μm were induced after ~3 weeks of water curing. Control cubes were tested for compressive strength at different ages. Without any intervention the high volume pozzolan concrete gradually filled the cracks. The hypothesis is that this was done with newly-synthesized CSH gel (a product of the ongoing pozzolanic reaction). The cracks were completely filled-in after ~4.5 months, see Figure 4.



Figure 4. Photo of former cracks in concrete of EMC Cement, taken 5 months after formation in February 2013. The photograph shows that the former cracks have undergone a complete self-healing process without any intervention. During the observation period, continuous strength-development was also recorded by virtue of the ongoing pozzolanic reaction.

REFERENCES

- Johansson, K., Larsson, C., Antzutkin, O. N., Forsling, W., Rao, K. H. and Ronin V. ,1999
 “Kinetics of the Hydration Reactions in the Cement Paste with Mechanochemically Modified Cement by ^{29}Si Magic-Angle-Spinning NMR Study”, *Cement and Concrete Research*, Vol. 29 (1999) pp. 1575-1581.
- Justnes, Harald ,2011
 “Concrete with high volume of supplementary cementing materials and admixtures for sustainable and productive construction”. Indian Concrete Industry, ICI Update, Vol 2, Feb 2011, No 2, pp 12-26, see http://www.emccement.com/pdf/EMC_ICI_02_11_ex.pdf
- Justnes, Harald, Elfgren, Lennart and Ronin, Vladimir 2005
 “Mechanism for Performance of Energetically Modified Cement versus Corresponding Blended Cement”, *Cement and Concrete Research*, Vol. 35 (2005) pp. 315-323.
- Justnes, H., Dahl, P.A., Ronin, V., Jonasson, J.-E., and Elfgren, L.,2007
 “Microstructure and performance of energetically modified cement (EMC) with high filler content”. *Cement and Concrete Composites*, Vol 29 (2007), pp 533-541. Elsevier.
- Pike, C., Ronin, V., and L. Elfgren, 2009
 “High volume pozzolan concrete: Three years of industrial experience in Texas with CemPozz”. *Concrete Infocus Magazine*, 2009, vol.8, nr. 2. March/April, pp. 22-27.
- Rao, K. H., Ronin, V. and Forsberg, K. S. E., 1997
 “High Performance Energetically Modified Portland Blast-furnace Cements”, Proceedings of the 10th *International Congress of the Chemistry of Cement* (Ed. by H. Justnes), Gothenburg, Sweden, June 1997. Inform Trycket AB, Gothenburg, 3ii104, 9pp. (ISBN 91-630-5497-5).
- RILEM, 1985
 “Determination of the Fracture Energy of Mortar and Concrete by means of three-point bending tests on notched beams”. *Materials and Structures*, Vol 18, No 106, pp 285-290.
- Ronin, Vladimir, 2005
 “Process for Producing Blended Cements with Reduced carbon Dioxide Emissions”, US Patent nr. 6, 936,098 B2.
- Ronin, Vladimir and Jonasson, Jan-Erik, 1994
 “Investigation of the Effective Winter Concreting with the Usage of Energetically Modified Cement (EMC) - Material Science Aspects.” *Report 1994:03*, Division of Structural Engineering, Luleå University of Technology, Luleå, Sweden, 1994, 24 pp.
- Ronin, Vladimir; Jonasson, Jan-Erik; and Hedlund, Hans, 1997
 “Advanced modification technologies of the Portland cement based binders for different high performance applications. Proceedings of the 10th *International Congress on the Chemistry of Cement* (Ed. by H. Justnes), Gothenburg, Sweden, June 1997. Inform Trycket AB, Gothenburg, 2ii077, 8pp. ISBN 91-630-5496-5.

Alkali Resistance of Textile Reinforcement for Concrete Façade Panels



Lic. Eng. Natalie Williams Portal
CBI Swedish Cement and Concrete Research Institute
SE-504 62 Borås, Sweden
E-mail: Natalie.WilliamsPortal@cbi.se



Dr. Mathias Flansbjer
SP Technical Research Institute of Sweden
Box 857 SE-501 15 Borås, Sweden
E-mail: mathias.flansbjer@sp.se



Dr. Kristian Tammo
CBI Swedish Cement and Concrete Research Institute
Box 118 SE-221 00 Lund, Sweden
E-mail: Kristian.Tammo@cbi.se



Prof. Katarina Malaga
CBI Swedish Cement and Concrete Research Institute
SE-504 62 Borås, Sweden
E-mail: Katarina.Malaga@cbi.se

ABSTRACT

Textile reinforced concrete has been proven to be a suitable solution for the production of thin and lightweight façade panels. Despite it being researched over the past decade, its long-term durability is not sufficiently characterized. This paper presents experimental results from accelerated aging and direct tensile testing of various textile reinforcement alternatives according to ISO 10406-1. Based on the results, a large degeneration of the glass and basalt fibre bars was observed after 30 days of immersion. As for carbon fibre grids, no significant difference in ultimate tensile force was noted before and after immersion.

Key words: Textile reinforced concrete, Fibres, Testing, Aging.

1. INTRODUCTION

The building construction industry is in need of sustainable materials and solutions. A novel building material, such as textile reinforced concrete (TRC), could be used to meet this demand. TRC is typically a combination of fine-grained concrete and multi-axial textile grids or bars, which has been fundamentally researched over the past decade. TRC can be utilized to build slender and lightweight façade elements primarily due to the fact that the concrete cover mandated for conventional steel reinforcement can be minimized as the risk of corrosion is eliminated. Despite these improvements, many questions pertaining to the long-term durability arise when attempting to implement such innovative building materials. Durability performance is most accurately measured in real-time (Mechtcherine, 2012); however, usually having time as a constraint, accelerated aging tests or calibrated numerical models (Cuypers, Orłowsky et al. 2007) are typically used to predict the long-term performance. Accelerated testing according to ISO 10406-1 pertaining to fibre-reinforced polymer (FRP) bars and grids was performed in this work. One drawback of this test method is such that the prescribed boundary conditions are thought to inadequately model the realistic conditions encountered by a TRC façade panel.

Future parametric studies are suggested to investigate the variability of the controlling factors in this test, i.e. temperature or pH level of the pore solution, which cause the deterioration of the various reinforcement alternatives.

This paper presents the outcome of accelerated aging and direct tensile testing of various textile reinforcement alternatives performed at CBI Swedish Cement and Concrete Research Institute and SP Technical Research Institute of Sweden. This study was part of the research project *Tekocrete II - Energy efficient thin façade elements for retrofitting of Million Programme housing: TRC textile reinforced concrete façade elements* co-funded by Formas-IQS. Glass and basalt fibre bars, as well as carbon fibre grids were immersed into a high alkali environment (pH 14) with elevated temperature (60°C) for 30 days according to ISO 10406-1. Direct tensile tests of the reinforcement specimens were conducted before and after exposure to observe the degree of stiffness and tensile strength loss due to aging. Both physical and mechanical changes of the textile reinforcement are evaluated and compared in this work.

2. EXPERIMENTAL SETUP

2.1 Materials

Three different textile reinforcement alternatives, namely glass and basalt fibre bars and a carbon fibre grid, were included in this study as described in Table 1. The basalt fibre bars have a spiral wrapping which provides a deformed profile and the surface is coated with sand grains in order to increase the bond capacity. Similarly, the glass fibre bars are covered by a thin layer of resin which incorporates small sand grains. The carbon fibre grid is epoxy coated and has a relatively smooth surface.

Table 1 – Description of tested materials

| ID | Description | Coating | Supplier/Product |
|----|------------------------------|---------|--------------------------------------|
| A | Glass fibre bar $\phi 6$ mm | Yes | Sto Scandinavia AB, StoFiberBar C6 |
| B | Basalt fiber bar $\phi 6$ mm | Yes | Sudaglass Fiber Technology Inc. |
| C | Carbon fibre grid 40x40 mm | Yes | Sto Scandinavia AB, StoFRP Grid C390 |

2.3 Aging test

The alkali resistance of the textile reinforcing grid or bar was investigated as per ISO 10406-1. Linear pieces of textile reinforcing grid with extraneous parts cut away or bars were immersed in an alkaline solution (pH 14) while being exposed to a temperature of 60°C \pm 3°C for 30 days. The solution used was composed of 8.0 g of NaOH and 22.4 g of KOH in 1 L of deionized water. In order to prevent the infiltration of the solution via the ends of the linear pieces, both ends of the test specimens were sealed by epoxy resin. The specimens were immersed in the alkaline solution contained in plastic cylinders. The plastic cylinders were sealed and placed in a climate chamber at a temperature according to the aforementioned boundary conditions. After 30 days, the aged specimens underwent tensile testing and were visually compared to non-aged reference specimens.

2.2 Tensile test setup

The tests were carried out using an Instron 1273 and the force F was recorded by a load cell with a rated capacity of 250 kN and accuracy within 1%. The deformation was measured by a Messphysik Videoextensometer ME46 and pattern recognition technique. The measuring length was chosen as approximately 100 mm. The force and deformation were recorded in a data acquisition system with a sampling rate of 10 Hz. The specimens were preloaded with a force of 0.1 kN. The tests were controlled by the cross-head displacement of 3 mm/min, corresponding

to a strain rate of approximately $5 \times 10^{-3} \text{ min}^{-1}$ within the measuring length. The temperature at testing was approximately $23 \text{ }^\circ\text{C}$.

The anchorage system at each end of the grid or bar simply consisted of a steel tube filled with epoxy resin. In this way, the tensile force is transmitted from the steel tube to the bars by shear stresses in the epoxy. The steel tubes had a length of 100 mm, outer diameter of 15 mm and an inner diameter of 12 mm. The epoxy resin used was NM Injection 300 from Nils Malmgren AB.

3. EXPERIMENTAL RESULTS

3.1 Observations after aging

The specimens were weighed and visually inspected after removal from the alkaline solution. Photos of the test specimens before and after alkaline aging are shown in Figure 1.

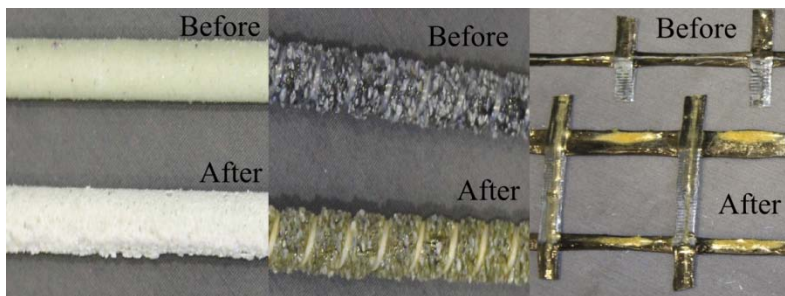


Figure 1 – Photo of test specimens before and after alkaline aging of glass fibre bars, basalt fibre bars and carbon fibre grid (left to right).

For glass fibre bars, the outer surface layer with embedded sand was very porous and came loose easily, which could, in turn, lead to a reduced bond capacity. As for basalt fibre bars, only the colour was observed to change from black to a brownish colour. The emergence of brownish areas with small bubbles at the surface of the carbon fibre grid was noted after alkaline aging.

3.2 Tensile test results

A total of five tests were conducted for each alternative before and after alkaline aging. The load-strain relationships for all alternatives are depicted in Figure 2.

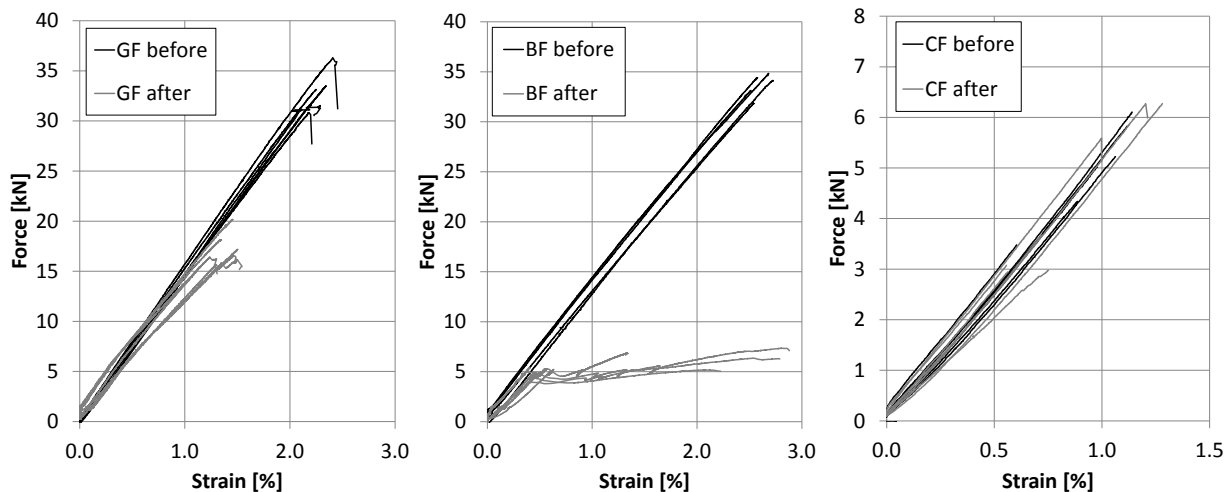


Figure 2 – Load-strain curves before (black) and after alkaline aging (grey) for glass fibre (GF) bars (left), basalt fibre (BF) bars (middle) and carbon fibre (CF) grid (right).

A large degeneration of the glass and basalt fibre bars was observed after 30 days of aging. The stiffness and the ultimate tensile force of the glass fibre bars were reduced by approximately 11 % and 48 %, respectively, while those corresponding to the basalt fibre bars were reduced by 24 % and 80 %, respectively. As for the carbon fibre grids, no significant difference in the ultimate tensile force was noted before and after immersion. The observed scatter may be rather explained by the difference in size and shape of the cross section and the straightness of grid samples.

For the glass fibre bars and the carbon fibre grids no major difference in failure mode could be observed before and after aging. The glass fibre bars splintered along the entire free length and as for the carbon fibre grids, the failure occurred at the location of cross points. Conversely, there was a clear difference in failure mode for the basalt fibre bars before and after aging. Before aging, the samples splintered along the free length. After aging, the failure was much more localized and a pull-out of the basalt fibres from the matrix occurred which is indicated by the horizontal part of the load-strain relation in Figure 2.

4. CONCLUDING REMARKS AND FUTURE WORK

To determine the alkaline resistance of FRP, accelerated testing according to ISO 10406-1 is often used. However, this method describes the relative difference in durability between different samples, but does not predict the actual durability of the material and specifies no requirements to be met. For instance, an unreasonably large degeneration of the glass and basalt fibre bars was observed after 30 days. The prescribed boundary conditions are unlikely to occur in a façade panel and can therefore be considered to yield an upper bound solution. In view of that, this presented study will be subsequently expanded to include the evaluation of the impact of varying the temperature and pH in order to better characterize realistic durability limitations for given textile reinforcement materials. For instance, a temperature of 60°C can be considered as a constant parameter while the pH level of the immersion solution can vary from 12-7. If the specimens were to deteriorate in a neutral solution (7), then it would be made clear that the temperature is a controlling parameter. Alternatively, a similar parametric study can be made to observe the impact of varying the temperature while maintaining a realistic pH level (~12).

REFERENCES

- Cuypers, H., Orlowsky, J., Raupach, M., Büttner, T., Wastiels, J., 2007,
 “Durability aspects of AR-glass-reinforcement in textile reinforced concrete, Part 2: Modelling and exposure to outdoor weathering” *Advances in Construction Materials*, Springer Berlin Heidelberg: 389-395.
- ISO 10406-1:2008(E)
 “Fibre-reinforced polymer (FRP) reinforcement of concrete – Test methods – Part 1: FRP bars and grids.” International Organization for Standardization, 2008.
- Mechtcherine, V., 2012,
 “Towards a durability framework for structural elements and structures made of or strengthened with high-performance fibre-reinforced composites.” *Construction and Building Materials* **31**: 94-104.

Alkali-Silica Reaction in Reinforced Concrete Structures Part I: Material Properties and Crack Orientation



Ricardo Antonio Barbosa
PhD student – Section for Construction Materials
DTU Civil Engineering – Brovej, Building 118, DK – 2800 Kgs. Lyngby
ranba@byg.dtu.dk



Kurt Kielsgaard Hansen
Associate Professor, PhD – Section for Construction Materials
DTU Civil Engineering – Brovej, Building 118, DK – 2800 Kgs. Lyngby
kkh@byg.dtu.dk



Linh Cao Hoang
Professor, PhD – Section for Structural Engineering
DTU Civil Engineering – Brovej, Building 118, DK – 2800 Kgs. Lyngby
linho@byg.dtu.dk



Erik Stoklund Larsen
MSc, PhD – Head of Construction
The Danish Road Directorate – Niels Juels Gade 13, DK – 1022 København K
esl@vd.dk

ABSTRACT

Numerous reinforced concrete structures in Denmark may potentially suffer from severe alkali-silica reaction (ASR) and some are already severely damaged. However, the influence of drilling and crack orientation on material properties of concrete cores drilled out from actual severely damaged structures is not sufficiently illuminated in the literature. Therefore, this paper deals with the consequences of ASR and crack orientation on the compressive strength and splitting tensile strength of concrete cores drilled out from a severe ASR damaged bridge structure. Preliminary results performed at DTU Civil Engineering indicate that the compressive strength and the splitting tensile strength are strongly depending on the crack orientation on concrete cores. The preliminary results are based on strength tests of approximately 55 concrete cores.

Key words: ASR, crack orientation, compressive strength, splitting tensile strength.

1. INTRODUCTION

In Denmark research on alkali-silica reaction (ASR) started already back in the 1950's. The Danish research in 1950-1960 revealed that unfortunately, most aggregate sources in Denmark contain reactive components, opaline and/or calcedonian flint, leading to an always high risk of developing ASR in Danish concrete structures. In 1961 preventive measures regarding the content of reactive components in the concrete were already published [Plum,1961]. These measures are still used in Denmark, but they were unfortunately first adopted by the Danish concrete industry several decades later with the publication of "Basisbetonbeskrivelsen for bygningskonstruktioner" in 1987 [Basisbetonbeskrivelsen, 1987]. Therefore, several concrete structures in Denmark are made of concrete containing sufficient reactive components in aggregates in order to potentially cause ASR. The Danish Road Directorate has estimated that approximately 600 road and railway concrete bridge structures potentially may suffer from alkali-silica reaction.

Most research in Denmark and around the world can basically be divided into three fields of research: 1) the mechanism behind ASR, the controlling and critical parameters of the reaction and how the reaction evolves, 2) identification of ASR in structures and 3) how to repair ASR damaged concrete structures. However, there is very limited research on the load carrying capacity and material properties of actual ASR damaged bridge structures. With the support of The Danish Road Directorate an on-going PhD project at DTU Civil Engineering focus on investigation of actual ASR damaged bridge structures. This paper provides preliminary results concerning the influence of ASR and crack orientation on the material properties of concrete drilled out from an actual severe ASR damaged bridge structure.

2. BACKGROUND

The concrete cores used for determination of material properties were drilled from beams cut from a cantilever part of a fly over bridge located north of Aarhus. The bridge was constructed in 1976 and consisted of three spans. The middle span is located above a highway and the side spans are located above hillsides at the bridge ends. The bridge was constructed in reinforced concrete, where the bridge deck is not provided with shear reinforcement. The bridge deck is cast together with two longitudinal pre-stressed main beams. Visual inspections performed on the bridge showed comprehensive fine wet longitudinal cracks and white precipitations in the cantilever part and in the pre-stressed main beams. In this part water and de-icing salts were accumulated on the top of the bridge deck leading to perfect conditions of ASR due to bad drainage and locally leakage of the water proof membrane.

3. MATERIALS AND METHODS

In 2013, the concrete beams used for drilling cores where cut from the northern cantilever beam above hillsides at the bridge end in order to avoid traffic complications in the highway. The beams had a width of approximately 0.3 m, a length of 1.3 m and a height which varied from 0.45 m at the end up to the pre-stressed main beam to 0.27 m up to the edge beam. In total 12 beams were cut from the northern cantilever beam. Two of the beam surfaces were impregnated with fluorescent epoxy without vacuum due to its size in order to visualize possible crack patterns in the beam. Figure 1 shows the fluorescent impregnated side view of the ASR damaged concrete beam surface under ultra-violet light. The cracks patterns are orientated horizontally to the bridge deck. The beams were not provided with shear reinforcement, and this crack orientation was expected since the ASR induced expansion is not restricted in the vertical orientation.

Concrete cores of 100 mm in diameter and between 100 and 200 mm in length were drilled out both horizontally and vertically, thus obtaining cores with cracks perpendicular and parallel to the drilling direction. Surprisingly almost all concrete cores were drilled in one piece despite of comprehensive cracks, thus providing a hypothesis that the reaction product, alkali-silica gel, in the Danish reactive components possibly acts like a strong glue binding the concrete together. The concrete cores were used for compressive strength testing and splitting tensile strength testing. Both tests were deformation controlled with a loading rate of 0.5 mm/min. This differs from the European standards [DS/EN 12390-3:2009] [DS/EN 12390-6:2002], where compressive strength and splitting tensile strength tests are performed as load controlled. All concrete cores reported in this paper were tested approximately 3 weeks after drilling.

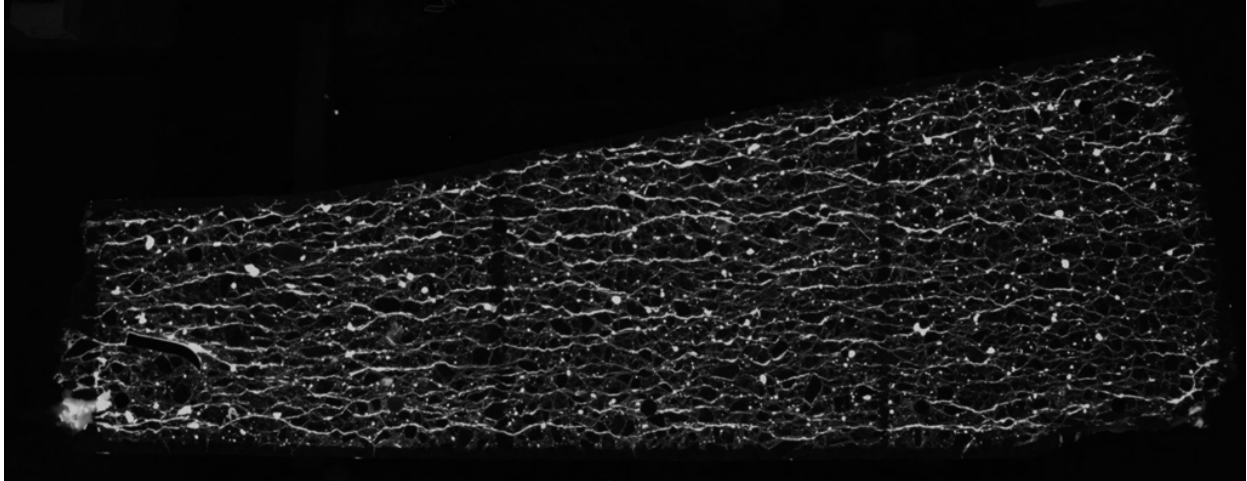


Figure 1: Fluorescent impregnated cantilever beam surface seen under ultra-violet light. The figure shows comprehensive ASR induced horizontal cracks (i.e parallel to the surface of the bridge deck). The dimensions of the beam are shown in the text.

4. RESULTS AND DISCUSSION

4.1 Compressive strength

The length-diameter ratio of the concrete cores varied from 1.5 to 2.0. The concrete cores were converted to a concrete strength corresponding to D150/H300 mm concrete cylinder strengths according to [Vejregel, 2010]. Figure 2 (left) shows the compressive strength divided into cracks orientated perpendicular and parallel to the load direction. The compressive strengths are presented graphically as a box and whisker plot. The results show that the influence of the crack orientation on the compressive strength of concrete is significant. Concrete cores with cracks perpendicular to the load direction had smaller compressive strengths, in average 18.1 MPa, than concrete cores with cracks parallel to the load direction, in average 24.7 MPa. Further tests are being performed at DTU Civil Engineering in order to explain this remarkable difference in strength. The behaviour of the material during test also depended on the crack orientation. Concrete cores with cracks parallel to the load direction failed in a brittle manner, while concrete cores with cracks perpendicular to the load direction behaved more ductile. The ductile failure may be related to the compaction of the cracks. In practice the results show that the conventional way of drilling cores, vertical drilling, from non-shear reinforced bridge deck surprisingly provide the most conservative compressive strengths.

4.2 Splitting tensile strength

The concrete cores with crack orientation of 0, 45 and 90 degrees are all drilled out horizontally, and concrete cores with cracks orientated “out of plane” were drilled out vertically from the beams. Figure 2 (right) shows the splitting tensile strengths for the four crack orientations. The splitting tensile strengths for concrete cores with cracks “out of plane” are generally higher than all other crack orientations. Apparently, this splitting tensile strength corresponds to the strength of an almost “undamaged” concrete cross section. The scatter observed for the concrete cores with cracks of “0 degree” can be explained by the fact that in some tests the cracks are in alignment with the loading plane and in other tests they are not, thus having a higher strength. The cores with cracks orientations of 45 and 90 degrees have almost the same splitting tensile strengths. The splitting tensile test has in earlier published experiments been reported to provide results that are less indicative for the effects of ASR on the concrete properties [Siemens 20002]. During the splitting tensile test the crack failure will not follow the weakest section in

the concrete, but it will follow a predetermined plane between the two loading plates resulting in higher splitting tensile strengths.

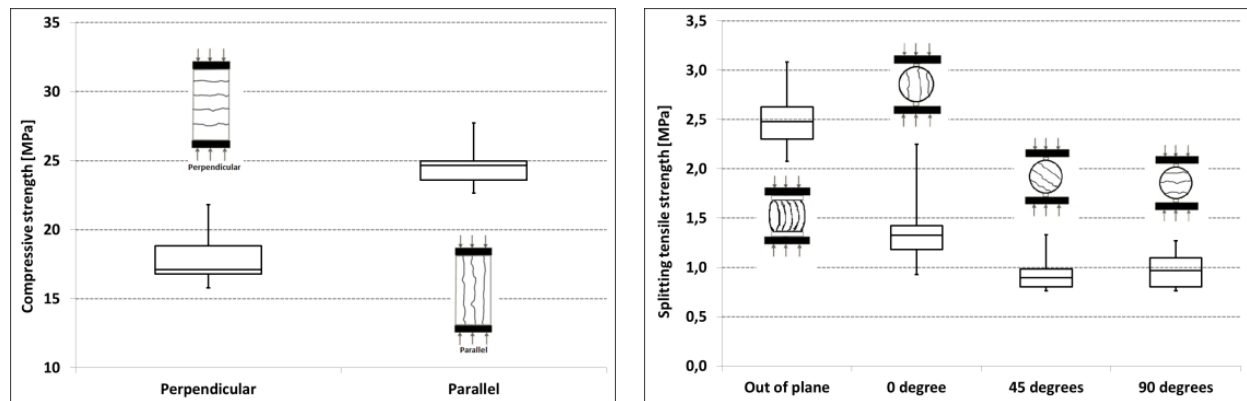


Figure 2: Left: Compressive strength of concrete cores divided into cracks orientated perpendicular (5 compressive tests) and parallel (6 compressive tests) to the load direction. Right: Splitting tensile strength of concrete cylinders divided into four crack orientations: out of plane (12 splitting tensile tests), 0 degree (10 splitting tensile tests), 45 degrees (11 splitting tensile tests) and 90 degrees (11 splitting tensile tests).

5. CONCLUSION

The compressive strength and splitting tensile strength results presented indicate that drilling and thereby crack orientation are very significant for the strength measured. Anisotropic material behaviour as a result of different crack orientations is observed. Further tests must be performed in order to clarify if this tendency is the same for other non-shear reinforced bridge structures.

ACKNOWLEDGMENT

Thanks for the support given by The Danish Road Directorate, COWI and Rambøll. The authors also thank MSc students Christian Gottlieb and Damien Lawrence Hannerz for their great work and interest during their MSc work.

REFERENCES

- Basisbetonbeskrivelsen for Bygningskonstruktioner. Byggestyrelsen (1987), Copenhagen (In Danish).
- DS/EN 12390-3:2009
 “Testing hardened concrete – Part 3: Compressive strength of test specimens”, The Danish Standards Association, 2009
- DS/EN 12390-6:2002
 “Testing hardened concrete – Part 6: Tensile splitting strength of test specimens”, The Danish Standards Association, 2002
- Plum, N.M., 1961
 ”Alkaliudvalgets vejledning 1 – Foreløbig vejledning i forebyggelse af skadelige alkaliske reaktioner i beton”, The Danish National Institute of Building Research, 1961 (In Danish).
- Siemens, T., Han, N. and Visser, J., 2002
 “Unexpectedly low tensile strength in concrete structures”, Heron, Vol. 47, No. 2, 2002, Special issue on ASR-ISSN 0046-7316
- Vejregel 2010
 ”Vejledning til belastning- og beregningsgrundlag”, The Danish Road Directorate, 2010

Alkali-Silica Reaction in Reinforced Concrete Structures

Part II: Shear Strength of Severe ASR Damaged Concrete Beams



Ricardo Antonio Barbosa
PhD student – Section for Construction Materials
DTU Civil Engineering – Brovej, Building 118, DK – 2800 Kgs. Lyngby
ranba@byg.dtu.dk



Kurt Kielsgaard Hansen
Associate Professor, PhD – Section for Construction Materials
DTU Civil Engineering – Brovej, Building 118, DK – 2800 Kgs. Lyngby
kkh@byg.dtu.dk



Linh Cao Hoang
Professor, PhD – Section for Structural Engineering
DTU Civil Engineering – Brovej, Building 118, DK – 2800 Kgs. Lyngby
linho@byg.dtu.dk



Iben Maag
MSc, Coordinator at Maintenance of Bridges
The Danish Road Directorate – Niels Juels Gade 13, DK – 1022 København K
ibma@vd.dk

ABSTRACT

The published experimental research on the shear strength of ASR damaged concrete beams has shown that both reductions as well as increases in shear strength of laboratory test specimens can be obtained. This paper deals with the shear strength of severely ASR damaged beams without shear reinforcement cut from an actual bridge structure. The test results indicate that the shear strength of the severe ASR damaged concrete beams is higher than the predicted shear strength based on the compressive strength of the ASR damaged concrete, and the Eurocode 2 design formula. The shear test results also indicate that the shear strength of the beams was not reduced even by severe ASR damages compared to calculations based on the original concrete compressive strength estimated from thin section analysis.

Key words: ASR, bridge structure, concrete beams, shear strength, pre-stress, reinforcement, compressive strength, Eurocode 2

1. INTRODUCTION

The Danish Road Directorate has estimated that approximately 600 road and railway bridges in Denmark may potentially suffer from alkali-silica reaction (ASR) and some are already severely damaged. However, knowledge regarding the material properties and load carrying capacity of these ASR damaged structures is very limited. An on-going PhD project at DTU Civil Engineering supported by The Danish Road Directorate focuses on the material properties and the load carrying capacity of ASR damaged bridges.

The majority of the reported results in the literature concerning the shear strength of ASR damaged beams are obtained from laboratory conditioned specimens. The degree of damage, type of reactive aggregate and conditioning are different in all tests, thus leading to significant challenges in the interpretation and comparison of the test results.

In Denmark a research project initiated in 1984 investigated the shear strength of non-shear reinforced beams stored for different periods in a sodium chloride solution at 50 °C [1]. This method of accelerating ASR has since been criticized by Hobbs [2], because the alkali ions are introduced from all surfaces having different crack patterns compared to beams in a more natural exposure. The test results showed that the shear strength of the severely ASR damaged beams was not reduced but increased up to 78 % beyond the capacity of non-deteriorated reference beams. Despite of compressive strength loss, it was stated that the loss in compression strength is compensated by the pre-stress induced in the reinforcement as a result of the ASR expansion. In [3] the shear strength of non-shear reinforced beams was also reported to increase compared to corresponding reference beams. Once again this increase in shear strength was attributed to the effect of the pre-stress induced in the reinforcement. As an additional hypothesis, the reaction product, alkali-silica gel, was considered to have a positive effect on the shear strength by acting as strong glue binding the cracks together. Contrary, in [4] a loss in shear strength of 11.7 to 25 percent is reported. The overall conclusions from these tests are generally very contradictory and it is questionable whether these test results can be related to the actual shear strength of existing ASR damage structures.

Therefore in this paper the influence of ASR on the shear strength of severe ASR damaged concrete beams cut from an actual bridge structure is investigated. The shear tests were conducted on 3 beams and results are compared with the Eurocode 2 (EC2) design formula.

2. EXPERIMENTAL PROGRAM

The experimental program consisted of three severe ASR damaged beams, with length of 7.6 m and a depth of 0.74m. The beams were cut from a bridge structure in 2010 in connection with the demolition of the bridge structure due to limited knowledge concerning the influence of ASR on the load carrying capacity. From 2010 to 2013 the beams were stored and in 2013 they were tested at DTU Civil Engineering.

The beam geometry is shown in Figure 1 (left). The beams widths were reduced before the test in order to reduce the shear resistance without significant reduction of the bending resistance. The reinforcement at the bottom of the beams consisted of 3 Ø 25 mm bars and the reinforcement at the top varied from 1 to 3 Ø 20 mm.



Figure 1: Left: Specimen geometry and reinforcement ratio in one of the tested beams. $bw = 0.39$ m, $B2 = 0.60$ m, $H2 = 0.13$ m, $h = 0.74$ m, $V = 45^\circ$ and $d = 0.68$ m. Right: Asymmetrical three point bending test rig with the length of 5.6 m between supports.

The beams were tested in asymmetrical three point bending, see Figure 1 (right). Both ends of two of the beams were loaded until failure. After the first test was performed the length between test supports was decreased from 5.6 to 3.7 m and the non-tested end of the beam was

loaded until failure. In total 5 shear tests were obtained from the 3 beams. In all tests, the shear span to depth ratio, a/h , was 2.38 and in order to prevent anchorage failure the anchorage length was 1.0 m. The load was applied by a hand-operated 500 kN jack in about 1 hour. The load was increased stepwise with a rest period between the load steps, allowing stabilization of the first time-dependent effects. Deflections were measured at five points along the beam and also the so-called digital correlation (DIC) system ARAMIS was used to monitor deformations and crack propagation during testing.

3. RESULTS AND CALCULATIONS

The test results are summarized in table 1. All beams failed in shear with formation of diagonal crack in the web. The shear strength of the beams varied from 231 to 291 kN. This difference in shear strength may possibly be explained by the difference in reinforcement ratio at the top of the beams and thus different ASR induced pre-stress in the longitudinal reinforcement.

In order to verify whether the ASR induced expansion have caused a pre-stress in the longitudinal reinforcement, tests were performed on the top longitudinal reinforcement before reduction of the width of the beams. Measurement of possible strains in the longitudinal reinforcement was performed with strain gauges glued locally to the reinforcement and then cutting the reinforcement. The results based on 8 strain measurements showed that the extension or pre-stress in the longitudinal reinforcement was depending on the reinforcement diameter. Strains measured on \varnothing 20 mm reinforcement were in average 1.28 ‰ (based on 5 measurements) and strains measured on \varnothing 25 mm reinforcement were in average 0.89 ‰ (based on 3 measurements). Converting these strains into normal forces, the average normal force for \varnothing 20 mm reinforcement was 84.7 kN and for \varnothing 25 mm reinforcement was 91.5 kN, assuming a modulus of elasticity of 210 GPa. The results showed an increase in strain for smaller reinforcement diameter and decrease in normal forces for smaller reinforcement diameter.

Table 1: Summary of test results.

| Specimen ID | Top reinforcement | Mean $f_{c,Parallel}$ [MPa] | $V_{u,test}$ [kN] | $V_{u,EC2}$ [kN] | $V_{u,test}/V_{u,EC2}$ |
|-------------|-------------------------|-----------------------------|-------------------|------------------|------------------------|
| B1-T 1 | 2 x \varnothing 20 mm | 21.2 | 291 | 242 | 1.20 |
| B1-T 2 | 3 x \varnothing 20 mm | 21.2 | 240 | 253 | 0.95 |
| B2-T 1 | 1 x \varnothing 20 mm | 21.2 | 266 | 231 | 1.15 |
| B2-T 2 | 1x \varnothing 20 mm | 21.2 | 231 | 231 | 1.00 |
| B3-T1 | 1 x \varnothing 20 mm | 21.2 | 286 | 231 | 1.24 |

Notations: $f_{c,Parallel}$: Mean concrete compressive strength, ASR cracks parallel to load direction. $V_{u,test}$: Tested shear strength. $V_{u,EC2}$: Calculated shear strength, according to EC2.

3.1 Comparison of test results with calculations

The shear test results have been compared with calculations by use of the EC2 design formula. The purpose of using this formula is based on a practical point of view, since the EC2 is the basis of shear strength verification in most European countries. According to EC2, the shear strength of beams without shear reinforcement is calculated as:

$$V_u = \max \left\{ \begin{array}{l} (0.18k(100\rho_l f_c)^{1/3} + 0.15\sigma_{cp})b_w d \\ (0.035k^{3/2}\sqrt{f_c} + 0.15\sigma_{cp})b_w d \end{array} \right. \quad (1)$$

where $k = 1 + (200/d)^{1/2} \leq 2$ (d in mm), $\rho_l = A_{sl}/(b_w d) \leq 0,02$ and $\sigma_{cp} = N/A_c < 0.2f_c$. According to EC2, N is the axial force in the cross-section due to loading or pre-stressing where $N > 0$ for

compression. Due to the current beam geometry, $b_w d$ in Eq. (1) is given as the cross section area of the beam corresponding to the effective depth and taking into account the flanges.

The compressive strength, f_c , of the ASR damaged concrete is as reported in [5] depending on the orientation of the ASR induced cracks. The mean compressive strength of D100 mm concrete prisms with ASR cracks orientated parallel to the load direction is higher, 21.2 MPa, than the compressive strength of concrete prisms with cracks orientated perpendicular to the load direction, 13.9 MPa. In the calculations the mean compressive strength of cores with ASR cracks orientated parallel to the load direction has been used. It may be argued that an effective strength somewhere between 13.9 and 21.2 MPa may be more representative for the diagonal compressive strut developed in the web of the beams due to shear action.

In Table 1 the calculated shear strength according to EC2 are summarized. In general, the test results are above the calculated shear strength where the ASR induced pre-stress in the longitudinal reinforcement is taken into account. The ratio of tested shear strength over calculated shear strength varies from 0.95 to 1.24. The ASR induced pre-stress in the longitudinal reinforcement seems to compensate for the loss of compressive strength caused by ASR. The original concrete compressive strength has been estimated to be 40 MPa based on thin section analysis. This means that the original shear strength according to Eq. (1) will amount to approximately 225 kN (no effect of pre-stressing in this case). It can be seen that apparently no significant reduction of shear strength has occurred, even by severe ASR damages with approximately 50% reduction in the concrete compressive strength.

4. CONCLUSION

The influence of ASR on the shear strength of beams cut from an existing severely damaged bridge structure without shear reinforcement has been investigated. Strain measurements have shown that the ASR induced expansion has caused a significant pre-stress in the longitudinal reinforcement. The tested shear strength of the ASR damaged beams is generally higher than calculations based on EC2 using the compressive strength of the ASR damaged concrete and with inclusion of the pre-stressing effect. The tested shear strength is comparable with the shear strength of the undamaged structure obtained from calculations using the original compressive strength. The results thus indicate that as far as the shear strength is concerned, the pre-stress induced by ASR expansion can significantly compensate for the loss of compressive strength.

REFERENCES

- [1] The Road Directorate, 1990
Load carrying capacity of structural members subjected to alkali-silica reactions, Ministry of Transport, Denmark, 1990
- [2] Hobbs, D.W., 1988
Alkali-silica reaction in concrete, American Society of Civil Engineers, Thomas Telford Ltd, London, 1998.
- [3] Ahmed, T., Burley, E. and Rigden, S., 1998
The static and Fatigue Strength of Reinforced Concrete Beams Affected by Alkali-Silica Reaction, ACI Materials Journal; 95(4); 376-387
- [4] Chana, P.S. and Korobokis, G.A., 1991
The structural performance of reinforced concrete affected by alkali-silica reaction: Phase I. British Cement Association, Contractor Report 267, 1991
- [5] Barbosa, R.A., Hansen, K.K., Hoang, L.C. and Larsen, E.S., 2014
Alkali-silica reaction in reinforced concrete structures, Part I: Material properties and crack orientation, XXII Concrete Research Symposium, Reykjavik, 2014

STRUCTURAL BEHAVIOUR AND DESIGN
Cont.

Safety Levels in Industrial Steel Fibre Concrete Floors



Prof. Dr. Johan Silfwerbrand
 KTH Royal Institute of Technology
 SE-100 44 Stockholm
 E-mail: jsilfwer@kth.se

ABSTRACT

Steel fibre concrete (SFC) is a versatile alternative for industrial floors, but unfortunately, there is no common view on how to design and construct SFC floors. In Sweden, there are two competing alternatives, one is based on Swedish traditions and safety concepts and one is based on continental or Belgian concepts. Comparisons show that the Swedish design method is substantially more conservative. This paper identifies the differences and estimates their importance on the safety level on pile-supported industrial SFC floors.

Key words: Design methods, Industrial Concrete Floors, Safety Level, Steel Fibre Concrete.

1. INTRODUCTION

Industrial concrete floors are not always given the same level of consideration as the surrounding industrial building despite the fact that well-performing, even, damage-free, aesthetically appreciating floors with crack control are of great importance for any client and owner. One problem is that industrial floors on ground are regarded as non-structural, i.e., they are not regarded as load-carrying structures. This might be true for floors of the static type slabs-on-grade but is hardly valid for pile-supported slabs.

Steel fibre concrete (SFC) is a versatile alternative for industrial floors, but unfortunately, there is no common view on how to design and construct SFC floors. In Sweden, there are two competing alternatives, one is based on Swedish traditions and safety concepts and one is based on continental or Belgian concepts. At the Stockholm fib symposium in 2012, a unique Swedish-Belgian paper was published (Destrée & Silfwerbrand, 2012). It compared the design of a pile-supported fibre concrete slab. The comparison showed that the calculated load-carrying capacity was considerably higher for the Belgian design than the Swedish design. The differences are due to differences in material test methods, interpretation of material test results, and yield-line pattern. This paper describes the differences and highlights their importance.

2. DESIGN OF INDUSTRIAL CONCRETE FLOORS

2.1 General considerations

All serious design methods for SFC floors have to cover the following steps:

1. Determination of the flexural tensile strength of fibre concrete.
2. Determination of the flexural moment capacity of the fibre concrete cross section.
3. Determination of the design flexural moments for actual geometry and loading case at Ultimate Limit State (ULS).
4. Comparison between flexural moment capacity and design flexural moment.
5. Design against punching shear.
6. Design in the Serviceability Limit State (SLS) for crack and deformation control under both short term and long term loads.

The four first steps are compulsory. Step 5 ought to be checked but experience shows that it is rarely the design case in practical cases. Before dealing with step 6, all parties involved in the project (client, designer, contractor, and material deliverer) have to agree on an acceptable level of cracking. Industrial concrete floors with a crack-free guarantee require expensive solutions (e.g., posttensioning) and can seldom be motivated regarding real requirements on the floor.

2.2 The Swedish design method

The Swedish design method for industrial SFC floors has been developed during the last 25 years (Skarendahl & Westerberg, 1989, SCA, 1995, SCA, 1997, SCA, 2008). The flexural tensile strength of fibre concrete is based on tests on prismatic fibre concrete specimens. From the beginning tests on slender SFC beams through 4-point bending were used (Figure 1, left). During recent years, this test method has successively been replaced by the European standard test method using 3-point bending on a notched less slender (fat) beam (Figure 1, right). The advantages and disadvantages with the two test methods have been discussed by Silfwerbrand (2008). The design value of the flexural tensile strength of SFC is determined through characteristic values divided by the partial safety factor for SFC.

The flexural moment capacity is determined taking the cross section height and the design value of the flexural tensile strength of SFC into account. In cases with additional conventional reinforcement, a contribution from the steel is superposed to the capacity (SCA, 2008). The design flexural moments are determined using the yield-line theory and the failure modes shown in Figure 2. The design criterion implies that the flexural moment capacity exceeds the design flexural moment. Finally, steps 5 and 6 in Section 2.1 are checked but they are omitted here due to limited space.

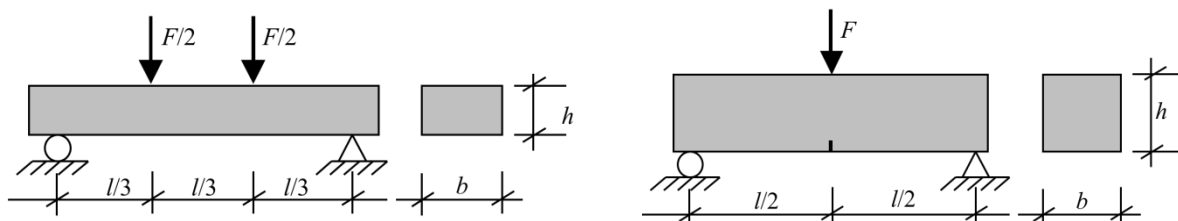


Figure 1 – The old Swedish test method (SCA, 1997) and the new European test method SS-EN 14651 (2005) for determining flexural strength of SFC.

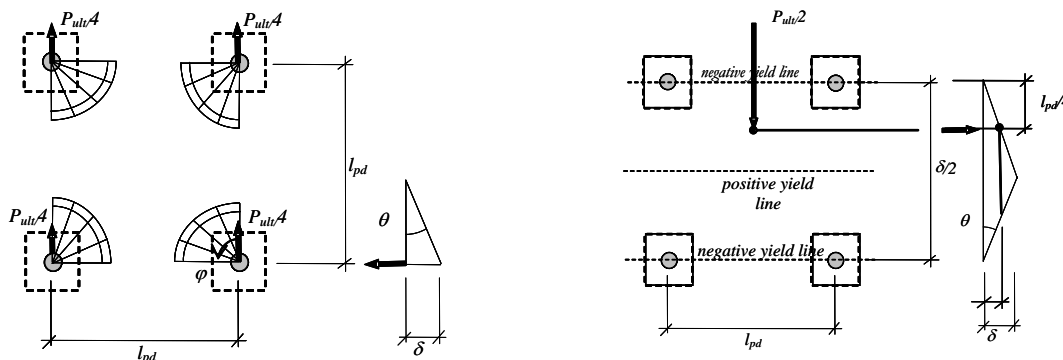


Figure 2 – Two different flexural failure modes for pile-supported slabs (SCA, 2008). In the Belgian design method, the negative yield lines are running at the periphery of the pile heads on the side that is closest to each other.

2.3 The Belgian design method

The Belgian design method for industrial SFC floors (Destrée, 2010) has both similarities and differences with the Swedish design method. The most important differences are the following ones:

1. The flexural tensile strength is not based on prismatic beams but on round slabs.
2. The design values of the strength are determined using German guidelines (DafStb, 2005).
3. The failure mode is based on an assumption that the yield lines coincide with the periphery of the pile heads and not the centre of the pile (cf. Figure 2). This leads either to a shorter lever arm and, thus, a reduced design flexural moment, or a smaller loaded area and, thus, a reduced design load.

3. ESTIMATION OF SAFETY LEVELS IN INDUSTRIAL SFC FLOORS

In general, safety against failure is given by the following equation:

$$\frac{R/\gamma_R}{F \cdot \gamma_F} \geq 1 \quad (1)$$

where, R = resistance or capacity, F = load, γ_R = partial safety factor for resistance, and γ_F = partial safety factor for load. The total safety level R/F can be determined as the product $\gamma_R \gamma_F$. Both factors can in turn be expressed as a product of factors regarding, e.g., geometry and calculation method.

In Table 1, a crude comparison between the Swedish and the Belgian design method for pile-supported industrial SFC floors regarding safety levels is shown. Please, note that the estimation of the various factors is very approximate. We know that the Belgian yield-line pattern used for estimating the design moment is less conservative than the Swedish one, but the values in the table are just estimations. A similar reasoning can be made on the other factors. Very little research has been devoted to the beneficial membrane and arch effect. However, we know that the arch effect increases with increasing ratio between thickness and pile spacing and since the Swedish method will lead to thicker slabs this condition will make the arch effect more pronounced in the Swedish design.

Table 1 – Estimated partial coefficients for two different design methods.

| Category {1} | Item {2} | Symbol {3} | Swedish design method {4} | Belgian design method {5} | {4}{5} |
|---------------------|---------------------------------------|----------------------|---------------------------|---------------------------|--------|
| Load side | Load | a | 1.5* | 1.5* | 1.0 |
| | Design moment | b | 1.3 | 1.0 | 1.3 |
| | Calculation method | c | 1.1 | 1.1 | 1.0 |
| Resistance side | Flexural tensile strength (from test) | A | 1.5 | 1.1 | 1.36 |
| | Design strength value | B | 1.5* | 1.5* | 1.0 |
| | Moment capacity | C | 1.3 | 1.0 | 1.3 |
| | Calculation method | D | 1.1 | 1.1 | 1.0 |
| Neglected phenomena | Safety margin due to arch effect | α | 1.7 | 1.5 | 1.13 |
| | Safety margin due to membrane effect | β | 1.1 | 1.1 | 1.0 |
| Overall | Total safety | $abcABCD\alpha\beta$ | 12.9 | 4.9 | 2.6 |

Note. * This value is given in the design method and, thus, not estimated.

The total safety factors may be considered as very high, but they are neither exceptionally high, nor unnecessarily high. We know that material testing of SFC leads to high scatter. Furthermore, there are often additional scatters regarding slab thickness and fibre content at site. Last, but not least, the yield-line theory that is used in design is hardly an exact description of the real failure mode. If scatters on strength, loads, and geometry all contribute in an unbeneficial way, a high total safety factor is needed.

4. CONCLUDING REMARKS

The design of industrial concrete floors does not follow the same rigorous procedures as the design of elevated concrete slabs. For pile-supported SFC slabs, there are at least two competing design methods that give considerably different solutions for the same conditions and prerequisite. In this paper, the author has tried to quantify this difference in terms of a total safety factor. The Swedish design method is substantially more conservative than the Belgian one but we do not know if the Swedish method is too conservative or the Belgian one is too uncertain. It is possible that beneficial effects (e.g., arch and membrane effects) that are neglected in the current design methods could counterbalance the rather venturesome assumptions that are made in the Belgian design method.

REFERENCES

- DAfStb, 2005,
 “Richtlinie Stahlfaserbeton”. (“Guidelines on Steel Fibre Concrete”). Deutschen Ausschuss für Stahlbeton, Berlin, Germany. (In German).
- Destrée, X., 2010,
 “Steel Fibre Reinforced Concrete in Free Suspended-Elevated Slabs”. Paper No. 12 in ACI SP 268 “Fiber Reinforced Concrete in Practice”. American Concrete Institute, Farmington Hills, MI, USA.
- Destrée, X., & Silfwerbrand, J., 2012,
 “Steel Fibre Reinforced Concrete in Free Suspended Slabs: Case Study of the Swedbank Arena in Stockholm”. Proceedings, fib Symposium on “Concrete Structures for Sustainable Community”, Stockholm, Sweden, June 11-14, 2012, pp. 97-100.
- Silfwerbrand, J., 2008,
 ”Codes for SFRC Structures – A Swedish Proposal”. Proceedings, fib Symposium “Taylor Made Concrete Structures”, Amsterdam, The Netherlands, May 19-21, 2008, 6 pp.
- SS-EN 14651:2005, 2005,
 “Test Method for Metallic Fibred Concrete. Measuring the Flexural Tensile Strength (Limit of Proportionality (LOP), Residual)”. Swedish Standards Institute, Stockholm, Sweden, 28 pp.
- Swedish Concrete Association, 1995,
 ”Stålfiberbetong – Rekommendationer för konstruktion utförande och provning” (“Steel Fibre Concrete – Recommendations for Design, Construction, and Control”). Concrete report No. 4, 1st Edition, Stockholm, Sweden. 132 pp. (In Swedish).
- Swedish Concrete Association, 1997,
 ”Stålfiberbetong – Rekommendationer för konstruktion utförande och provning” (“Steel Fibre Concrete – Recommendations for Design, Construction, and Control”). Concrete report No. 4, 2nd Edition, Stockholm, Sweden. 135 pp. (In Swedish).
- Swedish Concrete Association, 2008,
 ”Industrigolv – Rekommendationer för projektering, materialval, produktion och underhåll” (“Industrial Floors – Recommendations for Design, Material Selection, Production, and Maintenance”). Concrete report No. 13, Stockholm, Sweden. (In Swedish).

Industrial bridge building- An effective bridge construction process through an integrated design and construction process



Daniel Ekström
PhD Student
Division of Civil and Environmental Engineering
Chalmers University of technology, Sweden
daniel.ekstrom@wspgroup.se



Rasmus Rempling
Assistant Professor
Division of Civil and Environmental Engineering
Chalmers University of technology, Sweden
rasmus.rempling@chalmers.se



Mario Plos
Associate Professor
Division of Civil and Environmental Engineering
Chalmers University of technology, Sweden
mario.plos@chalmers.se

ABSTRACT

This PhD-project aims to develop and industrialise bridge building, in order to achieve a more efficient and sustainable bridge construction process. The advancements of several key areas - materials science and technology, design and analysis methods, production techniques and information and communication technology - have resulted in a vast potential to rationalise the process and renew the designer's role. Initially, the project will define effective bridge construction criteria's by means of interviews and case-studies. The work should result in an integrated design and production process. This project is a collaborative project, involving: Swedish Transport Administration, WSP and Chalmers.

Keywords: Industrial bridge construction, sustainable, efficient process, structural design

1. BACKGROUND

An effective building industry creates possibilities for an increased value for society, i.e. the same or higher quality to a lower price or a higher quality from the same costs as today. Furthermore, an effective building industry should of course not only consider costs; solutions should also be chosen from the view of a sustainable society. The solutions can range from process to details, but the leading character should relate to productivity and innovation. The productivity in the building industry is lagging behind other industries. This is evidenced by increasing costs and lead time (time for planning and execution of a building project). A market driven innovation is lacking because of deficient incentives, insufficient competitiveness and because demands of quality and function are not clearly formulated. The main client in Sweden is the Swedish Transport Administration, which thereby has a unique position that influences the productivity and innovation capacity of the building industry.

Poor productivity and innovation capacity of the building industry leads to misused investments in new bridges. The investments are mainly misused due to non-integrated design and production processes and long lead-time for both planning and execution of projects. In addition to less value for invested money, the ineffectiveness causes disturbance for stakeholders in society.

Productiveness and innovations are clearly related and will never reach a final state. Instead a continuous development of the processes, methods and products of the building market is needed. A development that should incorporate the advancements of other areas such as: materials science and technology, design and analysis methods, production techniques, as well as the rapid development in information and communication technology.

If an effective and sustainable bridge building process was clearly defined, a design process that combines aspects of structural resistance and production can be developed and integrated into the building process. This new design process should include the above mentioned advancements and consider already established innovations.

2. PURPOSE AND AIM

The purpose of this project is to develop and make bridge building more effective where the general requirements not only define an effective and sustainable building process, but also includes an innovative design process that combines aspects from structural and production points of views.

The overall aim is to make the bridge building process more effective by integration of the structural design process and the bridge production process. This will be achieved by fulfilment of the following objectives:

- Derive criteria's that defines an effective and sustainable bridge building process.
- Study the system of communication in the building process where the use of Building Information Modelling (BIM) is especially interesting.
- Study and develop the structural design process to promote technical innovations and information modelling.
- Disseminate the results continuously in order to get feedback from researchers and industry and to generate impact on the Swedish Transport Administration and industry.

3. STATE OF THE ART OF SWEDISH RESEARCH ON EFFECTIVE BRIDGE CONSTRUCTION

In the last decade or two, industrial production has shifted its focus from being generally connected with mass production towards increased customer value through adopting the philosophies of Lean production. Mass production is a concept that never been suited to bridges and this shift in focus has therefore enabled a large amount of industrial concepts to be adopted for industrial bridge construction.

Frequently mentioned techniques and methods that characterize industrial construction are standardisation, modularisation, prefabrication or off-site fabrication, as well as on-site fabrication, pre-assembly, mechanisation, automation and the use of different building systems. Many of these techniques and methods, if not all, can be applied in bridge construction. And of course, the goals to generate products at low cost, to produce higher quality products at the same cost and to reduce the overall construction time while maintaining the quality and environmental requirements are applicable also to industrial bridge construction.

It also can be seen in Swedish literature that the perception of the term industrialized building can vary between different authors. Not seldom, industrialization is mentioned as the solution to the lack of productivity in the construction industry, but still it may not be clear to the industry what the terms of industrialization and industrialized construction actually represents.

Some research argues that industrial development is reached mainly through modernising of traditional construction methods (industrialization) while other argues that it is reached by developing new methods or materials from scratch (industrial construction approach). Of course, there are also those who mean that it is more a question of the distinction between pre-fabrication and construction on-site and its degree of industrialisation, and states that there is no difference between the two mentioned approaches.

There can also be found agreement within the industry. One is that there are a lot of different actors, components and parties involved and that industrial construction clearly are multi-disciplinary. In such a multi-disciplinary environment, information- and communication technology (ICT) plays a key-role to generate the possibility to work efficiently within and in between all the involved disciplines.

Based on the TFV-concept presented by Koskela (2000), which is one comprehensive theory for the construction industry, Harryson (2002) presented three cornerstones of industrial bridge construction which was identified as process development, productivity development and product development, the three P's. Serving as the natural link and generating a continuous circle of development between the three P's is ICT. The rapid progress of development and increased knowledge about the use and strategies about how to implement the use of ICT/BIM into industrial construction, this might be the single most important factor for developing new and successful industrial concepts.

Recent research at Luleå University of Technology presents two strategies that normally are undertaken to minimize the complexity of construction, which are standardization of products and standardization of processes, Larson et al (2013). It is also stated that it have been proved difficult to achieve standardization in both due to the lack of utilising the experiences and innovative ideas from contractors in early stages of design. Some core elements to support standardization and increase the industrialization of infrastructure construction is identified in the article, and also some barriers and its actors which has the power to eliminate them. Many of the core elements which are identified are related to long term actions, such as processes, rather than short term actions, such as projects. Here, integration between design and production is

identified as one of the five largest core elements. Notably, and very interestingly, three out of the five largest perceived barriers is considered to be able to be eliminated by the client's role.

4. SCIENTIFIC APPROACH

To meet the specified objectives, the scientific approach will include: literature review of several related research areas; qualitative studies, such as observing projects of best practice; quantitative studies, such as studying the processes of today; and using case studies for deriving research questions and develop show cases.

5. EXPECTED OUTCOME

The project should result in an innovative bridge building process that:

- decrease the time used for planning and production,
- includes information and communication technologies,
- facilitates a continuous improvement of productiveness, product development and innovation,
- creates incitement for an industrial driven productiveness, product development and innovation,
- and creates incitement for the industry to develop standards and modular thinking of products.

REFERENCES

Harryson, P., (2002)

Industrial Bridge Construction – merging developments of process, productivity and products with technical solutions, Licentiate Thesis, Chalmers

Harryson, P., (2008)

Industrial Bridge Engineering - Structural developments for more efficient bridge construction, PhD-thesis, Chalmers

Koskela, L., (2000)

An exploration towards a production theory and its application to construction. VTT Publications 408, Technical Research Centre of Finland, Espoo

Larsson, J., Eriksson, P-E., Olofsson, T., Simonsson, P., (2013)

Industrialized construction in the Swedish infrastructure sector: core elements and barriers, *Construction Management and Economics*

Olofsson, I. (2010)

Structural engineering potentials and applications for effective industrial bridge construction, Report, Chalmers

Simonsson, P., (2008)

Industrial Bridge Construction with cast in place concrete – New production methods and Lean Construction philosophies, PhD-thesis, Luleå

Full-Scale Test to Failure of a Prestressed Concrete Bridge in Kiruna



Niklas Bagge¹
PhD Student



Thomas Blanksvärd¹
Ass. Professor



Gabriel Sas¹
Ass. Professor



Lars Bernspång¹
Ass. Professor



Björn Täljsten¹
Professor



Anders Carolin²
Bridge Engineer,
PhD



Lennart Elfgren¹
Em. Professor

¹ Luleå University of
Technology
SE-971 87 Luleå
name.name@ltu.se

² Trafikverket
SE-972 42 Luleå
anders.carolin@trafi
kverket.se

ABSTRACT

To calibrate methods for condition assessment of prestressed concrete (PC) bridges, tests are planned for a 50 year old five-span bridge with a length of 121 m in Kiruna in northern Sweden. Both non-destructive and destructive full-scale tests will be performed. This paper summarises the test programme, which comprises evaluation of the structural behaviour of the bridge, the residual forces in the prestressed steel, methods for strengthening using carbon fibre reinforced polymers (CFRP) and the shear resistance of the bridge slab.

Key words: Assessment, Pre-stress, Shear Resistance, Strengthening, Fibres, Reinforcement, Repair, Structural Design, Testing.

1. INTRODUCTION

Our bridge stock is growing at the same time as it is getting older. In order to enable optimal management methods, it becomes increasingly important to develop reliable models for condition assessment. There is a lack of knowledge about the structural behaviour, formation of cracks and the actual load-carrying capacity of prestressed concrete (PC) bridges. In this paper a programme for destructive and non-destructive full-scale testing of a PC bridge, the Kiruna Bridge, will be presented. The main tests are planned to be carried out in June 2014.



Figure 1. Photograph of the Kiruna Bridge, view from south (2014-02-19).

2. THE KIRUNA BRIDGE

The Kiruna Bridge, located in Kiruna in northern Sweden, is a 121.5 m long continuous PC beam bridge. It was constructed in 1960 and due to deformation of the ground, caused by mining activities, the owner (LKAB) decided to permanently close it in October 2013.

The bridge consists of five spans with the lengths 18.00, 20.50, 29.35, 27.15 and 26.50 m, see Figure 1-2. The western part (84.2 m) is curved with a radius of 500 m and the eastern part (37.2 m) is straight. Furthermore, the bridge has an inclination of 5.0 % in longitudinal direction and 2.5 % in transverse direction. The cross-section is 15.5 m wide with three longitudinal beams with a height of 1.92 m. The concrete quality was K 300 ($f_{ck} = 21.5$ MPa) in the substructure and K 400 ($f_{ck} = 28.5$ MPa) in the superstructure, and the reinforcing steel was Ks 40 ($f_{yk} = 410$ MPa) and Ks 60 ($f_{yk} = 620$ MPa). The prestressed reinforcing steel system BBRV was used with

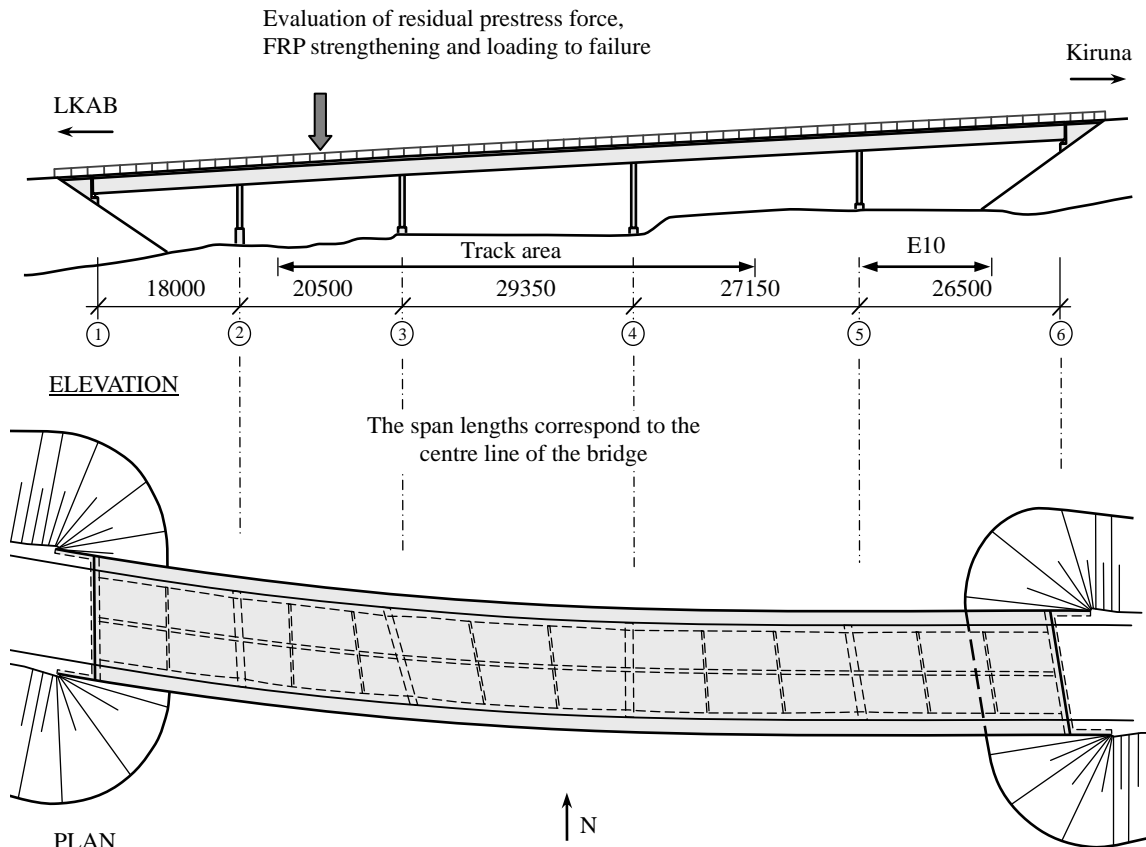


Figure 2. Geometry of the Kiruna Bridge and locations of the experimental study.

the quality denoted St 145/170 ($f_{yk} = 1450 \text{ MPa}$, $f_{uk} = 1700 \text{ MPa}$).

3. TEST PROGRAMME

The European route E10, passing under the span 5-6, will still be in use at the time of testing and therefore the tests will mainly be located in the spans 2-3, see Figure 1-2. The condition and the residual prestressed force will be investigated. Furthermore, two different techniques to increase the flexural moment resistance, using carbon fibre reinforced polymers (CFRP), will be studied in span 2-3 during the loading to failure. Finally, investigation of the shear resistance of the bridge slab is planned to take place.

3.1. Evaluation of residual prestressed force

In order to evaluate the residual force in the prestressed steel, non-destructive testing can be utilised. Measuring the evolution of strains on the bottom surface of the longitudinal beams, when isolating a concrete block by gradually saw cutting on each side of the strain gauge, the actual prestressed force can be determined (Kukay et al., 2010). Based on the load, the cross-section properties and the measured strain, when the saw cut no longer influences the concrete strain, the prestressed force can be calculated.

The cracking moment test (Osborn et al., 2012) will be utilised for calibration of the non-destructive testing. The bridge will be loaded until formation of cracks, the cracks will be marked and then the bridge will be unloaded. Crack opening displacement (COD) gages will be attached across the cracks and the bridge will be reloaded. The strain corresponding to reopening of the cracks will be used to determine the prestressed force.

3.2. CFRP strengthening and loading to failure of bridge beams

The bridge will be strengthened by two methods: (1) prestressed CFRP laminates applied to the northern and southern longitudinal beams and (2) near surface mounted (NSM) CFRP bars applied to the central longitudinal beam, see Figure 3.

The objective of the strengthening is to increase the flexural moment resistance, with the intention to obtain a shear related failure of the bridge. As it is a lack of knowledge about the behaviour at combined flexural and shear failure, especially for full-scale structures, the results from the testing programme are of importance for calibration of models for assessment of the

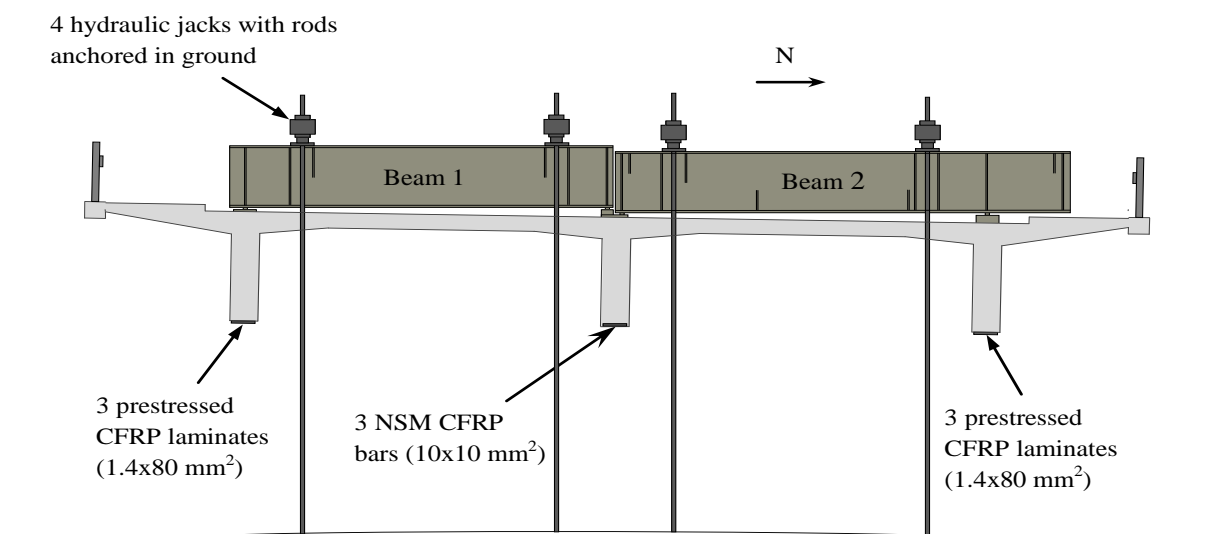


Figure 3. Arrangement for test of the load-carrying capacity in span 2-3 of the Kiruna Bridge.

shear force resistance, where the theoretical background appreciably differ between some of the most commonly used codes. Moreover, the testing in span 2-3 is aimed for investigation of the robustness of the structure and its ductility.

3.3. Shear capacity of bridge slab

In order to provide additional data for calibration of models for the shear resistance, the concrete slab is planned to be tested in span 2-3, after the testing procedure described in in previous section. The load will be applied approximately 800 from the centre of the northern longitudinal beam, using the hydraulic jack and rods anchored in the ground as illustrated in Figure 3. The test-setup will be based on the Load Model 2, LM2, in the Eurocode (CEN, 2003), specified by two load plates with the distance of 2.0 m between their centres and the dimensions 350 and 600 in the longitudinal and transversal direction, respectively. In contrast to the description in Eurocode, the arrangement will be placed perpendicular to the longitudinal axis of the bridge.

It is not uncommon that stirrups are required in bridge slabs according to the Eurocode. We will try to study how necessary this is from a structural point of view.

ACKNOWLEDGEMENT

The authors gratefully acknowledge financial support from Trafikverket/BBT, LKAB/HLRC, SBUF and Luleå University of Technology (LTU). They also thank their colleagues in the Swedish Universities of the Built Environment (LTH, Chalmers and KTH) for fruitful cooperation.

REFERENCES

CEN, 2003,

“Eurocode 1: Actions on structures – Part 2: Traffic loads on bridges”, European Committee for Standardization, Brussels, Belgium, SS-EN 1991-2:2003, 176 pages.

Kukay, B., Barr, P.J., Halling, M.W., Womack, K., 2010,

“Determination of the Residual Prestress Force of In-Service Girders using Non-Destructive Testing”, Structures Congress 2010, Orlando, Florida, USA, May 2010, pp. 709-716.

Osborn, G.P., Barr, P.J., Petty, D.A., Halling, M.W., Brackus, T.R., 2012,

“Redsidual Prestress Forces and Shear Capacity of Salvaged Prestressed Concrete Bridge Girders”, Journal of Bridge Engineering, Vol 17, No. 2, March 2012, pp. 302-309.

Prefabricated elements and structures: Developments, tests and experiences.



Dr. Per Goltermann
 Technical University of Denmark, Building 118,
 DK – 2800 Lyngby
 E-mail: pg@byg.dtu.dk

ABSTRACT

Danish concrete structures are often built with prefabricated elements, joined together on the site and this provides a large challenge to constantly improve and optimize the elements, the joints and the models. DTU Byg has been active in the development, testing and modelling of new elements, joints and models and a number of results and experiences are presented in the paper.

Key words: Reinforcement, prefabricated elements, joints, testing.

1. INTRODUCTION

The design and construction of new buildings, houses and offices in Denmark will often use prefabricated elements, joined together on site to create complete load carrying structures. There is a constant interest in producing less expensive elements, in using fewer of cheaper materials and in developing and documenting easier, faster to implement onsite and more robust joint designs. The joining represents also one of the largest risks of faulty execution, which could endanger the structural safety. The Danish Technical University's Department for Civil Engineering (DTU Byg) has been active in development and documentation of such new element and joint designs in recent years.

The development of deck elements has focused on superlight SL-deck element /Hertz, Castberg and Christensen, 2014/, /Hertz, 2013/, /Christensen and Hertz, 2012/, which resulted in the spin-off company Abeo, where production has already begun, however, there has also been substantial activities in design of wall elements and in design of joints between walls.

2. PREFABRICATED WALL ELEMENTS

Prefabricated walls are reinforced, but there are some discussions about the amount of reinforcement required: Should walls be normally reinforced for bending or should they just contain the necessary amount of reinforcement to transfer loads and provide a fair distribution of cracks. Many Danish producers prefer the concept of lightly reinforced walls, where load-carrying capacity for eccentric, vertical loads in combination with wind loads is ensured by the concrete's tensile strength as described by EN 1520. Reinforcement is in such designs only used for distributing shrinkage cracks and ensuring safety during transport and erection and will often consist of a reinforcement mesh of $\phi 4\text{mm}/250\text{mm}$ (often of class A according to EC2) in the middle of the cross-section. This may be combined with additional reinforcement of class A or B around windows and doors, just as some sections as e.g. integrated beams over windows or doors may require more reinforcement.

It would, however, be a significant benefit if such lightly reinforced walls could have some of the same advantages as more heavily reinforced walls have, e.g. a possibility for using yield line theory for evaluating the capacities against transverse loads.

Three teams of project students /Franck and Odgaard, 2012/, /Bresemann and Odgaard, 2012/, /Sadiki and Reenberg, 2013/ at DTU Byg have therefore tested and evaluated lightly reinforced walls, exposed to transverse loads. The test walls (30 in total) were all 2,6 m x 4,0 m, with a thickness of 100 mm and were produced by EXPAN. The test setup at DTU Byg (Figure 1), supported the wall on all four sides and loaded it from behind by airbags.

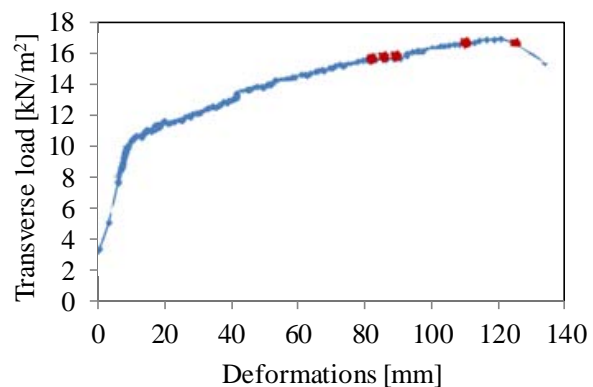


Figure 1 – Marking cracks in a tested wall element J and the load-displacement curve. Red starts indicate rupture of reinforcement /Sadiki and Reenberg, 2013/, /Youtube, 2013/.

The tested element designs covered lightly reinforced, lightly reinforced with additional, more concentrated reinforcement in specific zones (around the windows) and normally reinforced walls. It was found that yield lines develop in all cases, but that reinforcement tended to rupture before the peak load is reached (Figure 1), especially in the cases using class A steel or very low reinforcement amounts. This makes the use of the yield line theory dubious in such cases. Distributed reinforcement (mesh) and additional reinforcement in zones could, however, be combined in the estimation of load carrying capacity. Predictions from the yield line theory were lower than corresponding experimental capacities, probably due to the effect of large displacements. Large displacements increase load-carrying capacities to an extent, difficult to estimate by simple methods, but should be possible by numerical methods.

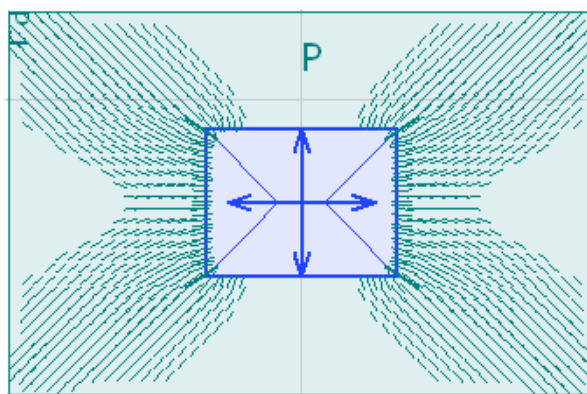


Figure 2 – Simulation of crack pattern in element J with Strusoft /Sadiki and Reenberg, 2013/.

Initial attempts to carry out such a numerical simulation with potential cracks and potentially large deflections have been made with the commercial program StruSoft. This was found to give a fairly good prediction of crack patterns (Figure 2) and deflections at moderate loads. The program could, however, not take yielding of the reinforcement into account and was therefore unable to predict the full load carrying capacities. Estimating behaviour and capacity of a partly cracked wall with transverse loading and yielding in some of the reinforcement is still very difficult even with more advanced and complicated models and programs as Abaqus /Mehlsen, 2011/ and has not been achieved yet in a reliable manner.

3. JOINTS BETWEEN PREFABRICATED WALL ELEMENTS

The traditional joint design between prefabricated concrete walls consists of U-shaped stirrups reaching out from the two elements into the joint, where a vertical reinforcement bar is inserted to tie the two rows of U-shaped stirrups together before the concrete or mortar is cast in the joint. This activity is time consuming and may involve rough on-site bending or straighten of the U-stirrups (against the rules) and makes joint quality and strength major sources of uncertainty for the final structure safety. Easy to use joint designs may be a solution to these problems

Danish producers (EXPAN and The Danish Element producers association BEF) and universities (DTU Byg and ASE) have therefore been active in developing, testing and modelling a number of alternative joints in recent years. Alternative joint designs may involve inserts, SE-joints, wireboxes and other approaches. Testing is required in this situation necessary, first as a screening of the joints eventual suitability and later as documentation for performance.

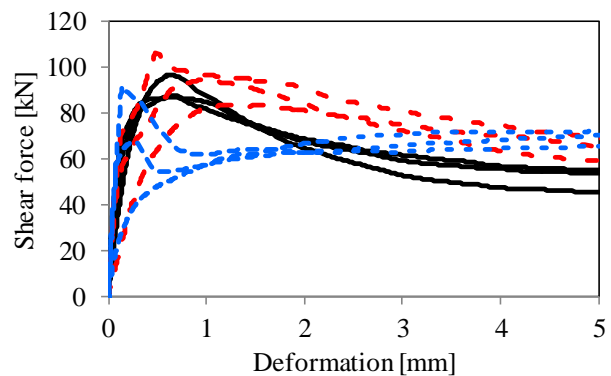


Figure 3 – Test bench (left) with test specimen and load-deformation relation for three different joint designs (U-stirrups and alternatives in a smooth joint) /Nielsen and Nordkvist, 2014/

A number of student projects /Andersen and Poulsen, 2002/, /Frederiksen and Madsen, 2011/, /Nielsen and Nordkvist, 2013/ /Christensen and Pedersen, 2014/ have focused on these problems, resulting in a large number of tests (113 large tests plus the material tests until now). The standard test element is app. 2,08m x 0,8-0,9m x 0,15m and shaped as two L-shaped standard parts, so the main difference between two different test series will be a) the surface in joints (toothed, partly toothed or smooth) or b) how elements are actually joined (glue, mortar or concrete and U-stirrups, SE-joints or wireboxes or something different). The test bench with a test element is shown in Figure 3. The tests have identified some good and some poor joint designs and form a good basis for further developments.

4. CONCLUSIONS.

The use of lightly reinforced wall elements is safe and the capacity against transverse loads is quite sufficient to withstand the wind loads. It may seem safe to use yield line method, if one only compares estimated capacities to experimental capacities, but when the reinforcement ruptures before the peak load is reached, then it is doubtful to use that method.

The new and old designs of joints provide an added and valuable insight into the behavior of joints. This will undoubtedly lead to additional testing and further develop of new joint types.

REFERENCES

- Andersen, H.B. and Poulsen, D.G., 2002
 “Liner anvendt i præfabrikerede betonelementer, Hovedrapport og forsøgsrapport (Lines used in prefabricated concrete elements, Main report and test report)”, DTU, December 2010.
- Bresemann, P. and Odgaard, R., 2012
 “Tværbelastede betonplader- brudlinjer i svagt armerede plader (Transversely loaded concrete slabs – yield lines in lightly reinforced slabs)”, DTU, January 2012
- Christensen, C.O. and Pedersen, A.V., 2014
 “Nye samlinger i betonelementbyggeri (New joint in precast concrete constructions)”, DTU, to be handed in in June 2014.
- Christensen, J. and Hertz, K,D, 2012
 “Super-Light Prefabricated Deck Element Integrated in Traditional Concrete Prefabricated Element Construction”, IASS Annual Symposium., Seoul, 2012
- Franck, O.E.G. and Flesborg, E., 2010
 “Tværbelastede betonplader - Deformationer og bæreevner (Transversely loaded concrete slabs – Deformations and loadcarrying capacities)”, DTU, December 2010
- Frederiksen, M.S. and Madsen, K., 2011
 “Elementsamlinger med wirebokse (Element joints with wireboxes)”, ASE, July 2011.
- Hertz, K., 2011
 “Super-light concrete with pearl-chains”, Magazine of Concrete Research, pp.655-662, October, 2009,
- Hertz, K.; Castberg, A. and Christensen, J., 2014
 “Super-light concrete decks for building floor slabs”, Structural Concrete, 2014.
- Mehlsen, H., 2011
 “Analyse af armerede betonplader ved brug af et pseudomateriale (Analysis of reinforced concrete slabs by use of a pseudomaterial)”, DTU, February 2011
- Nielsen, R. S. and Nordkvist, R.T., 2014
 “Styrker af elementsamlinger (Strength of element joints)”, DTU, February 2014.
- Sadiki, M. and Reenberg, A.M., 2013
 “Tværbelastede vægelementer (Transversely loaded wall elements)”, DTU, February 2013
- Youtube, 2013
http://www.youtube.com/watch?feature=player_detailpage&list=PL4E15BC544A7D8478&v=b7kliTrKYNg

Experiment on Concrete Beams without Shear Reinforcement



Eyþór Rafn Þórhallsson
Associate Professor.
Dept. of Civil Engineering,
Reykjavik University,
Menntavegi 1,
101 Reykjavik, Iceland



Sigurður Rúnar Birgisson
Research Assistant.
Dept. of Civil Engineering,
Reykjavik University,
Menntavegi 1, 101 Reykjavik, Iceland

ABSTRACT

In this paper testing of eighteen reinforced concrete beams without shear reinforcement is compared to three building codes; American Concrete Institution Building Code Requirements for Structural Concrete (ACI), European Standard Eurocode 2 and Model Code 2010. The findings were that the three codes gave different estimates for shear resistance. EC2 and Model Code calculated shear design value lower than the value when the first shear crack appeared. In all instances the ACI code gives the lowest estimate of the shear resistance and is thus well on the safe side. The new shear approximations in Model Code give 5% to 20% lower values than calculated according to EC2.

Keywords: Shear resistance, Experiment, a/d ratio, Reinforced concrete beams, Design code formulas.

1. INTRODUCTION

Concrete beams nowadays are reinforced both with and without shear reinforcement. If concrete beams are equipped with shear reinforcement (or stirrups as they are called), the beams can resist considerably higher shear forces than without stirrups. In most cases the beam members have a flexural reinforcement that is placed in the tensile zone of the beams to resist flexural moment.

Shear failure in concrete structures are very hazardous since they can rarely be predicted and often happen explosively. Tests have been carried out for decades to study this phenomenon and these studies have led to the rules used nowadays to estimate the shear resistance of concrete beams. The behaviour of RC structures is still however still partly unsolved with calculations made to estimate shear strength mainly being based on empirical equations.

Form of shear failure is different between members depending on several factors such as quantity of longitudinal reinforcement, geometry and load configuration. The shear span/effective depth ratio (a/d ratio) defined in Figure 1 is however one of the most significant factor influencing the behaviour of shear failure since it controls the slenderness of the member.

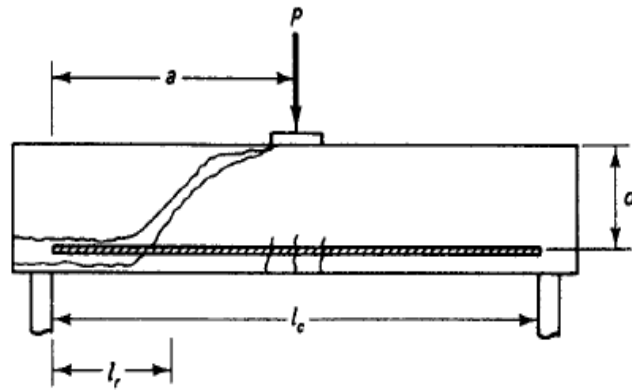


Figure 1 – Diagonal tension failure of concrete beam, cracking development (Nawy, 2009).

Nawy stated that “Fundamentally, three modes of failure or their combination occur: flexural failure, diagonal tension failure, and shear compression failure (web shear)”. This research contributes to knowledge of diagonal tension failure as shown in Figure 1. This type of failure occurs when the diagonal tensile strength is lower than flexural strength of a beam. First, vertical flexural cracks starts to develop at midspan which is followed by bonding failure between the reinforcing steel and surrounding concrete at the support. In continuation of that, diagonal cracks start to develop between loading and support points. As the cracks stabilize, they widen into principal diagonal tension cracks which extend to the top of the beam. This type of failure usually causes only relatively small deflection at failure and the shear span/effective depth ratio varies from 2.5 to 5.5 for beams suffering from concentrated loading (Nawy, 2009).

The purpose of the experiment was to compare the results to four building codes; American Concrete Institution Building Code Requirements for Structural Concrete (ACI 318-08, 2007), European Standard Eurocode 2 (EN 1992-1-1, 2004), European pre-Standard Eurocode 2 (ENV 1992-1-1, 1991) and the new Fib Model Code 2010 (Fib, 2012) to see which of these codes give the best prediction to the shear resistance test performed.

2. RESEARCH AND RESULTS

Six series of concrete beams were cast, three of each series (A, B and C), a total of 18 beams specimen. The beams were only equipped with longitudinal flexural reinforcement, not stirrups.

Two variables were in the research, different height of beams (105, 131, 164, 189, 236 and 335 mm) and different longitudinal reinforcement ratio, that is the relative cross section area of the longitudinal reinforcement (A_s) against the effective concrete cross section ($b_w \cdot d$) (1.55, 1.48, 1.41, 1.39, 1.35 and 1.31 %).

The length and height was the same for all beams, 1.25m and 0.25m respectively. Concrete type was C25/30 with measured compression strength 31.4 MPa.

The flexural reinforcement was bent up at the ends for internal anchoring to prevent slipping of the bars in the concrete. For support there were 80mm steel rolls and 50mm rolls were used under the steel beam. The load was manually controlled and increased little by little until shear failure was reached. Computer equipment continuously monitored and recorded the load and the deflection for the middle of the concrete beam.

Table 1 - Test results and shear force values from four codes

| Beam type | a/d | 1 st shear crack | V at failure | ENV2 | EC2 | MC 10 | ACI |
|-----------|------|-----------------------------|--------------|-------|-------|-------|------|
| | | KN | KN | KN | KN | KN | KN |
| BS-335 | 1.14 | 86.0 | 168.6 | 145.9 | 116.7 | 110.2 | 54.3 |
| BS-236 | 1.86 | 61.2 | 64.6 | 66.4 | 54.1 | 51.8 | 37.2 |
| BS-189 | 2.39 | 45.6 | 48.5 | 41.8 | 39.8 | 37.1 | 28.8 |
| BS-164 | 2.81 | 39.4 | 47.0 | 34.9 | 34.2 | 30.7 | 24.6 |
| BS-131 | 3.68 | 35.1 | 35.1 | 27.6 | 26.5 | 22.5 | 18.8 |
| BS-105 | 4.81 | 25.8 | 25.9 | 21.8 | 20.5 | 16.3 | 14.3 |

The results are shown in Table 1. Six beams were tested, three beams in each category. The a/d ratios are shown in the second column. In the third column the shear force at first noticed shear crack are shown. In the fourth column shear forces at failure are shown. In the next four columns design calculated shear force are listed. All the values are calculated without safety factors and mean tested compression strength of the concrete is used.

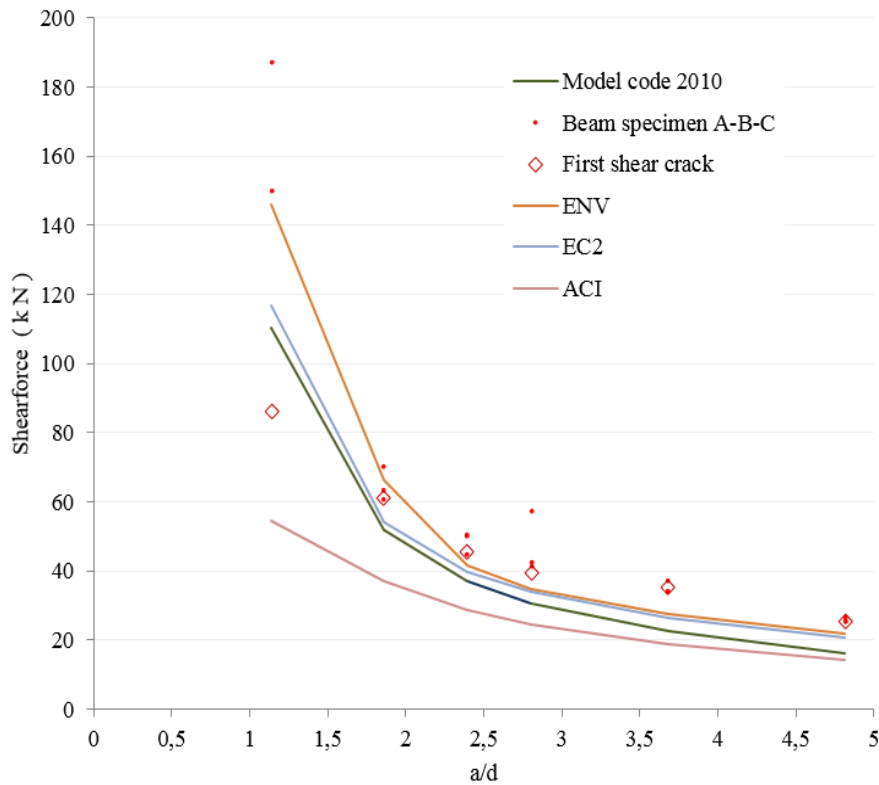


Figure 2 - Shear resistance load estimation of the American Concrete Institution building code, European pre-Standard Eurocode 2, European Standard Eurocode 2 and Model code 2010 with beam specimen failure loads and load at formation of first shear crack.

The ACI code predicted safely the formation of first shear crack and failure of the concrete beam. The EC code and MC 10 predicted failure of all beams. But for the deepest beam type BS-335 both of these codes gave higher shear design values than observed first shear crack in the beam.

Four different shear design formulas are plotted in Figure 2 according to beam properties as well as experimental values at the failure and at first shear crack. Concrete strength is taken as an

average of the cylinder compressive strength test (31.43 MPa). No partial safety factors are used.

The ACI code has the most conservative values and the difference between these four codes becomes much more apparent in deeper beams. The ENV 1992-1-1 code which is outdated now is the most unreliable and fails to predict failure of the deepest beam. EC2 can safely predict failure of the beams but not for the first shear crack. Same can be said for the Model Code prediction.

With a closer look at the ENV, EC and MC10 lines in figure 2, where they begin to rise at $a/d \approx 2$ or lower, the shear strength rises due to additional strength factor. All of these codes allowed for shear increase near support because of strut or arch action when a/d is under 2 but as can be seen on the figure the first observed shear crack for the deepest beam were under these design values. The codes therefore are inefficient to predict the appearance of the first shear crack but continue to predict the failure.

3. CONCLUSION

When the shear resistance is calculated, using the mentioned codes, for the cross section in the experiment, the conclusion is that the ACI code is the most conservative one and estimates the lowest shear resistance of those four codes. The ENV estimates the greatest shear resistance for all beams. It can be mentioned that the ACI code does not take into account the size effect or the effect of the longitudinal reinforcement like the EN, Model Code and ENV. It can be argued whether the ACI code underestimates the shear resistance too much.

Improvements that have been made to the European pre-Standard shear resistance equation have resulted in a more exact estimate of real shear resistance, especially in deeper beams. The new shear approximations in Model Code 2010 give 5% to 20% lower values than calculated according to EC2. It is noticeable that changes that have been made to the shear resistance equation show a better estimation and fit to reality than the predecessor of EN, the ENV code.

It can be said that all four building codes are safe to design with, even though one shear force measurement exceeded the shear resistance estimate for the ENV code if taken into account characteristic concrete strength and safety factors.

REFERENCES

- ACI 318-08. (2007). ACI 318-08: Building Code Requirements for Structural Concrete and Commentary. Farmington Hills: American Concrete Institute.
- EN 1992-1-1. (2004). *Eurocode 2: Design of concrete structures - Part 1-1: General rules and rules for buildings*. Brussels: CEN.
- EN 1992-1-1: General rules and rules for buildings. (2004). Brussels: Comité Européen de Normalisation.
- ENV 1992-1-1. (1991). *Eurocode 2: Design of concrete structures - Part 1: General rules and rules for buildings*. Brussels: CEN.
- Fib. (2012). *Model Code 2010 - Final draft, Volume 2*. Lausanne, Switzerland: The International Federation for Structural Concrete, Bulletin 66.
- Nawy, E. G. (2009). *Prestressed Concrete (5th ed.)*. Upper Saddle River, NJ: Prentice Hall.

AGGREGATES AND ADDITIVES

**RILEM Technical Committee, AAA (2014 – 2019)
Avoiding Alkali Aggregate Reactions in Concrete
Performance Based Concept.**



Prof. Børge Johannes Wigum
Norcem Brevik
Postboks 38
3991 Brevik
NORWAY
E-mail: borge.wigum@norcem.no

ABSTRACT

Development and assessments of test methods, in order to avoid deleterious Alkali Aggregate Reactions (AAR) in concrete, have been the focus of three previous RILEM Technical committees (TC). A fourth TC has recently been established and will during the next five years focus on further development and assessment of; Performance based testing concepts, the relationship between results from laboratory and field and the establishment of exposure sites, and finally the assessment and testing of potential alkalis released from certain types of aggregates.

Key words: Alkali Aggregate Reactions, Durability, Testing, RILEM.

1. INTRODUCTION

1.1 Background of the previous work

The 3rd RILEM¹ Technical Committee (TC 219-ACS)² on Alkali-Aggregate Reactions (AAR) has been active since 2007. The committee terminated its activities early this year (2014). Initial work by the first two RILEM TCs; 191-ARP and its predecessor TC 106, concentrated on the assessment of the alkali-reactivity potential of aggregates. However, in recognition that damaging expansion involves interaction between all the main components of a concrete mix, more recent investigation in the 3rd TC 219-ACS has focused on the evaluation of particular mix combinations, i.e. involving adequate assessment of the effect of the cement/binder. The work in the last committee has been divided into the following activities and sub-committees:

- **AAR-1 Petrographic method**

Further development of the Petrographic method (AAR-1) and development of a Petrographic Atlas.

(Rapid classification of aggregates).

- **AAR-2 Accelerated mortar bar test**

Further development of the Accelerated mortar bar test (AAR-2).

(Rapid classification of aggregates based on alkali exposure).

- **AAR-3 Concrete prism test (38°C)**

Further development of the Concrete prism test (38°C) (AAR-3), with further development of this test as a Performance test.

(“True” testing of aggregates, later in combination with various binders; on-going).

¹ RILEM – International union of laboratories and experts in construction materials, systems and structures

² RILEM Technical Committee TC 219-ACS. Alkali-Aggregate Reactions in Concrete Structures

- **AAR-4.1 Accelerated concrete prism test (60°C)**
Further development of the Accelerated concrete prism test (60°C) (AAR-4), with further development of this test as a Performance test.
- **AAR-5 Screening test for carbonates**
Developing a screening test for alkali carbonate reactive aggregates.
- **AAR-6.1 (Diagnosis & Prognosis)**
Producing a report on Diagnosis and Prognosis.
- **AAR-6.2 (appraisal & repair)**
Producing a report on Appraisal and Repair.
- **AAR-7.1 (ASR specification)**
Producing ASR specification.
- **AAR-8 (releasable alkalis)**
Developing a method for releasable alkalis from aggregates.
- **AAR-9 (modelling of structures)**
Producing a report on modelling of structures.

Many of these developed RILEM methods have been or are intended to be published in the journal; *Materials and Structure*, during this year (2014).

2. THE NEW COMMITTEE

The establishment of a new, 4th Technical Committee on AAR (TC AAA)³ has been accepted by RILEM and has scheduled its first kick-off meeting during autumn this year (2014). The TC will be chaired by Professor Børge Johannes Wigum (*Norcem – HeidelbergCement Group, Norway*), and the secretary will be Dr Jan Lindgård (*SINTEF, Norway*).

The purpose of this new TC is to develop and promote a performance based testing concept for the prevention of deleterious AAR in concrete. Strong emphasis will be put on the implementation of the RILEM methods and recommendations as national- and international standards.

2.1 The Work Packages (WPs)

WP1 - Performance testing and accelerated testing in laboratory.

Avoidance of AAR in future structures is of great importance, and the ways to achieve this will be covered by the work programme proposed by this TC. Development of performance test methods to examine the potential alkali reactivity of particular concrete mixes to be used in a project has already been focused on in the work programme of a previous TC, i.e. TC 219-ACS. In that work programme, it was taken into account the mitigating effect of supplementary materials such as fly ash or slag etc., or the specification of low alkali levels in the mix. By using such mitigation measures, a much wider selection of aggregates can be used safely while increasing the sustainability of the concrete and aggregate industry. Although such draft performance tests have been under preparation, there is still a necessity to finalize and validate these test methods by international inter-laboratory trials and correlate the performance test results with field exposure sites. Performance testing of special types of concrete (e.g. containing lightweight or recycled aggregates, fibres etc) also needs to be studied further. As soon as the necessary validation is finished, it is the intention to publish these methods as RILEM Recommendations. This WP1 will be headed by Dr Terje F. Rønning, (*HeidelbergCement Northern Europe, Norway*).

³ Avoiding alkali aggregate reactions in concrete - Performance based concept.

WP2 - Performance testing and laboratory vs. field; Exposure site.

An important additional tool in validation of the performance testing concept is to make an assessment of the link between the accelerated results from the laboratory and behaviour of these concrete mixtures in real field structures. This will be carried out by compiling the main findings from exposure sites worldwide, preparing an overview of "lab-field correlation" from exposure sites and real concrete structures in services. One main objective is to establish a link between outdoor exposure sites dedicated to AAR investigations and located in different parts of the world, in order to generate an international database on the effect of environmental conditions on the kinetics of AAR. Ultimately, this will allow the development of new specifications for reducing the risk of deleterious expansion and cracking development in concrete structures due to ASR in different environments. This WP2 will be headed by Professor Benoît Fournier (*Université Laval, Québec, Canada*).

WP3 - Performance testing; Assessment of detailed alkali household in concrete, including internal aggregate release, recycling and external supply.

One of the important “missing links” in the international AAR research is how to measure the amount of potential alkalis to be released from various types of aggregates in the laboratory, under accelerated conditions. It is also of important to evaluate the potential alkali recycling which in some instances have been reported. This is of particular importance for massive structures having long-service life, e.g. dams, where the contribution of alkalis from aggregates is believed to produce damaging AAR despite the fact that the concrete has been designed to meet current specifications for avoidance of AAR. Various test methods have already been proposed, and it is the intention in this proposed TC to finalise and validate a test method for alkalis released by aggregates, while compiling results from exposure sites and concrete structures worldwide in order to assess the “true” level of alkali released from various aggregates. As soon as the necessary validation is finished, it is the intention to publish this method as a RILEM Recommendation. This WP3 will be headed by Dr Esperanza Menéndez Méndez (*Institute of Construction Science, “Eduardo Torroja” (CSIC), Spain*).

It is well known that synergistic reactions such as freezing and thawing and delayed ettringite formation (DEF) can exacerbate the effects of AAR and can complicate its diagnosis and management. It is however *not* the intention in this proposed TC to include these issues.

3. PROPOSED TERMS OF REFERENCE

The proposed TC will work for the full 5 years of its allowed life, based upon the nature of the performance tests. Much of the ground work for these performance tests has been carried out by the previous TC 219-ACS, in the form of draft test methods and State-of-the-Art Reports. However, due to the nature of AAR, being a slow reaction, it is necessary to validate these performance test results with exposure site measurements which necessitate the full 5 year term to reach reliable correlations.

The objective of finalizing and validating the performance testing concepts to avoid AAR in future structures will be achieved by organised international inter-laboratory trials and round-robin testing. This will make use of the wide body of expertise available through the participating members and their entities.

The main objective of estimating the alkali release from aggregates is to achieve an assessment of the total (reactive) alkali content in concrete. A proposed RILEM AAR-8 test method is considering different test parameters of measurement. It is necessary to investigate and obtain more experience with a common method that takes into account different parameters like,

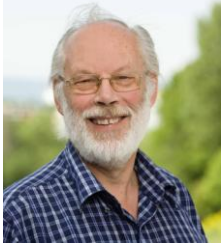
different temperatures, size of aggregate particles, extraction solution, etc. The analysis of different aggregates could give information about the more realistic test method to estimate the potential contribution of alkalis in the field concrete. It is necessary to carry out a round robin test to analyse the possible dispersion of the method and the accuracy of the results. For the round robin test, a period of two years is necessary for the selection of different types of aggregate, test them and analyse the results to extract conclusions. Finally, the validated test methods that reliably estimate the total alkali content of concrete will be published as a RILEM recommendation.

Many of the members will be invited from TC 219-ACS on AAR, though new members are encouraged and will be welcome. The TC is aiming to have a wide international membership which helps to promote the eventual international use of RILEM methods and recommendations. Thus, much communication will be by e-mail and making use of web-site solutions. However, physical meetings will still be the centre of its activities and wherever possible these will be co-ordinated with major relevant international conferences to facilitate attendance. Meetings will also be arranged in locations where laboratories are carrying out performance testing and/or have established outdoor exposure sites. The TC also aims to apply new ways of electronic communication during the meetings, enabling participation of members without physically being at the venue of the meeting.

Influence of Aggregates on Compressive Strength and E-modulus of C45/55 Concrete



Bård M. Pedersen
Senior Principal Engineer, PhD
Norwegian Public Roads Administration
N-0033 OSLO
E-mail:baard.pedersen@vegvesen.no



Reidar Kompen
Senior Principal Engineer, MSc
Norwegian Public Roads Administration
N-0033 OSLO
E-mail:reidar.kompen@vegvesen.no

ABSTRACT

An investigation on the impact of aggregate type on the compressive strength and E-modulus of C45/55 concrete has been carried out. The investigation involved 8 ordinary Norwegian aggregates in combination with CEM II/A-V and CEM I. The results showed, as expected, a very large impact of aggregates on the E-modulus, with differences in measured E_c of 17 GPa at 90 days. More surprisingly, the variation spectre in compressive cube strength was as large as 27 MPa at 28 days, increasing to 44 MPa at 1 year. Both the compressive strength and to an even larger degree the E-modulus are strongly correlated to the Los Angeles value of the aggregates.

Key words: Aggregates, compressive strength, E-modulus, Los Angeles value

1. INTRODUCTION

The most common type of concrete for bridges in Norway is B45 SV-40 according to the NPRA Handbook 026, which means strength class C45/55 and maximum water/binder-ratio of 0.40. Subsequent to the introduction of Norcem Anleggsement FA around 2008 as the new main cement for bridge concrete, increasing numbers of reported problems in achieving the prescribed characteristic strength at 28 days were reported. Even though the new cement type, which is a 42.5 CEM II/A-V with 15-20 % fly ash, has a slower strength gain than the previous Norcem Anleggsement and lower strength potential at 28 days, these problems were not expected. All available laboratory reports had shown that the strength potential of this new cement was sufficient for production of C45/55 based on water/binder ratios in the range from 0.38 - 0.39. Hence, there is an obvious need for stronger focus on aggregates and to what extent the type of aggregate influences the compressive strength.

It is known from previous investigations that the mechanical properties of the aggregate has a major influence on the E-modulus of concrete, but to a much lower degree influences the compressive strength /Smeplass 1992/. /Järvenpää 2001/ has, however, reported that the Los Angeles value of aggregates may have a relatively large impact on the compressive strength of concrete. For bridge concrete in strength class C45/55, the general attitude in Norway has been that the aggregate normally is so much stronger than the cement paste that even the poorest aggregates hardly causes any limitations in achieving the prescribed strength.

The reported investigation, which was initiated based on the reported problems to achieve the prescribed 28 days compressive strength, included in total 8 different combinations of aggregates. The aggregates were mainly chosen from well-known large aggregate resources from different regions of Norway. A working hypothesis was that the mechanical properties of concrete, particularly the E-modulus, may be related to the Los Angeles value of the aggregate. The Los Angeles value tested according to EN 1097-2 test gives a quantification of the resistance to fragmentation, or actually a combination of fragmentation and abrasion resistance.

2. MATERIALS AND MIX DESIGN

1.1 Aggregates

The coarse (8/16 mm) fractions in aggregate combinations 1, 5 and 8 were produced by crushing hard rock of granite, basalt and gabbro, respectively. All 0/8 mm fractions and all 8/16 mm fractions except from aggregate combinations 1, 5 and 8 were produced from glaciofluvial deposits. Detailed technical descriptions including petrography of all the aggregates may be found in the full report by /Pedersen & Kompen 2013/.

1.2 Cements and other materials

Norcem Anleggsegment FA (ANL FA) was chosen as main cement for this investigation. This cement is classified as a CEM II/A-V 42.5 according to EN197-1. In addition, Aalborg Rapid was used in combination with aggregate combinations 5, 6 and 7. This cement is classified as CEM I 52.5 according to EN 197-1.

Other materials utilized were: BASF Glenium 151 super plasticizer and BASF Micro Air air entraining agent. In addition, Elkem compacted silica fume was used in all mixtures.

1.3 Mix design

All concretes were proportioned with a constant volume fraction between cement paste and aggregates of 34.8:65.2 %, and with a constant volume fraction between fine (0/8 mm) and coarse (8/16 mm) aggregates of 53/47 %. The water/binder ratio was 0.39 for all mixes. 4 % silica fume by cement weight was added to all mixes, using an activity factor of 2.0. All concretes were air entrained with a target value of 4-5 % air. The amount of super plasticizer was varied in order to achieve a slump in the range of 150-200 mm.

3. RESULTS AND DISCUSSION

Compressive strength results for all aggregates in combination with ANL FA are shown in Figure 1 (left), while Figure 1 (right) also include results for the combinations with Aalborg Rapid. The maximum variation in compressive strength at 28 days was 27 MPa, increasing to 44 MPa at 1 year, which is surprisingly high. The results shown in Figure 1 (right) shows, as expected, that Aalborg Rapid gives a faster strength gain up to about 28 days, but then flattens out. The ANL FA cement has a slower strength gain due to the much slower chemical reaction of the fly ash. Based on these rather limited results the differences in compressive strength seem to be larger for ANL FA than for Aalborg Rapid.

The variation spectre in E-modulus as can be seen in Figure 2 (left) was more in line with the expectations, with a maximum difference in E_c at 28 days of 15 GPa, increasing to 17 GPa at 90 days. The E-modulus values are relatively stable over time, with only a slight increase with time. As can be seen in Figure 2 (right), the high strength cement Aalborg Rapid gives slightly higher E_c than ANL FA cement, in particular at relatively “early” ages up to 28 and 90 days.

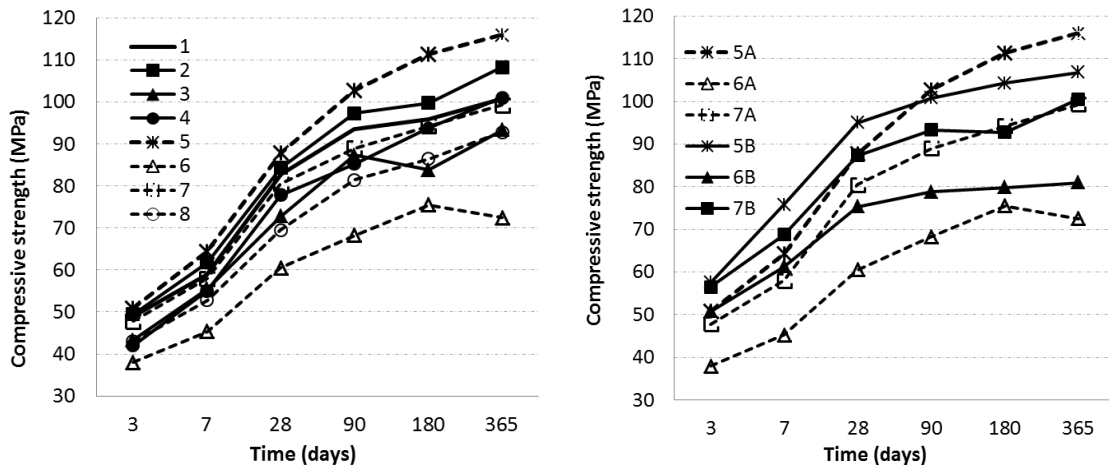


Figure 1 Compressive cube strength vs time. Left: CEM II/A-V (ANL FA) in all concretes. Right: CEM II/A-V (ANL FA) in A-series, CEM I (Aalborg Rapid) in B-series.

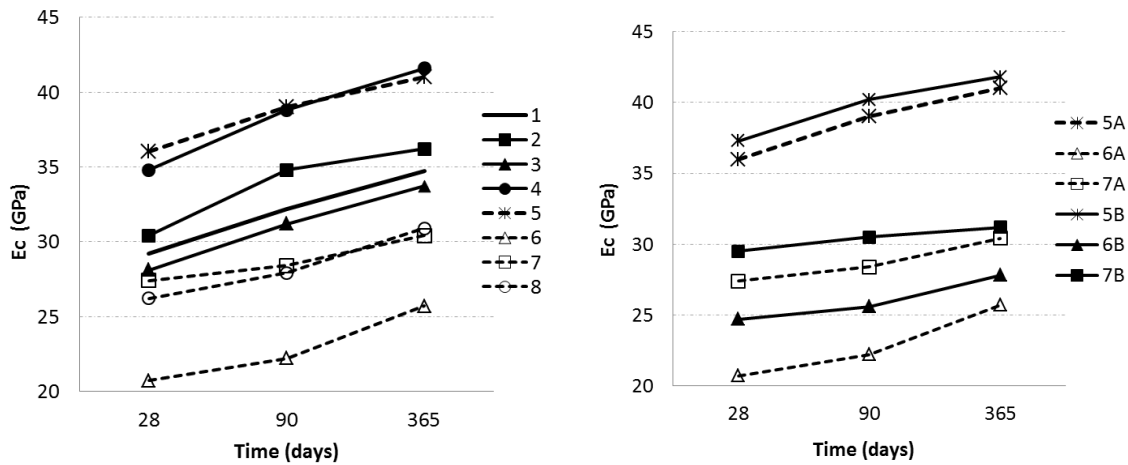


Figure 2 E-modulus vs time. Left: CEM II/A-V (ANL FA) in all concretes. Right: CEM II/A-V (ANL FA) in A-series, CEM I (Aalborg R) in B-series.

The aggregate factors influencing the mechanical properties of concrete are believed to be rather complex and include parameters such as shape and angularity, surface texture, free mica content, surface dust etc. in addition to mechanical strength of the aggregates. However, simple analyses based on the presented results have shown that both the compressive strength and to an even larger extent the E-modulus are strongly related to the mechanical strength of the aggregates expressed by their Los Angeles values. Plots of compressive strength at 28 days vs LA- values and E_c at 28 days vs LA-values are shown in Figure 3, left and right respectively. The LA-values used in the calculations are mean values of fine and coarse aggregate fractions. Based on the presented results, the mechanical properties of the coarse aggregates seem to be only slightly more important than the properties of the fine aggregates. Note that the standard test fraction for the LA-test is 10/14 mm. This means that the values for the coarse fractions represents “measured values”, while the values used for the fine fractions (0/8 mm) are measured on coarser fractions.

The Eurocode 2 “Design of concrete structures EN-192-1-1” gives an equation for calculating the E-modulus based on the compressive strength f_{cm} . Based on our results, this equation

generally seems to overestimate the E_c . Our measured E_c values were in the range from 58 to 92 % of the calculated E_c values.

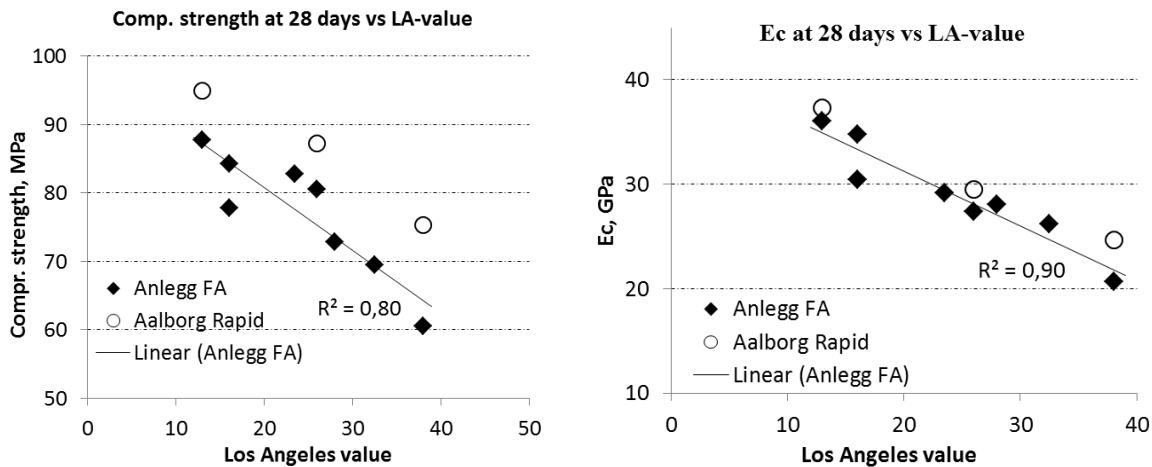


Figure 3 Compressive cube strength at 28 days vs Los Angeles-value (left) and E-modulus at 28 days vs Los Angeles value. Regression lines for the series with Norcem Anlegg FA (CEM II/A-V).

4. CONCLUSIONS AND FURTHER WORK

The study has confirmed the large impact of aggregates on the E-modulus of concrete. The E_c is strongly correlated to the Los Angeles value of the aggregate at all ages. More surprisingly, the study has revealed that even the compressive strength of C45/55 concrete is strongly dependent on the aggregate choice. Also the compressive strength of the concrete is correlated to the Los Angeles value of the aggregate, even though the correlation is not as strong as for E-modulus.

The Norwegian Public Roads Administration has a general requirement of LA₃₅ or better for concrete aggregates. However, this requirement has not been followed up on a regular basis up to now. Further work may show if the Los Angeles value is such a strong quality parameter that it may serve as a criterion to differentiate aggregates for different purposes.

REFERENCES

Järvenpää, H., 2001

“Quality characteristics of fine aggregates and controlling their effects on concrete”, doctoral thesis, Helsinki University of Technology, Finland.

Pedersen, B., Kompen, R., 2013

“Trykkfasthet og E-modul for SV-40 betong. En studie av tilslagets effekt”, Statens vegvesens rapporter nr 177, Oslo 2013.

Smeplass, S., 1992

“Effekt av tilslagstypen på betongens trykkfasthet og E-modul”, Materialutvikling Høyfast betong rapport nr. 5,6. SINTEF-rapport STF70 A92051.

How to evaluate filler from crushed rock aggregates for concrete production



Prof. Dr. Björn Lagerblad,
Senior Researcher Swedish Cement and Concrete Research Institute SE-
10044 Stockholm, Sweden
E-mail: bjorn.lagerblad@cbi.se



Jaume Cirera Riu,
Assistant Researcher, Swedish Cement and Concrete Research Institute. SE-
10044 Stockholm, Sweden
E-mail: jaume.cirerariu@cbi.se



Dr. Hans-Erik Gram,
Senior Researcher, Cementa AB, P.O. Box SE-472 10 Stockholm, Sweden
E-mail: hans-erik.gram@cementa.se

ABSTRACT

In fresh concrete, the filler fraction (0-0.125 mm) is of vital importance for workability. With the use of superplasticizer, it is possible today to use quite large amount of fillers. This has made it possible to make self-compacting concrete and other special concretes.

How to use the fillers and the amount of fillers depends on the size distribution and quality of the filler. Basically, the filler should be round and the distribution of filler and cement should be continuous. The size shall not overlap too much with that of the cement. Fillers from crushed rocks consist of minerals and the filler particles depend on the mineralogy and texture of the rock type. This work treats different methods, including paste rheology, to evaluate the quality of the filler fraction. By using good quality filler, it is possible to reduce the amount of cement in concrete.

Key words; aggregates, mix design, rheology, sustainable

1. INTRODUCTION

The filler is part of the micro mortar (of the concrete) and consists of filler, cement and water. In the fresh micro mortar, cement is also a particle. The particles in the fresh micro mortar should, like the particles in concrete, follow a smooth distribution curve to give a good rheology and workability. Micro fine filler (smaller than cement) can reduce the amount of cement with almost half and still have the same strength of concrete (Lagerblad & Vogt 2005, Vogt 2010). Crushed rocks normally give rather large amounts of filler. Thus the quality of the filler will be of vital interest. In this context we regard filler as all particles that pass the 125 μm sieve. If the quality and size distribution of the filler is good one can save cement in the concrete but if the quality is bad the concrete will have bad workability. Good filler is round/cubic, while bad filler has particles that are flaky or elongated. The filler normally consist of free minerals. Often, bad filler is characterized by free mica sometimes as clay minerals. The basic problem is that it is difficult to analyze the fine particles, especially the ultrafine particles.

The particle distribution can be analyzed by a laser sieve but this method does not reveal the particle shape. The laser sieve assumes that all particles are round. This means that flaky particles appear larger than they are. The laser sieve can, however, be combined with measurements of the specific surface (BET-surface). Most of the BET surface is given by the ultrafine particles. Flaky particles give a larger surface per weight unit than round or cubic particles. Thus ultrafine clays result in a high BET surface. Thus by considering the ratio between amount of ultrafine particles given by the laser sieve and the BET surface one can obtain the shape of the ultrafine particles. A good micro filler and shows large amount of fine filler but shows a low BET-surface.

The larger filler particles can be studied under the microscope. However, particles in sizes less than 63 μm are difficult to analyze in thin sections. It is possible to study the filler particles in a SEM, but this is costly, difficult and time consuming. Easier and a more simple method is needed. Both a laboratory method and a field methods in order to determine quality is needed.

2. TEST METHODS OF FILLER

The task is to evaluate filler and the filler quality for concrete production. The micro mortar is basically a water-particle suspension where cement too is a particle. Basically good filler should give good flow with as little water as possible. For a good workability a concrete shall contain a large amount of micro mortar for workability but at the same time the micro mortar should also contain small amount of cement and water for durability and environmental reasons.

The simplest way to study the filler quality is as a water suspension. There are two methods, the Puntke and flow spread method, described in the literature (Hunger & Brouwers 2009) to measure the flow of filler-water suspensions. The two methods and micro mortar rheology are treated in Cirera (2014)

The outflow method is based on a mini cone. Filler and water are mixed in a mixer. Water is successively added and at a specific amount of water the suspension water saturated and with more water it will flow and spread. When more water is added the spread will increase. The start of the spread is similar to the Puntke value.

The Puntke test measures the amount of water needed for a specific volume of filler to be water saturated. The filler/water mix is shaken or vibrated. In our tests we use a vibrator. When the surface appears smooth and shiny the mix is regarded to be water saturated. Both methods measure the amount of water needed to fill voids and to wet all surfaces. Figure 1 shows a test where different amounts of 0-63 μm and 63-125 μm are tested. Two materials are tested where K104 is a better filler than K101. The results show that more water is need for both ends. For the coarse particles this is probably due to packing. The lack of finer particles gives larger voids Sample K101 contains large amounts of free mica, which is known to give both bad packing and bad rheology (Lagerblad et al 2008). For the finer particles, it is probably due to the larger surface, which need to be wetted. This is probably due to free micas in the clay fraction. When the fine fraction contains free mica it normally does so in all of the fine fractions. Figure 1B shows packing values of 0.125 to 0.250 mm. Void volume of 0.63 to 0.125 and smaller fractions give uncertain values. The packing here can be correlated with both with the amount of free mica and the Puntke value.

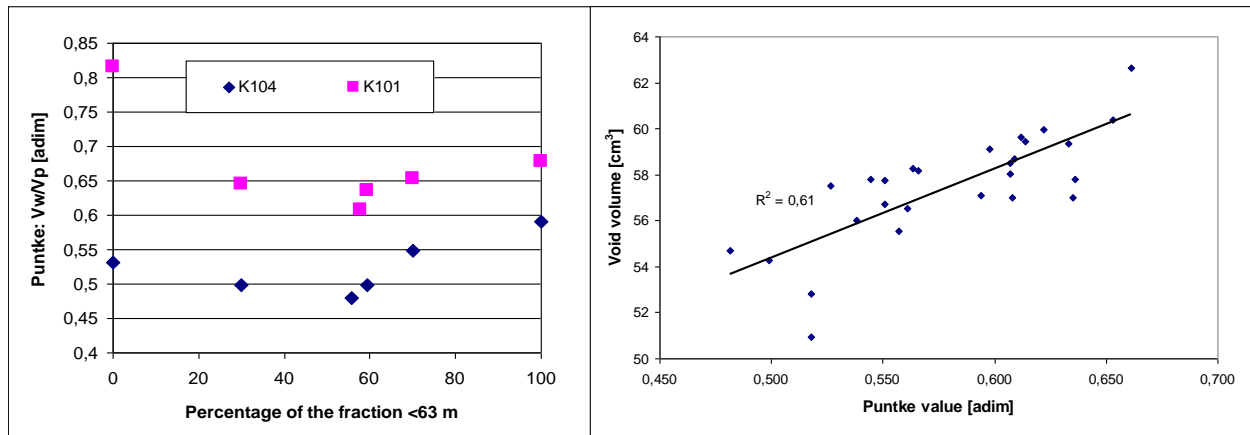


Figure 1. Water saturation according to the Puntke value. A; According to grain size distribution. B; Void volume according to loose packing.

The filler can also be classified in a rheometer (MCR 300, physica). In this case a micro mortar is produced. In Lagerblad et al (2008) a micro mortar with a D_{max} of 0.25 mm was tested. The cement paste consisted of 36.1 vol. % of cement and 63.9 vol. % water. Fine material was successively added with a constant w/c. The results showed that when the amount of filler was more than 15 vol. %, the quality of the fine material was of great importance, both as regard yield stress and plastic viscosity. The amount of free micras and high clay contents indicated by a high BET surface was important.

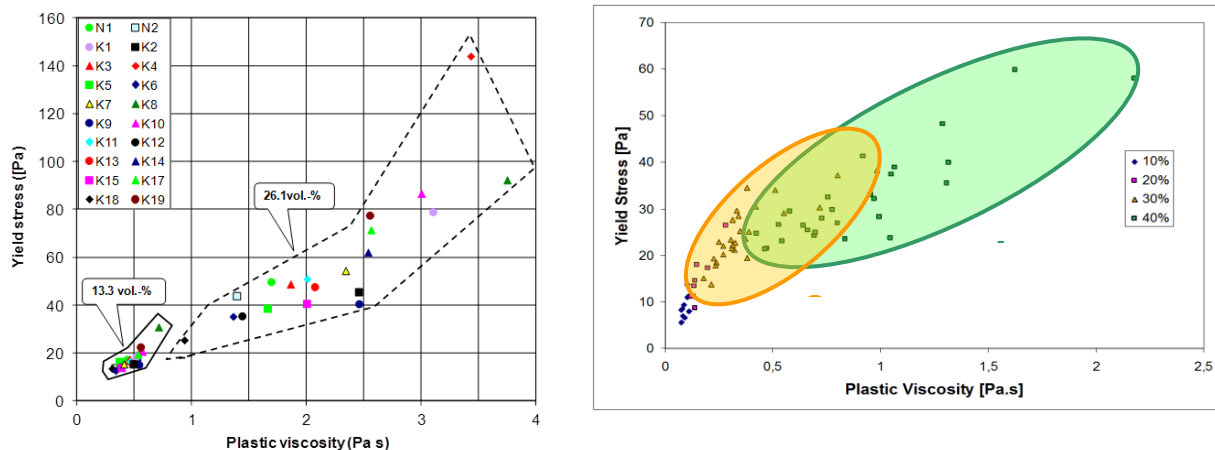


Figure 2. A, Rheological data of micro mortar containing 13.3 and 26.1 volume % of fines < 0.25 mm. From Lagerblad et al 2008. B; Rheological data of micro mortar containing 10, 20, 30, and 40 volume % of filler < 0.125 mm. 60 volume % 0.063-0.125 and 40 volume % < 0.063 mm. From Cirera Riu 2014.

The results show that with less than a certain amount of filler the quality of the filler is of less importance as regard rheology, but with larger amounts it is of vital importance. As the volume of filler and the proportions of 63-125 and < 63 μ m is the same the micro mortar, the 40 % value gives an indication of quality.

Figure 3 shows a comparison between the rheology of the micro mortar and the Puntke value. There is a general correlation. One must however consider that many of the values with a high plastic viscosity have a high BET surface indicating clay minerals. The Puntke is not sensitive to clays. Figure 3 B shows an experiment where additional filler is added to a concrete mix. The filler comes from air sieving of a crushed granite rock with good fines. The mass of the fines are

less than 0.2 mm in size. This shows it is important to find out the quality of the filler and good filler can be used to optimize concrete with a lower cement content. The filler in concrete, however, requires somewhat more superplasticizer and it is more viscous.

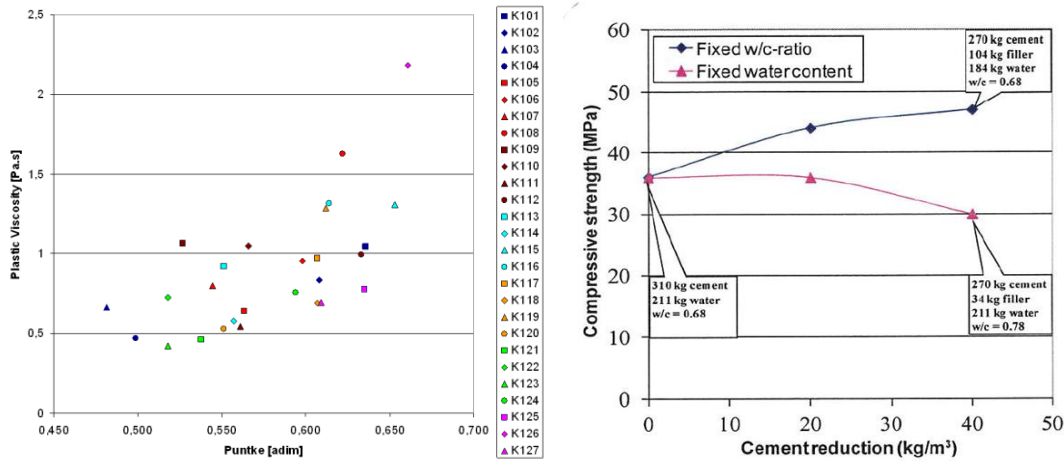


Figure 3. A; Relationship between plastic viscosity (40 volume % filler) and Puntke value. B; Effect on concrete compressive strength and amount of filler. A fixed w/c ration demands increased amounts of superplasticizer.

REFERENCES

Cirera, J. (2014).

Quality of fine materials from crushed rocks in sustainable concrete production. Minor Thesis, UPC BarcelonaTech, Barcelona (Spain).

Hunger, M., Brouwers, H.J.H., (2009)

Flow analysis of water-powder mixtures: application of specific surface area and shape factor, Cement and Concrete Composites 31, s 39-59. 2009

Lagerblad, B., Vogt, C., (2004)

Ultrafine particles to save cement and improve concrete properties, CBI report, 1:2004, 2004

Vogt, C., 2010

Ultrafine particles in concrete-influence of ultrafine particles on concrete properties and applications to concrete mix design, Doctoral Thesis in Concrete Structures, Royal Institute of Technology, TRITA-BKN. Bulletin 103, Stockholm 2010

Particle packing of aggregates for concrete mix design: Models and methods.



Yahya Ghasemi
 PhD-student
 Div. Structural and Construction Engineering, Luleå University of
 Technology
 S-971 87 Luleå
 E-mail: yahya.ghasemi@ltu.se



Tekn Lic, Niklas Johansson
 PhD-student
 Cementa AB
 P.O. Box 104, S-624 22 Slite
 Div. Structural and Construction Engineering, Luleå University of
 Technology
 S-971 87 Luleå
 E-mail: niklas.johansson@cementa.se
 niklas.johansson@ltu.se

ABSTRACT

An optimized aggregate particle packing density- used as a base for concrete mix design- provides economic, environmental and technical advantages. The particle packing density can be determined by many methods and predicted by different models. This paper reviews common packing and procedures and compares predictions of three packing models. It was found that the models tend to show different packing densities and percentage of ingredients at maximum packing for the same mixture. A test setup is proposed to determine the accuracy of each model's prediction.

Keywords: Aggregate, Testing, Mix design, Dry packing

1. INTRODUCTION

The prediction of the packing density for aggregate mixture, together with fine particle (i. e. matrix) modelling, is essential in concrete mix design. It is known that besides particle size distribution, the packing density of the aggregates is influenced by the packing process and also the shape of the grains /Proske & Ramge 2004/. Over the past few decades, several mathematical models have been introduced for the purpose of predicting packing of granular mixes. This study aims to compare three common particle packing models. The models were used on 4 mixtures of aggregate fragments with known aggregate distribution and packing density for each fragment. In addition to that, the paper will briefly review four common dry packing methods and aims to illustrate how the variation in packing process affects the outcome of packing density.

2. PACKING MODELS

2.1. Modified Toufar Model

In this model, the packing density and characteristic diameter of each material are used to calculate the packing densities of particle combinations /Goltermann et al. 1997/. Modified Toufar model can be used for estimating packing of a multicomponent system. However, according to /Fennis 2011/.calculations of multi-component mixtures based on this procedure tends to underestimate the packing density.

2.2. 4C Model

4C is a computer program developed by Danish Technological Institute and is based on the Linear Packing Density Model (LPDM). The factors that are taken into account include particle size distribution of the mixture and packing densities of each size class. The accuracy of the model depends on interaction formulas which are relations derived from the packing density of two-component mixtures /dti.dk; Glavind, et al. 1999/.

2.3. Compressible Packing Model

De Larrard /1999/ introduced the concept of virtual compactness that is defined as the packing that can be obtained by placing the aggregates one by one in a mixture in such a way that the minimum amount of space is left. The actual packing density can be derived from virtual packing density by use of compaction index K. The value of K depends on the compaction energy applied in the process of packing.

3. PACKING METHODS

Several methods exist for packing process; one method is suggested by de Larrard /1999/ using vibration+compaction method. According to vibration+compaction approach, the aggregates should be poured in a cylinder that is closed with a 20 kg steel piston and the whole set should be put on a vibration table and submitted to the following vibration sequences: 2 min,40 s and 1 min at amplitudes 0.4 mm, 0.2 mm and 0.08 mm respectively.

American standard ASTM C29 enforces conducting rodding or jiggling method. Rodding method is defined as filling one third of a cylinder and rodding the layer of aggregate with 25 strokes and continuing with filling the two-thirds and again rodding as above and finally, filling the cylinder to overflowing and rodding again. Jiggling procedure includes filling the container in three approximately equal layers and compacting each layer by placing the measure on a firm base and raising the opposite sides alternately about 50 mm and allowing the measure to drop on the surface blow. Each layer should be compacted by dropping the measure 50 times, 25 times on each side.

Moreover, European standard EN-1097:3 suggests using loose packing by means of pouring the aggregates in a standard cylinder from the distance of maximum 50 mm.

Obviously the selection of the method affects the packing density. Among the packing models compiled for particle packing prediction, compressible packing model (CPM) takes the effect of packing method into account by means of a compaction factor index- K -which was suggested to have the value of 4.1, 4.5, 4.75 and 9 for loose packing, rodding, vibration and vibration+compression respectively. Figure 1 shows the effect of compaction index on packing density of a mixture based on CPM.

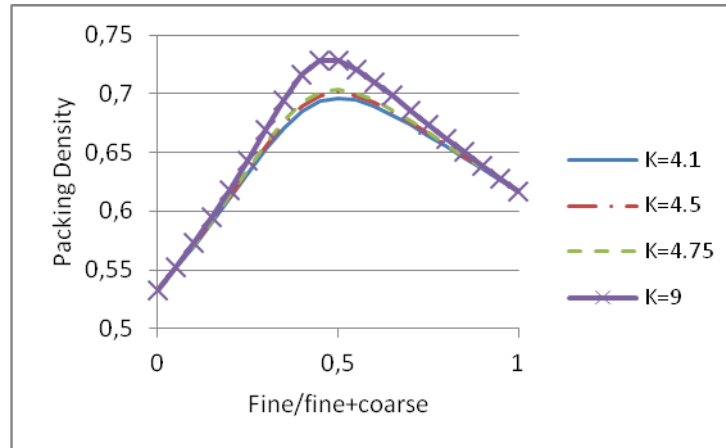


Figure 1: Effect of K value on compaction. Actual packing densities of two classes were measured on loose packing.

4. EXPERIMENTS AT LTU

In order to examine the reliability of the models, a series of tests have been designed. The experiment will include mixing different types and fragments of aggregates to construct binary mixes. The fines will be mixed with coarser aggregates in steps by replacing 10 % of coarse materials by fines in each step. The trend for mixture packing density will be drawn and can be compared to the results obtained from mentioned models. Eventually, models will be calibrated based on the lab results. As a reliable model was found or compiled, the mixtures with higher packing density will be used for making concrete samples with the aim of measuring the workability of mixtures. The experiments will be done on loose packing in a standard cylinder. As a part of the research, effect of packing method on packing density will be studied.

5. THEORETICAL COMPARISON OF THE MODELS

Examples of results for theoretical comparison of models' predictions made so far are presented in Figure 2. Each model suggested a different optimum contribution of the aggregates to the mixture and moreover, the models did not agree on the maximum packing density that can be obtained in the mixtures. 4C and Toufar model tend to almost merge as the finer aggregates became dominant in the mixture. The predicted packing from CPM was significantly different from 4C and Toufar. In the mixtures with crushed aggregate the difference between 4C and CPM was about 3 % while for the mixture of crushed and natural the difference was increased up to 7 %. CPM tends to predict higher packing density than the other two model whereas 4C showed the least packing density.

6. FINAL COMMENTS

As it can be seen in Figure 2, the models led to different proportions of aggregates for the same mixture, also the maximum predicted packing densities were unlike. It is noticeable that the models tend to agree on the packing density as the finer material became dominant in the mixture (above 60% of fine material). However, the maximum packing density of a mixture is usually achieved when fine materials had 40 to 60% share of aggregate mixture, where the models showed the highest deviations from each other. That emphasizes the need of further studies on experimental data in order to calibrate the existing models or compiling a new one.

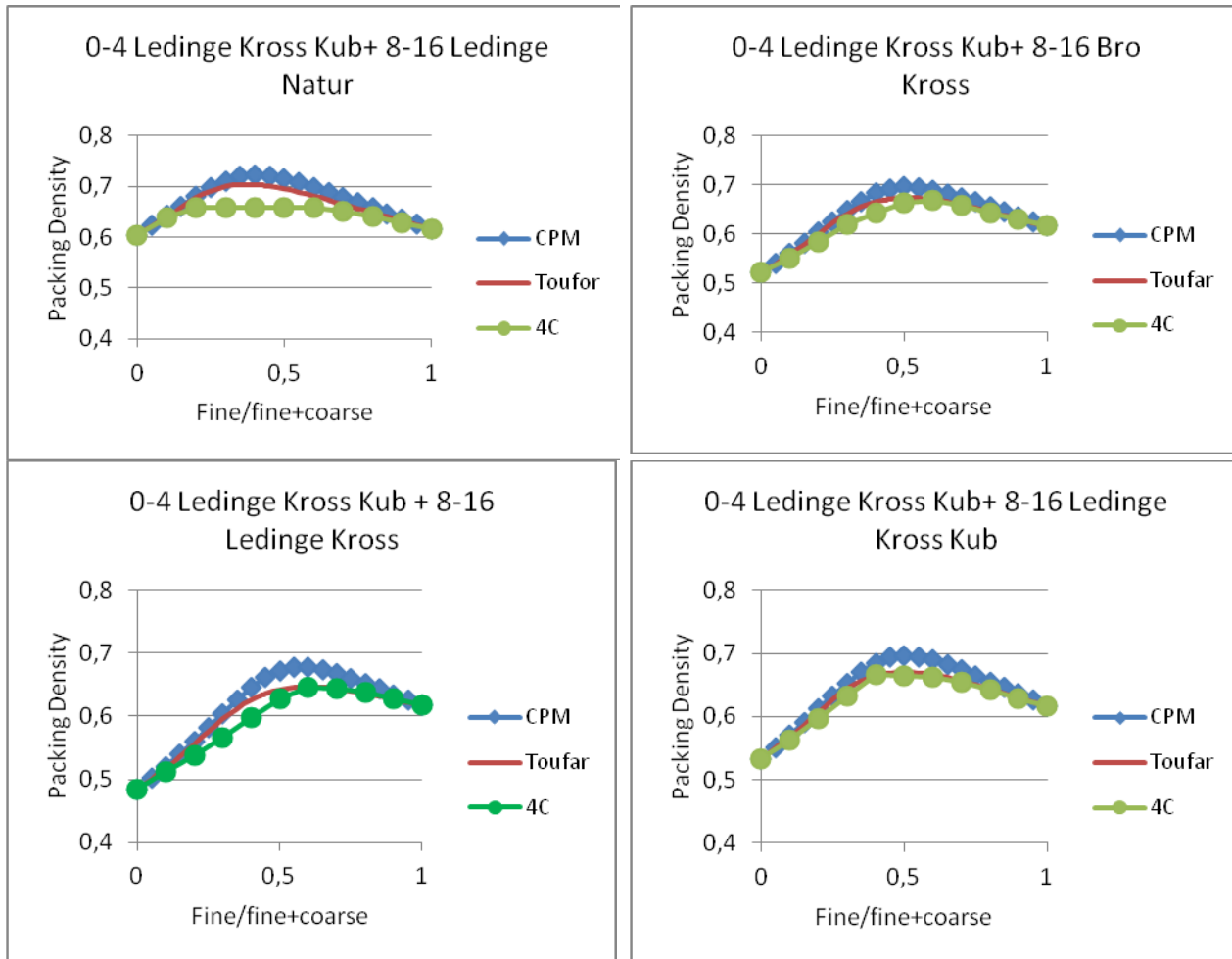


Figure 2: Comparison of packing models for four available aggregate combinations. Actual packing density of fragments were measured in the lab.

REFERENCES

ASTM C 29

“Standard test method for bulk density and voids in aggregates”. ASTM International.

Fennis, S. A. A. M., 2011

“Design of ecological concrete by particle packing optimization” Dissertation, Delft University of Technology.

Glavind, M., Olsen, G.S., Munch Petersen, C., 1999

”Packing calculations and concrete mix design”. Danish Technological Institute

Goltermann, P., Johansen, V., Palbol, L., 1997

“Packing of aggregates: an alternative tool to determine the optimal aggregate mix.” ACI Materials Journal, Vol 94, pp. 435-443

Larrard, F. de., 1999

“Concrete mixture proportioning: a scientific approach.” London: E & FN Spon.

Proske, T., Range, P., 2004

“Influence of the particle shape on the packing density of aggregates.” Darmstadt Concrete – Annual Journal on Concrete and Concrete Structures, 19.

SS-EN 1097-3:1998

“Tests for mechanical and physical properties of aggregates-Part3: Determination of loose bulk density and voids”. SIS..

Crushed fine aggregate for concrete production



Tekn Dr. Hans-Erik Gram
Cementa AB
P.O. Box 472 10, Stockholm
E-mail: hans-erik.gram@cementa.se



Tech. Lic. Mikael Westerholm
Cementa AB
P.O. Box 472 10, Stockholm
E-mail: mikael.westerholm@cementa.se



Prof, Dr. Mats Emborg
Div. Structural and Construction Engineering,
Luleå University of Technology
SE-971 87 Luleå
Betongindustri AB
Box 47312
SE-100 74 Stockholm
E-mail: mats.emborg@ltu.se / mats.emborg@betongindustri.se

ABSTRACT

Fine aggregate from crushed bedrock needs to meet requirements to be suitable for concrete production. Besides chemical requirements, particle shape, grading and mineral composition are crucial if a cost effective concrete with low environmental impact is to be produced. Different methods to evaluate particle shape of fine aggregate are studied, e.g. flow measurements and loose packing. Also the fines and methods to evaluate its suitability are addressed in the paper. The results show that some methods can be used to evaluate the effect of different crushing, e.g. cone crusher vs. vertical shaft impact crushers and different rotor speeds, as well as to estimate if they are suitable for concrete production in terms of workability.

Keywords: Aggregate, Shape, Mix design, Fresh concrete.

1. INTRODUCTION

The main type of fine aggregates (0-8 mm) used in concrete in Sweden is glaciofluvial material from eskers. However, the authorities are restricting their use for environmental reasons and in some regions they are becoming scarce as deposits are empty and the only realistic alternative to natural fine aggregates is crushed rock. The main difference between the two aggregate types is

the particle shape as the crushed particles are flakier and the surface is rougher than the ones of natural aggregates. Another important difference is the particle distribution curve – the crushed rock contains higher or much higher amounts of fine particles, i. e. the fillers.

All these differences imply a more complicated concrete production as the less favourable particle shape and the higher filler content calls for higher water demand in the concrete which in turn also calls for a higher cement content and/or increased use of superplasticisers.

Regarding the crushed rock, the most common production method is cone crushing, which normally produces good coarse aggregates but the smaller the aggregate size, the less favourable is the particle shape. The alternative, the VSI-crushers, are able to produce better particle shapes and this is true for sizes down to the size where the aggregate becomes a single mineral.

Thus, in the research, it is of interest to evaluate the rock crushing methods with regard to fresh concrete performance and also to evaluate methods of documenting the particle features.

2. DRY TESTS METHODS

As long as the particles are larger than a certain size they are rather easy to characterize by means of sieving, flakiness studies, loose (or compressive) packing or flowing properties i. e. dry test methods. Figure 1 shows example of loose packing to determine the air voids of some Swedish aggregate fraction 0,125 – 2 mm. Flowing properties are studied with the same equipment, see Figure 2. Here the time of emptying the container is documented. Moreover, Figure 3 shows equipment to document flakiness index and corresponding results. Interesting and clear differences between the commercial available aggregates can be found in the figures and it is generally concluded that the precision of the dry test methods is rather good when the particles are bigger than 0,125 mm.

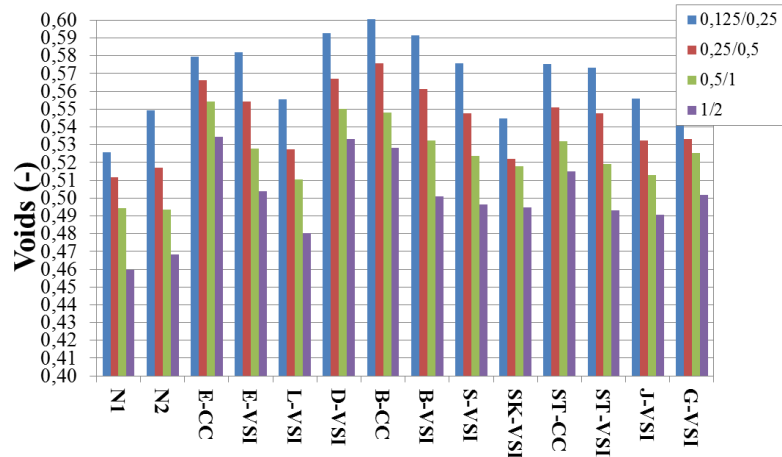
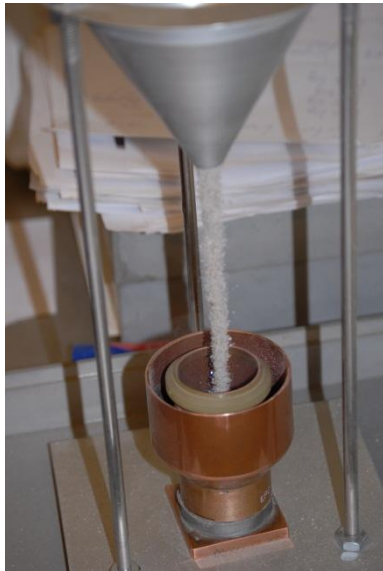


Figure 1 - Loose packing for determining the void volume of fine aggregates batches in the fractions 0,125-0,25 mm (blue), 0,25-0,5 mm (red), 0,5-1 mm (green) and 1-2 mm (violet). The two from left are natural aggregates, the rest are crushed manufactured with different methods.

Flow time

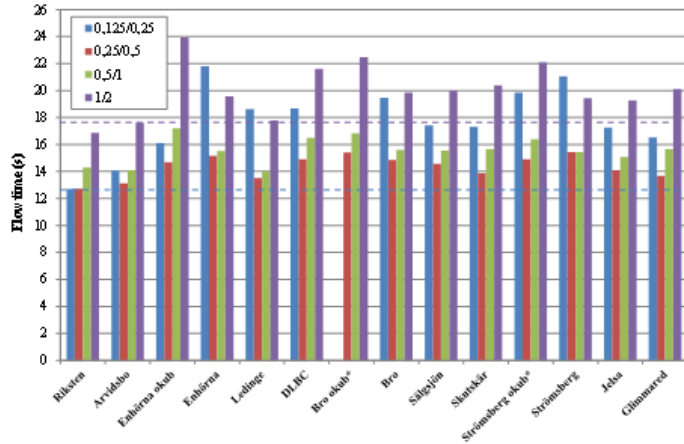


Figure 2 – Flow time measurements of the same fractions as in Figure 1.

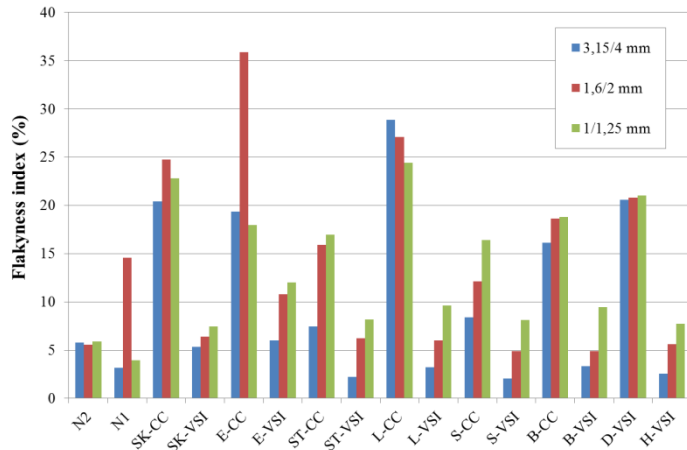
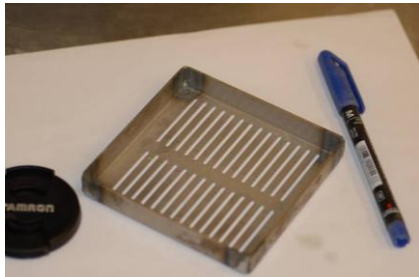


Figure 3 – Determining the Flakiness Index; aggregate type, see Figure 1, fractions 1 – 4 mm

3. WET TESTS METHODS

Regarding particles passing the 0,125 mm sieve, the natural types normally occupy less than 10-15% of the volume of cement in the concrete. The filler properties of natural aggregates, influencing the rheological properties of the concrete, are mainly linked to the clay content, i.e the BET surface. On the other hand crushed fine aggregates normally imply a much bigger volume of particles < 0,125 mm; up to 50-70 % of the cement volume, i. e. its impact on the concrete properties is important. Thus, it is recommended to characterize the fillers in a micro mortar composition consisting of cement, filler, water and maybe also superplasticizer, see Figure 4.

Micro mortar has been composed with two water to powder ratios of 1,204 and 1,505 (volume) and the volume of the cement was 49 % of the total powder volume. The spread of the micro mortar has been determined in a small slump cone with a bottom diameter of 38 mm, see figure 4. The spread for 0 mm and 62 mm has been calculated and is presented in Table 1. It is seen that the higher water to powder ratio, the higher is the water demand for the studied filler.

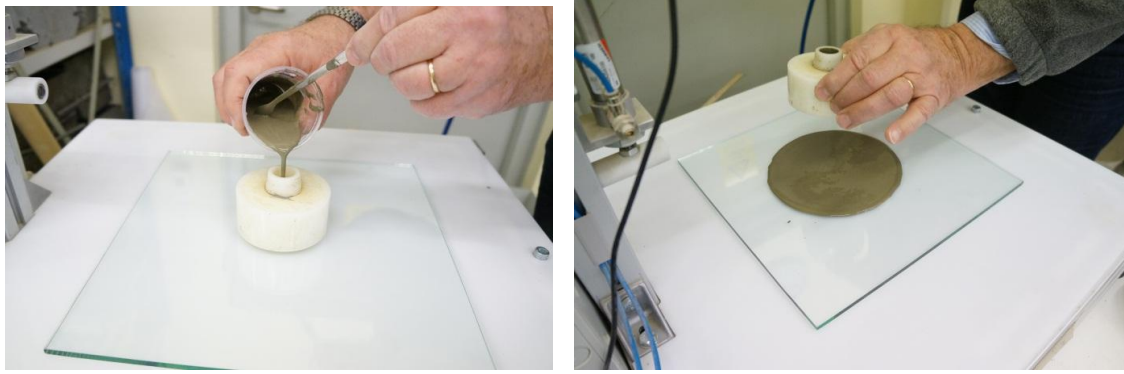


Figure 4 – Micro mortar tests made with a mini slump cone with a bottom diameter of 38 mm.

Table 1 Results from tests with micro mortar

| SPREAD | N1 | N2 | E-CC | E-VSI | L-VSI | D-VSI | B-CC | S-VSI | SK-VSI | ST-CC | J-VSI | G-VSI |
|--------|-------|-------|-------|-------|-------|-------|-------|-------|--------|-------|-------|-------|
| 0 mm | 0,884 | 1,012 | 0,877 | 0,922 | 0,937 | 0,993 | 0,96 | 1,011 | 1,006 | 1,02 | 0,955 | 0,932 |
| 62 mm | 1,406 | 1,325 | 1,41 | 1,382 | 1,373 | 1,337 | 1,358 | 1,326 | 1,329 | 1,32 | 1,361 | 1,361 |

4 CONCLUSIONS AND SUMMARY

The grading curve for fine aggregates does not give enough information on how a material will influence the rheological properties of concrete. In the present paper some simple test methods are presented and results using them show differences between the studied fine aggregates. This will enable aggregate producers to gain more knowledge of how their products will behave in concrete and it will facilitate the choice of new fine aggregates for the concrete producers.

The study from which some results are presented here is a part of a larger effort to achieve reliable mix design methods considering influences of aggregate features more accurately, see e. g /Johansson and Emborg, 2014/, /Ghasemi and Johansson, 2014/

REFERENCES

Ghasemi Y and Johansson N, 2014

“Particle packing of aggregates for concrete mix design: Models and methods”.
Proceedings from the NCR Conference Reykjavik Aug 2014, 4 pp

Johansson N and Emborg M, 2014

“Methods to Optimize Aggregate Composition – Evaluation by Concrete
Experiments”, Proceeding from the NCR Conference Reykjavik Aug 2014, 4 pp

Lagerblad B., Westerholm M., Fjällberg L., Gram H-E. 2008,

“Bergkrossmaterial som ballast I betong”, CBI RAPPORT 1:2008, pp 1-121.

LABORATORY AND FIELD TESTING

A Norwegian Concrete-Ice Abrasion Laboratory



Stefan Jacobsen
Professor
Dept of Structural Eng., NTNU
N-7491 Trondheim
stefan.jacobsen@ntnu.no

ABSTRACT

A laboratory for simulation of abrasion by ice movement on concrete structures with a circular ice surface moving horizontally back and forth while forced on a concrete specimen was developed. The specimen is fixed in a holder with roller bearings, thermal control and horizontal and vertical load cells. The exposure parameters (ice pressure on concrete, movement, temperature) are controlled and adjusted to set values with a feed-back system. The average rate of concrete abrasion, or wear was in the order of 0.05 mm/km at ≈ 0.1 m/s average sliding velocity, 1 MPa ice pressure and -10 °C on a high performance concrete with $w/b = 0.30$ and granitic aggregate. Higher abrasion on paste than on aggregate is shown with structured light scanning and this feature is the same as in full scale ice abrasion. The resulting abrasion profile on the concrete from the reciprocal ice movement is explained by effective wear length variations. Static friction coefficient peaks were $\approx 0.15 - 0.2$ whereas the dynamic friction coefficient was $\approx 0.02 - 0.03$ during a typical (sinusoidal) reciprocal ice movement experiment.

Key words: Frost action, aggregate, binder

1. INTRODUCTION AND BACKGROUND

Ice movement can occur onto and along concrete structures in water such as bridges, piers, lighthouses, oil-platforms, sea wind mill foundations, concrete dams, canals etc. Depending on concrete and ice conditions the ice abrasion depth can amount to several mm/year as seen on older Baltic Sea lighthouses /Houvinen 1990/. However, the 90 MPa concrete in the Canadian Confederation Bridge has abrasion of only 0.3 mm/year /Newhook 2007/, see Figure 1.



Figure 1 - 0.3 mm/year concrete ice abrasion on 90 MPa concrete of the Canadian Confederation Bridge, left: pier, right: $\sim 15 \times 10$ cm close-up /Newhook 2007/.

2. WEAR BY ICE ON CONCRETE STRUCTURES AND IN LABORATORY

Field studies have shown that ice abrasion occurs both in zones where ice is sliding, and in zones with brittle crushing of the ice against the concrete /Houvinen 1990, Newhook 2007, Jansson 1988, Hara 1995/. The depth of concrete-ice abrasion, or wear, is proportional to length of ice movement, as observed both in lab and field /Houvinen 1990, Newhook 2007, Itoh 1988,

Møen 2011/. Early lab experience /Itoh 1988/ also indicated that wear increases with increasing normal pressure of the ice on the concrete. Archard's law /Archard 1953a, Archard 1953b/ thus seems to apply in field and lab and can be written as /Basu 2011/:

$$W = k_1 p/H \quad (1)$$

W [m/m]: wear depth/ice movement, k_1 : unitless wear coefficient, p : ice pressure (MPa), H : material hardness (MPa). Eq.(1) is an inverted version of Archard since it describes the wear of the harder material concrete by abrasion of the softer material ice. At present we assume it is most correct to use concrete hardness in Eq.(1) though also ice hardness plays an important role. In /Houvinen 1990/ it was proposed that concrete compressive strength can be used instead of hardness in an expression similar to Eq.(1). However, his very simple empirical model does not include the basic load parameter ice pressure and is therefore too limited for service life prediction. Assuming that the concrete Hardness should be used, the wear coefficient k_1 in Eq.(1) may be estimated based on concrete-ice abrasion experiments and concrete hardness data. In /Kirkhaug 2013/ a concrete with $w/b = 0.30$ had a wear rate due to concrete-ice abrasion of $0.05 \text{ mm/km} = 50 \times 10^{-6} / 10^3 = 5 \times 10^{-8}$ at $-10 \text{ }^\circ\text{C}$, 1 MPa ice pressure and average sliding speed 0.1 m/s measured in our lab described below. Paste hardness for a similar mortar was found to be $\approx 1 \text{ GPa}$ /Wang et al 2009/ measured with nano indentation. This gives k_1 in the order of 5×10^{-5} . However, the granitic aggregate particles had hardness $\approx 15 \text{ GPa}$ as measured with nano indentation /Wang et al 2009/ so then $k_1 \approx 75 \times 10^{-5}$. The wear coefficient should thus be somewhere in the range $5 - 75 \times 10^{-5}$ for this concrete and test. Concrete ice abrasion mechanics and fracture mechanisms have been treated in a separate study /Jacobsen & Scherer 2013/

3. LABORATORY DEVELOPMENT

A test machine has been designed and is presently in operation at our concrete laboratory simulating concrete-ice abrasion by forcing a circular ice surface towards the surface of a concrete specimen while moving the ice back and forth and controlling ice pressure, average speed, temperature etc. Figure 2 shows a concrete specimen (100 by 50 by 310 mm) in a holder with load- and temperature control.

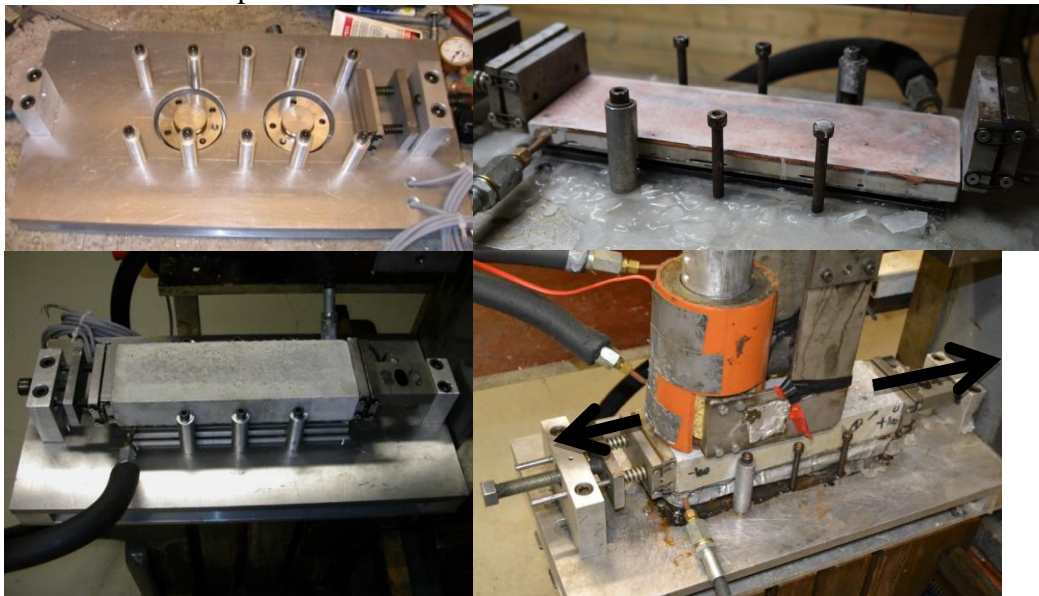


Figure 2 – Concrete specimen holder with load cells (top left), copper-epoxy-steel coiled support and heat transfer plate (top right), concrete specimen and horizontal load cell (low left) and in operation with ice moving (low right) (Photos E.Møen, J.R. Kirkhaug, N.S. Greaker)

During the reciprocal ice movement on top of the 100 x 310 mm concrete specimen surface both average horizontal speed and vertical force are controlled, see figure 2. The ice pressure is applied to the concrete surface by a feeding step motor. The ice is consumed at high rate as the concrete is abraded: ≈ 400 mm length of ice is consumed to abrade ≈ 0.1 mm of concrete in a few hours of test. So even though pure ice crystals can have very high strength compared to the tensile strength of the concrete /Jacobsen&Scherer 2013/ and the harder concrete is abraded by the softer ice, Eq.(1) is an inverted Archards law in our case. Figure 2 (upper right) shows control of concrete temperature and reaction forces via a copper-epoxy-steel coiled sandwich support- and heat transfer plate. The plate exchanges heat by cooling liquid while allowing measurement of vertical and horizontal reaction forces via load cells. In our experience this is very important: unless accurate temperature control there will be ice-on-ice sliding and no ice-abrasion. The bottom steel plate of the copper-epoxy-steel sandwich rests on steel roller bearings on another lower steel plate that transfers loads to two vertical and one horizontal load cell (Fig.2 upper and lower left). The ice is forced vertically on the concrete with a feeding step motor, transferring the ice-load via a spring-loaded piston acting on the $\varnothing = 74$ mm ice cylinder kept inside a cylindrical ice holder (Fig.2, lower right photo).

3. CONCRETE-ICE ABRASION MEASUREMENTS AND FEATURES

Figure 3 shows the ice abrasion wear profile of a B60 concrete as detected with structured light scanning using an ATOS III (www.gom.com) after 2,5 km of ice abrasion /Greaker 2013, Sætre 2013/. The concrete had w/b = 0.37, 5 % silica fume, 6.4 % fresh air void content, granitic normal density aggregate with maximum size of 8 mm, 73 MPa 10 cm cube strength and 34 volume % cement paste /Skjølsvold 2011/. Before start of ice abrasion exposure the concrete surface was grinded with a hard metal grinder. (The same grinder normally used to ensure parallel test surfaces in compressive strength- and E-modulus testing.) A scan made before ice abrasion exposure showed no wear of the kind seen in figure 3. The average B60 concrete ice abrasion rate measured by digital indicator was 0.08 mm/km which is slightly larger than observed on a B70 concrete with w/b = 0.30: 0.05mm/km /Kirkhaug 2013, Skjølsvold 2011/. The central parts of the surface in Figure 3 show the plane surfaces of the aggregate particles in relief towards the surrounding cement paste that is abraded slightly deeper. Thus each aggregate particle is less abraded and increasingly exposed as the surrounding cement paste is abraded by the ice. The ice abrasion test therefore reproduces high paste abrasion like in field, see figure 1. Figure 3 also shows that the abrasion is larger along the central part of the tested surface. The longer effective abrasion path along the central line due to circular ice is thus the main reason for the higher wear in the central parts of Figure 3. Preliminary results with roughness calculations based on the data from the scanner indicate that converging surface roughness values of the mortar can be obtained by suitable selection of sampling density from the scans. Further work on this is in progress. Two objectives of the concrete specimen holder shown in Figure 2, in addition to temperature control, are to control the ice pressure (which is forced onto the concrete specimen by the step-motor and the steel spring charged load cylinder above the specimen), and to measure friction during test. The way the system is programmed gives a possibility of logging friction at high frequency so that continuous development during an abrasion experiment can be sampled, including variations within each reciprocal movement cycle. Friction was measured on a moulded surface of a well cured, air entrained OPC mortar of w/c = 0.60 with 40 volume % paste and 8 mm maximum aggregate size granitic aggregate from Årdal, Norway. The ice was granular, made by freezing tap water in plexiglas pipes. The temperature was -10°C , the average sliding speed ≈ 0.17 m/s in a (sinusoidal) reciprocal cycle ($\approx 2 \times 0.2$ m sliding / ≈ 2.3 sec), average ice pressure 1 MPa. During the first two hours of this reciprocal movement the static coefficient of friction had maximum values $\approx 0.15 - 0.2$ right after stop and before turning of the ice movement direction. The minimum dynamic friction

coefficient was reached at maximum speed of the reciprocal movement and was in the order of 0.02 – 0.03.

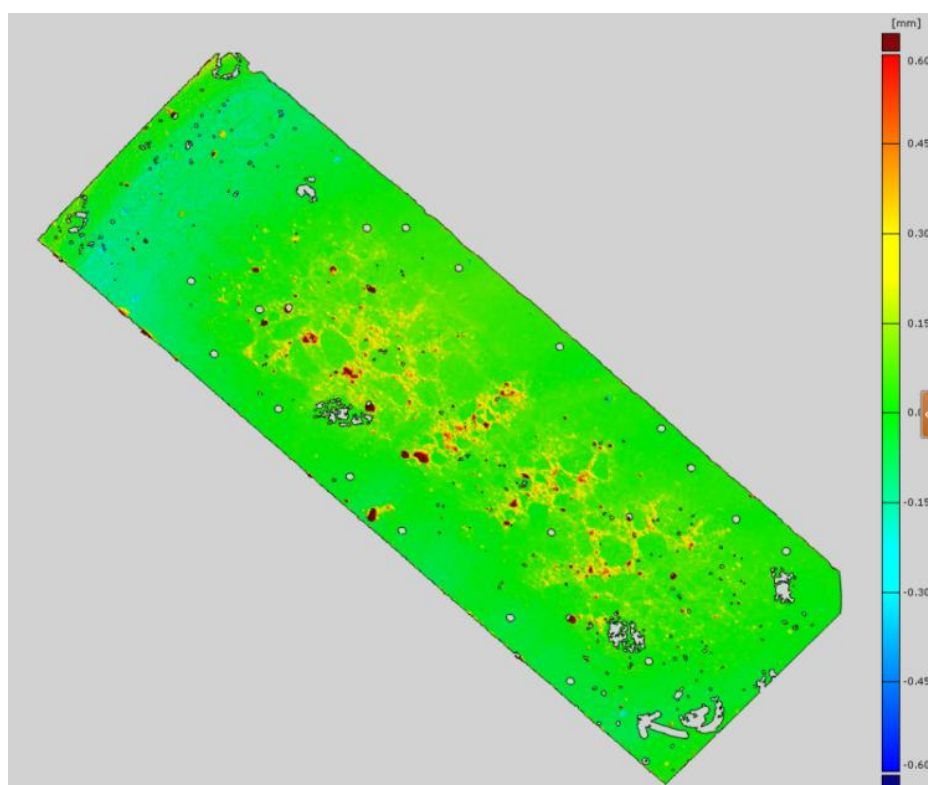


Figure 3– Concrete-ice abrasion by 3D scan (ATOS III/GOM Inspect) of a cut concrete surface of a B60 MPa normal density concrete after 2.5 km ice abrasion at -10 °C, 1 MPa average ice pressure, 0.25 m/s average sliding speed. Average concrete ice abrasion rate by digital indicator = $0.2\text{mm}/2.5\text{ km} \approx 0.08\text{ mm/km} = 8 \times 10^{-8}$ (Data by J. R. Kirkhaug, K. Sætre, NTNU)

REFERENCES

- Archard J.F. (1953a) J.Appl.Physics 24, 981-988
 Archard J.F. (1953b) Nature V.172 918-919
 Basu B. Kalin M. (2011) 1st Ed, Am. Cer Soc. published by J.Wiley&Sons 522 p.
 Greaker N.S. (2013) Project report, Norw Univ of Science and Techn.NTNU, Trondheim, 72 p
 Hara, F, Saeki, H., Sato, H.M., Takahasi, Y., Tachibana H. (1995) Consec'95, E&FN Spon, V1, 485-494
 Huovinen S (1990) Dr.thesis, VTT Publication 62, Finland, pp. 110
 Itoh Y., Yoshida, A., Tsuchiya. M., Katoh, K., Sasaki, K., and Saeki, H. (1988) 20th Ann Offsh. Techn. Conf. Houston, Texas, May 2-5, 1988. (OTC 5687), pp. 61-68
 Jacobsen S. & Scherer G.W (2013) Princeton University/NTNU/Kvaerner, 61 p.
 Jansson J.E. (1988) Proc 7th Int Conf Offsh Mech Arct.Eng, Am S Mech Eng V3 225-231
 Møen E (2011) Presented at Norwegian Concrete day, Trondheim
 Kirkhaug J.R. (2013) MSc thesis Norw. Univ. of Sc.& Techn. Dept. Str. Eng., 114 p.
 Newhook J.P. and McGuinn D.J. (2007) Engineering Summit 1997-2007 Proc. Can. Soc. For Civ. Eng. 145-157
 Skjølsvold O. (2013) Sintef report SBF 2013 F0107 11 p.
 Sætre K. (2013) Project Rep., Norw Univ of Sci.& Techn.NTNU, Trondheim, 29 p
 Wang X, Jacobsen, S., He, J.Y., Zhang, Z., Lee, S.F., Lein, H.L. (2009) Cem Con Res 39 (8) 701-715

Impact Testing of Reinforced Concrete Slabs



Ari Vepsä, M.Sc. (Eng.),
Senior scientist,
VTT Technical research centre of Finland,
Kemistintie 3, Espoo, P.O. Box 1000,
02044 VTT,
ari.vepsa@vtt.fi



Ilkka Hakola, M. Sc. (Eng),
Principal scientist,
VTT Technical research centre of Finland,
Kemistintie 3, Espoo, P.O. Box 1000,
02044 VTT,
ilkka.hakola@vtt.fi

ABSTRACT

Resistance against large passenger aircraft crash has become one of the design criteria for new nuclear power plants to be built in Finland. This resistance is shown by numerical models or semi-empirical or analytical formulas. In order to be reliable, these predictive methods have to be validated against empirical results. Scarcity of publicly available results led VTT Technical research centre of Finland to start its own medium scale impact testing campaign on reinforced concrete slabs. Numerous external organizations have joined the campaign along the way. The tests are funded and designed jointly with the results shared between the participants.

Key words: Nuclear, Reinforcement, Testing

1. INTRODUCTION

The purpose of the protecting structures of a nuclear power plants reactor building, commonly built of reinforced and in some cases of prestressed concrete, is to protect those systems inside the building that are essential for nuclear safety against various internal or external hazards. Largely due to 9/11 terrorist attacks, large passenger aircraft crash has been included as one of the possible external hazards. In Finland, for example, resistance against such a crash has become one of the design criteria for the new nuclear power plants to be built in future. This resistance is verified with numerical models or semi-empirical or analytical formulas. In order to be reliable, these predictive methods have in turn to be verified against empirical results. Scarcity of publicly available results led VTT to launch its own medium scale impact test campaign in 2004, into which numerous external organizations have joined since then. The tests carried out are funded and designed jointly with each participant getting all the results. Some of the tests are collectively agreed as “public“, meaning that they can be used by the participants in academic journal articles and conference papers.

So far testing has had its focus mainly on global bending and local perforation behaviour of reinforced concrete slabs when impacted with soft or hard projectiles. The soft projectiles simulate the fuselage of an aircraft and are considered to be much more deformable than the slab used as a target. When impacting against a reinforced concrete slab, a soft projectile makes the target to bend, giving raise to a fear that the bending reinforcement of the slab yields and ultimately ruptures destroying the load bearing capacity of the structure at this point. The hard projectiles in turn simulate the motors, landing gear and other hard parts of an aircraft and are considered to be much less deformable than the target they are impacted against. These hard projectiles cause local penetration, and in the worst case, perforation of the target slab.

2. TEST BED

All the tests have been carried out with a test bed developed and operated by VTT. The test bed consists of the launching, or the gun, part and the target support system. The launching part is basically a huge air-gun with pressurized air used for accelerating the projectile into its target velocity. This launching part consists of a pressure chamber, inside which the air pressure is increased into its test-specific target value, and a barrel part, inside which a steely piston is placed and above which a projectile is placed on rails. When released, the air pushes the piston inside the barrel towards the target. At the same time, a fin of the piston, protruding through a narrow longitudinal slit on the barrel, pushes the projectile. The piston is caught with a steel structure designed for this purpose before it hits the target. The projectile in turn hits the target which is placed between two halves of a steel supporting frame that rests on wooden planks and is supported horizontally with steel pipes attached to a bedrock. A schematic drawing of the test bed is shown in Figure 1.

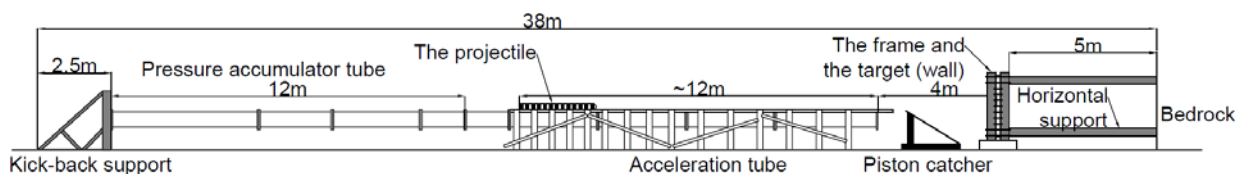


Figure 1 – Schematic drawing of the test bed used in the impact tests at VTT.

3. TEST TYPES

As of beginning of May 2014, 77 tests have been carried out with reinforced concrete slabs using the test bed described in the previous chapter. These tests have been carried out within international projects called Impact I - III and IRIS_2010. 37 of these tests have been bending behaviour tests with soft projectiles, 37 punching behaviour tests with hard projectiles and in 3 tests, the focus has been in the combined effect of bending and punching with the projectile being closer to a soft one than a hard one. In addition to the concrete slab tests, 97 tests have been carried out within the Impact as well as other projects using a so called force-plate set-up in which the concrete slab is replaced as a target by a smaller steel plate with force transducers attached behind it to measure the impact force.

3.1 Bending behaviour tests with soft projectiles

In the bending behaviour tests, most of the parameters of both the projectile as well as the target have been varied along the years. The parameters of the projectile that have been varied include the type (with/without wings, hollow/water-filled), dimensions ($\phi_0=200-256$ mm, $t=2-4$ mm), material (aluminium/stainless steel), mass (42/~50 kg) and the impact velocity (103-163 m/s). As for the target, the varied parameters include its dimensions (2300*2000*150 mm / 2100*2100*150 mm), supporting (simple, 1- or 2-way), bending reinforcement (ϕ_6 mm c/c 50 mm / ϕ_8 mm c/c 55 mm), shear reinforcement (none / ϕ_6 mm closed stirrups with $A_s=20.78$ –

52.57 cm²/m²) and the concrete material properties ($f_{c,Cube} = 33.8-70.1$ Mpa, $f_t = 2.47-4.47$ Mpa, $E = 21497-31625$ MPa).

The most common type of projectile used in the bending tests is a stainless steel pipe with an end cap welded in the front. Water filled projectiles have also been used frequently in testing to simulate the effect of the fuel tanks. The amount of water inside these water filled projectiles has commonly been roughly half of the total mass of the projectile. Schematic drawings of these two typical soft projectile types are shown in Figure 2.

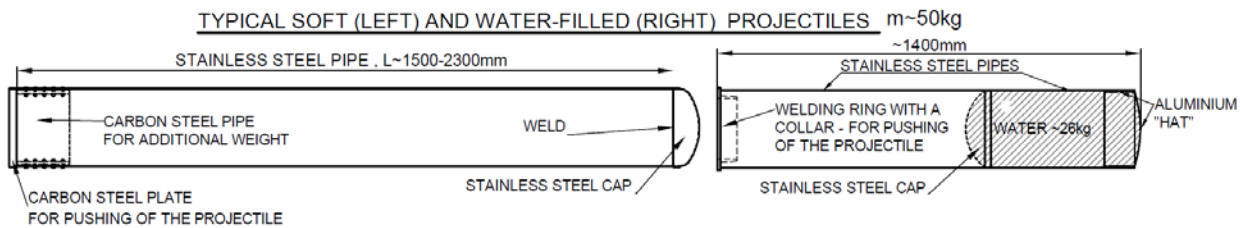


Figure 2 –A typical soft (on the left) and water-filled (on the right) projectile used in the bending behaviour tests at VTT.

The quantities that are measured in the bending behaviour tests are the impact velocity, displacements, strains on the reinforcement rebars, strains on the front surface of the slabs and support forces with the ones underlined being the most important.

3.2 Punching behaviour tests with hard projectiles

The dimensions of all the slabs tested for punching behaviour have been 2100*2100*250 mm. The supporting has been simple 2-way supporting with the span width being 2000 mm. The projectile, shown in Figure 3, has also remained unchanged with only the impact velocity being varied between 59-163 m/s. The parameters of the target that have been varied in the tests include bending reinforcement ($\phi 10$ mm c/c 90 mm, $2\phi 10$ mm c/c 90 mm, $\phi 16$ mm c/c 90 mm), shear reinforcement (none/ $\phi 10$ mm c/c 90 mm T-headed bars/ $\phi 12$ mm c/c 90 mm T headed bars / $\phi 12$ mm c/c 90 mm C-shaped stirrups with or without hooks), prestressing (none/ $2*10\phi 26.5$ mm St1080/1230 Dywidag bars without prestressing/ ~ 5 Mpa / ~ 10 MPa with or - without grouting), 1.5 mm thick steel liner at the backside (no/yes, with or without stiffeners) and concrete material properties ($f_{c,Cube} = 41.2-70.5$ MPa, $f_t = 2.85-4.10$ MPa and $E = 22155-32500$ MPa).

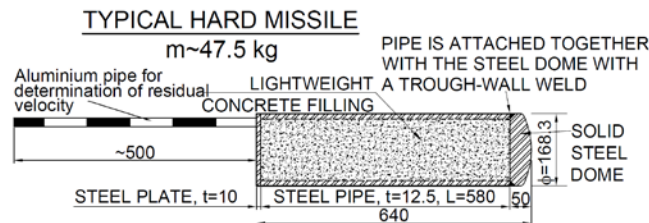


Figure 3 –A hard projectile used in the punching behaviour tests at VTT.

The main output parameters of interest are the residual velocity of the projectile in case it perforates the slab and the penetration depth in case it does not and the areas of scabbed concrete at the front and the backside of the slab. In addition to the aforementioned quantities, as well as those already mentioned in sub-chapter 3.1, the quantities measured include also the change in the prestressing force in some of the prestressing tendons and the strains acting on the steel liner in case there is such.

3.3 Material tests

Most of the materials used in the tests are subjected to static strength tests. Uniaxial tensile tests are carried out for reinforcement rebars, prestressing tendons and the projectile as well as the liner material. Each batch of concrete is tested for unconfined compression strength, splitting tensile strength (Brazilian tests) and Young's modulus. In addition, one batch of concrete has been subjected also for confined compression strength tests.

4. AN EXAMPLE OF THE TEST RESULTS AND THEIR USAGE

The main benefit of the test results is achieved when used as reference data against which the predictions given by different models and methods are compared and corrected, if need be. From the viewpoint of concrete as a material, one can study the effect of the material properties on the behaviour of the tested slab. As an example, the graph on the left in Figure 4 shows a second order predictive function fitted on the measured maximum displacements as a function of impact velocity at one location of the slab for bending tests. As expected, not all the points lie exactly on the curves. Since, ignoring the impact velocity, the concrete material properties are the main differences between the tests, they should explain the difference between the measured results and the fitted curve. To study this, the graph on the right shows this difference between the measured and the predicted maximum displacements as a function of Young's modulus of concrete. The R^2 values in the graphs are the squares of the Pearson product-moment correlation coefficient, which is a measure of linear dependence between two variables. While the Young's modulus does not explain the difference fully, it does it at least by parts and also more satisfactorily than the compressive strength or the splitting tensile strength.

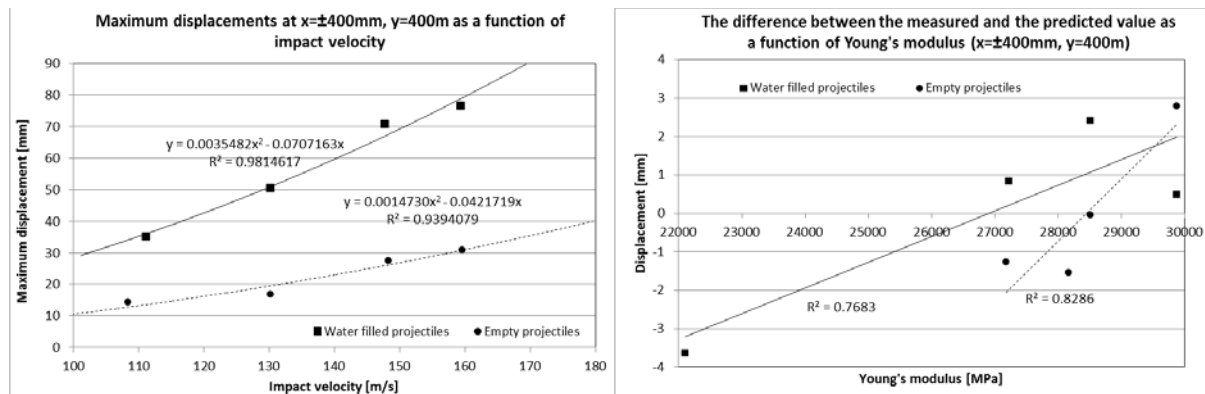


Figure 4 –Left: The maximum displacements as a function of impact velocity at one location measured in some of the bending behaviour test. Right: The difference between the measured and the predicted maximum displacement as a function of Young's modulus of the batch of concrete used.

5. CONCLUSIONS

The main benefit of the tests is achieved when used as reference data against which the predictions given by different models and methods are compared. By doing this, the predictability of the used methods and models can be assessed and the methods and models improved or changed if there appears need for that. Validated methods and models can then be used for an actual problem: a large passenger aircraft crash against NPP reactor building.

Updated Temperature-Stress-Testing-Machine (TSTM): Introductory tests, calculations and verification



PhD Student Anja B. E. Klausen
COIN, Department of structural engineering, NTNU
NO-7465 Trondheim
E-mail: anja.klausen@ntnu.no



Professor Terje Kanstad
COIN, Department of Structural Engineering, NTNU
NO-7465 Trondheim
E-mail: terje.kanstad@ntnu.no



PhD Øyvind Bjøntegaard
COIN, Norwegian Public Road Administration
E-mail : oyvind.bjontegaard@vegvesen.no

ABSTRACT

The Temperature-Stress Testing Machine (TSTM) System at NTNU is well established, but the software for logging and management is new. Introductory tests, calculations and evaluations are on-going to verify the test equipment and reproducibility.

The verification of the TSTM System includes comparisons of test results with a specially designed 1D-calculation program performed with Excel and Visual Basic, as well as with the 2D program CrackTeST COIN and the 3D FE program Diana.

Furthermore, a mechanical test series of four different concretes with varying fly-ash content has been carried out to identify the model parameters needed for the theoretical approach.

Key words: Early age concrete, cracking, thermal dilation, autogenous deformation, stress measurements, stress calculations.

1. INTRODUCTION AND OBJECTIVE

Hydration reactions in the concrete during the hardening phase always cause volume changes, and these volume changes are proven to be a considerable challenge. If these movements are restrained by the subgrade and/or adjoining structural parts, stresses will build up in the hardening concrete, which again may lead to cracking. In the literature, autogenous deformation and thermal dilation are shown to be the major driving forces to stress generation and cracking in real concrete structures. The amount of stress generated by autogenous deformation and thermal dilation in a given time interval is dependent on the degree of restraint and the visco-elastic properties of the concrete.

The Temperature-Stress Testing Machine (TSTM) System at NTNU is well established /Bjøntegaard 1999/, and consists of a Dilation Rig and a TSTM, Figure 1. The Dilation Rig

measures free deformation, i.e. thermal dilation and autogenous deformation, while the TSTM is constructed to measure the stress generation of concrete through the hardening phase. Although the TSTM System at NTNU is well established, the software for logging and management was updated within COIN's "Focus area 3.1: Crackfree concrete structures" in 2009-2012. In addition, the instrumentation system was improved to achieve the necessary accuracy and robustness of the system. The update was initiated to open for more extensive materials output and selectable degree of restraint (R) during the test. Verification tests, calculations and evaluations are on-going to verify the test equipment and reproducibility.

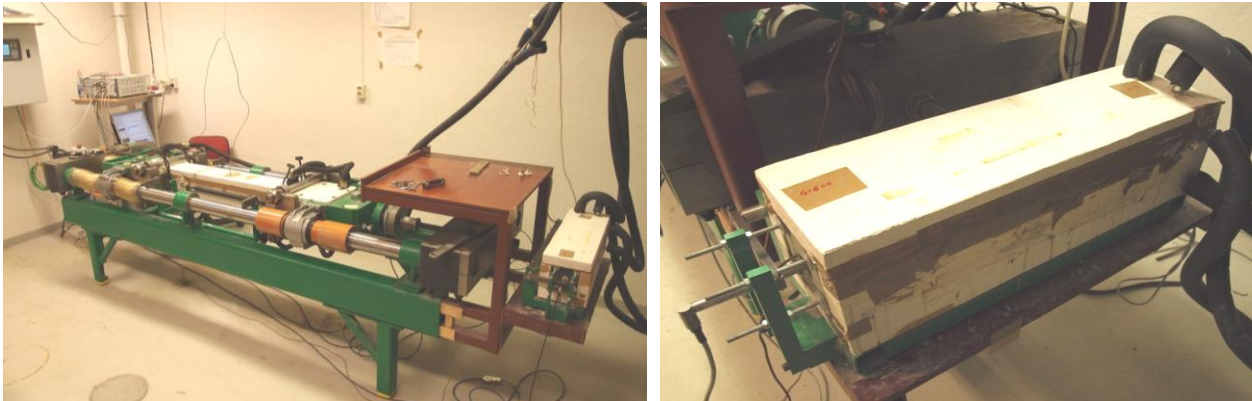


Figure 1 – The TSTM system at NTNU (left), the Dilation Rig (right)

2. EXPERIMENTAL EQUIPMENT AND TEST PROCEDURES

The total length of the dog-bone shaped specimen in the TSTM is 1200 mm, while the length which is controlled by the steering system is 700 mm, Figure 2. In both Rigs in the TSTM System, 6 mm copper pipes with circulating water are placed on the outer side of the formwork. The copper tubes are connected in series to a cooling/heating regulator (Julabo FP33). The temperature system makes it possible to prescribe and apply realistic or isothermal temperature histories to the two concrete specimens. After casting, the concrete surfaces are covered with an aluminium foil before the whole system is isolated. The TSTM System is located in a conditioned room which holds a temperature of 20 °C.

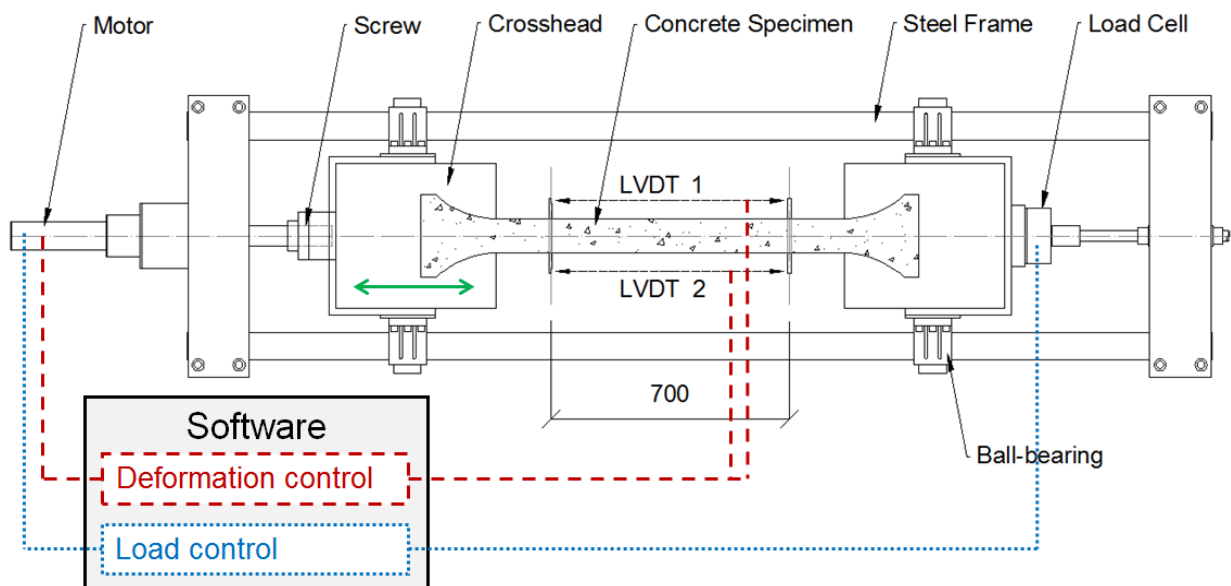


Figure 2 – The updated TSTM at NTNU

Previously, the TSTM was deformation-controlled: A feedback system was connected to the deformation transducers (LVDTs) as well as to a high precision screw moving the left crosshead, Figure 2, providing zero strain over the mid 700 mm span and, thus, a 100% restraint condition for the concrete specimen.

After the update, the TSTM is both deformation-controlled and load-controlled, see Figure 2. The magnitude of the crosshead movement induced by the software-control of the screw is decided by: 1) the length change in the concrete measured by the LVDTs, 2) the load measured by the Load Cell, and 3) the user defined parameters in the software. The update of the TSTM makes it possible to select both a chosen degree of restraint and a chosen temperature history, and thus directly simulate the stress development in a selected section of a concrete structure.

3. TEST RESULTS AND CALCULATIONS

Due to the recent update of the TSTM System, verification tests, calculations and evaluations are currently being carried out to verify the test equipment and reproducibility.

Figure 3a presents five free deformation tests in the Dilation Rig, where the given concrete specimens are subjected to a realistic temperature history. The measured free dilation show good reproducibility. The corresponding measured stress generation in the TSTM for two of the tests are shown in Figure 3b.

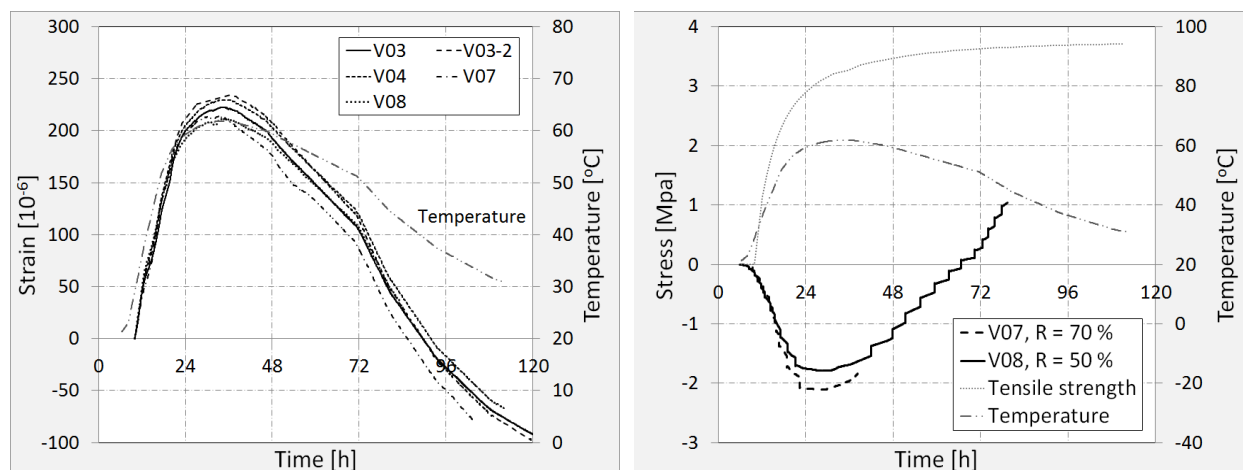


Figure 3 – a) Free Dilation (left) and b) Stress Development (right) results from the verification tests performed with a realistic temperature development in the concrete specimens

As a part of the on-going verification, three different calculation methods are tried out. The calculations simulate the stress generation in the TSTM at a given degree of restraint with free dilation measurements from the dilation rig as input data. The investigated calculation methods are; 1) a created Excel workbook /Microsoft Office, 2010/ containing calculations based on linear viscoelasticity with age adjusted effects, 2) analyses in the special-purpose 2D program CrackTeST COIN /JEJMS Concrete AB, 2012/, and 3) analyses in the multi-purpose 3D Finite Element Method program DIANA /TNO DIANA BV, 2010/. In addition to the verification tests, a mechanical test series of four different concretes with varying fly-ash content has been carried out to identify the model parameters needed for the theoretical approach. Figure 4 shows measured stress versus calculated stress development in the TSTM for verification test “V08”. Based on the comparisons so far, the created Excel calculations as well as DIANA and

CrackTeST COIN offer good agreement with the stress- and strain development in the TSTM Rig.

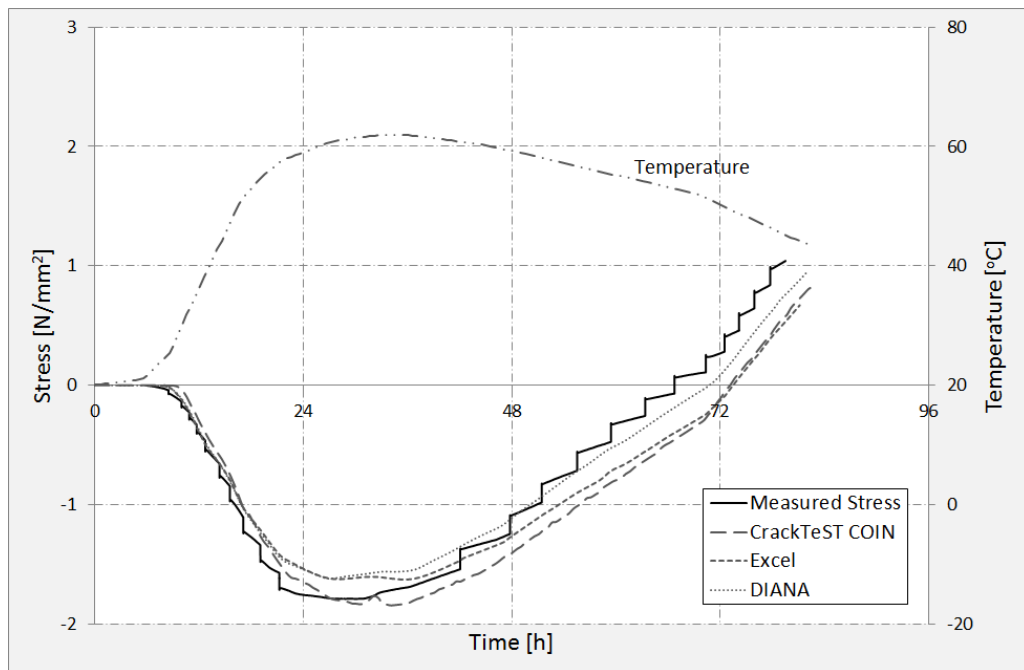


Figure 4 – Measured and calculated stress development in the TSTM

ACKNOWLEDGEMENTS

The paper is based on the work performed in COIN - Concrete Innovation Centre (www.coinweb.no) - which is a Centre for Research based Innovation, initiated by the Research Council of Norway (RCN) in 2006. The Centre is directed by SINTEF, with NTNU as a research partners and with the present industrial partners: Aker Solutions, Norcem, Norwegian Public Roads Administration, Rescon Mapei, Skanska, Spenncon, Unicon, Veidekke and Weber Saint Gobain.

REFERENCES

Bjøntegaard, Øyvind, 1999

Thermal Dilation and Autogenous Deformation as Driving Forces to Self-Induced Stresses in High Performance Concrete. PhD Thesis. The Norwegian University of Science and Technology (NTNU), Trondheim, Norway, 1999

JEJMS Concrete AB, 2009-2012

CrackTeST COIN, Version 1.2, Sweden, 2009-2012

Jonasson, Jan-Erik and Westman, Gustaf , 2001

RELAX - Conversion of creep data to relaxation data by the program RELAX. Luleå University of Technology, Luleå, Sweden, 2001

Microsoft Office, 2010

Microsoft Excel, Version: 14.0.6123.5001, 2010

TNO DIANA BV, 2010

Manual -- Release 9.4.3

Laboratory testing of early age shotcrete bond strength



Techn.Lic. Lars Elof Bryne
 Vattenfall Research and Development AB, Älvkarlebylaboratoriet
 SE - 814 70 Älvkarleby
 E-mail: lars-elof.bryne@byv.kth.se



Prof. Dr. Anders Ansell
 KTH Royal Institute of Technology, Concrete Structures
 SE - 100 44 Stockholm
 E-mail: anders.ansell@byv.kth.se

ABSTRACT

Shotcrete (sprayed concrete) differs from ordinary concrete through its application technique and the addition of accelerators which gives immediate stiffening. A method for laboratory bond strength testing of very young shotcrete on hard rock is presented. The technique does not depend on coring or other mechanical operations that disturb the shotcrete and loading is done without applying a tensile force to the soft material. The friction during the pull out testing is also minimized. The method can now be used to obtain reliable material parameters for young and hardening shotcrete, to be used for accurate analyses of structural shotcrete.

Key words: Additives, Admixtures, Aging, Binders, Mix Design, Testing.

1. INTRODUCTION

For shotcrete (sprayed concrete) on hard rock the bond to the subsurface is perhaps its most important property. Early high bond strength is especially important for its capability to prevent rock fallout and also for its resistance towards shrinkage strains and vibration damage from e.g. rock blasting during the tunnelling process. The physical properties of the hardening shotcrete and the bond it forms to the rock during the first hours after spraying depend on the set accelerator used and the micro structure that is formed and it thus differs from ordinary concrete, through its application technique and the material properties obtained. The bond strength possible to reach on hard rocks surfaces thus depend on the type of rock, condition of the rock surface, method of spraying, i.e. wet-mix or dry-mix method, and also the skill of workers handling the spraying equipment.

2. BOND STRENGTH TESTING

Testing the bond strength of very young shotcrete is difficult, without disturbing the bond that is to be measured. A reliable testing technique cannot have the problems associated with core drilling and other mechanical operation that also can cause friction during pull-out testing. It is also difficult to attach load carrying pull-out couplings to the shotcrete prior to it reaching adequate tensile strength. There are three main principles for bond strength testing of shotcrete on hard rock in the direction perpendicular to the substrate (Bryne et al., 2013, 2014), here

shown in Figure 1. The most common method (a) is pull-out of cores, pre-drilled through the concrete and the outer layer of the rock, see e.g. (SSI, 2008). The method is well established for use on fully hardened sprayed concrete on hard rock in situ, but unsuitable for testing of young shotcrete for the reasons mentioned. The second method (b) can be used also with very young concrete but it only gives an indirect measure of the bond strength. At testing shotcrete covered steel discs are pulled through the shotcrete with a force that depend on the membrane effects and tensile strength of the shotcrete. The third technique (c) is based on prepared slabs with pre-drilled cores that are fixed during spraying and then pulled out in the reversed direction. The pull-out force is thus directly proportional to the bond stress and there is no disturbance from coring or other mechanical cutting operations and the friction during pull-out can practically be reduced to zero. A new method based on this technique have been developed and tested for use with young and hardening shotcrete, see Bryne et al. (2011, 2013, 2014).

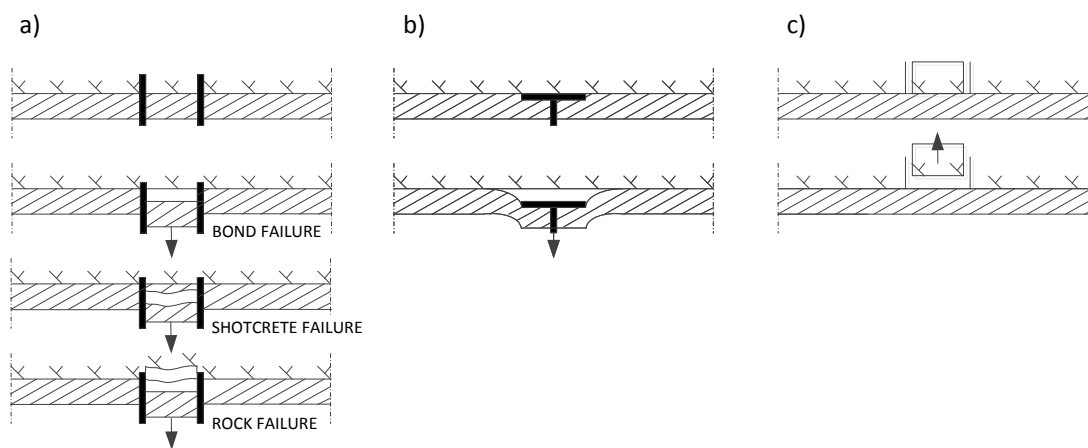


Figure 1 – Principal methods for shotcrete bond strength testing. Pull-out of drilled test cores (a), pull-out of shotcrete covered steel discs (b) and pull-out in the reversed direction of a substrate core (c). From (Bryne et al., 2013).

3. LABORATORY TESTING

The new test method is intended for use in laboratory environment but it is not possible to use the method with concrete on a rock wall since the pull-out equipment must be installed in the direction of pull. It can, however, be used in situ with test specimens sprayed and stored under tunnelling conditions. In the following the test procedure is only briefly summarized but details are given by Bryne et al. (2013, 2014).

3.1 Shotcrete material properties

The composition of the tested shotcrete is given in Table 1, based on the Swedish cement type “Anl ggningscement” (CEM I 42.5 N – SR 3 MH/LA). The water-cement ratio was 0.45 and an alkali-free set accelerator was added in the nozzle during spraying, at 3–5 % of the cement weight.

3.2 Test set-up

Granite slabs $600 \times 600 \times 40 \text{ mm}^3$ with nine symmetrically placed, circular $\phi 100 \text{ mm}$ holes were used for the tests. Prior to spraying the slab was placed in a wooden frame and $\phi 95 \text{ mm}$ granite cores were positioned and fixed in the holes. The cores were equipped with steel coupling rings fastened with a strong adhesive, as seen on the concrete core in Figure 2. The gap between holes

and cores were covered with a plastic plate so that the effective diameter in contact with the shotcrete became $\phi 83$ mm. Prior to testing the slab surface was sprayed to a thickness of 60 mm. A pull out tester with load cell and strain gauge (LVDT) were used to pull up the cores, as shown in Figure 2.



Figure 2 – Core of concrete adhered to a coupling steel disc. Pull out tester with load cell and strain gauge (LVDT). From (Bryne et al., 2013, 2014).

Table 1 – General mix and main ingredients for tested shotcrete.

| Material | Density (kg/m ³) | Content (kg/m ³) |
|-------------------|---------------------------------|---------------------------------|
| Cement | 3150 | 495 |
| Silika Densified | 2230 | 19.8 |
| Water | 1000 | 221 |
| Superplasticiser | 1100 | 3.5 |
| Aggregate, 0-2 mm | 2650 | 394 |
| Aggregate, 0-8 mm | 2650 | 1183 |

4. RESULTS

The bond tests were conducted within a shotcrete age span of 2–72 hrs., for samples stored at two different temperatures, +7°C and +20°C. The results are shown in Figure 3 where curves (see Bryne et al., 2014) have been fitted to the test results, from three tests at each shotcrete age. It can be seen that the sprayed samples are within the interval of 0.3–1.7 MPa for granite, given by Hahn and Holmgren (1979) and it show good agreement with other observations, see the compilation by Bryne et al. (2014). The results indicate that slightly higher bond strength can develop during lower temperatures.

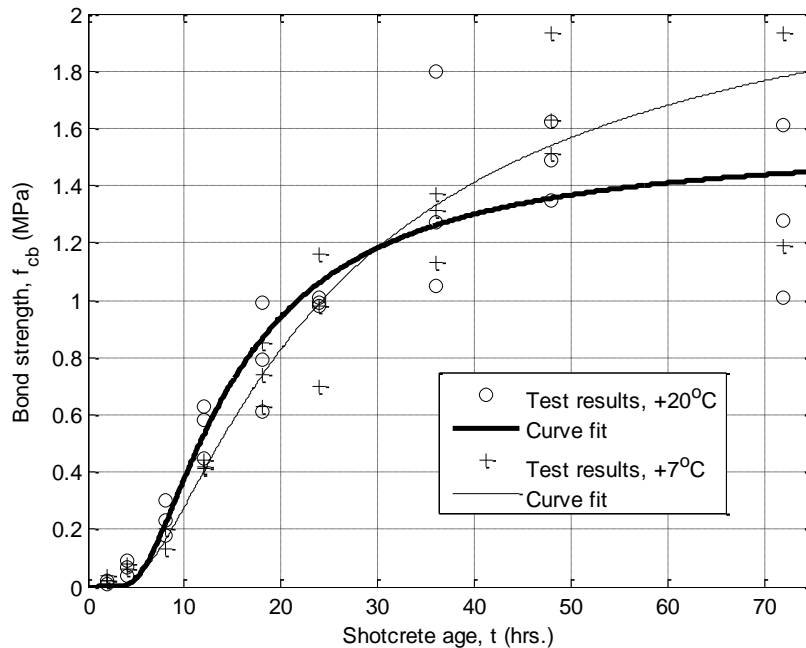


Figure 3 – Bond strength for shotcrete at +7°C and +20°C. From (Bryne et al., 2014).

5. CONCLUSIONS

The newly developed bond strength test method is suitable for use in laboratory environments where it has been tested with cast concrete (Bryne et al., 2013) and shotcreted (Bryne et al., 2014) samples. Test results could be obtained already from a couple of hours after spraying or casting. The method show significantly lower scatter in the results compared with ordinary pull-out tests performed on fully hardened shotcrete in situ. As part of the test series a comparison of relative strength increases for bond and compressive strengths (see Bryne et al., 2014) show that the bond generally develops faster than corresponding compressive strength. This is of great interest for future analysis of stresses that occur in young shotcrete on hard rock and important for the resistance towards vibrations and shrinkage.

REFERENCES

- Bryne, L.E., Ansell, A., Holmgren, J., 2013, “Laboratory testing of early age bond strength between concrete for shotcrete use and rock”, *Nordic Concrete Research*, 47, 81–100.
- Bryne, L.E., Ansell, A., Holmgren, J., 2014, “Laboratory testing of early age bond strength of shotcrete on hard rock”, *Tunnelling and Underground Space Technology*, 41, 113–119.
- Bryne L.E., Holmgren J., Ansell A., 2011, “Experimental investigation of the bond strength between rock and hardening sprayed concrete”, In: *6th International Symposium on Sprayed Concrete*, Tromsø, Norway, 77–88.
- Hahn, T., Holmgren, J., 1979, “Adhesion of shotcrete to various types of rock surfaces and its influence on the strengthening function of shotcrete when applied on hard jointed rock”, In: *International Society for Rock Mechanics, 4th International Conference*, Montreux, Switzerland.
- SSI, 2008, “Testing sprayed concrete – Part 4: Bond strength of cores by direct tension”, *SS-EN 14488-4:2005+A1:2008*, Swedish Standard Institute, Stockholm, Sweden.

Demonstration of wireless monitoring in rock mass, compacted bentonite and reinforced concrete



Edgar Bohner
Dr.-Ing., Senior Scientist
VTT Technical Research Centre of Finland
P.O. Box 1000
FI-02044 VTT, Finland
edgar.bohner@vtt.fi



Janne Häkli
Senior Scientist
VTT Technical Research Centre of Finland
P.O. Box 1000
FI-02044 VTT, Finland
janne.hakli@vtt.fi



Timo Lehikoinen
Research Team Leader
VTT Technical Research Centre of Finland
P.O. Box 1000
FI-02044 VTT, Finland
timo.lehikoinen@vtt.fi

ABSTRACT

The feasibility of reliable wireless data transmissions over distances of several metres through dense materials was investigated within a project on wireless monitoring systems. By means of the project it could be shown that specially developed wireless sender units were able to transmit a signal carrying data from a temperature sensor through rock mass, compacted bentonite and reinforced concrete in the range of decimetres to several metres. The latest developments by VTT in the field of wireless sensor and network systems offer a large potential for sensor-based performance and condition monitoring of (infra)structures.

Key words: wireless sensor, monitoring, concrete, rock mass, nuclear, testing

1. INTRODUCTION

Wireless network systems (WNS) offer manifold opportunities in transmission of data provided by sensor-based performance and condition monitoring of structures. However, the applicability, functionality, durability and serviceability of the systems are still unknown if applied to very harsh and severe conditions as e.g. when used in concrete or underground structures. Very demanding conditions exist inside underground repositories for nuclear waste, usually located inside very dense natural materials (e.g. crystalline rock, clay or salt) and designed to be

especially tight due to construction of engineered barrier systems made of compacted bentonite and reinforced concrete.

Therefore the goal of the project was an experimental trial providing information to assess the feasibility of wireless sensor data transmission for monitoring the condition of rock mass, compacted bentonite and concrete. Crystalline rock, bentonite and concrete are materials which prevent the penetration of electromagnetic waves at the common transmission frequencies of wireless systems. High moisture contents and pH values in combination with possible deformations leading to cracking and the formation of fracture zones give extremely harsh conditions for the sensors and the devices required for the signal transmission.

2. WIRELESS SENSING IN DEMANDING ENVIRONMENTS

Data is most commonly transferred wirelessly using electromagnetic waves. There are two basic mechanisms for transferring information wirelessly using radio waves: far field communication and near field communication. The common radio transmission and reception are an example of the far field case; the transmitting and receiving antennas are located far apart in terms of the wavelength λ used and they operate independently of each other. The data is received by receiving the transmitted radio wave. When the antennas are close to each other, they operate in the near field and the antennas are electromagnetically coupled. The data is transferred through this coupling from the transmitter antenna to the receiving antenna.

The transmission through rock, concrete and bentonite is difficult because of the high attenuation by the medium. The high attenuation is caused by the conductivity of the material – the electric field is strongly attenuated by the conductive material components such as water or metals. The attenuation can exceed 10 – 200 dB/m, i.e. the signal power is attenuated by a factor of 10^{-1} – 10^{-20} per metre depending on the conductivity of the material and the frequency used. The attenuation increases rapidly with the increasing frequency. The solution to obtain a reasonable data transfer range in spite of the high attenuation is to use a very low frequency, the lower the more conductive the material is.

The antennas for transmitting and receiving radio waves are typically at least of the order of $\lambda/2$ in size; at low frequencies the wavelength and the antennas become very large. Therefore, a different approach to wireless data transfer is needed – magnetic coupling in near field /McCaffrey et al. 2013/. The antennas used are loops and coils which can be made considerably smaller than the corresponding electric antennas. An additional significant advantage is that the magnetic field is not attenuated by the electrical losses caused by the conductivity making the signal propagation almost insensitive to the medium. Magnetic materials and highly conductive materials e.g. metals cause signal attenuation due to magnetic losses and eddy currents, respectively. Furthermore, the near field coupling between the antennas decreases rapidly with increasing distance between the antennas limiting the achievable communication range regardless of the medium. In order to investigate the possibilities of wireless sensor data transfer experiments were done with a simple transmitting sensor with a ferrite coil antenna and with a receiver using a loop antenna.

3. EXPERIMENTAL PROGRAMME

For the experimental tests, temperature sensors connected to data transmission units were embedded in blocks of compacted bentonite (sensor coverage 0.6 m, bulk density about 1900 kg/m³), concrete and reinforced concrete (sensor coverage 0.35 m) as well as mounted to tunnel walls at three locations inside VTT's underground research laboratory (rock thickness between 7 to 17 m), see Figure 1. Outside of the blocks or in an adjacent tunnel respectively, the antenna

unit was placed in a distance of approx. 1 m from the blocks or the tunnel walls. The concrete was a normal strength concrete K30-2 #16mm S2 /SFS-EN 206-1 2005/ with a maximum aggregate size of 16 mm. The reinforcement bars had a diameter of 5 mm and formed a mesh on all sides of the block with bar spacing of 150 mm. As a reference of the measurements traditional wired temperature sensors were placed next to the wireless sensors inside the concrete blocks.

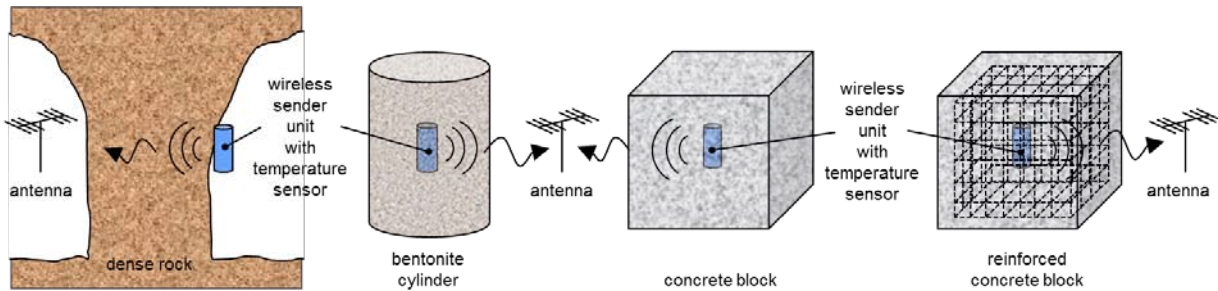


Figure 1 – Experiment test setup, from left to right: transmission through rock mass (wall thickness 7 to 17 m), a cylinder made of compacted bentonite (height 1.35 m, diameter 1.28 m), a concrete block ($77 \times 77 \times 77 \text{ cm}^3$), and a reinforced concrete block ($77 \times 77 \times 77 \text{ cm}^3$).

To investigate the wireless sensor data transmission through rock, bentonite and concrete a simple experimental setup was assembled. The setup consisted of the temperature sensor, transmitter at 125 kHz with a ferrite coil antenna, a receiver with a 2.1 m diameter loop antenna and a 9 V battery for the energy supply. The hardware setup is illustrated in Figure 2 together with the sensor electronics and its' waterproof plastic casing, and the receiver loop antenna.

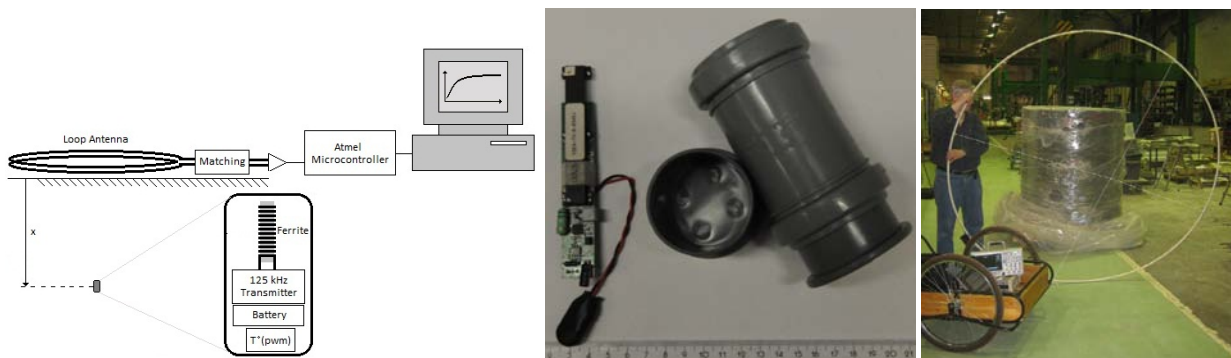


Figure 2 – Experiment hardware setup, from left to right: block diagram, sensor and casing, the receiver loop antenna.

4. RESULTS

The research showed that the specially developed wireless sender units were able to transmit a signal provided by a temperature sensor through several metres of rock mass. Data transmissions were successfully received from the wireless sensors embedded in the compacted bentonite block and the concrete and reinforced concrete blocks with a cover depth of 0.6 m, and 0.35 m respectively. As shown in Figure 3, the signal was continuously received from both concrete blocks, starting with concrete casting and ending after 18 days when the 9 V battery expired. Some data loss during the first day occurred due to a failure in recording. It can be observed from Figure 3 that the fresh concrete with its high content of unbound water did not attenuate the radio signal significantly, nor did the reinforcement mesh.

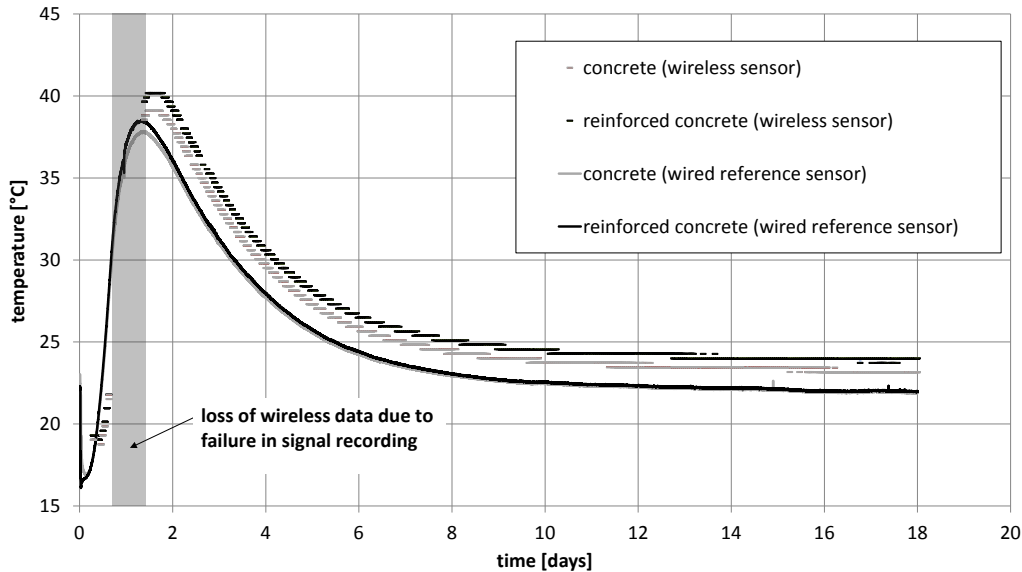


Figure 3 – Temperature development inside the concrete block and the reinforced concrete block, caused by concrete hydration during the first 18 days after casting. The data was obtained using wireless and wired temperature sensors.

5. CONCLUSIONS AND OUTLOOK

The project provided essential information about the feasibility of wireless network systems for sensor-based performance and condition monitoring of structures. Signal transmissions through moist rock mass and highly-compacted or dense mineral-based building materials were possible. Furthermore, signal passage through commonly used reinforcement steel meshes inside concrete components was feasible. The experiments were carried out with a simple transmitting sensor and receiver prototype. The results obtained and the past results /McCaffrey et al. 2013/ show that sensor data can be transmitted from inside challenging materials, e.g. up to several metres in range using magnetic coupling at 125 kHz.

The project has proved that the latest VTT technology in the field of wireless sensor and network systems offers a large potential for sensor-based performance and condition monitoring of (infra)structures. The rudimentary test setup can be upgraded for more rugged design, reduced power consumption, increased sensor lifetime, and with more sophisticated sensor elements for monitoring also other environmental parameters in addition to temperature.

Further developments of the wireless sensor and network systems have already started by replacing the attached battery with modern sources of energy, based on either inductive energy transmission or energy harvesting technologies.

REFERENCES

McCaffrey, C.; Hakli, J.; Hirvonen, M.; Huhtinen, I.; Nummila, K.; Lehtikoinen, T., 2013

"Magnetically coupled wireless communication for buried environmental sensor", *Environment and Electrical Engineering (EEEIC), 2013 12th International Conference on*, pp.341, 345, 5-8 May 2013

SFS-EN 206-1, 2005

"National Building Code of Finland, B4 Concrete Structures", Annex 3: National Annex to Standard SFS-EN 206-1, 2005

STRUCTURAL BEHAVIOUR AND DESIGN
Cont.

Impact of the combined effect of fibre orientation and volume fraction on the mechanical properties of fibre reinforced concrete



Elena Vidal Sarmiento
PhD student
Norwegian University of
Science and Technology
Department of Structural
Engineering
N - 7491 Trondheim
elena.sarmiento@ntnu.no



Mette Rica Geiker
Professor
Norwegian University of
Science and Technology
Department of Structural
Engineering
N - 7491 Trondheim
mette.geiker@ntnu.no



Terje Kanstad
Professor
Norwegian University of
Science and Technology
Department of Structural
Engineering.
N - 7491 Trondheim
terje.kanstad@ntnu.no



Max A. N. Hendriks
Professor
Norwegian University of
Science and Technology,
and Delft University of
Technology
max.hendriks@ntnu.no
M.A.N.Hendriks@tudelft.nl

ABSTRACT

Variations in the fibre orientation are generally accepted to have great impact on the mechanical performance of fibre reinforced concrete (FRC), while less or no attention is generally paid to local variations of the fibre volume fraction. The present paper discusses the applicability of a single parameter, the fibre efficiency μ , integrating contributions of both the fibre orientation and the local volume fraction, to be related to the post-cracking response of the material. The formulation of the fibre efficiency parameter allows the evaluation of the impact of the two contributions. The results demonstrate that the volume fraction, and not exclusively the orientation, has a great impact on the mechanical response of FRC.

Key words: Fibres, SCC, Structural Design, Fibre efficiency

1. INTRODUCTION

The heterogeneity of FRC is often accounted for in the prediction of the post-cracking response of the material by evaluating variations in the fibre orientation, see e.g. Ferrara, Özyurt et al. (2011), Grünewald, Laranjeira et al. (2012) or Svec, Zirgulis et al (2013). However, less or no attention is paid to the significance of local variations of the fibre volume fraction, assuming that a uniform distribution of fibres is generally achieved. The present paper discusses the need to incorporate the contributions of both the local fibre orientation and the local volume fraction in the relationship with the mechanical performance of FRC.

2. MATERIALS AND METHODS

2.1 Experimental set

An experimental series is presented to illustrate the relationship between the local performance of fibres and the residual strength. The series includes 18 beams with dimensions $0.6\text{m} \times 0.15\text{m} \times 0.15\text{m}$. The fibre reinforcement corresponded to 40kg/m^3 (0.5vol.%) of hooked-end steel fibres. The length and diameter of fibres were 60mm and 0.75mm, respectively. The beams were sawn at different locations from a total of 6 slabs ($1.2\text{m} \times 1.2\text{m} \times 0.15\text{m}$) cast with a fixed discharging point. A radially spread flow, characteristic from casting slabs (Ferrara,

Özyurt et al. 2011, Abrishambaf, Barros et al. 2012), aligned fibres orthogonally to the flow. As a result, the sawn beams cover a wide range of different fibre distribution and orientation. A description of the mix design, casting process and fresh concrete properties can be found in Svec, Zirgulis et al. (2013).

All specimens were scanned by means of a Computed Tomography (CT) scanner. The scanned images were post-processed to compute the position of all fibres. The mechanical response in flexure was studied by performing three-point bending tests according to EN 14651 (CEN 2005). In order to capture the structural effect due to differences in the fibre distribution, the beams were tested with the bottom cast surface on the tensile edge. Large variations of the residual flexural strength were registered between the specimens (CV=41% for the residual flexural strength at 2.5mm crack width). The basis of this large scatter must be ascribed to variations of the fibre dispersion. Relating the local fibre properties to the residual flexural strength is the main objective of the proposed approach.

2.2 The fibre efficiency parameter

The fibre efficiency parameter μ is proposed by the authors in order to link the local fibre properties to the mechanical performance of the material. The parameter incorporates the contributions of both the fibre orientation and the local volume fraction, and is formulated as the linear combination:

$$\mu = w_1(\alpha) + w_2\left(\frac{v_f}{\bar{v}_f}\right) \quad (1)$$

where w_1 and w_2 are normalized weights (with $w_1+w_2=1$) for the orientation and volume fraction components, respectively; α is the orientation term, v_f is the local volume fraction; and \bar{v}_f is the volume fraction for the concrete batch. In absence of any digital information of the fibres (Zirgulis, Geiker et al. 2013), fibre orientation can be deduced from the formulation by Soroushian and Lee (1990), which relates orientation to fibre counts over cross-sections. Local volume fraction can be assessed by separating fibres from a crushed concrete slice.

When the locations of the fibres in a specimen are known, as it is after a CT-analysis, local volume fractions can be directly computed and the fibre orientation of a certain volume can be described by the second order orientation tensor (Advani and Tucker 1987, Ferrara, Ozyurt et al. 2011, Şanal and Özyurt 2013, Svec, Zirgulis et al. 2013). The efficiency of fibres on bridging a crack depends on their orientation with respect to the crack plane. This relative orientation refers to the angle between the dominant fibre direction and the direction normal to the crack plane, which is formulated as:

$$\cos\theta = \mathbf{a}_1 \cdot \mathbf{n} \quad (2)$$

where \mathbf{a}_1 is the eigenvector associated to the largest eigenvalue of the orientation tensor, \mathbf{n} is the vector normal to the crack plane, and θ is the angle between the two vectors. Under these conditions, eq. (1) can be reformulated as:

$$\mu = w_1(\cos\theta) + w_2\left(\frac{v_f}{\bar{v}_f}\right) \quad (3)$$

3. RESULTS AND DISCUSSION

In this section a linear relationship between the residual flexural tensile strength $f_{fl, res2.5}$ and the fibre efficiency parameter μ is proposed for the present series of beams. $f_{fl, res2.5}$ is the flexural strength at 2.5mm crack mouth opening displacement obtained during the 3-point bending test. The relationship $\mu - f_{fl, res2.5}$ is deduced from the linear regressions of the experimental data set.

Processing the results from CT-scan provides the fibre orientation and volume fraction for any discrete volume of a specimen. Four alternative volumes in the vicinity of the notch (Fig. 1) were studied in order to define the relevant volume in which fibre properties and, therefore μ , must be assessed to be related to the mechanical properties of the material. As an example, the results from one of the beams are presented in Table 1, where differences between the zones relate mainly to the volume fraction, most likely caused by the downward settlement of fibres.

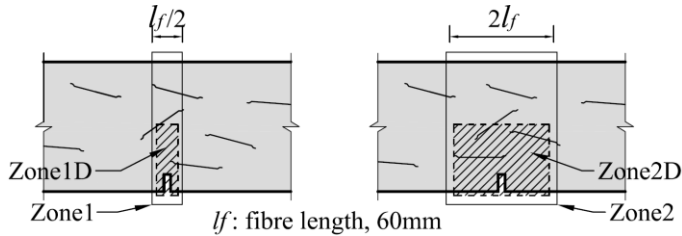


Figure 1 - Alternative volumes considered for defining parameter μ . The zones extend over the thickness of the specimen.

Table 1- Fibre orientation ($\cos\theta$) and volume fraction (v_f) over the different zones.

| Zone | $\cos\theta$ | v_f (%) |
|---------|--------------|-----------|
| Zone 1 | 0.68 | 0.40 |
| Zone 1D | 0.66 | 0.53 |
| Zone 2 | 0.70 | 0.39 |
| Zone 2D | 0.67 | 0.49 |

The relative impact of the contribution from orientation and from volume fraction in the relationship with the mechanical properties can be studied during the assessment of the weight parameters w_1 and w_2 (eq. (3)). The linear fit of the experimental data has been compared for different combinations of w_1 and w_2 . As an example, Figure 2 illustrates the data sets resulting by computing the two extreme combinations: orientation only ($w_1=1, w_2=0$) and volume fraction only ($w_1=0, w_2=1$).

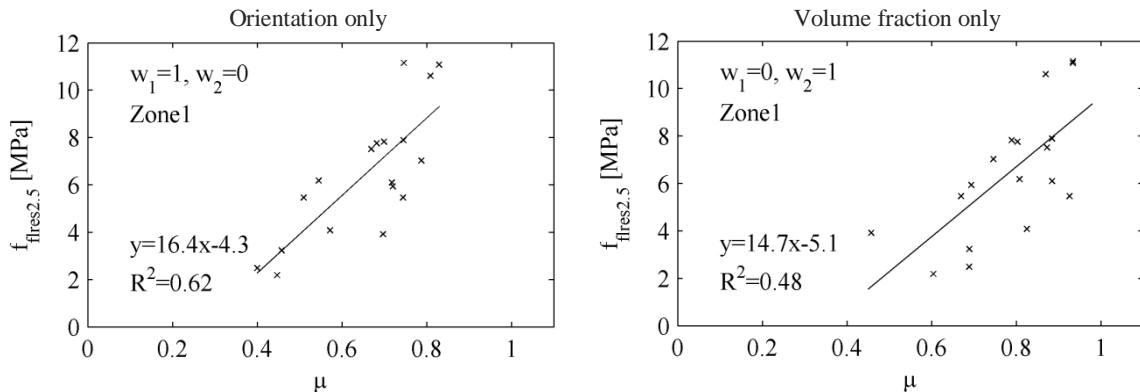


Figure 2 - Relationship between the fibre efficiency parameter μ and the residual flexural tensile strength $f_{fl,res2.5}$ for the two extreme combinations of the normalized weight factors, defined over Zone1.

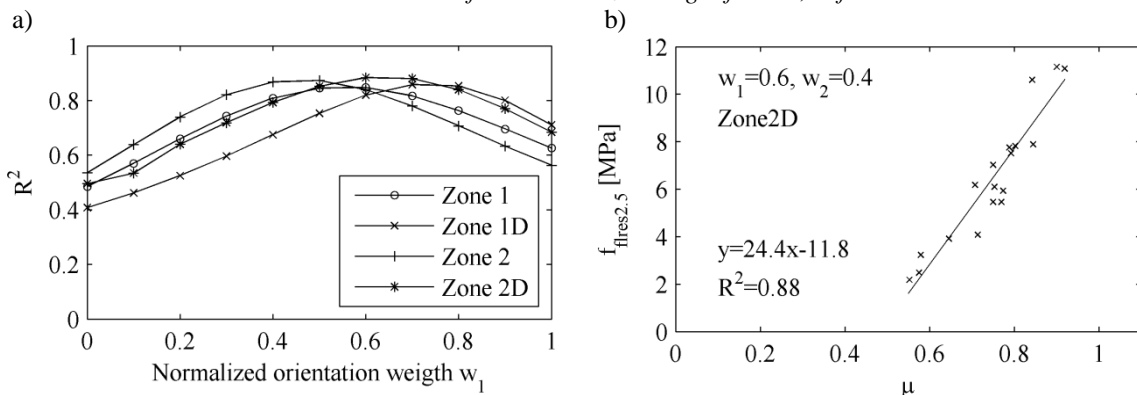


Figure 3 - a) Variation of the coefficient of determination R^2 with the normalized weight w_1 ; b) relationship between the fibre efficiency parameter μ and the residual flexural tensile strength $f_{fl,res2.5}$, defined over Zone2D.

The goodness of the linear regressions for the different relevant volumes and combination of weight factors has been evaluated based on the coefficient of determination R^2 (Fig. 3a). The relevant volume and w_1, w_2 -combination satisfying the criteria of best linear fit (i.e. maximum

R^2) are “Zone 2D” and $w_1=0.6$, $w_2=0.4$, respectively. This result highlights the great impact of variations in the volume fraction, and not exclusively in orientation, when defining the post-cracking response of FRC. Finally, the linear regression from Figure 3b is therefore proposed to relate the residual flexural strength and the fibre efficiency parameter for the present study.

4. CONCLUSIONS

This paper discusses the need to incorporate the contributions of both the fibre orientation and the local volume fraction in the relationship with the mechanical performance of FRC. The results demonstrate that a poor agreement with the residual flexural strength is obtained when considering only orientation ($w_1=1$ and $w_2=0$) or only volume fraction ($w_1=0$ and $w_2=1$). In contrast, a good correlation results from considering a combination of the two aspects. For the present study, it is concluded that the residual flexural strength is for 60% explained by variations in the fibre orientation, and for 40% by variations in the local volume fraction.

ACKNOWLEDGEMENTS

The paper is based on work performed in COIN - Concrete Innovation Centre (www.coinweb.no) - which is a Centre for Research based Innovation financed by the Research Council of Norway and industrial partners (2007-2014).

REFERENCES

- Abrishambaf, A., J. Barros, V. M. C. F. Cunha and F. N. M. Cunha, 2012
 "Assessment of fibre orientation and distribution in steel fibre reinforced self-compacting concrete panels". BEFIB2012 - Fibre reinforced concrete. Guimaraes, Portugal.
- Advani, S. G. and C. L. Tucker, 1987
 "The Use of Tensors to Describe and Predict Fiber Orientation in Short Fiber Composites." Journal of Rheology 31(8): 751-784.
- CEN, 2005
 Test method for metallic fibre concrete - Measuring the flexural tensile strength (limit of proportionality (LOP), residual), European Committee for Standardization. EN 16451.
- Ferrara, L., N. Özyurt and M. Prisco, 2011
 "High mechanical performance of fibre reinforced cementitious composites: the role of “casting-flow induced” fibre orientation." Materials and Structures 44(1): 109-128.
- Grünewald, S., F. Laranjeira, J. C. Walraven, A. Aguado de Cea and C. Molins Borrell, 2012
 Influence of fibre orientation on the performance of steel fibre-reinforced concrete. BEFIB 2012 - Fibre reinforced concrete. Guimaraes, Portugal.
- Şanal, İ. and N. Özyurt, 2013
 "To what extent does the fiber orientation affect mechanical performance?" Construction and Building Materials 44(0): 671-681.
- Soroushian, P. and C.-D. Lee, 1990
 "Distribution and Orientation of Fibres in Steel Fiber Reinforced Concrete." Materials Journal 87(5): 433-439.
- Svec, O., G. Zirgulis, J. E. Bolander and H. Stang, 2013
 "Influence of formwork surface on the orientation of steel fibres within self-compacting concrete and on the mechanical properties of cast structural elements". S. t. C. a. C. Composites.
- Zirgulis, G., M. R. Geiker, O. Svec and T. Kanstad, 2013
 Potential methods for quality control of fibre distribution in FRC SCC. 7th RILEM International Conference on Self-Compacting Concrete. Paris, France.

Elastic Modulus of Concrete with Icelandic aggregates.



Sveinbjörn Sveinbjörnsson
Senior concrete specialist. Mannvit.
Grensarsvegi 1.
108 Reykjavik, Iceland



Þórdís Björnsdóttir
Civil Engineer B.Sc. Reykjavik University,
Menntavegi 1.
101 Reykjavik. Iceland



Guðbjartur Jón Einarsson
Civil Engineer M.Sc. Mannvit.
Grensarsvegi 1.
108 Reykjavik, Iceland



Eyþór Rafn Þórhallsson
Associate Professor. Dept. of Civil Engineering,
Reykjavik University,
Menntavegi 1,
101 Reykjavik, Iceland

ABSTRACT

In this paper an Icelandic research on the effect of Icelandic basalt used as aggregate in concrete are discussed in detail since Icelandic aggregate have shown to lower the elastic modulus of concrete with Icelandic basalt being considerably more porous than basalt in continental Europe.

The results of measurements of elastic modulus are compared with the modulus calculated using methods from Eurocodes and newly released fib Model Code. The results of these comparisons indicate that reduction factors for use of dense aggregate stated in national annexes to the Eurocodes are too high. With Fib Model Code, however, reduction factors have to be specified for the use of dense and porous Icelandic basalt as aggregate.

Key words: Elastic modulus, concrete, basalt, Eurocode, Model Code

1. INTRODUCTION

In this research elastic module of Icelandic concrete is investigated to clarify the reduction factors stated in the national annexes of Iceland. In the Eurocode 2 standard (EN 1992-1-1: General rules and rules for buildings, 2004) the following formula is given for the calculation of elastic modulus for concrete with quartzite aggregates:

$$E_{cm} = 22 \cdot \left(\frac{f_{ck} + 8 \text{ MPa}}{10} \right)^{0.3} \quad (1)$$

This value should be reduced by 10% for limestone aggregates and 30% for sandstone aggregates, but increases by 20% for basalt aggregates.

According to the Icelandic national annexes to the Eurocodes the elastic modulus stated in the latter should be lowered by 10% (multiplied by a reduction factor 0,9) when dense aggregates

are used, and by 40% (multiplied by a reduction factor 0,6) when porous aggregates are used (Icelandic National Annexes to Eurocodes, 2010).

In Iceland basalt is practically the only mineral used as aggregate in concrete. Icelandic basalt differs from basalt from continental Europe in that it is much more porous, The porosity of Icelandic aggregates, measured as water absorption, is 3-8%, but 0,5% in neighbouring countries (Wallevik & Iversen, 1992).

In fib Model code 2010 (fib Model Code for Concrete Structures 2010, 2013) the following equation for elastic modulus is stated:

$$E_{ci} = 21.5 \cdot \alpha_E \cdot \left(\frac{f_{ck} + 8 \text{ MPa}}{10} \right)^{0.3} \quad (2)$$

where the factor α_E is different for the type of aggregate used; 1.2 for basalt, 1.0 for quartzite, 0.9 for limestone and 0.7 for sandstone.

2. RESEARCH AND RESULTS

The following data is from ongoing research project at Mannvit, an engineering firm, in collaboration with Reykjavík University and the Icelandic Roads Authority (Vegagerðin) (Sveinbjörnsson, 2013). Samples of concretes were obtained from various concrete producers; in addition two samples were made in the laboratory of Mannvit. The aggregates used in the concrete samples were from various mines and thus had different characteristics such as porosity.

The elastic modulus was measured in accordance to the test methods stated in the standard ISO 1920-10:2010. For each sample the compressive strength was measured on three cylinders and elastic modulus and Poisson-ratio measured on two.

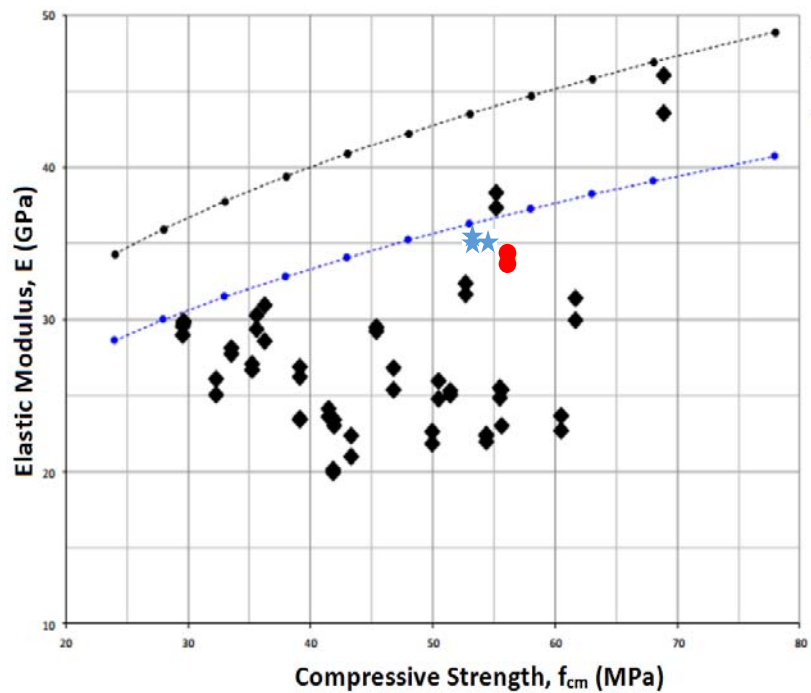


Figure 1: Compressive strength as a function of Elastic Modulus

In Figure 1 the measured elastic modulus is shown for various concrete samples is shown, basalt aggregates as diamonds, quartzite as stars and granite-gneiss as circles, as well as the elastic modulus calculated according to Eurocode 2, the top line being the value for basalt aggregates and the bottom for quartzite aggregates.

In Figure 2 the measured elastic modulus from five concrete producers (marked from 1 to 5) is compared to the elastic modulus calculated according to Eurocode 2 and multiplied with the reduction factors 0.9 and 0.6.

In Figure 3 the measured elastic modulus is compared to the elastic modulus calculated according to fib Model Code. The reduction factors for limestone (0.9) and sandstone (0.7) are used since the value stated for basalt in Model Code does not fit the Icelandic basalt.

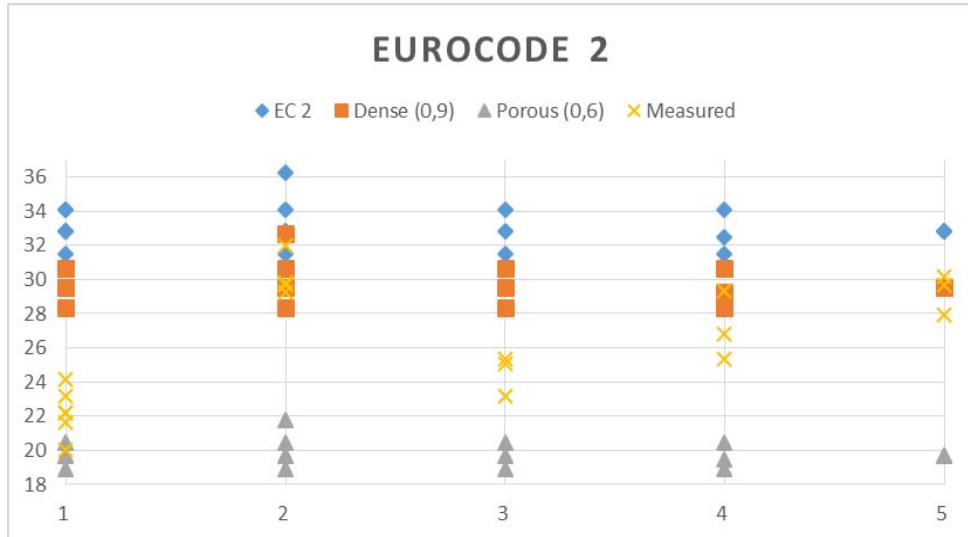


Figure 2: Measured elastic modulus is compared to the elastic modulus calculated according to Eurocode 2

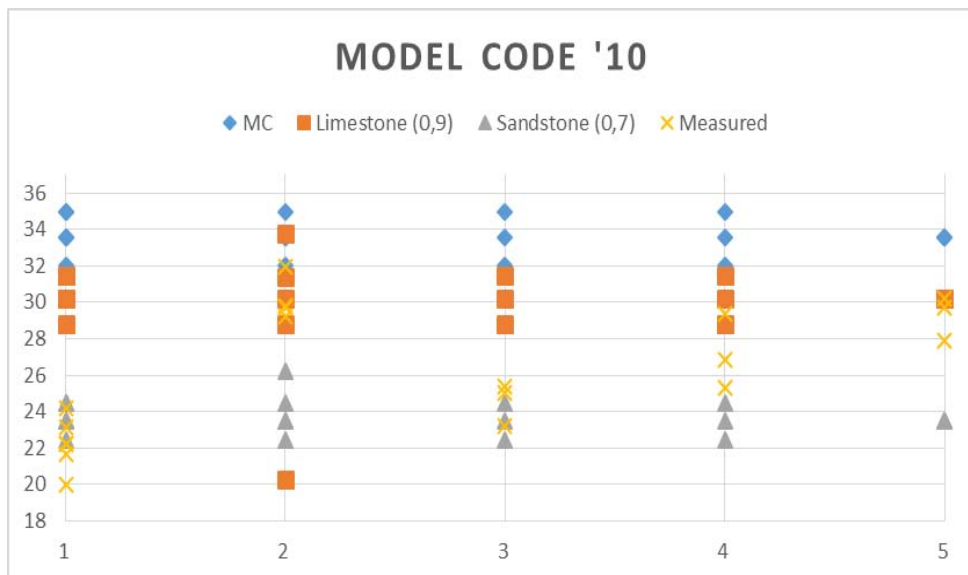


Figure 3: Measured elastic modulus is compared to the elastic modulus calculated according to fib Model Code

3. CONCLUSION

In Figure 2 measured values and values calculated according to EC2 and the Icelandic National Annex are shown. When the reduction factor 0.9, for dense aggregates, is used 5 samples of 20 have a measured value higher than the calculated value. With the reduction factor 0.6, for porous aggregates, all 20 samples have a higher measured value than calculated.

In Figure 3 measured values and values calculated according to Model Code 2010 are shown. With the factor $\alpha_E = 0.9$, for limestone, only 2 values of 20 had a measured value higher than the calculated value and with $\alpha_E = 0.7$, for sandstone, 5 samples still had a higher calculated value than measured.

As stated above Icelandic basalt differs from basalt in continental Europe and there for the rules and equations stated in Eurocode 2 for basalt aggregates do not fit the Icelandic aggregate. The national annexes for EC2 notes two reduction factors but does not state when to use each one. With only 5 of 20 samples having a higher measured value than calculated when the reduction factor for dense aggregate indicates that the value 0.9 might be too high.

As for Model Code 2010 reduction factors for Icelandic basalt, much like the ones stated in the national annexes for EC2, are necessary if the equations from the standards are to be used for concrete made with Icelandic basalt.

As mentioned Icelandic basalt is more porous than basalt from elsewhere in Europe. Results of the measured porosity on the elastic modulus indicated that porosity ratio in aggregates has considerable effect on the elastic modulus of the concrete.

ACKNOWLEDGEMENT

The authors greatly appreciate the financial support from the Icelandic Roads Authority, the Housing financing fund and Aalborg Portland in Iceland.

REFERENCES

- Björnsdóttir, Þ. (2013). *Fjaðurstuðull steinsteypu*. Reykjavík: Reykjavik University.
- EN 1992-1-1: *General rules and rules for buildings*. (2004). Brussels: Comité Européen de Normalisation.
- fib Model Code for Concrete Structures 2010. (2013). Berlin: Ernst&Sohn.
- Icelandic National Annexes to Eurocodes*. (2010). Reykjavík: Staðlaráð Íslands.
- Sveinbjörnsson, S. (2013). *Fjaðurstuðull steinsteypu - Rannsóknarverkefni. Áfangaskýrsla*. Reykjavík: Mannvít.
- Wallevik, Ó. H., & Iversen, K. (1992). *Hástyrkleikasteypa úr íslenskum efnum: kostir, notagildi, efniseiginleikar og framleiðsla*. Reykjavík: Rannsóknarstofnun byggingariðnaðarins.

Tailor-made Concrete Structure with the use of Digital Fabrication



Thomas Juul Andersen
 Team Manager, Cand. Arch.
 Danish Technological Institute
 Gregersensvej, DK-2630 Taastrup
 tja@dti.dk

ABSTRACT

In the early spring 2014 a sculptural concrete structure saw the daylight. The structure marks the end of the large EU FP7 project TailorCrete and it tell the story of the technological developments within the research project. This involves digital architecture, advanced robot technology for the prefabrication of non-standardized formwork and reinforcement, and advanced form filling with self-compacting concrete.

Key words: Non-standardized Formwork, Reinforcement, Digital Architecture, Self-Compacting Concrete, Digital Fabrication, Robot Technology, Sustainability.

1. INTRODUCTION

I August 2009 a huge European project under FP7 called New Industrial Technologies for Tailor-made Concrete Structures at mass customized Prices (acronym: TailorCrete) was launched. The project addressed the weak link between the possibilities in digital 3D-modelling using advanced CAD-software (Computer Aided Design) and the possibilities in physical fabrication of the needed formwork and reinforcement to enable the realization of digital architecture. Today, the creation of complex concrete structures is extremely costly as the fabrication and processing of formwork and reinforcement is still a very labour intensive process. Thus, the main idea behind the TailorCrete concept is to close this gap by introducing robots, programmed from the 3D CAD designs via advanced CAM-technologies (Computer Aided Manufacturing) for the processing of formwork and reinforcement.

After 4½ years of research and development the end of the project was marked by the construction of a full-scale sculptural concrete structure (referred to as the Demonstrator). The Demonstrator which is located in Aarhus in Denmark demonstrates a great part of the technological developments within the project. This involves digital architecture, advanced robot technology for the prefabrication of non-standardized formwork and reinforcement, and advanced form filling with self-compacting concrete.

2. PREFABRICATED NON-STANDARDIZED FORMWORK AND REINFORCEMENT

The Demonstrator is designed by the Turkish architectural company Superpool. The design is generated with the use of the latest digital 3D-modelling tools which has resulted in an advanced geometry which would be very difficult to fabricate with the use of traditional available methods. In the following the process of how the technological developments in TailorCrete were used to fabricate the non-standardized formwork and reinforcement needed to construct the Demonstrator is described.

2.1 Fabrication of Milled Formwork using Robot Technology

One of the major challenges in the future manufacturing of non-standardized concrete structures is to introduce new and more cost-effective ways to fabricate the needed non-standardized formwork. An interesting opportunity is to exploit digital fabrication techniques in the development of new formwork systems. In TailorCrete a new formwork system has been developed based on robot milling technology and light-weight formwork materials.

Typically expanded polystyrene (EPS) is used as the formwork material in connection to milled formwork. EPS is both cheap, easy to mill, easy to handle due to the low weight and still strong despite the high content of air in the material. Furthermore, clean EPS can be recycled entirely into new EPS and thus ensure a minimum amount of waste. The material comes in blocks which are milled into its final shape. Milled EPS formwork has been used in a number of architecture projects the last 10-15 years, e.g. in connection to the construction of the Spencer Dock Bridge in Dublin, Ireland, and a concrete pavilion in Glostrup, Denmark in connection to the Danish R&D-project Unique Concrete Structures. These projects showed some of the potential of milled formwork, but also pointed out some weaknesses. Among these the lack of reusability of the EPS – recycling was not an interesting option because of the time-consuming task of separating the EPS and its coating.

For the construction of the Demonstrator a new formwork system based on milling was developed involving optimized robot milling strategies and reusable formwork in order to address specific challenges regarding milled formwork gained through previous experiences:

- Optimizing the cost-effectiveness
- Minimizing the amount of milled material
- Ensuring reusability of the formwork and recycling the waste material
- Achieve acceptable release properties as well as smooth concrete surfaces.

Through previous cases and experiments it is evident that in order to optimize the cost-effectiveness of milled formwork one key factor is to reduce the milling time. The solution is to find the right balance between the choice of milling tool, milling strategy, and surface quality. With the use of advanced 5-axis strategies for robot milling it has proven to be possible to reduce the milling time up to a factor of 6 compared to traditional 3-axis strategies.

In order save volumes of block material a new formwork substructure were developed specially for the milled formwork. One of the advantages of the substructure is that it split the non-standard geometries into a standard grid which is easier to control in the design process and at the building site. Furthermore, all the EPS-blocks used for the Demonstrator were pre-cut using a hot-wire before milling. Instead of considering the front- and back formwork as two separate pieces they were considered as one piece which was cut in the approximate angle corresponding to the cavity for the concrete structure.

When casting directly against milled EPS formwork the surfaces of the concrete become rough and de-moulding can be very difficult, especially when high curvatures defines the geometry. Previous experiments has shown that applying a liquid coating to the milled surfaces can result in smooth concrete surfaces – but the disadvantage with liquid coatings is that the formwork often breaks in the de-moulding process and it is very difficult to separate the coating from the EPS which could enable recycling of the EPS. To address these challenges a new system involving a flexible membrane attached on the milled EPS was developed. The most promising membrane turned out to be a 0.5 mm. silicone membrane. This relatively thin membrane is easy

to handle and attach to the milled EPS using a new developed attachment method. Besides providing the concrete with a smooth surface and ensure good release properties, the membranes also ensure reusability of the milled formwork. After casting onto the milled EPS with the silicone membrane attached the concrete can easily be detached and both EPS and membrane can be reused. When reusability is not necessary the EPS is still clean after casting and thus can easily be recycled into new EPS.

For the Demonstrator the reusability of the milled formwork was demonstrated by using 90% of the formwork twice. This was possible since the Demonstrator was designed with a rotation line along the centre and thus the two halves are the same except for the lowest part which contains two different endings of the structure.

2.2 Robot Bending and Binding of Reinforcement

Another major challenge within the area of non-standardized concrete structures is to optimize both production and usage of reinforcement and thereby be able to shape the reinforcement with high precision and at a lower price. In the research steel fibres, carbon fibres, textile reinforcement, and traditional steel reinforcement has been investigated. For the Demonstrator traditional reinforcement has been used, and the research has focused on the possibilities to automate the production using digital fabrication techniques.

The research has explored the potential of using robots to bend and assemble traditional reinforcement. In order to handle the complete production of a reinforcement structure, a prototype of a production setup with two robots has been designed. Robot 1 is taking care of the tasks involving feeding, bending and transportation of rebars and is mounted with a gripping tool and a cutting tool. Robot 2 is mounted with a binding tool. Furthermore a flexible fixture is used to hold the reinforcement structure during production. In order to ensure a collision free process a mathematical model of rebar deflection developed and verified, and thus the system can simulate the gravity impact on the rebars during bending and handling.

The setup with 2 robots enables automated fabrication of reinforcement meshes, and can handle rebars of 8, 10 and 12 mm. It was used to fabricate complex double curved rebars for the parts with very high curvature surfaces on the Demonstrator. The rest of the reinforcement for the Demonstrator was single curved rebars fabricated using traditional methods.

3. ON-SITE PROCESSES

3.1 Assembling of prefabricated parts

In order to simplify the on-site processes every prefabricated piece was given a specific number referring to the final position in the structure. Further, all milled formwork parts were transported in a container where each block was positioned corresponding to the order of use on the site to optimize the logistics.

Assembling of both the milled formwork and the robot bend reinforcement was very easy due to high precision of the digital fabrication. The position of the tie-rods was planned already in the design phase, and thus it was possible to pre-drill the holes needed in the formwork using robot technology. A special cone for curved structures was used in the connection between formwork and tie rods.

3.2 Casting and de-moulding

The Demonstrator was cast in 4 stages. The first 3 castings involved a special designed SCC. A small hole on top of the formwork was made for the inlet, and here a thin hose was lowered – as

well as a camera in order to follow the casting. The SCC was designed with a high plastic viscosity but low yield stress and it was cast very slowly in order to achieve nice surfaces. The final casting – the horizontal deck – was cast using slump concrete. This part had no counter-formwork and thus the upside was shaped in hand.

De-moulding of the formwork turned out to be more challenging than in the previous laboratory tests. First the release properties of the membrane had changed during the time of weather exposure, thus there was no easy release between concrete and rubber membrane as observed in laboratory tests. Second the attachment points of the membranes were not accessible during de-moulding since they were located along the sides of the EPS. If the attachment points had been located on the backside the EPS could have been pulled out and the membrane easily removed sideways. Despite these problems, all EPS-parts could be reused but 90% of the membranes had to be replaced for the second casting.

The final concrete surfaces of the Demonstrator had a very high quality in terms of smoothness and very few blow holes. Some places the formwork had slightly misaligned during assembling and casting which can be seen when looking closer but this doesn't affect the overall nice appearance of the Demonstrator.

4. CONCLUSIONS

Within the TailorCrete project a new formwork system based on robot milling technology has been developed, and by the construction of the Demonstrator it has been demonstrated FSD demonstrated been achieved to

- Optimize the cost-effectiveness of the milling process by introducing advanced 5-axis milling strategies.
- Minimize the amount of milled material by the development of a fixed grid substructure, and by using hot-wire cutting before milling.
- Ensure reusability of the formwork and recycling the waste material by introducing a flexible membrane to separate the concrete from the EPS.
- Achieve smooth concrete surfaces due to the flexible membrane – but not possible to achieve acceptable release properties to the milled formwork. A method on how to de-mould a complex structure using correct positioned fixing points for the membrane on the milled EPS has been described for future castings.

Furthermore, assembling of both the milled formwork and the robot bend reinforcement was very easy due to high precision of the digital fabrication, and slow casting with special designed SCC resulted in concrete surfaces of high quality.

REFERENCES

Verhaegh, R.W.A, 2010,

“Free Forms in Concrete”, Eindhoven University of Technology, 2010, p. 28.

Andersen, T.J., Greisen, J.R. and Thrane, L.N, 2013

Tailormade concrete structures: Architectural opportunities in robot fabricated concrete formwork, *Facade Tectonics Journal*, Number 8: February 2013 Conference Proceedings, California, USA.

Thrane, L.N., 2007

Form Filling with Self-Compacting Concrete, PhD Thesis, Department of Civil Engineering, Technical University of Denmark, 2007.

Simulation of Experimental Research of Concrete Beams Prestressed with BFRP Tendons



Andri Gunnarsson, M.Sc - Structural engineering
Efla, Consulting engineers
Hofdabakka 9, 110 Reykjavik
E-mail: andri.gunnarsson@efla.is



Eythor Rafn Thorhallson, associate Professor
Reykjavik University
Menntavegi 1, 101 Reykjavik
E-mail: eythor@ru.is



Prof. Jonas Thor Snaebjornsson
Reykjavik University
Menntavegi 1, 101, Reykjavik
E-mail: jonasthor@ru.is

ABSTRACT

Fiber reinforced polymer (FRP) have over the past years become a noteworthy choice as a reinforcement for concrete structures. The main reason being their good resistance to chemicals and weathering. Basalt fiber reinforced polymer (BFRP) is the latest FRP material considered as reinforcement for concrete. Experimental results from three studies, considering prestressed BFRP reinforced concrete (RC) beams, were reviewed and simulated using the finite element (FE) program ANSYS. The key finding was that the non-linear FE models created in ANSYS to simulate the experimental tests gave an acceptable comparison to the experimental results regarding failure mode, failure force and stress distribution.

Key words: BFRP tendons, ANSYS simulation, prestressed concrete beams, FRP.

1. INTRODUCTION

For several years now, research has been conducted on the use of prestressed BFRP tendons as longitudinal reinforcement for concrete beams at Reykjavik University. The three most recent studies are presented in Gunnarsson (2013). These experiments had a similar main theme, which was to compare the testing capacity and theoretical calculations for prestressed concrete beams reinforced with BFRP tendons. In the research project presented herein, the experiments conducted in the above mentioned studies were simulated in the FE program ANSYS, release 14,0. The main objective of this study is to see how an advanced FE program copes with evaluating the bearing capacity and prediction of failure modes for concrete beams reinforced with prestressed BFRP tendons.

Ibrahim and Mahmood (2009) created an FE model in ANSYS to simulate experimental testing of shear capacity for six RC beams strengthened with FRP laminates. Comparisons between experimental results and the ANSYS FE model were then carried out with regard to load deflection curves, crack patterns and failure loads. All these comparisons showed good agreement. One of Ibrahim and Mahmood (2009) main conclusion was that their FE model could be used in additional studies to develop design rules for the use of FRP laminates as strengthening material for RC members. Kim, Shi and Green (2008) studied ductility and

cracking behaviour of prestressed concrete beams strengthened with prestressed CFRP sheets by constructing FE model in ANSYS. Their main conclusion was that the ANSYS model presented acceptable crack widths under service loads when compared to the tested beams. However, the FE model did not represent the stiffness of the beams well enough after the beams started cracking and some differences were also noticed in the ductility indices between the test beams and the FE model.

2. FINITE ELEMENT MODELLING

Four models were created in ANSYS to simulate the four experimental set-ups from the experimental work mentioned in the introduction. All the models consist of concrete beams prestressed with BFRP tendons. They have all the same cross section, similar prestress force (P) and material properties (concrete strength, f_c , reinforcement ratio, ρ , and reinforcement area, A_f). The only significant variable is the length (a/d ratio) of the beams. This is represented further in Gunnarsson (2013). The elements used to create the models are: Solid65 for prestressed concrete, Link180 for reinforcement and Solid187 for supporting cylinders. Both the beams and

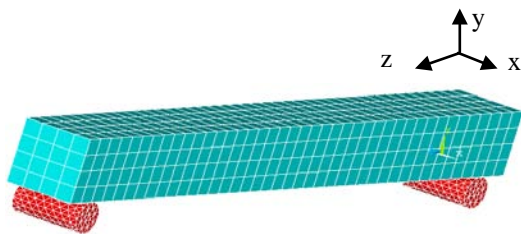


Figure 1 –Model created in ANSYS

supporting cylinders are modelled as volumes but the reinforcement is modelled as a line. An example of one model is shown on Figure 1. A perfect bond between reinforcement and concrete was assumed and the BFRP tendons were defined as linear elastic until failure but the concrete was defined as a nonlinear material. Therefore, a nonlinear rate independent stress-strain curve was defined. The plastic behaviour

of the yield surface was represented by kinematic hardening. The von Mises failure criterion was then chosen to implement a multi-linear stress-strain curve.

According to Kachlakev, Miller, & Yim (2001) the element size is recommended to be one to three times bigger than the maximum aggregate size, which is 19 mm in this study. Hence, the concrete beams were meshed with rectangular elements of the size $b \cdot h \cdot l = 50 \cdot 50 \cdot 50mm$. To constrain the beams, the bottom side of the supporting cylinders was constrained in all directions and movements of the concrete beams in the X-direction were constrained. The tendons were constrained at both ends and cooled down through temperature definitions to provide a pre-stressing effect. The load is then applied to the beams as a controlled displacement at certain element nodes, to emulate the experimental results.

The analyses for this study were defined as quasi-static. According to Kachlakev et al. (2001) numerous load steps are recommended to make it easier for the solution to converge and to capture the correct failure load. Two to three load steps were defined for each model. The convergence criterion was defined for the displacement using a tolerance of five times the default limit. Numerous sub steps were then defined for each load step. A failure was detected when the solution stopped converging for the last load step or when the model suffered from extreme deformation in a particular sub step.

3. RESULTS AND DISCUSSION

Results for one of the four models created are displayed below. A comparison of load deflection curves from ANSYS and from the experiments is displayed in Figure 2. The beam model created in ANSYS began to crack under a 14 kN load and then the tendons started to take over the tension force. The maximum loading reached 32.6 kN with a maximum deflection of 93 mm.

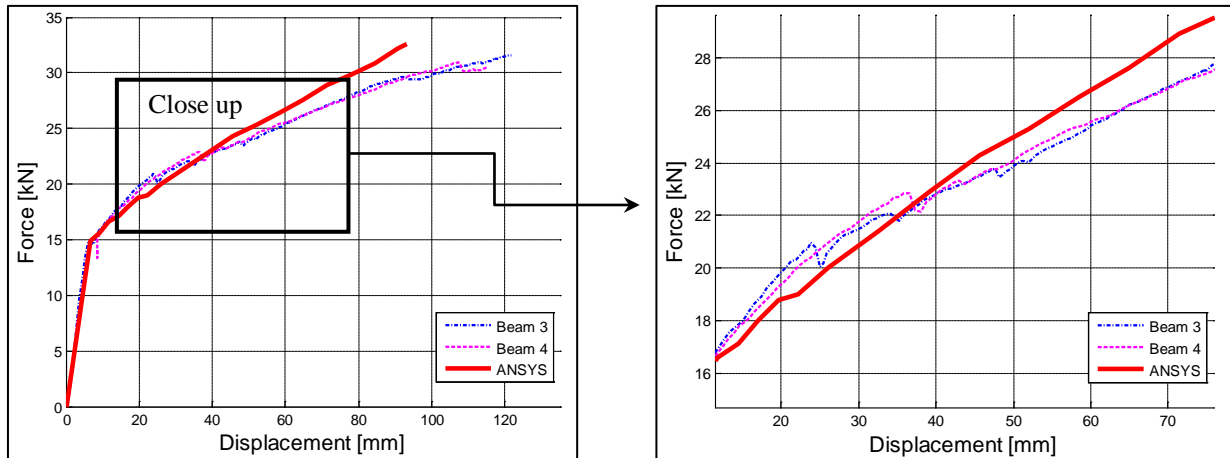


Figure 2 – Comparison between load-deflection curves for ANSYS and experimental results

The load deflection curves from ANSYS follow the curves from the real tests quite well up to yield zone of concrete (Figure 2). After the concrete starts to yield, the ANSYS curves follow the test curves approximately one third to half way of the failure displacement. There the slope of the test curves decreases, suggesting reduction in the stiffness of the beams, while the ANSYS curves are almost linear until failure. This leads to higher failure force and less deformation of the ANSYS models.

The cracking behaviour recorded in ANSYS is shown in Figure 3. First, vertical flexural cracks started to develop at midspan. They were followed with a formation of diagonal tension cracks and multiple sloping flexural cracking beside the loading points.

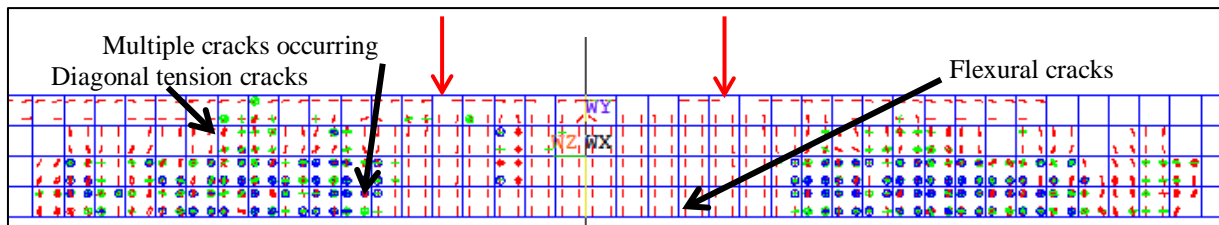


Figure 3 – Close up of the cracking behaviour for the modelled beam at failure.



Figure 4 – Cracking behaviour for the test beam at failure (Gunnarsson, 2013).

In Figure 4 an example of a failure crack from test beam is shown for comparison. The cracking behaviour detected in the ANSYS models is quite similar to the behaviour of the real tests. The failure cracks (Figure 4) occurring in the tests also have a similar slope and position as the diagonal tension cracks (Figure 3) that were formed in the ANSYS models. The same applies to the flexural cracks where they can be detected. The cracking load estimated for the test beams is 15-30% lower than in the ANSYS models. The cracking load for the test beams was estimated visually from just one side and is therefore rather uncertain. In ANSYS this can, however, be estimated with good accuracy and the observed difference is thus not unexpected. In Table 1, experimental results for shear capacity of all the beams considered in this study, $V_{exp.}$, are

compared with predicted values from ANSYS, V_{ansys} . As presented in Table 1, the experimental results and the results from the ANSYS simulations fit quite well although the ANSYS usually gives somewhat higher results.

Table 1 – Comparison of experimental and predicted shear capacity for test beams.

| ANSYS model | f'_c [MPa] | P [kN] | a/d - | A_f [mm ²] | ρ - | $M_{at\ failure}$ [kNm] | V_{exp} [kN] | V_{ansys} [kN] | V_{exp}/V_{ansys} - |
|-------------|-----------------|-------------|------------|-----------------------------|-------------|----------------------------|-------------------|---------------------|--------------------------|
| Model 1 | 60,4 | 78 | 5,3 | 156 | 0,0052 | 23,5 | 29,5 | 32,9 | 0,90 |
| | 60,4 | 78 | 5,3 | 156 | 0,0052 | 26,6 | 33,5 | 32,9 | 1,02 |
| | 60,4 | 78 | 5,3 | 156 | 0,0052 | 23,1 | 29,0 | 32,9 | 0,88 |
| Model 2 | 57,1 | 78 | 10,67 | 156 | 0,0052 | 25,3 | 15,8 | 16,3 | 0,97 |
| | 57,1 | 78 | 10,67 | 156 | 0,0052 | 24,7 | 15,5 | 16,3 | 0,95 |
| Model 3 | 67,4 | 84 | 2,63 | 156 | 0,0052 | 30,6 | 77,5 | 77,5 | 1,00 |
| | 67,4 | 84 | 2,63 | 156 | 0,0052 | 28,4 | 72,0 | 77,5 | 0,93 |
| Model 4 | 61,7 | 84 | 7,63 | 156 | 0,0052 | 26,4 | 23,1 | 26,2 | 0,88 |
| | 61,7 | 84 | 7,63 | 156 | 0,0052 | 26,6 | 23,2 | 26,2 | 0,89 |
| Average | 61,5 | 81 | | | | 26,1 | | | 0,93 |

It is not unexpected to find that the ANSYS models are stiffer than the actual test beams. The ANSYS models are based on simplified description of behaviour as they for instance assume a perfect bond between tendons and concrete. The same applies to the concrete elements which is not the case in reality where the arrangement of the aggregate and the microstructure of the concrete affect the true material stiffness. Debonding of the BFRP tendons, under high tension force, could also explain the decrease in the stiffness of the test beams but the ANSYS model does not simulate that behaviour. This is considered to be the main reason for the deviation seen in Figure 2. However it must be noted, that the tendons were anchored at the ends in the experimental beams. Internal lengthening of the tendons inside the beam would therefore cause debonding of the tendons. This indicates that the maximum strain in longitudinal BFRP tension reinforcement needs to be controlled. Based on this study no more than 4 to 5% strain should be allowed in BFRP tendons to maintain bond between concrete and reinforcement.

ACKNOWLEDGEMENTS

Special thanks are due to former students of Reykjavik University that provided access to their research data: Sindri Hlifar Guðmundsson civil engineer M.Sc., Björgvin Smári Jónsson civil engineer M.Sc. and Jónas Ásbjörnsson civil engineer B.Sc.

REFERENCES

- Gunnarsson, A. (2013). *Bearing capacity, relaxation and finite element simulation for prestressed concrete beams reinforced with BFRP tendons* (Master's thesis, School of science and engineering, Reykjavik University, Iceland). Retrieved from <http://hdl.handle.net/1946/16126>
- Ibrahim, A., M., & Mahmood, M., Sh. (2009). Finite Element Modeling of Reinforced Concrete Beams Strengthened with FRP Laminates. *European Journal of Scientific Research*, 30(4), 526–541.
- Kachlakev, D., Miller, T., & Yim, S. (2001). *Finite element modeling of reinforced concrete structures strengthened with FRP laminates* (Final report No. SPR 316). Salem, OR: Oregon Department of Transportation.
- Kim, Y., Shi, C., & Green, M. (2008). Ductility and Cracking Behavior of Prestressed Concrete Beams Strengthened with Prestressed CFRP Sheets. *Journal of Composites for Construction*, 12(3), 274–283. doi:10.1061/(ASCE)1090-0268(2008)12:3(274)

Influence of strain softening on spalling of concrete due to blast load



Jonas Ekström,
Ph.D. Student
Chalmers University of
Technology
412 96 Göteborg, Sweden
jonas.ekstrom@chalmers.se



Rasmus Rempling,
Assistant Professor
Chalmers University of
Technology
412 96 Göteborg, Sweden
rasmus.rempling@chalmers.se



Mario Plos,
Associate Professor
Chalmers University of
Technology
412 96 Göteborg, Sweden
maio.plos@chalmers.se

ABSTRACT

A society needs a certain readiness for different emergency situations, such as explosions within the urban community but also civil safety shelter in the case of war. Therefore, the ability to evaluate and to strengthen existing buildings exposed to new demands is of great importance. Many experiments and numerical analyses indicate that structures of fibre reinforced concrete yield a more favourable response during dynamic load conditions compared to plain concrete. In this study the effects of spalling of a concrete wall subjected to blast loads were studied for plain concrete modelled with an elastic-plastic material model. The results from the analysis show that spalling occur when cyclic loading from a pressure wave gradually increase the plastic strains in the concrete.

Key words: wave propagation, strain-softening, concrete, spalling

1. INTRODUCTION

In society there is a certain need of readiness for different emergency situations, such as unprovoked explosions within the urban community or even in case of act of war. In these situations, important buildings, and especially civil safety shelters are fundamental for the readiness. In Sweden, the building stock is ageing and the focus lies upon maintaining existing buildings rather than demolishing and rebuilding. Therefore, the ability to evaluate and to strengthen existing buildings exposed to new demands is of great importance. In an on-going research programme at Chalmers University of Technology, financed by the Swedish Contingency Agency, MSB, structural behaviour of concrete structures subjected to blast and fragment loading is studied. The current project is focusing on the behaviour of fibre reinforced concrete with and without main reinforcement bars.

During shock dynamics - such as blast and impact loading - the time frame where the structural response takes place is relatively short. In structural evaluation related to static condition, the time frame from unloaded structure to fully loaded structure can span over a few seconds, short term load, and up to hours or years, intermediate and long term load. For shock dynamics the time duration from the load origin to the peak stress of the structure can be as short as a fraction of a millisecond. During this time span the structural response can be very different compared to a static load case. Fracture modes which never occur for a static load can turn out to be the most

critical response. However, both in static and in dynamic response similar structural properties and material properties are considered as favourable.

For a structure subjected to high dynamic loads, such as explosions or impacts, a high ductility of the structure is usually considered as favourable, (Johansson & Laine 2012). The argument for this is that a high ability to withstand large deformations can give the structure a good ability to absorb the high energy content of the load. Regarding concrete structures, fibre reinforced concrete is a material that can be designed to have a high ductility during fracture of the material, compared to plain concrete. For this reason it is generally argued that fibre reinforced concrete provides an increased ability to withstand high dynamic loads when used in a structure, compared to a structure designed with plain concrete. Many experiments and numerical analyses indicate that structures of fibre reinforced concrete have a higher resistance against damage propagation in the structures with regard to damage critical for the internal function of persons, such as thrown pieces of concrete into the interior of the protective structure, (Foglar & Kovar, 2013); this phenomenon is called spalling of concrete.

In order to protect the inhabitants of a building or a shelter it is important that the material do not spall. Spalling can occur when a compression wave reaches a free surface from where a release wave will start to propagate in the opposite direction, (McVay 1988). The gradient between applied load and the time duration will create a tensile stress when the release wave propagates back in the structure, see Figure 1. If the tensile stress reaches the tensile capacity the damage, which can lead to spalling, will be initiated. However, a fully open crack where no tensile stress can be transferred between the two sides will not occur instantaneously. For brittle material with a much higher resistance against compressive stresses than tensile stresses, such as concrete, spalling occurs in a higher extent than for instance for metals.

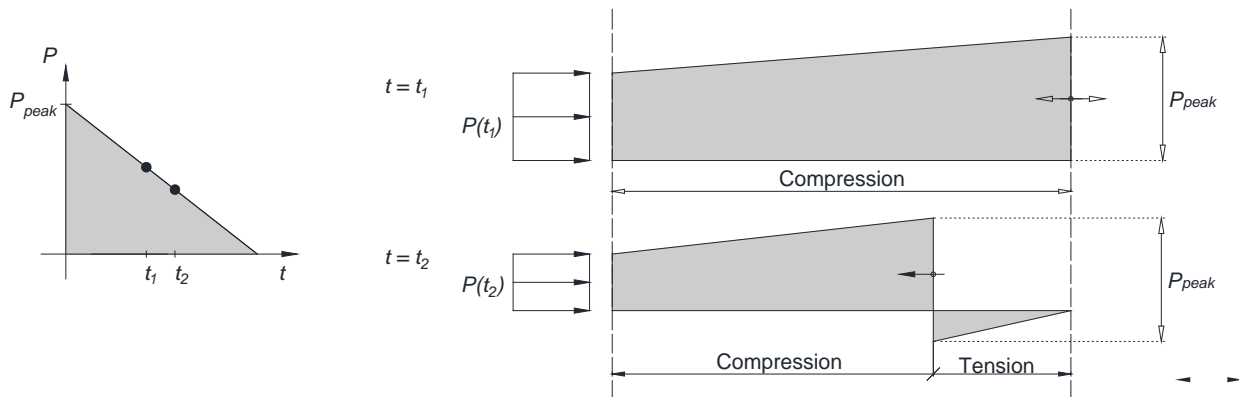


Figure 1 Stress distribution when a compression wave reaches the free edge (above), and when crack initiation occurs due to release wave (below).

Numerical models can be a powerful tool to understand the behaviour of a structure subjected to high dynamic loads. Different parameters of the load and the geometry can be evaluated and the structural behaviour can be studied from the time the load is applied until the final state of the structural response. As comparison, for experimental studies, the final stage of the response is usually the only state which can be studied in detail.

The aim of this study is to better understand the phenomena of spalling in plain concrete and fibre reinforced concrete. Furthermore, focus is set on how a finite element model with smeared crack approach and homogenous material response behaves when the increased ductility in tension of fibre concrete is modelled using a modified strain softening law. The effect of spalling in a concrete wall subjected to blast loads was studied for plain and fibre reinforced

concrete. A semi-analytic approach was used to understand the phenomena of spalling in concrete, crack propagation during spalling, the effects with regards to different concrete materials and the limitations and abilities of a finite element model which experiences spalling damages.

2. METHOD

Wave propagation in a plain concrete wall element was studied with the simplified theoretical approach by a 1-dimensional rod. The applied load was simplified to a plain pressure wave with linear decrease of the pressure after peak pressure, see Figure 2. The load was chosen such as spalling is achieved, both in the simplified theoretical approach, (McVay 1988) , and for the numerical model. The load corresponds to a hemispheric charge of 1500 kg TNT at a distance of 5 m calculated according to (ConWep 1992). The concrete is considered as an elastic-plastic material with a weak discontinuity to describe the crack localization. The softening law is defined to resemble plain concrete. For plain concrete a linear softening law is used. The stress-strain relation to describe the softening branch is smeared out over a fracture zone equal to 3 times the maximum aggregate size, (Weerheijm & Van Doormaal 2007). With assumed maximum gravel size of 16 mm the crack band width becomes 48 mm. Yielding only occurs for tension when the tensile capacity is reached. Unloading and compression of elements will be elastic for any state. The fracture energy is calculated according to (fib Model Code 2010). The structural model is a spring and mass model with proportional stiffness damping based on the linear elastic stiffness matrix. The analysis is carried out with non-linear explicit analyses in MATLAB[®]. The numerical model and input for model geometry, material model and external load applied on the structure are presented in Figure 2.

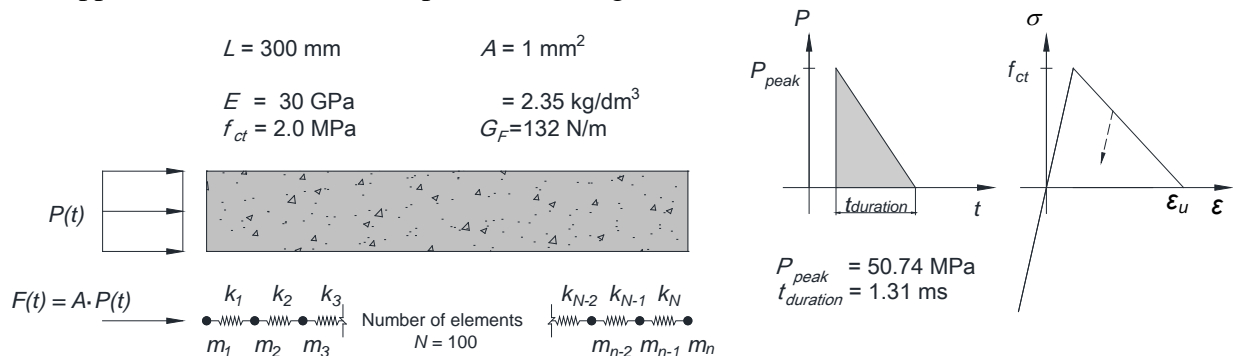


Figure 2 – Studied wall segment, numerical model, applied load and material response.

3. RESULTS

The plastic strains from the numerical analysis are presented in time steps of $\Delta t = 2L/c$. Thus, during one time step, a stress wave can travel the distance of twice the wall thickness. In the theoretical model spalling occurs during the first cycle when the release wave travels back towards the left side of the wall, i.e. $\Delta t/2 < t < \Delta t$. With the analysed wall and the applied load the first spalling crack occurs 92 mm from the right side with the theoretical approach presented in (McVay 1988). Because of the load duration and the linear decrease of pressure additionally spalling cracks should be able to form each 92 mm. In the numerical analysis the crack initiation during the first cycle occurs 97 mm from the right side of the wall. However, the growth of the plastic strain is small in this element. When the release wave propagates back towards the left side a higher plastic strain is reached in the following elements. The development of the plastic strain stops when the second compression wave propagates from the left side of the wall towards the right side. During the second release wave the plastic strain grows a bit more. For each cycle a higher maximum plastic strain is reached and the strain localizes to a few elements, see Figure 3a. The stress-strain relation of the material point where the highest plastic

strain is attained is presented in Figure 3b. This point corresponds to $x = 167$ mm and the stress-strain response shows the cycles for which the plastic strains gradually increases.

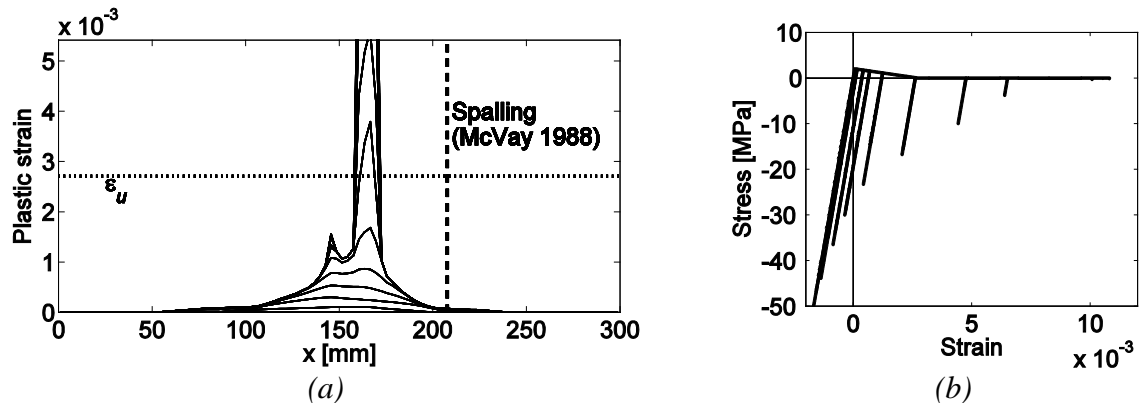


Figure 3 (a) Distribution of plastic strain during different time steps Δt , and (b) stress strain response in the strain localization zone.

4. DISCUSSION

When the tensile strength of a material and the material softening is taken into account the damage propagation which leads to spalling will be different compared to an approach where a crack is considered as fully developed as soon as the tensile strength is reached. According to the numerical analysis, with elastic-plastic material, spalling occurs after cyclic development of the plastic strain. The load duration, i.e. the pressure-time gradient, affects the number of cycles needed to develop the final strain localization. Continuation of the study will include the effects of spalling when a damage model is used and the effects of fibre concrete modelled with increased ductility of the softening branch in tension.

REFERENCES

ConWep 1992

“Collection of conventional weapon effects calculations based on TM 5-855-1.

Fundamentals of Protective Design for Conventional Weapons”, U.S. Army Engineer Waterboys Experiment station, Vicksburg (VA, USA)

fib Model Code for Concrete Structures 2010

Wiley-VCH Verlag GmbH & Co. KGaA, Weinheim, Germany, 2013

Foglar, M., & Kovar, M. 2013

“Conclusions from experimental testing of blast resistance of FRC and RC bridge decks”.

International Journal of Impact Engineering, 59, 18–28. doi:10.1016/j.ijimpeng.2013.03.008

Johansson M., & Laine L. 2012

”Bebyggelsens motståndsförmåga mot extrem dynamisk belastning, Del 3 – Kapacitet hos byggnader” Myndigheten för samhällsskydd och beredskap. Publ.nr MSB142, Karlstad

McVay M. K. 1988

“Spall damage of concrete structures”, Department of the army, Technical Report SL-88-22, Vicksburg, MS, USA

Weerheijm, J., & Van Doormaal, J. C. a. M. 2007

“Tensile failure of concrete at high loading rates: New test data on strength and fracture energy from instrumented spalling tests”. International Journal of Impact Engineering, 34(3), 609–626. doi:10.1016/j.ijimpeng.2006.01.005

AGGREGATES AND ADDITIVES

Cont.

Technique and use of Crushed Concrete from Precast Elements as Aggregate in Concrete Production



Peter Billberg
M.Sc. (Eng.), PhD.
Project Manager
Consolis Group Material Development Centre (GMDC)
P.O. Box 92145
SE-120 08 Stockholm
E-mail: peter.billberg@consolis.com



Patrick Rogers
MEng (Chem), AMIChemE
Assisting Researcher
Swedish Cement and Concrete Institute, CBI
Drottning Kristinas väg 26
SE-100 44 Stockholm
Email: Patrick.Rogers@cbi.se



Katja Fridh
M.Sc., PhD.
Building Materials
Department of Building and Environmental Technology
Faculty of Engineering, LU, Lund University
P. O. Box 188
SE-221 00 Lund
E-mail: katja.fridh@byggtek.lth.se

ABSTRACT

A two-year project is formed by Strängbetong, CBI, Cementa, Abetong, SBUF and Lund University. The project will focus on optimizing the use of crushed concrete from precast production as aggregate in new concrete. A constant proportion of ca. 3-6% of the produced concrete is, for different reasons, wasted. It is important to avoid deposition of this concrete waste and instead recycle it back into production. Aspects included in the research program are crushing techniques, particle characterization, concrete proportioning, fresh and hardened concrete properties as well as how to increase the CO₂-uptake of the crushed concrete while stored.

Key words: Aggregate, CO₂-uptake, Crushed Concrete, Durability, Mix Design, Particle Analysis, Rheology, SCC.

1. INTRODUCTION

There are a number of different reasons why a proportion of concrete is discarded in the precast element production. For example, when producing hollow-core (HC) slabs, the start and end of

the long slab has to be cut off. It is also common that these types of elements have to be cut longitudinally or diagonally in order to fit the architectural design. Approximately 3-6% of the total produced concrete is wasted. Other sources are demolished concrete and railway sleepers taken out to be replaced by new ones. But if focusing on precast production, the wasted concrete is often uniform with the same strength and w/c-ratio which is very favourable when using it as aggregate.

Interest in recycling all the wasted concrete back into new concrete production is high. The demand from society in terms of reuse of waste concrete from a production instead of depositing it will increase in the future. The importance of this topic is illustrated by the extensive research published in literature, e.g. /Collins 1998, CUR 1997, Hansen 1986, Hoffmann 2012, Karlsson 1997/.

2. AIM AND GOAL

The aim with this project is to crush hardened concrete waste from different types of precast elements and evaluate how to use it as aggregate in production of new concrete. The focus is set on self-compacting concrete (SCC) only. Central issues to investigate are how the crushing technique will influence the particle shape, the resulting particle size distribution (PSD) curve and how to create an optimal curve. Another interesting aspect is to evaluate if the powder fraction is reactive and if it can be used as powder for SCC. Studies will show possible limits in the use of crushed concrete as aggregate in terms of durability and relative to the demands according to EN 206-1. A special focus will be set on how to increase the speed of CO₂-uptake while the material is stored.

The overall project goal is to gain an understanding into the handling and processing aspects in order to achieve a 100% reuse of the discarded concrete back into production.

3. PROJECT GROUP

The group of partners in this project are represented by a research centre: The Swedish Cement and Concrete Research Institute (CBI), by academia: Lund University (LU), by industry: Cementa AB, Strängbetong AB (project leader) and Abetong AB, and by a research funding body: The Development Fund of the Swedish Construction Industry (SBUF).

As described in more detail in the following section, the industrial partners (Strängbetong and Abetong) will contribute with crushing and fractioning the waste concrete and delivering it to the research partners. At later stages they will also provide possibilities to perform full-scale tests in their factories. CBI and Cementa will carry out the laboratory tests while LU will focus on the CO₂-uptake.

4. PROJECT OUTLINE

The work will be split into several stages. Concrete from hollow core slabs and concrete from older rejected and replaced railway sleepers will be crushed.

4.1 Crushing

The technique when crushing a material such as hardened concrete has to be controlled in order to achieve an optimized PSD-curve /Karlsson 1997/ and to enable 100% to be used in production of new concrete. Materials will be HC-slabs from Strängbetong and railway sleepers from Abetong. The waste concrete will first, at each respective factory, be separated from reinforcement and other imbedded items and then coarsely crushed. The material will then be transported to a secondary crusher facility to be further crushed and fractionized. The fractions

will be 0-4 mm, 4-8 mm and 8-16 mm. These fractions are then sent to the other partners for tests and evaluations. During the second year of the project, it is planned to also crush concrete in a VSI-crusher to obtain more cubicized particles.

4.2 CO₂-uptake

The different fractions mentioned will be stored in various ways, and methods of how to increase the air penetration without any mechanical need will be tested. The purpose is to quantify the CO₂-uptake and how to increase this relative to time.

4.3 Particle characterization

Both coarse (> 4 mm) and fine aggregates (< 4 mm) will be characterized in terms of particle size distribution, particle shape and porosity. The characterization will be done in such a way that the parameters can be used as input to the proportioning software which is under development by CEMENTA.

4.4 Fresh concrete tests

How the crushed concrete works as aggregate in SCC will be evaluated systematically. Proportioning will be done with both fine and coarse crushed particles in combination with the aggregate normally used in the respective factories.

Use of the finest crushed powder particles < 0.125 mm on SCC fresh properties (rheology) will be evaluated in a special project study. This will first be done on mortar and then scaled up to concrete. Systematic tests on replacing the normally used limestone powder with recycled powder will be carried out. The use of this powder material in hollow-core concrete (very stiff consistency) will also be done.

Some of the questions to be answered are how the crushed material influences the required paste volume, superplasticizer demand and the slump loss.

4.5 Hardened concrete tests

Besides the obvious tests of compressive strength and strength development, also porosity and shrinkage will be investigated. Durability tests will focus on freeze-thaw resistance, carbonation and chloride transport.

4.6 Production tests

After the extensive laboratory studies, concrete with recycled aggregate will be tested in full-scale elements in the factories. Different batches with various amount of fine and coarse aggregate (5% or 10%) will be tested. This will not be done in real production but in order to produce elements, from which samples can be taken for characterization of hardened properties. Both fresh and hardened properties will be recorded and compared with today's production. Focus for the fresh properties are workability and slump-loss.

4.7 Logistics

It will be investigated how to store the crushed concrete in a way as to optimize the logistics. Is it possible to store it under a roof and then use it in combination with "normal" aggregates for production of new concrete? Another question is how to ensure that the material is saturated with water after the carbonation process is finished, and what is the consequence if this cannot be achieved? New surfaces are activated during crushing and possible unhydrated cement will come to surface. What does this mean when storing fine fractions, should it be treated as cement?

5. DISSEMINATION OF RESULTS

The results from this two-year project will be disseminated both nationally in Sweden in relevant journals and also on information days by Cementa and CBI. Some results from part of the project, e.g. on use of fine recycled powder for SCC and/or on CO₂-uptake will be submitted to international journals. A project report for SBUF will be written in form of guidelines.

REFERENCES

Collins, R., 1998,

“Recycled aggregate pushing back the barriers”, *Quarry Management*, 25, pp. 23-26.

CUR, CSTC, and Eerland Recycling, 1997,

“Use of Recycled Materials as Aggregates in the Construction Industry – State-of-the-Art in Europe”, Report on Brite EuRAM III Industrial and Materials Technologies, Contract BRRT-CT-0048.

Hansen, T. C., 1986,

“Recycled aggregates and recycled aggregate concrete second state-of-the-art report developments 1945-1985”, *Materials and Structures*, Vol. 19, Issue 3, pp. 201-246.

Hoffmann, C., 2012,

“Recycled concrete and mixed rubble as aggregates: Influence of variations in composition on the concrete properties and their use as structural material”, *Construction and Building Materials*, 35, pp. 701-709.

Karlsson, M., 1997,

“Recycling of Concrete - A preliminary study”, Chalmers University of Technology, Division of Building Technology, Göteborg, p. 58.

Engineering Properties of Palm Kernel Shell Fiber Reinforced Concrete



Kayode Bamikole OLAWUNI
MS, Civil Engineering
Eastern Mediterranean University,
Gazimagusa, TRNC via Mersin 10, Turkey.
kayode.olawuni@cc.emu.edu.tr
kayode.olawuni@yahoo.co.uk



Özgür EREN
Professor
The Chair, Civil Engineering Department,
Eastern Mediterranean University,
Gazimagusa, TRNC via Mersin 10, Turkey.
ozgur.eren@emu.edu.tr

ABSTRACT

In this study, Palm Kernel Shell (PKS) partly replaced with conventional aggregates. The effect of PKS and steel fibers were experimented. Several concrete mixes were prepared with different PKS coarse aggregates amount of 25%, 50% and 75% that replaced by mass of 10 mm size conventional coarse aggregates. PKS fine aggregates amount of 10%, 7.5% and 5% replaced by mass of conventional fine aggregates. This procedure was imitated for target mean strength of 30MPa. The compressive strength, Schmidt hammer and splitting tensile strength of concretes was performed at the curing age of 28 days.

Key words: aggregates, fiber, mix design, testing.

1. INTRODUCTION

Palm tree, mostly found in the Asia and Africa, are the mother of Palm Kernel Shell (PKS). Over four decades, counted as agricultural waste dumped near the local factory. For many years, PKS has no negative effect to weather condition and exposure. About three decades ago, the importance of PKS was unleashed and unwrapped by researchers. Having discovered its' properties, researches has been carried out to test how useful it is. Over the years, the carried out tests and experiments showed that PKS can successfully served in the construction industries as a lightweight aggregate concretes and also as sub base materials for road construction[Basri et.al. 1999]. During the crude palm oil processing, the fruit's flesh then melted through a steaming treatment. The residual nuts crashed to extract the seeds or Kernels. This is achieved either by manual or mechanical cracking. The crashed shells are Palm Kernel Shells (PKS), a virgin biomass with a high calorific value [ASTM D5865-02. 2002]. It was reported that almost 4 million tons of PKS were produced annually in Malaysia [Alengaram et.al. 2013].

1.1 Palm Kernel Shell

This palm kernel shell is the hard endocarp that surrounds the palm kernel seed. It is light and naturally size. Many researchers have proved its importance in different ways ranges from construction industries According to the previous study; PKS as lightweight aggregate were used as coarse aggregates in making lightweight aggregate concrete. However, this study considered PKS lightweight aggregates as both fine aggregates and coarse aggregates for lightweight concrete production.

2. MATERIALS

2.1 Natural Aggregates

Crushed limestones used for both fine and coarse aggregates are termed as natural aggregates.

PKS Aggregates

The PKS aggregates obtained from agricultural waste from Nigeria.



Figure 2.1 (a) PKS Coarse Aggregate



(b) PKS Fine Aggregate

2.2 Water

The water used in all mixes was potable water from the pipeline in the material laboratory of the University.

2.3 Cement

A well-preserved type 32.5 Portland cement was used.

2.4 Steel Fibre

Double hook-end hybrid steel fibres of length 60 mm, diameter 0.4 mm and an aspect ratio of 150 were used in this study. The aspect ratio is high due to the hybrid nature of the steel fiber.

3. MIX PROPORTIONS.

Table 3.1 – Concrete Mix Proportions [BS EN 206-1].

| Mix ID | Cement(g) | Water(g) | S/Fiber(g) | Normal Aggregate (g) | | | | PKS Aggregate (g) | |
|--------|-----------|----------|------------|----------------------|------|------|------|-------------------|------|
| | | | | Fine | 10mm | 14mm | 20mm | Fine | 10mm |
| CMix | 390 | 225 | - | 900 | 260 | 390 | 216 | - | - |
| C250M1 | 390 | 225 | 19.5 | 810 | 195 | 371 | 216 | 90 | 65 |
| C50M2 | 390 | 225 | 39 | 833 | 130 | 351 | 216 | 68 | 130 |
| C75M3 | 390 | 225 | 59 | 855 | 65 | 332 | 216 | 45 | 195 |

4. RESULTS AND DISCUSSION

4.1. Workability

The mixtures have the same water/cement ratio. The increase in the slump was due to the PKS aggregates added the more the percentage of PKS coarse and fine aggregates used in proportion of conventional aggregates, the more the slump recorded.

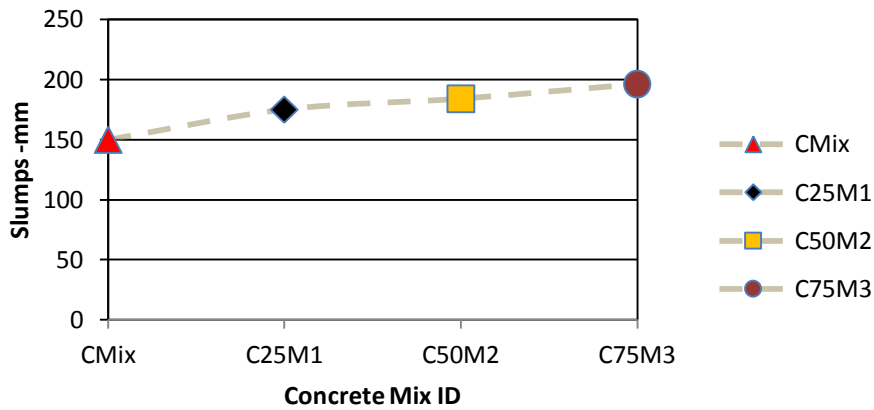


Figure 4.1: The PKS concrete slumps.

4.2. Compressive Strength

The percentage of the palm kernel shell has effect on the concrete compressive strength. These results indicated that all the concrete specimens containing PKS aggregates have low compressive strength.

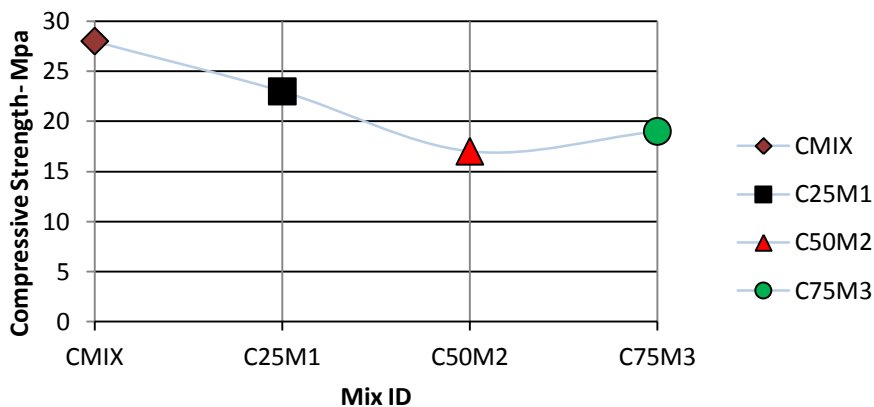


Figure 4.2: Compressive Strength.

4.3. Splitting Tensile Strength.

The control mix has splitting strength of 3.76 MPa. However, specimen with less PKS percentage has recorded higher value of 2.58 MPa.

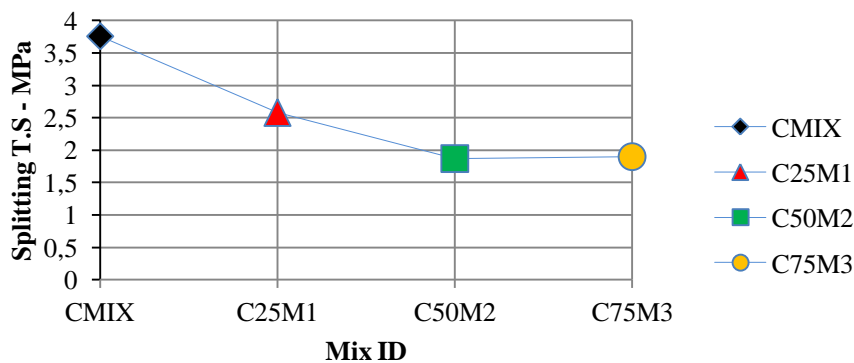


Figure 4.3: Splitting Tensile Strength.

4.4. Rebound (Schmidt) Hammer Test.

The result of this test shows that specimen without PKS has less surface strength than those with PKS aggregates. Irrespective of the amount of PKS present in each sample, the specimen that has PKS almost has the same measurement of surface hardness. The specimen with highest PKS replacement has the highest surface hardness. However, specimen with 25% and 50% PKS replacement has almost the same surface hardness.

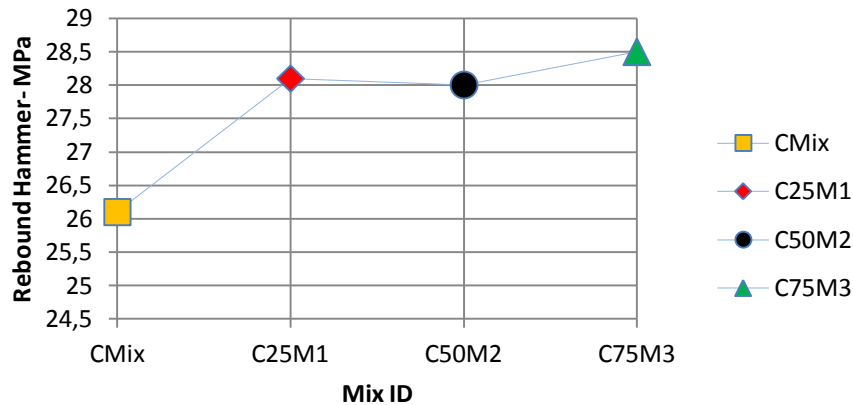


Figure 4.4: Rebound Hammer Test.

5.0 CONCLUSION

Based on the results of the experiments above, the following conclusions were drawn.

1. The entire mix has the same water/cement ratio. However, the increase in slump was due to the percentage of PKS present in the concrete [Fig. 4.1].
2. The reduction in compressive strength of the samples was due to the percentage of PKS present in the sample. In addition, C25M1 that contained 25% PKS coarse and 10% PKS fine aggregates has recorded more compressive strength [Fig. 4.2].
3. The reduction in splitting tensile strength was recorded. This was due to the present of PKS in the concrete samples. C25M1 has higher splitting tensile strength than C50M2 and C75M3. However, C75M3 has recorded more strength than C50M2 due to the present of high percentage of hybrid steel fiber and low PKS fine aggregate [Fig. 4.3].
4. The samples C25M1, C50M2 and C75M3 have more surface strength than CMix. This shows that concrete with PKS replacements has more surface strength than concrete that has no PKS aggregate. [Fig. 4.4].

REFERENCES

- Alengaram, U.J., Al Muhit, B.A., Jumaat, M.Z., 2013
Utilization of oil palm kernel shell as lightweight aggregate in concrete. Science direct, construction and building materials, 2013(38) 161-172.
- ASTM D5865-02, 2002
Standard test method for Gross Calorific value of Coal and Coke.
- Basri, H.B., Mannan, M.A., Zain, M.F.M., 1999
Concrete using waste oil palm shells as aggregate. Cement and concrete research 1999; 29(4): 619-622
- BS EN 206-1
Standard Method for design of fresh concrete mix.

Pioneering Methods for Control of Aggregates using Machine Vision, Spectroscopy and Statistical Modelling



Thorgeir S. Helgason M.E.Sc. Managing Director
 Petromodel ehf, Ofanleiti 2,
 IS - 103 Reykjavik
 E-mail: thorgeir.helgason@petromodel.is



Dipl.-Ing. MMag. DDr. Vera Hofer Professor
 Institute for Statistics and Operations Research,
 University of Graz, Universitätsstr. 15,
 AT - 8010 Graz
 E-mail: vera.hofer@uni-graz.at



Dipl.-Ing. Dr.techn. Holger Bach Project Manager
 Petromodel ehf, Sparbersbachgasse 13,
 AT - 8010 Graz
 E-mail: holger.bach@petromodel.is

ABSTRACT

PETROSCOPE-4D is a measuring equipment that uses machine vision for measuring the 3D size and shape and VIS-spectroscopy for the petrographic composition of aggregates and is based on patented methods, and it offers a statistics module to predict physical and mechanical properties. The combined testing with these two methods allow for a groundbreaking way to monitor the quality of aggregates. Most recently, these new solutions have been used in large research projects on the endurance of railway ballast for Austrian Railways (ÖBB) and are now being evaluated by ÖBB for uptake as a new regular quality control tool.

Key words: Aggregates, Concrete, Control, Modelling, Petroscope, Testing

1. INTRODUCTION

The establishing of Petromodel ehf and the technical solutions of the company are based on the governing principles of materials science (Helgason 1990; Hofer et al. 2006). The development started with an equipment to measure the „internal structures“ of aggregates, in just one run, and is now in its third version as PETROSCOPE-4D (Helgason et al. 2006); also the company developed the statistical software Techmodel to predict mechanical properties of the same aggregates and this software is now being updated for third time and offered as an add-on module with PETROSCOPE-4D.

2. PETROSCOPE-4D –MEASURING FUNDAMENTAL PROPERTIES IN ONE RUN

The instrument (Fig. 1) consists of a feeder module that delivers the sample particle-wise to the spectrometer. For each particle, spectral data is obtained – mainly in the visible range ($\lambda = 350 - 1100$ nm). The subsequent 3D camera scan determines each particle's precise shape with an accuracy of approx. 0.15 mm. A powerful software, PS4D-TEST&VIEW (Fig. 2), then calculates the particle's volume, surface area, sieve size, its form (shape) characteristics according to Zingg (1935), and angularity using Powers' (1953) approach as adopted by Lee et al. (2007) for use in the PETROSCOPE-4D. At the same time, gradually, sample-based values are being calculated (Fig. 3): Distribution of particle sizes, angularity classes, form classes and rock types, both based on volume (i.e. mass) and number of particles. And finally, flakiness index (EN 933-3) and shape index (EN 933-4) are calculated.

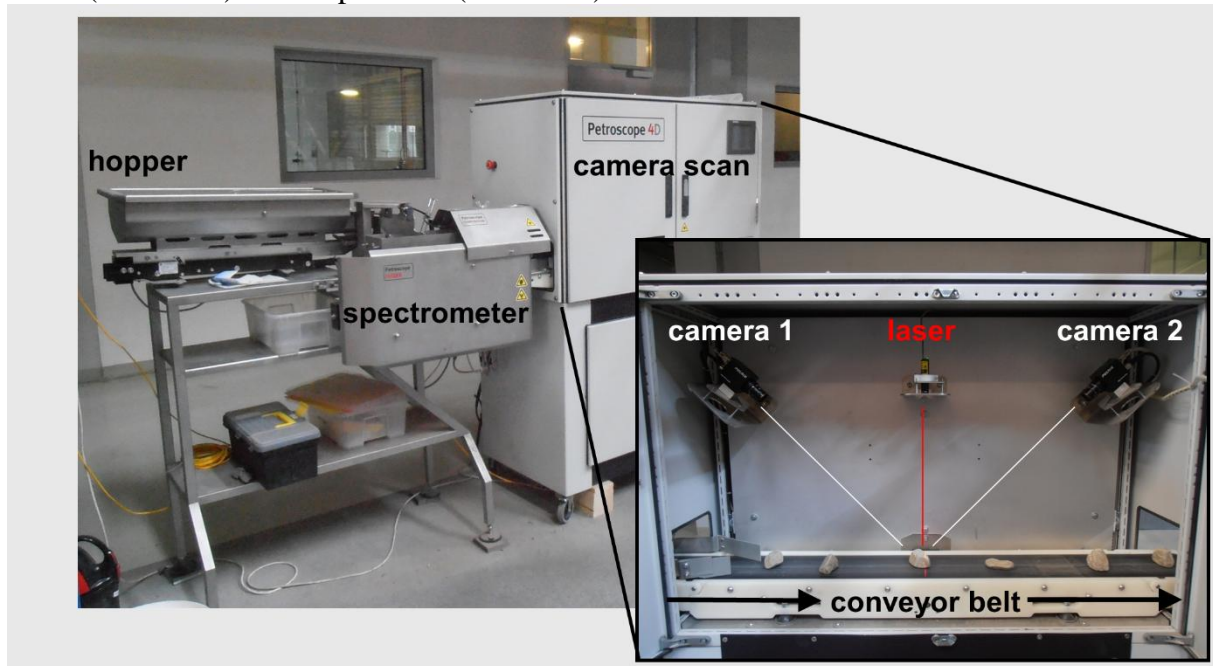


Figure 1 – PETROSCOPE-4D - general layout.

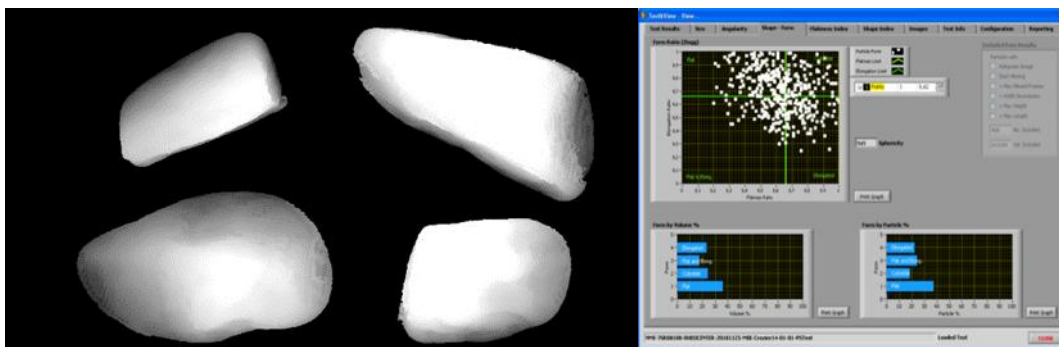


Figure 2 – PS4D-TEST&VIEW showing rendered 3D-models of measured particles (left) and a screenshot (right).

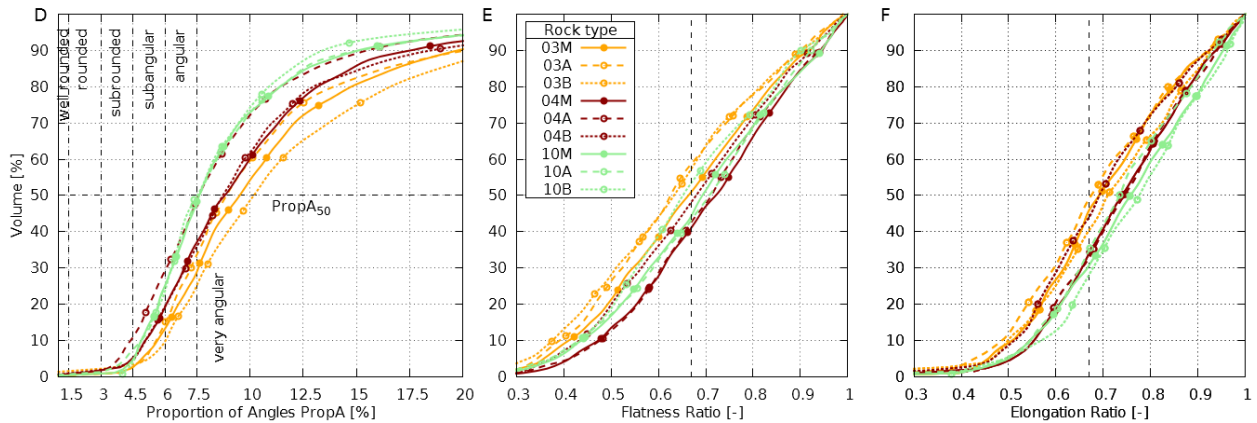


Figure 3 – Cumulative curves of angularity class, flatness ratio and elongation ratio for nine samples of railway ballast with different rock types and varieties from three quarries in Austria.

3. PS4D-STATISTICS – PREDICTING MECHANICAL PROPERTIES

First step is to prepare reference samples for the quarry, area or country, and then to measure the mechanical parameters of these samples as well as the above mentioned fundamental properties using the PETROSCOPE-4D. Then, the powerful statistical add-on software, PS4D-STATISTICS estimates the respective mechanical values of new samples (Hofer et al 2013) as soon as they have been tested with PETROSCOPE-4D. As an example, for ÖBB, models have been established (Fig. 4) for predicting the LA-coefficient (EN 1097-2, clause 5), micro-Deval coefficient (EN 1097-1) and a modified version of the impact value (EN 1097-2, clause 6) for 14 quarries with nine different rock types in Austria (Hofer and Bach 2013).

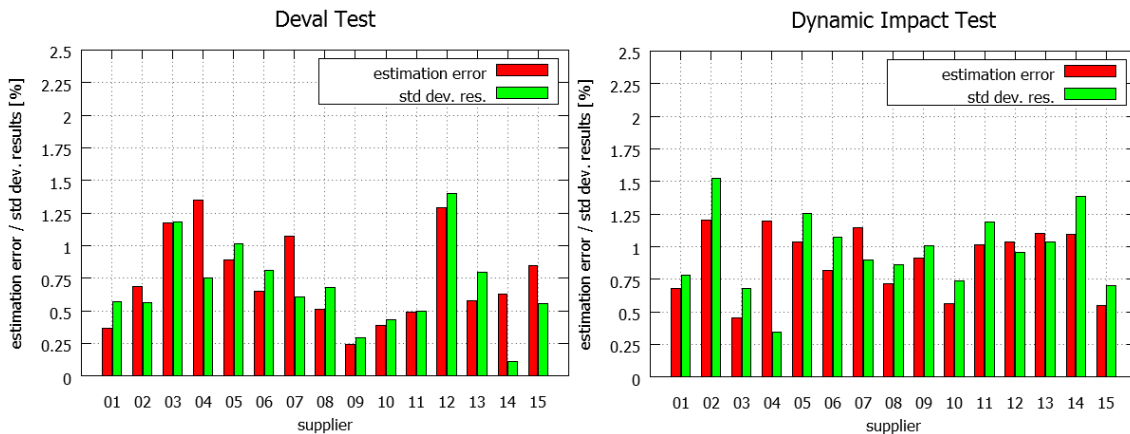


Figure 4 – Estimation error of PS4D-STATISTICS (measured minus predicted value; left bar) and standard deviation (right bar) of measured results for two test series, the micro-Deval coefficient (left) and impact value (right).

4. GROUNDBREAKING QUALITY CONTROL METHOD

The use of PETROSCOPE-4D and PS4D-STATISTICS allows for a totally new way of control in the aggregates industry. This methodology is described, in the case of railway ballast, in a submitted paper (Hofer and Bach 2012). It is also important to stress here that the new testing solutions described can in fact be used for Factory Production Control (FPC) of e.g. concrete aggregates (EN 12620); this is so as “testing within FPC may use either the standard reference tests or other test procedures which have been shown to correlate with those tests.” (FprEN 16236:2011). Besides what is said in this paper regarding correlation of test results (e.g. Fig. 4),

formal validation on the particle size distribution has been performed in USA (Daniel and Lowe 2011) and on flakiness index in Iceland (Gudjonsson 2010). These validations have shown that PETROSCOPE-4D simulates the old methods very well, besides giving totally new results including 3D data for numerical particle models and particle packing modelling.

REFERENCES

Daniel, J.S. & Lowe, J., 2011.

Petroscope Evaluation. Final report submitted to New Hampshire Department of Transportation by Department of Civil Engineering, University of N.H., 10 pp. + appendix.

Gudjonsson, S., 2010.

Results of the validation measurements. Report to the Student Innovation Fund, Iceland, 10 pp. + appendix.

Helgason, T.S., 1990.

Characteristics, properties and quality rating of Icelandic volcanic aggregates. Proceedings of the 43. Canadian Geotechnical Conference, St. Foy, Quebec, 339-346.

Helgason, T.S. et al., 2006.

Apparatus and method for analysis of size, form and angularity and for compositional analysis of mineral and rock particles. World Intellectual Property Organization, publication no. WO 2006/027802 A1. Priority date, 7 September 2004.

Hofer, V., Pilz, J. & Helgason, T.S., 2006.

Statistical Classification of Different Petrographic Varieties of Aggregates by Means of Near and Mid Infrared Spectra. *Mathematical Geology*, 38 (7), 851-870.

Hofer, V. & Bach, H., 2012.

Statistical monitoring for continuous quality control of railway ballast. Preprint submitted to *European Journal of Operational Research*, 25 August 2012, 13 pp.

Hofer, V., Bach, H., Latal, C., Neubauer, AC, 2013.

Impact of Geometric and Petrographic Characteristics on the Variability of LA Test Values for Railway Ballast. *Mathematical Geosciences* 45(6), 727-752

Hofer, V. & Bach, H., 2013.

Analyse des Gleisschotters. Report in German to ÖBB-Infrastruktur AG, Austria, 19 pp. + appendices.

Lee, J.R.J., Smith, M.L., Smith, L.N., 2007.

A new approach to the three-dimensional quantification of angularity using image analysis of the size and form of coarse aggregates. *Engineering Geology* 91 (2-4), 254-264

Powers, M.C., 1953.

A new Roundness Scale for Sedimentary Particles, *J Sediment Petrol*, 23 (2), 117-119.

Zingg, T. 1935.

Beitrag zur Schotteranalyse - Die Schotteranalyse und ihre Anwendung auf die Glattalschotter, Dissertation, Abteilung für Naturwissenschaften an der ETH Zürich, Switzerland, 140 pp.

Research project on manufactured sand for concrete



Rolands Cepuritis
Norcem AS, R&D Department c/o Dept. of Structural Eng., NTNU
Richard Birkelands vei 1A,
NO-7491 Trondheim
E-mail: rolands.cepuritis@norcem.no



Stefan Jacobsen
Dept. of Structural Eng., NTNU
Richard Birkelands vei 1A,
N-7491 Trondheim
E-mail: stefan.jacobsen@ntnu.no



Ernst Mørtsell
NorBetong AS
Heggstadmyra 6,
NO-7080 Heimdal
E-mail: ernst.mortsell@norbetong.no



Sverre Smeplass
Dept. of Structural Eng., NTNU
Richard Birkelands vei 1A,
N-7491 Trondheim
E-mail: sverre.smeplass@ntnu.no



Børge J. Wigum
Depat. of Geology and Mineral Resources Eng., NTNU
Sem Sælands vei 1,
N-7491 Trondheim
E-mail: borge.j.wigum@ntnu.no

ABSTRACT

The paper very briefly reports on progress made in an industrial PhD-project on crushed sand production for concrete investigating how to control the variability with respect to fresh concrete properties. This includes production of model materials from a wide range of relevant Norwegian bedrocks using a new technology (VSI and air-classification), particle characterisation and studies of fresh concrete rheology. The model material production is described and some preliminary results on characterisation are presented. The further work will include development of micro-proportioning technology to exploit the best properties of fillers and adapt these to different types of cement and other binders.

Key-words: Aggregate, Crushed sand, Manufactured sand, Crushed fines, Quarry fines, Static air-classification, Fresh concrete, Rheology.

1. INTRODUCTION AND BACKGROUND

The global aggregate demand is increasing while the available natural (fluvial and glaciofluvial) sand resources traditionally used for concrete production are scarce /Danielsen 2008/. There is therefore a need for research to prepare the concrete industry to use sand produced by crushing rock.

This article briefly introduces the recent R&D work regarding crushed sand that is completed and still in progress by the authors in a close cooperation with the workgroup under the FA

(focus area) 2.3 “High quality manufactured sand for concrete” within the COIN (Concrete Innovation Centre) project (www.coinweb.no).

2. IMPORTANCE OF FINES FOR RHEOLOGY OF FRESH CONCRETE

In order to quantify the impact of the different fractions of sand on rheology of fresh concrete a series of experiments were performed comparing the rheology of concrete by exchanging the fractions 0-0.125, 0.125-2, 2-5 and 5-8 mm using 5 different types of sand (both crushed and natural). The properties of the different sand types were characterized in terms of petrography and physical properties (PSD, density, shape *etc.*).

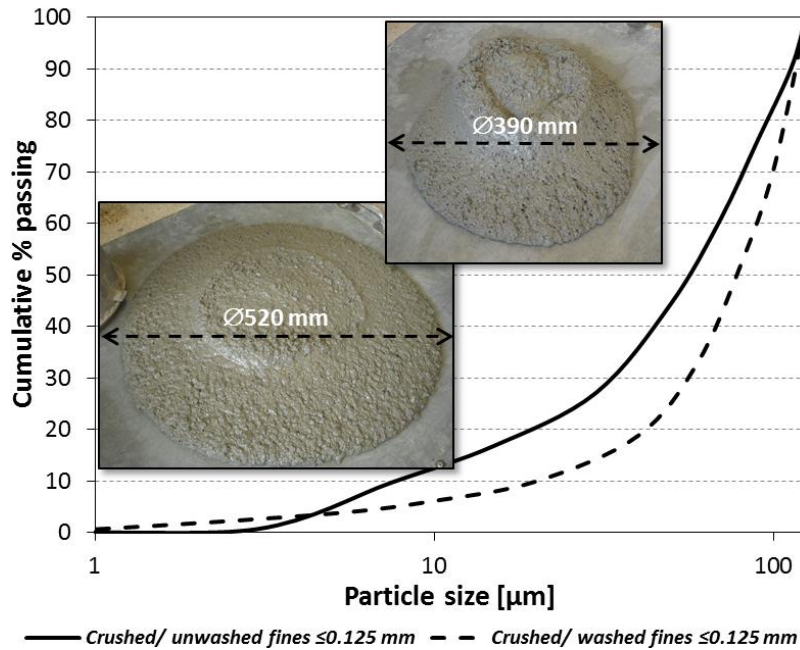


Figure 1 – Influence of crushed sand fines grading on the slump value of fresh concrete; constant w/c ratio of 0.5 and amount of cement (389 kg/m^3), and constant dosage of polycarboxylate based superplasticiser was used for the both mixes.

It was found that exchanging the 0-0.125 mm fraction had by far the largest effect on workability. Figure 1 shows an example from the experiments with exchanging different materials in different fractions. The figure shows the effect of two different crushed fines ($\leq 125 \mu\text{m}$) when everything else is kept constant. The two fines were obtained from the same deposit but one of them was washed, *i.e.* a type of controllable adjustment of the particle size distribution, or classification which is an often used term. As seen from Figure 1, this has a large effect on the concrete workability, affecting the slump flow by 130 mm. Fines constituted only 3.3% (57 kg/m^3) of the total volume of 0/16 mm aggregates. The

reduced flow value of the finer grading can be explained by the adsorption of the free water or surface coverage of lubricating phase on a larger total surface area /Smeplass 2004/ (or reduced packing density /De Larrard 1999 and Sedran 1999/), thus leaving less water available for the lubrication of the cement paste itself.

3. DEVELOPMENT OF NEW CRUSHED SAND PRODUCTION TECHNOLOGY

A set of model-materials (crushed fillers) that represent a wide range of geological variety in Scandinavia have been produced from 10 different rock-types that are used for aggregate production in Norway: granite/ gneiss, mylonitic quartz diorite, quartzite, limestone, dolomite, basalt, anorthosite, and aplite. The final processing included one step of Barmac VSI crushing to generate fines and screening off 0/2 mm crushed sand before using a three step air-classification as shown in Figure 2.

Figure 3 shows an example of a PSD of one of the 0/2 mm materials coming from the VSI crushing and the subsequent fractions after the air-classification according to the flow-chart in Figure 2.

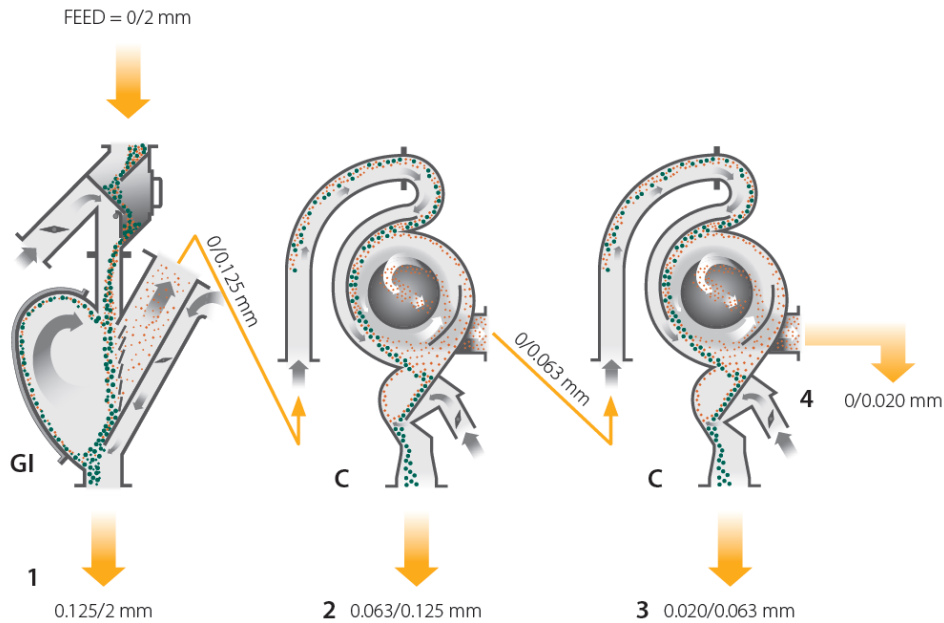


Figure 2 – Flow sheet of the air-classification experiments carried out at the Metso Minerals air-classification lab in Lebanon, PA, USA.

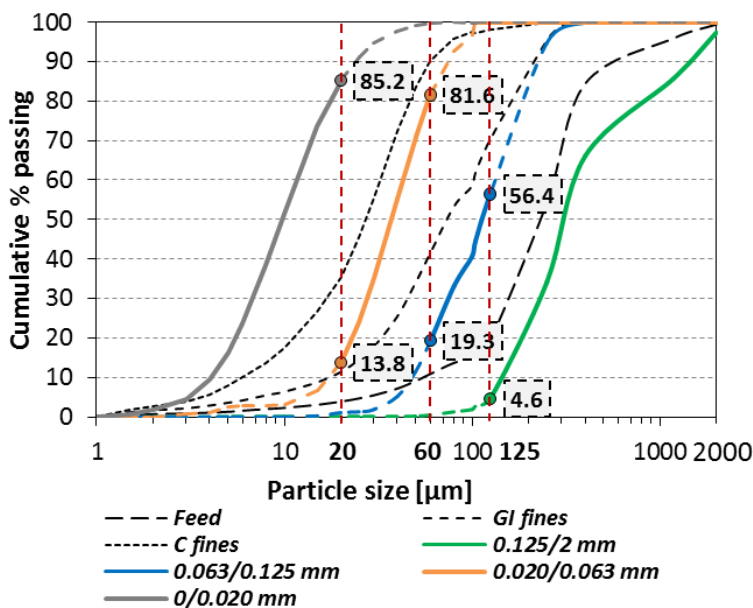


Figure 3 – Typical results of the air-classification experiments for one of the limestone 0/2 mm crushed sands.

4. CONCLUDING REMARKS: FROM MANUFACTURED TO ENGINEERED SAND FOR CONCRETE

By further developing state-of-the art proportioning methods /De Larrard 1999 and Mørtzell 1996/ with increased account of the aggregate properties, the use of crushed aggregate in everyday concrete production will be improved. The following benefits of the increased use of crushed sand, and thus of the ongoing PhD work, will result:

The 10 model materials made in the above process are at present being characterized (PSD, porosity, specific surface, mineralogy, particle shape, particle density *etc.* /Cepuritis et.al. 2013/) before further investigations on rheological properties are carried out.

The goal of the described research approach is to be able to have as good control as possible of the most important aggregate parameters on a scale as close as possible to both full scale aggregate and concrete production.

- No need to landfill crushed fine quarry waste what means less environmental impact and more sustainable aggregate production industry;
- Less wear of the road infrastructure and less noise- due to reduced transportation distances;
- Preservation of natural sand deposits which usually are potential recreational areas with beautiful nature and great biodiversity;
- Preservation of river beds which is another possible place for natural sand extraction;
- Preservation of natural sand deposits which are in a lot of cases "filter" for the ground water (important for drinking water supply).

The study will thus hopefully benefit competitiveness of cement-, aggregate- and concrete industries as well as the user of concrete on site, i.e. contractors, and the owner of the end-product since availability of quality aggregate is fundamental for proportioning and rheology of sustainable, quality concrete in Norway and worldwide.

ACKNOWLEDGEMENTS

COIN project FA 2.3 and the authors would like to use the opportunity to acknowledge Metso Minerals for their deep end enthusiastic involvement in this exciting project. In particular the teams of Research and Test centre in Tampere, Finland and air-classification laboratory facility in Lebanon, PA, US as well as crushing process specialist Tero Onnel, product manager for cone crushers Jouni Mahonen and sales engineer Sven-Henrik Norman for their administrative efforts. The research project would not have been possible without the support from the industrial partners Norstone AS, Franzefoss Miljøkalk AS, Verdalskalk AS, Franzefoss Pukk AS, Elkem Tana AS, Gudvangen Stein AS, Heli Utvikling and Nord-Fosen Pukkverk AS who have supplied the materials for the study. Authors would also like to acknowledge the Inorganic Materials group at National Institute of Science and Technology (NIST) in particular Kenneth A. Snyder, Edward J. Garboczi and Chiara (Clarissa) F. Ferraris for their help and hospitality. In addition, special thanks with respect to providing many interesting ideas and sharing valuable practical experience, should be accredited to Randy Weingart who is pursuing the pioneering work of Advanta® crushed concrete sand development as the director of materials management and research at Luck Stone in the US.

REFERENCES

- Cepuritis, R., Wigum, B.J. and Jacobsen, S., 2013. Crushed aggregate fines for SCC: specific surface & pore size study. In: Wang, K., Shah, S.P. and Khayat, K., eds., Proceedings of The Fifth North American Conference on the Design and Use of Self-Consolidating Concrete, Chicago 12th to 15th of May.
- Danielsen, S.W., 2008. Concrete aggregates from crushed hard rock - why, - where, - how? In: Wigum, B.J., ed., 2008. Manufactured sand – Workshop, Stavanger, Norway, October 30th and 31st 2008. Summary of Presentations. Oslo: SINTEF.
- De Larrard, F., 1999. Concrete mixture proportioning: a scientific approach. London: E & FN Spon.
- Mørtzell, E., 1996. Modelling the effect of concrete part materials on concrete consistency. PhD. D. Norwegian University of Science and Technology (In Norwegian).
- Sedran, T., 1999. Rhéologie et rhéométrie des bétons. Applications à la formulation des bétons autonivelants. Ph.D. Ecole Nationale des ponts et Chaussées (In French).
- Smeplass, S., 2004. Fresh concrete – proportioning. In: Jacobsen S., ed. et al, 2012. TKT 4215 Concrete Technology 1. Course compendium. Norwegian University of Science and Technology. Ch. 4.

Discrepancies in Measured and Modelled E-modulus due to Porous Aggregates. Some Experiences from tests on Icelandic Concrete



Johann A. Hardarson

B.Sc.

ICI Rheocenter, Reykjavik University & Innovation Center Iceland

Arleynir 2-8

IS-112 Reykjavik

E-mail: johann09@ru.is



Thordur I. Kristjansson

B.Sc., M.Sc.

ICI Rheocenter, Reykjavik University & Innovation Center Iceland

Arleynir 2-8

IS-112 Reykjavik

E-mail: thordur.k@nmi.is



Olafur H. Wallevik

Dr. Ing. Prof.

ICI Rheocenter, Reykjavik University & Innovation Center Iceland

Arleynir 2-8

IS-112 Reykjavik

E-mail: wallevik@ru.is

ABSTRACT

Six concrete mixes were made containing: granite, limestone and porous basalt aggregates. Compressive strength and E-modulus tests were carried out. The results show discrepancies in E-modulus compared to those obtained from models, especially when using limestone aggregate and reduction of E-modulus with increasing porosity.

Key words: Elastic Modulus of Concrete, Aggregate, Porous Aggregates, Saturated Surface Dry.

1. INTRODUCTION

Elastic modulus (E-modulus) describes a linear relationship between stress and strain i.e. where Hooke's law applies ("Hooke's law (physics)," n.d.). Concrete however exhibits a non-linear relationship between stress and strain. To simplify calculations engineers attempt to define its E-modulus, using various models. The most common definition of E-modulus for concrete, used in this article, is known as the secant modulus (Neville & Brooks, 2010).

In practice, E-modulus of concrete is measured and empirical equations then fitted to the results. Eurocode 2 (EC2) presents a formula to calculate the E-modulus of concrete (E_{cm}) from the

mean value of concrete cylinder compressive strength (f_{cm}), or from equation (1) (EN 1992-1-1, 2004),

$$E_{cm} = 22 \left(\frac{f_{cm}}{10} \right)^{0.3} . \quad (1)$$

The experiments presented in this paper is intended to elucidate the effect of porosity in aggregates on the E-modulus of concrete. The difference in porosity will be quantitated by the moisture content (MC) of aggregates in saturated surface dry (SSD) condition.

2. MATERIALS AND METHODS

Six mixes were made using different combination of aggregates. The mass-ratio of fine aggregates (< 4.0 mm) was the same in all mixes, 47% of total aggregates. This made the accumulative particle size distribution fairly homogeneous, except maybe for the basalt mix no. 4 (see fig. 1). Abbreviations and aggregate composition can be seen below.

| | |
|---------------|---|
| Granite: | Norwegian granite aggregates. |
| Limestone: | Dune sand and limestone aggregates from Abu Dhabi (United Arab Emirates). |
| Basalt no. 1: | Basalt aggregates from Icelandic inland quarry. |
| Basalt no. 2: | Basalt from Icelandic seabed quarry + inland sand. |
| Basalt no. 3: | Basalt aggregates, Icelandic seabed quarry. |
| Basalt no. 4: | Basalt aggregates from Icelandic inland quarry. |

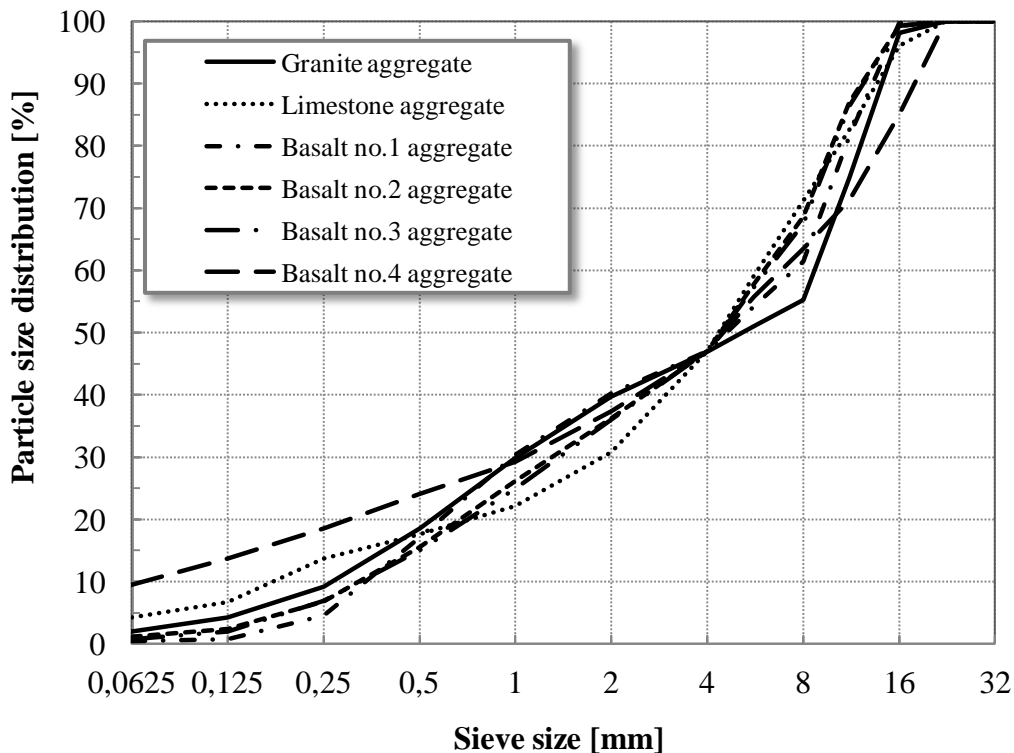


Figure 1 – Cumulative particle size distribution of mixes containing various aggregates.

Cement content in all the mixes was 315 kg/m^3 and water content 174 kg/m^3 , maintaining a water-to-cement ratio of 0.55 and a paste volume of 27.7%. The amount of superplasticizer in

each mix was arrived at with acceptable workability in mind. E-modulus test were done according to the standard (*ISO 1920-10*, 2010). Additional info for mixes can be seen in table 1.

Table 1 – Various values, measured prior to casting

| | SPC-25 ^a (kg/m ³) | Air (%) | Slump (mm) | G-yield (A) | H-plastic ^b (A·s) | SSD ^c (%) |
|--------------|---|------------|---------------|----------------|---------------------------------|-------------------------|
| Granite | 1.0 | 4.1 | 215 | 0.68 | 1.87 | 0.3 |
| Limestone | 1.5 | 3.3 | 190 | 0.73 | 2.10 | 0.6 |
| Basalt no. 1 | 1.0 | 4.3 | 235 | 0.64 | 1.50 | 1.7 |
| Basalt no. 2 | 2.2 | 5.5 | 185 | - | - | 2.9 |
| Basalt no. 3 | 2.0 | 4.2 | 185 | - | - | 3.0 |
| Basalt no. 4 | 1.9 | 3.2 | 170 | 0.92 | 5.21 | 4.8 |

a . Omnicon SPC 25 (polycarboxylic ether)

b. Plastic viscosity

c. Weighted average MC in SSD condition

3. RESULTS AND DISCUSSION

Table 2 shows the results from both 7th and 28th day compressive strength as well as E-modulus. Calculated values, using equation from EC2, are based on 28th day compressive strength.

Table 2 – Measured values, after casting, and compared to calculated E-modulus

| | 7 th day ^c Compressive st. (MPa) | 7 th day E-modulus (GPa) | 28 th day ^d Compressive st. (MPa) | 28 th day E-modulus (GPa) | E-modulus ^e from EC2 (GPa) |
|--------------|--|---|---|--|---|
| Granite | 30.9 | 29.4 | 40.5 | 29.4 | 33.5 |
| Limestone | 31.4 | 35.9 | 41.7 | 39.4 | 33.8 |
| Basalt no. 1 | 31.5 | 28.9 | 42.0 | 30.8 | 33.8 |
| Basalt no. 2 | 37.9 | 27.9 | 47.0 | 28.3 | 35.0 |
| Basalt no. 3 | 38.8 | 27.8 | 51.0 | 29.6 | 35.9 |
| Basalt no. 4 | 41.8 | 19.2 | 54.6 | 22.3 | 36.6 |

d. Mean value of concrete cylinder compressive strength.

e. Value calculated according to equation (1) and without modification factor.

Article 3.1.3 in EC2 states that equation (1) is valid for quartzite aggregates, but the outcome should be reduced by 10% for limestone and increased by 20% for basalt (*EN 1992-1-1*, 2004). It is clear from table 2 that the EC2 model drastically underestimates the E-modulus with respect to limestone aggregates, especially if the reduction factor is used. There is a known discrepancy between EC2 values for E-modulus and measured results, using Icelandic aggregates. This is attributed to the prevailing porosity of Icelandic aggregates, MC in SSD condition from 3 to 8% (Jónsson, 2006). In fact the Icelandic National Annex (INA) to EC2 suggests a correction factors to multiply the values obtained from (1), 0.9 for non-porous aggregates and 0.6 for porous aggregates (*INA to EN 1992-1-1*, 2010). The measured results, for basalt 1-4, fairly agrees with the EC2 model if the correction factors from INA are used.

Figure 2 shows the measured E-modulus plotted as a function of MC in SSD condition. If the values obtained from granite and limestone aggregates (values with low MC) are ignored, a fairly good linear correlation emerges between porosity and E-modulus.

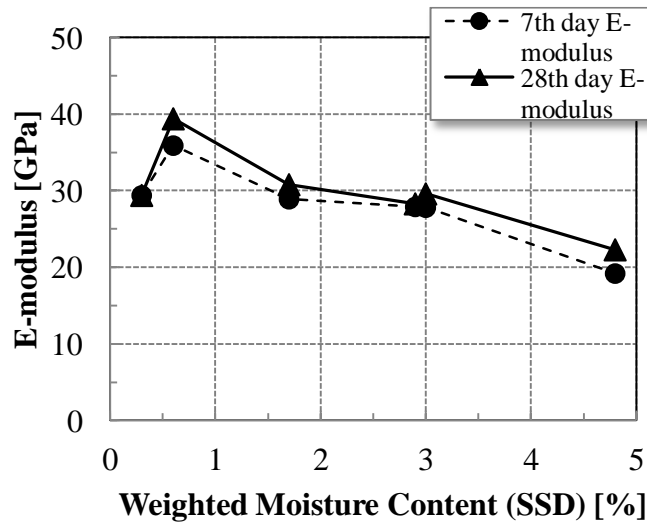


Figure 2 – E-modulus of concrete as a function of aggregate MC in SSD condition

4. CONCLUSIONS

The results indicate substantial discrepancies in measured E-modulus for concrete made from limestone aggregates, compared to estimates based on mean concrete cylinder strength according to EC2.

The measured results from concrete with Icelandic aggregates, basalt 1-4, fairly agrees with the EC2 values if the correction factors from INA, based on aggregate porosity, are applied.

If the values obtained from granite and limestone aggregates are ignored, a fairly good correlation can be seen between aggregate porosity and E-modulus of concrete.

REFERENCES

- EN 1992-1-1:2004: Eurocode 2: Design of concrete structures - Part 1-1: General rules and rules for buildings.* (2004). Brussels: CEN.
- Hooke's law (physics). (n.d.). *Encyclopedia Britannica*. Retrieved May 21, 2014, from <http://www.britannica.com/EBchecked/topic/271336/Hookes-law>
- Icelandic National Annexes to Eurocodes.* (2010) (1st ed.). Staðlaráð Íslands (e. Icelandic Council for Standardization).
- ISO 1920-10:2010 - Testing of concrete -- Part 10: Determination of static modulus of elasticity in compression.* (2010). Geneva: ISO.
- Jónsson, G. (2006). *Formbreytingar í steinsteypu - fjaðurstuðull og skrið - (e. Deformations of Concrete - E-modulus and Creep)* (No. 93). Reykjavík: The Icelandic Building Research Institute.
- Neville, A. M., & Brooks, J. J. (2010). *Concrete Technology* (Second Edition.). England: Pearson Education Limited.

BINDERS, ADMIXTURES, MIX DESIGN AND RHEOLOGY

Analysis of Shear Rate inside a Concrete Truck Mixer as a Function of Drum Charge Volume and Plastic Viscosity



Jon E. Wallevik
B.Sc, M.Sc, Ph.D.
Innovation Center Iceland
Arleynir 2-8
IS-112 Reykjavik
E-mail: jon.w@nmi.is



Olafur H. Wallevik
M.Sc, Ph.D., Prof.
Innovation Center Iceland
Arleynir 2-8
IS-112 Reykjavik
E-mail: wallevik@ru.is

ABSTRACT

In this work, the shear rate is analysed inside a concrete truck mixer. This is done both as a function of concrete drum charge volume and plastic viscosity. The work shows that the shear rate decreases in an exponential manner with increasing drum charge volume. It is also shown that the shear rate decreases with increasing plastic viscosity.

Key words: Concrete truck mixer, mixing energy, drum charge, plastic viscosity.

1. INTRODUCTION

In addition to the mixing energy applied to fresh concrete (i.e. shearing during mixing) [Banfill P.F.G. 2004, Orban, J. 1986, Banfill, P.F.G 1992], the shear history after mixing is also important. This applies especially for binder rich self-compacting concrete. This is due to the influence that the binder has on the overall concrete in terms of thixotropic- and structural breakdown behaviour. The two processes, structural breakdown and thixotropy is well explained in [Wallevik, J.E 2009]. Because of this, the shear rate is analysed inside a drum of a concrete truck mixer. In this manner, one can better understand the effect of transport of fresh concrete, from the ready mix plant to the building site. The shear rate analysis is done as a function of drum charge volume 2.6 m^3 , 5.3 m^3 and 8.6 m^3 . In addition to this, the effect of plastic viscosity is also analysed.

The concrete drum under consideration is the KARRENA 9/5. It is used for example at the premix plant Steypustöðin ehf in Reykjavik. The KARRENA 9/5 has a geometrical drum volume of 15.7 m^3 , but the max rated drum capacity is 9 m^3 . The range of drum speed is between 0 and 14 rpm (i.e. from 0 to 0.23 rps). In this work, the drum speed is set at 0.12 rps. This is about the half of the max drum speed and is meant to represent the rotation during transport (or roughly so). The inclination of the drum relative to the horizontal, is 11 degrees. In the right illustration of Figure 1, is the computational mesh shown for the KARRENA 9/5 drum. On this note, all analysis done here is with the CFD simulation software OpenFOAM.

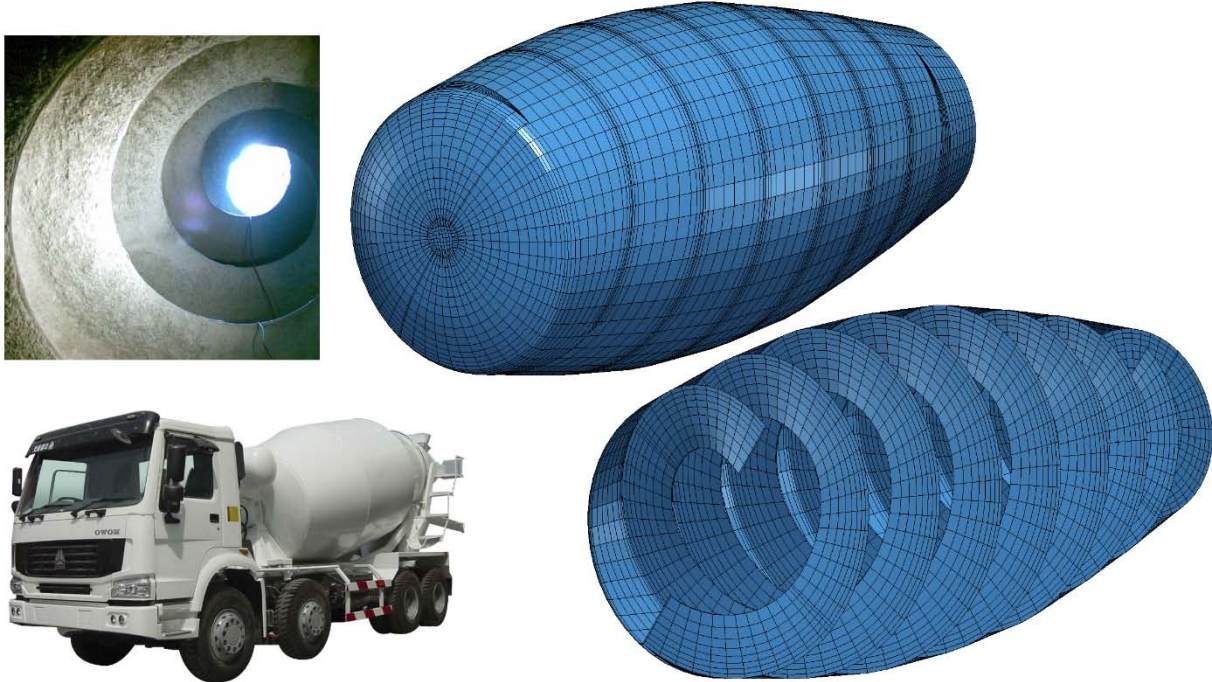


Figure 1 – To the left: Inside a KARRENA 9/5 drum (top); A concrete truck mixer (bottom). To the right: Computational mesh of the KARRENA 9/5 drum.

2. EXPERIMENTAL

As mentioned above, the CFD software used is the OpenFOAM 2.1.0. It is licensed under the GNU General Public License (GNU GPL) and is available at www.openfoam.org. It is written in C++ and as such, an object-oriented programming approach is used in the creation of data types (fields) that closely mimics those of mathematical field theory [Weller H.G 1998]. OpenFOAM uses unstructured mesh system in Cartesian coordinate system. The no-slip boundary condition (i.e. the Dirichlet boundary condition) is used at all wall boundaries. This is not so unrealistic, as used drum has usually rough surfaces due to older hardened concrete attached to the inside drum wall. An example of this is shown in the top left illustration of Figure 1.

Instead of physically rotating the computational mesh at 0.12 rps, the mesh is kept fixed and the gravity-field \mathbf{g} is rather rotated at this rate. This means that instead of the drum is rotating on a stationary Earth surface, the drum is stationary and the Earth is rotating around the drum. In taking this step, the system (i.e. the computational domain) represents no longer an inertial reference frame [Holton, J.R 1992] (i.e. is now a rotating reference frame). This means that the Coriolis force and the centrifugal force have to be included into the governing equation.

The constitutive equation used here, consists of the Generalized Newtonian Model [Tanner, R.I. 1998], or in short GNM. In [Feys, D 2012], the benefits of the modified Bingham model is discussed for SCC. As such, it is uses as a material model. It should be noted that in this preliminary work, both the yield stress and the so-called c -parameter are set equal to zero.

For 3D incompressible flow where the GNM is valid, it can be shown that the shear rate is calculated as $\dot{\gamma} = \sqrt{2\dot{\boldsymbol{\epsilon}}:\dot{\boldsymbol{\epsilon}}}$. The term $\dot{\boldsymbol{\epsilon}}$ is the rate-of-deformation tensor. In this work, the volume averaged shear rate is used. It is given by

$$\bar{\dot{\gamma}}(t) = \frac{1}{V} \iiint_V \dot{\gamma}(x, y, z, t) dx dy dz \quad (1)$$

The term V is the volume of the concrete sample inside the drum (i.e. the drum charge volume, either 2.6 m^3 , 5.3 m^3 or 8.6 m^3) and the integration $dV = dx dy dz$ is over the same concrete sample. If the shear rate would be constant within the concrete sample, the *volume averaged shear rate* would be the same as the *shear rate*.

3. RESULTS

Figure 1 shows the shear rate Equation (1) plotted as a function of time for the 9 cases, $\mu = 40$, 60 and 100 Pa·s at charge volume of 2.6, 5.3 and 8.6 m^3 . At the start of each simulation, the concrete sample is stationary and therefore the shear rate begins at 0 s^{-1} . With start of rotation, there are some wave generation occurring due to the fact that the concrete sample is being pushed into the front of the drum by the helix geometrical shape of the drum. After about 5 to 10 seconds, equilibrium is obtained in this pushing process, and the wave generation stops.

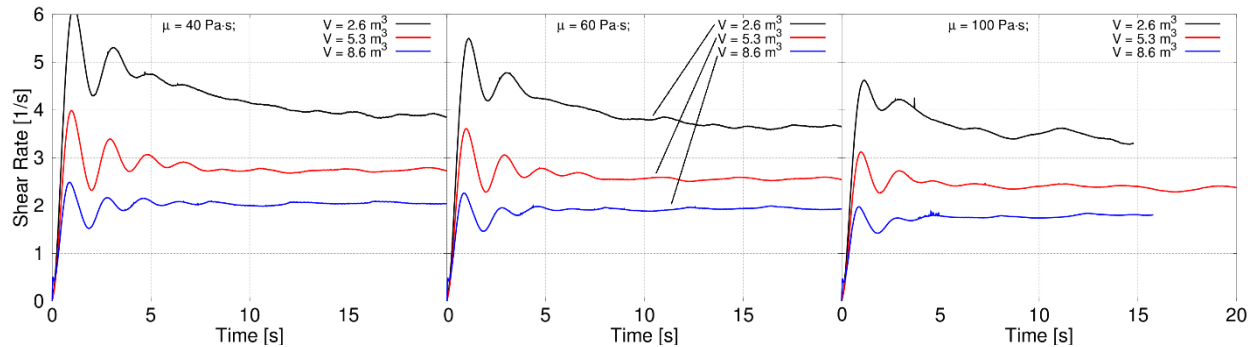


Figure 2 – Volume averaged shear rate Equation (1) plotted as a function of time.

What is interesting to note about the results in Figure 2 is that the shear rate (by Equation (1)) is less dependent on the plastic viscosity and more dependent on charge volume. By time integrating Equation (1) as shown with the following

$$\dot{\gamma}_t = \frac{1}{(20\text{s}-10\text{s})} \int_{10\text{s}}^{20\text{s}} \bar{\dot{\gamma}}(t) dt \quad (2)$$

and thereafter plotting the results as a function of charge volume and plastic viscosity μ , Figure 3 is obtained. There, it is clearly shown how the shear rate decreases in an exponential manner with increasing charge volume. It also shows how little effect the plastic viscosity has on the shear rate, relative to the volume concrete inside the drum. It should be noted that the integration in the above equation, started at 10 seconds and not at 0 seconds. This is due to the fact that equilibrium in shear rate is obtained at 10 seconds (or roughly so) in Figure 2, which represents shear rate during transport, from the ready mix plant to the building site.

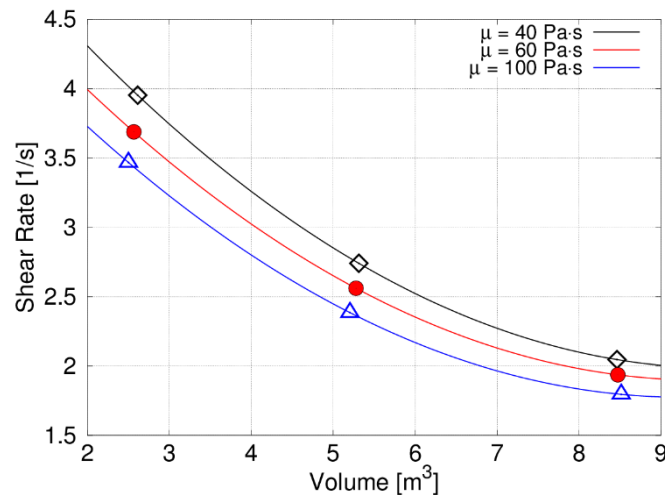


Figure 3 – Shear rate (by Equation (2)) as a function of charge volume and plastic viscosity μ .

4 CONCLUSION

The shear rate of concrete, inside the concrete drum, decreases in an exponential manner with increasing charge volume. This behaviour can be considered important to note for concretes sensitive to shear history. That is, during the transport of such concretes, from the ready mix plant to the building site, a different rheological condition might be present during casting of the same concrete mix design (i.e. of the same such concrete family).

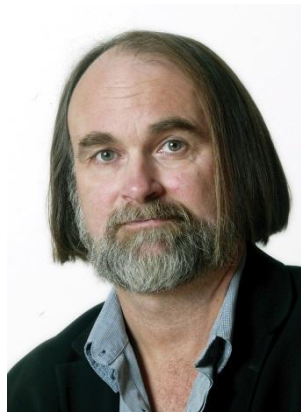
REFERENCES

- Banfill, P.F.G. 1992
 “Structural breakdown and the rheology of cement mortar”, Proc. XIth Int. Congress on Rheology, Elsevier, 1992, pp. 790-792.
- Banfill, P.F.G. & Swift, D.S. 2004
 “The effect of mixing on the rheology of cement-based materials containing high performance superplasticizers”, Annual Transactions of the Nordic Rheology Society, vol. 12, 2004.
- Feys, D., Wallevik, J.E., Yahia, A., Khayat, K.H. & Wallevik, O.H., 2012
 “Extension of the Reiner-Riwlin equation to determine modified Bingham parameters measured in coaxial cylinders rheometers”, Mater. Struct., vol 46, 2012, pp. 289-311.
- Holton, J.R., 1992
 “An Introduction to Dynamic Meteorology”, 3rd edition, Academic Press Inc., USA, 1992.
- Tanner, R.I. and Walters, K., 1998
 “Rheology: An Historical Perspective”, Elsevier Science B. V., Netherlands, 1998.
- Orban, J., Parcevaux, P., Guillot, D., 1986
 “Influence of shear history on the rheological properties of oil well cement slurries”, Proc. 8th Int. Congress on the Chemistry of Cement, vol. 6, 1986, pp. 243-247.
- Wallevik, J.E., 2009
 “Rheological properties of cement paste: thixotropic behavior and structural breakdown”, Cement and Concrete Research, vol. 39, 2009, pp. 14 - 29.
- Weller H.G., Tabor G., Jasak H., Fureby C., 1998
 “A tensorial approach to computational continuum mechanics using object-oriented techniques”, Comput. Phys. vol. 12, 1998, pp. 620 - 631.

SCMs and plasticizers: A study on their effects on the rheology and early age hydration of blended cements



Dr. Serina Ng
Research Scientist
Richard Birkelandsvei 3
7465 Trondheim, Norway
E-mail: serina.ng@sintef.no



Prof. Dr. Harald Justnes
Chief Scientist
Richard Birkelandsvei 3
7465 Trondheim, Norway
E-mail: harald.justnes@sintef.no

ABSTRACT

The dispersing effectiveness of five admixtures was investigated in two blended cement systems containing fly ash and calcined marl respectively. Investigations were performed employing rheological studies using Physica MCR 300 rheometer, hydration profiling up to 24h via isothermal calorimetry and packing density analysis through centrifugal consolidation. It was found that the rheological and hydration properties of fly ash blended cements mainly deviated from that of an ordinary cement by the degree of fly ash replacement, whereas calcined marl affected the cements both by adsorbing large quantity of water and consuming the plasticizers from solution, rendering them unavailable for dispersion.

Key words: Admixtures, Blended cements, Plasticizers, Rheology, Hydration

1. INTRODUCTION

Creation of a green and eco-friendly environment is a very distinct trend in the concrete industry nowadays. One of the methods in achieving this is through the usage of supplementary cementitious materials (SCMs) in replacement of the CO₂ rich clinker phases /Cement Technology Roadmap 2009/ present in cement. This replacement can and have generated many changes in the concretes, both involving chemical and mechanical properties /Alonso 2013/. To combat this change, a study to gain a better understanding of two key features; rheology and early age of hydration of such systems was undertaken as part of the ongoing workgroup 'Binders with low emission and reduced resources consumption' in the COIN consortium.

For this purpose, five different commercial plasticizers were investigated in two different blended cements systems, fly ash (FA) and calcined marl (CM). The polymers include a

lignosulfonate (LS), a naphthalene sulphonated - formaldehyde polycondensate (NSF) and three different polycarboxylic ethers (PCEs). High amounts of SCMs replacement, namely 20, 40 and 60% replacement by weight of OPC were investigated. A commercial FA cement containing ~20% FA was utilized as a comparison.

This paper gives a summary of the results obtained.

2. MATERIALS AND EXPERIMENTAL

An ordinary Portland cement, a fly ash and a marl calcined at 850 °C were employed in this investigation. The OPC and FA were supplied by Norcem A.S. (Brevik, Norway), while the calcined marl was from Saint-Gobain Weber (Oslo, Norway). As dispersants, five commercial plasticizers were investigated, namely a purified sodium LS (Borregaard AS, Sarpsborg/Norway), a NSF (Sika AS, Sketten/Norway), and three sets of PCEs (NRG, SX and SRN from Mapei Escon AS, Sagstua/Norway). All materials were utilised as per obtained.

For preparation of the blended cements, the OPC and FA/CM were manually mixed in the ratio of 4:1, 3:2 and 2:3 to produce blended cements with FA/CM content of 20, 40 and 60% respectively. These blended cements were denoted as FA20, FA40, FA60, CM20, CM40 and CM60 respectively. Pure OPC and FA/CM were investigated too. The w/b utilised was 0.36.

Rheological analysis was performed employing the principles of a parallel plate rheometer, whereby viscosity, yield stress and flow resistance of the pastes were determined. The flow resistance (FR_2) which represented the amount of work performed to shear the paste was calculated from the area under the down flow curve measured over the range of shear rates from 2 to 150s⁻¹. The packing density and water demand were examined by the centrifugal consolidation method, while the heat of hydration of the cement slurries was studied by isothermal calorimetry.

3. RESULTS AND DISCUSSION

3.1 Rheological properties of blended cements

In general, in the neat pastes, fly ash and calcined marl behaved totally opposite to each other when added into the binder system. Addition of fly ash increased the fluidity of the cement pastes, while a reduction was observed when the cement clinkers were replaced with calcined marl (Figure 1a). The former can be justified by the dilution effect of relatively inert fly ash samples, which increased the availability of water in the system for improved rheological behaviour. In the FA cement, its behaviour mimicked that of an OPC owing to the increased surface area designed to compensate for the lower FA reactivity by the producer. On the other hand, the high sorption of water by calcined marl resulted in a drastic decrease in flow.

In presence of plasticizers, similar trend in the interactions of the blended cements with plasticizers was observed relative to the OPC. In general, PCEs dispersed the cement pastes better than NSF and LS. The addition of LS increased the FR_2 of the cement pastes (decrease fluidity of the paste) with increasing dosages as a result of interference in the hydration of C₃A with gypsum.

More specifically, despite the fluidity of the FA blended cements, no bleeding of the cement pastes was detected even for FA60 except when 0.2%bwob of NRG was added. The FA particles were relatively inert and acted as fillers during the first 24h of hydration. Minimal dissolution of FA particles occurred in the paste and is relatively negligible as compared to the bulk reaction of the cement clinkers during early age. Upon addition of plasticizers, the

plasticizing effectiveness was as follow: $SX \geq NRG > SRN > NSF > LS$. Whereas the ability to maintain flow resistance over time was $SRN > SX > NRG > LS \approx NSF$. At higher FA amounts, the interaction of FA particles with plasticizers increased. However, interaction with clinker phases remained dominating. All in all, the NRG was found to be the most effective plasticizer for FA blended cement (Figure 1b).

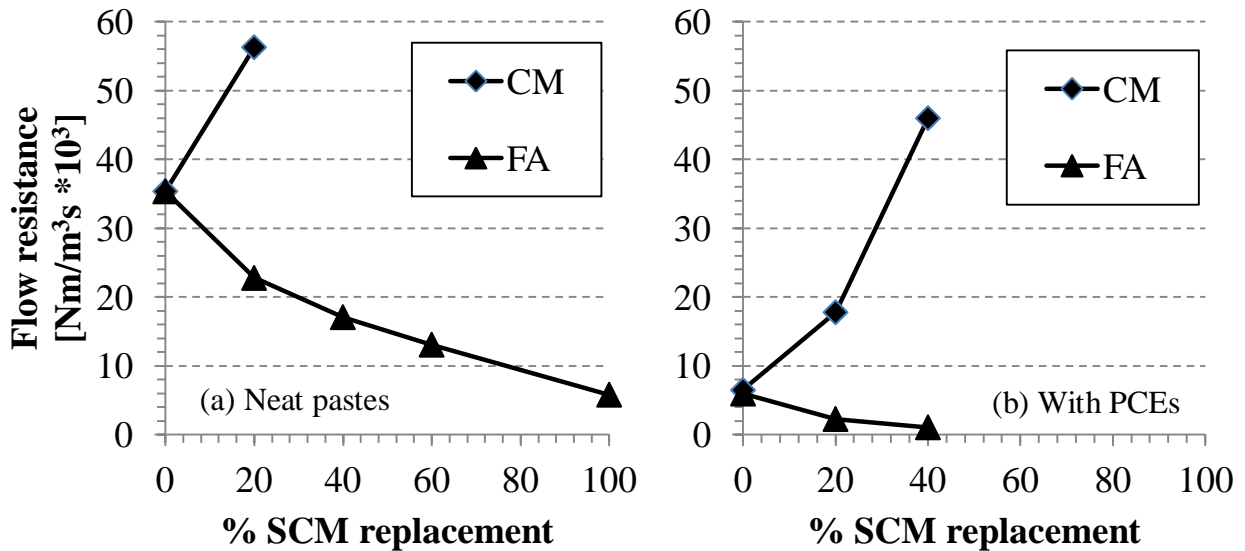


Figure 1 – (a) FR_2 of neat blended cements as a function of SCM replacement (FR_2 of FA cement = $36,200 Nm/m^3s$), (b) FR_2 of blended cements containing 0.2 %bwob of the optimal polymer, NRG or SX, $w/c = 0.36$. No flow for CM60 while FA60 was too fluid for measurements.

In the calcined marl blended cements, calcined marl does not render inert but instead competes with the cement clinkers for plasticizers. The degree of competition varied according to the characteristic of the plasticizers. SX, possessing an intermediate side chain length and charge density proved to be the best dispersing agent here, whereby it was effective from a dosage of only 0.1%bwob in CM20 (Figure 1b). The plasticizing effectiveness of the plasticizers was $SX > NRG > SRN > NAPH > LS$. The effectiveness of the dispersing agents on retaining slump flow was $SRN \approx SX > NRG > LS > NAPH$.

3.2 Heat of hydration of blended cements

Pure FA showed negligible amount of heat released up to 24h. In FA blended cements, a decrease in the cumulative heat of hydration of the cements was observed with increasing fly ash content. The trend in the effectiveness of plasticizers (degree of retardation and change in total heat released) was similar to that observed in an ordinary Portland cement. Pre-blended fly ash cement displayed similar hydration profile as the ordinary Portland cement.

Pure CM, on the other hand, displayed thrice the amount of heat released as that for a pure FA sample. This, in comparison to the heat evolved in cement hydration was however, negligible. In neat blended cements up to a loading of 40% CM, no retardation was observed. Replacement by 60% CM altered the hydration profile of the cement, indicating formation of different hydration products. Addition of plasticizers only affected and retarded the hydration of the cement pastes from a threshold dosage of 0.4% bwob.

4. CONCLUSION

Two very different SCMs, fly ash and calcined marl were investigated here with a series of five different plasticizers. As observed, they behave totally different and care must be taken in the application of both SCMs. Application wise, usage of a dosage of less than 0.2% bwob of plasticizer is recommended in FA blended cements to prevent excessive retardation which can lead to a premature decrease in early strength of the concrete. Whereas, in a CM blended system, more than 0.2% bwob of plasticizer is recommended. At higher replacement percentage, up to 0.8%bwob of plasticizers is needed to disperse the cement. A better method would thus be to synthesize new plasticizers specific for these systems, in the effort to produce an overall low cost and efficient system.

As a general outlook, a ternary cement blend of these two SCMs with cement clinker could be probed as a new binder material. In such a situation, the water retaining capacity of the calcined marl can be compensated by the fly ash, while the gain in initial strength of the paste can be covered by the calcined marl. It will be interesting to investigate the influence of superplasticizers on such a system.

REFERENCES

- Cement Technology Roadmap 2009, "Carbon emissions reduction up to 2050, World Business Council for Sustainable Development", 2009
- Alonso M. M., Palacios M., Puertas F., 2013, "Compatibility between polycarboxylate-based admixtures and blended-cement pastes", *Cem. Concr. Comp.* 35, 2013 pp. 151–162

Hydrostatic pressure to measure sedimentation and bleeding



Ya Peng
MSc, PhD student
Dept of Structural Eng., NTNU
N-7491 Trondheim
ya.peng@ntnu.no



Klaartje de Weerd
Postdoc, Research Scientist
Dept of Structural Eng., NTNU, Sintef
N-7491 Trondheim
klaartje.d.weerd@ntnu.no



Bård Pedersen
Senior principal Engineer
Norwegian Public Roads Administration (NPRA)
N-0033 Oslo
baard.pedersen@vegvesen.no



Stefan Jacobsen*
Professor
Dept of Structural Eng., NTNU
N-7491 Trondheim
stefan.jacobsen@ntnu.no
(* corresponding author)

ABSTRACT

The lower viscosity and high matrix volume of Self-Compacting Concrete (SCC) compared to ordinary concrete can lead to instability in the form of particle segregation, sedimentation and bleeding. This is a problem for the exploitation of all the benefits from the use of SCC for the ready mix industry and contractors. A sensitive HYdroStatic Pressure Test (HYSPT) was developed at the concrete laboratory of NTNU to detect the density differences over time and depth in fresh cement paste and matrix due to sedimentation and bleeding. Based on the comparison with dp/dt plots from HYSPT and the measurements on in-situ solid fraction, HYSPT is validated to be applicable to evaluate the sedimentation process and flocculation state of the paste or matrix. Furthermore, the sedimentation rate by HYSPT measurements was found to coincide with bleeding measurements and estimates from the Kozeny-Carman equation. By the use of HYSPT, the stabilizing effect of various powders and admixtures was analyzed and compared. HYSPT helps to understand the basic mechanism of the stability and can be looked upon as a good tool to study the stability of cement paste and the effect of different materials, such as chemical admixtures and powder additives, on stability.

Key words: stability, sedimentation, bleeding, hydrostatic pressure

1. INTRODUCTION

Self-compacting concrete (SCC) has been described as one of the most innovative developments in the field of concrete technology for its reduced construction costs and improved working

environment /De Shutter 2008/. Unfortunately, SCC cast in-situ in Norway has stagnated at a very low market share. One of the main reasons is probably the low stability and robustness against fluctuations in the concrete production /Vikan 2008/. The origin of the problem is the density difference between the particles and the fluid phase. Consequently, 100% effective solutions for stable SCC, which are usually attempted by adding powder and/or Viscosity Modifying Admixtures (VMA), are hard to achieve. This paper develops and investigates a new test method measuring hydrostatic pressure as a means to detect and characterize the stability of pure and filler modified cement paste (matrix) of various compositions to proceed in the development of more stable SCC.

2. HYDROSTATIC PRESSURE TEST (HYSPT)

Fig. 1 shows the test system with two pressure sensors connected to glass siphons leading into the cylinder filled with a sample of fresh paste or matrix. The accurate pressure sensors (Endress+Hauser Cerabar-S PMC71) compensate for atmospheric pressure variation so that a pure hydrostatic pressure signal is produced. The sensors are connected to an electronic controller which monitors the sensor and transfers the data to the computer.

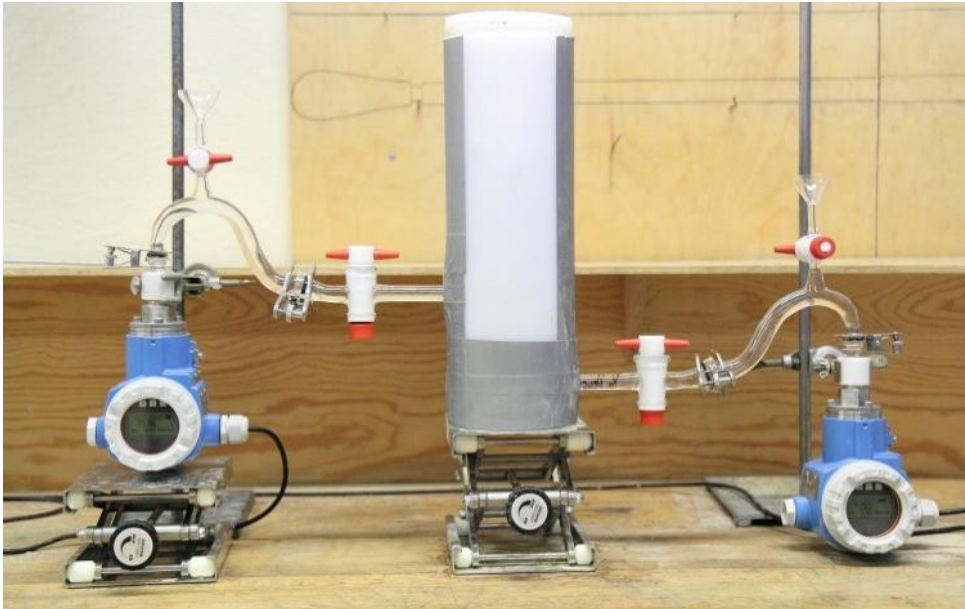


Fig. 1: hydrostatic pressure test set up for cement paste sedimentation measurement

HYSPT relies on the mainly restricted Stokesian settlement of particles causing changes in the solid fraction and thus the fresh density at a given height and time. Generally, the hydrostatic pressure at the given height of a homogeneous suspension can be calculated as the sum of the pressure due to the fluid and particles above the measurement position $P_m = \rho_m g h$, where ρ_m is the mixture density and h is the height of the suspension above the measurement level. Accordingly the density and thus the volume fraction of the suspension can be calculated by monitoring the hydrostatic pressure. During sedimentation the densities at the different levels of the suspension are not constant but increase from top to bottom. Hence, the above simple equation does not hold any longer and other assumptions are needed, for example taking into account bleeding and flocculation. The Richardson-Zaki Equation (R-Z), which explains the particle sinking velocity v_p in a hindered system as given in Eq. (1):

$$v_p = v_t(1 - \Phi)^n \quad (1)$$

Where v_t is the Stokes terminal sinking velocity of the particle in the laminar flow condition, Φ is the solid volume fraction, n is a coefficient depending on the particle Reynolds Number and will normally be 4.65. However, for high concentrated suspensions with serious flocculation, v_p would increase as opposed to in a dispersed system. Therefore, R-Z is too simplified to take into account both flocculation and solidification for all types of cement and limestone mixes. A detailed study of the development and interpretation of the system was recently given /Peng 2014/ including effect of varying powder types and use of admixtures, especially SP, which influence the particle flocculation state and thus change the “effective” particle sizes and sedimentation.

3. HYSPT APPLICATION

Fig. 2 shows an example of the application of HYSPT to detect the particle movement and flocculation state of cement paste. The sedimentation process of four cement pastes with the same solid volume fraction and mixing procedure ($\Phi=0.388$, $w/c=0.5$, cement type Norcem standard cement, CEM I according to EN-197-1) were compared. The sedimentation rate and the time to reach the plateau indicate the flocculation state of the mixtures. It can be seen that, compared with the reference cement paste without SP (polycarboxylate type in this case, PCE) and VMA (PCE0VMA0), the individual addition of SP (PCE0.6VMA0) induces a lower sedimentation rate; the individual addition of VMA (PCE0VMA2.0) results in a higher sedimentation rate; while the combined addition of both SP and VMA (PCE0.6VMA2.0) causes the lowest sedimentation rate. The quite different sedimentation rates were concluded to be a result of particle flocculation /Peng 2013a/. VMA increases the viscosity of the fluid phase in cement paste /Peng 2013a/ but induces a higher particle sinking velocity. This is mainly due to the flocculation of the high-concentrated mixture. However, the addition of SP overshadows the negative effect from VMA on stability, so the increased viscosity by VMA and the dispersing effect from SP contribute to stabilize the cement paste more.

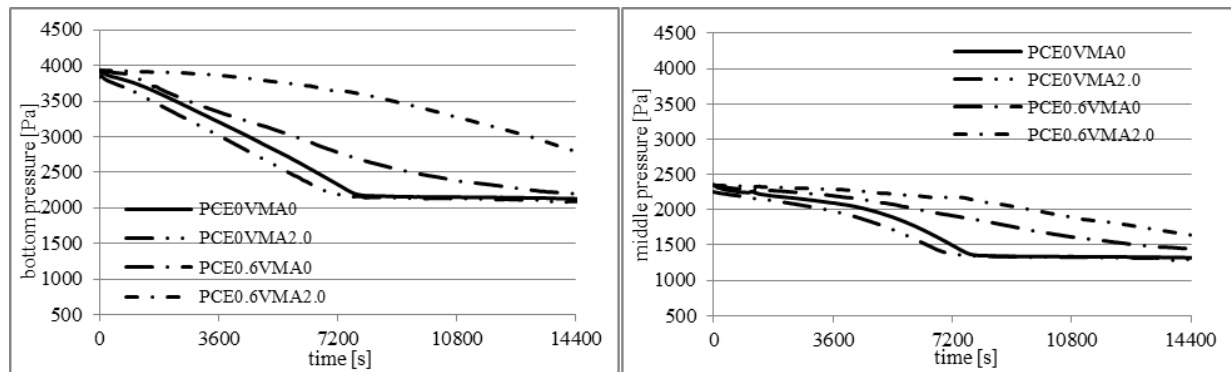


Fig. 2: The pressure vs time curves of cement pastes with or without admixtures including SP and VMA (the number after the admixture is the liquid dosage) [4]

Except for evaluating the sedimentation and flocculation state of cement paste and filler modified paste /Peng 2013b, Peng 2013c/, HYSPT was also applied to investigate bleeding of cement paste or matrix /Peng 2013a/. Also parallel measurements with HYSPT, in situ volume fraction measurements and bleeding tests shows that it is possible to use the HYSPT results to evaluate the bleeding rate based on proper assumptions /Peng 2013a/. As presented above, the addition of some additives such as SP improves the behaviour compared to the Richardson-Zaki Equation. However, they also result in a softer bleeding front and opaque bleeding, which make many classic bleeding measurement methods inapplicable. The evaluation of this turbid bleeding layer could be a difficulty of stability evaluation for cement paste. More recently it was found /Peng 2013a/ that the bleeding rate calculated from dp/dt at the position close below the

bleeding front by HYSPT are in the same magnitude as the measured bleeding rate from some parallel bleeding measurements. This is one of several interesting aspects for further research to develop robust and stable SCC.

4. CONCLUSION AND FURTHER RESEARCH

The investigations on stability of cement paste contribute to a better understanding of concrete stability, especially for SCC. The instability of cement paste is a result of particle sedimentation and is mainly affected by the solid fraction, various particle sizes or mineralogy, the fresh properties of the fluid phase, the flocculation between particles and density differences between particles and fluid. The sedimentation of cement paste is more complicated than that of the suspensions with inert particles because of the reaction between particles and fluid phase. These effects, effects of system design and effects of varying material qualities were investigated in a number of experiments in /Peng 2013a/. However, we are now ready to further develop HYSPT to be able to investigate the stability of real SCC.

ACKNOWLEDGEMENTS

The support from the COcrete Innovation Center (COIN) and the NTNU concrete laboratory, as well as the discussion with Prof. Erik J. Sellevold, Dr. Tor Arne Hammer and Prof. Sverre Smeplass are gratefully acknowledged.

REFERENCES

- De Schutter D., Bartos P. J.M., Domone P., Gibbs J. 2008
 “Self-Compacting Concrete”, Whittles Publishing, Scotland, UK, 2008
- .Peng Y. 2014
 “Sedimentation and bleeding of fresh cement paste”, Doctoral thesis in NTNU, 2014:89
 ISBN 978-82-326-0102-8 (printed), 2014:89 ISBN 978-82-326-0103-5 (electronic),
 2014, Trondheim, Norway
- Peng Y.; Jacobsen S. 2013a
 “Influence of water cement ratio, admixtures and filler on sedimentation and bleeding of cement paste”, Cement Concrete Research, V.54, 2013, pp.133-142
- Peng Y.; Jacobsen S., Weerdt K. De; Pedersen B. 2013b
 “Model and methods for stability of fresh cement pastes”, ASTM-Advances in Civil Engineering Materials, V.3, 2013, pp.1–24, doi:10.1520 /ACEM20130097. ISSN 2165-3984
- Peng Y., Jacobsen S., Pedersen B., Rudberg E.A., De Weerdt K. 2013c
 “Filler and plasticizer effects on sedimentation and bleeding of cement paste”, submitted to Materials and Structures, Dec. 2013
- Vikan H. 2008
 “Means of improving concrete construction productivity – State of the art”, COIN Project report 8, 2008, ISBN 978–82–536–1068–9, 17p

Attenuation of Vibrations in Fresh Concrete



Ahmad A. Ghadban
M.S. in Civil Engineering
Ph.D. Student and Graduate Research Assistant
Kansas State University
2118 Fiedler Hall, Department of Civil Engineering
Manhattan, KS, 66506
E-mail: aghadban@ksu.edu



Mohammed Albahtiti
M.S. in Civil Engineering
Ph.D. Student and Graduate Research Assistant
Kansas State University
2118 Fiedler Hall, Department of Civil Engineering
Manhattan, KS, 66506
E-mail: bahtiti@ksu.edu



Kyle Riding
Ph.D. in Civil Engineering
Associate Professor
Kansas State University
2118 Fiedler Hall, Department of Civil Engineering
Manhattan, KS, 66506
E-mail: riding@ksu.edu



David Lange
Ph.D. in Civil Engineering
Professor
University of Illinois at Urbana-Champaign
205 N. Mathews Ave.
Urbana, IL 61801
Email: dlange@illinois.edu

ABSTRACT

A study is being conducted with the aim of relating the rheological properties of fresh concrete to vibration attenuation during consolidation. Concrete vibration attenuation measurements were carried out by measuring the concrete acceleration using a submersible accelerometer at different depths and distances from an immersion vibrator in a large cylindrical concrete sample. The acceleration decreased at a decreasing rate as the distance from the centre of vibration was increased, with the highest acceleration measured close to the tip of the vibrator. Results showed

that concretes with high viscosities transmitted more wave energy than concretes with low viscosities.

Key words: Rheology, Testing, Vibration, Immersion Vibrator, Plastic Viscosity, Yield Stress

1. INTRODUCTION

Concrete is often vibrated during placement to consolidate the concrete to ensure adequate bond with the reinforcing steel, ensure homogeneity between layers placed, and fill all voids in the form. Under-vibration can result in incomplete consolidation, whereas over-vibration can result in segregation and loss of air entrainment needed for freeze-thaw durability. The rheological properties of concrete play a critical role in the amount of vibration energy needed to achieve full consolidation, the spacing of vibrator insertion or placement, and the amount of time needed for vibration.

Relatively little work has been done to date to understand the effects of rheology on concrete vibration attenuation. Tattersall and Baker (1988) constructed an apparatus to measure the rheological properties of concrete during vibration in a form vibrator. They concluded that the efficiency of vibration is mainly controlled by the peak velocity of vibration. Teranishi and his colleagues investigated the effect of the rheological properties of fresh concrete on the sinking behaviour of coarse aggregate in concrete under vibration. They found that the higher the volume of coarse aggregate the lower the segregation of concrete. This makes intuitive sense since concretes with high volumes of coarse aggregate tend to have high yield stresses and plastic viscosities (Teranishi, Tanigawa, Mori, & Terada, 1995). Another paper published by Banfill and his colleagues attempted to predict the radius of action of internal immersion vibrators in fresh concrete using the mathematics of wave propagation. They used the rheological properties of concrete for that purpose and they were able to produce acceptable correlations between experimental and analytical data (Banfill, Teixeira, & Craik, 2011). However, they did not attempt to use large sample size which might have resulted in boundary effect. They also did not conduct experiments on concretes with different rheological properties. The objective of this study is to relate the rheological properties of concrete to the attenuation of vibrations in large masses of fresh concrete.

2. MATERIALS

One mortar mixture and three different concrete mixtures were used in this study. The mortar mixture used was made with an ASTM C150 Type III cement and a natural siliceous sand. One concrete mixture was made in the laboratory using an ASTM C150 Type III cement, a natural siliceous sand, and a limestone coarse aggregate. Two additional concrete mixtures were used and were made and delivered by a local ready mixed concrete supplier. They were made with an ASTM C150 Type I/II cement, a natural siliceous sand, coarse aggregate, an air entraining admixture and a superplasticizer. Rheological properties of the ready mixed concrete mixtures were varied by altering the water-cement ratio and the superplasticizer dosage. A hydration stabilizing admixture was added to all concrete mixtures in order to maintain nearly-constant rheological properties throughout the entire testing period.

3. METHODOLOGY

3.1 Rheology measurements

The rheological properties of the concrete mixtures were measured regularly during each test using an ICAR Rheometer. The ICAR Rheometer was used to measure the mortar and concrete static yield stress (i.e. yield stress without prior shearing history), dynamic yield stress (i.e. yield

stress after breaking the thixotropic effect), and plastic viscosity (Amziane, Ferraris, & Koehler, 2005).

3.2 Vibration attenuation measurements

The laboratory made mortar and concrete mixtures were placed in cylindrical cardboard tubes with a diameter of 0.6 m and height of 0.81 m to measure their vibration attenuation. The ready-mixed concrete mixtures were placed in cylindrical tubes with a diameter of 1.52 m and height of 0.81 m. A 25.4 mm diameter immersion vibrator (230 Hz frequency) was inserted in the centre of the cardboard tube 203 mm into the concrete, as shown in Figure 1. The vibrator was attached to two steel rods which were connected to a stand in order to ensure fixity of the vibrator location during testing. A three-axis submersible accelerometer was attached to a steel stand to control the accelerometer location. The accelerometer was inserted into the concrete to measure the concrete acceleration with depth and distance in the radial direction away from the vibrator. The acceleration was measured in the radial, tangential and vertical directions at each point measured.



Figure 1 – Vibration testing apparatus

4. RESULTS AND DISCUSSION

Measurements showed that the immersion vibrator used emitted large radial vibrations while tangential direction vibrations were lower but also strong. The higher radial wave measurements are compressive whereas the tangential ones are shear waves. The particles in a fluid such as fresh concrete are not close enough to sufficiently support propagation of shear waves. Vertical vibrations were also detected but were very small to make any significant contribution towards breaking down the yield stress of the concrete. Figure 2 shows a comparison in terms of the radial vibration measurements between the ready-mixed stiff concrete with a slump of 76 mm and the ready-mixed fluid concrete with a slump of 222 mm. Each curve represents the radial peak accelerations with distance and depth from the centre of vibration. The behaviour along the depth of concrete can be observed from Figure 2 (a) where the acceleration readings peaked near the depth of the tip of the immersion vibrator. This is because the vibrator was fixed at one end and free at the other end causing a pendulum effect at the free end, located 203 mm deep in the concrete. In the case of fluid concrete, Figure 2 (b) demonstrates a more erratic behaviour with higher measured accelerations.

Experiments using water, mortar and concrete were conducted in an attempt to understand the erratic acceleration behaviour measured in the fluid concrete mixture. Figure 3 shows a comparison between the acceleration measured with water, mortar and concrete. Figure 3 (a) shows that the rheological properties of mortar and concrete are comparable, with concrete being slightly of higher viscosity. The acceleration measurements showed that the peak acceleration decreased at a decreasing rate as the distance from the centre of vibration was increased. The decrease in concrete acceleration with distance from the vibrator looked very

uniform for the case of water and mortar, but also showed erratic behaviour for the case of concrete. This indicated that the reason for this erraticism is coarse aggregate. The coarse aggregate particles could easily move in a fluid mixture, impacting the accelerometer and causing misleading results.

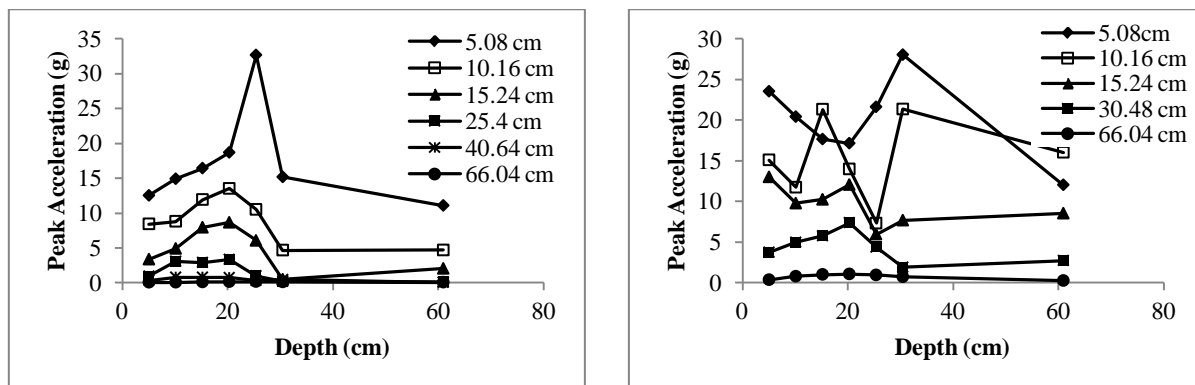


Figure 2 – Radial vibrations in 121.92 cm diameter tubes. a) Stiff concrete. b) Fluid concrete

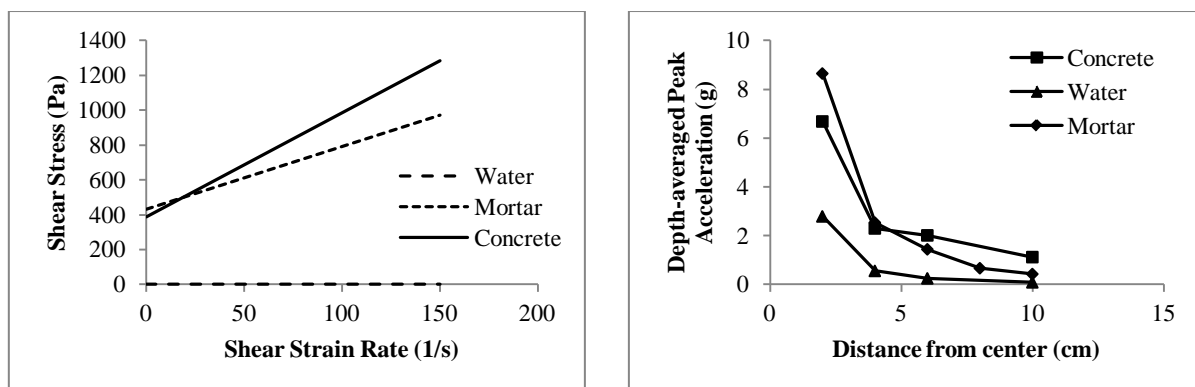


Figure 3 – a) Rheological properties and b) Tangential vibrations in 61 cm diameter tubes

5. CONCLUSIONS

The main conclusion from this study is that concretes with higher viscosities transmit more of the wave energy than concretes with lower viscosities. Also, the transmitted wave generally becomes negligible beyond 254 mm and 406 mm away from the centre of vibration.

REFERENCES

- Amziane, S., Ferraris, C. F., & Koehler, E. P. (2005). Measurement of Workability of Fresh Concrete Using a Mixing Truck. *Journal of Research of the National Institute of Standards and Technology*, 55-66.
- Banfill, P. F., Teixeira, M. A., & Craik, R. J. (2011). Rheology and vibration of fresh concrete: Predicting the radius of action of poker vibrators from wave propagation. *Cement and Concrete Research*, 41, 932-941.
- Tattersall, G. H., & Baker, P. H. (1988). The effect of vibration on the rheological properties of fresh concrete. *Magazine of Concrete Research*, 40(143), 79-89.
- Teranishi, K. K., Tanigawa, Y., Mori, H., & Terada, K.-i. (1995). Study on sinking behavior of coarse aggregate in fresh concrete subjected to vibration. *Transactions of The Japan Concrete Institute*, 17, 1-8.

Methods to Optimize Aggregate Composition – Evaluation by Concrete Experiments



Tekn Lic, Niklas Johansson
 PhD-student
 Cementa AB
 P.O. Box 104, S-624 22 Slite
 Div. Structural and Construction Engineering
 Luleå University of Technology
 S-971 87 Luleå
 E-mail: niklas.johansson@cementa.se / niklas.johansson@ltu.se



Prof. Dr. Mats Emborg
 Div. Structural and Construction Engineering,
 Luleå University of Technology
 S-971 87 Luleå
 Betongindustri AB
 P.O. Box, 473 12 Stockholm
 E-mail: mats.emborg@ltu.se / mats.emborg@betongindustri.se

ABSTRACT

A proper mix design optimizes the environmental impact and the cost effectiveness of a concrete. A minimum cement paste content is desirable without deteriorate the concrete properties. Thus, cement paste content is dependent on the packing properties of the aggregates. Three methods to optimize the aggregate composition have been evaluated by concrete tests for crushed and natural aggregates: one curve fitting method and two particle packing methods. It is shown that the methods suggest very different aggregate compositions and they can't handle fine crushed aggregate that consumes a lot of mixing water.

Key words: Aggregate, Mix design, Fresh concrete, Cement paste

1. INTRODUCTION

The environmental impact and the cost effectiveness of concrete highly depend on the cement paste content as cement is responsible for a major part of the CO₂ emissions in a concrete (more than 50% according to Fennis /2010/. Water cement ratio, binder types, aggregates and admixtures have a big impact on the cement paste content in the concrete and it is of interest in mix design to optimize the paste content without deteriorate the concrete properties. Moreover, 60-70% of the concrete volume consists of aggregate i. e. its properties and composition has a large influence on the concrete performance. The aggregate properties can be described in many ways for example, sieve curve, flakiness index, packing density, flow value and surface texture. The composition of different aggregate fractions in the concrete can be based on optimization curves and/or particle packing models where it is thus striven for a low void ratio of the particles lead to a reduced cement paste content /Fennis 2010/.

2. METHOD

2.1 Aggregate characterization

In the study, particle density, water absorption, sieve curve, flakiness index, loose particle packing and compressive particle packing were tested for each fraction of the following aggregates chosen since they have clear different performance regarding water demand and particle shape:

- a) 0-4 mm manufactured sand
- b) 0-8 mm natural sand
- c) 4-8 mm crushed and cubisized rock
- d) 8-16 mm crushed and cubisized rock
- e) 8-16 mm crushed rock
- f) 8-16 mm natural stone

. The compressive particle packing value was determined by filling a 5 litre cylinder in three levels. Each level was compacted by 80 hits on a jolting table.

2.2 Methods to optimize aggregate composition

Three methods of optimizing the aggregate composition were studied.

Fuller curve /Fuller and Thompson, 1907/ is an optimum sieve curve, often used in traditional concrete mix design. Required input is the sieve curve of each aggregate fraction, i.e. no packing.

Toufar model is a particle packing model that was initially developed for binary systems but can also be used for three aggregate fractions /Goltermann, et al. 1997/. Input data required is sieve curve and particle packing value of each aggregate fraction

4C-packing is a computer software based on the Linear Density Packing Model /Stowall, et al. 1986/ The software was developed by DTI in Denmark and can be used as a concrete mix design tool. Input data needed is particle density, sieve curve and particle packing value of each aggregate fraction. There is also a parameter called Mu-value that needs to be decided. The Mu-value quantifies the so called loosening effect and will normally be in the range of 0,07-0,13. /Pade, et al. 2009/ Spherical particles have higher Mu-value than flaky particles.

2.3 Concrete trials

Concrete recipes were created based on the suggested optimum aggregate compositions from the three methods. The following aggregate combinations were tested.

- I. 0-8 mm natural sand + 8-16 mm natural stone (aggregate b and f above).
- II. 0-4 mm manufactured sand + 4-8 mm crushed and cubisized rock + 8-16 mm crushed and cubisized rock (a, c and d).
- III. 0-4 mm manufactured sand + 4-8 mm crushed and cubisized rock + 8-16 mm crushed rock (a, c and e).

Concrete with two w/c (0,40 and 0,65) were tested with a fixed dosage of superplasticizer per cement weight. Concrete batches of 20 litres were mixed and slump, density and air content were documented on the fresh concrete. For each concrete the cement paste content was varied, keeping the w/c ratio thus changing the consistency.

3. RESULTS

3.1 Aggregate properties

The properties of the aggregates used in this study are shown in Table 1, where it is observed that there is a big difference between the aggregates regarding loose packing. The difference is smaller for compressive packing since the crushed materials get more compacted.

Table 1 – Aggregate properties. Packing values are presented as % by volume.

| | Density (kg/m ³) | Flakiness index (%) | Loose Packing (%) | Comp. Packing (%) | Loose vs Comp. Packing (%) |
|--------------------------------|---------------------------------|---------------------------|-------------------------|-------------------------|----------------------------------|
| a) 0-4 mm manufactured sand | 3020 | - | 61,7 | 76,4 | 23,8 |
| b) 0-8 mm natural sand | 2650 | - | 66,3 | 76,8 | 15,8 |
| c) 4-8 mm crushed + cubisized | 3100 | - | 54,4 | 61,1 | 12,3 |
| d) 8-16 mm crushed + cubisized | 2950 | 14 | 53,3 | 59,7 | 12,0 |
| e) 8-16 mm crushed | 3110 | 22 | 48,5 | 55,5 | 14,4 |
| f) 8-16 mm natural | 2660 | 4 | 60,5 | 64,8 | 7,1 |

3.2 Aggregate compositions

The aggregate properties above were used as input data in the methods described in Section 2.2. The outcome, i. e. the optimum composition is presented in Table 2. The Mu-value in 4C-packing was 0,10 for natural aggregates and 0,07 for crushed aggregates.

Table 2 – Optimum aggregate composition presented as % by weight for combination I - III.

| Aggregate Composition | Fuller | Toufar | | 4C-packing | |
|-----------------------------|--------|------------|-----------|------------|-----------|
| | | Loose Pack | Comp Pack | Loose Pack | Comp Pack |
| I | | | | | |
| 0-8 mm natural sand | 61% | 43% | 50% | 50% | 42% |
| 8-16 mm natural | 39% | 57% | 50% | 50% | 58% |
| II | | | | | |
| 0-4 mm manufactured sand | 55% | 43% | 55% | 40% | 58% |
| 4-8 mm crushed + cubisized | 12% | 20% | 14% | 0% | 0% |
| 8-16 mm crushed + cubisized | 33% | 37% | 31% | 60% | 42% |
| III | | | | | |
| 0-4 mm manufactured sand | 55% | 50% | 66% | 64% | 75% |
| 4-8 mm crushed + cubisized | 0% | 19% | 11% | 0% | 4% |
| 8-16 mm crushed | 45% | 31% | 23% | 36% | 21% |

It is shown that there are big differences in optimum aggregate composition depending on method and packing technique. The compositions in bold characters were used in the concrete trials where compressive packing values were chosen for 4C-packing based on the instructions in the user's manual. /Pade, et al. 2009/. The most realistic aggregate compositions were chosen from the Toufar model.

3.3 Concrete results

The results from the concrete trials show that the methods work quite well for natural aggregates with quite spherical particles. The required cement paste content to reach 200 mm slump was low. With aggregate-combination II according to Table 2, the aggregates have an impact on required cement paste content especially at low w/c ratios, see Figure 1. The 0-4 mm manufactured sand that was used is a poor material for concrete production since it consumes a lot of mixing water. As curve optimization and particle packing models do not take the water

demand into account, there is a risk that the suggested percentage of fine aggregates will be too high and the need for cement paste gets high.

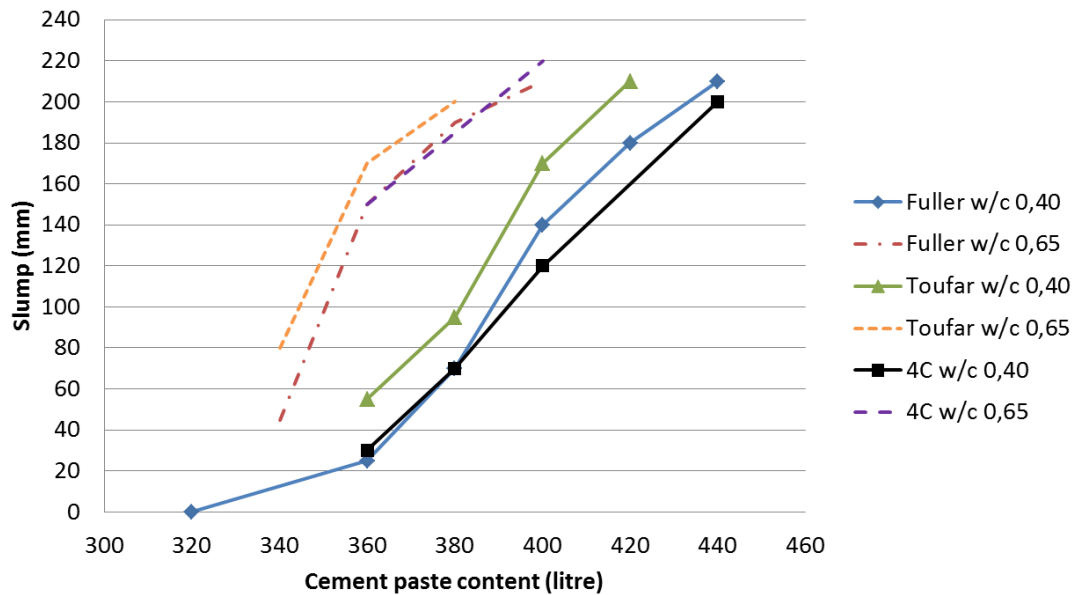


Figure 1 – Slump as a relation to cement paste volume for concrete with aggregate combination II. Fuller: 55% 0-4 mm ; Toufar 43% 0-4 mm ; 4C 58% 0-4 mm.

REFERENCES

Goltermann, P., Johansen, V., Palbøl, L., 1997

”Packing of aggregates: An Alternative Tool to Determine the Optimal Aggregate Mix”, ACI Materials Journal, Vol 94 (5), pp 435-443.

Fennis, S.A.A.M., 2010

”Design of ecological concrete by particle packing Optimization”, TU Delft. Doctoral thesis, 256 pp.

Fuller, W.B., & Thompson, S.E., 1907

”The laws of proportioning concrete”, Transactions of the American society of civil engineers 33, pp 222-298.

Pade, C., Nyholm Trane, L., Kaasgaard, M., 2009

”4C-packing – User’s manual”, Version 3.0, Danish Technological Institute, 24 pp.

Stovall, T., Larrard, F.de., Bull, M., 1986

”Linear Density Packing Model of Grain Mixtures”, Powder Technology, Vol 48, pp 1-12.

FIBRES

Strengthening of Concrete with Carbon Fibre Reinforced Polymer (CFRP) Grids Bonded by Cementitious Binders



Katalin Orosz
 Tec. Licentiate, Ph.D student
 Division of Structural Engineering
 Luleå University of Technology
 97 187 Sweden
 katalin.orosz@ltu.se

ABSTRACT

Knowledge of the tensile behaviour of the strengthening material is important to estimate the shear capacity of the strengthened structure. In this paper, the tensile behaviour of externally bonded carbon fibre polymer (CFRP) grids has been studied. Bonding agent was either quasi-brittle polymer-modified mortar (PMM) or strain-hardening (“ductile”) mortar, instead of the typical epoxy resin. Uniaxial tensile and wedge-splitting tests were conducted to investigate the tensile-, and post-cracking behaviour, toughness, and ductility. The strain-hardening mortar enhanced both the load bearing- and in particular, the deformation capacity, surpassing the benefits of the PMM. The “ductile” mortar has also shifted the overall behaviour from brittle towards a more ductile failure.

Keywords: Concrete, Strengthening, CFRP, Testing, Strain Hardening, Tensile Behaviour, Cracking, Brittleness, Deformation Capacity

1. INTRODUCTION

Externally bonded fibre-reinforced polymer (FRP) systems have shown to be a robust and durable way to repair, or strengthen concrete structures. Epoxy, as the most common bonding agent, provides excellent force transfer, and bonds well to the base substrate to the strengthening material. However, the epoxy-bonded systems exhibit certain inherent weaknesses, such as low compatibility with the concrete substrate, degradation in strength and stiffness around 85 °C, and toxicity both during application and when subjected to fire. Epoxies also require a minimum application temperature often above 10 °C, and create sealed surfaces, potentially resulting in moisture and freeze/thaw problems.

In recent years, alternative, inorganic bonding agents have been of interest for strengthening applications. Cementitious bonding agents, when combined with FRP, have the potential to become a high-performance strengthening system, without the drawbacks of the epoxy. Inorganic binders provide excellent protection to the FRP against UV-degradation, fire, or vandalism. Contrary to epoxy, they can be applied in colder temperatures or climates. They show a better compatibility with the base concrete in terms of chemical or thermal compatibility, shrinkage properties, and they do not create diffusion-closed surfaces.

In this research, a strengthening system comprised of a carbon fibre grid, and a fine-grained mortar phase as binder has been investigated, with focus on the tensile behaviour of the material. Both quasi-brittle and strain-hardening mortars have been used. The strain-hardening mortar used was a custom engineered cementitious composite (ECC) that contained a low (1%) fraction of short, oiled PVA fibres and a high percentage (44%) of fly ash.

2. TESTING

2.1. Background

The toughness of concrete is usually evaluated by means of the post-failure behaviour in tension, the stress versus crack width relation – the tension softening behaviour. It is a basic property of the concrete described by (a) tensile strength, (b) shape of the softening curve, and (c) fracture energy, which corresponds to the area under the stress versus crack width curve /Hillerborg, Modéer et al. 1976/. Knowledge of these parameters enables estimations of shear capacity and brittleness in compression and tension.

The experimental work presented here consists of two test series; uniaxial tensile tests carried out on dogbone-shaped specimens, to characterize the tensile properties of the bare composite strengthening material, and wedge-splitting tests to investigate the post-cracking behaviour and the interaction between the strengthening material and the base concrete.

The standard uniaxial tests are very sensitive for brittle or quasi-brittle materials. It is difficult to ensure that cracking will happen in the prescribed (and monitored) test field, preferably in the middle of the web of a dogbone specimen. There is a high risk of cracks initiating where the web meets the bulk end of the specimen. While the more robust wedge-splitting test method is not a direct tensile test, it does provide valuable data on the tensile behaviour. It is a fracture mechanics test method that has proven to be suitable for obtaining both splitting tensile strength and an estimation of the fracture energy. One significant advantage of the WST is its stability; it always results in stable crack propagation /Østergaard, Stang et al. 2002/. Its limitations are that it does not create a uniform tensile field, since the specimen undergoes bending because of the way the load is applied. In addition to that, the WST does not *directly* characterize the tensile properties of the concrete, unless an inverse analysis is performed. Without inverse analysis, the test can still be used to determine the fracture energy and if desired, fracture toughness.

2.2. Experimental set-up

In the uniaxial tensile tests, the bare strengthening material was investigated, without considering the interaction with a real structure to be strengthened. Crack development and the influence of the ductility of the applied mortar on the behaviour in tension were investigated. Both quasi-brittle polymer-modified mortars (PMM) and strain-hardening mortars (ECC - engineered cementitious composites) have been tested. Two different grids with different grid spacings, and three chosen grid orientations (0° - longitudinally placed grid, 90° - transversally placed grid, 15° - rotated grid) were tested in different combinations.

Dimensions of the dogbone-shaped test specimens were 160 x 160 x 980 mm, with a representative test section of 400 x 160 x 20 mm. The CFRP grid was placed in the mid-plane of the specimens. The number of the CFRP tows in the representative test section, tensile direction, were 7 (“small”, S-grid, spacing 24x25mm) and 4 (“medium”, or M-grid, spacing 42x43 mm). The specimens were fixed in self-centering, custom-made clamps.

The wedge-splitting test is an extension of the uniaxial test because the strengthening is applied on a concrete surface. The behaviour of the CFRP grid reinforcement in two different directions (0° and 45°, respectively) together with both quasi-brittle and strain-hardening mortars has been investigated and evaluated. External dimensions of the plain concrete test specimen were 500 x 500 x 100mm, after strengthening with a representative test section of 400 x 420 x 140mm where 140mm is the total thickness after strengthening on both sides. The CFRP grid was applied on both sides, placed between two 10 mm thick layers of mortar. Tests were run

deformation-controlled, i.e., through the crack opening displacement kept constant. During the test, vertical load and crack opening displacement (COD) are recorded; hence the splitting load can be calculated. More details on both test set-ups can be found in /Orosz 2013/.

3. RESULTS

Figure 1 presents the uniaxial tensile test results. Quasi-brittle and strain-hardening mortars are compared and related to the linear elastic behaviour of the pure CFRP grid. For more details, see /Orosz 2013/.

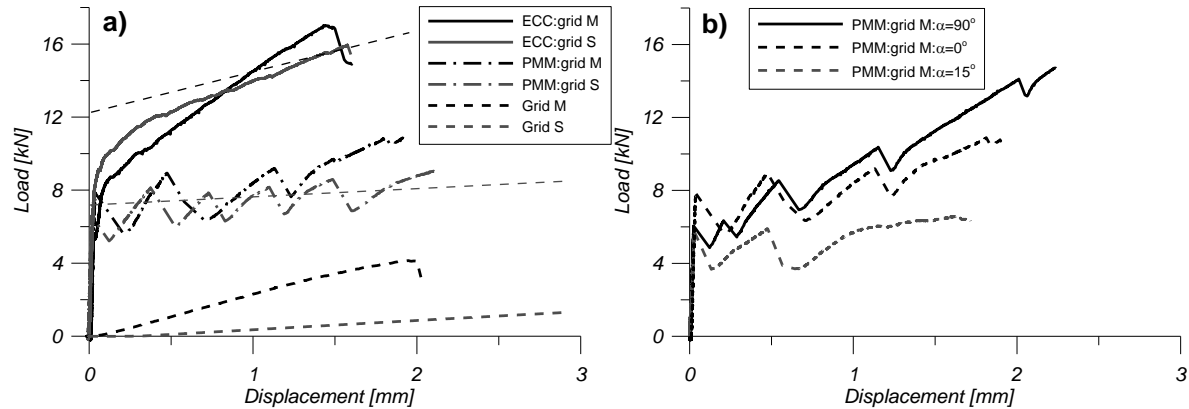


Figure 1 – All dogbone specimens with grid S and M placed in longitudinal (0°) direction; (b) Effect of grid orientation, transverse – 90° , longitudinal – 0° and rotated – 15°

Behaviour of all specimens was nearly identical up to first cracking, irrespective of which mortar is used. After first cracking, ECC specimens show a significant strain hardening behaviour with both grids which is represented as the contribution of the mortar compared to the shifted lines of the bare grid. These curves are smooth due to the fibre-bridging characteristics of the cracks in ECC, due to its PVA fibre content. The plots of the quasi-brittle mortars are more jagged and have a significant drop in load carrying capacity right after the first crack (and after further crack formation). This shows that the increased ductility of the ECC mortar has a positive effect on the interaction with the CFRP. It seems to prevent premature failure of the CFRP grid which was observed in the specimens with brittle mortars, with significantly reduced axial tensile strength.

Figure 2 shows the wedge-splitting test results. Figure 2a illustrates the effect of the grid orientation for the strain-hardening, while Figure 2b for the quasi-brittle mortar. The apparent better performance of the grid when not rotated respective to the governing crack may be due to the joint shape and associated deformation capacity of the grid joints when loaded in a certain direction. The resulting crack opening vs. splitting force plots show that the (splitting) tensile strength of concrete can be significantly improved with the strengthening, resulting in an increase of 30-110% in peak splitting load compared to the unstrengthened reference specimen. The strain-hardening mortar has given significantly higher failure loads and similarly to the uniaxial tests, it prevented pronounced drops in load capacity. Ductility is significantly enhanced by all grid-mortar combinations resulting in an extreme increase of fracture energy – which is directly proportional to the area under the curves.

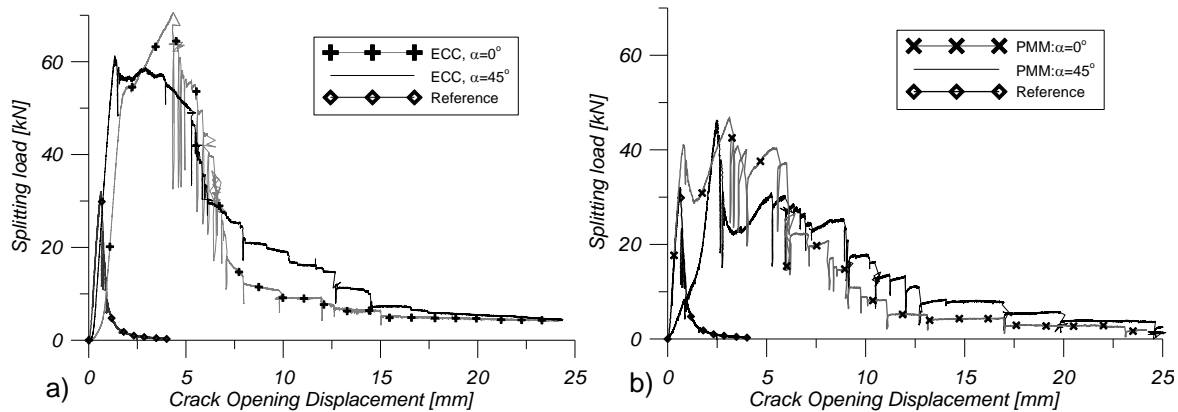


Figure 2 – WST: COD vs. splitting force diagrams for specimens with highest peak load per series, against reference specimen (plain concrete)

4. CONCLUDING REMARKS

The strengthening system performed excellent in terms of load-carrying capacity. Both the dogbone and the wedge splitting tests resulted in specimens failing with FRP rupture in accordance with earlier results from /Blanksvärd 2007/ indicating that there is a good bond within the system, both on the concrete-composite interface and within the mortar and the grid component.

Furthermore, the strain-hardening mortar has been found to enhance both the load bearing- and in particular, the deformation capacity. It has also been shown that the strain-hardening mortar is capable to shift the overall behaviour from brittle towards a more ductile, hence, more predictable failure.

REFERENCES

Blanksvärd, T., 2007

"Strengthening of concrete structures by the use of mineral based composites".

Licentiate Thesis, Luleå University of Technology, Luleå, Sweden

Hillerborg, A., M. Modéer and P. E. Petersson, 1976

"Analysis of crack formation and crack growth in concrete by means of fracture mechanics and finite elements." Cement and Concrete Research Vol. 6, No. 6, pp. 773-781.

Orosz, K., 2013

"Tensile behaviour of mineral-based composites". Licentiate Thesis, Luleå University of Technology, Luleå, Sweden

Østergaard, L., H. Stang and J. F. Olesen, 2002

"Interpretation and inverse analysis of the wedge splitting test". Fracture Mechanics Beyond 2000. A. Neimitz. United Kingdom, EMAS Publications. II: pp. 593-600.

Design, testing and evaluation of a fullscale post-tensioned steelfibre reinforced flat slab



Prof. Terje Kanstad
Department of structural engineering,
NTNU,
N-7491 Trondheim
E-mail: terje.kanstad@ntnu.no



Dr. Steinar Trygstad
THiLT Engineering AS,
N-6002 Ålesund
E-mail: steinar@thilt.no

ABSTRACT

A full-scale failure test of a post-tensioned and fibre reinforced flat-slab has been carried out. The structural system consisted of 2 by 2 spans (2 x 8,5m and 2 x 6,5m), and the slab was reinforced with tendons and 0,38 volume % steel fibres (30kg/m³). The load was uniform water-pressure, and strains and deflections were measured. The test is related to ongoing standardization work, and the major result is that the experimental capacities are considerably on the safe side if characteristic strength values and elastic theory for calculation of moment distribution are used. This holds both for the German design rules for fibre reinforced concrete (DIN-EN), for *fib* Model Code and the Norwegian guideline-proposal.

Key words: Fibres, Modelling, Structural Design, Testing.

1. INTRODUCTION

For fibre concrete lack of standards and design guidelines is a limiting factor for general use in load carrying structures, and soil supported slabs and sprayed concrete for tunneling and rock stabilization are presently the only considerable markets. But the situation is improving, and standardization work in the Nordic countries [Kanstad, T. et al., 2011], launching of *fib* Model Code 2010 with fibre chapters both for materials and structural design [*fib* 2013], and *DIN-EN-1992: DafStb* Guideline Steel fibre reinforced concrete (Draft 2012) [DIN-EN 1992-1-1: 2012] are some major achievements. Furthermore has the CEN committee for revision of Eurocode 2 (CEN/TC 250/SC 2/WG 1) established a sub-committee for fibre concrete (TG2), with the purpose of writing an annex to Eurocode 2 which should be included in the next revision. To support the ongoing standardization work full-scale tests and reference projects are needed, and the current full-scale test was carried out in the spring 2013. While the major objective by the project was to verify the structural behaviour and the load carrying capacity, more specific objectives were to investigate the shear capacity around the central column, the moment capacity and the moment and shear-force (re)distribution due to cracking. Furthermore, it was interesting to compare results obtained by elastic analysis versus yield line (plastic) analyses, observe the ductility of the structural system, and investigate the in-situ residual tensile strength determined on saw-cut beams versus the strength of standard three-point bending tests (EN14651).

2. SLAB LAYOUT AND TEST ARRANGEMENT

The slab, shown in Figure 1 below, was first designed according to common practice with prestressing tendons and ordinary shear and longitudinal reinforcement bars, but the ordinary reinforcement was skipped and replaced by 0,38 volume % fibres (30kg/m^3). Hooked end steel fibres with length 50mm, 0,8mm diameter, and tensile strength 1550N/mm^2 were used. The slab was loaded with uniform water-pressure over the entire slab inside a bin made of formwork and watertight sheets. Furthermore the structure was instrumented with LVDTs for strain and deflection measurements. The deflections were recorded in three points in the column and field strips, while the strain development was recorded in 24 points. A load cell was placed below the slab over the central column to investigate the effect of cracking on the load distribution (ie the redistribution of moments and shear forces) in the slab. For further details see [Hallberg et.al. 2013]

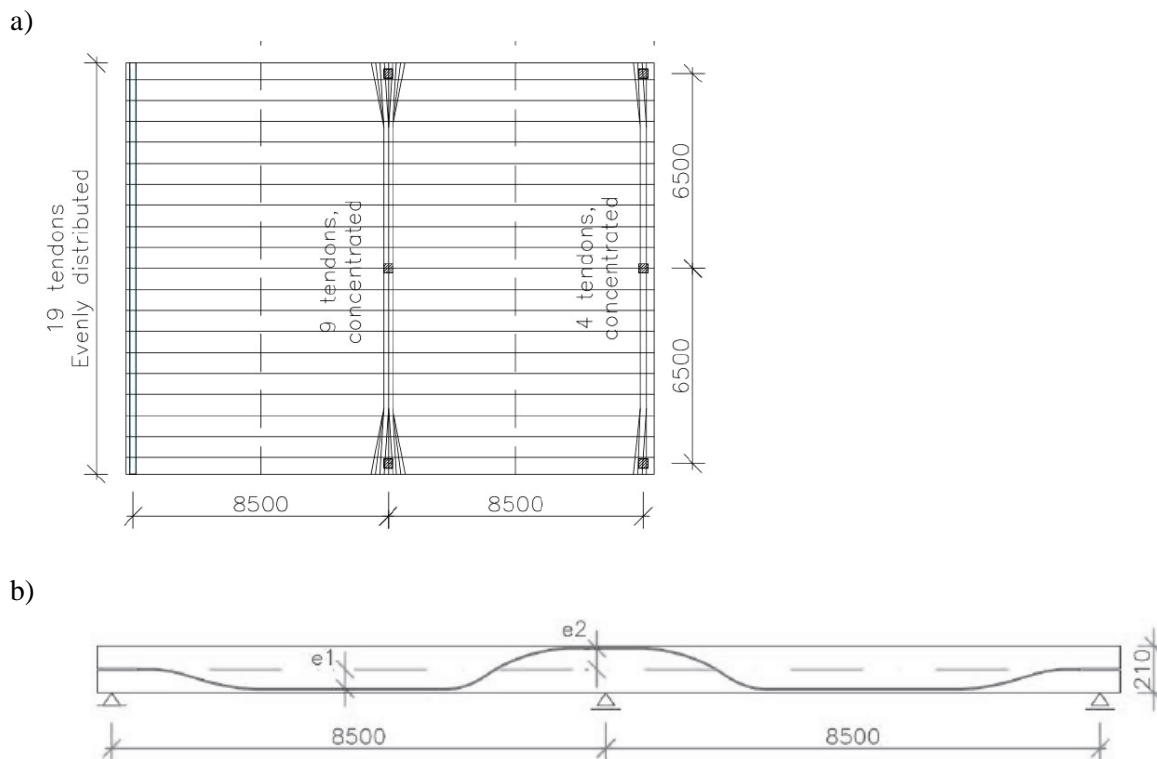


Figure 1. Structural system, geometry and tendon layout of the full-scale test-slab[3]

3. TEST RESULTS AND CALCULATED MOMENT AND SHEAR CAPACITIES

Recording of the measurement data started when the water load was applied, and strains due to selfweight and prestressing are therefore not included in this paper. However, the calculated strains at the initial stage are less than $0,1\text{E-}3$, and the amount of cracking was rather small at this stage. Furthermore shrinkage and temperature effects are also neglected, which, can be justified by limited horizontal restraint, and low age at testing (29 days).

The moment capacity of the slab was first calculated with moment distribution based on elastic theory and assumptions of constant moments over the width of defined strips. The moment capacities of the different sections were calculated without safety factors in accordance with

commonly used stress and force resultant principles. The stress in the prestressing steel is set to 1340MPa assuming 10% loss, and the compressive strength is set equal to the average measured cylinder strength which is 47,7MPa, while different approaches were used for determination of the residual tensile strength. Alternatively yield line analysis has been used, and thereby has redistribution of the forces been accounted for. The decisive yield line pattern is shown in Figure 2a, and in this case the calculated moment capacity is considerably larger due to the fully utilized capacity both in the span and over the mid support although the stress resultants and the moment capacity expression remain the same. Use of yield line analysis can be justified by the ductile behavior illustrated in Figure 2b. The moment capacity was calculated using constant residual tensile strength over the entire tensile zone equal to 0,37 times the residual flexural strength at 2,5mm CMOD as recommended in the literature. Comparing the calculated and experimental values in Figure 3, it is seen that the experimental results are considerably on the safe side if elastic theory is applied and either characteristic ($f_{res}=0,97\text{MPa}$) or average residual tensile strength ($f_{res}=1,54\text{MPa}$) are being used. The calculated capacity for the two cases corresponds to 45 and 60% of the water load at failure. If the characteristic value is adjusted with the maximum value of the redistribution factor as proposed in *fib* Model Code 2010[3] (1,4 times the characteristic value) or for the failure zone size as proposed in DIN-EN 1992-1-1[Kanstad, T. et al., 2011] (0,87 times the average value), the calculations based on elastic theory are still considerably on the safe side. It is worth noting that this is achieved despite of considerably lower capacity of the saw-cut beams compared to the standard beams.

Another important point to consider is the strength contribution from the tendons might be larger than assumed above since their stress is increasing somewhat in the critical sections due to large deflections and frictional forces. A rough estimate based on several methods referred in [Kanstad, T., 1990] indicates that a deflection of 50mm might result in a prestress increase of 50MPa which corresponds to about 4% of the assumed prestress. When we take into account that the total tensile forces in the prestressing steel is of comparable size related to the total forces in the fibre concrete after cracking, it can be stated that the uncertainty in residual fibre concrete forces still is decisive for this evaluation. When yield line analysis was used, the calculated moment capacity is considerably larger, and close agreement between theory and experiment is achieved. Still one should remember that it is not common practice, and not generally allowed, to use yield line analysis for load carrying elevated slabs.

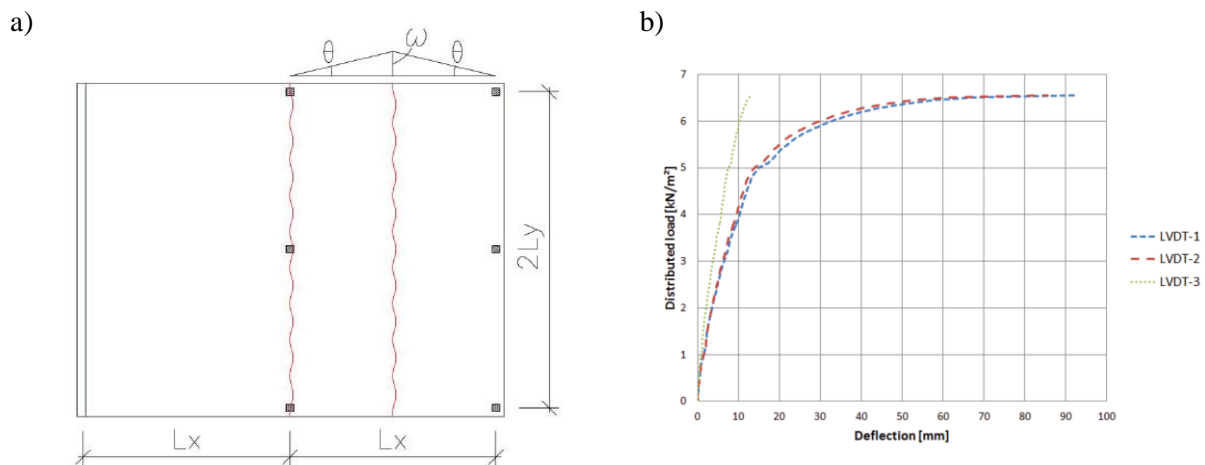


Figure 2. (a) Yield line pattern used for the moment capacity calculations. (b) Recorded load deflection relation

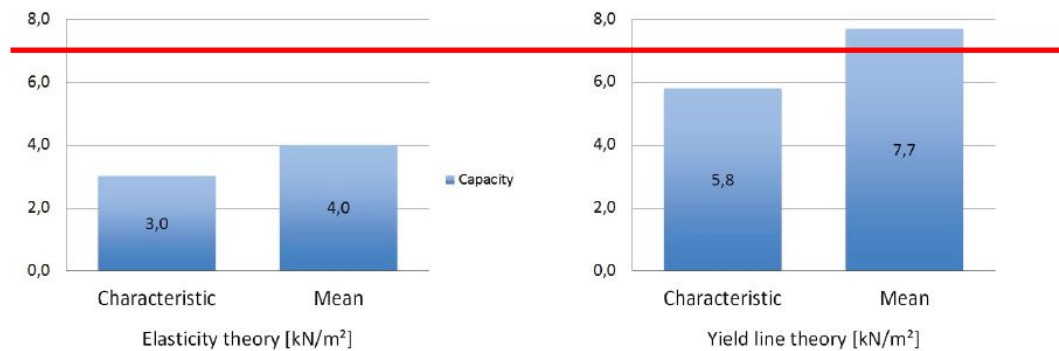


Figure 3. Calculated (bars) and observed moment capacity(line) based characteristic or mean strength

5. CONCLUSIONS

- A fullscale fibre reinforced post-tensioned flat slab was tested to failure. The objectives were related to ongoing standardization work, and valuable test results and experience was achieved.
- The test results are considerably on the safe side related to calculated capacities if characteristic strength values and elastic theory are used
- If yield line analysis is used and redistribution of forces is accounted for, very good agreement between theory and experiment is achieved
- The results, and especially the ductility considerations, are interesting for the robustness and the ductility requirements in the future Eurocode 2-annex for FRC
- The current approach, with a relatively low degree of pre-stressing and low amount of fibres, can be recommended for further development and use in elevated slabs

ACKNOWLEDGEMENT

These companies contributed to the project: Spenneteknikk Construction AS, Betong Øst, Dyrøy betong, Mapei, Innovation Norway and NTNU. The evaluation of the test is supported by COIN.

REFERENCES

DIN-EN 1992-1-1: 2012

DafStb Guideline Steel fibre reinforced concrete (Draft 2012).

fib International Federation for Structural Concrete, 2013

fib Model Code for Concrete Structures 2010. Lausanne, Switzerland.

Hallberg, M.A., Hanssen, H.E., 2013

Post-Tensioned Fibre Reinforced Flatslab, MSc Thesis, Dept of Struct Eng, NTNU,.

Kanstad, T. et al., 2011

Proposal for Norwegian guidelines for design, execution and control of fibre reinforced concrete structures, COIN report, Sintef Building and infrastructure.

Kanstad, T., 1990

Nonlinear analysis considering time dependent deformations and capacity of reinforced and prestressed concrete. Dr.ing.thesis, Department of concrete structures, NTNU.

[6] Trygstad, S. 2013

Full-Scale Test. Prestressed Tendons and Steel Fibres in a Flat Slab. Spenneteknikk Construction AS. Ålesund.

COIN's 15 MPa Target Fibre Concrete: Materials Development Towards High Residual Flexural Strength



Gunrid Kjellmark

Research Engineer, COIN – Concrete Innovation Centre (www.coinweb.no) at SINTEF Building and Infrastructure, Rich. Birkelands v3, N-7465 Trondheim, Norway, gunrid.kjellmark@sintef.no



Tor Arne Martius-Hammer

Centre Director, COIN – Concrete Innovation Centre (www.coinweb.no) at SINTEF Building and Infrastructure, Rich. Birkelands v3, N-7465 Trondheim, Norway, tor.hammer@sintef.no



Terje Kanstad

Professor, Department of structural engineering, The Norwegian University of Science and Technology, Rich. Birkelands v1A, N-7491 Trondheim, terje.kanstad@ntnu.no

ABSTRACT

During the research work within COIN's fibre concrete project, several types and combinations of structural fibres have been tested, and a residual flexural strength of 18MPa was reached by optimized mix design, using a packing theory based on the "Andreassen-equation" from 1934 /Elkem 2014/. As these concretes are quite expensive, continued work was conducted using a more economical mix design and experiments on how the w/b-ratio influences the residual flexural stress were conducted. The tested concretes included 1.0, 1.5 or 2.0 vol.-% steel fibres. Reasonably good casting properties and a clear bending-hardening behaviour were achieved for all of them. Using a w/b-ratio of 0.35 and 2 % (160kg) 60mm steel fibres, an average residual flexural strength at 2.5 mm crack width of 18.9 MPa was reached which is clearly above the COIN target.

Key words: Fibres, Mix design, SCC, Workability, Residual flexural strength

1. INTRODUCTION

1.1 General

The main objectives by the present work conducted within COIN's fibre project (FA 2.2), are to investigate how fibres can be utilized in load carrying concrete structures, and to develop and verify a ductile high tensile strength all-round concrete with a target residual flexural tensile strength of 15 MPa, set by the COIN partners. The materials development started with a Ph.D.-study /Sandbakk 2011/, and has continued with experimental work at SINTEF and NTNU /Sarmiento 2012, Martius-Hammer 2012/. To reach this goal of a high residual tensile strength concrete where a major part of the traditional reinforcement can be left out, type and amount of fibres, fibre distribution and fibre-matrix bond should be optimised.

2. MATERIALS, MIX DESIGN AND TEST METHODS

The present mix design approach was to design a superflowable and stable SCC before fibre addition; with a slump flow of approximately 800 mm without any segregation, which is able to handle 2-3 % by volume of fibres and still achieve sufficient flowability, without additional

superplasticiser. The particle packing program "EMMA" developed by Elkem AS /Elkem 2014/, based on the "Andreassen-equation", was used to achieve this.

Further, a more economic mix design with lower amounts of cement, silica, special filler materials, and conventional aggregate materials was developed, based on the packing theory. This mix (denoted *M60 B35 SCC*) was the base for the experiments reported in the present paper. The nominal recipes are given in Table 1.

Table 1 - Nominal recipes (kg/m³)

| | VC55 | VC45 | VC35 |
|--------------------|--------|--------|--------|
| CEM I 42.5 R | 296.3 | - | |
| CEM II/A-V 42,5N | - | 380.0 | 491.3 |
| Microsilica | 29.6 | 30.4 | 24.6 |
| Fly ash | 44.4 | 0 | 0 |
| Water | 195.6 | 198.4 | 189.2 |
| Sand 0/8 mm | 1111.7 | 1263.2 | 1622.4 |
| Sand 0/2 mm | 600.4 | 422.3 | 0 |
| Super plasticizer | 4.44 | 5.7 | 7.37 |
| Anti-foaming agent | 0.30 | 0.38 | 0.49 |

All concretes were mixed without fibre addition for approximately 7 minutes, followed by fresh concrete measurements approximately 10 minutes after water addition. Then the fibres were added followed by another 2 minutes of mixing, and the fresh concrete measurements were repeated. Slump flow (SF) and flow time (t_{500}) were measured according to EN 12350-8:2010, while the fresh concrete density was measured according to NS-EN 12350-6:2009. Compressive strength and hardened concrete density were measured on $\varnothing 100 \times 200$ mm cylinders according to NS-EN 12390-3 and NS-EN 12390-7, and the results are reported as the average of three specimens.

The residual flexural stress versus crack mouth opening displacement (CMOD) was measured by a three points bending test on $150 \times 150 \times 550$ mm beams with a 25 mm deep notch, according to EN 14651. During testing, the vertical displacement in the middle of the beam, δ , was measured, and the corresponding CMOD (crack mouth opening displacement) calculated by the formula given in the standard. The residual flexural tensile strength at CMOD = 2.5 mm (f_{R3}) is used as the decisive parameter in the following.

The five types of fibres described below have been used, and because of different geometry and materials, they are believed to influence the workability and residual flexural strength differently. All concretes contained 1% or more of the 60mm long F1 or F3 fibre.

F1 Hooked end 60 mm long, ordinary strength steel fibres with aspect ratio $l/d=65$

F3 Double-hooked end 60 mm long, high strength steel fibres with aspect ratio $l/d=65$

F4 Hooked end 35 mm long, ordinary strength steel fibres with aspect ratio $l/d=65$

F5 Straight 13 mm long steel fibres with 0.16 mm diameter, $l/d=81$

F6 Straight 6 mm long steel fibres with 0.16 mm diameter, $l/d=38$

3 RESULTS

3.1 Residual flexural strength versus fibre content for concretes with w/c-ratio 0.55

Figure 1 shows the flexural stress versus CMOD and flexural strength versus nominal fibre content for concretes with a w/c-ratio of 0.55, and compressive strength in the range 43-50 MPa. Eight of the ten mixes reached a residual flexural strength of approximately 10 MPa, while two of the mixes deviate from the others with 13.2 (1%F1 + 1% F5) and 15.0 MPa (2% F1), respectively. With regard to the concretes containing 1.5 % of fibres, the mix containing macro steel fibres (F1) only, performed better (11.1 MPa) than the three mixes with combinations of steel fibres (F1 + F4/F5/F6), which gave results in the range 10.1 – 10.4 MPa.

Also for 2% of fibres, the concretes containing F1 fibres, only, performed better than the other combinations. Among the concretes with fibre cocktail, the combination of long steel fibres (F1)

and 13 mm (F5) fibres gave the strongest concrete. Note however, that concretes containing 2 % of fibres challenges the degree of compaction and workability, and this might be the explanation of the larger scatter observed. Another plausible explanation might be the failure mechanism which can be different for concretes with large fibre volumes compared to ordinary fibre concrete /Kanstad 2012/.

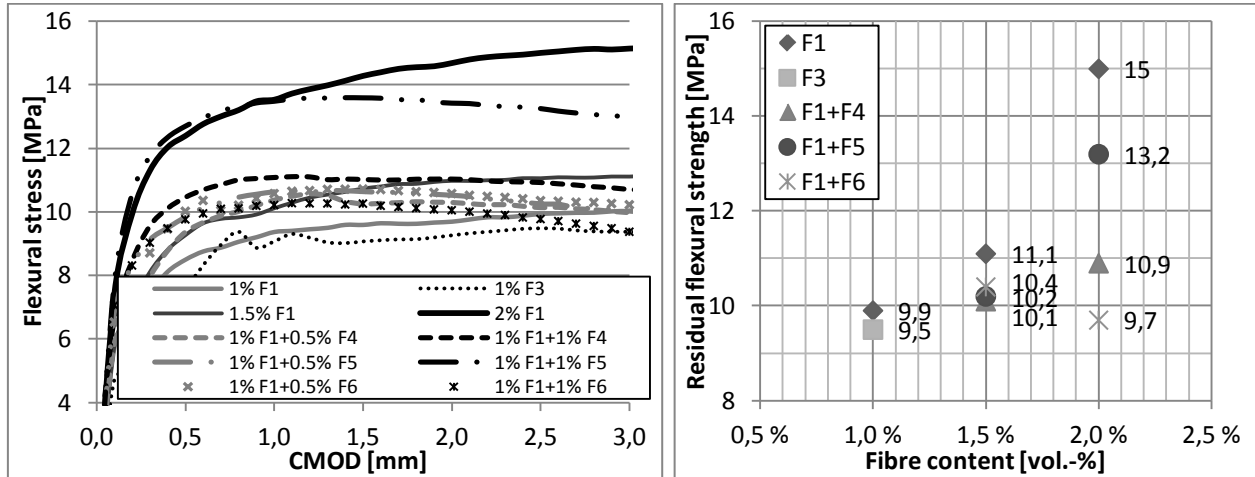


Figure 1: Flexural stress versus CMOD (left) and Residual flexural strength (f_{R3}) versus nominal fibre content (right) for concretes with a w/c-ratio of 0.55.

3.2 Residual flexural strength versus compressive strength (w/b-ratio)

Figure 2 shows the relationship between residual flexural strength and concrete compressive strength. In general, the residual flexural strength increase with increasing compressive strength, i.e. by reduced w/b-ratio /Grünewald 2004/. However, for the concretes with combinations of F1-fibres and micro fibres F5 the effect is less pronounced, and for concretes with F1 and F4 fibres the residual strength even seems to decrease after a certain compressive strength is reached. One reason could be that the fibres break as a result of increased bondage with reduced w/b-ratio. Further tests are needed in order to verify this. Finally it should be noted that the two highest residual strength values (at 2.5 mm CMOD) are reached with w/b=0.35 and 2 % 60mm end hooked steel fibres, respectively 18.9 MPa with the F1 fibres and 17.3 MPa with the F3 fibres.

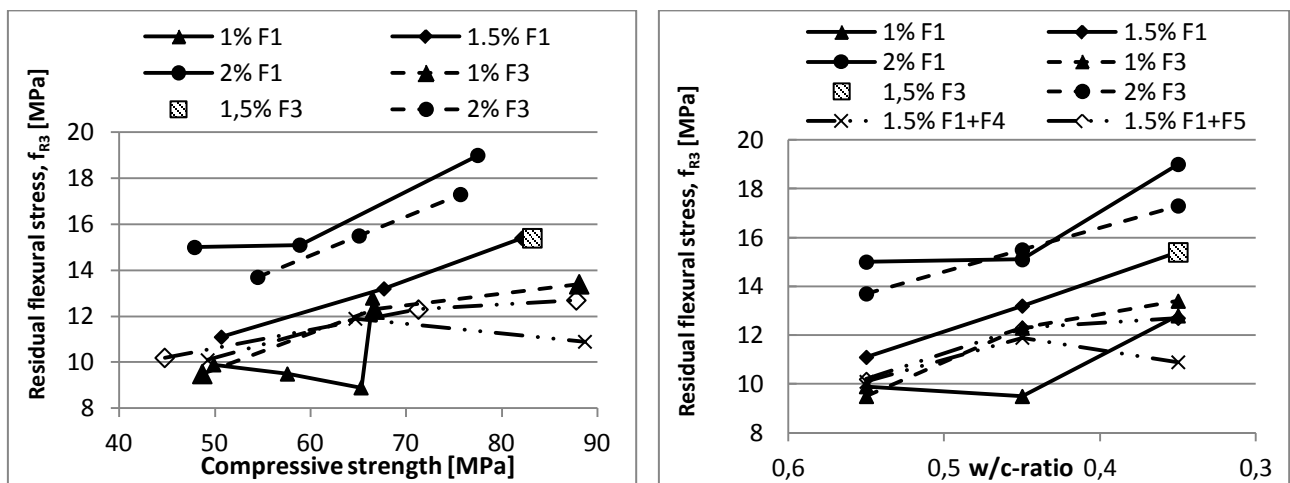


Figure 2: Residual flexural stress versus compressive strength (left) and Residual flexural stress versus w/c-ratio for increasing concrete strength.

4 CONCLUSIONS

The present experiments have given increased general knowledge, understanding and experience on the behaviour and performance of both fresh and hardened fibre reinforced concrete. The COIN target residual flexural strength of 15 MPa has been reached by several approaches with 18.9 MPa as the highest value, but the high necessary fibre dosages are challenging due to fresh concrete behaviour and fibre efficiency. All the investigated concretes (fibre volume 1 % or larger) have clear bending-hardening behaviour. It is shown that it is possible to reach the COIN target residual flexural strength of 15 MPa with a well composed concrete and fibre volumes of 2 % or higher, and a compressive strength in the range of ordinary concrete for buildings.

The tested concretes have a certain flowability and compactable properties that do not require vibration and the mass stays relatively homogenous. However, the present work has revealed that the standardized slump flow test does not reflect the actual castability of the concrete, as the long fibres remains in the middle of the slump flow table, even though the concretes had reasonable workability. The most promising high residual tensile strength concrete with $w/b=0.35$ and 2 % steel fibres will be used for testing of full-scale structural elements during the spring 2014 to gain further experience and for mapping of the flowability and strength properties.

ACKNOWLEDGEMENTS

The paper is based on the work performed in COIN - Concrete Innovation Centre (www.coinweb.no) - which is a Centre for Research based Innovation, initiated by the Research Council of Norway (RCN) in 2006. COIN has an annual budget of NOK 25 mill, and is financed by RCN (approx. 40 %), industrial partners (approx 45 % of which ¼ is cash) and by SINTEF and NTNU (in all approx 15 %). The Centre is directed by SINTEF, with NTNU as a research partners and with the present industrial partners: Kværner, Norcem, the Norwegian Public Roads Administration, Mapei, Skanska, Unicon, Veidekke and Weber Saint Gobain.

REFERENCES

Elkem Silicon materials (2014)

[online] Available from: <http://www.elkem.com/en/Silicon-materials/Support/Software-EMMA/>

Grünewald, S. (2004):

Performance-based design of self-compacting fibre reinforced concrete. PhD-thesis, Delft University of Technology, Netherlands, June 2004.

Kanstad, T., Sandbakk, S., Geiker, M.R. and Martius-Hammer, T.A. (2012):

Flowable fibre reinforced concrete: materials development, fibre distribution and structural properties. Proceedings from the ERMCO conference, Italy, 2012.

Martius-Hammer, T.A., Kjellmark, G., Kanstad, T. (2012):

Mix design of structural fibre reinforced self-compacting concrete with high fibre content. Proceedings of the Fifth North American Conference on the Design and Use of Self-Consolidating Concrete, Chicago, Illinois, USA, May 2012.

Sandbakk, S. (2011):

Fibre reinforced concrete – Evaluation of test methods and material development. PhD-thesis, Department of structural engineering, NTNU, Trondheim, Norway, April 2011

Sarmiento, E.V., Zirgulis, G., Sandbakk, S., Geiker, M.R., Kanstad, T. (2012):

Influence of concrete flow on fibre distribution, orientation and mechanical properties of fibre reinforced concrete. BEFIB 2012 - 8th RILEM International Symposium of Fibre Reinforced Concrete. Rilem publications 2012 ISBN 978-2-35158-132-2. s. 119-120

An Initial Investigation of the Possibility to Use Basalt Fibres for More Durable Concrete Structures in Norwegian Fish Farming



Ali Mohammadi Mohaghegh
PhD Candidate
Ålesund University Collage
P. O. Box 1517, N-6025
Ålesund
Corresponding author:
almo@hials.no



Johan Silfwerbrand
Professor
Department of Civil and
Architectural Engineering
KTH Royal Institute of
Technology,
SE 100 44 Stockholm



Vemund Årskog
Associate Professor
Ålesund University College
P. O. Box 1517, N-6025
Ålesund

ABSTRACT

Reinforcement corrosion in concrete structures in the harsh environment of the humid and cold climate of the Norwegian west coast is one of the most challenging problems pertaining to the design and construction of marine concrete structures. Using new materials with a higher strength and durability than steel reinforcement can be a good solution in such circumstances. In our study we investigate the use of new forms of macro fibres termed MiniBars made from basalt fibres. The paper presents our preliminary findings indicating that basalt fibres might provide more sustainable reinforcement in concrete barges.

Key words: Reinforcement, Fibres, Corrosion, Sustainable, Fish Farming Barges

1. INTRODUCTION

Development of commercial fish farming in Norway started around 1970. Today, aquaculture is one of the main industries on the west coast of Norway (Fao.org, 2014). In 2010, around 62% of Norwegian fish export with the value of 33.4 billion NOK was from aquacultures (Mathisen, 2012). But the concentration of fish in the farms can be harmful to the local environment (Mathisen, 2012). One approach to solve this problem is moving the fish farms to more exposed areas, further from the coast (Mathisen, 2012). A well-functioning feed barge is the basis for such fish farms and using concrete barges could be an economical option for this purpose. The barges are used as storage units, but also for workshops and homes for the workers, so safety and long term performance are important issues.

The results of a probability-based durability analysis on exposed parts of a concrete barge show that after a period of 15 years, the probability of failure in the form of depassivation exceeds 10%, while the critical chloride concentration has already reached to the reinforcement after a service period of 12 years (Årskog et al, 2004). It shows that the cover thickness specified according to Eurocode is not sufficient to protect the reinforcement from corrosion. There are two possible solutions to this problem; one is to increase the cover thickness and the other one is using corrosion resistant reinforcement. In barges the dead weight of whole structure is an important parameter in design and construction, because it affects both the total cost and the load bearing capacity. Therefore, increasing the cover thickness is not a good solution. Replacing steel reinforcement with fibre reinforced polymer (FRP) rebars in combination with basalt fibres could be another solution. When stainless steel reinforcement is used, the minimum cover due to environmental condition can be reduced and the same concept can possibly be applied for the FRP rebars.

Basalt fibres as raw material for producing basalt fibre reinforced polymer (BFRP) are non-toxic, environmental friendly and cheaper than carbon, silica and other type of fibres (Patnaik, 2009). Also it has a high resistance to corrosion, acidic and alkaline environments (Patnaik, 2009). BFRPs for structural applications exist in the form of bar, basalt macro fibre and fabric. MiniBar is a kind of macro fibre; it has average diameter of 0.66 mm and cut length of 43 mm. It is made from basalt continuous fibres (BFC) with the diameter of 17 μm and an epoxy based vinyl ester resin used as binder, see Figure 1 (Patnaik, 2013). Measurement shows a tensile strength of 1080 MPa and modulus of elasticity of 44 GPa for the fibres (Patnaik, 2013).

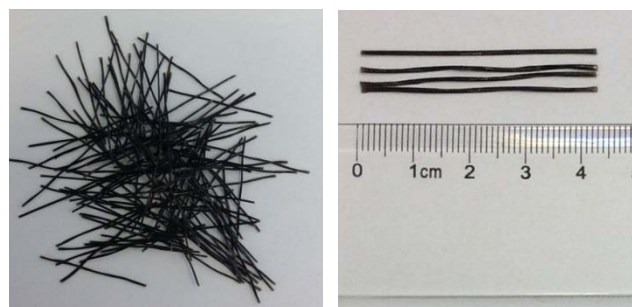


Figure 1- Geometry of MiniBars, the length of fibres, as it can be seen is, around 43 mm

The density of basalt macro fibre is 1900 kg/m^3 which is approximately the same density as concrete; therefore it will have an equal distribution in the fresh concrete mixture (Patnaik, 2013). According to DNV-OS-C502 the maximum amount of fibres is limited to 2% by

volume but because of equal distribution of fibres there should be a possibility to use higher amounts of fibres.

Figure 2 shows the relation between the fibre volume fraction and the concrete modulus of rupture, based on results from flexural tensile strength (FTS) testing. The average compressive strength of the concrete was 68 MPa. As it can be seen, a FTS of 16 MPa was obtained for fibre volume fraction of 4%.

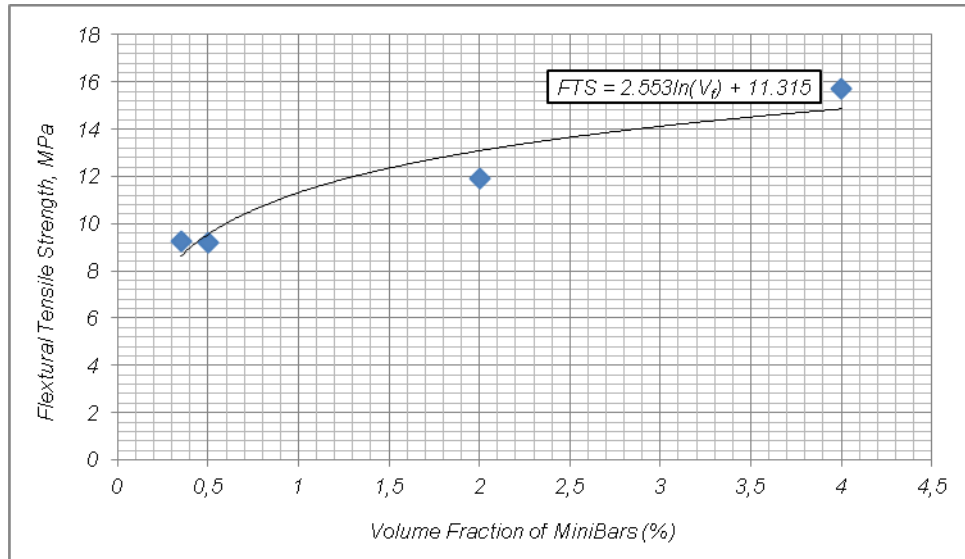


Figure 2- Flexural tensile strength against volume fraction of MiniBars (Patnaik, 2013)

2. CONCLUDING REMARKS AND FURTHER WORKS

A Sustainability approach in design and construction of concrete structures is highly desirable in order to reduce the ecological impact from the concrete construction industry. Basalt macro fibres and generally BFRPs with higher strength, high corrosion resistance and lower density could be a very good alternative to steel reinforcement for concrete structures in marine environment. Due to the high corrosion resistance of BFRPs, the concrete cover can be decreased, leading to a reduction in the volume of concrete and weight for a given structure. Because of the higher FTS of basalt fibre concrete, a part of reinforcement could be eliminated. Transportation and labour cost of construction could be decreased by using BFRPs pertaining to its higher strength and lower density. As a result, the ecological impact could be reduced.

The only published information about basalt fibre concrete is limited to experimental results which have been performed by Akron University (Patnaik, 2013). In those experiments ACI and ASTM have been used as testing standards and the maximum aggregate size is limited to 20. According to DNV, the maximum aggregate size for offshore applications must be less than 16 mm, therefore there is a need to perform the experiments according to European test standards and with the local aggregates. Regarding cost and economy, self-compacting concrete (SCC) for marine applications may be an interesting option, but there is no available information about basalt fibre (BF) SCC. Also there is a lack of information pertaining to chloride ingress in BF concrete. In order to investigate the chloride resistance of basalt macro fibre concrete, the NT BUILD 492 testing method could be a good option. To have an optimized structural system a hybrid system of BFRP bars and basalt macro fibres as reinforcement is necessary; therefore tests on hybrid structural elements made by both of them

are needed. As the first step we have planned for a testing program on fresh and hardened BF-SCC. The tests will be performed according to NS-EN 12350, 12390, 14488, ASTM C 1399 and NT BUILD 492. The aim of the first series of experiments is to characterize the properties of the fresh and hardened concrete. In the second step we are going to test hybrid elements aimed for marine structures.

3. ACKNOWLEDGEMENT

The first author greatly appreciates the information provided by ReforceTech Company

REFERENCES:

- CEN, (2004).
Eurocode 2: Design of concrete structures - Part 1-1: General rules and rules for buildings. EN 1992-1-1. Standard Norge.
- DNV, (2012).
Offshore Concrete Structures. DNV-OS-C502. DET NORSKE VERITAS AS.
- Fao.org, (2014).
FAO Fisheries & Aquaculture National Aquaculture Sector Overview (NASO).
[Online] Available at: http://www.fao.org/fishery/countrysector/naso_norway/en
[Accessed 28 Apr. 2014].
- Mathisen, S. (2012).
Design criteria for offshore feed barges. Master Degree. NTNU
- Patnaik, A. (2009).
Applications of Basalt Fiber Reinforced Polymer (BFRP) Reinforcement for Transportation Infrastructure. Department of Civil Engineering, The University of Akron, OH44325-3905.
- Patnaik, A. (2013).
Gen 3.1 MiniBar Reinforced Concrete (MRC). NO-1383 Asker, Norway:
ReforceTech Basalt Fiber Reinforcement Technology
- Årskog, V., Ferreira, R. and Gjørsv, O. (2004).
Durability analysis and performance of concrete barges. CONSEC04, Seoul, Korea.

Experimental Investigation on Rebar Corrosion in Combination with Fibres



Carlos Gil Berrocal
PhD-student
Chalmers University of
Technology
412 96 Göteborg, Sweden
carlos.gil@chalmers.se



Karin Lundgren
Professor
Chalmers University of
Technology
412 96 Göteborg, Sweden
karin.lundgren@chalmers.se



Ingemar Löfgren
PhD,
Thomas Concrete Group AB
412 54 Göteborg, Sweden
ingemar.lofgren@tcg.nu

ABSTRACT

In this paper, early results from an on-going project aimed at investigating the influence of fibre reinforcement on corrosion of rebar are presented. Resistivity of mixes containing fibres was reduced when compared with plain concrete while chloride migration seemed to remain unaffected. On the mechanical properties, results showed that while the flexural behaviour was greatly enhanced by addition of fibres up to 0.5% vol., the variation in compressive strength was negligible regardless of the fibre type. Early results from the main experiments indicated a tendency of earlier corrosion initiation with increasing crack width, and that the initiation time was somewhat delayed for the fibre reinforced specimens.

Key words: cracking, chlorides, corrosion, fibres

1. INTRODUCTION

Civil engineering structures like bridges and harbour piers require the use of a dense concrete (low w/c ratio), thick concrete covers and strict crack width limitations due to the risk for chlorides to cause reinforcement corrosion. In practice, this leads to large reinforcement amounts which often cause complications in production, but still with difficulties in controlling the surface crack width due to the large concrete cover. Fibre reinforcement has been extensively used in applications such as buildings, floors or slabs on grade for crack control (Bentur and Mindess 2007). Therefore, it would be beneficial to use fibres, in complement to the traditional reinforcement, also in civil engineering structures where their crack limiting effects are of interest.

However, the use of fibres in combination with conventional reinforcement in chloride environments raises questions due to the limited research available in this field. Some of these questions are related to the influence fibres may have with respect to chloride ingress and moisture transport. The main issues that have yet to be dealt with are the potential risk of galvanic corrosion due to the different steel types used in the fibres and in the traditional reinforcement, and the risk of higher corrosion rates due to lower resistivity of steel-fibre reinforced concrete. In an on-going Ph.D. project at Chalmers University of Technology, the

authors investigate the durability of concrete structures with regard to chloride induce corrosion when fibre reinforcement is combined with conventional reinforcement.

2. EXPERIMENTAL PROGRAMME

The main task in the project consists of a long-term experimental campaign specifically conceived to answer the aforementioned questions. The experiments include a total of 56 beam specimens with dimensions 100×180×1100 mm and reinforced with 3 Ø10 mm diameter rebar as illustrated in Figure 1. The reinforcement was placed to get a clear concrete cover of 30 mm and the separation between bars was kept to 45 mm to allow the fibres to easily flow through them and ensure a more homogenous material.

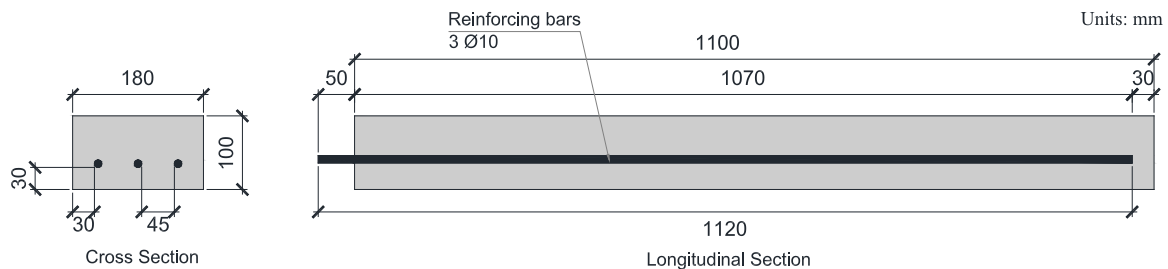


Figure 1. Geometry of the test specimens

A single concrete mix and three types of fibres were used to cast four different types of concrete, hereafter referred as to: *plain*, for ordinary concrete; *steel*, for steel-fibre reinforced concrete; *hybrid*, for a combination of steel and micro polyvinyl-alcohol fibre reinforced concrete; and *synthetic*, for macro polyvinyl-alcohol fibre reinforced concrete. Table 1 shows the mixture proportion and fibre dosages used in each mix. Further parameters varied are the loading conditions, including sound specimens (never cracked) and specimens cracked and subjected to cyclic loading (bond degradation), sustained loading, or no loading. Also the influence of surface crack width is studied with openings ranging from 0.1 to 0.4 mm. Six specimens are kept immersed in potable water as a reference while the rest are exposed to an accelerated process of natural corrosion by partial immersion in 10% Cl⁻ solution and cycles of 14-day wetting and 14-day drying. Moreover, companion specimens to study chloride ingress, chloride migration and resistivity of concrete, as well as compressive strength and flexural behaviour of fibre concrete were cast.

Table 1. Mixture proportions, kg/m³

| Component | | | | |
|--------------------------------------|-------|-------|--------|-----------|
| Cement (CEM I 42,5N SR 3 MH/LA) | | | | 360 |
| Limestone filler (Limus 40) | | | | 165 |
| Fine aggregate (Sand 0/4) | | | | 770 |
| Coarse aggregate (crushed 5/16) | | | | 833 |
| Effective water | | | | 169 |
| Superplasticizer – Glenium 51/18 | | | | 5.76 |
| Air entrainer – MicroAir 105 | | | | 0.72 |
| Fibre (Volume, %) | Plain | Steel | Hybrid | Synthetic |
| Steel – Dramix [®] 65/35-BN | - | 0.5 | 0.35 | - |
| PVA – Kuralon [™] RFS400 | - | - | 0.15 | - |
| PVA – Kuralon [™] RF4000 | - | - | - | 0.75 |

3. RESULTS AND DISCUSSION

Some results are shown in Figure 2, as can be seen, the addition of fibres in low dosages had a marginal effect on the compressive strength of concrete. Similarly, no significant variation was observed in the chloride migration coefficient for the different mixes. These results are in agreement with those from (Sanchez, Alonso, and Barragán 2009) or (Teruzzi et al. 2004) who concluded that the interfacial zone between fibres and the cement paste does not act as a preferential path for the ingress of detrimental agents. Resistivity tests, on the other hand, revealed a clear influence of fibres on this property. Resistivity of series containing steel fibres is invariably reduced with lower values for higher fibre contents. Moreover, synthetic series, with PVA fibres, also show a decrease in resistivity with respect to their ordinary concrete counterpart. Similar results are reported in (Roque et al. 2009), indicating that PVA fibres, despite their high resistivity ($\sim 3.5 \cdot 10^5 \Omega\text{m}$) and unlike other fibres such as polypropylene, may reduce the resistivity of concrete.

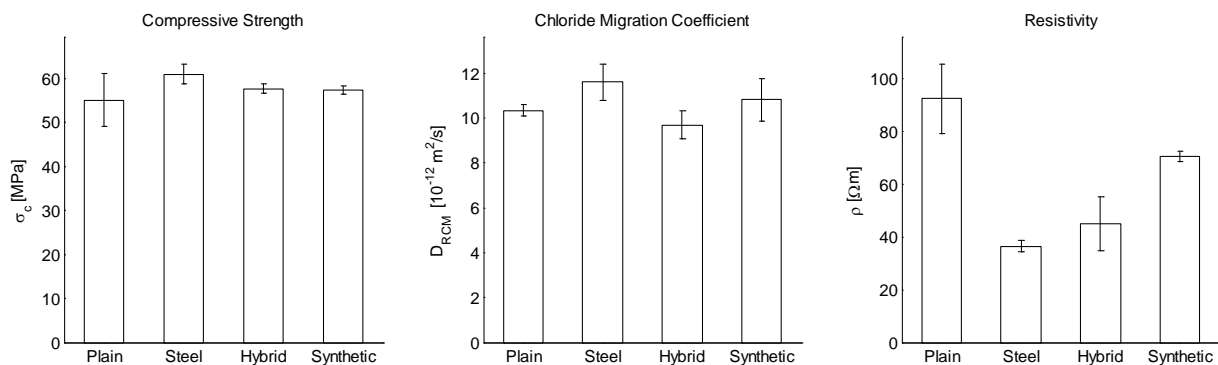


Figure 2. Results on material tests for compressive strength, chloride migration coefficient and resistivity of concrete (mean values and standard deviation for 3 specimens)

The flexural behaviour of fibre reinforced concrete was studied by means of three-point bending tests according to (RILEM TC 162-TDF 2002). Figure 3 evidences the enhanced flexural behaviour of fibres in terms of toughness while the increase in tensile strength is negligible.

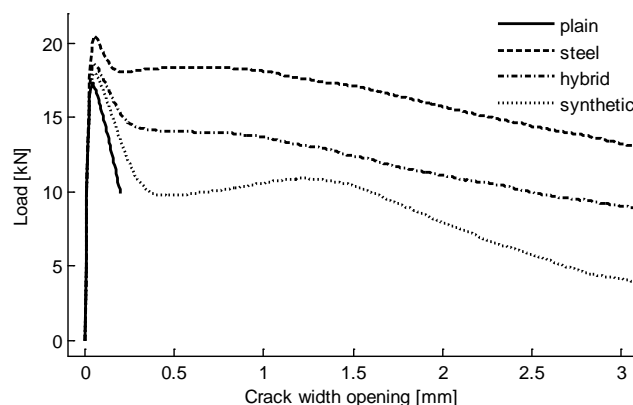


Figure 3. Load versus crack mouth opening displacement for three-point bending beam tests (Averaged curves for 6 specimens each)

In the long-term experiments, half-cell potential (HCP) are continuously monitored using an embeddable reference electrode. HCP describes the thermodynamic state of a metal's surface and, alone, does not provide information about the corrosion rate. However, it can indicate whether the reinforcement is actively corroding or in a passive state and it may suggest a range of corrosion rates. A proposed range to determine the probability of corrosion can be found in

(ASTM C876-91 1999). Based on that, the corrosion initiation times of each mix are shown in Figure 4 for varying crack width and for 3 different loading conditions. Note the difference in scales for loaded and unloaded series; the shorter initiation times for the loaded specimens are due to the cracks being kept open, while the values of the crack width in the other two series was the measured ones *before* unloading. A clear tendency is observed where larger crack widths led to earlier corrosion, except for the loaded specimens, where corrosion generally started soon after the first exposure to chlorides regardless of the crack opening. Additionally, a slight delay in the corrosion initiation time is observed for the fibre-reinforced mixes.

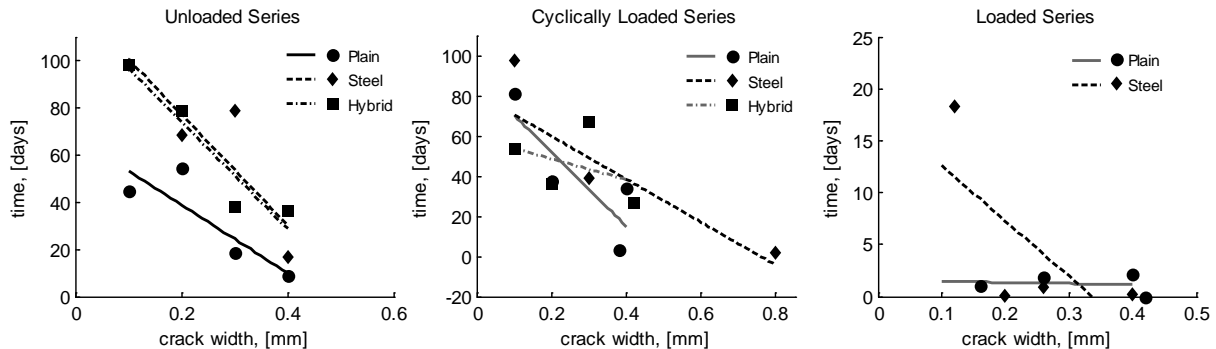


Figure 4. Corrosion initiation times for different loading conditions

4. CONCLUSIONS

The results from this investigation indicate that controlling the crack width is crucial in order to delay the initiation of corrosion in reinforced concrete structures. Fibre reinforcement can effectively control the crack width and provides a considerable improvement of the tensile properties of concrete in terms of toughness. Besides, given the same surface crack width, results show that corrosion initiation was somewhat delayed for fibre-reinforced mixes. On the physical properties, no adverse effect is detected regarding the chloride migration coefficient for FRC. Conversely, electrical resistivity is greatly decreased by the presence of steel fibres, and even in the case of PVA fibres, results show a reduction. Today, this fact represents the major impediment to use fibre reinforcement in combination with conventional rebar in chloride environments, as there are concerns that a reduced resistivity will increase the corrosion rates. Therefore, further investigations are required to address this issue.

REFERENCES

- ASTM C876-91. 1999. "Standard Test Method for Half-Cell Potentials of Uncoated Reinforcing Steel in Concrete." 91 (Reapproved).
- Bentur, Arnon, and Sidney Mindess. 2007. *Fibre Reinforced Cementitious Composites*. 2nd ed. Abingdon, United Kingdom: Taylor & Francis.
- RILEM TC 162-TDF. 2002. "Test and Design Methods for Steel Fibre Reinforced Concrete - Bending Test." 35 (November): 579–82.
- Roque, Reynaldo, N Kim, Byoungil Kim, and George Lopp. 2009. *Durability of Fiber-Reinforced Concrete in Florida Environments*. Tallahassee, FL.
- Sanchez, M., M.C. Alonso, and B. Barragán. 2009. "Durability Performance of Plain and Fiber Reinforced Self-Compacting Concrete." *CPI- Concrete Plant International-2*: 62–64.
- Teruzzi, T., E. Cadoni, G. Frigeri, S. Cangiano, and G. A. Plizzari. 2004. "Durability Aspects of Steel Fibre Reinforced Concrete." In *6th RILEM Symposium on Fibre-Reinforced Concretes*, 625–34.

SUSTAINABILITY AND AGEING

Re-usage of Concrete Elements – to determine their new possible environment



Dr. Martin Nilsson
Luleå University of Technology
Division of Structural Engineering
SE-971 87 Luleå
Email: Martin.Nilsson@ltu.se

ABSTRACT

40% of the energy consumption in Sweden is used in the construction industry. Recycling – including re-usage, recycling and energy recovery – could possibly reduce this energy consumption. Re-usage gives the largest energy savings, evaluated by calculating the recycling potential. Designing for disassembly means planning how structures can easily be disassembled into original components and then recycled. Concrete elements must be designed, documented and assessed regarding reinforcement, cutting locations and degradation, respectively, for a safe re-usage in new environments. A plan is designed for how to assess concrete elements and for which new environments they can be used in.

Keywords: structural design, recycle, design for disassembly, sustainable construction, condition assessment

1. INTRODUCTION

The concept Sustainable development was introduced by the World Commission on Environment and Development (“Brundtland Commission”) in 1987. They stated that

“Sustainable development is development that meets the needs of the present without compromising the ability of future generations to meet their own needs” /Brundtland Commission, 1987/.

Within the construction industry instead the concept sustainable construction is used. Its definition according to the International Council for Research and Innovation in Building Construction (CIB) reads /Kilbert, J. C., 2008/:

“Creating and operating a healthy built environment based on resource efficiency and ecological design.”

To meet this, the construction industry must change its behaviour. In Sweden the construction industry stands for about 40% of the total energy consumption. The operation phase is one of the three largest energy consumption phases in the life of a constructional work. The other two are the construction phase and the demolition/dismounting phase. In recent years a lot of effort has been put into decreasing the energy consumption in the operation phase, i.e. passive or low energy buildings. When decreasing the energy consumption during the operation phase, the others have to be more in focus.

When a construction comes to its end it is usually demolished or dismantled. Sometimes parts or materials are reclaimed in new structures, but to a very little extent. Concrete is sometimes crushed and reclaimed as ballast or road aggregates. If this is not the case, the material is dumped, which is not the best regarding energy consumption and sustainable development. Therefore, demolishing must be replaced with dismantling leading to recycling of whole structural elements.

1.1 Problem, purpose and limitations

Recycling decreases the energy consumption and it is a concept including re-usage, material recycling and energy recovery, where re-usage gives the largest energy saving. For this reason the concept design for disassembly has been established. Some guidelines can be found in e.g. Scotland, USA and Sweden /Thormark, 2001/ about design for disassembly, but nothing about how elements – read concrete – can be re-used.

The purpose of this work is to investigate for what other environments and loads old concrete elements can be re-used. The sub-purpose is to create an template/guide how to determine the new environment for an old concrete element

The remaining life of on element is set to when the carbonation or chloride threshold value reach the reinforcement and the corrosion starts. The environmental influence treated here is only the energy consumption, not emissions such as CO₂, NO_x or SO₂.

2. THEORY

Recycling

If an element or material is not re-used, recycled or burned up the life of the material is a straight line: raw material extraction ⇒ manufacturing ⇒ design ⇒ usage ⇒ demolition ⇒ disposal landfill. To get a closed cycle for materials, demolition must be replaced with dismantling and recycling, either of whole constructions, parts of constructions, materials for new parts or materials. Recycling contributes to save raw materials, reduce energy usage, decrease of emissions harmful to the environment and decrease the usage of ground for disposal landfill.

To express, measure and compare environmental aspects of recycling its potential can be calculated /Thormark, 2001/. This indicates the saving obtained by recycling and differs whether the material is re-used, recycled or burned up, where re-usage gives the highest value. The recycle potential can be calculated in energy, mass of raw material, money, emissions etc. The potential is calculated as

$$R_{\text{pot}} = \sum_{i=1}^n I_{p,i} L_{t,i} - E_{r,i} \quad (1)$$

where R_{pot} is the recycling potential, n is the number of materials, $I_{p,i}$ is the environmental impact of manufacturing the new material replacing the old, $L_{t,i}$ is the remaining life of the reclaimed material in per cent of the thought life of the material being replaced, $E_{r,i}$ is the energy consumed in the recycling process.

3. RE-USAGE OF CONCRETE ELEMENTS

When re-using a concrete element it is important to assess its condition /fib bulletin 71, 2013/ and to have knowledge about the amount and location of the reinforcement. If the element has

been degraded its new possible environment must be determined, which means changed exposure class /Eurocode 2, 2008/ or changed loading.

Different environments demand different concrete cover to protect the reinforcement. The degradation is due to chloride entrainment or carbonation, which can be estimated according to /Svenska betongföreningen, 2007/. One template for determination of new exposure class with respect to carbonation is seen in Figure 1. The similar is done with respect to chloride entrainment. If the carbonation or chloride entrainment reaches the reinforcement it will corrode. Then the time of corrosion has to be determined to estimate how much is left of the reinforcement. With knowledge about possible corrosion one can determine the load carrying capacity of the element.

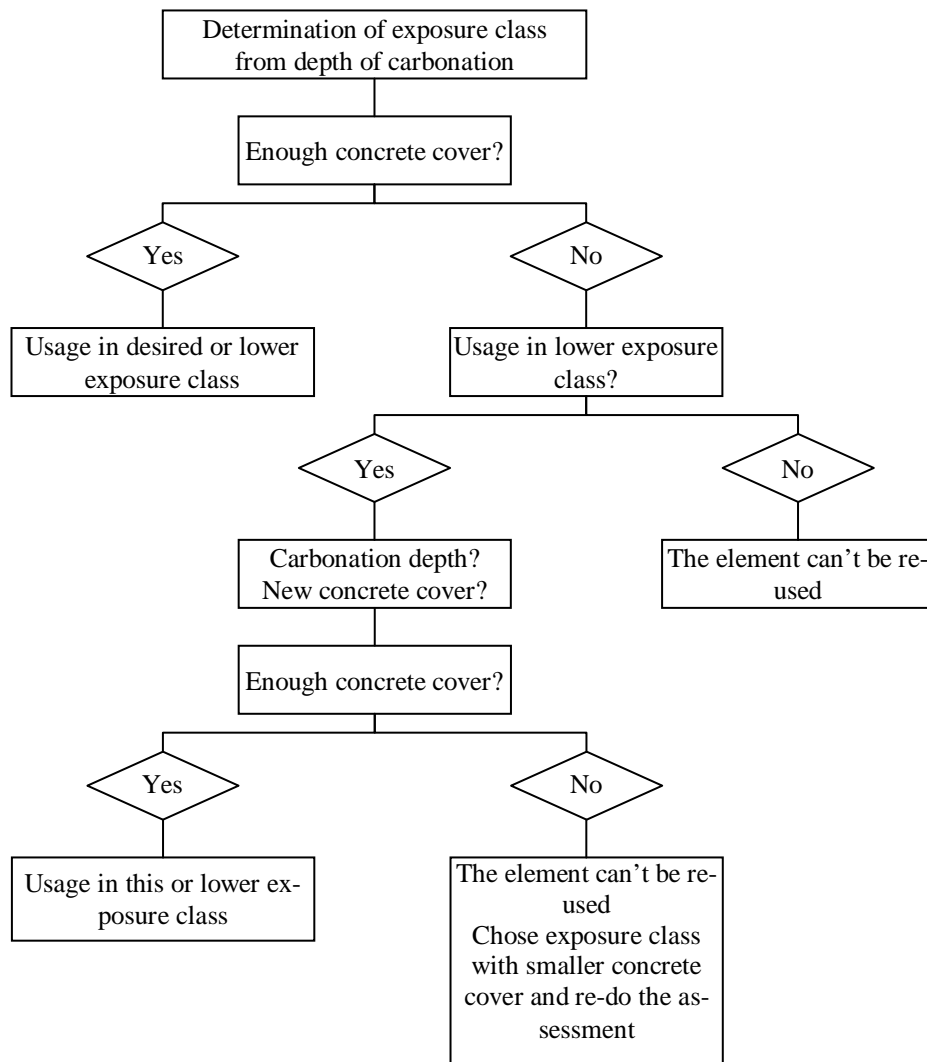


Figure 1 – New exposure class with respect to depth of carbonation /Ekergård, Y., 2012/

Simply supported one-span elements are easy to re-use. They only need to be assessed regarding chloride entrainment, carbonation, possible corrosion and load carrying capacity. However, if the element is clamped in one or two ends or continuous one has to be more careful. For example, a beam that before cutting is

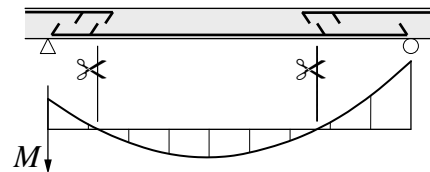


Figure 2 – Bending moments and cutting location in a continuous concrete beam

location where the span moment equals zero to get the same shear forces and bending moments as before cutting, Figure 2. But, one also must look at the reinforcement content and location in order to estimate the load bearing capacity.

4. DISCUSSION AND CONCLUSIONS

By assessing the carbonation and the chloride entrainment it is possible to estimate what is left of the concrete cover or if the reinforcement is corroding. Then it is possible to determine the new concrete cover and thereby the new exposure class and possible new environment. When re-using concrete elements, one saves in planning, design, manufacturing and transportation of new elements and loses in planning, design, assessment, possible cutting and transportation of the old elements. The net saving is however positive, especially regarding environmental emissions since re-usage leads to less raw material usage and less manufacturing and processing.

A sustainable construction should be designed for as little energy consumption as possible during its whole life span and with a high possibility for re-usage. To make it more possible to re-use concrete elements in the future the following guiding principles should be noticed: 1. initial properties (concrete, reinforcement, exposure class, concrete cover etc.), 2. external environmental properties (chlorides, carbon dioxide); 3. plan for cutting and possible test locations; 4. possible tests of the fresh element (carbonation and chloride entrainment resistances); 5. which assessments must be done (chloride profile, carbonation depth and resistance, concrete quality etc.), 6. what equipment is needed for the dismounting.

REFERENCES

Brundtland Commission, 1987

Our Common Future, Report of the World Commission on Environment and Development, World Commission on Environment and Development, 1987. Published as Annex to General Assembly document A/42/427, Development and International Co-operation: Environment August 2, 1987.

Ekergrård, Y., 2012

Återvinning av betongelement – att bestämma ett elements nya miljö (Recycling of concrete elements - to determine the new environment of an element). Luleå, Sweden: Luleå University of Technology, Master thesis, LTU-EX-2012-41450916

Eurocode 2, 2008

Design of concrete structures – Part 1-1: General rules and rules for buildings. European standard EN 1992-1-1

fib bulletin 71, 2013

Integrated life cycle assessment of concrete structures, State-of-art report, Task Group 3.7, International Federation of Structural Concrete (fib), ISBN 978-2-88394-111-3

Kilbert, J. C., 2008

Sustainable constructions green building design and delivery. Canada: John Wiley & Sons, Inc.

Svenska Betongföreningen, 2007

Vägledning för livslängdsdimensionering av betongkonstruktioner (Guidance for design of life length of concrete structures). Betongrapport 7, 2007

Thormark, C., 2008

Projektera för demontering och återvinning (Design for disassembly and recycling). Stockholm: AB Svensk Byggtjänst.

Thormark, C., 2001

Recycling Potential and Design for Disassembly in Buildings. Lund: Byggnadskonstruktion, Lunds Tekniska Högskola.

ZeroWaste: Turning waste into a new, sustainable resource for concrete



Dr. Per Goltermann
Technical University of Denmark, Building 118,
DK – 2800 Lyngby
E-mail: pg@byg.dtu.dk



Dr. Lisbeth Ottosen
Technical University of Denmark, Building 118,
DK – 2800 Lyngby
E-mail: lo@byg.dtu.dk



Dr. Pernille Erland Jensen
Technical University of Denmark, Building 118,
DK – 2800 Lyngby
E-mail: pej@byg.dtu.dk



Dr. Gunvor Marie Kirkelund
Technical University of Denmark, Building 118,
DK – 2800 Lyngby
E-mail: gunki@byg.dtu.dk

ABSTRACT

The ZeroWaste research group at the Department of Civil Engineering at the Technical University of Denmark (DTU Byg) was established two years ago and covers the broad range of expertise, required for turning waste materials into attractive, new materials. Members of the group have, prior to that, developed methods for removal of heavy metals and phosphorous from waste incineration, sewage sludge and other bio ashes, providing the basis of to make these ash types an attractive, new material for the building sector. Initial results for upgrading and using different types of ashes are presented in the paper, including an approach for involving large number of project students in the work.

Key words: Waste, environment, new concrete types, puzzolans, design, testing.

1. INTRODUCTION

The production of waste in Denmark is fairly large and corresponds to 1.45 tons/person/year. A substantial part of the waste is already recycled or incinerated, and only a small part is deposited. Incinerating waste is beneficial as it will 1) generate energy and heating for the large cities, 2) reduce volume and weight and 3) in the case of e.g. sewage sludge also remove health hazards from pathogens and organic contaminants.

Table 1 - Main waste productions in Denmark with 5.6 mio inhabitants /Miljøstyrelsen 2011/.

¹The material is normally incinerated.

| Origin | Mio ton/year | Solid material | Recycling |
|---------------------------------|------------------|--------------------|-----------|
| Building industry (Concrete) | 5.0 (1.2) | 5.0 (1.2) | 90% |
| Coal fired power plants | 1.2 | 1.2 | 90% |
| Household waste | 3.4 ¹ | 0.7 ¹ | 85% |
| Sewage plants | 0.8 ¹ | 0.009 ¹ | |

In comparison to this, the use of concrete in the industrialized world is app. 1 m³/person/year each requiring 1.5-2.0 tons aggregates and 3-400 kg cement and puzzolans (flyash). In addition to this, large amounts of materials are required for road construction, landfills, expansion of harbor areas etc. The large amounts of waste materials and required resources show that both waste handling and construction can benefit from mutual involvement from both sectors. The waste must, however, be turned into environmentally safe, attractive and renewable resources and preferably be used to reduce the cement consumption and improve the concretes. DTU Byg decided therefore to establish a strong and multidisciplinary research group ZeroWaste Byg (www.zerowaste.byg.dtu.dk), to deal with these problems and possibilities.

2. THE ZEROWASTE GROUP

The group consists of 11 faculty members plus 3 PhD students and covers the fields of building materials, structures, deterioration, indoor and outdoor environments, codes and standards, testing, product optimization and other civil engineering fields and has established an efficient code of cooperation (e.g. all questions are welcome and will be answered and all members must both contribute and benefit). The ZeroWaste group follows a number of basic dogmas for the research and development:

- The build environment is placed centrally in a sustainable material cycle of the society Research and innovation is focused on replacement of natural raw materials with secondary resources
- Building technology is rethought and materials are redesigned for today's as well as tomorrow's demands

- There is no compromise on the quality of the construction materials
- There is no compromise on environmental impact

Team members have already developed electro-dialytic to upgrade the incinerated materials to higher environmental safety by removing heavy metals and salts processes /Ottosen et al. 2006/, /Kirkelund et al. 2013/. A recent innovation has also made it possible to remove the phosphorous from the sewage ash /Ottosen et al. 2013/, which can fulfill the future Danish requirements of recycling the phosphorous /Danish Government 2013/. These new methods provide a potentially cost efficient way of cleaning and upgrading the ashes and their economy will be influenced by a) avoiding deposit taxes (often saving 80€/ton or more), b) capturing heavy metals (price unknown), c) capturing phosphorous from sewage ash to use as fertilizer (value above 100€/t sewage ash) and d) costs of establishing and running the plant. These methods also results in a number of new and interesting materials to use in concrete or other applications.

3. INITIAL RESULTS

The research in the ZeroWaste group initially focused on reuse of sewage sludge ash and later on other ash types. The relevant topics to investigate are many, as e.g. 1) replacement of cement or sand by fly ash, 2) water requirement for the mix, 3) effects on mix stability, 4) coloring of mix, 5) to wash or not to wash ash prior to use, 6) difference between stored ashes from the deposit and fresh ashes, 7) effect of grinding of the ashes, 8) setting time, 9) development of strength, 10) corrosion protection, 11) chloride binding, 12) indoor climate effects and 13) aesthetic impression. In order to work efficiently with this, a semester based R&D plan has been set up.

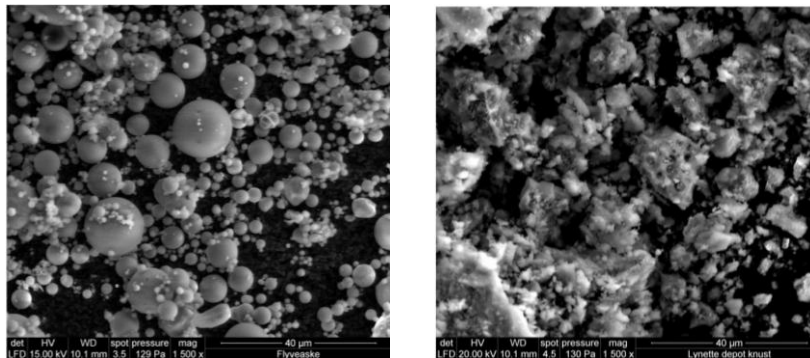


Figure 2 – SEM pictures of coal flyash (left) and milled sewage sludge ash from Lynetten (right). The scale of the two pictures are the same / Carlsen and Petersen 2013/.

The group has supervised app. 30 project students in the past two years, organized in project families (independent projects sharing a common semester focus based on the R&D-plans). The students have so far put 15-20.000 hours of work dealing with different aspects of the use of the ashes, both from incinerations plants and from sewage treatment plants and produced many valuable results. This enables not only efficient supervision, but leads also to many useful results, as the group of students work together with the R&D group and produces app. 5000 hours of work per semester. The results of each semester's student projects have had an impact on the R&D and use of project families facilitates cooperation with the industry significantly.

One important result was that the ash should be ground in a mill in order to improve its structure and to reduce the required amount of water and improve the strength of the mix, probably due to the changes in the ash structures, although the ground ash will still not have the same structures

as coal fly ash, as seen on Figure 2. Tests have indicated that up to 20% of the cement may be replaced while the strength is maintained at reference level with up to 10 % and a structurally acceptable level up to 20 % (Figure 3). Other tests have shown that replacing sand with ash may increase the strength.

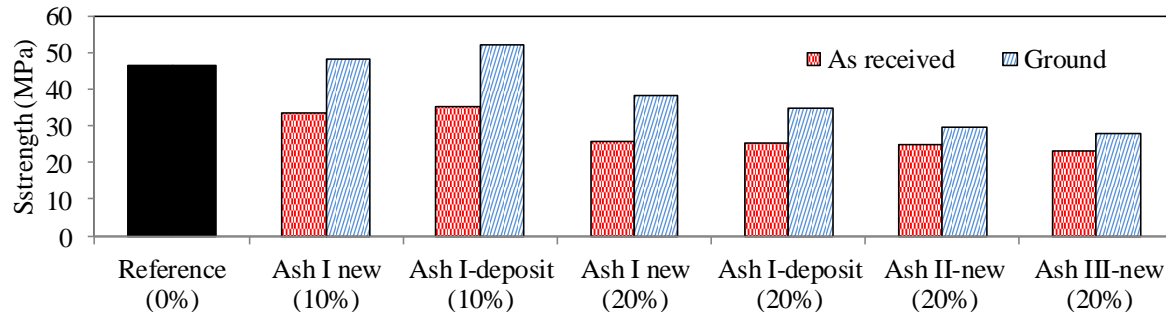


Figure 3 – Compressive 7 days strength in different mixes with constant water content and three different sewage ash types (results from student projects 2012-13).

The tests show sewage sludge ash has no pozzolanic effect, but additional tests show that other ashes can have a pozzolanic effect.

4. CONCLUSIONS

The techniques to extract the heavy metals from the ashes make these environmentally safe to use. The extraction of phosphorous from sewage ash provides a good and renewable source of phosphorous. This transforms ashes from environmentally dangerous waste materials to safe and renewable resources for the concrete mix and for construction activities. A methodology for testing new ashes in concrete is being developed, based on an interdisciplinary approach on the issue.

REFERENCES

- Carlsen, A.B. and Petersen, S.R., 2013
 "Slamaske i beton. Undersøgelse af anvendelsesmuligheder", DTU, January 2013
- Danish Government, 2013,
 "Danmark uden affald. Genanvend mere – forbrænd mindre". ISBN 978-87-93026-07-0.
- Miljøstyrelsen, 2011
 "Affaldsstatistik 2009 og Fremskrivning af affaldsmængder 2011-2050", Orientering fra Miljøstyrelsen Nr. 4, 2011
- Kirkelund G.M., Damoe A.J., Ottosen L.M., 2013
 "Electrodialytic removal of Cd from biomass combustion fly ash suspensions". Journal of Hazardous Materials 250-251: 212-129.
- Ottosen L.M., Lima A.T, Pedersen A.J., Ribeiro A.B., 2006
 "Electrodialytic extraction of Cu, Pb and Cl from municipal solid waste incineration fly ash suspended in water". J Chem Technol Biotechnol 2006; 81: 553–9.
- Ottosen, L.M., Kirkelund, G.M. and Jensen P.E., 2013
 "Extracting phosphorous from incinerated sewage sludge ash rich in iron or aluminum". Chemosphere 91(7), 963-969.

Effects of aging concrete in support structures for hydroelectric machinery



Doctoral student, M.Sc. Tobias Gasch
KTH Royal Institute of Technology, Concrete Structures
SE - 100 44 Stockholm
E-mail: tobias.gasch@byv.kth.se



Researcher, Dr. Richard Malm
KTH Royal Institute of Technology, Concrete Structures
SE - 100 44 Stockholm
E-mail: richard.malm@byv.kth.se

ABSTRACT

At many of the Swedish hydropower plants, cracks have been observed in the concrete power station. Although the presence of cracks in these massive concrete structures does not pose an immediate threat to the structural safety, it of course affects its durability. Besides this, and perhaps as important in this application, the presence of cracks reduces the structural stiffness which affects the operation of the machinery. A case study is presented, where cracks have been found in the concrete support. Furthermore, analysis methods to evaluate the status of the concrete support; mainly through the use of finite element analysis are proposed.

Key words: Aging, Cracking, Modelling, Shrinkage

1. INTRODUCTION

The hydropower industry in Sweden is currently in a phase of managing and operating its aging power plants, most of which were built during the mid 20th century. This includes maintenance of aging concrete structures, not only the large water retaining concrete dams but also the concrete structures of the power stations. Especially, the status and integrity of the concrete surrounding and supporting hydroelectric generators and turbines are of importance in order to maintain a continuous and safe operation of the power plant. A detailed study is needed, since the machine manufactures and operators often regard the concrete support structure as a rigid boundary. A reduced structural stiffness due to damaged and aging concrete will thus have a significant influence on the how the rotating machinery behaves.

A typical layout of a power station is shown in Figure 1a), where the water enters the station through the penstock (1). At the end of the penstock there is a turbine runner, which is turned by the flowing water. The shaft from the turbine goes up into the generator, which produces the electricity. The generator is supported by a concrete support structure, illustrated as (5) in the figure. It should be noted the design of the power house and the concrete support structure surrounding the unit can vary significantly between different power stations. A vertical cross-section of a typical concrete support structure is illustrated in Figure 1b), together with some components of the hydroelectric unit and its steel beam support brackets.

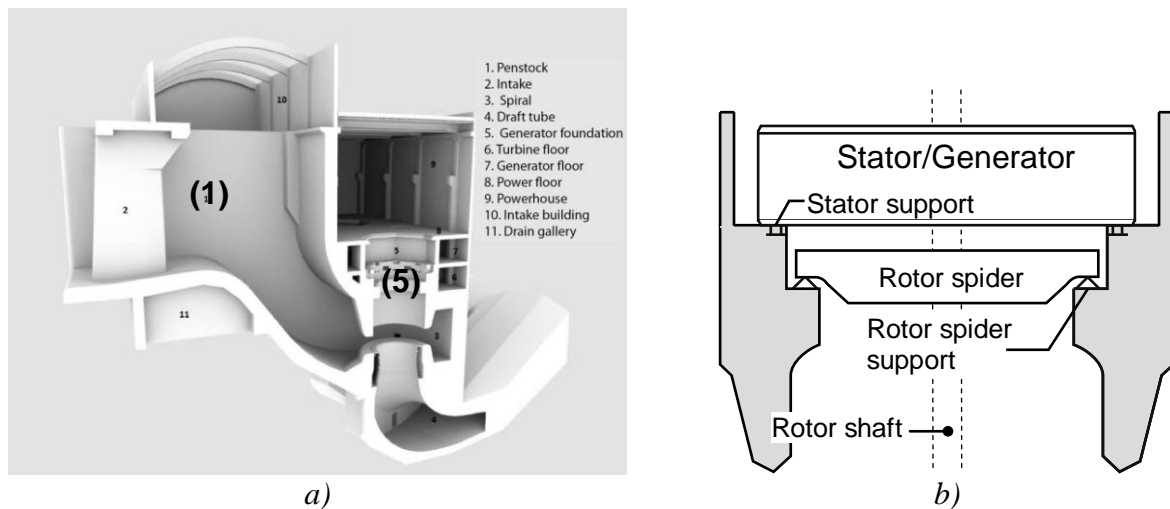


Figure 1 – Schematic layout of a hydropower station (a), from (Paavola, 2011), and a vertical cross-section of the concrete support structure (b).

2. TYPICAL LOADS ON THE REINFORCED CONCRETE STRUCTURE

The focus in this study is on the reinforced concrete support structure for the generator, shown in Figure 1. The concrete is subjected to various loading conditions during its lifetime of which the most important are described in the following sections.

2.1 Environmental

During operation, the hydroelectric unit produce heat which causes the temperature in the generator chamber to be significantly higher than in the ambient air. Typically, the temperature in the generator chamber varies between 25-34°C, whereas the temperature in other parts inside the power station varies between 15-24°C, depending on season. Also, an increase in temperature inside the generator chamber during operation leads to expansion of the large steel support brackets, causing further loading on the concrete, as investigated in (Rhen, 2007). Furthermore, environmental effects related to drying of the concrete such as creep and shrinkage, will affect the long-term behaviour of the structure. Especially since the cross section is up to 2 m thick and the thickness also varies considerably, causing internal restraint forces.

At some hydropower stations, deterioration process related to the environmental conditions (e.g. AAR) has also been observed in the concrete. However, such effects are not considered in the current study.

2.2 Mechanical

The concrete support structure is designed to carry the mechanical loads of the hydroelectric unit, both permanent and transient, which are transferred from the unit via the steel support brackets at several interconnections. Permanent loads can be summarised as the self-weight of the unit and its components, e.g. runner turbine, rotor shaft, generator, stator, bearings and support brackets. In a perfectly operated and balanced unit the transient loads from the unit would be small. However, this is often not the case, as for example mechanical unbalances and electromagnetic forces introduce a whirl in the rotating system, increasing the vibrations that are transferred to the concrete support structure. Hydraulic and mechanical forces in the runner also contribute to the vibrations. A more thorough description of loads that act on the concrete support structure due to operation and also various fault causes of the unit is given in (Malm et. al., 2013) and (Gasch et. al., 2013).

3. CASE STUDY OF STRUCTURAL DAMAGE AT A HYDROPOWER STATION

A case study of a hydropower plant located in the southern parts of Sweden is used to show some typical structural damages observed in-situ. Two different kinds of cracks are shown in Figure 2, at the interconnections between the power unit and the concrete support structure.

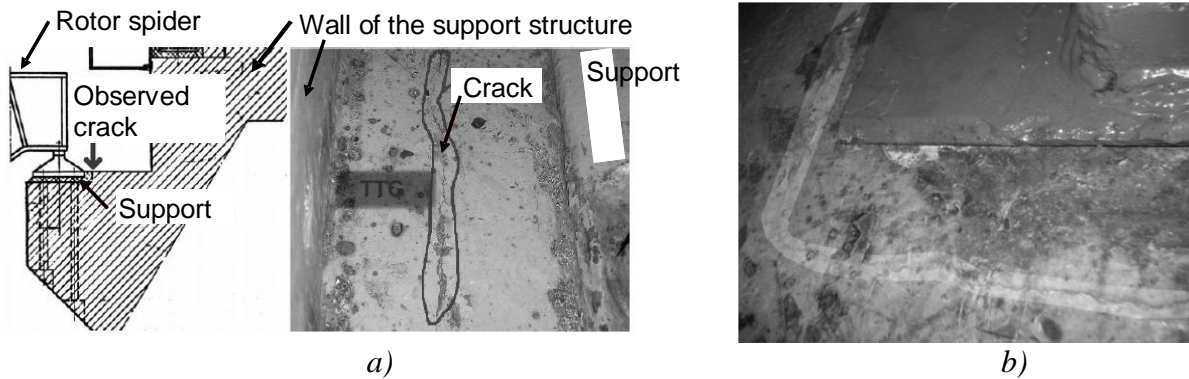


Figure 2 – Cracks observed in-situ at a rotor spider support (a) and a stator support (b), photos from (Larsson, 2008) and (Rhen, 2007).

To show that the observed cracks can be explained by the loads described in section 2, a finite element model of the concrete support structure was created in the finite element software Abaqus, see (Malm et. al. 2013). The model included the coupled effect of mechanical loads, thermal loads and drying shrinkage together with a non-linear material model to account for cracking in the concrete. Drying of the concrete was described according to the model of Yunping et. al. (1994) with a coupling from humidity to shrinkage as proposed by Ljungkrantz et. al. (1994). The material non-linearity was described with a plastic-damage model as proposed by Lubliner et. al. (1989) with modifications by Lee and Fenves (1998). Several simulations were carried out for different loading conditions and results are presented in (Malm et. al., 2013). In Figure 3, results from one simulation are presented. The distribution of humidity after 20 years is shown in Figure 3a) and a typical temperature distribution in Figure 3b). Coupling of these two environmental loads with the mechanical loads from the unit resulted in a crack pattern as illustrated in Figure 3c). Note that the mechanical loads were only taken as the permanent loads and steady-state values of the transient loads, i.e. no dynamic loads, in the presented simulation.

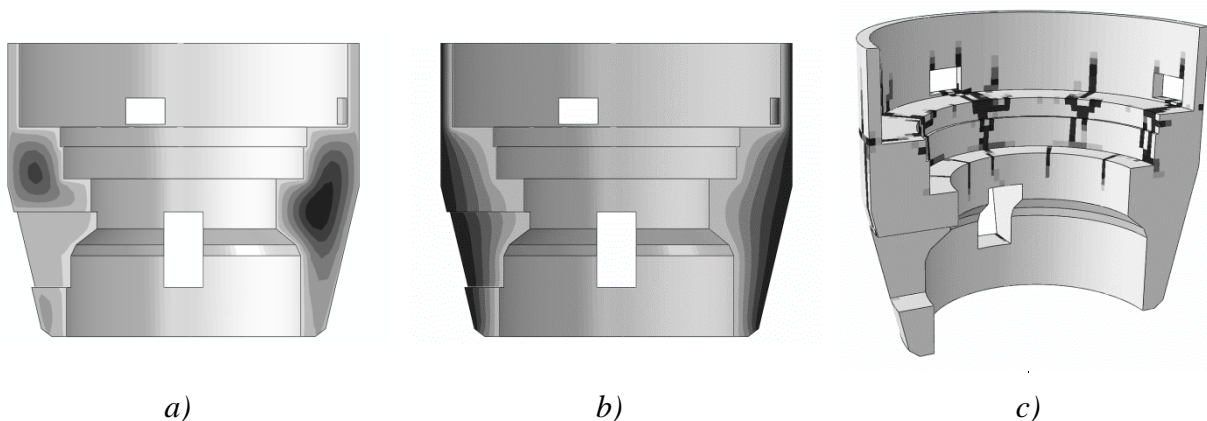


Figure 3 – Results from the FE-model, RH distribution (a), a typical temperature distribution (b) and plastic strains in the concrete (c).

4. CONCLUSIONS

The performed finite element analyses showed that drying shrinkage induced cracking inside the concrete support structure, especially around the supports of the stator and the rotor spider, as the cracks observed in-situ shown in Figure 2. They further showed that a variation in temperature, both due to cyclic seasonal variations and operation patterns, induced further cracking of the reinforced concrete structure. This additional cracking mainly manifested itself as radial cracks.

The effect of this type of structural damage to the concrete support structures to the operation of hydroelectric machinery is currently being studied and some initial results are presented by Gasch et. al. (2013).

ACKNOWLEDGEMENT

The research presented in this article was supported by Elforsk AB and "Swedish Hydropower Centre - SVC". Elforsk AB is the Swedish power Companies R&D association and SVC has been established by the Swedish Energy Agency, Elforsk and Svenska Kraftnät together with Luleå University of Technology, KTH Royal Institute of Technology, Chalmers University of Technology and Uppsala University. www.svc.nu.

REFERENCES

- Gasch, T., Nässelqvist, M, Hansson, M., Malm, R., Gustavsson, R., Hassanzadeh, M., 2013, "Cracking in the concrete foundation for hydropower generators - Part II", Elforsk Report 13:64, Elforsk, Stockholm, Sweden.
- Larsson, M., 2008, "Fundament för vattenkraftgeneratorer - analys av krafter och deformationer", M.Sc Thesis, Luleå University of Technology, Luleå, Sweden (In Swedish).
- Lee, J., Fenves, G., 1998, "Plastic-damage model for cyclic loading of concrete structures", *Journal of Engineering Mechanics*, 124, 892-900.
- Ljungkrantz, C., Möller, G., Peterson, N., 1994, "Betonghandbok – Material", 2nd Edition, Svensk Byggtjänst, Stockholm, Sweden (In Swedish).
- Lubliner, J., Oliver, J., Oller, S., Oñate, E., 1989, "A plastic-damage model for concrete", *International Journal of Solids and Structures*, 25, 299-326.
- Malm, R., Hassanzadeh, M., Gasch, T., Eriksson, D., Nordström, E., 2013, "Cracking in concrete supports for the generator in hydropower stations - Analyses of non-linear drying diffusion, thermal effects and mechanical loads", Elforsk Report 13:63, Elforsk, Stockholm, Sweden.
- Paavola, J., 2011, "FEM-Modellering av en vattenkraftstation – Utvärdering av beräkningar i 3D", M.Sc Thesis, Luleå University of Technology, Luleå, Sweden (In Swedish).
- Rhen, M., 2007, "Förslag till dimensionerande lastfall för generator- och bärlagerarmkors-upplag. Rotor- och temperaturdynamiska laster", Elforsk Report 07:54, Elforsk, Stockholm, Sweden (In Swedish).
- Yunping, X., Bazant, Z.P., Molina, L., Jennings, H.M., 1994, "Moisture diffusion in cementitious materials - moisture capacity and diffusivity", *Advanced Cement Based Materials*, 1, 258-266.

Numerical modelling of alkali silica gel in mesoscopic scale



M.Sc. TABET Mohamed
Laboratoire de Recherche en Génie Civil « LRGC »
University Mohamed Khider Biskra, BP 145 RP, 07000 Biskra, Algeria
E-mail: m.tabet@univ-biskra.dz



Prof. GUETTALA Abd El Hamid
Laboratoire de Recherche en Génie Civil « LRGC »
University Mohamed Khider Biskra, BP 145 RP, 07000 Biskra, Algeria
E-mail: guettalas@yahoo.fr

ABSTRACT

In this article we treat a pathological problem to lead us to a better understanding of the phenomena of ASR; the modelling of ASR has been represented in a relative element of volume (REV) in mesoscopic scale. The method used to estimate the formation of ASG is the kinematic estimation of the ASR where it generates in the end an expansion, thus modelling give us a bigger range of understanding of the rheology behaviour of a concrete with ASR. The numerical model adopted to validate the effect of the expansion of alkali silica gel in terms of strain/stress is a phenomenological one, where it gives us sustainable results with the rheological models.

Key words: Aggregate, Alkali silica reaction (ASR), Alkali silica gel (ASG), rheology, expansion, Relative element volume (REV).

1. INTRODUCTION

The causes of deterioration of concrete are many whose alkali-silica reaction (ASR) or alkali - granular reaction (AAR). The alkali reaction is a chemical reaction between certain types of silica and silicate which can be present in aggregates of the concrete, and the alkaline solution of the pore as they may be from different sources, such as cement, chemical adjuvants...etc. The reaction product is an amorphous gel, which expands in the presence of water creates a swelling pressure generating cracks leads to deterioration of the concrete. Although much work has been done to determine the properties of silica gel formed (Leeman 2013) which is the key point to determine the damage induced from ASG. However modelling silica gel must be in order to explain the rheological behaviour of concrete affected by ASR, knowing the complication that takes to seize the mechanical and chemical mechanism. The product of the chemical reaction (ASG) is a fundamental aspect of this reaction, thus the transport of alkali ions in pore solutions of reagents grains showed that alkalis ions move towards the reactive grains precisely the contour of the grains and aggregates, in cement paste / Aggregate borders. Modelling studies have been based on two assumptions to predict the ASR, which involves the dissolution / diffusion of silica and the formation of gel and swelling of the gel in presence of humidity (Grimal 2010).

2. NUMERICAL MODELING OF ASR:

Mesoscopic models were originally proposed to estimate the expansion of material samples to laboratory conditions, currently used for the expertise of potential swelling materials.

Furusawa (1994), describe the mechanism as topochemical reaction kinetics of the diffusion of hydroxyl ions OH^- in the reactive aggregate, where he idealized the shape as a sphere, and deduced from 2nd Fick's Law.

$$\frac{\partial C}{\partial t} = D \left(\frac{\partial^2 C}{\partial z^2} \right) ;$$

Zhuang (2013), following the same reasoning as Furusawa and Xi et al, introducing an increase of the ASG product volume from the reactive layer over the granulate.

$$V_{\text{ASG}} = n_{\text{ASG}} \cdot V_{\text{ASG}}^{\text{mol}} ;$$

The contribution of the aggregate size and shape in the asymptotic expansion of the material is written by the difference between the volume total of gel product and partly absorbed by the porous area.

$$\epsilon_{\text{ASG}} = \frac{V_{\text{ASG}} - V_{\text{pores}}}{V} ;$$

Likewise the numbers of aggregates N_g reacting are calculated as a volume fraction of the entire volume fraction of the structure.

$$N_g = \frac{\phi_i \cdot \phi_g \cdot V}{\frac{4}{3} \pi \cdot Rq} , \quad Rq = \frac{D_i + D_{i+1}}{4} ;$$

The assumptions made in this work states that the reaction has semi-infinite source of alkalis, a fixed amount of solute material diffusing in from one end. Limited source diffusion requires a constant amount of alkalis.

$$\text{Na}_2\text{O}_{\text{eq}} = \text{Na}_2\text{O} (\%) + 0.658 \text{K}_2\text{O} ;$$

The initial condition and boundary conditions are set:

$$C(x, 0) = 0 , \quad \int C(z, t) dz = C_0 , \quad C(x, \infty) = 0 ;$$

The solution to Fick's 2nd Law under these conditions is:

$$C(z, t) = \frac{C_0}{\sqrt{\pi Dt}} e^{\left(\frac{-z^2}{4Dt} \right)}$$

According to 1st Law of Diffusion, the Flux of alkalis can be described by the following equation:

$$J = -D \frac{\partial C(z, t)}{\partial z}$$

J.C.Maxwell explain that the quantity which passes through the volume in the case of fluxes, and the integration of the flux, over a volume, the results of this operation is called the surface integral of the flux. It represents the quantity which passes through the surface.

Then the volume of alkali-silica gels can be described by:

$$V_{\text{ASG}} = N_g \cdot V_{\text{ASG}}^{\text{mol}} \cdot 4 \pi Rq^2 \int_0^t J dt$$

The expansion evolution developed by Larive (1997) is adopted in this work knowing the dependency of the ASR the temperature. The ASR expansion of the ASG can be described as above by:

$$\epsilon_{\text{ASR}} = \frac{V_{\text{ASG}} - V_{\text{pores}}}{V} \cdot \xi(T, t) , \quad \xi(T, t) = \frac{1 - e^{-\frac{t}{\tau_c(T)}}}{1 + e^{-\frac{t - \tau_L(T)}{\tau_c(T)}}}$$

$$\tau_c(T) = \tau_c(T_0) e^{U_c \left(\frac{1}{T} - \frac{1}{T_0} \right)} , \quad \tau_L(T) = \tau_L(T_0) e^{U_c \left(\frac{1}{T} - \frac{1}{T_0} \right)}$$

3. MODELLING USING FINITE ELEMENT METHOD:

In this work, the implementation of this model adopted is modelled by Freefem.

The 2D implementation of the REV and the numerical calculation of the generated expansion is inserts and modelled using the power of FE to analyze the effect of the expansion on the structure of the REV.

Table.1 – Parameters used in the modeling of ASR

| Parameter | Values |
|---|-----------------------|
| Volume fraction of reactive aggregats | 20 |
| Spicemens size / mm ³ | 100 x 100 x 400 |
| Mortar porosity / % | 13-16 |
| Diffusion coefficient of Na + in the cement paste / (m ² /s) | 8.9×10^{-13} |
| Molar gel volume / (cm ³ /mol) | 21.5 |
| Concentration of Na ₂ O / (mol/L) | 0.327 |
| Average size of aggregates (mm) | 4.75-9.5 |
| Temps de calcul (jours) | 16 |
| Poisson Coefficient of aggregates | 0.23 |
| Young Modulus of aggregats / Gpa | 54.0 |
| Poisson Coefficient of paste cement Young | 0.217 |
| Modulus of paste cement / Gpa | 28.46 |
| Ambient temperature T ₀ / C° | 21.0 |
| Temperature T/C° | 60.0 |
| The characteristic time $\tau_c(T_0)$ /day | 1 |
| The latency time $\tau_L(T_0)$ /day | 2 |
| U _c The activation energie of $\tau_c(T)$ /K | 5400 |
| U _L The activation energie of $\tau_L(T)$ /K | 9500 |

4. RESULTS

According to the model adopted previous calculation, and numerical simulations of ASR was carried out to estimate the applicability of the model with the temperature dependency, proposed by Larive (1997). The expansion was calculated according to the proposed model. The calculation results were compared to the results of Zhuang model, as shown in (Figure.1, 2).

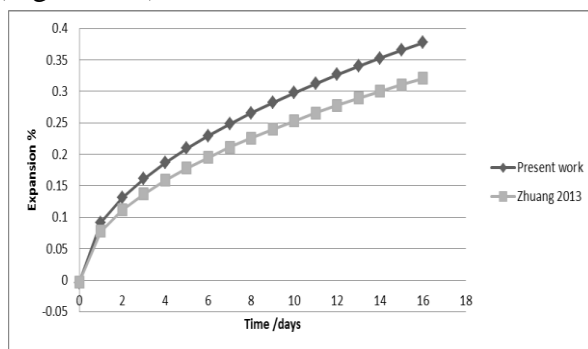


Figure 1 – ASR expansion %

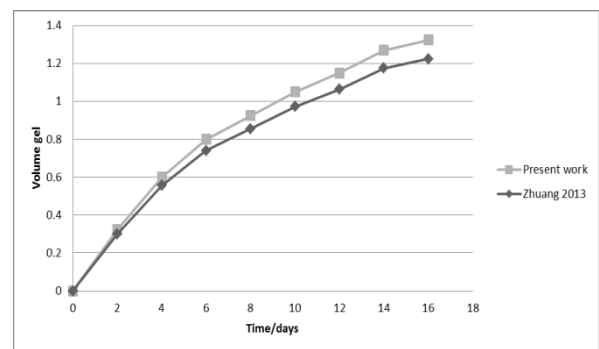


Figure 2 – ASR gel volume calculated /10⁻³ mole

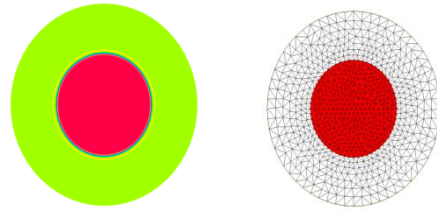
4.1 Analysis of the expansion on a REV

To ease the modelling of ASG some simplifications have been made to implement an efficient FE model to let us comprehend in an effective way the behaviour of a concrete affected by ASR. For this investigation, a plane strain model is adopted, thus two-dimensional segment of REV of spherical shape is chosen.

Results focused around the proposed model will be stood out from those achievable utilizing the

current situation with practice model (Zhuang, 2013) with a development of the direct kinematics response which depends on the temperature.

Fig.3: Cross section of REV and presentation of the impact of ASG.



The results show the mechanism of deformation and damage at the mesoscopic scale (see Figure.4), where the stress is maximum at the gel silica formed / aggregate (see Figure.1) interface; after a short time the mechanical resistance of loose aggregate join the critical threshold and deformed without returning to its linear elastic behaviour, unlike the silica gel formed and the cement paste which they have mechanical properties reduced compared to the aggregates (see Table.1).

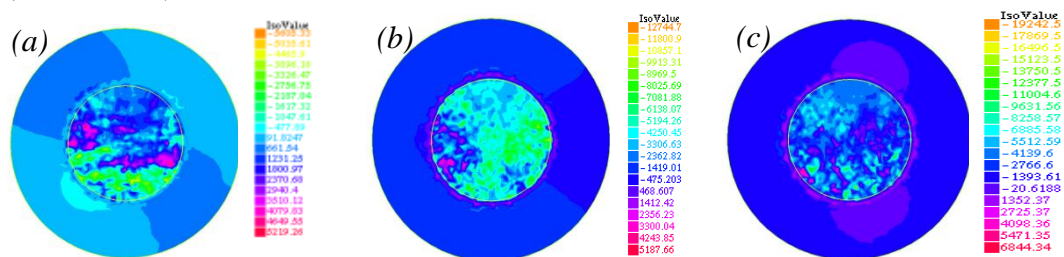


Fig.4: (a, b, c) Stress response of the expansion of ASG;

As we said the (see Figure.5) show the deformation caused by the expansion of the gel formed by the alkali silica reaction is primarily focused and concentration on the aggregate. This results showed that the rheological behaviour of concrete component (aggregates, cement paste, silica gel formed, grains, ...) must increasingly subjected to a variety of in-depth research.

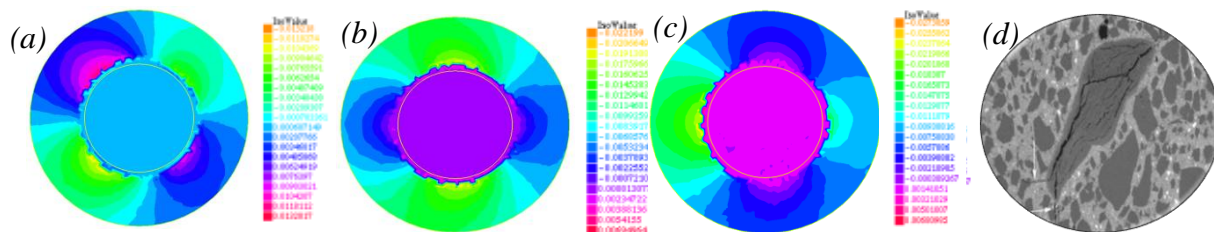


Fig.5: (a,b,c) Strain response of the expansion of ASG; (d) A chert aggregate particle with extensive internal cracks due to ASR [79]

REFERENCES

- Grimal, E et. al, 2010,
 “Concrete Modeling for Expertise of Structures Affected by Alkali Aggregate Reaction,”
 Cement and Concrete Research, 40, 502–507.
- Leeman, A.,2013,
 “E-Modulus of the Alkali–silica-Reaction Product Determined by Micro-Indentation”.
 Journal of Construction and Building Materials 44 (2013)221-227.
- Xu, W, 2013,
 “Calculation of alkali silica reaction (ASR) induced expansion before cracking of
 concrete”. Journal of Wuhan University of Technology. 28(1), pp.110- 116.

EARLY PROPERTY DEVELOPMENT IN CONCRETE



Gitte Normann Munch-Petersen
Civil engineer, senior lecturer
VIA University College
Chr. M. Østergaardsvej 4
DK-8700 Horsens
E-mail: gin@viauc.dk



Christian Munch-Petersen
Civil engineer, MSc
Emcon a/s
Ordrupvej 60
DK- 2920 Charlottenlund
E-mail: cmp@emcon.dk

ABSTRACT

The Freiesleben Maturity function is widely used for planning of execution. We tested if for concrete with and without fly ash. The test showed surprisingly that the maturity function in general is not valid. We found that curing at high temperature gave a significant decrease in strength. Fly ash appears to reduce this decrease somewhat. We also examined the resistance against chloride penetration for the different concrete types. The resistance was reduced at high temperatures for concrete without fly ash. For concrete with fly ash, it was the opposite; concrete with fly ash obtained higher resistance by heat curing.

Key words: Additions, Chlorides, Execution, Testing.

1. INTRODUCTION

In Denmark, planning of execution parameters like strength development is based on the Freiesleben Maturity function. The maturity function is used to calculate the properties of concrete at both short and long term, even though the development is only tested for 2 days according to the test method for the maturity function /TI-B 103 (94)/.

In recent years there has been a growing recognition that concrete properties in the long term cannot be seen independently of the temperatures during curing. At very high temperatures (above 60-70 °C), there is even in some cases seen a subsequent total destruction of the concrete (DEF - Delayed Ettringite Formation). It is possible that even at lower and more common temperatures a smaller, partial degradation of the concrete will take place.

2. TESTS

The tests carried out comprise curing of concrete in a temperature range from 20 °C to 70 °C. Three commercially concrete types were used with varying content of fly ash. The cement was the Danish Rapid cement, which is a CEM I 52,5 N (LA) with a C₃A less than 8%.

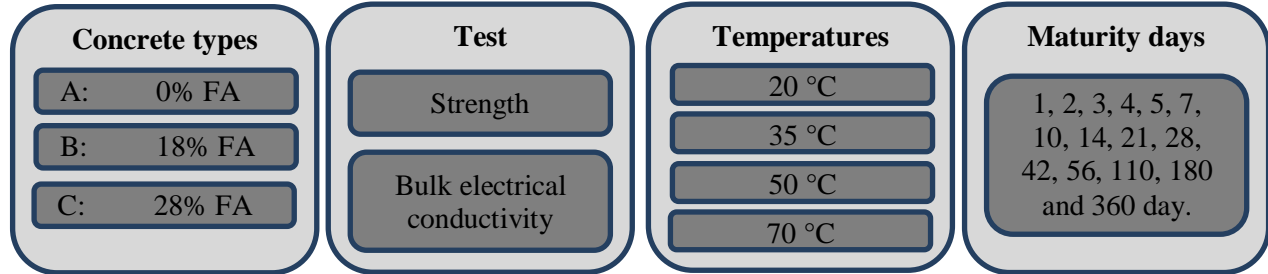


Figure 1 – Test programme

The specified day is the maturity day.. The function is based on The Arrhenius function. This has the consequence, that if the maturity function was correct a given mix would obtain the same properties at the same maturity days. Any deviation from this is therefore a symptom on the maturity function being wrong.

3. RESULTS AND DISCUSSION

The influence of temperature on strength development

Curve fitting were made on strength development curves from the experimental data. The exponential equation proposed by /Freiesleben Hansen and Pedersen 1985/ was used:

$$f_c = f_{\infty} \cdot \exp \left[- \left(\frac{\tau}{M} \right)^{\alpha} \right]$$

- $f_{c,\infty}$ the total strength development for M tending to infinity [MPa]
 f_c the strength at the maturity M, [MPa]
 M concrete maturity in hours [h]
 τ time constant [h]
 α curvature parameter [-]

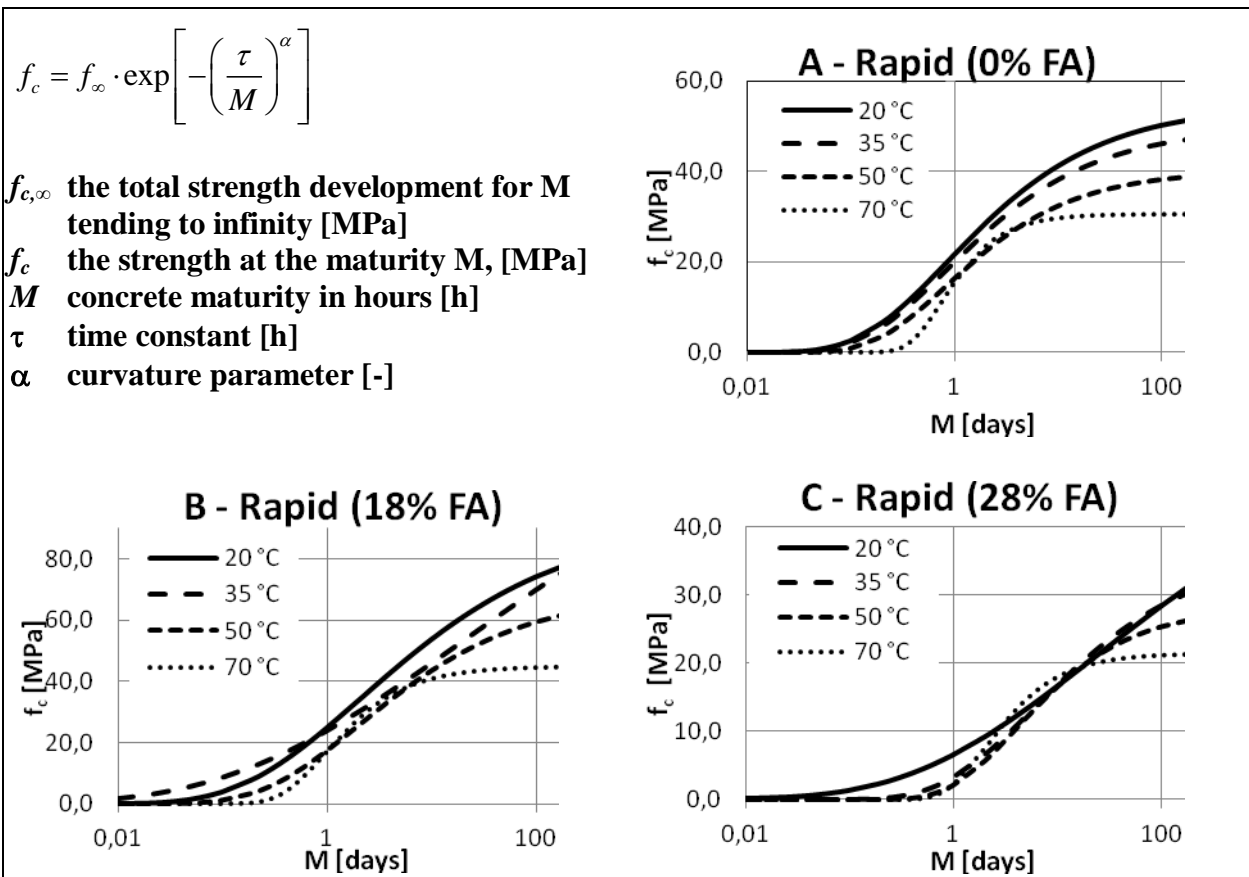


Figure 2 – Strength development

For all three types of concrete, it applies that the 28 days of strength obtained at 20 °C was not obtained for concrete cured at 70 °C, and for concrete type A and B the strength were not obtained even if the concrete is stored at 50 °C.

Generally, the strengths at 50 and 70 °C were significantly lower than the strengths of 20 and 35 °C. Strength curves for 20 and 35 °C were almost identical, if uncertainties in the measurements were included.

Our measurements show the maturity function of the tested concretes, only with considerable uncertainty can be considered to be only fairly valid up to 35 °C.

4. BULK ELECTRICAL CONDUCTIVITY -

Curve fitting were made of resistance development curves from the experimental data using test equipment according to /ASTM C1760 – 12/ The instrument is called “Merlin” from Germann Instruments.



It was assumed that the curves with good approximation could be described by the exponential equation shown in figure 4:

Figure 3 – “Merlin from” German Instrument

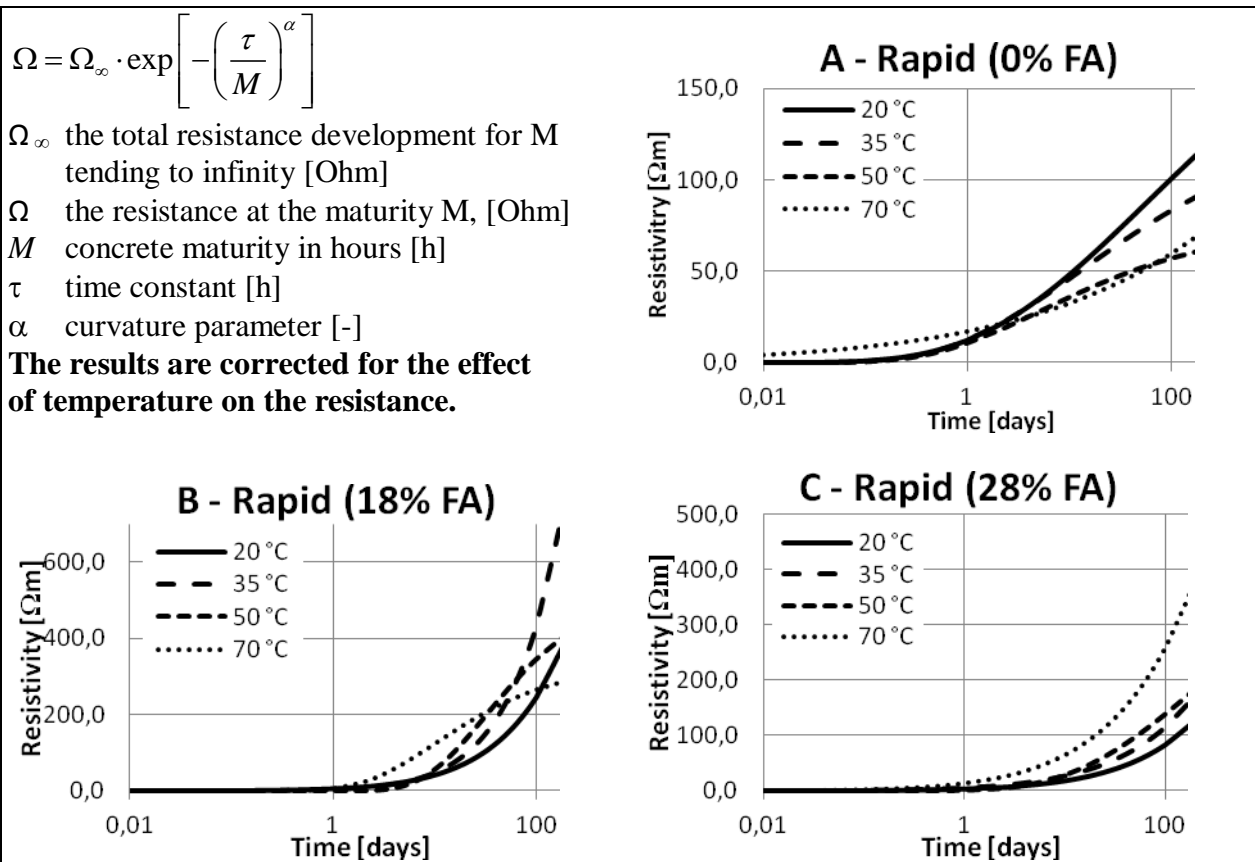


Figure 4 – Development in resistivity

The conductivity of the pore fluid affects the measured specific electrical conductivity of the concrete. Therefore, one cannot compare the measurements on concrete if there is a big difference in pore fluids conductivity. Concrete with fly ash can have a reduced conductivity of the pore fluid, which will reduce the conductivity measurement, although the actual diffusivity is not reduced. The conclusion must be that, since there are different levels of fly ash in the 3 types of concrete, the development may be compared, while the absolute level cannot be compared without additional studies of the actual diffusivity at a couple of selected dates. Unfortunately, this has not been possible within the project's limited budget.

For concrete type A (without FA) it was seen that at almost all dates the resistance was higher the lower the curing temperature. This corresponds well with the strength development.

For concrete type B, containing 18% FA, it was seen that the resistance at the early dates was highest at 70 °C, but the curve flattens after 15 days while the other curves were still increasing. After 360 days the resistance at 20 °C were twice that at 70 °C and at 35° C the resistance was three times that at 70 °C.

By comparing compares the concrete of A and B, there was a tendency that the resistance was significantly effected (meaning that the maturity function was correct in this situation) when cured at temperatures up to 50 °C.

For concrete type C containing 28% FA, it was seen that the rising temperature, gave higher resistance, ie. curing at high temperatures of concrete with high content of fly ash encouraged the develop of the resistance (chloride resistance).

4. RESULTS AND DISCUSSION

Based on this very small series of test it can be concluded, that the traditional Danish maturity function does not give reasonable results for strength development at temperatures higher than 35 °C. For the electrical resistance (correlated to chloride penetration parameters) the maturity function does not give reliable estimations after 10 days for any temperature. Even if the maturity function was developed on concrete without additions, it seems that concrete with fly ash performs somewhat more according to the maturity function.

The electrical resistance can for some mixes with fly ash become substantial higher at elevated curing temperatures.

More – much more – research is needed on this subject.

REFERENCES

ASTM C1760 – 12

Standard Test Method for Bulk Electrical Conductivity of Hardened Concrete

Freiesleben Hansen and Pedersen 1985

Curing of Concrete Structures,” CEB Information Bulletin 166,May, 42 p.

TI-B 103 (94)

Prøvningsmetode - Aktiveringsenergi i den relative hastighedsfunktion, Teknologisk Institut, Byggeri

BINDERS, ADMIXTURES, MIX DESIGN AND RHEOLOGY
Cont.

In-situ XRD Studies of Phase Evolution during Hydration of Portland Cement Paste with Lignosulfonates



Dr. Tobias Danner
NTNU* – Department of
Materials Science
Sem Sælandsvei 12,
N - 7491 Trondheim
danner@nt.ntnu.no



Prof. Dr. Harald Justnes
NTNU – Department of
Materials Science
Richard Birkelands vei 3
N – 7491 Trondheim
harald.justnes@sintef.no



Prof. Dr. Mette R. Geiker
NTNU – Department of
Structural Engineering
Richard Birkelands Vei 1a
N – 7491 Trondheim
mette.geiker@ntnu.no



Alessia Colombo, M.Sc.
NTNU – Department of
Structural Engineering
Richard Birkelandsvei 1a
N – 7491 Trondheim
alessia.colombo@ntnu.no

* NTNU – Norwegian University of Science and Technology

ABSTRACT

The effect of two lignosulfonates, one softwood (LSs)- and one hardwood based (LSh), on the early hydration of three Portland cements was studied with isothermal calorimetry and in-situ XRD. In-situ XRD proved to be a good method for detecting the influence of LS on the evolution of single phases during the hydration of cement. In the presence of lignosulfonate the hydration of C_3S was retarded while ettringite formation was accelerated. LSh retards the C_3S hydration more than LSs, but has less influence on the ettringite formation.

Key words: in-situ XRD, Lignosulfonate, Admixtures, Binders,

1. INTRODUCTION

This research is part of a larger project in cooperation with Borregaard (Sarpsborg, Norway), SINTEF and international partners (Ecole des Mines d'Alès, University of Sheffield, the University of Melbourne and Chalmers University). One of the goals is to tailor Lignosulfonate (LS) in order to make it a suitable plasticizer in new concrete formulations with blended cements where traditional plasticizers do not work. Modified LS by Borregaard show a water reduction of 8-25 % in normal concrete (Reknes & Petersen, 2003, Kauppi et al., 2003)]. However the addition of LS also delays the setting time and strength development (Ramachandran, et al, 2002). A better understanding of the mechanisms of retardation is necessary to know which parts of the molecule should be modified to improve the performance of LS.

In-situ XRD can be applied to qualitatively follow the hydration of single phases simultaneously in a more component system like OPC by plotting the peak area (Quennoz & Scrivener, 2013) or peak intensities against hydration time. Changes in phase content during the hydration of cement pastes can be observed and e.g. be correlated with heat flow. Moreover it is possible to monitor the phase development already from the first 5-15 minutes after mixing the paste which can be important when working with admixtures.

2. EXPERIMENTAL

2.1 Materials

Three Portland Cements named A (Norcem Standardsement; CEM I. 42.5 R), B (Norcem Anleggsement; CEM I, 52.5 N) and C (Cemex Rapid sement; CEM I. 52.5 R) were used. Representative batches were obtained by using the cone and quarter technique.

As plasticizers, two low sugar Ca-lignosulfonates (LS) based on Softwood (LSs) and Hardwood (LSH) were provided in form of a powder by Borregaard (Sarpsborg, Norway). From the powder 1% solutions was prepared for accurate dosing.

2.2 Experimental Procedure

Cement pastes with a constant water to cement ratio of 0.4 were prepared. The LS was directly added with the mixing water in a concentration of 0.2 % and 0.4 % by dry weight of cement (bwoc). Mixing was performed by hand with a plastic spatula, the batch size was 10.5 g and the mixing time was 90 sec.

Isothermal calorimetry of cement pastes with and without lignosulfonate addition was carried out at 20 °C using a TAM Air (TA Instruments).

In-situ XRD was performed using a Bruker D8 Advance. The paste was smeared in the sample holder and the sample surface was flattened by stripping off the excess material with a glass plate. The sample was then placed in an MRI Physikalische Geräte GmbH sample chamber, and data was collected at room temperature and constant relative humidity of 96 %. One scan took about 13 min, and a total of 110 scans are collected during 24 h. A typical level plot (2-D plot of $^{\circ}2\theta$ against time of hydration) where the intensities of phases are defined as colours (greyscale) is shown in Figure 1.

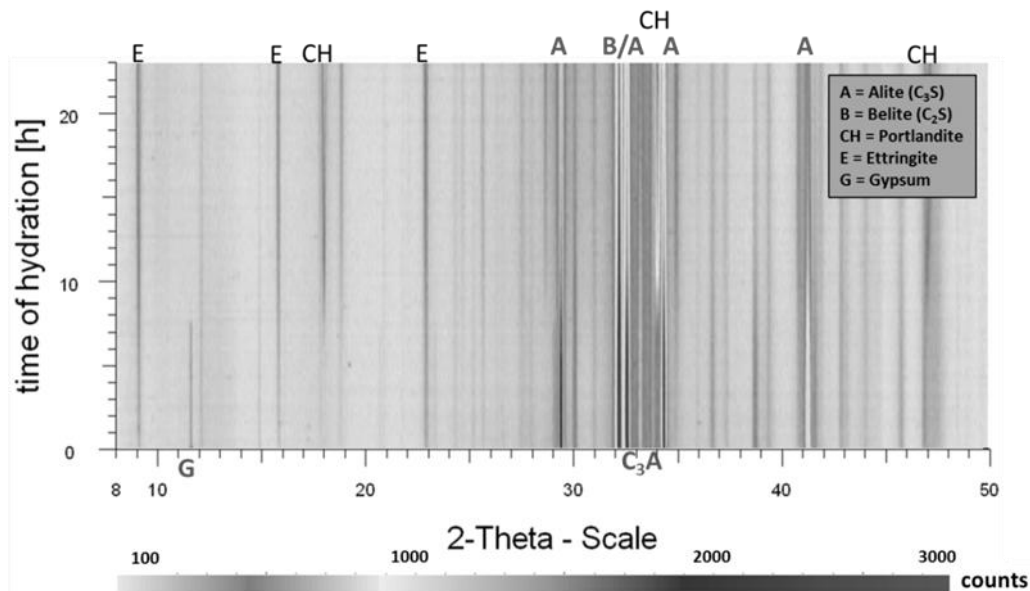


Figure 1 – in-situ XRD level plot of cement A hydrated for 24 hours at 23 °C. No addition of LS

To qualitatively analyse the phase development of the single phases the peak intensities of specific non overlapping peaks were plotted against hydration time to monitor changes in phase content.

3. RESULTS

Figure 2 (Left) shows the phase development of the main clinker phases (C_3S & C_3A) as well as the main hydration products ettringite and portlandite combined with the heat flow curve during the first 24 h of hydration of cement A without LS.

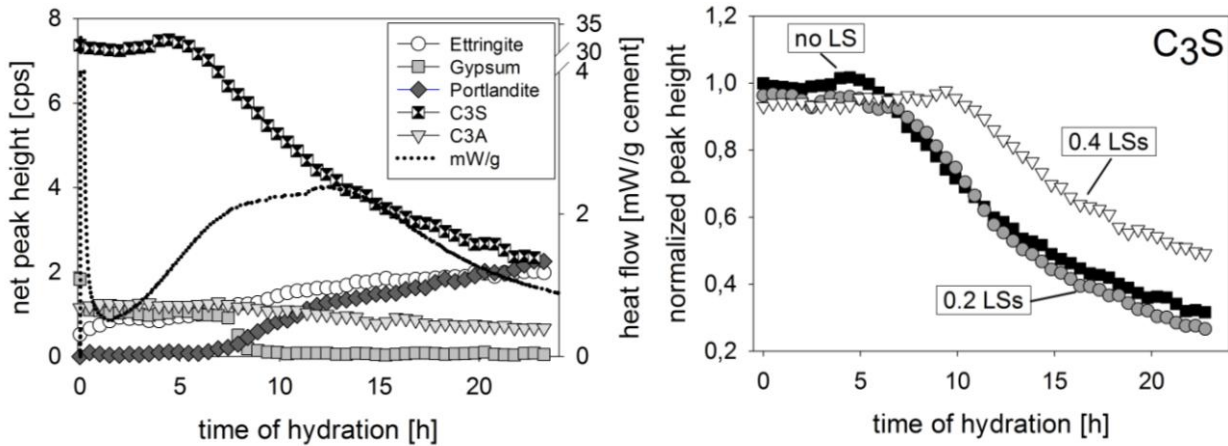


Figure 2 – *Left*: Net peak height of clinker phases and crystalline hydration products combined with the heat flow during the hydration of cement A with no addition of LS. *Right*: Normalized net peak height of C_3S phase in cement A during the hydration without LS and with 0.2 % and 0.4 % LSs bwoc.

Within the first 15 minutes a fast dissolution of gypsum is detectable as can be seen in Figure 2 (left). The net peak height of gypsum is immediately decreasing from 2 to about 1 cps. This is accompanied with an initial first ettringite formation corresponding to the initial heat flow measured with calorimetry. The peak intensities of C_3S start decreasing between 5-6 h of hydration during the acceleration period in the heat flow. The first maximum of the acceleration period coincides about with the first detection of crystalline portlandite after around 7 hours. Between 7-8 h gypsum is also dissolved completely and ettringite peak intensities seem to increase again steady after almost reaching a plateau between about 1.5-6 h of hydration. Initial C_3A reaction is too fast to catch with XRD and the second decrease in intensity starts with the sulphate depletion. Possible AFm phases are either not crystalline enough to be detected or present in too small amounts to be visible with the resolution of the diffractograms. When adding LSs to the mixing water a retardation of the acceleration period in calorimetry can be observed. Comparing the peak intensities of C_3S (normalized to starting value) in the systems with and without LS it is visible that by addition of 0.4 % LSs the C_3S hydration is delayed by about 4 hours (Figure 2 - right) while 0.2% LSs has almost no effect. Correspondingly, portlandite formation is also retarded. C_3A hydration (not shown) follows a similar trend as C_3S . By comparing the evolution of ettringite with and without lignosulfonate it was observed that ettringite formation is accelerated with LS. This is in agreement with Bishop & Barron, 2006. The hardwood based lignosulfonate has a similar effect on the phase development of cement pastes. In general it is slightly more retarding than the softwood based lignosulfonate. With in-situ XRD it could be observed that the C_3S hydration of cement A is retarded by about 4 h already at a concentration of 0.2 % LSh. At a concentration of 0.4 % LSh the C_3S hydration is delayed by about 6 h. On the other hand LSh is less effective in accelerating the ettringite formation.

4. CONCLUSIONS

In-situ XRD can be a powerful tool to detect the influence of lignosulfonate on the hydration of single crystalline phases within a cementitious system and the effect on the formation of hydration products. The method provides a simple way of qualitatively presenting the retardation or acceleration of hydration reactions and it was shown that the hydration of C_3S is significantly retarded in the presence of 0.4 % LSs bwoc. Additionally early reactions like the acceleration of initial ettringite formation with LSs were detected. Together with calorimetry it can be shown how the single phase development contributes to the heat flow. The first maximum in the main hydration peak observed with isothermal calorimetry coincides with the first detection of portlandite by XRD.

5. ACKNOWLEDGEMENT

Borregaard and the Norwegian Research Council are acknowledged for financial support. We especially want to thank Rolf Andreas Lauten (Borregaard) for managing this project and his contributions in fruitful discussions. Furthermore the authors would like to thank Klaartje De Weerd (NTNU & SINTEF) and Serina Ng (SINTEF) for discussing the results and giving input and ideas for further experiments.

REFERENCES

- Bishop, M. & Barron, A.R.; 2006,
 “Cement Hydration Inhibition with Sucrose, Tartaric Acid, and Lignosulfonate: Analytical and Spectroscopic Study”, *Industrial & Engineering Chemistry Research*, Vol.45, No. 21, pp. 7042-7049, 2006
- Kauppi, A., Banfill, P.F.G., Bowen, P., Galmiche, L., Houst, Y, Lafuma, F.; 2003
 “Improved superplasticizers for high performance concrete”, *Proceedings of the 11th International Congress on Chemistry of Cement*, Durban, South Africa, 11-16 May 2003, (Grieve, G., Owens, G., editors) Vol 2, pp. 528-536
- Quennoz, A. & Scrivener, K.L.; 2013
 “Interactions between alite and C3A-gypsum hydrations in model cements”, *Cement and Concrete Research*, Vol.44, pp. 46-54, 2013
- Ramachandran V.S., Paroli, R. M., Beaudoin, J. J., Delgado, A. H; 2002
 “Retarding and Water Reducing Admixtures”, in *Handbook of Thermal Analysis of Construction Materials*, NoYes Oublications, 2002, pp. 221-238
- Reknes, K. & Petersen, B.G.; 2003
 “Novel lignosulphonate with Superplasticizer performance, In: *Proceedings 7th CANMET/ACI International Conference on Superplastizicers and Other Chemical Admixtures in Concrete* (Malhotra, V.M., Editor) Berlin, Germany, 2003, pp. 285-299

The Initial Setting Time of Ground Granulated Blastfurnace Slag GGBS and Its Relation to the Modulus of the Alkali-Activating Solution



Helén Jansson, Ass. Prof.
Chalmers Univ. of Techn.
Div. of Building Technology
SE-412 96, Gothenburg
Email: helen.jansson@chalmers.se



Tang Luping, Prof
Chalmers Univ. of Techn.
Div. of Building Technology
SE-412 96, Gothenburg
Email: tang.luping@chalmers.se

ABSTRACT

In this study the initial setting time of water glass activated slag was investigated by the traditional Vicat method. It was found that the initial setting time is mainly influenced by two parameters; 1) the specific surface area of the material and 2) the modulus of the water glass used for the activation. The IR and ^{29}Si -NMR spectroscopies were used to identify the structures of the water glass activator. The results show that the silica configuration is highly dependent on the modulus. The relationships between the initial setting time, specific surface area and silica structures are discussed.

Key words: alkali-activation, ground granulated blast furnace slag, water glass modulus, testing

1. INTRODUCTION

The most limiting factor for extended use of alkali-activated cementitious materials such as ground granulated blastfurnace slag (GGBS) is the difficulty in controlling the initial setting time (REFS). Maybe due to the lack of more systematically studies there is no clear and comprehensive picture of the main factors influencing the hydration and setting even if several, and sometimes contradictory, suggestions exist. Thus, the mechanism alkali-activated hydration is not fully understood, see for instance Refs./Shi et.al. 2006, Pacheco-Torgal et. al 2008a, Pacheco-Torgal et. al 2008b & Roy 1999/. In this study we have focused on two parameters; the specific surface area and the water glass modulus. The latter depends on the sodium content.

2. MATERIALS AND METHODS

In this study the initial setting time for two Swedish GGBS materials, Merit5000 and Hyttsand, was investigated by the Vicat method. These materials have exactly the same chemical

composition but differ in the specific surface area S (Merit5000 $S = 5000 \text{ cm}^2/\text{g}$ and Hyttsand $S = 3500 \text{ cm}^2/\text{g}$). For varying the specific surface different weight fractions of these slag products were blended. The materials were alkali-activated by water glass solutions of various moduli n ($\text{SiO}_2/\text{Na}_2\text{O}$, molar ratio). The water to binder ratio was kept constant to 0.5 for all samples. ^{29}Si (silicon) NMR experiments were performed on an 11.7 T Varian Inova spectrometer, operating at a ^{29}Si resonance frequency of 99.39 MHz. To avoid any background contribution from the probe and the NMR glass tube a RIDE /Kozminski et.al 2000, Schraml et. al 2013 & Woelk et.al 2002/ pulse sequence was applied. A Dionex ion chromatography (IC) system (Dionex ICS series) was used for quantification of free (uncomplexed) sodium ions (Na^+) in the water glass solutions of various moduli n .

3. RESULTS AND DISCUSSION

In figure 1A it is shown that the specific surface has a substantial influence on the initial setting time. The smaller the specific surface, the longer initial setting time. This is an expected behaviour since the initial setting time should be related to the initial flow and formation of hydrates that previously has been shown to be dependent on the fineness of the material /Yang et.al 2009/ , which, in turn, influences the rate of chemical reactions /Beltram 2009/

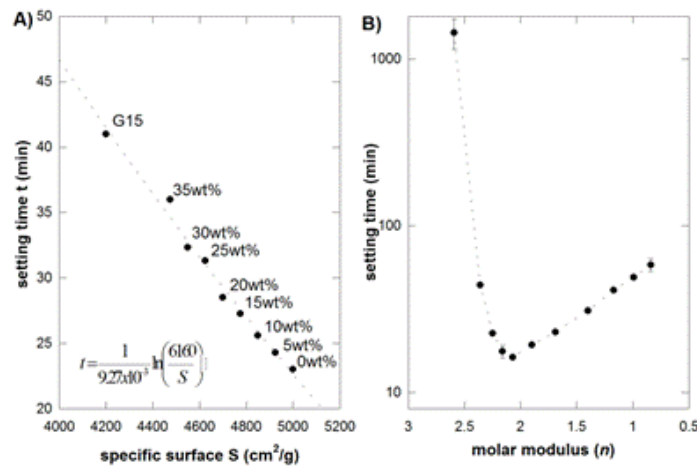


Figure 1 A and B show the initial setting time as a function of specific surface and water glass modulus, respectively

In case of a constant volume the initial setting time is related to the quantity of the hydration product /Beltram 2009/ and, consequently, also to the chemical reaction rate. Assuming that the calcium concentration is a function of the specific surface of the slag particles one can derive the following equation between the initial setting time t and the specific surface S :

$$t = \frac{1}{k} \ln\left(\frac{A}{S}\right) \quad (1)$$

where k is the chemical reaction coefficient and A is a constant describing the relation between S and the calcium concentration. By curve fitting, the values $k = 9.27 \times 10^{-3} \text{ (min}^{-1}\text{)}$ and $A = 6160 \text{ m}^2/\text{kg}$ were obtained. It should here be noted that any reduction of particle size (increased specific surface) during the dissolution phase was not taken into account.

Figure 1B shows how the initial setting time for Merit5000 changes by systematically varying the modulus n of the water glass used for the alkali-activation. As shown, the fastest initial setting time is obtained for the sample activated with $n = 2.07$ and longer initial setting times are

obtained at both lower and higher moduli. Even if such a behaviour has been observed at least once before /Bernal 2011/, the reason is not clear. Alkali-activation is known to be highly dependent on the chemical composition of the binder material, water content and the activator composition. Since both the binder material and water content are the same for all samples but the solutions used for the activation differed in the modulus a possible explanation could be that the water glass solutions itself, especially its modulus n , has an influence on the initial setting time of GGBS.

Table 1: Water glass characteristics

| Modulus n (molar) | pH | Na ⁺ (mM) from IC |
|------------------------|------|---------------------------------|
| 2.59 | 11.8 | 56.8 |
| 2.07 | 12.6 | 63.2 |
| 1.69 | 13.3 | 57.1 |
| 0.99 | 13.9 | 29.1 |

Table 1 shows how modulus n of water glass influences the pH of the solution. In general, pH affects the microstructure of the solution. With an increased pH larger molecular structures break up into smaller units, resulting in an increased viscosity as a consequence /Nordstrom et.al. 2011/. However, it has also been shown /Yang et.al. 2008/ that the viscosity reaches a minimum close to the value we obtained for the fastest initial setting time. Thus, it seems that there exists a relationship between the structure, which determines the viscosity, of the water glass solutions and the initial setting.

In a ²⁹Si NMR spectrum larger and smaller silica structures (units) are found at lower and higher values on the ppm scale, respectively. Figure 2 shows that going from higher to lower moduli n , peaks are moved to higher (less negative) ppm values and thus indicating that larger structural Si-units break up into smaller ones, as also suggested by the increased pH. As shown by infrared spectroscopy, the size of the structural units also have an influence on the degree of interaction of sodium ions with negatively charged sites (O⁻) located on the corners of the silica tetrahedrons /Halasz 2010 & Jansson 2014/. Table 1 displays that the content of free sodium ions (obtained by IC) is relatively low for the solution of lower modulus, indicating that large amount of sodium is bound to the negatively charged sites. During the hydration there is a competition between sodium from the solution and calcium ions from the slag for these negatively charged sites. On the other hand, the calcium concentration decreases with the increased pH (decreased modulus), resulting in a longer initial setting time. On the contrary, for the solution of the highest modulus $n = 2.59$ larger structural units are present and consequently very few charged sites (O⁻) are available for the calcium ions from the slag. This in turn also lead to a longer initial setting time. However, for the water glass with modulus $n = 2.07$ there is a maximum in the content of free sodium ions, which indicate that most uncomplexed charged sites on the silica structures are available in this solution. It is also at this concentration the fastest initial setting time is observed in figure 1B.

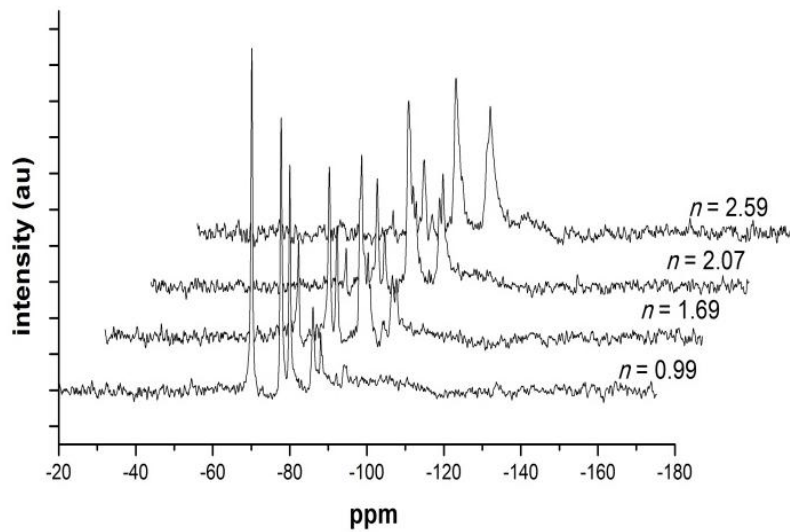


Figure 2: ^{29}Si NMR spectra for water glass solution of modulus $n = 0.99$ to 2.59 .

4. CONCLUSIONS

The initial setting time of water glass activated slag can be explained by the calcium dissolution from the particle surface. A smaller specific surface results in less calcium ions for the hydration products development.

The modulus of water glass solutions has a significant effect on the initial setting time. Change of modulus affects the pH and induces structural changes of the silica and calcium solubility. The fastest initial setting time occurs at the modulus $n = 2.07$ corresponding to pH 12.6 in this study.

REFERENCES

- Beltram, P., 2009 *Rates of chemical reactions: their measurement and mathematical expressions*, in *Fundamentals of chemistry*.
- Bernal, S.A., et al., 2011 *Cement & Concrete Composites*, **33**(1): p. 46-54.
- Halasz, I., et al., 2010 *Microporous and Mesoporous Materials*, **135**(1-3): p. 74-81.
- Jansson, H., et al., Submitted to CAM2014, RILEM conf. in China.
- Kozminski, W. and K. Jackowski, 2000 *Magnetic Resonance in Chemistry*, **38**(6): p. 459-462.
- Nordstrom, J., et al., 2011 *J. Colloid Interface Sci.*, **356**(1): p. 37-45.
- Pacheco-Torgal, F., J. Castro-Gomes, and S. Jalali, 2008a
Construction and Building Materials, **22**(7): p. 1305-1314.
- Pacheco-Torgal, F., J. Castro-Gomes, and S. Jalali, 2008b
Construction and Building Materials, **22**(7): p. 1315-1322.
- Roy, D., *Cem. Concr. Res.*, 1999. **29**(2): p. 249-254.
- Schraml, J., et al., 2013 *Magnetic Resonance in Chemistry*, **51**(7): p. 403-406.
- Shi, C., P.V. Krivenko, and D. Roy, 2006
Alkali-activated cement and concretes 2006: Taylor and Frances Group, London and New York
- Woelk, K., et al., 2002 *Journal of Magnetic Resonance*, **159**(2): p. 207-212.
- Yang, K.-H. and J.-K. Song, 2009 *J. Mater. Civ. Eng.*, **21**(3): p. 119-127.
- Yang, X., W. Zhu, and Q. Yang, 2008 *J. Solution Chem.*, **37**(1): p. 73-83.

Properties of Gypsum-free Portland Cement



Dr. Harald Justnes,
SINTEF Building and Infrastructure
Pb 4760 Sluppen
NO-7465 Trondheim, Norway
E-mail: harald.justnes@sintef.no

ABSTRACT

Ground Portland clinker can be set regulated by other soluble calcium salts than gypsum. Calcium nitrate reduced max temperature under semi-adiabatic conditions opening up for low-energy cement without changing clinker chemistry. Substituting calcium sulphate may also allow heat curing, or allow temperature in massive structures to exceed 70°C, without risking delayed ettringite formation. Mortar based on clinker with 3.5 % gypsum and 2.0% calcium nitrate, respectively, was heat cured at 80°C for 3 days and stored for 20°C thereafter. Linear expansion vs. time is steadily increasing for mortar with gypsum, while mortar with calcium nitrate is dimensional stable during 2 years water storage.

Key words: Admixtures, Binders, Rheology, Shrinkage

1. INTRODUCTION

Portland cement is Portland clinker interground with calcium sulphate mainly as set retarder for C₃A forming an initial layer of ettringite (Bullard et al, 2011), even though it is also known that sulphates accelerates the hydration rate of alite (Gunay et al., 2011) and partly counteracts early shrinkage by the ettringite formation in reaction with C₃A. Calcium formate (Cheung et al., 2011) and calcium nitrate (Justnes and Nygaard, 1997) are commonly used in Portland cement (i.e. with calcium sulphate) as accelerators, but no reports have been found on the effect of such calcium salts on Portland cement clinker without calcium sulphate. This paper shows some results where this is the case and discusses the potential implications that may arise from the changes in properties. More detailed discussion of results has been made by Justnes (2013a,b).

2. EXPERIMENTAL

Two different CEM I clinkers were tested. All chemicals used as set regulators where laboratory grades, with the exception of calcium nitrate obtained from the producer Yara International, Norway. Distilled water was used for pastes and ion exchanged water for mortars.

Clinker pastes (300 ml) were made by distilled water to w/c = 0.40. 3.5% gypsum of clinker 1 mass, and 3.0% of clinker 2 mass, (dosage according to corresponding commercial cement) was dry blended before water was added, while 2% of the other calcium salts by clinker mass were dissolved in the water before addition to the clinker. The pastes were prepared in a Braun MR5550CA high shear mixer. They were blended for 1 minute, resting for 5 minutes and mixed once more for 1 minute to stir up any false set.

The stepping up and down flow curves of the pastes were recorded by a rheometer MCR 300 by Physica starting from shear rate ($\dot{\gamma}$) 1 s^{-1} to 150 s^{-1} and immediately down again. This was repeated regularly from 10 to 90 minutes after resting with stirring up at 100 s^{-1} for 1 minute in between. A parallel plate set-up was used with a 1 mm gap and both upper and lower plate serrated to a depth of $150 \mu\text{m}$. Linear fitting of the downwards flow curve was done for the linear part from $\dot{\gamma}$ 99 to 43 s^{-1} resulting in the Bingham viscosity from the slope and yield point from the intercept with the ordinate axis.

The isothermal calorimetry of the same pastes as for the rheology tests (i.e. identical mix) were measured by a TAM air calorimeter as rate of heat evolution as well as cumulative heat. The paste samples were accurately weighed to about 6 g into glass vials and sealed before they were placed in the different channels in the calorimeter.

Mortars were made according to EN 196-1 for clinker 1 with 3.5% gypsum and with 2% calcium nitrate. Two $160 \times 40 \times 40 \text{ mm}$ prisms sets of 3 parallels were cast for each mix, where one set had cast in studs at the ends for length measurements. The spread of the mortars were measured immediately after mixing as well as just after casting the first set. One set was used to measure the 1 day strength after curing at $20 \text{ }^\circ\text{C}$ in the mold, while the set with studs was demolded and placed in a container with water that subsequently was placed in a room of 80°C for 3 days before it was again placed in a 20°C room and allowed to cool to ambient for further storage. Thereafter the lengths of the individual prisms were registered and the length change monitored monthly to see if there were any expansion due to delayed ettringite formation (DEF).

3. RESULTS AND DISCUSSION

The Bingham viscosity and yield point of clinker 1 paste derived from flow curves are plotted in Figure 1 a) and b) respectively when 3.5% gypsum is replaced with 2% calcium formate, acetate or nitrate. The viscosity of paste with gypsum increases with time due to formation of acicular crystals like ettringite and syngenite, while the other salts probably forms platelets of AFm type.

The isothermal calorimetry curves for clinker 1 paste are shown in Fig. 2 for a) for 2% calcium nitrate compared to nitrite and b) for 1% calcium acetate compared to 1.5% propionate. All salts gives sufficient open time to cast samples. Note that the double peak seen for gypsum due to $\text{AFt} \rightarrow \text{AFm}$ conversion is absent for the other salts as expected.

Properties of mortar based on clinker 2 with gypsum vs. calcium nitrate are listed in Table 1.

Table 1 – Properties of mortars made with clinker 2

| Mortar properties | w/ 3.5% gypsum | w/ 2% calcium nitrate |
|--|----------------------------|----------------------------|
| Fresh spread | 162 mm | 142 mm |
| 1 day σ_c 1 l steel mould ^a | $21.5 \pm 0.2 \text{ MPa}$ | $23.3 \pm 0.4 \text{ MPa}$ |
| 1 day mass 1 l steel mould ^a | $2305 \pm 9 \text{ g}$ | $2318 \pm 6 \text{ g}$ |
| 1 day σ_c 1 l styrofoam mould ^b | $52.5 \pm 0.7 \text{ MPa}$ | $53.6 \pm 0.0 \text{ MPa}$ |
| 1 day mass 1 l styrofoam mould ^b | $2310 \pm 3 \text{ g}$ | $2334 \pm 6 \text{ g}$ |
| 28 day σ_c 1 l styrofoam mould ^b | $59.6 \pm 0.2 \text{ MPa}$ | $70.9 \pm 0.4 \text{ MPa}$ |
| 28 day mass 1 l styrofoam mould ^b | $2345 \pm 15 \text{ g}$ | $2362 \pm 0 \text{ g}$ |

^aaverage and standard deviation of 3 parallels. ^baverage and standard deviation of 2 parallels.

As seen from Table 1 the 1 day strength of clinker 2 mortar with 2% calcium nitrate was slightly higher than mortar with 3% gypsum, both cured at 20°C in steel molds and semi-adiabatically in

styrofoam molds. The higher 1 day strength for mortar with 2% calcium nitrate cured in Styrofoam molds is achieved in spite of it reaching lower maximum temperature than mortar with 3% gypsum as seen in Fig. 3a. However, at 28 days the compressive strength was about 71 MPa for mortar with 2% calcium nitrate as compared to about 60 MPa for mortar with 3% gypsum as the same time as the difference in cube mass was less than 1% ruling out air content as explanation. The linear expansion of mortar with gypsum and calcium nitrate cured at 80 and 20°C for 3 days and the stored submerged in water for 2 years are plotted in Fig. 3b. Mortar with gypsum cured at 80°C is expanding, while the one with calcium nitrate is stable.

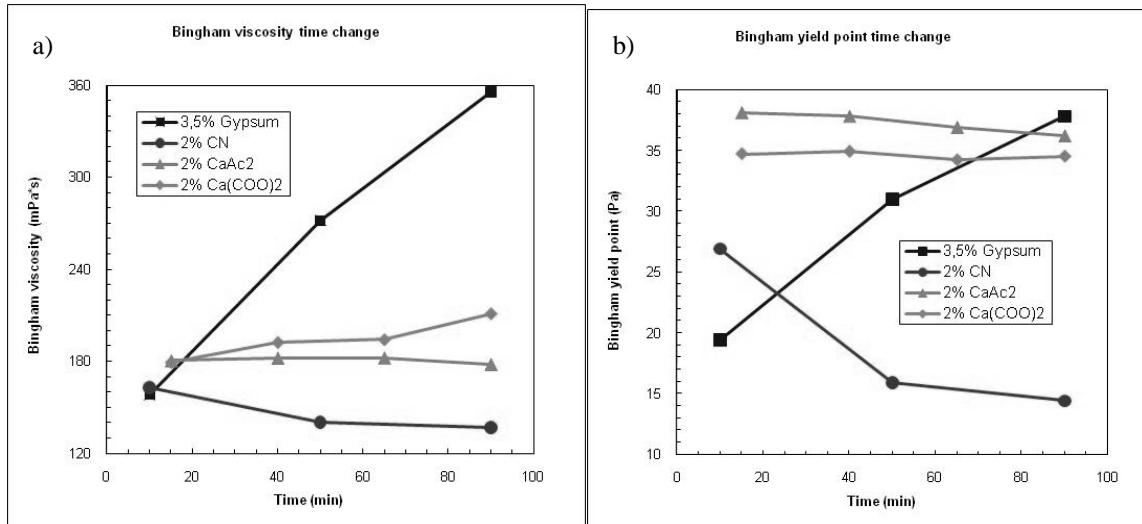


Figure 1 - Bingham viscosity (a) and yield point (b) as a function of time from water addition for clinker pastes made with 3.5% gypsum, 2% calcium nitrate (CN), 2% calcium formate, $\text{Ca}(\text{HCOO})_2$, and 2% calcium acetate dihydrate, CaAc_2 .

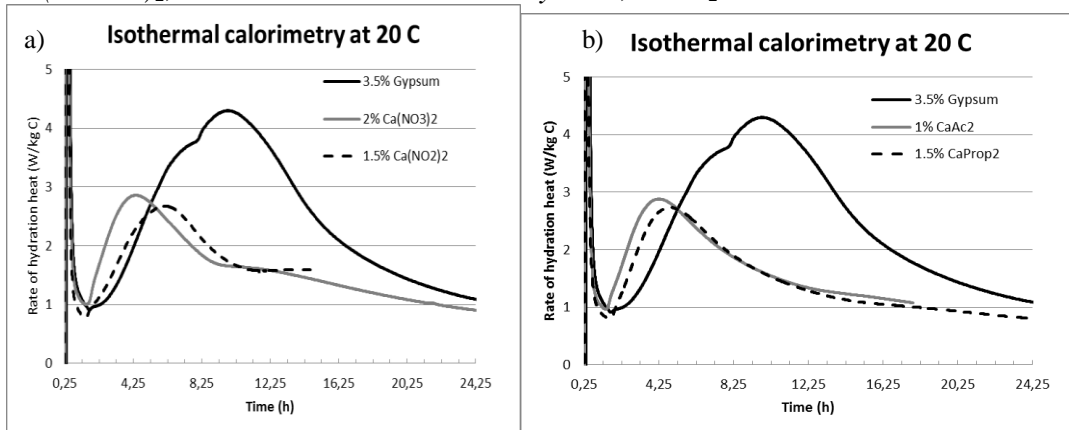


Figure 2 - Rate of heat evolutions first 24 h for clinker 1 pastes made with (a) 3.5% gypsum, 2% calcium nitrate, $\text{Ca}(\text{NO}_3)_2$, and 2% calcium nitrite, $\text{Ca}(\text{NO}_2)_2$, and (b) 3.5% gypsum, 1% calcium acetate, CaAc_2 , and 1.5% calcium propionate (CaProp_2).

4. CONCLUSIONS

Portland cement clinker can be set controlled by other soluble calcium salts than gypsum; proven for formate, acetate, propionate, nitrite and nitrate. The alternative calcium salts lead to a lower flow resistance of paste and mortar at equal w/c, and significantly less increase in flow resistance vs. time, than when gypsum is used.

Heat cured mortar with 3.5% gypsum is expanding while mortar set regulated with 2% calcium nitrate is dimensional stable for 2 years. Thus, gypsum-free cement can probably be allowed to

reach temperatures above 70°C either in massive structures or by extensive heat curing in precast element factories without the risk of detrimental delayed ettringite formation (DEF).

Semi-adiabatically cured mortar with 2% calcium nitrate gave 10°C lower maximum temperature than mortar with 3% gypsum and 11 MPa higher 28 days strength. Thus, it might be possible to make “low heat” cement for special applications (i.e. massive structures etc.) by simply replacing gypsum with calcium nitrate in the mill without altering the clinking process.

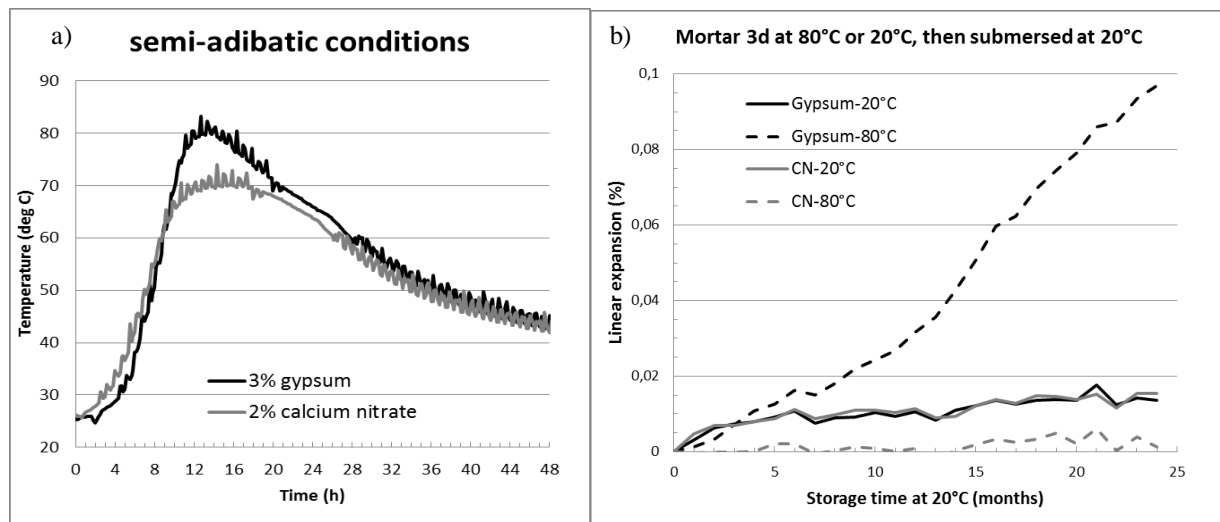


Figure 3 – a) Temperature evolution the first 48 h for clinker 2 mortar placed in 1 liter styrofoam molds with 3% gypsum and 2% calcium nitrate and b) linear expansion of mortars cured under different conditions.

ACKNOWLEDGEMENT

This paper has been supported by COIN - Concrete Innovation Centre (see www.coinweb.no). Financial support has also been received from Yara International, Oslo, Norway.

REFERENCES

- Bullard, J.W., Jennings, H.M., Livingston, R.A., Nonat, A., Scherer, G.W., Schweitzer, J.S. Scrivener, K.L. and Thomas, J.J., 2011. Mechanisms of cement hydration. *Cement and Concrete Research*, 41, 1208-1223.
- Cheung, J., Jeknavorian, A., Roberts, L. and Silva, D., 2011. Impact of admixtures on the hydration kinetics of Portland cements. *Cement and Concrete Research*, 41, 1289-1309.
- Gunay, S., Garrault, S., Nonat, A. and Termkhajornkit, P., 2011. Influence of calcium sulphate on hydration and mechanical strength of tricalcium silicate. *Proceedings of the 13th International Congress on Chemistry of Cement (ICCC)*, Ed. Palomo, A., Zaragoza, A. and López Agüi, J.C., 7 pp., Madrid, Spain, July 4-8, paper 423.
- Justnes, H. and Nygaard, E.C., 1997. The Setting Accelerator Calcium Nitrate - Fundamentals, Performance and Applications. *Proc. 3rd CANMET/ACI Intl. Symposium on Advances in Concrete Technology*, August 24-27, Auckland, New Zealand, ACI SP-171, 325-338.
- Justnes, H., 2013a. Aspects of replacing gypsum with other calcium salts in Portland cement, *Advances in Cement Research*, Vol. 25, Issue 1, February 2013, pp. 44-50.
- Justnes, H., 2013b. Properties of Gypsum-free Portland Cement, *Proc. 8th Intl. Symposium on Cement and Concrete (ISCC); Low Energy Manufacture and Effective Utilization*", Ed. Zhang Wensheng, Nanjing, China, 20-23 September 2013, Invited paper, 9 pp.

Cement hydration and development of texture and bond at interfacial zone between hard rock and shotcrete



Adjunct Prof. Dr. Björn Lagerblad
KTH Royal Institute of Technology, Concrete Structures
SE - 100 44 Stockholm
E-mail: bjorn.lagerblad@cbi.se



Techn.Lic. Lars Elof Bryne
Vattenfall Research and Development AB, Älvkarlebylaboratoriet
SE - 814 70 Älvkarleby
E-mail: lars-elof.bryne@byv.kth.se

ABSTRACT

Sprayed concrete differs from ordinary concrete through application technique and addition of set accelerator that gives immediate stiffening. The alkali free set accelerator consists of sulphate and aluminate and forms an ettringite network that gives a stiff but not hard matrix. This work has investigated the interaction between the early ettringite matrix and the proper cement hydration and the development of the interfacial zone between concrete and rock. This has been correlated to the development of the bond strength.

Key words: Shotcrete, admixture, interface, cement hydration.

1. INTRODUCTION

A strong bond between rock surface and sprayed concrete is of crucial importance, and contributes to a more durable and sustainable tunnel lining. The bond strength of sprayed concrete can be defined as the ability to adhere to a particular surface, e.g. rock or concrete. In a wider sense the concept of adhesion embraces different mechanisms where mechanical interlocking and adsorption can be mentioned among others (Kinloch, 1980). The bond or the texture of the interfacial zone is related to both the shooting of the concrete and the development of the shotcrete. This work treats wet mixed shotcrete, where a set accelerator reacts with the concrete in the air on the way to the projected surface. The most common type today are so called alkali free accelerators, which is a liquid substance mainly consisting of sulphates and aluminium. When mixed with concrete calcium from cement hydration ions are added and ettringite (a mineral) is formed. These reactions are treated in Lagerblad et al. (2010).

The purpose of this work was to increase the understanding of the development of the structure of the shotcrete at the contact zone and the development of bond strength. This has been done by investigating the development of the cement hydrates in Scanning electron microscope and by testing the bond strength from young age by a newly developed testing method. The structure of the interfacial zone and its development has also been investigated.

2. MATERIALS AND METHODS

A variety of testing techniques exist but almost none can be applied to very young and unhardened sprayed concrete. The most common technique is to pull-out cores, predrilled through the concrete and the outer layer of the rock (Holmgren et al., 1997), see Figure 1(a). An alternative technique is to pull steel plates through the concrete lining (O'Donnell and Tannant,

1997), see Figure 1 (b). In this experimental set up, normal sprayed concrete was used with composition comparable to standard concrete used for spraying (see Table 1), with a water-cement ratio of 0.45. Shotcrete mixed with an alkali-free set accelerator (Sigunit from Sika) with an amount of 3-5 wt. % of cement weight was used. A granite core with a flat sawn surface and a diameter \varnothing 95 mm was used in the pull-out test. Due to a protective device the effective cross section area of the bond test had a diameter of 83 mm. The tests were performed at both +7 and +20 °C and 50 % relative humidity.

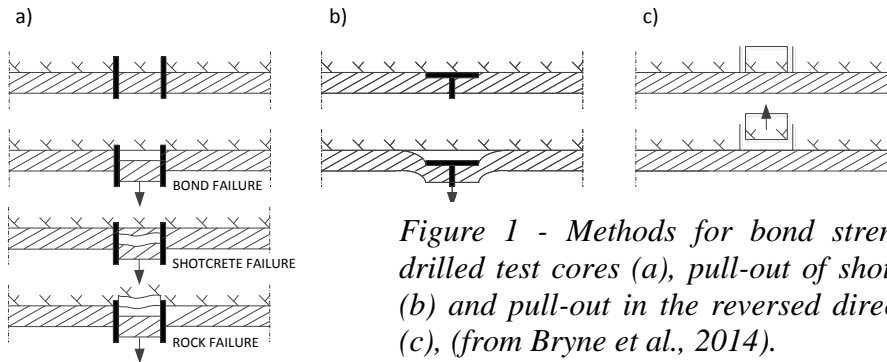


Figure 1 - Methods for bond strength testing. Pull-out of drilled test cores (a), pull-out of shotcrete covered steel discs (b) and pull-out in the reversed direction of a substrate core (c), (from Bryne et al., 2014).



Figure 2 - Surface with the ITZ of granite and shotcrete (left.) The half-moon shaped area on the upper part of the granite core shows the positions of shotcrete residuals. A slice containing granite core and epoxy with the interfacial zone just in between is shown in the upper part of the right photo.

The principle of the pull out methods is schematically described in Figure 1(c), where it can be seen that the direction of pull is reversed compared to the other two methods. This is possible since the method is intended for laboratory work where the substrate is represented by a slab of finite thickness, of e.g. rock or concrete. The cement is Swedish type “Anlæggingscement” (CEM I 42.5 N – SR 3 MH/LA). The set accelerator is an alkali free type, a liquid containing sulphate and aluminates (50 % dry content) by the name Sigunit (from Sika). The mix has a D_{max} of 8 mm and a w/c of 0.45. It also contains 5 % silica fume. The speed of hydration has been analysed by isothermal calorimetry (Figure 3) at 8 and 20 °C. The mix is equivalent to the concrete but with DIN-sand (0-2 mm) as aggregate. The results show that the acceleration period for the mix starts after around 3-4 hours at 20 °C and after around 6 hours at 8 °C. The set-accelerator is accelerating the reaction compared to normal cement hydration.

In the real shotcrete the concrete is warmer from the beginning and then gets colder. Moreover, the cement hydration presumably started in the concrete before it was shot. Thus the speed of hydration will be faster than in the calorimeter. The results show that up to 5-6 hours the strength of the paste is mainly achieved by the ettringite network resulting due to the set accelerator.

Later cement hydration will enhance the strength. The hydration of the cement of the interfacial zone was stopped with alcohol. A pull-out surface with the remaining paste is seen in Figure 2. After 24 hours the remaining alcohol was removed and the surface was dried and stabilised with epoxy and cured for at least 48 hours. An approximately 15 cm thin circular disc containing the

interfacial zone was then cut off from the granite core. A thin slice of the circular disc was cut out and finely ground and polished so that the interfacial zone could be examined in a scanning electron microscope (SEM), see Figure 2 (right) Five different hardening times have been evaluated: 2, 8, 12, 24 and 72 hours, respectively. Two samples per time, one from the test series at +7°C and one at +20°C were analysed.

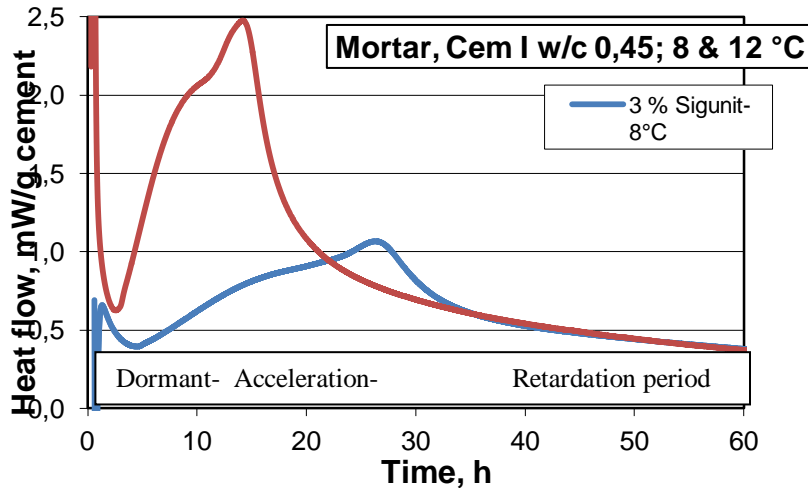


Figure 3-Energy release measured by isothermal calorimetry at 8 och 20 °C

3. RESULTS AND DISCUSSION

Figure 4 shows micrographs of the ITZ at 2, 8 and 24 h hardening times. After 2 hours, the binding matrix mainly consists of very small ettringite crystals. Presumably the texture was more homogeneous before drying. After 8 hours the gel (C-S-H) could be detected but no portlandite. The cement paste is now more homogeneous and the shrinkage is less. This indicates that the cement paste now has gained some strength. No individual ettringite crystals could be detected presumably due to the small grain size. After 24 hours the cement matrix is similar to that of ordinary cement paste. The hydration process in shotcrete is similar to that of ordinary concrete but the set accelerator effects the dormant period. In most cases no ettringite can be detected. No chemical interaction between the cement paste and rock can be observed.

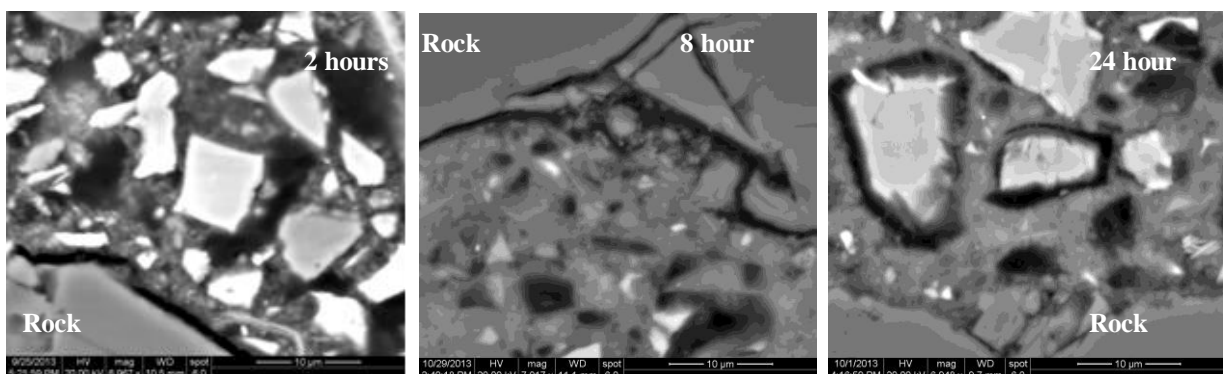


Figure 4 - SEM photos of cement paste at the interfacial zone. Flat polished epoxy impregnated samples over the interfacial zone between rock and shotcrete. The magnification is around 7000 x (30x30 μm)

Pull-out tests in Figure 5 shows that the bond strength is very weak during the first hours at both 7 and 20 °C. This coincides with the hydration of the cement and strength gain of the shotcrete.

In the beginning the strength is a result of the ettringite matrix and the bond is weak. The results show that it takes between 10 and 20 hours to get proper bond strength. The pull out test shows the strength at 7 °C starts somewhat later than at 20 °C but that the strength, with time, improves. This can be expected with experience from normal concrete.

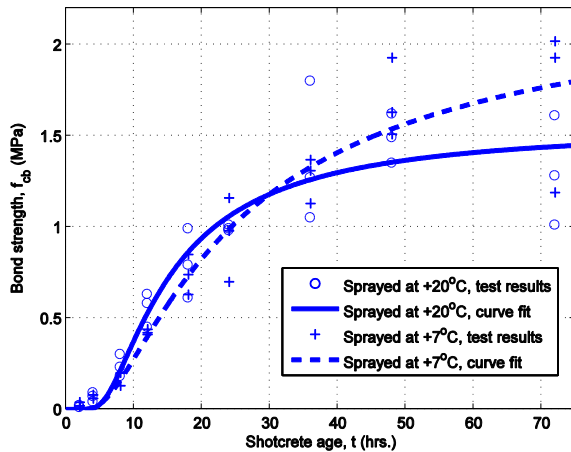


Figure 5 - Results from bond strength test of shotcrete on granite at +7°C and +20°C, respectively, (from Bryne et al 2014).

4. CONCLUSIONS

The presented, newly developed test method is well suited for laboratory work for studying the microscopical interaction between rock and very young shotcrete. Concluding, there is no strict chemical bond between the rock and the shotcrete. There are mainly physical adhesion forces and they are related to the properties of the two materials.

REFERENCES

- Bryne, L.E., Ansell, A., Holmgren, J., 2014,
 ‘Laboratory testing of early age bond strength of shotcrete on hard rock’, *Tunnelling and Underground Space Technology*, 41, 113–119.
- Holmgren, J., Alemo, J., Skarendahl, Å., 1997,
 Stålfiberbetong för bergförstärkning – provning och värdering (Steel fibre sprayed concrete for rock strengthening – testing and evaluation, in Swedish), CBI rapport 3:97, Cement och Betong Institutet, Stockholm.
- Kinloch, A.J., 1980,
 ‘The science of adhesion. Part 1 – Surface and interfacial aspects’, *Journal of Materials science*, 15, 2141–2166.
- Lagerblad, B., Fjällberg, L., & Vogt, C., 2010,
 ‘Shrinkage and durability of shotcrete’, *Proceedings, 3rd International Conference on Engineering Developments in Shotcrete*, Queenstown, New Zealand, 15-17 March 2010, pp 173-180.
- O’Donnell, J.D.P. Sr., Tannant, D.D., 1997,
 ‘Pull tests to measure the in situ capacity of shotcrete’, In: *CIM-AGM*, Montreal, 8p.

Impact of mixing on early hydration of cement paste with lignosulphonate



Alessia Colombo
PhD student
Norwegian University of Science
and Technology
Department of Structural
Engineering
N-7491 Trondheim
E-mail: alessia.colombo@ntnu.no



Tobias Alexander Danner
Postdoctoral fellow
Norwegian University of
Science and Technology
Department of Materials
Science and Engineering
N-7491 Trondheim
E-mail:
tobias.a.danner@ntnu.no



Klaartje De Weerd
Associate Professor
Norwegian University of Science
and Technology
Department of Structural
Engineering
N-7491 Trondheim
E-mail:
klaartje.d.weerd@ntnu.no



Mette Rica Geiker
Professor
Norwegian University of
Science and Technology
Department of Structural
Engineering
N-7491 Trondheim
E-mail:
mette.geiker@ntnu.no



Harald Justnes
Professor
Norwegian University of Science
and Technology
Department of Materials Science
and Engineering
N-7491 Trondheim
E-mail: harald.justnes@ntnu.no

ABSTRACT

As an initial phase of a project focused on effects of lignosulfonate plasticizers on fresh properties of cementitious materials, it was considered relevant to analyze the impact of different mixing procedures on the early properties of cement paste. Calorimetry was used to characterize the early property development. Procedures for mixing both inside and outside the calorimeter were compared. The variation in the time for the main hydration peak observed for different mixing procedures was of the same order of magnitude as variations caused by the addition of plasticizer. Thus, the mixing procedure should be carefully selected and kept constant during the whole experimental work.

Key words: Admixtures, Binders, Calorimetry, Lignosulfonate, Mixing

1. INTRODUCTION

The work reported in this paper is part of a broader research project involving Borregaard (Sarpsborg, Norway), SINTEF and several international partners (Ecole des Mines d'Alès, University of Sheffield, Chalmers University of Technology and University of Melbourne). The main objective of the project is the study of the impact of different lignosulfonate plasticizers on the fresh properties of cementitious materials.

It is known from literature that the mixing procedure can influence the strength development and the properties of cement paste /William et al. 1999; Geiker et al. 2006; Juilland et al. 2012/. As an initial phase of the project it was considered relevant to analyze the impact of different mixing procedures on the early properties of cement paste. The effect of the addition of different amounts of lignosulfonate was also considered. Samples were mixed using different procedures and the heat of hydration measured by isothermal calorimetry was compared for pastes varying in admixture content.

2. EXPERIMENTAL

With the purpose of investigating the very early reactions going on from the first minutes after the addition of water to the cement powder, it is necessary to mix the samples inside the calorimeter. The opening of the instrument in order to insert the samples would disturb the measurement of the initial hydration peak. Four different procedures (P1-P4, described in section 2.2) were then compared in order to choose the most suitable to get homogeneously mixed samples and reproducible results.

Two different procedures of mixing outside the calorimeter were also tested (P6, P7).

Cement paste is usually tested instead of concrete in order to save materials and working time. So as to ensure that the results obtained on cement paste can be comparable with concrete, it is useful to recreate a mixing process similar to the one that actually happens in a concrete system. In order to simulate the milling action of the aggregates on cement agglomerates, a high-shear mixing procedure has been performed (P6).

A hand-mixing procedure outside the calorimeter (P7) has also been evaluated, since it allows saving some material in comparison to procedure 6. Furthermore it was used for other analyses within the research project.

2.1 Materials

The cement paste used is a Portland cement CEM I 42.5 R produced by Norcem AS (Brevik, Norway), referred to as STD in the text, with w/c ratio of 0.4. Softwood sugar-free calcium lignosulfonate (LSs) produced by Borregaard (Sarpsborg, Norway) was added as plasticizer (1% solid).

2.2 Experimental procedure

Isothermal calorimetry was carried out at 20 °C in a TAM Air eight -channel isothermal calorimeter produced by Thermometric AB. Three series of samples were prepared with different amounts of LSs: series A without any LSs added, series B with 0.2% bwoc (by weight of cement) LSs and series C with 0.4% bwoc LSs.

An overview of the mixing procedures is given in Table 1. The samples mixed inside the calorimeter (P1-P4) were prepared mixing 4 g of cement powder with distilled water and superplasticizer. The total mass of the samples was 5.6 g. The samples were placed in 3456 TAM Air Admix ampoules (20 ml) where they were mixed automatically after being inserted in the calorimeter. Similar amounts were used for the paste mixed manually outside the calorimeter (P7).

High speed mixing (P6) was undertaken using a high-shear mixer from Braun (MR530) at intensity 6. The samples were prepared mixing about 280 g of cement powder with distilled water and superplasticizer. The mixing was performed by adding the cement powder to the water (in some cases mixed with lignosulfonate plasticizer), mix for ½ minute, resting for 5 minutes and mixing again for 1 minute.

Hand-mixing (P7): the samples were prepared mixing 15 g of cement powder with distilled water and/or superplasticizer. The total mass of the samples was 21 g. The samples were mixed manually with a spoon for 1 minute.

Table 1 - Mixing procedures

| Procedure | Inside calorimeter | Outside calorimeter | Mixing time | Method | Speed |
|-----------|--------------------|---------------------|------------------------|------------------|-----------|
| 1 | X | | 2 min | Stirrer | High |
| 2 | X | | 2 min | Stirrer | Low |
| 3 | X | | 3 min | Stirrer | Low |
| 4 | X | | 2 min | Manual | - |
| 6 | | X | 5 min resting 1 min | High-shear mixer | Very high |
| 7 | | X | 1 min | Manual | - |

3. RESULTS AND DISCUSSION

Figure 1 illustrates the effect of the addition of an increasing amount of plasticizer in samples mixed with the same procedure. The hydration curve of the sample without any admixture shows an initial heat peak straight after mixing, followed by an induction period, during which the rate of heat of hydration reduces. The second peak, generally attributed to the C_3S reaction, initiate after 2 hours and the maximum is reached after 10 hours. After 13 hours, a shoulder can be observed, which is commonly associated with changes in the AFm phase /Bensted and Barnes 2002/. In case of the samples with plasticizer, the shoulder is reduced when 0.2% bwoc LSs is added and it disappears for the sample with 0.4% bwof LSs. This proves that there is an interaction between C_3A and lignosulfonate which modifies the hydration reactions of cement. The second peak of hydration (or main hydration peak) is delayed of about 2 hours for 0.2% bwoc LSs and of about 5 hours for 0.4% bwoc LSs.

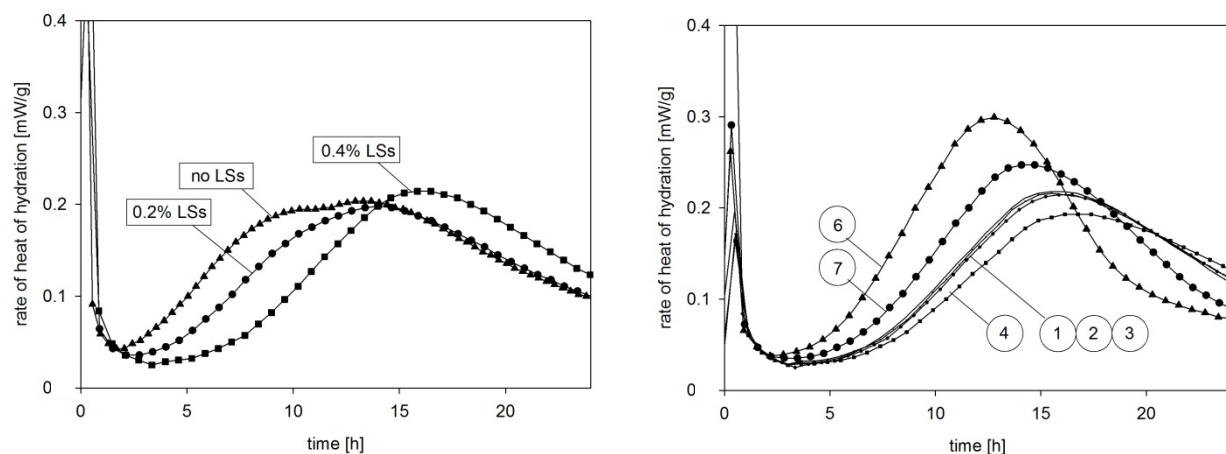


Fig. 1, 2 – On the left, rate of hydration over 1 day of STD cement pastes w/c 0.40 with 0/0.2/0.4 % bwoc LSs, mixed according to the mixing procedure 1 and, on the right, comparison between the rates of hydration over 1 day of STD cement pastes w/c 0.4 with 0.4% bwoc LSs, mixed according to all the procedures considered.

Figure 2 aims to compare the effect of different mixing procedures on the same sample to which 0.4% LSs was added. The mixing procedures inside the calorimeter (P1-P4) give similar hydration curves.

Both the curves obtained from mixing outside the calorimeter (P6, P7) display a higher and earlier main peak of hydration when compared to the first four procedures. In particular, with the high-shear mixing (P6) the highest hydration peak is obtained. The peak is measured about 2 hours in advance compared to the one achieved with procedure 7 and about 3.5 hours in advance compared to the average one achieved with procedures 1 to 4. High-shear mixing (P6) seems then to increase the speed of reaction, most likely because it leads to a better dispersion of particles.

Compared with the peak from procedure 6, the delay obtained with the other mixing procedures is of the same order of magnitude of the one caused by the addition of plasticizer to the system. For this reason it can be concluded that the mixing procedure has a relevant impact on the results. Therefore it is important to follow the same mixing procedure during the whole experimental work and to always take into account the mixing procedure used when comparing to other results from literature.

4. CONCLUSION

Different mixing procedures both inside and outside the calorimeter have been compared. The mixing procedures inside the calorimeter (P1-P4) give similar hydration curves. The higher and earlier main peak of hydration displayed with the procedures outside the calorimeter (P6, P7) may indicate better dispersion and higher degree of hydration of cement grains. Since the average delay in the hydration peak due to different mixing procedures is of the same order of magnitude of the one caused by the addition of plasticizer to the system, it can be concluded that the mixing procedure has a relevant impact on the results. Therefore it is important to follow the same mixing procedure during the whole experimental work and to always take into account the mixing procedure used when comparing to other results from literature.

5. ACKNOWLEDGEMENTS

Borregaard and the Norwegian Research Council are acknowledged for financial support. The authors especially want to thank Rolf A. Lauten (Borregaard) and Serina Ng (SINTEF) for discussing the results and giving useful suggestions for further experiments.

REFERENCES

- Bensted, J., Barnes, P., 2002,
 “Structure and performance of cements”
 2nd edition, Taylor&Francis, Oxon, New York
- Geiker, M., Bøhm, A., Kjeldsen, A., 2006,
 “On the effect of mixing on property development of cement pastes”
 International RILEM Conference, Volume Changes of Hardening Concrete, 20-23 August
 2006, Lyngby, Denmark (edt. Jensen et al.), pp. 303-310
- Juilland, P., Kumar, A., Gallucci, E., Flatt, R.J., Scrivener, K.L., 2012,
 “Effect of mixing on the early hydration of alite and OPC systems”
 Cement and Concrete Research, 42, 1175-1188
- Williams, D.A., Saak, A.W., Jennings, H.M., 1999,
 “The influence of mixing on the rheology of fresh cement paste”
 Cement and Concrete Research, 29, 1491-1496

FIBRES
Cont.

Ultra high performance fibre reinforced concrete as a waterproofing solution for concrete bridge deck renovations



Oldrich Svec
Building and Construction
Gregersensvej,
DK - 2603 Taastrup
E-mail: osv@teknologisk.dk



Claus Pade
Building and Construction
Gregersensvej,
DK - 2603 Taastrup
E-mail: cpa@teknologisk.dk

ABSTRACT

The ability of ultra-high performance fibre reinforced self-compacting concrete to act as a waterproofing on renovated concrete bridge decks is investigated. For such an application the concrete must exhibit specific features, such as deformability, low permeability and high strength. In this paper, the effect of the amount of steel fibres on the shrinkage crack distribution and on the workability of the material was investigated. The impact of a proper treatment of the underlying concrete layer on the bonding strength of the high strength concrete was also studied.

Key words: SCC, Fibres, Shrinkage, Cracking, UHPFRC, Waterproofing

1. INTRODUCTION

Majority of the existing concrete bridge decks in Denmark are currently being renovated by a traditional bitumen waterproofing. Such a renovation results in a lengthy and costly process. A typical traffic disruption due to the renovation is in the range of 3 months. A significant portion of that period is taken by the replacement of the waterproofing layers. Alternative waterproofing materials capable of reducing the duration or frequency of the renovations are therefore of a great interest. Ultra-high performance fibre reinforced concrete (UHPFRC) has been in the last decade investigated as an alternative waterproofing by e.g. Habert et.al. 2013. Insufficient knowledge of the material however restricts its wider adoption. This paper therefore aims to contribute to the knowledge by focusing onto the effect of fibre volume fraction on shrinkage crack distribution and workability of the concrete. This paper also focuses on the bonding strength of the UHPFRC with the underlying concrete.

2. MATERIALS AND METHODS

Mixture design of the UHPFRC used in the following studies followed ECO-UHPFRC presented in Habert et.al. 2013.

2.1 Concrete paving blocks 80 x 62 x 10 cm

Approximately 1 cm thick layer of the UHPFRC was cast onto 6 concrete paving blocks of dimensions 80 x 62 x 10 cm. Three different fibre volume fractions (0%, 4% and 8%) were used to study the effect of fibre amount on the shrinkage crack distribution. Concrete of the same fibre volume fraction was cast onto two separate concrete blocks. The specimens were covered by a plastic foil and left to harden. Subsequently, the shrinkage crack pattern of individual

specimens was studied by e.g. visual quantification and plane section analysis. Rheology of the UHPFRC was measured using the 4C-Rheometer (Thrane et.al. 2010).

2.2 Concrete blocks 30 x 30 x 7 cm

In total 10 blocks of dimensions 30 x 30 x 7 cm were cast of an ordinary bridge deck concrete. The blocks were left to harden for a period of 28 days. Six of the blocks were roughened by sand blasting, whereas four of the blocks were left with a very smooth surface. Two blocks of each surface type were covered with a very thin layer of dust. One day before casting, upper surfaces of all the blocks were soaked with water. Two of the sand blast blocks were treated with a mortar bonding agent. Approx. 3 cm thick layer of the UHPFRC was cast on top of all the blocks. The blocks were left to harden for 7 days. The bonding strength between the UHPFRC and the blocks was then measured by means of tensile and shear tests.

3. RESULTS

A minor parametric study of the UHPFRC workability for various fibre amounts was performed. Figure 1 presents results of the slump flow test performed using the 4C-Rheometer. The figure clearly indicates a decreasing workability of the concrete with increasing fibre volume fraction. A severe interlocking among the fibres was observed when the fibre volume fraction reached 8%. These observations are in line with Martinie et.al. 2010.



Figure 1 – Slump test of UHPFRC concrete for different fibre volume fractions.

3.1 Concrete blocks 80 x 62 x 10 cm

Figure 2 shows top views of the UHPFRC layer cast on the concrete paving blocks for 0% and 4% fibre volume fraction. The left figure indicates a clear pattern of relatively large shrinkage cracks. The right figure doesn't indicate any visible shrinkage crack pattern. The only crack was observed in the bottom right hand corner of the concrete block. The maximum thickness of the crack was in the range of 0.1 mm. The position and orientation of the crack indicates that it was primarily caused by an unfavourable local orientation of the steel fibres (Švec et.al. 2013).

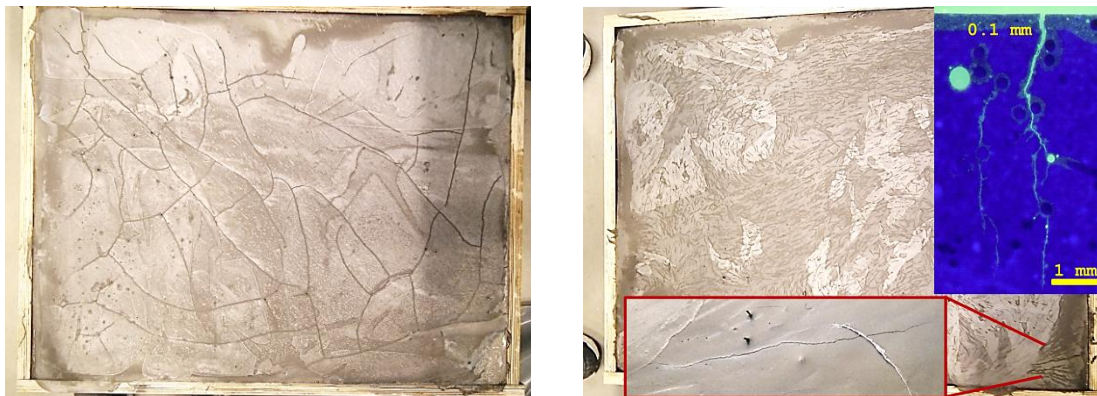


Figure 2 – Shrinkage cracks in UHPFRC. Fibre volume fraction: Left – 0%; Right – 4%.

3.2 Concrete blocks 30 x 30 x 7 cm

Delamination

The bonding strength between the concrete and the UHPFRC was negligible for all the specimens that were not treated by the mortar bonding agent. When a thin layer of dust was present on the concrete block, the UHPFRC completely delaminated. A severe delamination was also observed when the surface was intact, i.e. smooth (see Figure 3 for an example).



Figure 3 – An example of a severe delamination of the UHPFRC layer resulting in negligible bond strength.

The best results in the absence of the bonding agent were obtained when the surface of the concrete blocks was sand blast. When the surface of the blocks was penetrated by the mortar bonding agent (see Figure 4), the bonding exhibited a relatively high strength in the range of 4 – 5 MPa.



Figure 4 – A proper treatment of the substrate concrete before casting. The concrete surface was sand blast, moistened, and “penetrated” by a mortar bonding agent.

Shrinkage crack distribution

Similarly to Section 3.1, the effect of steel fibres on the shrinkage crack distribution was analysed for the concrete blocks of dimensions 30 x 30 x 7 cm. The block was cut and analysed by plane section analysis. Results of the analysis are presented in Figure 5. The top figure shows a photograph of the plane section. The bottom figure shows a sketch of all the cracks noticeable in the plane section. Thickness of the majority of the cracks was under 0.005 mm. All the cracks in the plane section were classified as micro-cracks, i.e. the UHPFRC can be seen as waterproof. Approximately 40 cracks were counted along the length (203 mm) of the plane section. The crack density was therefore approximately 0.2 cracks per millimetre.

4. CONCLUSIONS

A set of experiments was performed to analyse the ability of the UHPFRC to act as a waterproofing layer on the concrete bridge decks. The following main conclusions were drawn from the performed studies:

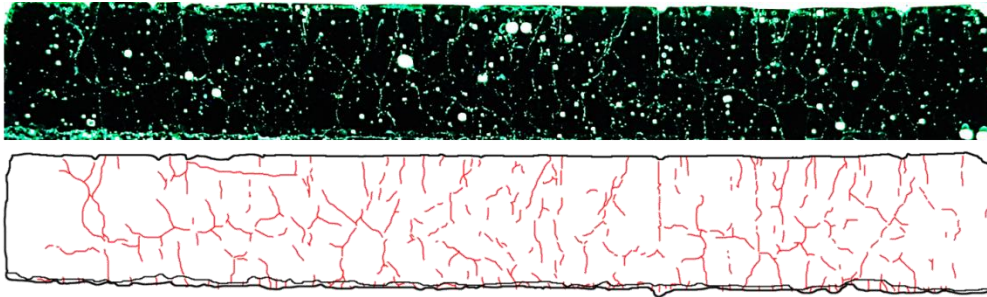


Figure 5 – Top: Plane section analysis of the UHPFRC cast onto a block of ordinary concrete. Bottom: Illustration of the crack pattern obtained from the plane section analysis.

- A proper surface treatment of the underlying concrete and a proper casting process is crucial to avoid delamination of the UHPFRC.
- Workability of the UHPFRC was reduced as the amount of steel fibres increased.
- Fibre volume fraction has a strong influence on the shrinkage crack distribution. A few large cracks were observed when no fibres were added. Many microscopic cracks were observed when a sufficient amount of steel fibres was added to the concrete.
- The distribution of shrinkage cracks is similarly to the fibre volume fraction influenced by the fibre orientation. To avoid shrinkage cracks, the excessive fibre orientation has to be avoided – i.e. the flowability of the concrete must be limited.

ACKNOWLEDGEMENT

The authors acknowledge support from the three-year (2013-2015) performance contract signed between the Danish Ministry of Higher Education and Science and the Danish Technological Institute titled “Ny teknologi til anlægskonstruktioner”.

REFERENCES

- Habert, G., Denarié, E., Šajna, A., Rossi, P., 2013, “Lowering the global warming impact of bridge rehabilitations by using Ultra High Performance Fibre Reinforced Concretes”, *Cement and Concrete Composites*, Volume 38, Pages 1-11, ISSN 0958-9465, doi: 10.1016/j.cemconcomp.2012.11.008
- Martinie, L., Rossi P., Roussel N., 2010, “Rheology of fiber reinforced cementitious materials: classification and prediction”, *Cement and Concrete Research*, Vol. 40, Issue 2, doi: 10.1016/j.cemconres.2009.08.032
- Thrane, L.N., Pade, C., Nielsen, C.V., 2010, “Determination of Rheology of Self-Consolidating Concrete Using the 4C-Rheometer and How to Make Use of the Results”, *Journal of ASTM International*, doi: 10.1520/JAI102003
- Švec, O., Žirgulis, G., Bolander, J.E., Stang, H., 2013, “Influence of formwork surface on the orientation of steel fibres within self-compacting concrete and on the mechanical properties of cast structural elements”, *Cement and Concrete Composites*, ISSN 0958-9465, doi: 10.1016/j.cemconcomp.2013.12.002

Strengthening of Concrete by Fibres and Fibre Reinforced Plastics



Prof., Dr. habil. sc. ing., Vitauts Tamužs
Institute of Polymer Mechanics (IPM), University of Latvia
23 Aizkraukles St., Riga, LV-1006, Latvia
tamuzs@pmi.lv

ABSTRACT

The strength, deformability and stability of concrete columns strengthened by composite sheets is considered in the first part of the presentation. The formulas for prediction of ultimate strength, ultimate strain, and the tangent modulus above the limit of nonlinearity are given. Comparison with the experimental data available in the published literature is done. Confined reinforced concrete columns are considered. The loss of stability of columns above the strength of plain concrete is analyzed and it is proved that FRP confinement is efficient only for columns having low or moderate slenderness ($\lambda < 40$).

In the second part of the presentation the strengthening of concrete by short metallic or synthetic fibres is considered.

Key words: concrete, fibres, strengthening, FRP (Fibre Reinforced Plastic)

The presentation shortly comprises the results obtained by author with collaborators in the IPM during the recent years.

1. STRENGTH, DEFORMABILITY AND STABILITY OF THE STRENGTHENED CONCRETE COLUMNS

1.1. The strength

The concrete column, wrapped by composite drastically change their behaviour: from very brittle material it turns to be quazi plastic (Figure 1).

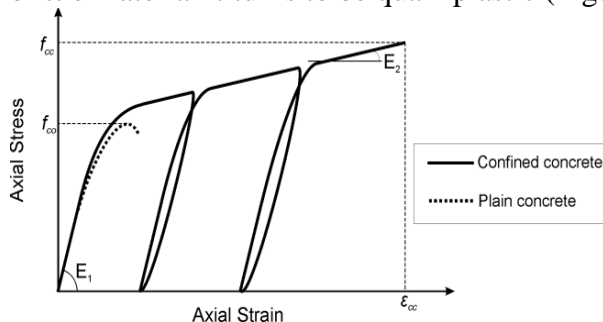


Figure 1 - Cyclic axial stress – strain curve of the confined concrete specimens.

Its behaviour is characterized by the following quantities:

- E_1 initial elastic modulus of the concrete;
- f_{co} ultimate compressive strength of the plain concrete, which coincides with the limit of nonlinearity of the confined specimens;
- f_{cc} compressive strength of the confined concrete;
- E_2 tangent modulus the confined concrete after axial stress exceeds f_{co} ;
- ϵ_{cc} ultimate axial strain of the confined concrete.

Above the limit of nonlinearity the tangent modulus of concrete and the Poisson ratio of the confined concrete begin to change in such way that the lateral pressure to the concrete increases and the loading paths for any concrete samples follows the master curve [Tamužs, V., Tepfers, R. and Spārniņš, E., 2006b].

The FRP jacket fails when the hoop strain reaches the limit value ε_{ju} . Consequently the compressive strength of confined concrete column f_{cc} is:

$$f_{cc} = f_{co} + 4|\sigma_{lu}| = f_{co} + \frac{4\sigma_{ju}h}{R} \quad (1)$$

where $\sigma_{ju} = \varepsilon_{ju}E_j$ is the hoop strength of the FRP jacket.

Apparently formula (1) at first was proposed in Fardis et al. (1981).

1.2. The deformability

Deformability of the confined concrete column. In the [Tamužs, V., Tepfers, R., Zīle, E. and Ladnova, O., 2006c] the expression of second tangent modulus E_2 was derived:

$$E_2 = 24 \cdot E_{lat} \cdot \left(\frac{f_{co}}{E_{lat}} \right)^{0.65}, \quad (2)$$

where $E_{lat} = \frac{E_j h}{R}$, but E_j , h modulus and thickness of the composite confinement ("jacket").

Knowing E_2 it is easy to find the ultimate strain

$$\varepsilon_{cc} = \varepsilon_{co} + 0.17 \cdot (\varepsilon_{ju} - \nu_0 \varepsilon_{co}) \left(\frac{E_{lat}}{f_{co}} \right)^{0.65}, \quad (3)$$

where ν_0 - initial Poisson's ratio, ε_{co} ultimate strain of plain concrete.

1.3. Behaviour of FRP-confined concrete columns reinforced by steel bars

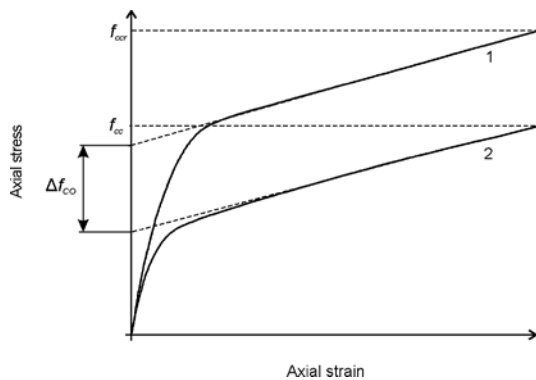


Figure 2 - Compressive behaviour of confined concrete columns with (1) and without (2) steel bar reinforcement.

stress of the steel:

$$\Delta f_{co} = n_s \cdot f_y \left(\frac{r}{R} \right)^2, \quad (4)$$

The longitudinal steel bar reinforcement considerably increases the limit of the nonlinearity of the confined concrete columns [Tamužs, V., Valdmanis, V., Gylltoft, K. and Tepfers, R., 2007]. This is caused by the axial stress redistribution between the concrete and reinforcement bars which lowers the stress level in the concrete.

The steel bars start to yield when the stress level reaches the plain concrete strength. During yielding the elastic modulus of the steel bars is zero and they no more contribute to the stiffness of the column. The increase of the limit of nonlinearity Δf_{co} (Figure 2) is proportional to the total cross-section area of the steel bars and yield

where n_s is the number of steel bars and r is the radius of the steel bars. It is assumed that $(r/R)^2 \ll 1$. The second tangent modulus of the reinforced concrete columns is the same as the second tangent modulus of the unreinforced columns.

Eq.(1) and Eq.(4) leads to the formula for the prediction of the compressive strength of the reinforced confined concrete columns:

$$f_{ccr} = f_{co} + \frac{4\sigma_{ju}h}{R} + n_s f_y \left(\frac{r}{R}\right)^2. \tag{5}$$

1.4. Stability of FRP-confined columns

Critical stress level σ_{cr} at the onset of instability for compressed hinged circular column can be written as follows: $\sigma_{cr} = \frac{\pi^2 E_t}{\lambda^2}$, where E_t is the tangent modulus and λ is the slenderness:

$\lambda = \frac{l}{\sqrt{I/A}}$, where l – length of the column between hinges, I , A – moment of inertia and area of the column cross-section.

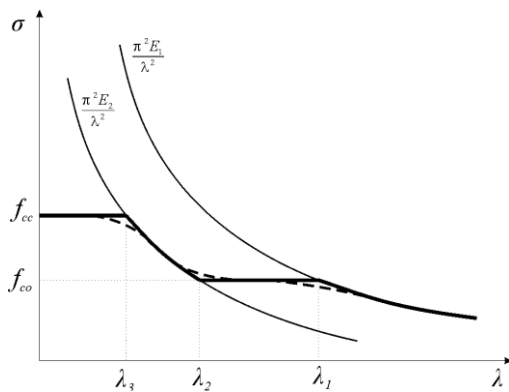


Figure 3 - Critical stress as a function of the slenderness for the confined concrete columns.

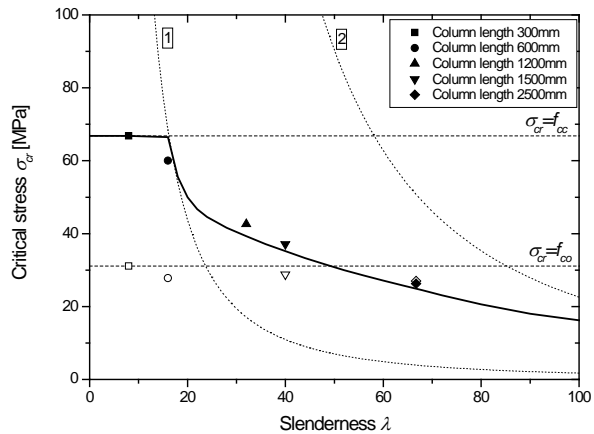


Figure 4 - Predicted and experimentally obtained values of the critical stress as a function of the slenderness. Closed symbols – results from the confined specimen tests, open symbols – results from the plain specimen tests. Solid line – prediction of the critical stress. Line 1 and 2 - Euler's hyperbolas with modulus E_2 and E_0 .

2. FIBRECONCRETE

A small amount of short steel or synthetic fibres added to concrete increases significantly the toughness and deformability of the concrete. To develop the mathematical model of the material it is necessary to estimate the bridging of cracks by the embedded fibres. For that aim it is necessary to test (pull out) the separate fibres embedded in concrete on different depth and angles.

On Figure 5 are shown the strain-force (Δ -P) curves on pullout tests for smooth and toothed steel fibresurface. The fibres are located on 20° relative to pullout direction [Zesers, A., J.Krūmiņš, J., 2014]

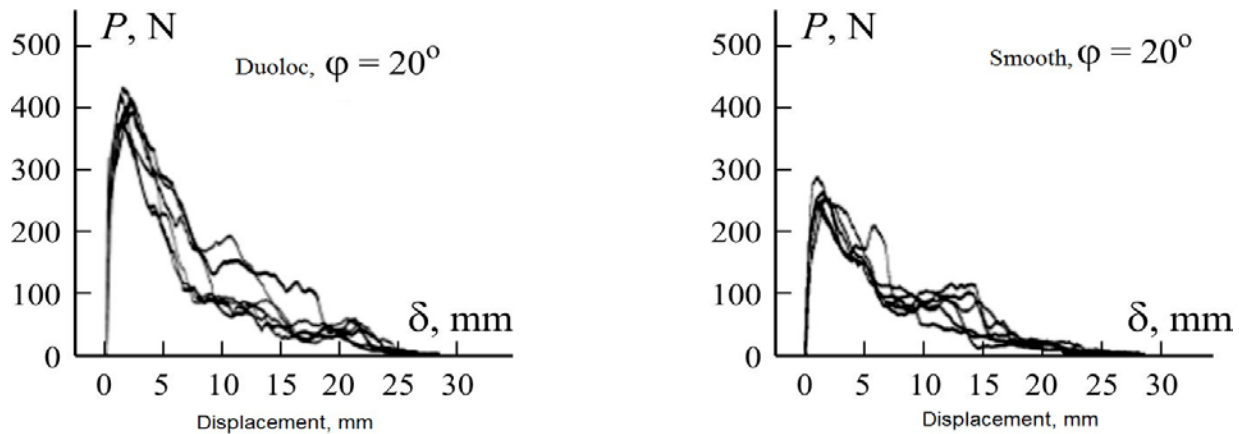


Figure 5 – Pullout curves of two fiber types inclined in 20°

Having $\Delta(P)$ curves it is possible to find the reduction of stress intensity factor as a function of the location of fibre, relative to the crack tip. [Zesers, A., Tamužs, V., 2014].

REFERENCES

- Fardis, M.N., Khalili, H., 1981,
 "Concrete encased in fibreglass-reinforced-plastic" J.Am.Concr. Inst. Proc., Volume 78, N° 6, 1981 pp. 440-446
- Tamužs, V., Tepfers, R., Zīle, E. and Valdmanis, V., 2008,
 "Mechanical behaviour of FRP-confined concrete columns under axial compressive loading". 5th International Engineering and Construction Conference (IECC'5), August 27-29, 2008. American society of civil engineers, International Committee, Los Angeles Section. 2008 17 p.
- Tamužs, V., Tepfers, R., Zīle, E., Valdmanis, V., 2013,
 "Mekaniska egenskaper hos CFRP-ömslutna runda betongpelare med tryckarmering av stål under axiell tryckbelastning", Bygg & Teknik 8/13, Stockholm, 2013 pp. 52-59
- Tamužs, V., Tepfers, R. and Spārniņš, E., 2006b,
 "Behavior of concrete cylinders confined by a carbon composite. 2. Prediction of strength". Mechanics of Composite Materials, Volume 2, 2006 pp. 165 - 178.
- Tamužs, V., Tepfers, R., Zīle, E. and Ladnova, O., 2006c,
 "Behavior of concrete cylinders confined by a carbon composite 3. Deformability and the ultimate axial strain". Mechanics of Composite Materials, Volume 42, N° 4, 2006 pp. 433 – 448.
- Tamužs, V., Valdmanis, V., Gylltoft, K. and Tepfers, R., 2007,
 "Behavior of CFRP-confined concrete cylinders with a compressive steel reinforcement", Mechanics of Composite Materials, Volume 43, № 3, 2007 pp. 191-202.
- Tamužs, V., Valdmanis, V., Tepfers, R., Gylltoft, K., 2008,
 "Stability analysis of CFRP-wrapped concrete columns strengthened with external longitudinal CFRP sheets". Mechanics of Composite Materials, Volume 44, № 3, 2008 pp. 199-208.
- Zesers, A., J.Krūmiņš, J., 2014,
 "Surface Properties of a Hooked Steelfiber and their Effects on the Fiber Pullout and Composite Cracking. I. Experimentl Study". Mechanics of Composite Materials, Volume 50, No. 3, 2014 (in press)
- Zesers, A., Tamužs, V., 2014,
 "Cracking Resistance of Short-Fiber-Reinforced Composites", Mechanics of Composite Materials, Vol. 50, No. 2, 2014 (in press)

Characterisation and observation of fibre orientation in flowable steel fibre reinforced concrete: Influence of formwork and reinforcement layout



Giedrius Žirgulis
Richard Birkelands vei 1a
NTNU, Trondheim
Norway
E-mail:
giedrius.zirgulis@ntnu.no



Prof. Terje Kanstad
Richard Birkelands vei 1a
NTNU, Trondheim
Norway
E-mail:
terje.kanstad@ntnu.no



Prof. Andrzej Cwirzen
Rakentajanaukio 4A
02150 Espoo Finland
E-mail:
andrzej.cwirzen@aalto.fi



Dr. Oldřich Švec
Gregersensvej 1
DK-2630 Taastrup
Denmark
E-mail:
osv@teknologisk.dk



Prof. Mette Rica Geiker
Richard Birkelands vei 1a
NTNU, Trondheim
Norway
E-mail:
mette.geiker@ntnu.no

ABSTRACT

In a comprehensive fibre orientation study numerical simulation results of slab and wall elements cast from flowable fibre reinforced concrete were compared to experimental results. Beams cut from the slabs and wall elements were analysed using computerized tomography (CT) and image analysis to characterise the fibre orientation. In addition some of the same beams were tested in bending. The influences of the following parameters were considered: wall versus slab element, formwork surface, reinforcement layout, formwork tie bars. The results showed that the numerical simulations agree well with the experimental observations.

Key words: Fibre reinforced SCC, fibre orientation, computerised tomography, image analysis, slab, wall, reinforcement bars.

1. INTRODUCTION

There are two reasons why fibres take preferred orientation in flow-able concrete, the wall effect and the shear stresses occurring during concrete flow (Martinie & Roussel, 2011). The wall is due to the physical restriction at the surface (for example mould) preventing fibres to orientate perpendicularly to the surface within a distance closer than about half the fibre length. The orientation of fibres is described using the fibre orientation factor (α), which is closely related to the number of fibres (N_f) crossing the investigated section of the fibre reinforced concrete (FRC) element (Žirgulis, Geiker, Švec, & Kanstad, 2013). The section for determining the number of fibres typically is chosen with respect to stress direction. For beams it is usually the cross-section of the beam. The fibre orientation factor (α) can be expressed as (Soroushian P, 1990):

$$\alpha = \frac{n_f A_f}{v_f} = \frac{N_f A_f}{A_c v_f} \quad (1)$$

Where: n_f is the number of fibres per surface unit; A_f is the cross-section area of one fibre; v_f is the fibre volume fraction, and A_c is the area of the concrete section in question.

In this paper analysis of the fibre orientation in slab and wall elements is described. The effect of surface quality, reinforcement and wall moulds tie bars on fibre orientation is investigated.

2. MATERIALS AND CASTING

2.1 Test setup

Six slab and two wall elements were cast. The size of the slabs was $1200 \times 1200 \times 150 \text{ mm}^3$ and the walls $1000 \times 1500 \times 150 \text{ mm}^3$. Four slabs had no reinforcement: two with slip surface (oiled laminated plywood), two with rough surface (formwork with glued sand), while the two later slabs were reinforced with 10mm diameter rebars with 200 mm spacing (Figure 1a). The wall formwork was tied using 4 tie bars as shown in (Figure 1b) and had a slip surface.

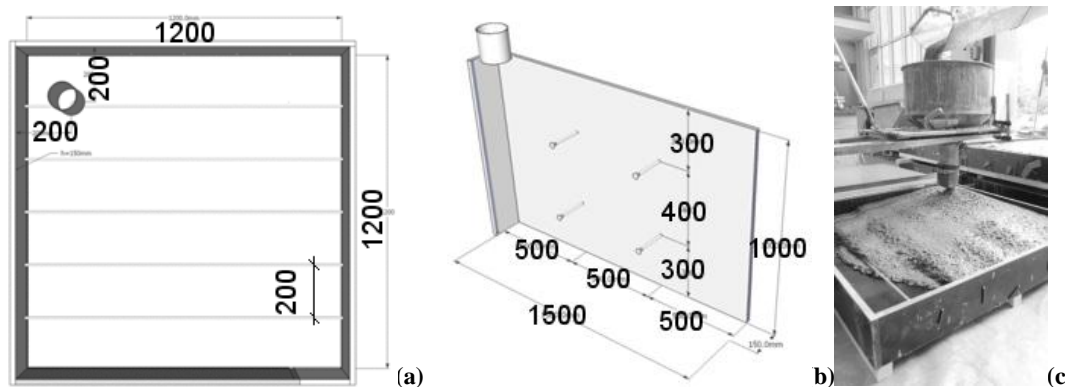


Figure 1– The dimensions of slabs and the rebar spacing in the reinforced slabs (a). The dimension of walls and the positions of tie bars (b). The funnel shaped barrel (c).

All slabs and walls were cast from one point delivering the concrete directly from the concrete truck into a funnel shaped barrel, which was supported by a forklift (Figure 1c). To investigate the orientation of fibres beams with size of $150 \times 150 \times 600 \text{ mm}^3$ were cut from the slabs and walls. The beams were later scanned in the CT scanner. The position of the beams is shown in Figure 2 and Figure 3. The cut beams from the unreinforced slabs were tested according to EN14651.

2.2 Mix composition

The mix composition of the concrete is given in Table 1. It contained 0.5% by volume of steel fibres. The fibres were made of cold drawn wire, had hooked ends, length of 60 mm, aspect ratio of 80, and a tensile strength of 1050 N/mm^2 according to the producer. The SCC was produced in a concrete mixing plant equipped with twin shaft compulsory mixer. The steel fibres were added manually after 1 minute of wet mixing. The mixing time was 3 minutes and the transportation from the concrete plant to the laboratory took approximately 15 minutes.

3. METHODS

3.1 Numerical simulations

Numerical simulations were run for each slab type and wall. The SCC was modelled as a free surface flow of a homogeneous Bingham plastic fluid with steel fibres assumed as thin rigid cylinders. The fibres were simulated as one by one. The model took into account the two-way coupled interaction between the fluid and the fibres, plastic collisions among the fibres, plastic collisions of the fibres with the formwork (Švec & Skoček, 2013). Each numerical simulation was run in parallel on 25 computer cores and lasted approximately 4 days. (Švec, Žirgulis, Bolander, & Stang, 2013).

Table 1– Composition and properties of concrete.

| | Density [kg/m ³] | Unit | Unreinforced slabs | Reinforced and walls | slabs |
|------------------------------------|---------------------------------|--------------------------------|-----------------------|-------------------------|-------|
| Cement, Norcem standard FA | 3010 | kg/m ³ | 388 | 388 | |
| Water | 1000 | kg/m ³ | 196 | 196 | |
| Silica fume, powder | 2200 | kg/m ³ | 19.4 | 19.4 | |
| Natural sand 0-8 mm | 2700 | kg/m ³ | 1182 | 1182 | |
| Crushed stone 8-16 mm | 3040 | kg/m ³ | 570 | 570 | |
| Super plasticizer, Glenium Sky 600 | 1193 | kg/m ³ | 4.66 | 4.66 | |
| Air entrainer Uamex 11 (1:7) | 1166 | kg/m ³ | 0.97 | 0.97 | |
| Air content | | m ³ /m ³ | 0.035 | 0.009 | |
| Steel fibres, [kg/m ³ | 7800 | kg/m ³ | 40 | 40 | |
| Matrix volume (< 0.125 mm) | | m ³ /m ³ | 0.364 | 0.364 | |
| Cement paste volume | | m ³ /m ³ | 0.334 | 0.334 | |
| w/(c+SF) (k=2) | | kg/kg | 0.47 | 0.47 | |
| Slump flow | | mm | 620 | 520 | |
| Mix density | | kg/m ³ | 2318 | 2486 | |

3.2 Computerised tomography (CT) and image analysis

The computerised tomography (CT) was conducted with a Siemens Somatom sensation 4 CT scanner using scanning voltage of 140kV. Open source software FIJI was used for image analysis of the CT scans (Schindelin et al., 2012). The threshold was applied to CT scanned images in order to separate the fibres. After this step the “skeletonise” plugin was applied, which thinned the diameter of fibres to one pixel. Later the “analyse skeleton” plugin was applied to produce the table of 3D coordinates of fibres end points. The thresholded CT images were also used to construct the 3D images of fibres. The data of 3D coordinates of fibre ends of the beams were used in specially written computer code for further numerical analysis of fibre orientation along and across the length of cut beams.

3. RESULTS AND DISCUSSIONS

The numerical simulation results showed the most pronounced fibre orientation in slabs cast on slip surface (Figure 2 left). This was reflected in the 3 point bending test results. The average value of the residual flexural strength at CMOD=2.5 mm for cut beams with the most favourable fibre orientation (A, Figure 2) from the slip surface slabs was 11.6 N/mm², while the corresponding value from the rough surface slabs was 6.5 N/mm². For beams with unfavourable (B, Figure 2) fibre orientation the values were 4.8 N/mm² and 5.3 N/mm², respectively. The large difference in residual flexural strength values of favourable and unfavourable orientation beams confirms that slip surface slabs had more defined fibre orientation.

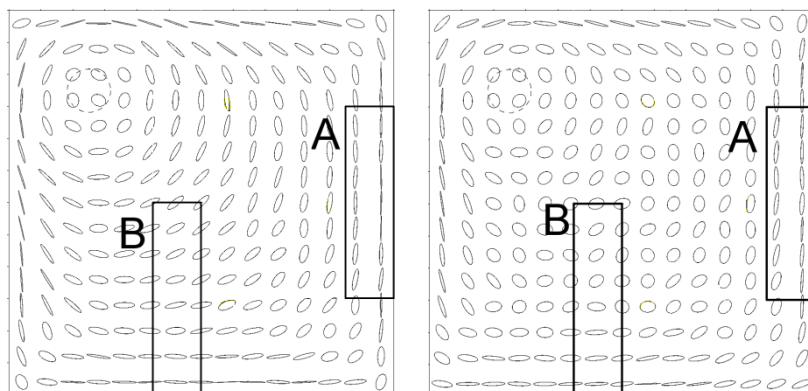


Figure 2– Simulated fibre orientation in lower layer of slabs cast on slip surface (left) and rough surface (right). (Švec, Žirgulis, Bolander, & Stang, 2013)

The analysis of fibre orientation in the beams cut from the reinforced slabs showed that the rebars affected the lower layer by increasing the fibre orientation towards the rebar. An increase in orientation parallel to the rebar was observed in front of the bar. There was no observed effect of rebars on the fibre orientation in the upper layers of the slabs.

The simulation (Figure 3 left) and CT (Figure 3 right) results of wall casting showed a good agreement as well. Both methods revealed zones of highly oriented fibres behind the formwork tie bars where fibre orientation followed the direction of the concrete flow. Multiple regions with unidirectional oriented fibres were observed in the wall. This potentially creates weak zones with respect to load (Figure 3).

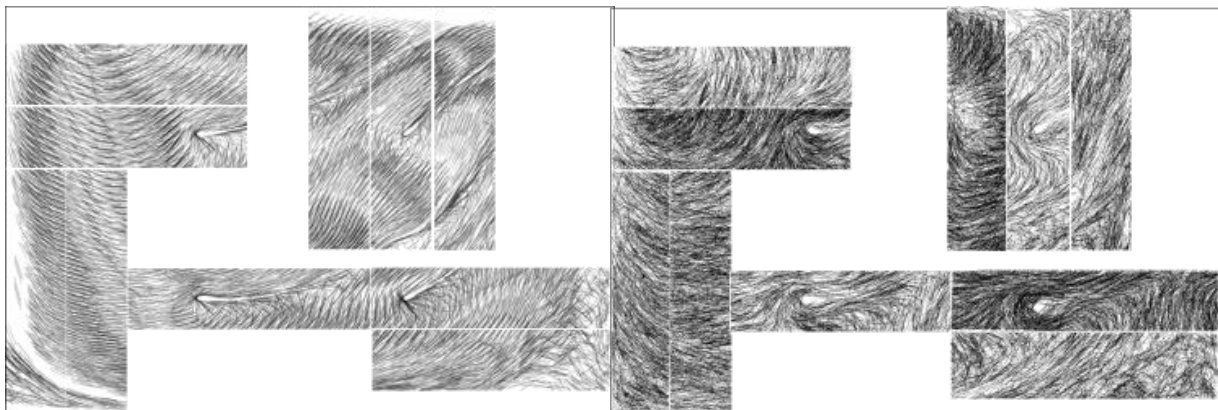


Figure 3 – Fibre orientation in the walls: numerical simulation (left), mapped by CT (right).

4. CONCLUSIONS

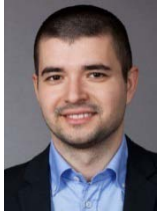
The fibres in slabs of flowable fibre reinforce concrete cast on slip surface were more oriented than in slabs cast on rough surface. Reinforcement affected the fibre orientation in lower layers of the investigated slabs.

Multiple regions with unidirectional oriented fibres were observed in the wall cast from flowable fibre reinforced concrete. Zones of highly oriented fibres were observed behind the tie bars.

REFERENCES

- Martinie, L., & Roussel, N. (2011). Simple tools for fiber orientation prediction in industrial practice. *Cement and Concrete Research*
- Schindelin, J., Arganda-Carreras, I., Frise, E., Kaynig, V., Longair, M., Pietzsch, T., Cardona, A. (2012). Fiji: An open-source platform for biological-image analysis. *Nature Methods*, 9(7), 676-682.
- Soroushian P, L. C. (1990). Distribution and Orientation of Fibers in Steel Fiber Reinforced Concrete. *ACI Materials Journal*, 87(5), 433–439.
- Švec, O., & Škoček, J. (2013). Simple navier's slip boundary condition for the non-Newtonian Lattice Boltzmann fluid dynamic solver. *Journal of Non-Newtonian Fluid Mechanics*, 1-24.
- Švec, O., Žirgulis, G., Bolander, J. E., & Stang, H. (2013). Influence of formwork surface on the orientation of steel fibres within self-compacting concrete and on the mechanical properties of cast structural elements. *Cement and Concrete Composites*.
- Žirgulis, G., Geiker, M. R., Švec, O., & Kanstad, T. (2013). Potential methods for quality control of fibre distribution in SCC. *Rheology and processing of construction materials*. RILEM proceedings PRO 90.

Experimental Program for Axially Loaded RC Walls with Openings Strengthened by FRP



Cosmin Popescu
M.Sc., Ph.D. Student
NORUT, Rombaksveien E-6 47, N-8517 Narvik, Norway
Department of Infrastructure Structures and Materials
E-mail: cosmin.popescu@norut.no



Gabriel Sas
Ph.D., Assistant Lecturer
Luleå University of Technology, Department of Structural Engineering
SE – 971 87 Luleå, Sweden
E-mail: gabriel.sas@ltu.se



Björn Täljsten
Ph.D., Professor,
Luleå University of Technology, Department of Structural Engineering
SE – 971 87 Luleå, Sweden
E-mail: bjorn.taljsten@ltu.se



Thomas Blanksvärd
Ph.D., Associate Senior Lecturer,
Luleå University of Technology, Department of Structural Engineering
SE – 971 87 Luleå, Sweden
E-mail: thomas.blanksvard@ltu.se

ABSTRACT

The presence of a new opening will decrease the axial capacity, thus, requiring upgrading. Satisfactory results were found when fiber reinforced polymers (FRP) was placed in the vicinity of the openings, being capable to restore the initial structural capacity. However, despite the considerable research carried out, there are still important research gaps that need to be further investigated. In this paper an experimental program aimed to study the influence of opening size and the strengthening pattern for RC walls will be presented. To achieve this aim, a two-level factorial experiment has been designed resulting in a total of nine wall specimens.

Key words: Repair, Strengthening, FRP, Structural Design, Openings, Walls

1. INTRODUCTION

Functionality modifications of structures are often encountered, as existing structures need to be adapted to the current living standard requirements. For example, new windows and doors require openings to be cut in reinforced concrete (RC) walls. The creation of these openings in walls will change the stress distribution and adversely influence the behaviour of the wall, thus a strengthening of the structure is imposed to recover the initial structural capacity. One repair and rehabilitation method that has received world-wide acceptance during the last two decades is the use of FRP as externally bonded reinforcement. Although considerable amount of research performed on RC walls with openings (Saheb and Desayi 1990, Doh and Fragomeni 2006, Lee 2008), all of them were designed as if the opening has been initially planned. Hence, the case of RC wall panels with cut-out openings is still unexplored. Mohammed et al. (2013) found that

the presence of the opening in a solid one-way panel lead to disturbance zones. The discontinuities causing high stresses will force the cracks firstly occur at the corners due to improperly reinforcing. From their results it can be concluded that applying FRP around the opening in different patterns the capacity could be improved by which reducing the principal stresses acting on the upper corners of the opening.

A research program is undergoing at Luleå University of Technology, Department of Structural Engineering where a number of concrete walls with different parameters will be tested. This paper aim to present the experimental program defined by design of experiments (DOE) technique.

2. EXPERIMENTAL PROGRAM

2.1 Test-rig for RC walls

Several researchers have put a tremendous effort into developing design equation for RC walls. In this study, one of our interests was to identify the characteristics of the test setup used previously and to decide which one will be useful for our case and to provide further improvements, if needed. In most cases, the bearing walls subjected to gravitational forces has been tested in one-way or two-way action. One-way panel refer to the panels restrained along top and bottom sides of the wall, thus being possible to develop a single out-of-plane curvature in vertical direction. Two-way panel refer to the panels restrained along three or all sides of the wall, where the wall deflects in double curvature in horizontal and vertical direction. In order to be on the safe side, the restraining elements provided only fixed translation and can freely rotate, thus creating a hinged connection. However, neither a perfect hinge nor a full rotation restrained could be achieved in laboratory environment, thus all design models present a high level of conservatism. Studying the previous test rig designs some particularities were observed on establishing the support conditions, thus being adopted in the current test program (see Fig 1).

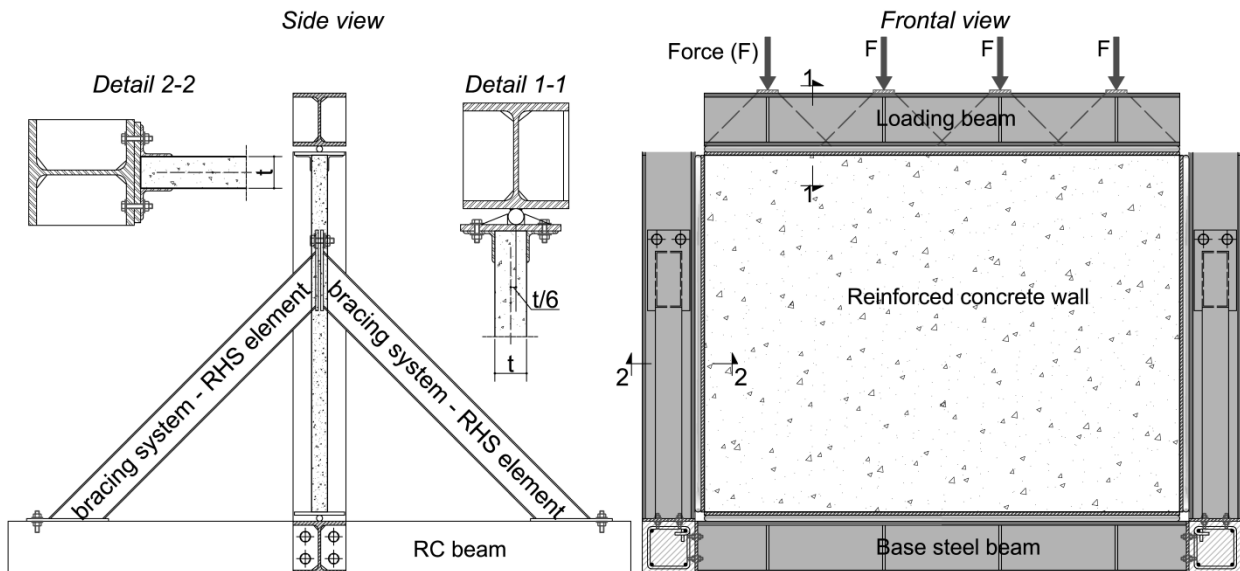


Figure 1 – General view of test setup

The test rig was designed in such way to simulate a hinged connection at the intersection between top/bottom element boundaries and the specimen. To achieve the hinged support a steel rod will be placed on a thick steel plate along the element edges. For lateral restraining conditions two clip angles has to be fixed on both sides of the element and connected to the main lateral columns. The boundary elements should be stiff enough to avoid any deformations. In order to assure a uniformly distributed load across the wall length, four actuators will transmit

the load through a loading beam. The height of the loading beam resulted to be 200 mm by assuming a 45° load distribution from the concentrated load. A total of four RHS beams will provide the lateral stability of the entire test rig.

3. Design of experiments

As shown by DeCoursey (2003), one-factor-at-a-time design would not give us any precise information about the interaction, and the results from that plan of experimentation might be extremely misleading. Thus, a better alternative is to conduct simulations by combining different levels of the factors, which is called a factorial design. By choosing a number of parameters and a fixed number of levels, experiments should be performed with all possible combinations. The parameters who can have a highly influence on the axial load of RC walls with openings were identified by studying different models available in the literature. Few models for predicting the axial capacity of RC walls with openings were found, however, the latest formula (1) proposed by Doh and Fragomeni (2006) was found to give satisfactory results. In equation (1) N_u represent the axial capacity of an identical panel without openings, k_1 and k_2 are constants derived using a standard regression analysis and the factor χ incorporate the effect of the size and location of the opening in the wall.

$$N_{uo} = (k_1 - k_2\chi)N_u \quad (1)$$

Parameters like eccentricity, side supports, slenderness, aspect ratio and reinforcement ratio have also influence on the ultimate axial strength of a solid RC wall. Those parameters have been intensively studied in the past, thus being out of scope for this experimental program. According to the theory behind factorial design, past experience should contribute in choosing the right parameters to be varied at maximum of two levels. Based on the results from the first stage of experiments, further tests can be designed logically and may well involve more than two levels for some parameters. Therefore, the first set of analyses will examine the impact of two parameters: (1) openings size and (2) strengthening pattern. For the first parameter small (S) and large (L) opening will be set as the min/max level and for the second one: (a) steel reinforcement placed around corners at 45° (st) as it has been initially designed and (b) externally bonded and near surface mounted FRP reinforcement (frp). Consequently, this will require $2^2=4$ different experiments for a complete factorial design. Besides these tests another three specimens (i.e. wall with and without cut-out openings) used as references will be tested until failure to demonstrate the effectiveness of strengthening alternatives. An important factor in experiments, namely replication, would be kept at low level. That means only two identical specimens from those strengthened with FRP will be cast and for the rest of them only one specimen. All tests resulted from DOE technique is shown in Figure 2.

3.1 Test specimens and material properties

Nine half scale specimens $L=1800$ mm (length), $H=1350$ mm (height) and $t=60$ mm (thickness) resulted from this plan of experimentation having an aspect ratio (H/L), slenderness ratio (H/t) and thickness ratio (L/t) of 0.75, 22.5 and 30, respectively. The cut-outs will represent a door opening centrally placed with 450x1050 mm and 900x1050 mm dimensions for small and large opening, respectively. For casting, normal concrete is intended to be used with a compressive strength class C25/30 used in daily practice. The steel reinforcement ratio is set to 0.2% which represents the minimum amount according to EC2 (EN1992-1-1). Half of this ratio should be located at each face of the wall.

An amount of reinforcement equivalent to that interrupted by an opening shall be added at 45° around corners for those elements intended to be strengthened with embedded steel reinforcement. For specimens FRP-strengthened, NSM bars at 45° will be mounted around corners and EBR sheets at the bottom part of the beam strip above the opening.

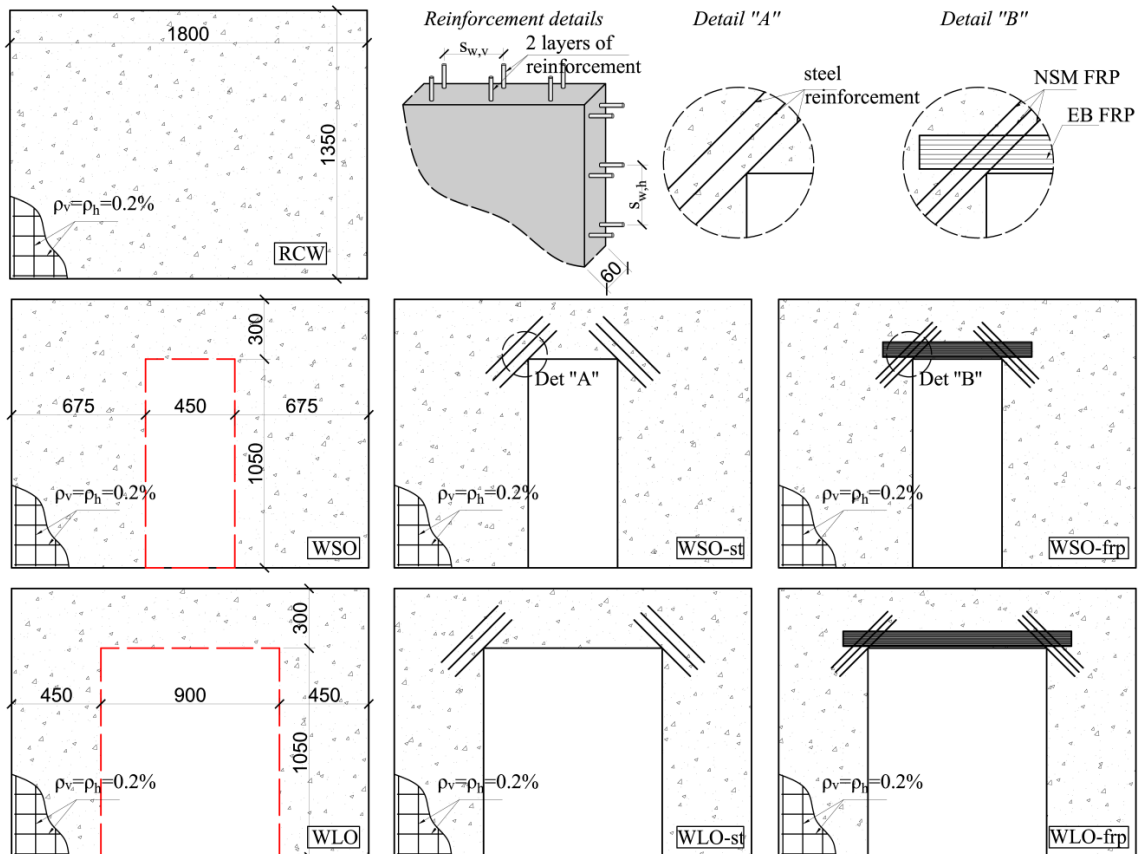


Figure 2 – Details of the specimens

4. CONCLUSION

The experimental program presented in this paper was conceived in accordance with factorial design technique. A total of nine wall specimens were proposed in order to study the influence of opening size and the effectiveness of the strengthening patterns. Two methods for strengthening of RC walls with openings have been proposed: (1) traditional by embedding steel reinforcement and (2) a modern technique using FRP materials.

REFERENCES

- Comité européen de normalisation, EN 1992-1-1, 2005,
 “Design of concrete structures Part 1–1 General rules and rules for buildings”, Brussels.
- DeCoursey, W.J., 2003,
 "Statistics and probability for engineering applications with Microsoft Excel", ebrary, Inc. Elsevier Science Publishers, Amsterdam; Boston: Newnes.
- Doh, J. H., and Fragomeni, S., 2006,
 "Ultimate load formula for reinforced concrete wall panels with openings", *Advances in Structural Engineering*, Vol. 9, No. 1, pp. 103-115.
- Lee, D.-J., 2008,
 "Experimental and theoretical study of normal and high strength concrete wall panels with openings", PhD Thesis, Griffith University, Australia.
- Mohammed, B., Ean, L. W., and Malek, M. A., 2013,
 "One way RC wall panels with openings strengthened with CFRP", *Construction & building materials*, Vol. 40, pp. 575-583.
- Saheb, S. M., and Desayi, P., 1990,
 "Ultimate strength of rc wall panels with openings", *Journal of Structural Engineering*, Vol. 116, No. 6, pp. 1565-1578.

Strengthening of concrete structures with FRP – a guideline



Björn Täljsten
Ph.D., Professor
Division of Structural Engineering, Luleå University of
Technology, SE-971 87 Luleå, and Sto Scandinavia AB,
Linköping, Sweden
bjorn.taljsten@ltu.se



Gabriel Sas, Ph.D
Luleå University of Technology
Department of Structural Engineering
SE – 971 87 Luleå, Sweden
E-mail: gabriel.sas@ltu.se



Thomas Blanksvärd, Ph.D.
Division of Structural Engineering, Luleå University of
Technology, SE-971 87 Luleå, and Skanska Sverige AB,
Göteborg, Sweden
E-mail: thomas.blanksvard@ltu.se

ABSTRACT

There is a need to retrofit existing concrete structures. There might be many different ways to increase the performance of a concrete structure. FRP (Fibre reinforced Polymer) strengthening might be one method to do so. This method is today commonly used over the world to upgrade concrete structures in its load carrying capacity. In this paper an overview of a Swedish guideline for FRP strengthening of concrete structures is presented. The guideline covers design for bending and shear as well as for confinement. The guideline also discusses the need of proper workmanship and choice of the right material for strengthening. In the guideline well worked out calculation examples can be found.

Keywords: Concrete, Retrofitting, Strengthening, Upgrading, FRP, Composite Material,

1. INTRODUCTION

Before a decision is taken regarding strengthening of concrete structures a proper assessment is recommended to make clear the reason for strengthening. Some common used methods to strengthen concrete elements are to increase the cross sectional area, external prestressing, shotcrete, change of static system etc. These methods normally have a good functionality and have also been used successfully for a long time. In the mid 70-ties a strengthening method using external bonded steel plates was developed. During the 70-ties and 80-ties the method was relatively commonly used in central Europe, US and Japan, (Täljsten, 1994). During the beginning of the 80-ties the use of FRP (Fibre reinforced Polymers) for strengthening of

concrete structures was researched, (Shinozaki et. al., 2007). The primary aims were to find methods and systems to improve the dynamic response on structures in relation to earthquakes. The effect was very positive and continued research in the area led to the development of unidirectional FRP laminates for external strengthening, (Meier et. al.1992). Today externally strengthening with FRP:s are commonly used and fully accepted around the world. In Sweden research in this area started in the end of the 80-ties at Luleå University of Technology. In this paper a brief summary of how to design for flexure, shear and confinement will be presented.

2. BENDING

2.1 General

FRP for strengthening are commonly used to increase the flexural capacity of concrete members. Strengthening can be done with laminates, sheets of NSM (Near Surface Mounted) reinforcement. In general laminates are most suitable for flat surfaces such as slabs, beams and walls. Sheets are used when greater flexibility is needed, e.g. curved surfaces, columns etc. In this section a brief presentation in design for bending is presented.

2.2 Design for bending

Calculation in SLS

In SLS a calculation regarding stresses and strains due to service load is carried out. Here a calculation is made to investigate if the structure is cracked or not and also a calculation of existing strain fields. Cross section data is then needed in coming calculation when the strain field at time for strengthening is calculated. In SLS calculations regarding deflections and crack widths are carried out if needed.

Design for strengthening in ULS

In Figure 1 a cross section of a rectangular strengthened concrete beam is shown. Where ε_{u0} is actual strain in the bottom fibre, ε_{c0} and ε_{s0} , strain in concrete respectively steel at time for strengthening. ε_f is the strain the FRP at ULS (or at level of calculation). $\Delta\varepsilon$ refers to the additional contribution from time of strengthening to ULS. In agreement with normal concrete design (EC2) the compressive strain in concrete, ε_c , should not exceed 3.5 ‰ in ULS. In the analysis (to calculate the FRP area) the expression in equation (1) is suggested. Where A_f and A_s is the cross sectional area of FRP and reinforcing steel respectively, M_d , moment capacity needed, f_y , yield stress of steel and E_f , Young's modulus of FRP. $\lambda = 0.8$ for $f_{ck} \leq 50$ MPa.

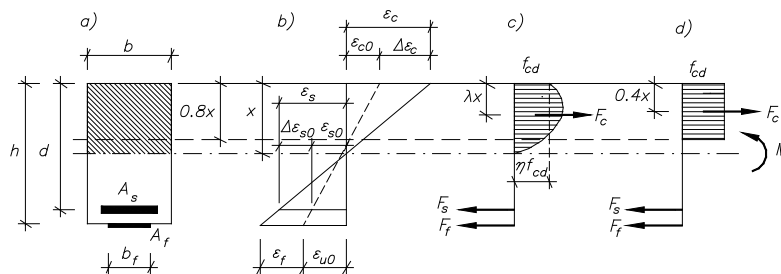


Figure 1 – Single reinforced cross section

$$A_f = \frac{M_d - A_s f_y \left(d - \frac{\lambda}{2} x \right)}{\varepsilon_f E_f \left(h - \frac{\lambda}{2} x \right)} \quad (1)$$

In the design often IC (Intermediate Crack) debonding is governed for laminates. For NSM often strain failure in the FRP or crushing of concrete is governed. In the design guideline ACI-4402R-08 form the basis for IC-debonding calculation, equation (2).

$$\varepsilon_{fd,ic} = 0.41 \sqrt{\frac{f_{cd}}{nE_f t_f}} \leq 0.9\varepsilon_{fu} \quad (2)$$

Where f_{cd} is design compressive strength of concrete and n number of layers of FRP. Furthermore the anchor length and the end peeling stresses need to be calculated, see (Täljsten et. al., 2011).

3. SHEAR

3.1 General

When strengthen concrete structures for shear is essential to anchor the strengthening material properly. Preferably is to enclose, W-wrap, a structure with a FRP sheet system. However, this is not always possible, e.g. for T-sections which is a common element to be strengthened. Here U-wrapped systems is recommended and if the end to the flange is mechanically anchored or if sufficient anchor length can be provided this is as effective as a W-wrap. Side wrapped, S-Wrap, is not recommended. Most common FRP systems for shear strengthening is sheet systems, but also laminates or NSM can and have been used.

3.2 Strengthening for shear

In the design model, see Figure 2, regarding strengthening for shear with FRP consider the contribution from concrete and steel. Calculation of contribution from steel and concrete follows EC2.

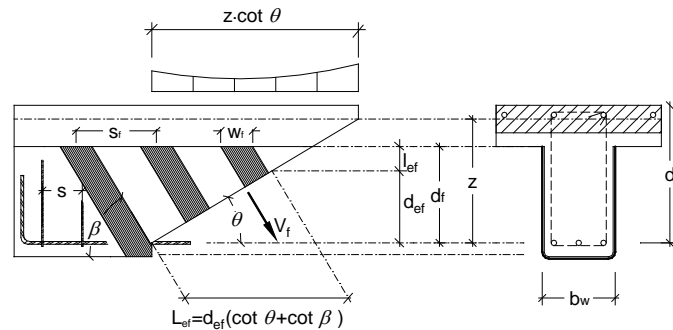


Figure 2 – Design model for FRP strengthening for shear

The contribution to the shear capacity can be calculated in (3) where the strain level is limited, see (Täljsten et. al. 2011)

$$V_{Rd,f} = A_f \varepsilon_{fd} E_{fd} L_{ef} \sin \beta_f \cos^2 \alpha \quad (3)$$

Where the anchor length l_{ef} , is calculated in (4) – which is the same expression as for the anchor length in bending. f_{ctm} is concrete tensile capacity.

$$l_{ef} = \sqrt{\frac{E_f t_f}{2f_{ctm}}} \quad (4)$$

4. CONFINEMENT

4.1 General

Using FRP for strengthening of columns has shown to be very efficient. The confinement effect is used in the calculation to create an increased compressive strength in the concrete.

For uniaxial loaded columns this calculation is very straight forward and easy to carry out. However, in the presented guideline also the effect of a bending moment is considered. The dominating strengthening system for confinement is sheet systems where FRP sheets are wrapped around a column. The system is most effective for circular columns but can also be used for rectangular columns with some reduction factors.

4.2 Strengthening of columns

The design for confinement when a combined normal force and a bending moment act on a axial member is best explained by Figure 3a) and 3b). Here we calculate different stages for a rectangular member, A to D, before and after strengthening. In Figure 3b we can notice the capacity before strengthening – the dashed curve, the need for strengthening, the X and the capacity after strengthening, the solid line.

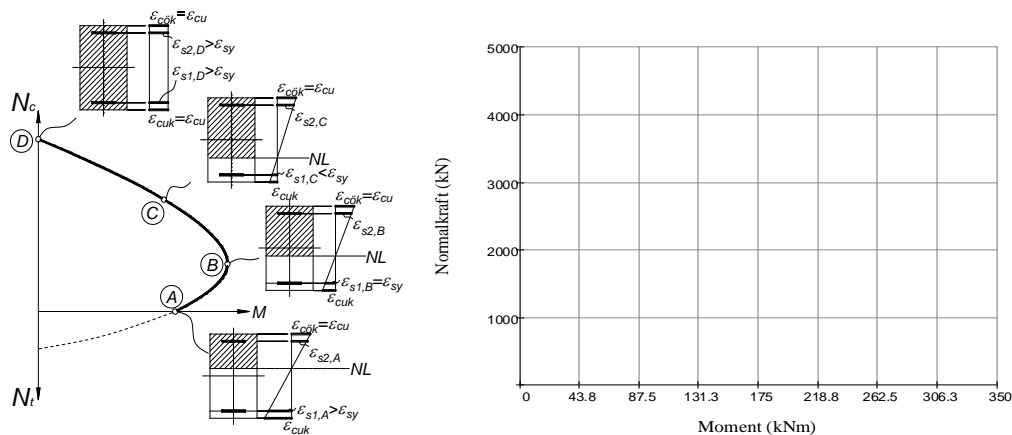


Figure 3 – Strengthening for confinement. a) General calculation, b) calculation for strengthening

5. DISCUSSION AND CONCLUSION

The brief presentation of the existing handbook used in Sweden shows the wide applicability of FRP strengthening. It also points out the most important and used areas for strengthening.

REFERENCES

- Meier U., Deuring M., Meier H., and Schwegler G. (1992), *Strengthening of Structures with CFRP laminates, Research and Applications in Switzerland*, Advanced Composite Materials in Bridges and Structures, Proceedings ACMBS 1, 1992, pp 243-251.
- Shinozaki, Hino, Aravinthan, Thiru, Pandey, Govinda Raj, and Mutsuyoshi, Hiroshi (2007) *Advancements in retrofitting reinforced concrete structures in Japan using FRP sheets*. ISBN 0-909375-78-X. Proceedings of the 23rd Biennial Conference of the Concrete Institute of Australia In: Concrete 07: Design, Materials & Construction: concrete for the future, 18-20 October 2007, Adelaide
- Täljsten B., 1994, *Plate Bonding, Strengthening of Existing Concrete Structures with Epoxy Bonded Plates of Steel or Fibre Reinforced Plastics*, Doctoral Thesis 1994:152D, ISSN 0348-8373, Luleå University of Technology, 1994, p 308.
- Täljsten Björn, Blanksvärd Thomas och Sas Gabriel (2011), *Handbok för dimensionering och utförande i samband med förstärkning av betongkonstruktioner med pålimmade fiberkomposit*, Luleå University of Tehcnology, p 186, ISBN 978-91-7439-146-6

SHRINKAGE AND DILATION

Laboratory evaluation of shrinkage in shotcrete sprayed on soft drains



Prof. Dr. Anders Ansell
KTH Royal Institute of Technology, Concrete Structures,
SE - 100 44 Stockholm
E-mail: anders.ansell@byv.kth.se



Techn.Lic. Lars Elof Bryne
Vattenfall Research and Development AB, Älvkarlebylaboratoriet
SE - 814 70 Älvkarleby
E-mail: lars-elof.bryne@byv.kth.se

ABSTRACT

The soft plastic drains used to lead away un-wanted water in hard rock tunnels are often covered with shotcrete (sprayed concrete) for mechanical protection. This soft surface gives little resistance to the shotcrete shrinkage which may lead to stress concentrations and severe cracking problems. With a recently developed test method the behaviour of shrinking shotcrete slabs on a plastic surface and with end restraints only have been investigated. The laboratory test set-up consist of instrumented granite slabs used for the monitoring of strains and corresponding stresses that are the result of drying shrinkage in the shotcrete.

Key words: Cracking, Fibres, Shrinkage, Testing.

1. INTRODUCTION

Shotcrete (sprayed concrete) is an important material for reinforcement of hard rock tunnels. Through the application technique and the addition of accelerators, which give immediate stiffening, the material properties becomes significantly different from ordinary, cast concrete of comparable strength. Shotcrete also has a relative high degree of shrinkage, partly due to the often large cement content. When sprayed on a rock surface the shrinkage strain is well distributed over the shotcrete lining leading to many thin cracks, if the tensile strength is exceeded. However, when sprayed on a softer surface that gives no or little restrain to shrinkage strains a few wide cracks can be the result. This is the case when shotcrete is sprayed on the soft plastic drains that are used to lead away un-wanted water in hard rock tunnels. A shotcrete cover is often applied for mechanical protection and also fire protection. Cracks of up to several millimetres wide have been observed in such drain constructions which shorten the life time due to fibre corrosion and fallout of parts of the shotcrete lining. This type of construction has previously been investigated in situ (Ansell, 2010), analytically (Ansell, 2011), and through laboratory testing by Bryne and Ansell (2011) and Bryne et al. (2014a-b). Results from the latter are here summarized, including tests with young and hardening shotcrete with and without glass fibre reinforcement.

2. SHOTCRETED DRAINS ON ROCK

The studied type of drain construction consists of soft 50 mm thick, 1500 mm wide mats of polythene with closed pores. The mats are placed vertically on the rock wall with steel bolts and are then shotcreted, often with an inner layer containing steel fibres and an outer un-reinforced layer (Holmgren, 2010). The lengths of these drains can either be the width of a single mat or in continuous sections covering up to 10–20 m of tunnel length. The shotcrete which often is 60 mm thick bonds to the rock on both sides of the drain mats only, resulting in an end-anchored shotcrete slab on top of a soft sub-surface. By using combinations of steel and glass fibres it may be possible to obtain shotcrete properties that combine early crack resistance with a ductile behaviour, which often is a structural load bearing requirement. One of the test series carried out with the method developed and tested by Bryne et al. (2014a-b), and described below, aimed at investigating the effect from added glass fibres.

3. LABORATORY TESTS

The recently developed test method is adopted for laboratory testing of shrinking shotcrete slabs with end-restraints. Shotcrete is sprayed on a plastic surface positioned on a granite slab so that the ends provide two areas that bond to the shotcrete and thus provides end anchorage. The granite slab is instrumented with strain gauges that provides information on the amount of compression and flexure that takes place due to the normal forces from the shrinking shortcrete.

3.1 Shotcrete material properties

Sprayed concrete slabs with or without glass fibres were used in the tests. The 6 mm long glass fibres were added for some test slabs in quantities of 5 or 10 kg/m³, for which relatively good workability was achieved (Bryne et al., 2014b). The shotcrete composition is given in Table 1, with a water to cement ratio of 0.45. The mix also contains a set accelerator at 3–5 % of the cement weight. Further details on the shotcrete composition are given by Bryne et al. (2014b).

Table 1 – General mix and main ingredients for tested sprayed concrete.

| Material | Density (kg/m ³) | Content (kg/m ³) |
|-------------------|---------------------------------|---------------------------------|
| Cement | 3150 | 495 |
| Silika Densified | 2230 | 19.8 |
| Water | 1000 | 220 |
| Superplasticiser | 1100 | 3.5 |
| Glass fibres | 2600 | 0-10 |
| Aggregate, 0-2 mm | 2650 | 394 |
| Aggregate, 0-8 mm | 2650 | 1183 |

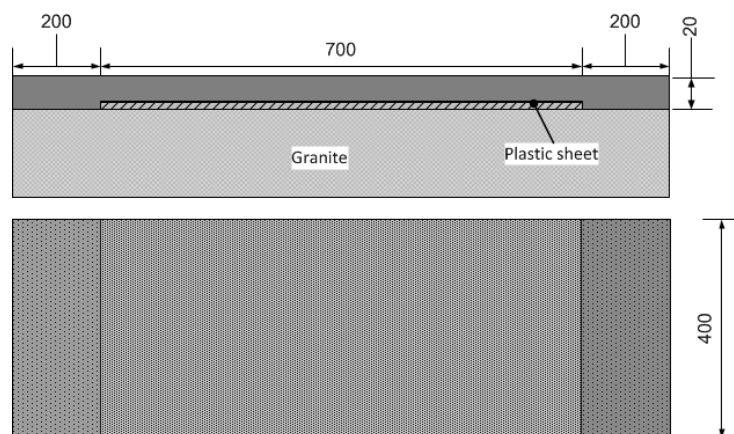


Figure 1 – End-restrained shrinkage test sample. The de-bonded length is 700 mm.

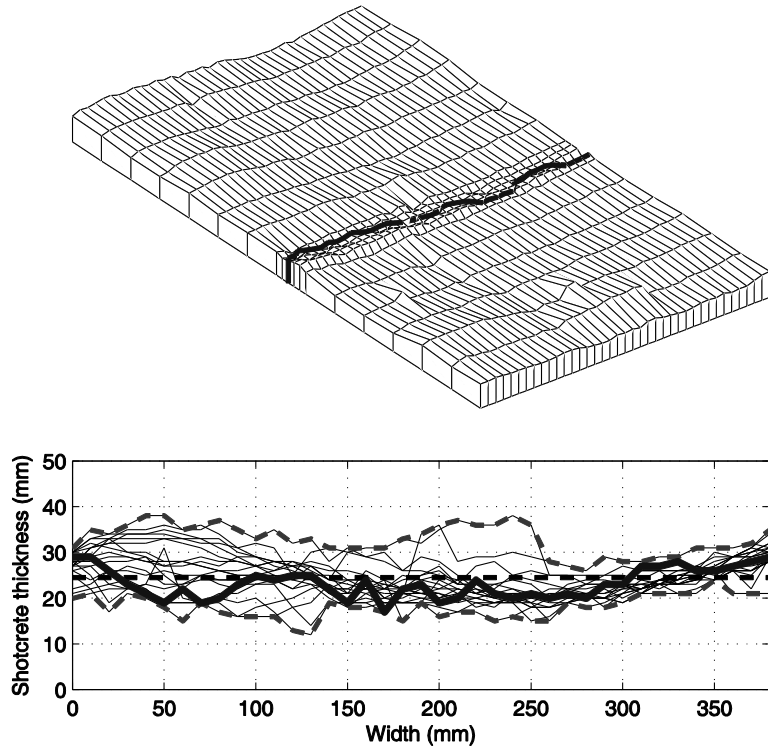


Figure 2 – Surface profile and shotcrete thickness for test slab no. 1. The crack is drawn with solid lines, the mean thickness with a straight dashed line. From Bryne et al. (2014b).

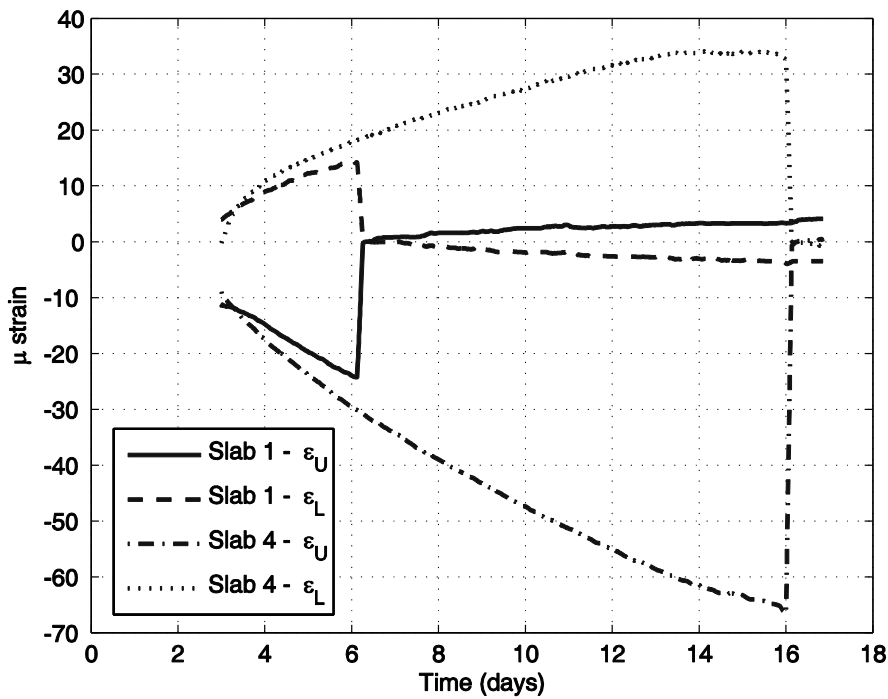


Figure 3 – Measured strains for test slabs 1 and 4, at upper (U) and lower (L) strain gauge positions. From Bryne et al. (2014b).

3.2 Test set-up

The test-setup is shown in Figure 1. A 700×400 mm² and 3 mm thick plastic sheet is placed on a 100 mm thick 1100×400 mm² granite slab, with two end areas 200×380 mm² to provide bond to the shotcrete. Strain gauges were mounted on each side of the slab, at its centre and 10 mm from the upper and lower edges. The newly sprayed shotcrete was covered with a wet jute cloth and a thin plastic sheet during 3 days of watering and thereafter kept in a climate chamber with RH of 50% and +20°C with continuous monitoring of the shrinkage strains.

4. RESULTS

Examples of test results are given in Figures 2-3. A total of six slabs were tested, see Bryne et al. (2014b). Profiles, average thickness and the position of a shrinkage crack are shown in Figure 2. It should be noted that the thickness along the crack is in this case close to the average thickness. Registered tensile and compressive strains for the granite slab are shown in Figure 3. It should be noted that test slab no. 1 is un-reinforced and cracks already after 6 days while slab no. 4 that contain 5 kg/m³ of glass fibres remains un-cracked up to 16 days.

5. CONCLUSION

The newly developed test method for young, hardening and shrinking shotcrete has been evaluated for use with cast and sprayed slabs, see Bryne et al. (2014a-b). The method is useful for investigating shrinkage properties of shotcrete material mixes, e.g. with various use of accelerators and fibre inclusion. The test results demonstrate how the build-up of strains and stresses develops until the first shrinkage crack appears. For the sprayed slabs tested the first cracks occurred already after 1–2 weeks which is in accordance with in situ observations (Ansell, 2010). The strain measurement corresponds to elastic restraining stresses that are in correspondence with the shotcrete strength at these ages (Bryne et al., 2014b). The registered strains are also comparable with the crack widths measured in situ.

REFERENCES

- Ansell, A., 2010,
 “Investigation of shrinkage cracking in shotcrete on tunnel drains”, *Tunnelling and Underground Space Technology*, 25, 607–613.
- Ansell, A., 2011,
 “Shrinkage cracking in sprayed concrete on soft drains in traffic tunnels”, In: *Sixth International Symposium on the modern use of wet mix sprayed concrete for underground support*, Tromsø, Norway, 27–38.
- Bryne, L.E., Ansell, A., 2011,
 “Restrained shrinkage tests of fibre concrete for shotcrete applications in hard rock tunnels”, In: *XXI Symposium on Nordic Concrete Research & Development*, Hämeenlinna, Finland, 489–492.
- Bryne, L.E., Ansell, A., Holmgren, J., 2014a,
 “Investigation of restrained shrinkage cracking in partially fixed shotcrete linings”, *Tunnelling and Underground Space Technology*, 42, 136–143.
- Bryne, L.E., Ansell, A., Holmgren, J., 2014b,
 “Shrinkage testing of end restrained shotcrete on granite slabs”, *Magazine of Concrete Research*, In press.
- Holmgren, J., 2010,
 “Shotcrete research and practice in Sweden: Development over 35 years”, In: *Third International Conference on Engineering Developments in Shotcrete*, Queenstown, New Zealand, 135–141.

Evaluation of Thermal Dilation and Autogenous Shrinkage at Sealed Conditions



Katalin Orosz
Tec. Licentiate, Ph.D student
Luleå University of Technology
katalin.orosz@ltu.se



Peter Fjellström
Tec. Licentiate
Luleå University of Technology
peter.fjellstrom@ltu.se



Dr. Jan-Erik Jonasson
Professor
Luleå University of Technology
jan-erik.jonasson@ltu.se



Dr. Mats Emborg
Professor
Luleå University of Technology
Head R&D Betongindustri Ltd.
mats.emborg@ltu.se
mats.emborg@betongindustri.se



Dr. Hans Hedlund
Adj. Professor
Luleå University of Technology
Skanska Sweden Ltd., Göteborg
hans.hedlund@skanska.se

ABSTRACT

As known, load independent deformations are of large importance in structural analysis, e. g. when estimating elongations, restraint stresses, or pre-stressing forces. Two models to describe thermal dilation (TD) and autogenous shrinkage (AS) have been evaluated, for a broader range of w/C ratios and cements types than before. In Model I, AS is determined solely based on the maturity model and TD incorporates two TD coefficients (TDC). In Model II, AS is dependent on both the maturity model and a separate temperature adjustment factor, while TDC is constant. For the more rapid-hardening cement, Model I did not give satisfactory results, whereas the usefulness of Model II to describe both AS and TD has shown to be limited, suggesting that a new model is needed.

Keywords: Concrete, Autogenous Deformation, Thermal Dilation, Free Deformation

1. INTRODUCTION

At LTU (Luleå University of Technology), two models have been used to describe free load independent concrete deformations. In Model I, the thermal dilation is determined by the use of an expansion coefficient and a contraction coefficient /Emborg 1990/. In Model I, autogenous shrinkage is dependent only on equivalent time/Hedlund 1996/. In Model II /Hedlund 2000/, autogenous shrinkage is dependent on both equivalent time and temperature, while the thermal dilation coefficient is constant. These models have proven to be suitable to describe the free deformations (the sum of autogenous shrinkage and thermal dilation) for concretes with w/C ratios around 0.40 using a “moderate heat” cement, see e.g. /Hedlund 2000/.

In this paper, the two models are evaluated for eight selected Swedish concretes representing a broader range of w/C ratios than before, at moisture-sealed conditions. Two recipes use AnlC, which is a “moderate heat” cement intended for civil engineering structures. Six recipes use BAS cement, which is a new “standard” cement intended mainly for housing purposes.

2. TESTING

The test procedure measuring the free deformation is described in /Hedlund 2000/. Two moisture sealed specimens are used, one with the concrete temperature about 20°C, and one following a real temperature simulating a concrete wall structure of about 0.7 m. The tested concretes are presented in Table 1, where SCC denotes self-compacting concrete.

Table 1 – Tested concrete recipes. BAS: CEM II/A-V 52,5 N containing about 4% LL and 16% fly ash, and AnlC: CEM I 42,5 N SR3 MH/LA.

| Recipe No. | Type | Cement content [kg/m ³] | w/C |
|------------|-------------|-------------------------------------|------|
| AnlC2 | Traditional | 455 | 0.40 |
| AnlC1 | Traditional | 340 | 0.55 |
| BAS1 | Traditional | 470 | 0.38 |
| BAS2 | Traditional | 360 | 0.55 |
| BAS3 | Traditional | 285 | 0.70 |
| BAS4 | SCC | 480 | 0.38 |
| BAS5 | SCC | 370 | 0.55 |
| BAS6 | SCC | 320 | 0.70 |

3. MEASUREMENT AND MODELING OF FREE DEFORMATION

The total free movement measured on the concrete sample located in the laboratory room at approximately 20°C is here denoted test A, and the test subjected to variable temperature is denoted test B. The registered free deformation is the sum of thermal dilation and autogenous shrinkage (Eq. 1). In Model I, two separate thermal dilation coefficients (α_E and α_C) are used (Eqs. 5-6).

$$\varepsilon_{tot} = \varepsilon_T + \varepsilon_{SH} \quad (1)$$

$$\varepsilon_{SH} = \varepsilon_{ref} \cdot \beta_{s0}(t_e) \cdot \beta_{ST}(T) \quad (2)$$

$$\beta_{s0}(t_e) = \exp\left(-\left[t_{s0}/(t_e - t_{start})\right]^{\eta_{SH}}\right) \quad (3)$$

$$\beta_{ST}(T) = a_0 + a_1 \cdot \left(1 - \exp\left[-T_c^{max}(t)/T_1\right]^{b_1}\right) + a_2 \cdot \left(1 - \exp\left[-T_c^{max}(t)/T_2\right]^{b_2}\right) \quad (4)$$

$$\varepsilon_T = \Delta T_c(t) \cdot \alpha_E \quad \text{for} \quad T_c(t) < T_{max} \quad (5)$$

$$\varepsilon_T = \Delta T_c(t) \cdot \alpha_C \quad \text{for} \quad T_c(t) > T_{max} \quad (6)$$

$$\alpha_T = \alpha_E = \alpha_C \quad (7)$$

where ε_{tot} [-] = measured strain; ε_T [-] = thermal dilation; ε_{SH} [-] = autogenous shrinkage; ε_{ref} [-] = reference ultimate shrinkage, a fitting parameter decided by the least square method; β_{s0} [-] = relative time development of shrinkage; t_e [s, h or d] = equivalent time of maturity; t_{start} [s, h or d] = start time of autogenous shrinkage specified as time after mixing; t_{s0} [s, h or d] and η_{SH} [-] = fitting parameters determined by least square method; $\beta_{ST}(T)$ [-] = temperature effect on autogenous shrinkage – for Model I, $\beta_{ST}(T) \equiv 1$; $T_c^{max}(t)$ [°C] = maximum temperature in the concrete sample up to time t ; t [s, h or d] = real time specified as time after mixing; a_0 [-], a_1 [-],

$a_2[-]$, $b_1[-]$, $b_2[-]$, $T_1[^\circ\text{C}]$, $T_2[^\circ\text{C}]$ = fitting parameters or chosen according to /Hedlund 2000/;
 $\Delta T_c(t)[^\circ\text{C}]$ = temperature difference in the concrete sample; $T_{\max}[^\circ\text{C}]$ = maximum measured
temperature for the concrete sample; $\alpha_E[^\circ\text{C}^{-1}]$ = thermal expansion coefficient; $\alpha_C[^\circ\text{C}^{-1}]$ =
thermal contraction coefficient; $\alpha_T[^\circ\text{C}^{-1}]$ = constant thermal dilation coefficient. α_E , α_C and
 α_T are fitting parameters. For Model II, $\alpha_T = \alpha_E = \alpha_C$.

The temperature dependent rate factor, or maturity function, affecting the hydration growth is described as

$$\beta_T = \exp\left[\frac{E}{R} \cdot \left(\frac{1}{293} - \frac{1}{T + 273}\right)\right] \quad (8)$$

where E = apparent activation energy [J/mole]; R = general gas constant = 8.314 [J/mole K].

The expression for the apparent activation energy is given as

$$\theta = \frac{E}{R} = \theta_{ref} \cdot \left(\frac{30}{T + 10}\right)^{\kappa_3} \quad (9)$$

where θ = “activation temperature” [K]; θ_{ref} [K] and κ_3 [-] are empirically constants usually determined from tests of strength growth at different temperature levels.

4. RESULTS

Examples of fitting parameters, by using the least square method, can be found in Table 2 (Model I) and Tables 3 and 4 (Model II). Complete results are presented in /Fjellström 2013/.

Table 2 – Evaluated parameters using Model I (Eqs. 2, 3, 5, 6, and 9). Complete results, see /Fjellström 2013/.

| Recipe | θ_{ref} [K] | κ_3 [-] | t_{s0} [h] | t_{start} [h] | ε_{ref} [10^{-6}] | η_{SH} [-] | α_E [$10^{-6}/^\circ\text{C}$] | α_C [$10^{-6}/^\circ\text{C}$] |
|--------|--------------------|----------------|--------------|-----------------|-----------------------------------|-----------------|---|---|
| AnlC2 | 3300 | 0.300 | 6 | 10 | -65 | 0.67 | 11.0 | 11.0 |
| BAS2 | 3150 | 0.275 | 6 | 30 | -165 | 1.00 | 10.2 | 10.2 |

Table 3 – Evaluated parameters using Model II (Eqs. 2, 3, 7, and 9). Complete results, see /Fjellström 2013/.

| Recipe | θ_{ref} [K] | κ_3 [-] | t_{s0} [h] | t_{start} [h] | ε_{ref} [10^{-6}] | η_{SH} [-] | α_T [$10^{-6}/^\circ\text{C}$] |
|--------|--------------------|----------------|--------------|-----------------|-----------------------------------|-----------------|---|
| AnlC2 | 3300 | 0.300 | 6 | 10 | -65 | 0.67 | 11.0 |
| BAS2 | 3150 | 0.275 | 6 | 35 | -116 | 1.00 | 9.7 |

Table 4 – Evaluated parameters using Model II (Eq. 4). Complete results, see /Fjellström 2013/.

| Recipe | a_0 [-] | a_1 [-] | T_1 [$^\circ\text{C}$] | b_1 [-] | a_2 [-] | T_2 [$^\circ\text{C}$] | b_2 [-] |
|--------|-----------|-----------|----------------------------|-----------|-----------|----------------------------|-----------|
| AnlC2 | 0.4 | 0.6 | 9 | 2.9 | 0.00 | 55 | 7.0 |
| BAS2 | 0.4 | 0.6 | 9 | 2.9 | 1.00 | 55 | 7.0 |

In terms of diagrams, an example of Model II (BAS2, representing the worst fit) is given in Figure 1. For all diagrams, see /Fjellström 2013/.

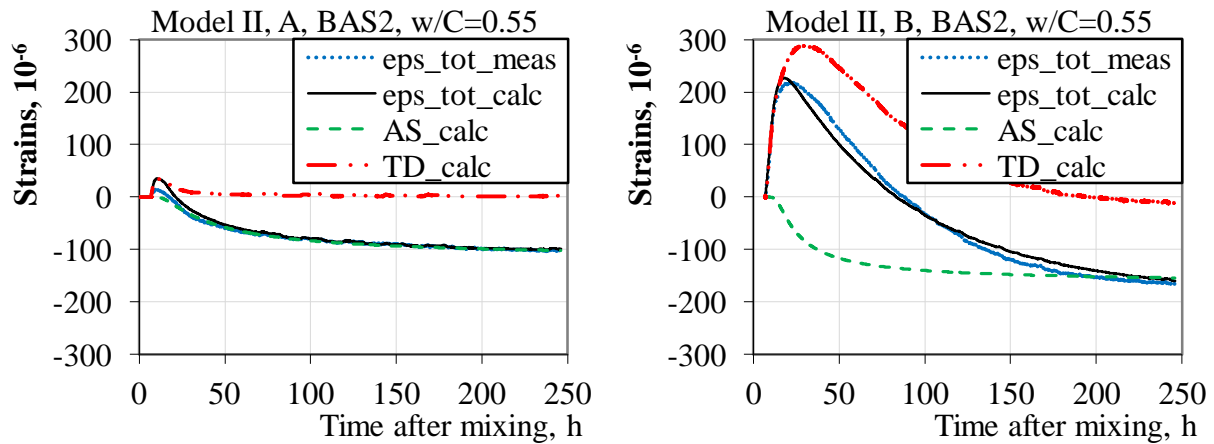


Figure 1 – Measured and calculated free deformations of BAS2 w/C=0.55 using Model II for a sample stored at $\sim 20^{\circ}\text{C}$ (A) and a realistic temperature curve simulating a 0.7m thick wall (B).

5. CONCLUDING REMARKS

The measured deformations are split into autogenous shrinkage and thermal dilation – using two models. Thermal dilation is adequately modelled with either of these models. However, for the more rapid hardening, the new BAS cement the autogenous shrinkage cannot be adequately described with Model I. By using Model II, a better fit can be achieved, but for certain concretes, the error is still unacceptably high. Furthermore, additional data presented in /Bjøntegaard 1999/ underline that, at more complex temperature variations, the autogenous shrinkage cannot be accurately described with either of the models used here. Therefore, a refined, or a new model is likely needed for more generalized temperature variations in young concrete.

REFERENCES

- Bjøntegaard, Ø., 1999
 "Thermal Dilation and Autogenous Deformation as Driving Forces to Self-Induced Stresses in High Performance Concrete". Doctoral Thesis, The Norwegian University of Science and Technology, Trondheim, Norway
- Emborg, M., 1990
 "Thermal Stresses in Concrete Structures at Early Ages". Doctoral Thesis, Luleå University of Technology, Luleå, Sweden
- Fjellström, P., 2013
 "Measurement and Modelling of Young Concrete Properties". Licentiate Thesis, Luleå University of Technology, Luleå, Sweden
- Hedlund, H., 1996
 "Stresses in high performance concrete due to temperature and moisture variations at early ages". Licentiate Thesis, Luleå University of Technology, Luleå, Sweden
- Hedlund, H., 2000
 "Hardening Concrete: Measurements and Evaluation of Non-Elastic Deformation and Associated Restraint Stresses". Doctoral Thesis, Luleå University of Technology, Luleå, Sweden

Shrinkage Properties of Cement Stabilized Gravel



Mia S. M. Lund
MSc, PhD Student
DTU Civil Engineering
Brovej, Building 118
DK - 2800 Kgs. Lyngby
msml@byg.dtu.dk



Kurt Kielsgaard Hansen
Associate Professor, PhD
DTU Civil Engineering
Brovej, Building 118
DK - 2800 Kgs. Lyngby
kkh@byg.dtu.dk

ABSTRACT

Cement stabilized gravel is an attractive material in road construction because its strength properties are accommodating the increasingly higher requirements to the bearing capacity of a base course. However, reflection cracking of cement stabilized gravel is a major concern. In this paper the shrinkage properties of cement stabilized gravel have been documented under various temperature and relative humidity conditions. Two cement contents corresponding to a 28-days compressive strength of 6.2 MPa and 12.3 MPa have been tested and compared. It is found that the coefficient of linear expansion for the two cement contents is $9.9 \times 10^{-6} \text{ }^{\circ}\text{C}^{-1}$ and $11.3 \times 10^{-6} \text{ }^{\circ}\text{C}^{-1}$, respectively. Furthermore, it is found that reflecting cracking can mainly be explained by temperature dependent shrinkage rather than moisture dependent shrinkage.

Keywords: Cement stabilized gravel, reflection cracking, temperature dependent shrinkage, coefficient of linear expansion, moisture dependent shrinkage.

1. INTRODUCTION

Semi-rigid pavements used for highways gained increasing popularity in Denmark during the 1970's. A semi-rigid pavement consists of a base course of cement stabilized gravel and an asphalt concrete layer. Some of the main advantages by using cement stabilized gravel compared to unbound gravel are improved bearing capacity and durability. However, during the 1980's the use of cement stabilized gravel was stopped due to the pavements from the 1970's beginning to show signs of reflection cracking. In recent years different methods have been developed attempting to prevent reflection cracking. The most common method is crack control where cracks are cut halfway through the layer of cement stabilized gravel at every 2 m. However, there is still a great lack in understanding the underlying phenomena which cause reflection cracking. This paper investigates the temperature and moisture dependent shrinkage properties of cement stabilized gravel.

2. METHODS

2.1. Specimen preparation

One type of 0-16 mm gravel material from Nymølle pit, Denmark, has been investigated. A sieve analysis performed in accordance with DS/EN 933-1:2012 classified the gravel as belong-

ing to Envelope B with an oversize of 7% on the 16 mm sieve, cf. EN 14227-1:2004. Figure 1 (left) shows the grain curve for the gravel material.

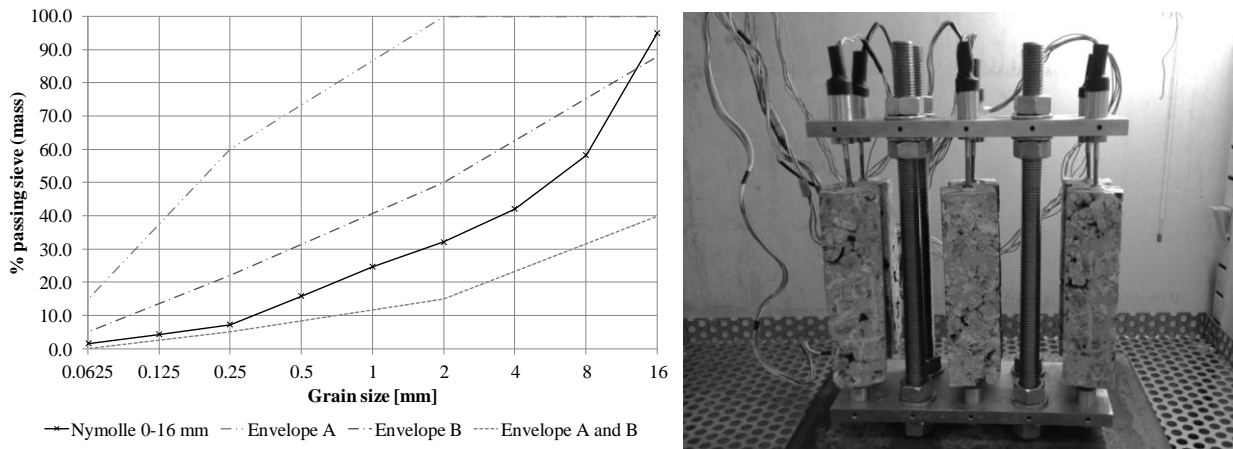


Figure 1 – Left: Grain size distribution of gravel (Nymølle 0-16 mm) with envelopes according to DS/EN 14227-1:2004. Right: Shrinkage setup in climate chamber. Six cement stabilized gravel specimens with dimensions of 4 cm x 4 cm x 15 cm were tested. Three of the specimens had a cement content of 4% and three had a cement content of 5%.

Two different cement contents of 4% and 5% of the dry material were chosen. The optimal water content was determined from proctor tests in accordance with DS/EN 13286-2:2012 by also including the influence of cement. The mixture was prepared by mixing gravel, low alkali cement and water in the right proportions for three minutes. The specimens were cast in accordance with EN 13286-50:2004 using the vibrating table compaction method. Split moulds with a diameter of 150 mm and a height of 300 mm were used. The minimum degree of compaction, which is defined as the ratio between the actual density of the specimen and the optimal density determined from proctor tests, was 97.4%. After 28-days of curing in a 20⁰C water basin a number of the cylinder specimens were cut into prisms with dimensions of 4 cm x 4 cm x 15 cm.

2.2. Experimental procedure

The compressive strength was measured on D150mm/H300mm cylinders on a TONI 3000 kN machine at a velocity of 3 and 5 kN/s for 4% and 5% cement content, respectively. Six cylinders of each cement content were tested after 28-days of curing in a 20⁰C water basin.

The shrinkage test was carried out in a SKANFRYS climate chamber with a temperature range of -10⁰C to +60⁰C and a relative humidity range of 10% to 95%. Extensometers with an accuracy of 2 μm and a measuring range of ±5 mm were used. Three specimens of each cement content were tested. The setup in the SKANFRYS climate chamber can be seen in Figure 1 (right). The specimens were mounted in vertical position in a steel frame.

Four different tests were carried out. In the first test the relative humidity was fixed at 65% and the temperature was varied between 5⁰C and 20⁰C. In the second test the relative humidity was fixed at 65% and the temperature was varied between 5⁰C and 40⁰C. In the third test the temperature was fixed at 20⁰C and the relative humidity was varied between 65% and 85%. In the fourth test the temperature was fixed at 20⁰C and the relative humidity was varied between 45%

and 85%. In all four tests the conditions were first changed when a steady deformation was obtained. Furthermore, two repetitions were made in all tests to underpin the observations.

3. RESULTS

The 28-days compressive strength of the cylinder specimens are shown in Table 1.

Table 1 – 28-days compressive strength, f_c , of specimens shown as average \pm standard deviation.

| Cement content [%] | 4 | 5 |
|--------------------|---------------|----------------|
| f_c [MPa] | 6.2 ± 0.6 | 12.3 ± 2.3 |

The calculation of the strain induced by the variation in either temperature or relative humidity was found as the difference in strain between the measured steady strain at e.g. 5^oC and 20^oC. The strain calculations for a temperature variation were corrected with respect to the deformation of the steel frame. This was done by estimating the coefficient of linear expansion of the steel frame itself by inserting an Invar steel bar in the frame. The deformation measured over the Invar steel bar was assumed to correspond to the deformation of the steel frame since the Invar steel bar has a negligible coefficient of linear expansion.

For the variation in temperature the coefficient of linear expansion was calculated as:

$$\varepsilon = \alpha \cdot \Delta T \quad (1)$$

where ε is the strain, α [^oC⁻¹] is the coefficient of linear expansion and ΔT [^oC] is the temperature change. Figure 2 shows the strain variation and corresponding variation in temperature and relative humidity for test no. 1 and no. 3.

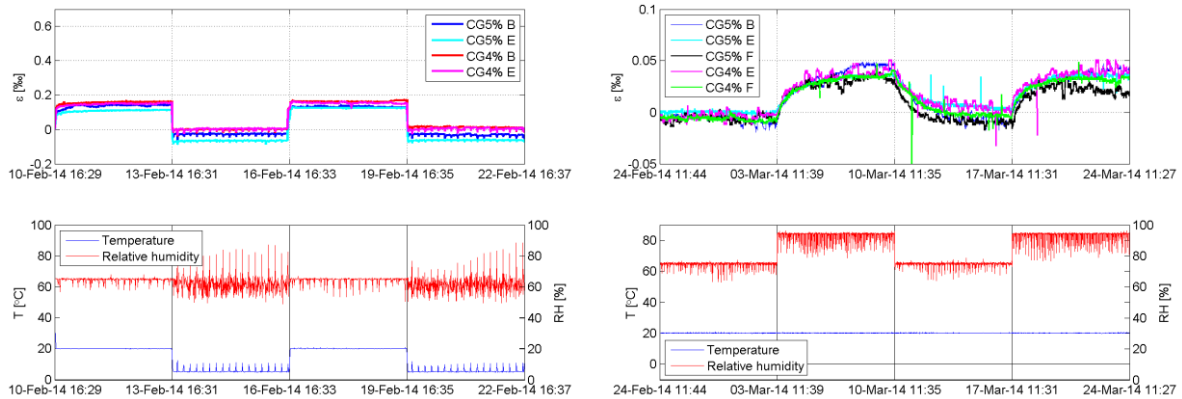


Figure 2 – Variation in strain, ε , for test no. 1: $RH = 65\%$ and $T = 5^{\circ}C - 20^{\circ}C$ (left) and for test no. 3: $T = 20^{\circ}C$ and $RH = 65\% - 85\%$ (right).

Table 2 shows the average results of strains and coefficients of linear expansion for each cement content. Obviously incorrect results have been omitted when calculating the average values.

Table 2 – Strains, ε , and coefficients of linear expansion, α , for various boundary conditions.

| No. | RH | T | 4 % cement | | 5 % cement | |
|-----|------------|---------------------------------------|------------------------------------|---|------------------------------------|--|
| 1 | 65 % | 5 ^o C to 20 ^o C | $\varepsilon = 1.5 \times 10^{-4}$ | $\alpha = 9.9 \times 10^{-6} \text{ }^{\circ}\text{C}^{-1}$ | $\varepsilon = 1.7 \times 10^{-4}$ | $\alpha = 11.2 \times 10^{-6} \text{ }^{\circ}\text{C}^{-1}$ |
| 2 | 65 % | 5 ^o C to 40 ^o C | $\varepsilon = 3.5 \times 10^{-4}$ | $\alpha = 9.9 \times 10^{-6} \text{ }^{\circ}\text{C}^{-1}$ | $\varepsilon = 4.0 \times 10^{-4}$ | $\alpha = 11.4 \times 10^{-6} \text{ }^{\circ}\text{C}^{-1}$ |
| | | | Average: | $\alpha = 9.9 \times 10^{-6} \text{ }^{\circ}\text{C}^{-1}$ | Average: | $\alpha = 11.3 \times 10^{-6} \text{ }^{\circ}\text{C}^{-1}$ |
| 3 | 65% to 85% | 20 ^o C | $\varepsilon = 3.6 \times 10^{-5}$ | - | $\varepsilon = 3.5 \times 10^{-5}$ | - |
| 4 | 45% to 85% | 20 ^o C | $\varepsilon = 8.5 \times 10^{-5}$ | - | $\varepsilon = 8.4 \times 10^{-5}$ | - |

4. DISCUSSION

Considering the tests where the relative humidity was kept constant and the temperature was varied it can be seen from Table 2 that the coefficient of linear expansion as expected is independent on the interval of the temperature variation. This is both observed for a cement content of 4% and 5% with an average coefficient of linear expansion of $9.9 \times 10^{-6} \text{ }^{\circ}\text{C}^{-1}$ and $11.3 \times 10^{-6} \text{ }^{\circ}\text{C}^{-1}$, respectively. A cement content of 4% and 5% corresponds to a 28-days compressive strength of 6.2 MPa and 12.3 MPa, respectively. An increment of 14% is observed when the cement content is increased from 4% to 5%. Considering the tests where the temperature was kept constant and the relative humidity was varied it can be seen that the size of the strains approximately doubles when the range of the relative humidity variation is doubled. This is both observed for a cement content of 4% and 5%. However, no unambiguous tendency is observed between the strains for a cement content of 4% and 5%. A slightly larger strain is observed for a cement content of 4% compared to 5% in both test no. 3 and no. 4. However, the small difference is rather explained by the uncertainty of the measurements than by an actual difference and the strains must be considered to be the same size of order.

The temperature and relative humidity intervals applied in the tests have been chosen in accordance with realistic values that pavements can be expected to be exposed to. Hence, it is of interest to compare the size of the strains induced by a variation in temperature and in relative humidity. From Table 2 it can be seen that the size of the strains induced by a variation in relative humidity is an order of magnitude less than the strains induced by a temperature variation. This means that the reflecting cracking observed in semi-rigid pavements is mainly expected to be due to the temperature dependent shrinkage properties of cement stabilized gravel.

5. CONCLUSION

The strain variation of cement stabilized gravel has been measured for two different cement contents under different temperature and relative humidity conditions. A coefficient of linear expansion of $9.9 \times 10^{-6} \text{ }^{\circ}\text{C}^{-1}$ has been found for cement stabilized gravel with a cement content of 4% which is corresponding to a compressive strength of 6.2 MPa. A slightly higher coefficient of linear expansion of $11.3 \times 10^{-6} \text{ }^{\circ}\text{C}^{-1}$ has been found for cement stabilized gravel with a cement content of 5% which is corresponding to a compressive strength of 12.3 MPa. Furthermore, the strains induced by a variation in relative humidity have been found to be an order of magnitude less than the strains induced by a variation in temperature. This indicates that the main cause of reflection cracking in semi-rigid pavements is temperature dependent shrinkage.

REFERENCES

DS/EN 933-1:2012

“Tests for geometrical properties of aggregates - Part 1: Determination of particle size distribution - Sieving method”, The Danish Standards Association, 2012

DS/EN 13286-2:2010

“Unbound and hydraulically bound mixtures - Part 2: Test methods for laboratory reference density and water content - Proctor compaction”, The Danish Standards Association, 2011

EN 13286-50:2004

“Unbound and hydraulically bound mixtures - Part 50: Method for the manufacture of test specimens of hydraulically bound mixtures using Proctor equipment or vibrating table compaction”, European Committee for Standardization, 2004

DS/EN 14227-1:2004

“Hydraulically bound mixtures - Specifications - Part 1: Cement bound granular mixtures”, The Danish Standards Association, 2004

Long-Term Shrinkage of Concrete using some Porous Icelandic Aggregates



Valgeir O. Flosason
B.Sc, M.Sc.
ICI Rheocenter, Reykjavik University & Innovation Center Iceland
Arleynir 2-8, IS-112 Reykjavik
E-mails: valgeir@steypustodin.is and valgeir@nmi.is



Eva L. Agustsdottir
B.Sc, M.Sc.
Ferill Engineering
Morkin 1
IS-108 Reykjavik
E-mail: eva@ferill.is



Olafur H. Wallevik
Dr.Ing., Prof.
ICI Rheocenter, Reykjavik University & Innovation Center Iceland
Arleynir 2-8
IS-112 Reykjavik
E-mail: wallevik@ru.is

Key words: Long term shrinkage, weight loss, basalt, porous aggregates, EC2.

ABSTRACT

In this work, the long-term shrinkage of concrete containing some Icelandic porous aggregates is examined. This was done by measuring the length change of concrete prisms in accordance with the ASTM C157/C157M-99 standard. The results indicate that concrete continues to shrink over long period of time, independent to evaporation caused by drying. The results also show that the measured shrinkage is considerably higher than estimated shrinkage according to the Eurocode 2 (EC2) prediction model. Due to this difference, deflection can be underestimated when designing concrete structures, as shrinkage influences deflection according to EC2.

Key words: Concrete, Shrinkage, Porous Aggregate, Deflection, Prediction Models.

1. INTRODUCTION

During its lifetime, concrete undergoes volumetric changes like shrinkage which is caused by several different mechanisms. The main mechanisms are believed to be capillary tension, surface tension, swelling pressure (also referred to as disjoining pressure) and movement of interlayer water from the C-S-H gel particles [Soroka I. 1979].

As concrete is usually restrained, shrinkage can cause tensile stresses in the concrete. If the tensile stresses become greater than the tensile strength of the concrete, cracking can occur which can cause several problems [Neville A.M and Brooks J.J 2010].

A great deal of data regarding shrinkage of concrete using Icelandic aggregates has been collected at the ICI Rheocenter in Iceland, for instance reported by Gudmundsson et. al [Guðmundsson J.G Mueller F.V and Wallevik O.H 2010]. According to this data, shrinkage of Icelandic concrete can amount to 1 mm/m in average which is somewhat higher than in many countries. This raises primarily two questions. The questions whether this is due to the Icelandic aggregates, as they have been shown to be very porous and of low elastic modulus [Þórðarson B.R and Wallevik Ó.H 1999, Gudmundsson J.G 2013] and why the concrete is still shrinking after long period of time despite no weight loss.

The main purpose of this research is to quantify the long-term shrinkage of concrete using Icelandic aggregates, compare the results to prediction models and determine the effects on structural properties such as deflection.

2. EXPERIMENTAL

In order to examine long-term shrinkage of concrete using Icelandic aggregates, several dozen mixes were performed [Ágústsdóttir E.L 2012] and the length change measured over long period. Table 1 shows three of the mixes performed. The aggregates used are Icelandic basalt with relatively high porosity (which is estimated from water absorption (WA) measurements). Two curing methods were applied; sealing the samples after demoulding to avoid evaporation, and storing the samples at 100% RH for 6 days after demoulding and then storing the samples at 50% RH.

Table 1: Mix designs of the selected mixes in the experiment

| Mix designs | | Mix A | Mix B | Mix C |
|-------------------------|-------------------|-------|-------|-------|
| Cement | kg/m ³ | 317 | 316 | 317 |
| Water | kg/m ³ | 146 | 174 | 206 |
| Sand 0/8 (WA = 4.0%) | kg/m ³ | 956 | 917 | 875 |
| Gravel 4/16 (WA = 3.2%) | kg/m ³ | 391 | 375 | 357 |
| Gravel 8/22 (WA = 3.2%) | kg/m ³ | 590 | 566 | 540 |
| Density | kg/m ³ | 2406 | 2350 | 2302 |
| Cement paste | v. % | 24.8 | 27.5 | 30.6 |
| W/c-ratio | | 0.46 | 0.55 | 0.65 |
| Measured air | v. % | 5.5 | 5.6 | 5.5 |
| Slump | mm | 165 | 180 | 180 |
| Compressive strength | MPa | 55.5 | 44.0 | 33.0 |

In addition to shrinkage measurements, the shrinkage of the samples was also estimated by using the prediction model according to EC2 [EN 1992-1-1:2004]. Also, the effects of shrinkage on deflection of concrete members were estimated according to EC2 and considered.

3. RESULTS

Figure 1 shows the shrinkage and the weight loss of the mix designs in table 1. The figure shows that the shrinkage is much higher when exposed to drying compared to the shrinkage of the sealed samples. Both the shrinkage and the weight loss are similar among mixes containing different w/c-ratio when the samples are sealed. However, when exposed to drying, both shrinkage and weight loss increase as the w/c-ratio increases as to be expected.

According to figure 1, the majority of the weight loss occurs within the first 90 days. Therefore,

the shrinkage up to 90 days will be interpreted as short-term shrinkage (STS), while the shrinkage taking place after 90 days will be interpreted as long-term shrinkage (LTS). Figure 2 accentuates the difference between short-term shrinkage and long-term shrinkage.

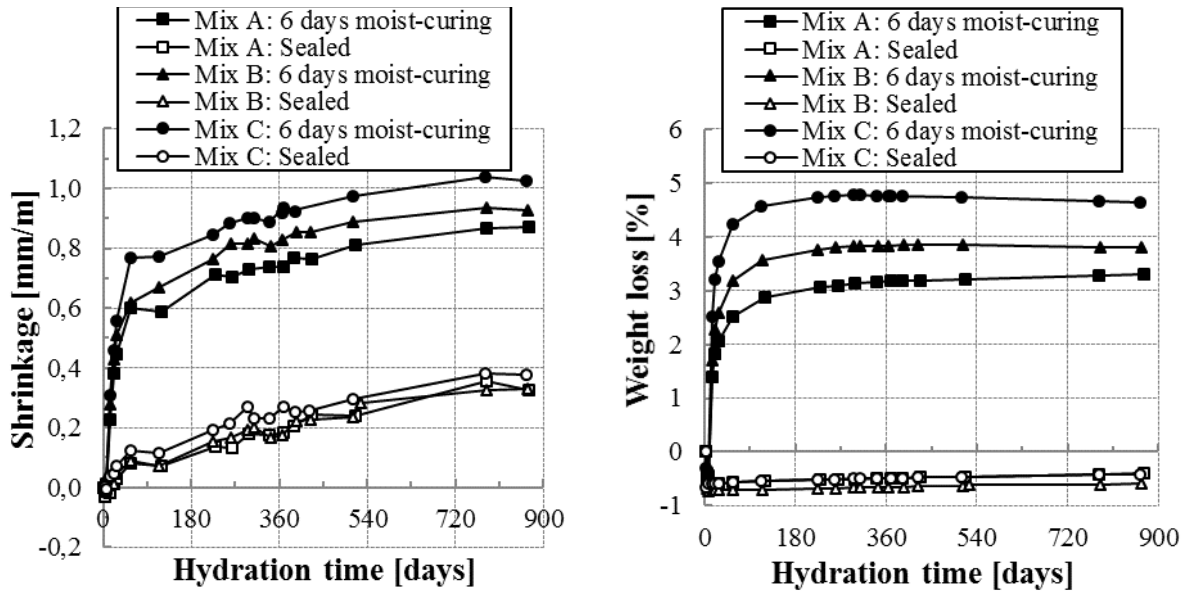


Figure 1: Shrinkage (left) and weight loss (right) of concrete containing Icelandic porous aggregates at different curing and w/c-ratios.

According to figure 2, avoiding drying of the samples significantly reduces the STS while it does not seem to affect the LTS, which indicates that the LTS is independent to the weight loss. The figure also shows how the LTS per year can be estimated by using the slope of the linear equation for the LTS.

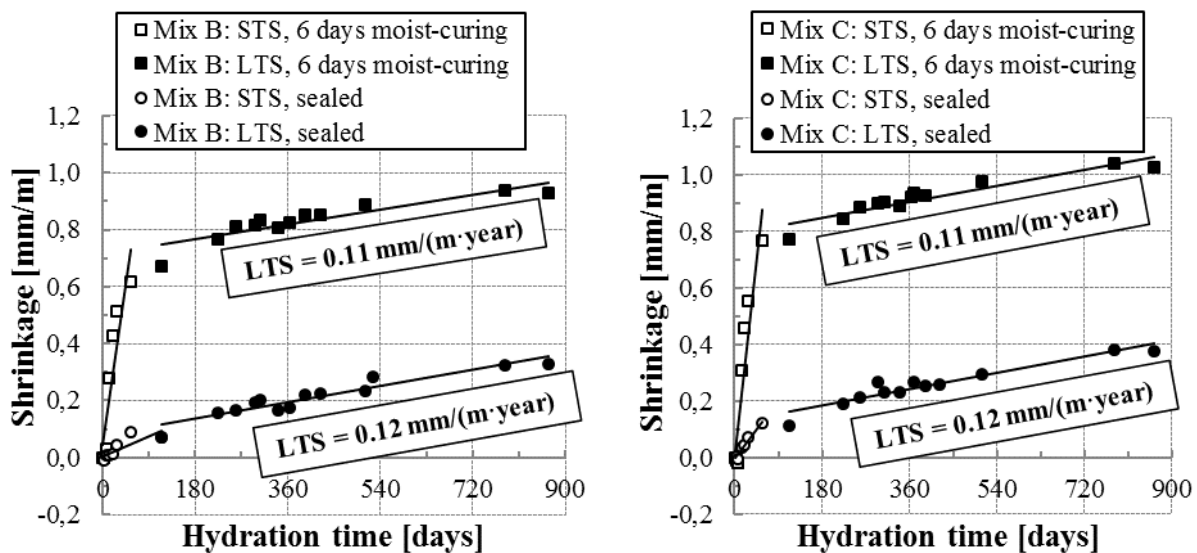


Figure 2: Long-term shrinkage of mixes B and C.

Figure 3 shows comparison of measured shrinkage and calculated shrinkage and also schematic illustration of the influence of shrinkage on deflection according to the EC2 prediction model. As the measured shrinkage exceeds the calculated shrinkage, the deflection would be underestimated by using the calculated total shrinkage value. According to [Flosason V.O

2014], the total long-term deflection can increase by approximately 29% when using measured shrinkage values compared to calculated shrinkage values when calculating the deflection according to EC2 (depending on the structural type and the load it will receive).

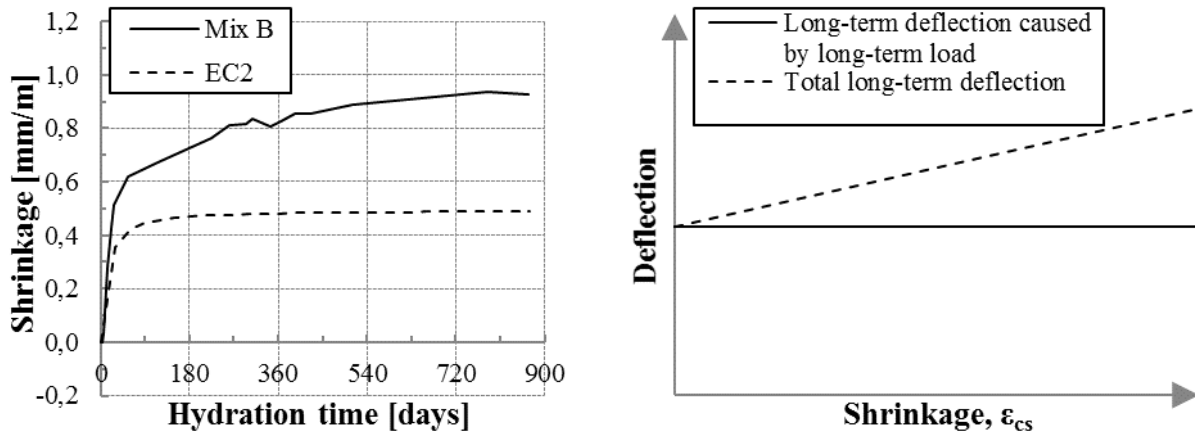


Figure 3: Comparison between measured shrinkage and calculated shrinkage (left) and schematic illustration of the effects of shrinkage on deflection (right) according to EC2.

4. CONCLUSION

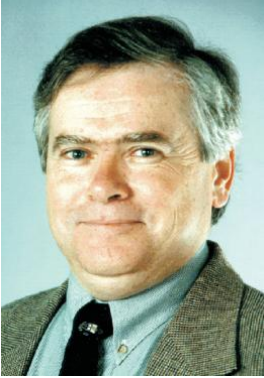
The results show that the LTS is not dependent on the type of curing which indicates that it is inevitable. Also, the magnitude of it seems to be similar among different w/c-ratios. As figure 3 demonstrates, increase in shrinkage can increase deflection according to EC2. The figure also shows that measured shrinkage of Icelandic concrete is much higher than the calculated shrinkage according to EC2. Due to this, it is recommended to create and apply some safety factors for the calculated shrinkage when using concrete containing Icelandic aggregates.

REFERENCES

- Ágústsdóttir, E.L. 2012
 “Rýrnun steinsteypu,” M.Sc. thesis, School of Science and Engineering, Reykjavík University, Iceland, 2012.
- EN 1992-1-1:2004
 “Eurocode 2: Design of concrete structures - Part 1-1: General rules and rules for buildings”. European Committee for Standardization, 2004.
- Flosason, V.O. 2014
 “Shrinkage of concrete using porous aggregates,” M.Sc. thesis, School of Science and Engineering, Reykjavik University, Iceland, 2014.
- Guðmundsson, J.G. Mueller, F.V. and Wallevik, O.H. 2010
 “7SR10030: Shrinkage of Icelandic concrete,” Innovation Center Iceland, Reykjavik,
- Guðmundsson, J.G. 2013
 “Long-term creep and shrinkage in concrete using porous aggregate - the effects of elastic modulus,” M.Sc. thesis, School of Science and Engineering, Reykjavík University, 2013.
- Neville, A.M. and Brooks, J.J., 2010
 “Concrete technology”, 2nd ed. Harlow, England; New York: Prentice Hall, 2010.
- Soroka, I. 1979
 “Portland cement paste and concrete”. London: Macmillan, 1979.
- Pórðarson, B.R. and Wallevik, Ó.H. 1999
 “Fjaðurstuðull íslenskrar steinsteypu: Mælingar á sýnum úr steypustöðvum”, Rannsóknastofnun byggingariðnaðarins, Reykjavík, 99-09, 1999.

Autogenous Deformation of High Performance Concrete-Pilot Study

Abdulaziz Alaskar, PhD student
35 St George Street
University of Toronto
Email: a.alaskar@mail.utoronto.ca



R Douglas Hooton,
Professor and NSERC/CAC Chair in Concrete Durability &
Sustainability
University of Toronto

Abstract

The combined autogenous deformation (AD) and thermal deformation (TD) of a high-performance mortar mixture was investigated under two thermal curing conditions: insulated and non-insulated. The w/cm was 0.36 and total binder content was 465 kg/m^3 and consisted of 8% silica fume and 25% slag. The insulated specimen exhibited increased strain, due to the higher temperature development.

Key words: Autogenous, deformation, swelling, shrinkage, mortar, temperature

1. INTRODUCTION

Due to its higher binder content and low w/cm, high performance concrete (HPC) is likely to undergo high heat of hydration as well as autogenous shrinkage resulting in rapid volume change. The risk of autogenous deformation in high performance concrete (HPC) can adversely influence the crack resistance and durability of reinforced concrete structures (Bentur, 2003; Jensen & Hansen, 2001). Development of internal strain by autogenous shrinkage of HPC at early ages is being investigated. The effect of the curing conditions, insulated and uninsulated, on the autogenous strain and temperature development were investigated.

2. EXPERIMENTAL PROGRAM

For the initial tests reported here, CSA A3000 General Use Portland cement, silica fume, and slag were used as binder. The silica fume and slag replacements of total binder content were 8% and 25%, respectively. The cement and the SCM material were mixed at a water/binder ratio of 0.36. The mortar mix proportions are shown in Table 1. Mortar mixing was completed according to ASTM C305 using graded ASTM silica sand. The autogenous deformation was tested according to a method proposed by Nawa et al. (Figure 1). An embedded strain gauge with built-in thermocouple was inserted vertically into the mortar in a cylindrical PVC mold 50mm diameter and 100mm height, as shown in Figure 1.

Table 1 Mix proportions

| Specimen ID | Regime Condition | Constituent (kg/m ³) | | | | | HRWR (mL/100k g binder) |
|-------------|------------------|----------------------------------|------------------|-------------|------|-------|-------------------------|
| | | Cement | Silica Fume(8%) | Slag (25%) | Sand | Water | |
| 465-UI* | Un-Insulated | 322 | 28 | 116 | 1237 | 167 | 700 |
| 465-I | Insulated | | | | | | |

465-UI: cement binder-regime condition (uninsulated)

The cylindrical mold was oiled to reduce the friction between the concrete and the mold wall. The wall was filled with mortar just after mixing. The samples were exposed to uninsulated and insulated conditions. The room temperature was controlled at 25+/-2 °C. The shrinkage and the temperature of the specimens were obtained every 15 seconds by data acquisition. The insulated specimen was surrounded with 25 mm thick insulation rigid board (FOAMULAR® C-200). Thermal resistance (R-value) of the insulation is 0.88 m²°C/W at 24 °C.

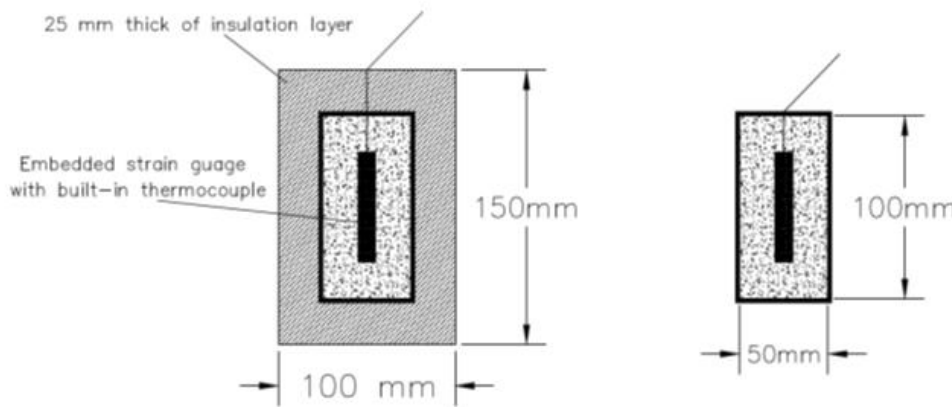


Figure 1 Measuring method of strain and temperature of mortar specimens.

3. RESULTS AND DISCUSSION

Figure 2 shows the measured autogenous deformation strain and temperature development versus time of both the insulated and uninsulated specimens. Temperature development of insulated specimen and uninsulated specimen were presented in Figure 2. At early age, autogenous swelling was thoroughly take place. The concrete expands as its temperature develops due to the generated heat of hydration during the cement and water reaction at early stage. The autogenous swelling can be attributed to the increases of expansion rate in comparison to the shrinkage due to the development of early age capillary pressure (Holt, 2001). The autogenous shrinkage of insulated and uninsulated specimens were almost identical from 4 to 12 hours of age (see Figure 2). The rate of autogenous shrinkage changed in conjunction with temperature evolution between 4 and 16 hours, following a slight increase by the insulated specimen beyond 16 hours. The measured autogenous shrinkage of the insulated specimen accounts for both autogenous deformation and thermal deformation (AD+TD). Therefore, further measurements were taken in place to separate the thermal and autogenous deformation by measuring the coefficient of thermal expansion (CTE) and multiplying it by the temperature difference between the insulated and uninsulated specimens and subtracting it from the total deformation (AD+TD) of the insulated specimen using Equation 1 to get AD (insulated). The CTE measurement was performed at 32 days of age after submerging the sealed specimen in a

preheated water bath at approximately 55 °C where it was kept for 24 hrs, following that, the thermal expansion strain was measured as 13.15 μ strain / °C..

$$\varepsilon_{(AD \text{ (insulated)})} = \varepsilon_{(AD+TD)} - CTE * \Delta T_{(Insulated-Uninsulated)} \quad \text{Equation 1}$$

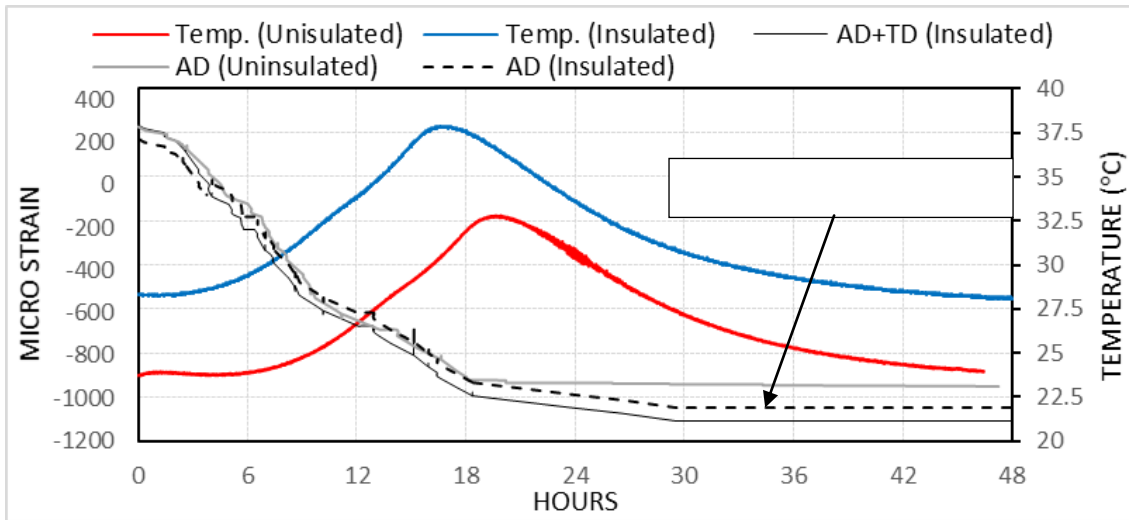


Figure 2 Autogenous deformation and temperature development

4. CONCLUSIONS

From this study on the effect of two levels of semi-adiabatic curing on development of the autogenous shrinkage in mortar, as expected, it was found that the autogenous shrinkage is significantly affected by temperature profile. It was found that the uninsulated specimen exhibited lower shrinkage strain beyond an age of 16 hours in comparison to the insulated specimen. The autogenous shrinkage and the rate of autogenous shrinkage development are higher at early age when the temperature is increasing. Even when corrected for the difference in temperatures, the insulated specimen exhibited higher autogenous deformation and that was likely due to the effects of thermal deformation and possible differences in degree of hydration resulting from the temperature difference.

REFERENCES

- Bentur, A. (ed.) (2003)
 “Early age cracking in cementitious systems”, State-of-the-art report by the RILEM TC 181-EAS Committee, RILEM Report 25, 2003.
- Holt, E. E. (2001).
 Early age autogenous shrinkage of concrete (Vol. 446). Technical Research Centre of Finland.
- Jensen, O. M., & Hansen, P. F. (2001).
 Autogenous deformation and RH-change in perspective. *Cement and Concrete Research*, 31(12), 1859-1865.
- Nawa, T., Horita, T., & Ohnuma, H. (2002).
 A study on measurement system for autogenous shrinkage of cement mixes. In *Concrete Floors and Slabs: Proceedings of the International Seminar Held at the University of Dundee, Scotland, UK on 5-6 September 2002* (Vol. 5, p. 281). Thomas Telford.

BINDERS, ADMIXTURES, MIX DESIGN AND RHEOLOGY
Cont.

Calcined Marl as Supplementary Cementing Material



B. Sc. Tone A. Østnor,
Research engineer
SINTEF Building and Infrastructure
Trondheim, Norway
E-mail: tone.ostnor@sintef.no



Prof. Dr. Harald Justnes
SINTEF Building and Infrastructure
Trondheim, Norway
E-mail: harald.justnes@sintef.no

ABSTRACT

Mortars (sand:cement = 3:1 and w/b = 0.50) were made where Portland cement was replaced with 0, 20, 35, 50 and 65 vol% calcined marl. The compressive and flexural strengths were determined after 1, 3, 7, 28, 90, 365 and 730 days curing at 90% RH and 23°C. The strength up to 28 days age was higher or equal to the reference for up to 50 vol% marl replacement of cement.

Mortars of all compositions were tested for durability starting after 90 days curing. The microstructure was characterized by SEM. Selected result are included in this paper.

Key words: Alternative binders, calcined marl, pozzolan, supplementary cementing material, durability, sustainability

1. INTRODUCTION

Marl, or calcareous clay, is considered "bad" clay for production of burnt clay products (e.g. bricks and light weight aggregate) since it is clay contaminated with substantial amounts of calcium carbonate that will form CaO after burning. This can lead to "pop outs" when calcium oxide reacts with water to calcium hydroxide during service.

Calcined marl has been proven earlier by Justnes et al (2011) to be an effective pozzolan in cementitious products. Thus, marl can be a large SCM resource that is not yet exploited to make blended cements or as mortar/concrete additive. Marl with 10-20% CaCO₃, or rather calcareous mudstone, was calcined at 800°C leaving 20% of the original CaCO₃ intact.

Calcined marl can be considered "industrial pozzolan" within the European cement standard (EN 197-1), and it may be feasible to make a pozzolanic cement with up to 55% clinker replacement (CEM IV/B) considering the 28 day strength and sufficient early strength documented in this paper.

2. MATERIALS AND EXPERIMENTS

2.1 Materials

The marl was provided by Saint Gobain Weber who calcined it in a rotary kiln close to industrial conditions. The calcined marl were ground to $d_{50} = 7 \mu\text{m}$. Normal Portland cement (CEM I 42.5R according to NS-EN 197-1) produced by Norcem Brevik, Norway, was used for

all the mortar mixes. The aggregate used was 0 – 8 mm crushed granite rock from Årdal, Norway. The superplasticizer used was Dynamon SP 130 supplied by Mapei AS, Norway.

2.2 Mortar mix designs

The mortars were made with 0, 20, 35, 50 and 65 vol% replacement of cement with marl to secure a constant volume of binder. The consistency of fresh mortar was determined using a flow table. The water-to-binder ratio (w/b) was 0.5 in all the mortars while the flow was maintained within ± 5 % of the reference by varying the amount of superplasticizer; 0.0, 0.2, 0.3, 0.5 and 0.9% (of binder weight) for the mortars with 0, 20, 35, 50 and 65 vol%, respectively. The mortar mixes were cast in 40x40x160 mm moulds and 100x200 mm cylinders. After 24 hours the prisms and cylinders were removed from the moulds and stored in a cabinet at 90 % RH and 23 ± 2 °C.

2.3 Experiments

The compressive and flexural strengths were determined after 1, 3, 7, 28, 90, 365 and 730 days of curing at 90% RH and 23°C. The capillary suction and saturation giving the total volume of capillary pores and amount of macro pores were measured, as well as electrical resistivity. Mortars of all compositions were tested for durability starting after 90 days curing with respect to chloride diffusion, expansion caused by sulphate attack (5% Na₂SO₄) at both +5°C and +20°C, as well as carbonation (accelerated by 1% CO₂ and 60% RH). Only some of the results will be presented in this paper due to limited space.

3. RESULTS

The average compressive and flexural strength for all mortars as a function of time are given in Table 1 together with standard deviations based on 5 and 3 parallels, respectively.

Table 1 Compressive (upper value) and flexural (lower value) strengths as a function of time for mortars where various amounts have been replaced by calcined marl.

| marl (vol%) | Average strength \pm standard deviation [MPa] at ages [days] | | | | | | |
|----------------|--|----------------|----------------|----------------|----------------|----------------|----------------|
| | 1 d | 3 d | 7 d | 28 d | 90 d | 365 d | 730 d |
| 0 | 22.0 \pm 0.3 | 40.4 \pm 1.0 | 46.2 \pm 1.0 | 53.5 \pm 0.6 | 61.1 \pm 1.6 | 67.9 \pm 0.9 | 72.9 \pm 2.4 |
| | 4.8 \pm 0.1 | 6.7 \pm 0.4 | 7.4 \pm 1.0 | 7.8 \pm 0.3 | 8.4 \pm 0.4 | 8.8 \pm 0.4 | 9.0 \pm 0.5 |
| 20 | 17.9 \pm 0.4 | 35.5 \pm 0.5 | 44.0 \pm 1.0 | 57.3 \pm 1.3 | 65.6 \pm 0.9 | 70.8 \pm 1.3 | 74.6 \pm 0.8 |
| | 3.8 \pm 0.3 | 5.9 \pm 0.2 | 7.2 \pm 0.2 | 7.4 \pm 0.2 | 7.7 \pm 0.6 | 9.0 \pm 0.5 | 9.1 \pm 0.2 |
| 35 | 14.0 \pm 0.1 | 31.2 \pm 0.4 | 42.5 \pm 0.6 | 57.0 \pm 0.8 | 62.8 \pm 1.6 | 68.4 \pm 1.0 | 68.9 \pm 2.9 |
| | 3.1 \pm 0.1 | 5.4 \pm 0.2 | 6.5 \pm 0.2 | 7.6 \pm 0.5 | 8.3 \pm 0.2 | 7.9 \pm 0.2 | 9.0 \pm 0.5 |
| 50 | 9.5 \pm 0.2 | 23.6 \pm 0.3 | 38.8 \pm 0.4 | 51.0 \pm 1.2 | 54.2 \pm 1.1 | 63.6 \pm 1.3 | 69.2 \pm 1.5 |
| | 2.2 \pm 0.1 | 4.5 \pm 0.2 | 5.9 \pm 0.3 | 6.5 \pm 0.3 | 6.8 \pm 0.4 | 8.3 \pm 0.9 | 9.4 \pm 0.3 |
| 65 | 5.7 \pm 0.1 | 15.8 \pm 0.3 | 27.6 \pm 0.1 | 38.1 \pm 1.2 | 43.5 \pm 1.0 | 55.9 \pm 1.3 | 67.8 \pm 0.7 |
| | 1.3 \pm 0.1 | 3.2 \pm 0.1 | 4.9 \pm 0.2 | 5.2 \pm 0.4 | 6.1 \pm 0.3 | 6.8 \pm 0.4 | 8.2 \pm 0.4 |

The average data with standard deviations extracted from capillary suction profiles of 4 parallel discs for each mortar mix are listed in Table 2 after 90 days and 2 years curing.

Table 2 Mortar properties extracted from capillary suction experiments

| Marl (vol%) | Capillary Porosity | | Air content ϵ_{air} [vol%] | | Average density of solids, | Dry Density |
|----------------|--------------------------------|----------|--|---------|-------------------------------|-------------------------------|
| | ϵ_{cap} [vol%] | | | | ρ_s [kg/m ³] | ρ_d [kg/m ³] |
| | 90 days | 2 years | 90 days | 2 years | 2 years | 2 years |
| 0 | 17.3 ± 0.4 | 16.8±0.3 | 3.4 ± 0.2 | 3.2±0.2 | 2660±3 | 2127±10 |
| 20 | 19.4 ± 0.2 | 19.0±0.1 | 2.4 ± 0.2 | 2.5±0.1 | 2692±3 | 2114±7 |
| 35 | 20.6 ± 0.2 | 20.4±0.1 | 2.1 ± 0.1 | 2.2±0.0 | 2706±2 | 2093±4 |
| 50 | 21.1 ± 0.1 | 20.9±0.2 | 2.1 ± 0.2 | 2.2±0.1 | 2683±13 | 2063±15 |
| 65 | 22.6 ± 0.1 | 21.8±0.1 | 2.3 ± 0.1 | 2.1±0.1 | 2680±2 | 2040±2 |

The chloride ingress profiles for mortars with different cement replacements by calcined marl are plotted in Figure 1, while the parameters obtained from the curve fitting are listed in Table 3.

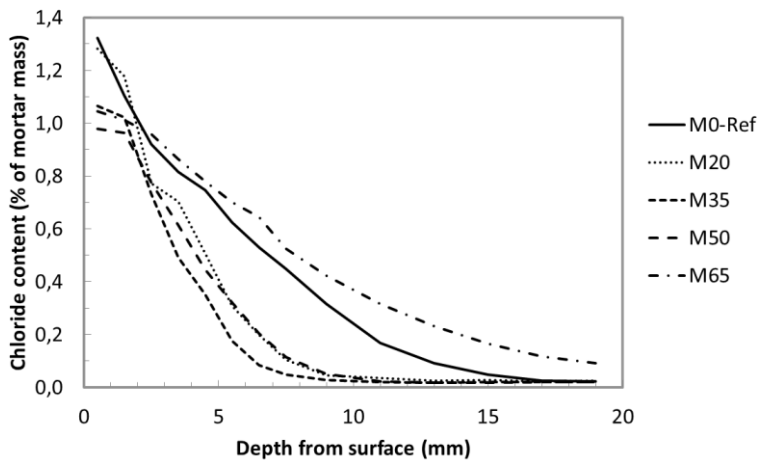


Figure 1 Chloride ingress in mortars where cement is replaced with 0 (M0), 20 (M20), 35 (M35), 50 (M50) and 65 (M65) vol% calcined marl after 35 days to 165 g NaCl/liter.

Table 3 Parameters obtained from curve fitting of the chloride ingress profiles according to mathematical solution of Fick's 2nd law of diffusion; the chloride surface concentration, C_0 (% of mortar mass), the apparent diffusion coefficient, D_{app} (10^{-12} m²/s) and the amount of chloride intrusion, ingress (g Cl/m² surface).

| Marl (vol%) | Parameters from Cl ⁻ profile | | |
|----------------|---|--|--------------------------------|
| | C_0 (%) | D_{app} (10^{-12} m ² /s) | Ingress (g Cl/m ²) |
| 0 | 1.29±0.11 | 8.2±1.9 | 188±37 |
| 20 | 1.68±0.10 | 1.9±0.2 | 119±0 |
| 35 | 1.54±0.10 | 2.0±0.2 | 105±2 |
| 50 | 1.32±0.04 | 3.3±0.2 | 117±3 |
| 65 | 1.18±0.03 | 16.1±1.4 | 227±11 |

The BSE images of mortar with 35 vol% cement replacement of calcined marl after 2 years curing in Figure 3 show to the left in the left images a cement grain that has reacted through and that is NOT decalcified with an inner CSH product with Ca/Si = 1.56. The products in the pores in the centre of images in Figure 2 are calcium aluminate hydrates (CAH), and the one to the right has composition 16.5 Ca, 8.3 Al, 1.1 Si, 0.4 S and 0.4 Fe in atom% by WDS. A Ca/Al = 2 corresponds to CAH compounds starting with C₄A in the short-hand notation of cement chemists (i.e. general AFm phases), including calcium monocarboaluminate hydrate.

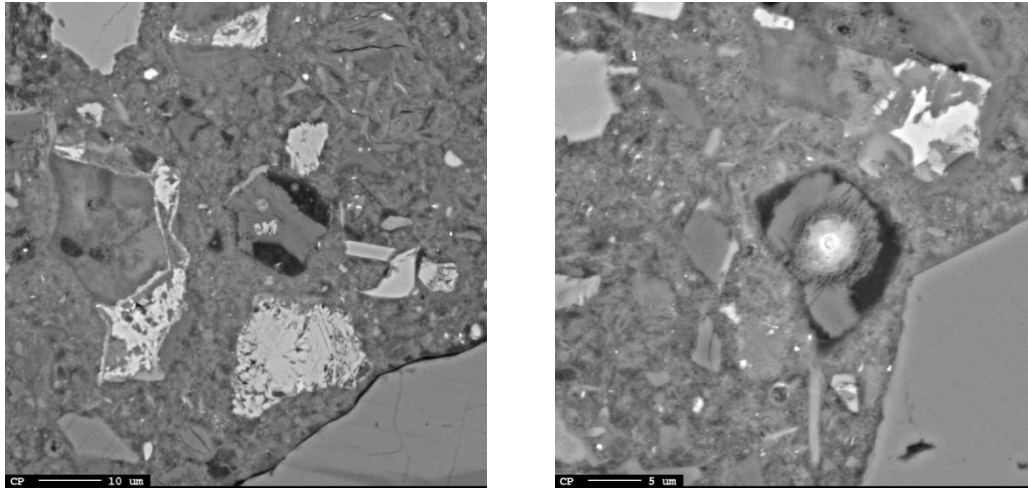


Figure 2 Mortar with 35 vol% cement replaced by calcined marl (M35) after 2 years curing showing calcium aluminate hydrate products crystallizing in voids.

4. CONCLUSIONS

Calcined marl – ordinary "blue" clay contaminated with calcium carbonate – can be an effective pozzolan in cementitious materials if calcined at the correct temperature. Marl is unsuitable for the clay product industry, and might thus be the high-volume available alternative pozzolan globally that the cement and concrete industry is looking for in order to reduce their carbon footprint.

Excellent strength at both 1 and 28 days relative to reference is obtained when up to 50 vol% is replaced by calcined marl.

The chloride ingress is drastically reduced relative to reference for mortars with $\leq 50\%$ marl replacing cement.

ACKNOWLEDGEMENTS

The paper is based on the work performed in COIN - Concrete Innovation Centre ([www.coinweb.no](http://coinweb.no)) - which is a Centre for research-based Innovation, initiated by the Research Council of Norway (RCN) in 2006. For more information, log on to: <http://coinweb.no/>

References

- Justnes, H., Østnor, T. and Danner, T.:
 "Calcined Marl as Effective Pozzolana", Proceedings of the International RILEM Conference on Advances in Construction Materials Through Science and Engineering, RILEM PRO 79, 5-7 September, 2011, Hong Kong, China, 8 pp.
- De Weerd, K. and Justnes, H.:
 "Microstructure of Binder from the Pozzolanic Reaction between Lime and Siliceous Fly Ash, and the Effect of Limestone Addition", Proceedings of 1st Int. Conf. on Microstructure Related Durability of Cementitious Composites, 13-15 October, 2008, Nanjing, China, pp. 107-116, RILEM Proceeding PRO 61.
- De Weerd, K., Kjellsen, K.O., Sellevold, E.J. and Justnes, H.:
 "Synergy between Fly Ash and Limestone Powder in Ternary Cements", Cement and Concrete Composites Vol. 33, Issue 1, January 2011, pp. 30-38.

Developing Pervious Concretes for Urban Stormwater Management in Nordic Environments



Erika Holt
Ph.D., Research Team Leader
VTT Technical Research Centre of Finland
P.O. BOX 1000
FI-02044 VTT, Finland
E-mail: erika.holt@vtt.fi



Hannele Kuosa
M.Sc. (Tech.), Research Scientist
VTT Technical Research Centre of Finland
P.O. BOX 1000
FI-02044 VTT, Finland
E-mail: hannele.kuosa@vtt.fi

ABSTRACT

Finland has been developing pervious concrete (PC) to mitigate impacts of climate change in urban environments. The work started in 2012 due to the needs of municipalities to have new solutions in their stormwater management programs. PC surfacing has not been earlier utilised in Finland due to the lack of quantitative dimensioning and performance uncertainties for winter durability. The laboratory program for PC has included studies of different material and recipe combinations, including performance evaluation of strength, porosity, water permeability and durability, prior to planning for in-situ demonstration constructions planned for year 2015.

Key words: Concrete, Pavement, Pervious, Permeability, Durability, Frost Action, Freeze-thaw, De-icing salt, Air entrainment, Mix design, Surfaces, Testing, Stormwater, Filtration.

1 INTRODUCTION

1.1 General

Several pavement surfacing materials have been investigated in the two-year “Climate Adaptive Surfaces” project /CLASS 2014/, aimed at providing alternative solutions for better urban stormwater management. The project has been funded by Tekes (the Finnish Funding Agency for Technology and Innovation), VTT and 16 industrial partners. The industries represent a wide value change, including 4 cities, a water handling organization, 3 designers, 2 associations and 6 material supplies, including Rudus Oy and Lemminkäinen Infra Oy. Close cooperation has also been made with the Swedish “Green-Grey” project, funded by Vinnova and coordinated by CBI.

Pervious concrete (PC) is one of the key solutions for development and performance assessment prior to implementation via the full-scale pilot demonstration constructions. PC has multiple environmental benefits: controlling stormwater runoff, mitigating impacts of climate changes in urban environments, restoring groundwater supplies, and reducing water and soil pollution. The research has had a concentrated effort on developing PC that is durable for arctic environmental conditions, while also being cost effective. The new materials combined with sub-base design are optimised during design, construction and maintenance, to allow for high water infiltration rather than over-burdening the stormwater collection systems or polluting nearby natural water bodies with urban run-off.

1.2 State-of-the-Art Results

Several State-of-the-Art reviews were performed /CLASS 2014/, prior to the laboratory and field studies with PC. One specific aim of the initial reviews was to plan the PC mix designs suitable with Finnish materials having high open porosity, high water permeability, high enough strength and especially good durability properties. The challenges in achieving these desired properties were identified. It was also found that there are no common methods for the testing of PC freeze-thaw resistance with and without de-icing salt. The main factor having an effect on the deterioration is the degree of water saturation achieved before and during the selected testing method. The freezing rate will also have an effect on the deterioration of PC. Too high freezing rate may not be suitable for the evaluation of the freeze-thaw durability of a pervious pavement material. In addition, a pavement's service life demand is normally not as high as for instance for structural bridge concrete. A 25 - 30 year service life is often acceptable for pavements which can be maintained or easily replaced. A high pavement water infiltration rate helps to maintain low water saturation of the PC. For this, it is essential to have a high enough total pore volume of the pavement sub-structure, and also good maintenance and cleaning practices over the lifetime. Cleaning will prevent too heavy clogging, thus avoiding unwanted water saturation.

Within the State-of-the-Art reviews, a clear problem was identified as the lack of suitable test methods for the measurement of the amount of entrained air pore amounts in fresh PC mix, which is needed for freeze-thaw durability. The methods to measure air content of normal concrete were found not to be applicable to PC, and thus new methods had to be developed, both for fresh and hardened states. In some cases plane sections and image analysis have been used. In addition to durability methods, other performance tests characterise PC density, open void content, water permeability, strength and effect on water quality.

2 MIXTURE DESIGNS

Several PC mixes were prepared, including casting of 0,5 m x 0,5 m slabs (h150 mm) and 150 mm cubes for laboratory studies. Before selecting the final mixes, preliminary mixes and studies were made, including thin section studies. (Figure 1d) These studies were necessary to select the right water/cement ratios, and the correct admixture dosage while adjusting the workability. A simple method was used for the workability estimation (see Figure 1a). No retarding admixture was included as the lab placing was immediately after mixing (at +20 °C), as opposed to field conditions where hydration control is often necessary. Also, no viscosity modifiers were included but rather relatively dry mixes and an effective compaction method were used (Figure 1b & 1c).

The main emphasis for the mixture design and samples was on ensuring durability for harsh Finnish winter exposure conditions. To study this, different PC mixtures were produced using two different cement types from Finnsementti, and then using either an air entraining agent, or a special 'polymer modifier' from Wacker Chemie AG. In all cases the target open porosity or void space was 20%, to ensure filtration and water permeability. Finnish crushed granitic aggregates from Rudus Oy were used. The final mix designs of the PCs are presented in Table 1. Additional studies were also done using pervious concrete paving blocks and pervious asphalt, though they are not reported here.

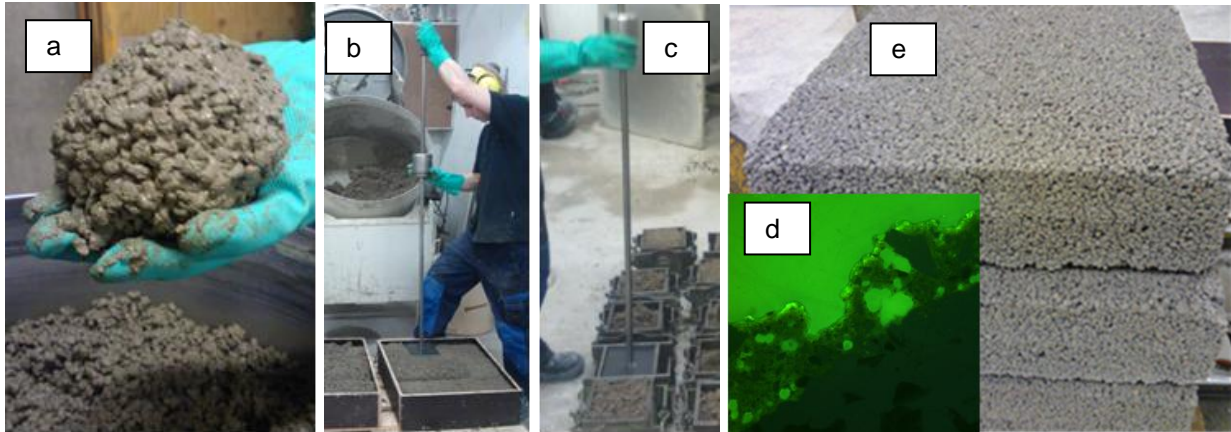


Figure 1 –a) PC workability verification; b) compaction of slabs; and c) cubes at laboratory by a Proctor-type hammer (4.5 kg) with a $150 \times 150 \text{ mm}^2$ metal plate; d) PC microstructure; e) PC0 slabs.

Table 1 – PC mix design.

| | PCA | PC0 | PC1 | PC2 | PC3 | PC4 |
|---|-------|-------|-------|-------|------|-------|
| CEM II/B-M (S-LL) 42,5 N (Plussementti) [kg/m^3] | 300 | 305 | 305 | 280 | 305 | 0 |
| CEM I 52,5 R (Pikasementti) [kg/m^3] | 0 | 0 | 0 | 0 | 0 | 305 |
| Total Aggregates [kg/m^3] | 1596 | 1565 | 1565 | 1534 | 1565 | 1565 |
| Extra fine gravel 0/1 mm [% of all aggregate] | 7 | 7 | 7 | 0 | 7 | 7 |
| Fine gravel 0/4 mm [% of all aggregate] | 0 | 0 | 0 | 7 | 0 | 0 |
| Gravel (water sieved) 4/8 mm [% of all aggregate] | 93 | 93 | 93 | 0 | 93 | 93 |
| Crushed aggregate 8/12 mm [% of all aggregate] | 0 | 0 | 0 | 93 | 0 | 0 |
| Water (effective) [kg/m^3] | 70 | 82 | 85 | 85 | 85 | 92 |
| w/c (effective) [-] | 0,27 | 0,27 | 0,28 | 0,28 | 0,28 | 0,30 |
| Plasticizer: VB-Parmix [% of cement] | 3 | 3 | 3 | 3 | 2 | 3 |
| Air entraining agent: AIRMIX [% of cement] | 0,1 | 0,1 | 0,1 | 0,1 | 0 | 0,1 |
| 'Polymer modifier': ETONIS 260 [% of cement] | 0 | 0 | 0 | 0 | 16 | 0 |
| Target Entrained air pores [%] | 2 - 4 | 2 - 4 | 2 - 4 | 2 - 4 | - | 2 - 4 |

3 RESULTS AND CONCLUSIONS

Fresh PC density was measured after compaction, and total void content (open voids + entrained air pores) was calculated based on the mix design. New fresh-test methods were developed to get fast information on the amount of entrained air pores as a percentage of cement paste. The results were compared to hardened PC air pore structure, assessed by thin-section microscopy.

A key parameter to measure was the PCs' freeze-thaw durability, both with and without de-icing salt. With salt the testing is done with the specimens ($h50 \times 150 \times 150 \text{ mm}^3$) in contact with NaCl solution (5 mm), while with only water, the testing is on immersed specimens. In both cases there is one freeze-thaw cycle in 24 h. PC deterioration was followed based the measurement of the scaling (with salt) or relative dynamic modulus of elasticity (with water), along with specimen weight. In the case of freeze-thaw without salt, splitting tensile strength was determined after the testing, and was compared with the splitting tensile strength of the reference specimens maintained in water. The water infiltration rate of PC slabs was measured by the ASTM Single Ring method (ASTM C1701/C1701M-09). Examples of some key results are presented in Table 2.

Table 2 – Example testing results.

| | PCA | PC0 | PC1 | PC2 | PC3 | PC4 |
|---|--|------------------------------------|-----------------------|----------|------|------|
| | 150 mm cubes | | | | | |
| Density (fresh) [kg/m ³] | 1956 | 1950 | 1938 | 1956 | 1926 | 1888 |
| standard deviation | (1 result) | 57 ¹⁾ | 21 | 16 | 16 | 18 |
| Porosity, fresh PC (open pores + entrained air pores) [%] | 23,9 | 24,3 | 23,8 | 23,6 | 23,6 | 26,5 |
| Entrained air pores (tentative method for fresh PC) [% of concrete] | - | 3,8 | 3,7 | 2,9 | 2,4 | 2,2 |
| Entrained air pores (tentative method for fresh PC) [% of cement paste] | - | 17,4 | 16,9 | 14,6 | 10,5 | 11,0 |
| Effective (pervious) voids [%] | ca. 20 | 20,5 | 20,1 | 20,7 | 23,6 | 24,2 |
| Compressive strength 28 d [MPa] | 22,5 | 12,2 ²⁾ | - | - | 15,9 | 15,4 |
| standard deviation | 3,1 | 2,0 | - | - | 0,8 | 0,1 |
| | h150 mm slabs (505 x 505 mm ²) | | | | | |
| Density (fresh) [kg/m ³] | - | 1984 ³⁾ | 1902 | 1843 | - | - |
| standard deviation | - | 57 ³⁾ | 8 | (1 cube) | - | - |
| Porosity, fresh PC (open pores + entrained air pores) [%] | - | Thin section study (see Figure 1d) | 25,9 | 28,0 | - | - |
| Entrained air pores (tentative method for fresh PC) [% of concrete] | - | - | - | 3,0 | - | - |
| Entrained air pores (tentative method for fresh PC) [% of cement paste] | - | - | - | 14,8 | - | - |
| Effective (pervious) voids [%] | - | - | - | 25,0 | - | - |
| Water infiltration (ASTM single ring method) [x10 ⁻³ m/s] | - | 6,3 | 0,4/2,5 ⁴⁾ | 6,1 | - | - |
| standard deviation | - | 0,1 | 0,1/0,1 | 0,4 | - | - |

1) Includes somewhat different compaction methods.

2) 150 mm cube strength, measured with Ø100 mm cores.

3) For the at RH 95% cured slab (Ø100 mm cores). Compaction with a roller in two layers, less intensive compaction than in all the other cases.

4) 2 castings

Additional laboratory studies are also done with a Filtration Simulation Rig testing (FS-Rig), where the hydraulic behaviour of the whole structure with PC as the surface material is studied. The FS-Rig has dimensions of 50 cm wide x 100 m length x 1 metre tall and is loaded with varying materials, such as subgrade soil, permeable sub-base, layering base course, geotextiles, drainage pipes, jointing material and/or surfacing PC. The primary criteria of the layered studies is the filtration rate, though studies also include evaluation of secondary parameters affecting the choice of pervious materials, such as the effect of clogging and maintenance cleaning on the water infiltration capacity, as well as stormwater chemical composition benefits due to filtration. The results are used in comparison to individual component tests and field studies on filtration performance of existing pervious pavements. Environmental and economic life cycle assessments are done for some of the most promising material layer systems.

The results of these studies are aiding urban planners and stormwater management experts in selection of the parameters and materials fulfilling Finnish design codes. New products are being developed for businesses, with a greater level of confidence for their performance, sustainability and cost. The results are also used in modelling of the stormwater handling expectations of the new pervious materials, both for current and future scenarios accounting for higher volumes of expected precipitation based on Finnish climate change predictions.

REFERENCES

CLASS. 2014. Climate Adaptive Surfaces – Project web page & published reports, VTT Technical Research Centre of Finland, <http://www.vtt.fi/sites/class/?lang=en> Visited 16.4.2014.

Finnish Clay based Pozzolan and Dehydrated Cement Paste as Cement Replacement Materials



M. Sc. Kalle Loimula
Research Scientist
VTT Technical Research Centre of Finland
Kemistintie 3, Espoo
P.O Box 1000
FI-02044 VTT, Finland
E-mail: kalle.loimula@vtt.fi

ABSTRACT

Cement manufacturing is responsible for serious amounts of worldwide CO₂-emissions. Emissions related to concrete structures can be reduced by a partial replacement of cement with a more environmentally friendly material when constructing concrete structures. In this study, a Finnish clay based pozzolan, two kaolins and dehydrated cement paste were used as cement replacement materials with heat treatments. All heat treated materials performed well as cement replacement materials. The heat-treated clay had the EN 450-1 required activity index at 28 days of age. Dehydrated cement paste and the heat-treated kaolins met the requirements at all test ages.

Key words: Additives, Pozzolans, Clays, Cement replacement materials

1. INTRODUCTION

It has been estimated that up to 5% of the global CO₂-emissions are caused by the cement manufacturing industry. Cement is needed for building concrete structures and can be partially replaced to reduce emissions related to these structures. /Worrell et al. 2001/ Pozzolans can be used as cement replacement materials. Pozzolans are siliceous or aluminous and siliceous materials that can react with calcium hydroxide to form calcium silicate hydrate (C-S-H). Calcium hydroxide is a hydration product in normal cement hydration and C-S-H is the binding phase in concrete, giving the structure its strength. /Taylor 1997/ Metakaolin is a well-known pozzolan. It is manufactured by heat treating kaolin clays (clays containing kaolinite). Kaolinite is a crystalline clay mineral and heat treatment at sufficient temperatures breaks down its crystalline structure to give an amorphous material with pozzolanic properties. Other clay minerals, than kaolinite, can also be heat treated to obtain materials with pozzolanic properties. /Siddique 2008, He et al. 1995/

In this study, two kaolins of different quality were heat treated to obtain metakaolins of different quality. Finnish clay containing no kaolinite was also heat treated in order to obtain a material with pozzolanic properties. These pozzolans and a commercial metakaolin were used as cement replacement materials and their performance was evaluated. Hydrated cement paste was also heat treated in order to regenerate reactive calcium silicates. The heat treated product was used as a cement replacement material and its performance was evaluated.

2. EXPERIMENTAL

The kaolins and clay were characterized with X-ray fluorescence (XRF) and X-ray diffraction (XRD) techniques. Elemental and mineralogical compositions were obtained. The thermal

behaviour of the kaolins and clay was characterized with thermogravimetry (TG-DTA). The heat treatment temperatures for these materials were chosen based on the TG-DTA curves.

For the kaolins and clay, heat treatments were chosen as 3h at 500, 600, 700 and 800°C. The hydrated cement paste had heat treatments of 2h at 250, 450 and 750°C. The heat treatment durations of 2 and 3 hours and heat treatment temperatures for hydrated cement paste were chosen based on literature. The heat treated products were further examined with XRD to determine the optimal heat treatment temperature for each material.

The optimal heat treatment temperature for both kaolins was concluded to be 600°C while the optimal heat treatment temperature for clay was found to be 800°C. Hydrated cement paste was heat treated in 750°C based on XRD analysis and literature.

The heat treated products along with commercial metakaolin were used as cement replacement materials, replacing 25% of the cement used in the reference mortar. Another reference mortar was made with 25% replacement with inert material (quartz). The mortars were tested for compressive strength at 7, 28 and 91 days of age /EN 196-1/. Activity indexes were calculated /EN 450-1/ and statistical analysis was performed on the compressive strength results. /Loimula 2013/

3. RESULTS

The mix designs, abbreviations and compressive strength results are presented in Table 1. Compressive strength values are averages of 9 measurements at all test ages.

Table 1 - Mix design data and compressive strength results.

| Abbreviation | Cement replacement material | Compressive strength 7d, MPa | Compressive strength 28d, MPa | Compressive strength 91d, MPa |
|--------------|-----------------------------|------------------------------|-------------------------------|-------------------------------|
| REF1 | - | 44.8 | 51.1 | 56.9 |
| REF2 | quartz | 20.2 | 24.4 | 30.9 |
| KAO1 | heat treated kaolin no.1 | 37.8 | 50.2 | 52.5 |
| KAO2 | heat treated kaolin no.2 | 47.3 | 63.3 | 68.7 |
| META | commercial metakaolin | 53.8 | 69.0 | 71.6 |
| CLAY | heat treated clay | 35.3 | 45.1 | 47.4 |
| HCP | heat treated cement paste | 46.1 | 52.5 | 52.4 |

Activity indexes were calculated according to Equation (1).

$$AI = \frac{CS}{CS_{REF}} \quad (1)$$

where,

AI = activity index

CS = compressive strength

CS_{REF} = compressive strength of REF1

Activity indexes for all test mixes at all test ages are presented in Figure 1.

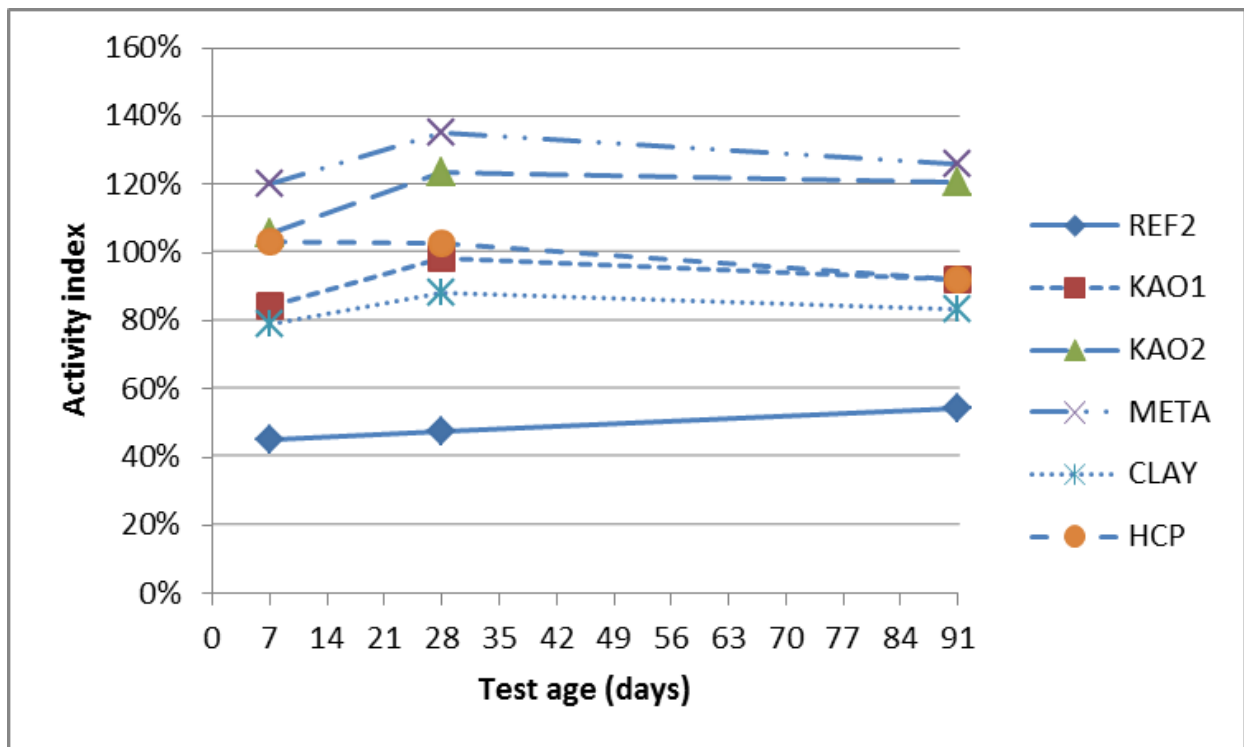


Figure 1 - Activity indexes for all test mixes at all test ages. Connection lines between data points do not have physical meaning.

An activity index of 100% equals the performance of mortar without any cement replacement (REF1). The requirement for activity indexes in standard EN 450-1 is 75 and 85% at 28 and 91 days, respectively. REF2 with inert cement replacement material failed to meet these requirements, as expected. CLAY with heat treated Finnish clay as a cement replacement material met the requirements at 28 days of age but performed slightly below requirements at 91 days of age. KAO1, KAO2, META and HCP met the requirements at both test ages.

An analysis of variance was performed on the compressive strength averages at all test ages to investigate if the differences between mortars are statistically significant. At 7 days, HCP and REF1 were statistically the same (95% confidence level). No statistical difference was observed between KAO2 and HCP either. At 28 days, HCP, REF1 and KAO1 were statistically the same. The difference between HCP and KAO1 at the age of 91 days was not statistically significant.

4. CONCLUSIONS

Heat treatment was successfully applied to kaolins, Finnish clay and hydrated cement paste to obtain cement replacement materials. Heat-treated Finnish clay performed adequately at 28 days of age as a cement replacement material but slightly failed to meet the requirements at 91 days of age. Heat-treated hydrated cement paste performed well as a cement replacement material at all test ages. The results of this project can be utilised when making more environmentally-friendly materials having a lower CO₂ burden, including new sources of binders and recycling of building materials. The products can meet durability and performance requirements according to existing standards.

REFERENCES

He, C., et al., 1995

“Pozzolanic Reactions of Six Principal Clay Minerals: Activation, Reactivity Assessments and Technological Effects”, *Cement and Concrete Research*, Vol. 25, 1995, pp. 1691-1702.

Loimula, K., 2013

“Applicability of Finnish Clay as a Raw Material for Pozzolans”, Master’s Thesis, Aalto University, School of Chemical Technology, 2013.

Siddique, R., 2008

“Waste Materials and By-products in Concrete”, Springer, 2008.

Taylor, H. F. W., 1997

“Cement Chemistry”, 2nd edition, Thomas Telford, London, 1997.

Worrell, E. et al., 2001

“Carbon Dioxide Emissions from the Global Cement Industry”, *Annual Review of Energy and the Environment*, Vol. 26, 2001, pp. 303-329.

NMR and Rheometrical study of Lime-Cement pastes



Marine Fourmentin
Laboratoire Navier
2, allée Kepler
FR - 77420 Champs-sur-Marne
marine.fourmentin@ifsttar.fr

Dr. Pamela Faure
Laboratoire Navier
2, allée Kepler
FR - 77420 Champs-sur-Marne
pamela.faure@ifsttar.fr

Dr. Didier Lesueur
Lhoist Recherche & Développement
Rue de l'Industrie, 31
B – 1400 Nivelles
didier.lesueur@lhoist.com

Dr. Ulrike Peter
Lhoist Recherche & Développement
Rue de l'Industrie, 31
B – 1400 Nivelles
ulrike.peter@lhoist.com

Dr. Philippe Coussot
Laboratoire Navier
2, allée Kepler
FR - 77420 Champs-sur-Marne
philippe.coussot@ifsttar.fr

ABSTRACT

Contrary to cement, which is widely studied, only few studies concentrate on lime-cement mixes, and even less discuss the effect of lime on cement setting. As these new materials appears increasingly in the industry, it is necessary to better understand the effect of hydrated lime on the setting of cement.

In this study, we followed the setting of different lime-cement mixtures by Nuclear Magnetic Resonance (NMR), which provide information on the porous structure, and by rheometry to monitor the elastic modulus. The correlation of these two methods clearly reveals the successive steps of setting and the significant impact of hydrated lime.

Key words: Cement, Lime, NMR, Rheology, Porous Media

1. INTRODUCTION

Current environmental problems constrains to a reduction of cement in the construction and to the use of more environmentally friendly materials. New binders consisting primarily of hydrated lime and cement are now developed with various applications (cellular concrete, hemp concrete, restoration of old monuments), as they combine strength at early age, thanks to the presence of cement, and flexibility thanks to the presence of lime. In view of developing the use of these materials on a larger scale, it is necessary to better understand the effect of lime on setting.

In this study, we followed the setting of a cement paste with two methods, which provide complementary information. On the one hand, NMR enables us to follow the amount of liquid

water and the evolution of the average pore size over time. On the other hand, we follow the mechanical properties by monitoring the elastic modulus during the setting.

2. RESULTS

All results presented here are for a simple cement paste with a water to cement ratio of 0.4.

2.1. Nuclear Magnetic Resonance (NMR)

NMR is a non destructive method that allows the detection of protons of water in a liquid state in a porous media by measuring their relaxation time (T_1) [1]. NMR measurements provide two important data. T_1 is assimilated to an average pore size in the sample, and the smaller the T_1 is, the smaller the pores are. T_1 distribution shows the various pore sizes in the sample and allows following pore size evolution. Plus, it provides quantitative measurements giving the amount of non-bounded water in the system. Protons in water that reacted with anhydrous cement grains to form hydrates are no longer detectable.

NMR was used to monitor the evolution of the structuration of a cement paste during its setting. First of all, the distribution of relaxation times shows at every moment a single peak meaning that there is a single "average pore size" in the sample. Looking at the distribution of relaxation times at various times of setting (fig.1a), we can see a progressive shift of the peak towards lower T_1 . The amount of water, which is proportional to the area under the peak, cannot easily be appraised here. Therefore, the evolution of T_1 value and total signal with time in the sample are represented (fig.1b).

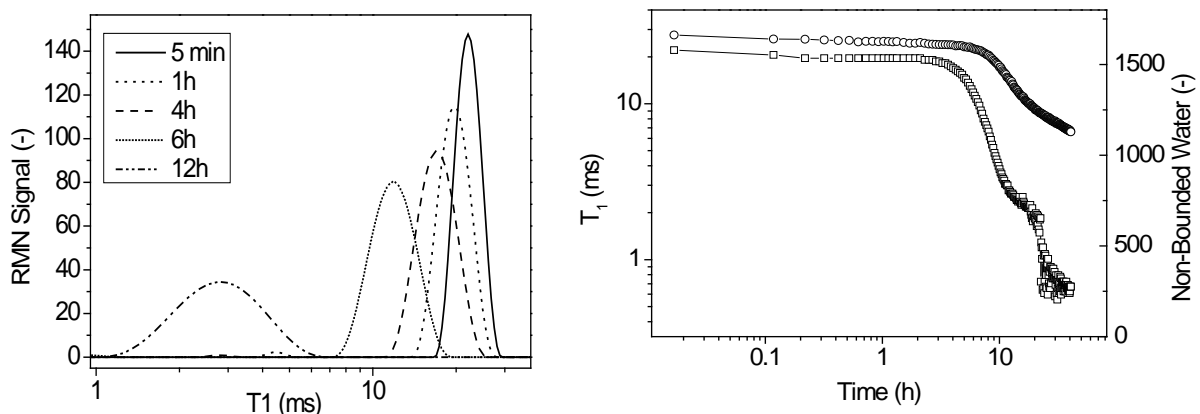


Figure 1. (a) Distribution of relaxation times at various successive stages of the setting (b) Evolution of porous structure (T_1 value, squares) and non-bounded water (circles) of the paste during the first 24h after mixing.

The total signal decreases significantly from 10 hours, which indicates water consumption at this time of the setting. T_1 decreases sharply from two hours to reach a hundredth of its initial value, which is representative of a high decrease of the average pore size.

2.2. Rheometry

A cement paste is a dense suspension that behaves like a yield stress fluid, which means that it can flow if a sufficient stress is applied on it. If a stress lower than the yield stress is applied, the material behaves like a solid, and an elastic modulus can be measured. If the stress is higher, the structure maintaining the paste breaks leading to a liquid behaviour. A critical deformation corresponds to the yield stress and will be used to understand the type of structure (long distance

interaction or short distance bond). Here, we focused on the solid behaviour of the cement paste and applied a constant low shear rate chosen in order to do a creep measurement.

In another study [2], two structures were observed in the cement paste with this method:

- A "smooth" structure which breaks at relatively high deformations (a few %), and which is characteristic of colloidal suspensions. In cement, this corresponds to the distant interactions between cement particles that allow the grains to form a percolation network in the paste.
- A brittle structure that breaks at lower deformations (0,05%) and which is associated to CSH precipitated at contacts between cement grains and thus forming brittle links.

It was observed that the yield stress in the structure at very low deformations increases with time of rest, as the CSH precipitate in the paste, while colloidal interactions are not modified. In order to follow the evolution of the structure of CSH, we decided to monitor the elastic modulus of the paste during setting. We applied deformation oscillations below the critical deformation of the brittle structure to measure the elastic modulus of the cement paste with time. Under such conditions, the evolution of the mechanical properties was monitored during setting without disrupting the structure. Elastic modulus increases continuously during the first 7 hours of the setting (fig.2).

3. INTERPRETATION

We can now compare our two previous methods (fig.2) and distinguish three phases during the setting of the paste.

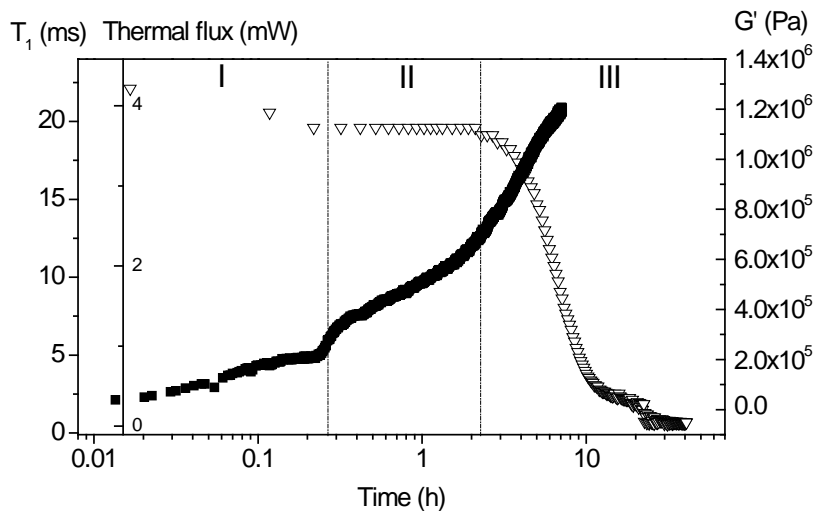


Figure 2. Evolution of porous structure (T_1 , empty triangles) and mechanical structure (G' , filled squares)

I: During this period, cement grains come in contact with each other and aggregate due to attractive forces between them [3]. This reorganization of the network due to attractive forces contributes to the slight decrease of pore size (T_1) as well as the strengthening of the material due to hydrates formed at contact points between cement particles (elastic modulus).

II: T_1 remains completely constant, which shows that there is no significant change in the porous structure, but the elastic modulus still increases. This could be explained by the precipitation of hydrates at the surface of cement grains, and particularly at the contact between cement grains, leading to the reinforcement of the structure. In this case, the porous structure is not impacted but the material still strengthens.

III: While hydration reaction starts and accelerates, T_1 value decreases sharply as hydrate start to precipitate in the pores. In fact, the development of hydrates is characterized by an increase of contact surface between water and solid structures and by a decrease of the volume of free water filling the pores. This explains the rapid decrease of the T_1 value. At the same time, we can observe a change of slope in the evolution of elastic modulus, which start increasing faster. This is the consequence of the precipitation of CSH in the pores, which increases contact surface between the grains and strengthens the structure.

The structural evolutions during setting can be summarized. (fig.3).

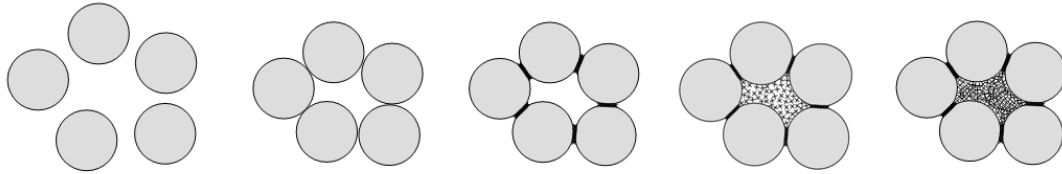


Figure 3. Structural evolutions during cement setting. Anhydrous cement grain is represented in grey, and the hydrates are represented by the black crosses. (a) represents the initial suspension of cement grains in water, (b) corresponds the formation of aggregates associated to step (I), (c) correspond to the strengthening at contact points between grains (II). (d) and (e) represent the progressive filling by hydrates during step (III).

4. CONCLUSIONS

Coupling NMR and rheometrical results give complementary results that provide information on the structure of the material during the successive steps of setting. These results were also in good agreement with isothermal calorimetry, which is a well known way to measure the energy released by cement hydration during setting. With these methods applied to lime-cement pastes, we were able, in a work in progress, to highlight and explain the significant impact of lime on cement setting.

REFERENCES

- [1] P. F. Faure, S. Rodts, « Proton NMR relaxation as a probe for setting cement pastes », *Magn. Reson. Imaging*, vol. 26, n° 8, p. 1183-1196, oct. 2008.
- [2] N. Roussel, G. Ovarlez, S. Garrault, C. Brumaud, « The origins of thixotropy of fresh cement pastes », *Cem. Concr. Res.*, vol. 42, n° 1, p. 148-157, janv. 2012.
- [3] S. P. Jiang, J. C. Mutin, A. Nonat, « Studies on mechanism and physico-chemical parameters at the origin of the cement setting. I. The fundamental processes involved during the cement setting », *Cem. Concr. Res.*, vol. 25, n° 4, p. 779–789, 1995.

Effects of the Composition and Amount of Paste on the Pumpability and Pump-stability of Flowable Concretes



Yared Assefa Abebe (M.Sc)
PhD Student
Institute of Building Materials Science
Leibniz Universität Hannover
E mail: yared.a@baustoff.uni-hannover.de



Prof. Dr.-Ing. Ludger Lohaus
Director of the Institute of Building Materials Science
Leibniz Universität Hannover
Appel Straße 9A, 30167 Hanover, Germany
E mail: Lohaus@baustoff.uni-hannover.de

ABSTRACT

Flowable concretes are generally susceptible to segregation, especially under the application of external forces like pumping pressures. In this paper, the influences of the composition and amount of pastes on the flowability, pumpability and pump-stability characteristics of concrete are presented. The amount of paste required for a specific aggregate composition was determined using the aggregates' paste requirement test. Subsequently, different paste compositions were used to investigate their influence on the pumpability and pump-stability of concrete using a pump resistance simulator (PuReSi) and a high pressure filter press (HPFP) respectively.

Key words: Rheology, Mix-design, Flowability, Pumpability, Pump-stability, Paste composition, Paste requirement

1. INTRODUCTION

The slender forms and immense heights of today's structures require concretes that are capable of flowing over long distances and through very tight spacing of reinforcements. Such flowable concretes are, however, very susceptible to segregation. This problem would further be aggravated with the application of pumping pressures, which might exacerbate the separation of the liquid phase (water or paste) from the solid phase (aggregates) paving the way for interlocking of the aggregates in the pumping lines /Kaplan, Larrard and Sedran 2005/. Design of a flow-able and yet stable concrete requires determining the right composition and amount of pastes for a specific aggregate composition. The paste content should be chosen in such a way that there is enough of it to coat the aggregates and to fill out the voids between them, also referred to as "excess paste volume" /Kennedy 1940/. Moreover, a certain amount of paste is needed as a lubricating layer to facilitate the movement of concretes in pumping lines. At the same time, the paste should be composed in such a way that it possesses the right properties so that the concrete has the desired flowability and stability, while satisfying the basic concrete design requirements such as maximum w/c ratio, minimum strength class etc. as required in the standards. In compliance with the segregation phenomenon that is more relevant to pumping (separation of the paste from the aggregates), the design of flowable concretes as introduced in this paper shall consider the concrete to be composed of a paste (Fines < 0,125 mm + Water + chemical admixtures) as the liquid phase and the combination of fine and coarse aggregates (particle size > 0,125 mm) as the solid phase.

2. EXPERIMENTAL INVESTIGATIONS

2.1 Paste characterisation

The flowability characteristics of the different paste compositions were investigated using the mini slump flow and packing density tests. The fines (V_F) are composed of CEM I 42,5 N cement (V_C) and fly ash (V_A) $\Rightarrow V_F = V_C + V_A$. Assigning the ratio $\frac{V_A}{V_C} = x \Rightarrow V_A = x \cdot V_C$ and $V_C = \frac{V_F}{1+x}$. The w/c-ratio of 0.6 is kept constant by using the following correlation with V_W/V_F .

$$w/c = \frac{\rho_w \cdot V_w}{\rho_c \cdot V_c} = \frac{\rho_w \cdot V_w}{\rho_c \cdot \frac{V_F}{1+x}} \Rightarrow \frac{V_w}{V_F} = \frac{w/c \cdot \rho_c}{1+x}$$

As shown in figure 1 (left), the flowability increases with increasing water – fines (V_W/V_F) and superplasticizer content (SP). However, there is a certain point from where a further increment, especially in SP, has no significant influence on the flowability. This point could be defined as the saturation point of SP /Cotardo and Hosni 2013/. Further addition of SP after this saturation point would instead lead to segregation of the paste. This saturation point can also be determined from the packing density tests as shown in fig.1 (right). After reaching the saturation point, the curves lie almost parallel to the saturation line, which theoretically indicates a complete filling of the voids with water /Wong and Kwan 2008/.

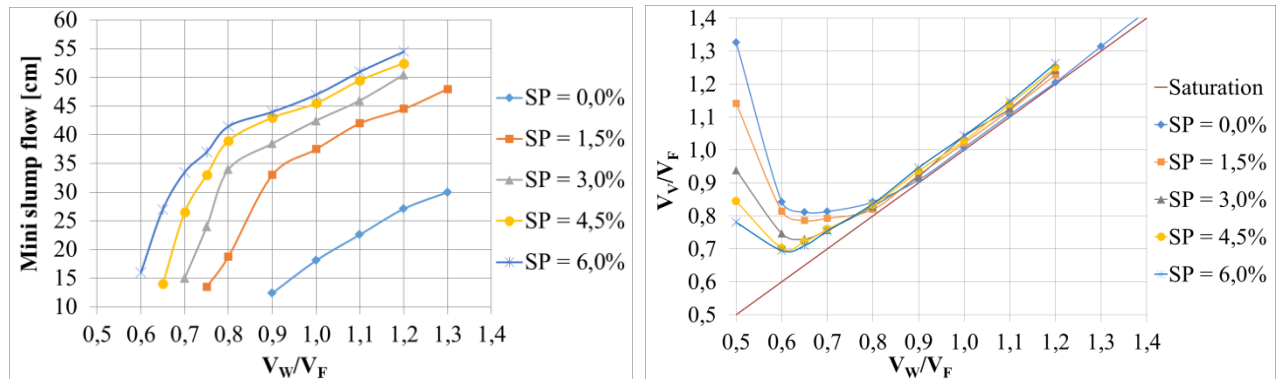


Figure 1 – Mini slump flow (left) and void ratio (right) for different V_W/V_F and SP combinations

2.2 Paste content determination

The type of aggregate used in this investigation has a maximum size of 8 mm with a gradation curve lying between the standard gradation curves A and B according to DIN 1045-2. The amount of paste that is needed to coat the aggregates and fill out the voids between them is determined using a test method developed for determination of paste volume for SCC /Huss 2010/. The dry aggregates in the container shall be completely filled with water and after a while the water will be completely sucked out. Afterwards, vibration will be applied in order to determine the maximum possible packing density of the aggregates. The mass difference between a wet aggregate (M_W) and a dry aggregates (M_D) gives the amount of water required to coat the aggregates' surface area (M_{WS}). $\Rightarrow [V_{WS} = M_{WS} = M_W - M_D]$.

Assuming that a saturated paste (V_P) comprises of water (V_W) and fines (V_F) $\Rightarrow [V_P = V_W + V_F]$ and based on the chosen water – fines ratio ($f = V_W/V_F$) from the mix design, a correlation could be found to determine the amount of paste needed to coat the aggregates surface (V_{PS}).

$$V_{PS} = V_{WS} + V_{WS}/f = V_{WS} (1+1/f) \quad (1)$$

The paste needed to fill the voids (V_{PV}) between the aggregates could be calculated by subtracting the absolute volume of the aggregate (V_G) from the total (bulk) volume (V_T).

$$V_{PV} = V_T - V_G \quad (2)$$

The total paste volume (V_P) is the sum of the paste needed to coat the aggregates surface (V_{PS}) and to fill the voids between them (V_{PV}).

$$V_P = V_{PS} + V_{PV} \quad (3)$$

As usual, a pore volume of 1.5 % – 2.0 % by volume of concrete is distributed proportionally between V_{PS} and to V_{PV} in the final calculation. A total paste volume of 385 dm³ was determined for the aggregate composition for a packing state based on vibration without additional weight.

2.3 Concrete pumpability and pump-stability characterisation

The pumpability properties are investigated using a specially developed pump resistance simulator (PuReSi) based on the principle of the sliding pipe rheometer /Kasten 2010/. It is equipped with a piston with built-in pressure sensor and a cable actuated position sensor. A pipe with a diameter of 125 mm will be filled with concrete directly above the pressure sensor to a height of 500 mm. Afterwards, three different weights of 20 kg, 40 kg and 60 kg shall be attached subsequently to the pipe in order to generate three different falling speeds, i.e. three different flow rates, thus enabling to establish a direct correlation between the flow rate (Q) and the pressure (P) /Yared and Lohaus 2014/.

The pump-stability or generally the stability of concrete under pressure is investigated using a high pressure filter press (HPFP). It has a diameter of 150 mm and a height of 300 mm. After setting up the HPFP in a compression machine, the applied load is increased linearly up to a maximum of 300 kN (ca. 170 bar) at a rate of 10 kN/min. Meanwhile, the amount of filtrate and the strain are measured continually.

Influences of paste composition

Despite the fact that all the four mixes shown in fig 2 have a comparable slump flow of about 620 mm, the mixes with lower V_W/V_F values and higher SP contents require significantly higher pressure for pumping. Moreover, the pressure requirement of these concretes increases drastically for an increased output. On the plus side, these mixes show the highest stability under pressure. This shows that finding the right mix for pumping is a delicate compromise between lowering the required pressure while attempting to attain a higher stability.

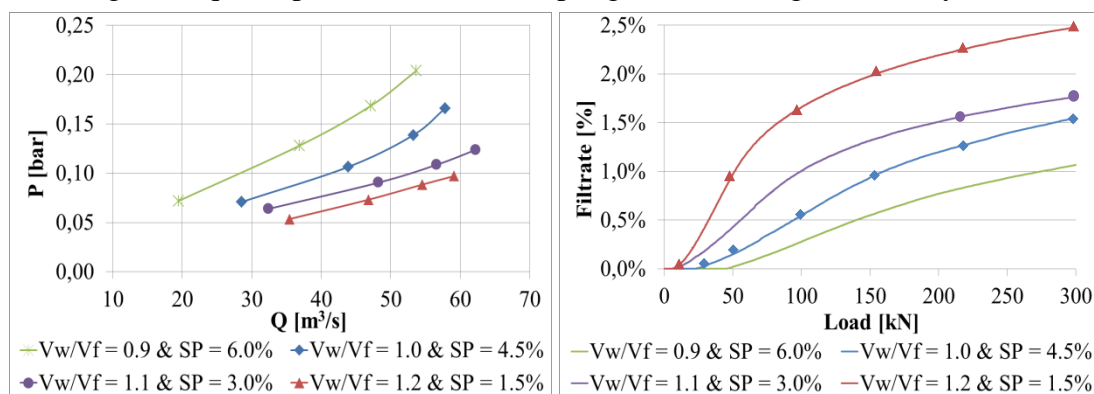


Figure 2
—
Influence
s of
 V_W/V_F
with
adjusted
SP

Influences of paste content

As shown in fig. 3, the effect of the different paste contents of 360, 385 and 410 dm³ with a constant $V_W/V_F = 1.0$ is not that much pronounced in relation to the required pressure. However, the stability of the concrete could be significantly undermined as a consequence

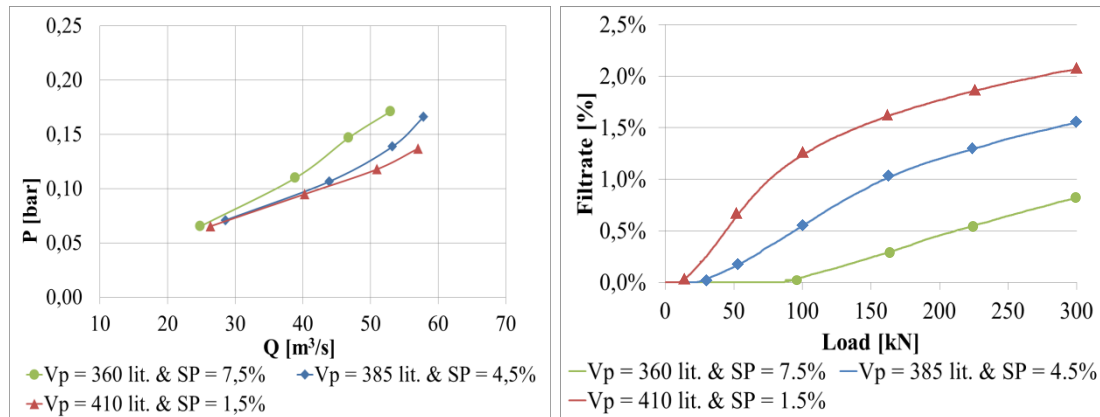


Figure 3 Influences of paste content with adjusted SP

3. CONCLUSION

The pastes in flowable concretes should generally reach a saturated state with the help of SP in order to guarantee the high flowability. However, the composition of the paste, even in the saturated state, could have significant influences on the pumpability and pump-stability of the concrete. As confirmed in the investigation, concretes exhibiting a similar slump flow could have completely different pressure requirements for the same flow rate. Generally, a favourable pumpability and pump-stability properties could be guaranteed by choosing a lower V_W/V_F value in combination with a higher SP content. In doing so, the paste content should be chosen in such a way that there is enough of it to satisfy the total paste demand of the aggregates. To this end, the applied investigation methods are of great importance to characterize and optimize flowable concretes with respect to their pumpability and pump-stability characteristics.

REFERENCES

- Cotardo, D., Hosni, A., 2013
 “Entwurfs- und Optimierungsstrategien für pumpfähigen Beton”, Diplomarbeit, Institut für Baustoffe, Leibniz Universität Hannover, 2013, in German
- Huss, A., 2010
 “Mischungsentwurf und Fließeigenschaften von Selbstverdichtendem Beton (SVB) vom Mehlkorntyp unter Berücksichtigung der granulometrischen Eigenschaften der Gesteinskörnung”, PhD Thesis, 2010, in German
- Kaplan, D., Larrard, F. d., Sedran, T., 2005
 “Avoidance of blockages in concrete pumping process”, ACI Material Journal, Vol. 102 No. 3, 2005 pp. 183 - 191
- Kasten, K., 2010
 “Gleitrohr-Rheometer - Ein Verfahren zur Bestimmung der Fließeigenschaften von Dickstoffen in Rohrleitungen”, PhD Thesis, TU Dresden, Shaker Verlag, ISBN 978-3-8322-9265-2, 2010, in German
- Kennedy, C., 1940
 “The design of concrete mixes”, ACI Journal Proceedings, Vol. 36, 1940, pp. 373-400
- Yared A. Abebe, Lohaus, L., 2014
 “Optimization and design strategies for pumpable, flowable and stable concretes”, 10th fib international PhD Symposium in civil engineering, Quebec, Canada
- Wong, H.H.C., Kwan, A.K.H., 2008
 “Packing density of cementitious materials: part 1 - measurement using a wet packing method”, Materials and Structures, Volume 41, Issue 4, 2008 pp 689-701

CRACKING, CREEP AND REPAIR

Analyses of Minimum Reinforcement for Crack Control



Prof. Dr. Mikael Hallgren
 Division of Concrete Structures
 KTH Royal Institute of Technology and Tyréns AB
 SE-144 00 Stockholm / SE-118 86 Stockholm
 E-mail: mikael.hallgren@tyrens.se

ABSTRACT

In order to control the width of a crack, a minimum amount of reinforcement has to be applied. Eurocode 2 gives a simple equation for calculating the required reinforcement for this purpose. However the equation may yield very high amounts of reinforcement. This paper presents a study where the effect of different amounts of minimum reinforcement has been tested in a series of numerical analyses. Based on the result of these analyses and on comparisons with Eurocode 2, Model Code 1990 and the previous Swedish code BBK04, a proposed modification of the Eurocode equation is presented.

Key words: Cracking, Minimum Reinforcement, Shrinkage, Non-linear Finite Element Analyses, Eurocode, Structural Design

1. INTRODUCTION

The minimum reinforcement to control cracks due to restrained shrinkage can be defined as the minimum amount of reinforcement required to distribute the imposed deformation to new cracks before the reinforcement which crosses the first crack yields. According to Eurocode 2, EN 1992-1-1, the minimum reinforcement required to control cracking can be expressed as:

$$A_{s,\min} = k_c \cdot k \cdot \frac{f_{ctm}}{f_{yk}} \cdot A_{ct} \quad (1)$$

where A_{ct} is the cross-sectional area of concrete in tension just before cracking
 f_{ctm} is the mean value of tensile strength of concrete
 f_{yk} is the characteristic yield strength of reinforcement
 k_c is a coefficient which takes account of the stress distribution within the section immediately prior to cracking. For pure tension $k_c = 1.0$
 k is a coefficient which allows for the effect of non-uniform self-equilibrating stresses, which lead to a reduction of restraint forces: $k = 1.0$ for webs with depth $h \leq 300$ mm and $k = 0.65$ for webs with depth $h \geq 800$ mm. Intermediate values may be interpolated.

This gives an equation which appears to be based on a physical model and which is easy to use for design. However, in the case of restrained shrinkage, A_{ct} is the area of the whole cross section in the structural member. Compared with previous national codes in many EU countries, Eq. (1) will then yield a much higher amount of minimum reinforcement for thick cross sections. This has raised the question in the construction industry whether the Eurocode equation is reasonable or not.

Eq. (1) is originally based on the CEB/FIP Model Code 1990. However, in Model Code 1990 the value of k is 0.8 for $h \leq 300$ mm and k is 0.5 for $h \geq 800$ mm, with interpolation for intermediate values of h . Eurocode 2 has, hence, introduced more conservatism.

In the previous Swedish Code BBK04, the minimum reinforcement for crack control was calculated on the basis of the effective concrete area $A_{ct,ef}$ instead of the whole cross-sectional area A_{ct} . $A_{ct,ef}$ is the area which is directly controlled by the reinforcement bar, i.e. the effective tension area which is equal to a height, which is twice the concrete cover plus the bar diameter, times the width of the cross section considered. Compared to Eq. (1), the coefficients k_c and k are both set equal to 1 in the corresponding BBK04 equation.

2. NUMERICAL SIMULATIONS

A series of numerical simulations of cracking of slabs due to restrained shrinkage (e.g. autogenous, drying and temperature shrinkage) were performed in the frame of a master thesis by Björnberg and Johansson (2013), who were supervised by the author of the present paper. The analyses were made with the non-linear finite element method based on the smeared crack approach. The material models included the non-linear behavior of concrete with cracking based on fracture mechanics, the non-linear behavior of reinforcement steel with plastic yielding and the bond slip between concrete and reinforcement.

Figure 1 shows the 2D model used for the simulations. The total depth of the slab, the concrete cover, the bar diameter, the bar spacing and the concrete strength class were varied. The spacing was calculated according to the requirements of minimum reinforcement in Eurocode 2, Model Code 1990 and a modified BBK04 equation were the effective tension area as given in Eurocode 2 was used. Based on the results, additional analyses with minimum reinforcement according to a proposed modification of the Eurocode 2 equation as presented in section 3 below were run. Altogether, 138 numerical simulations were performed.

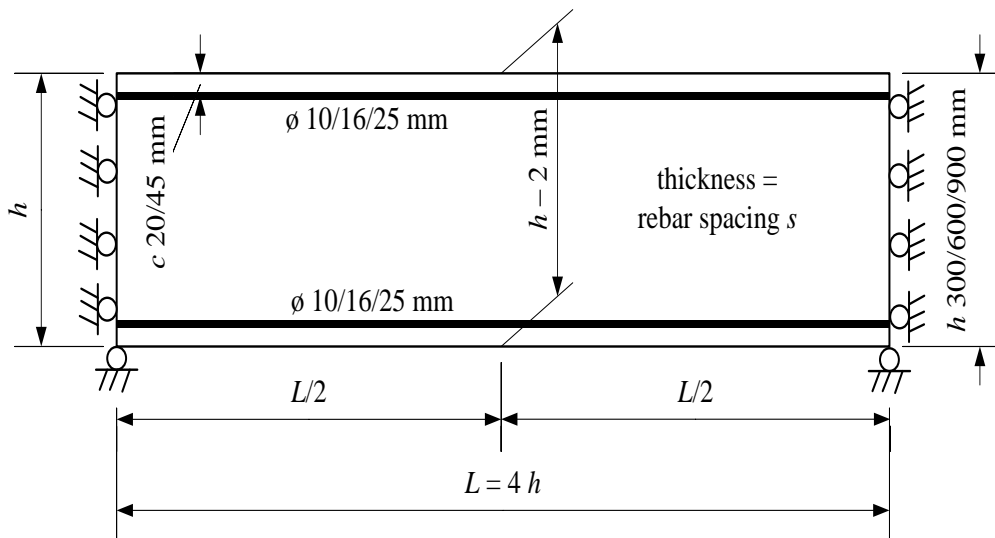


Figure 1 – 2D model used for the numerical simulations

Figure 2 shows some examples of the results. Three slab models with minimum reinforcement according to Eurocode 2 (EC2), Model Code 1990 (MC90) and the modified BBK04, respectively, were subjected to restrained shrinkage up to 1.6 ‰. In the models with minimum reinforcement according to EC2 and MC90, the reinforcement managed to distribute the

restrained shrinkage to new cracks. In the case according to the modified BBK04 method based on the effective tension area, the amount of reinforcement was not enough to redistribute the deformation to new cracks and the first crack grew wider.

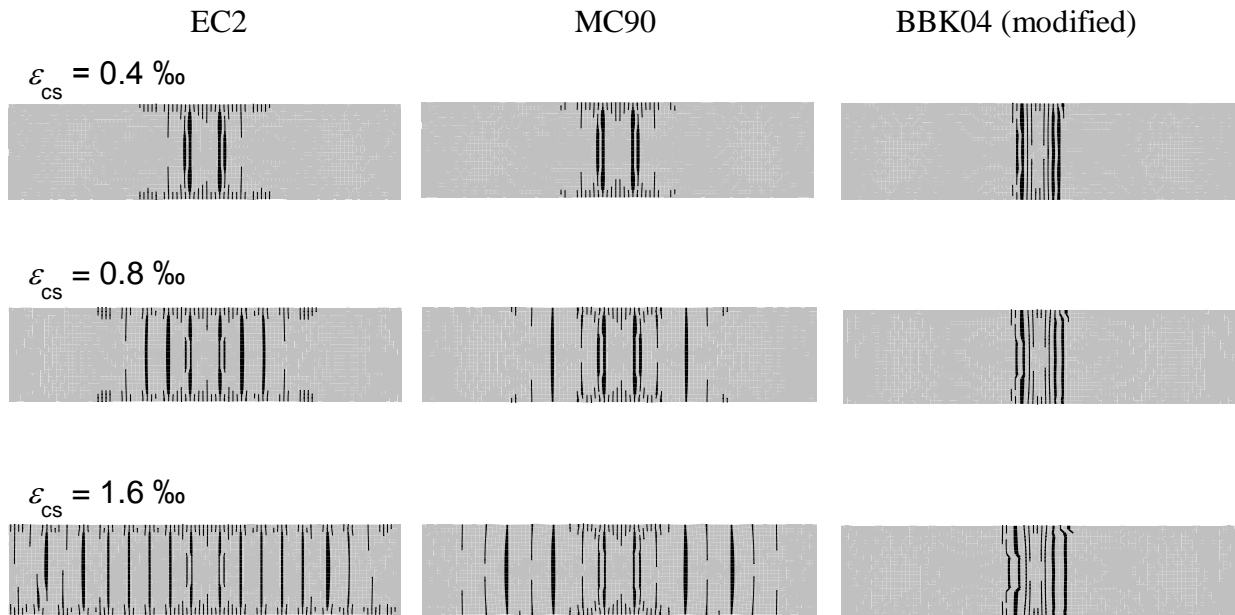


Figure 2 – Crack pattern slabs with minimum reinforcement according to the different codes and at various levels of shrinkage ε_{cs} . Example with slab depth $h = 600 \text{ mm}$, concrete C35/45, rebars $\phi 16 \text{ mm}$ and concrete cover $c = 20 \text{ mm}$.

In reason why the models with minimum reinforcement according to the method based on the effective tension area could not redistribute the deformation from the shrinkage to new cracks was that the reinforcement reached its yield strength in the section of the first cracks and before new cracks developed. In the models with minimum reinforcement according to EC2 and MC90, the stress in the reinforcement never reached the yield strength.

3. PROPOSED MODIFICATION OF THE EC2 EQUATION

Although the numerical simulations indicated that the choice of minimum reinforcement according to the Eurocode 2 equation was safe, the amount of required reinforcement for thick slab seemed to be unreasonably high. In order to check if it was possible to decrease the amount of required reinforcement, additional simulations with a modified Eurocode 2 equation were performed. The modification consisted of a proposed change of the coefficient k in Eq. (1), where the value of k is 0.9 for $h \leq 200 \text{ mm}$ and k is 0.4 for $h \geq 800 \text{ mm}$, with interpolation for intermediate values of h .

The proposal decreases the amount of required reinforcement for thick cross sections significantly. However, the additional numerical analyses with models based on the proposed modification of Eurocode 2 showed that this amount of reinforcement is sufficient to redistribute the shrinkage deformation to new cracks. Hence, the minimum reinforcement according to the proposal manages to give the required crack control.

Figure 3 shows the amount of minimum reinforcement according to the various methods as a function of the depth of the cross section. Two graphs are shown for cases with 20 mm concrete cover and 45 mm concrete cover, respectively. This illustrates the effect of concrete cover on the

minimum reinforcement according to BBK04. Furthermore, the proposed modification of the Eurocode 2 equation reduces the amount of minimum reinforcement with about 40 % for thick cross sections while still performing as required for crack control.

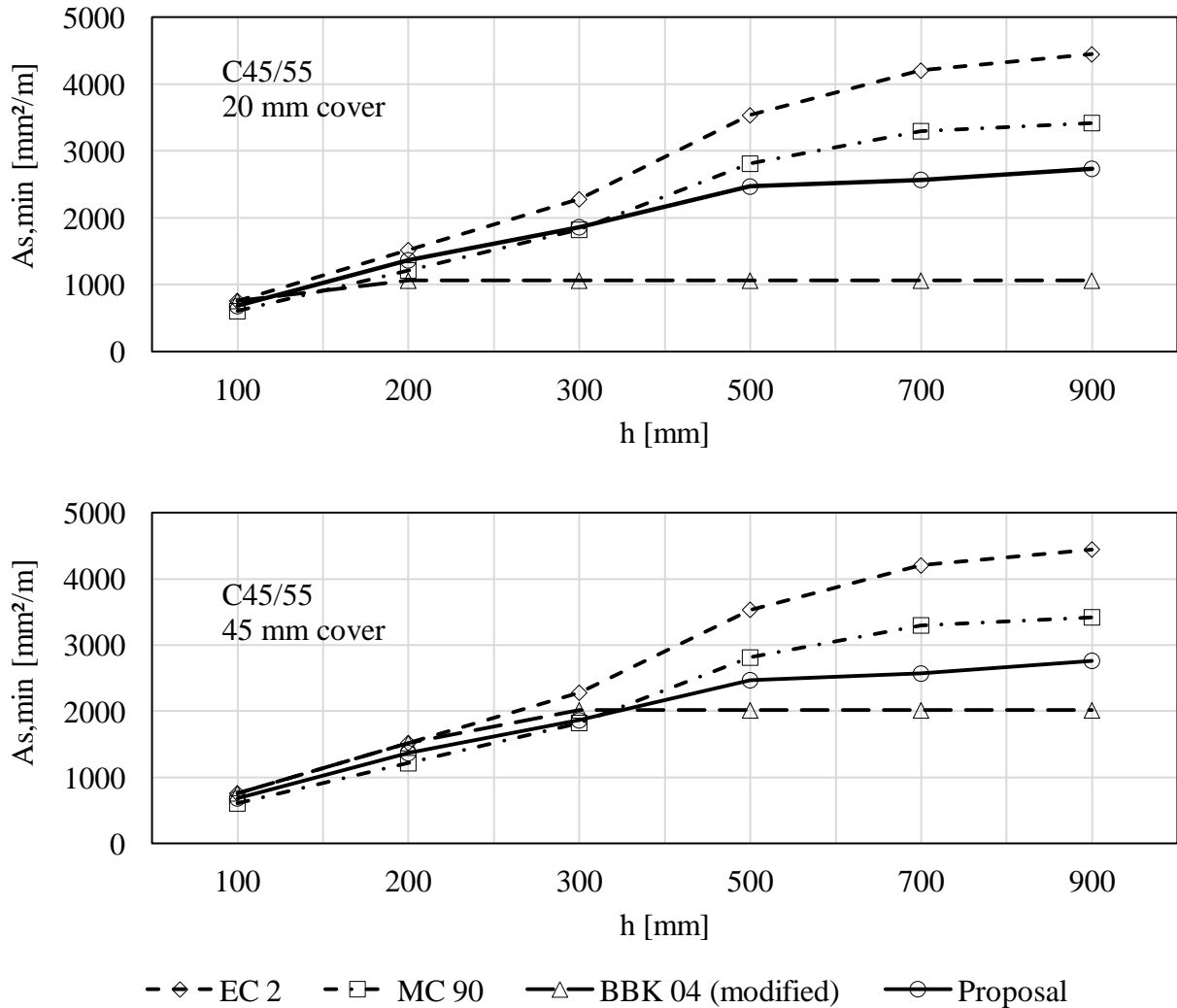


Figure 3 – Minimum reinforcement $A_{s,min}$ as function of the cross-sectional depth h for two different thicknesses of the concrete cover. Concrete strength class C45/55 in both cases.

4. CONCLUSIONS

The numerical analyses indicated that the demand of minimum reinforcement for crack control according to Eurocode 2 is too conservative for thick cross sections while the corresponding requirement according to BBK 04 may lead to extensive cracking without crack control, especially in cases with small concrete cover. The proposed modification of the coefficient k in the EC2 equation reduces the amount of reinforcement significantly. The numerical analyses indicate that the proposed modification still gives the required crack control.

REFERENCE

Björnberg M. & Johansson V., 2013

“Numeriska simuleringar av betongkonstruktioner med minimiarmering för sprickbredds-begränsning (in Swedish)”, TRITA-BKN, Master Thesis 387, Concrete Structures, KTH Royal Institute of Technology

Slabs on Ground Subjected to Concentrated Loads



Jan Arve Øverli
 Associate Professor, Ph.D
 Department of Structural Engineering
 Norwegian University of Science and Technology
 7491 Trondheim, Norway
 E-mail: jan.overli@ntnu.no

ABSTRACT

An experimental program is presented where a slab on ground was subjected to concentrated loading at the centre, the edges and at the corners. The concentrated loads introduced a radial crack pattern at the bottom of the slab and circular cracks formed at the top surface at some distance from the loaded area. The governing failure mechanism was a combination of bending and punching failure. Analytical solutions for the ultimate load capacity fit well with the results obtained in the tests.

Key words: Testing, cracking, structural design.

1. INTRODUCTION

Slabs on ground are often subjected to demanding service conditions. For industrial slabs and floors in buildings the owner and the builder often require crack free surfaces. Hence, in addition to have enough load capacity, it is important to keep control of cracking and crack widths. Typical loading which influence both serviceability and load capacity are concentrated loads from vehicles, columns or leg loads from storage platforms. From a structural point, slabs on ground are large planes lying on continuous support. The maximum bending moments are directly under the concentrated loads and introduce a radial crack pattern at the bottom of the slab. At higher load levels, circular cracks forms at the top surface at some distance from the loaded area. The response of the slab depends on many factors, e.g. loaded area, slab size, subgrade stiffness. These have been extensively investigated experimentally (Beckett 1990, Falkner, Huang and Teutsch 1995) and theoretically by many researchers (Westergaard 1948, Meyerhof 1962, Shentu, Jiang and Hsu 1997, Al-Nasra and Wang 1994, Losberg 1978, Rao and Singh 1986).

Design of slabs on ground are normally based on either elastic or plastic methods. In situations where cracking is unacceptable elastic methods should be used while plastic methods could be used in slabs where controlled cracking is acceptable. According to elastic theory, the problem was solved for concentrated loading by Westergaard (Westergaard 1948), when the loading was uniformly distributed over a small circular area. At ultimate limit state (ULS) the resistance of slabs subjected to concentrated loading is governed by bending failure, bearing strength or punching failure. Bending capacity can be calculated by means of conventional yield line theory. Meyerhof developed design equations for concentrated internal, edge and corner loads (Meyerhof 1962). The governing failure mechanism is cone-shaped with radial yield lines (from the loaded area) and a circular yield line forming some distance away from the loaded area

The aim of this study was to investigate slabs on ground subjected to concentrated loading. An experimental program was set up to find static capacities and to study the formation of cracks. Static load carrying capacities were compared to yield line solutions. The experimental work has

been carried out as part of a master thesis project at the Department of Structural Engineering at Norwegian University of Science and Technology (Heggen and Seglem 2010).

2. EXPERIMENTAL PROGRAM AND RESULTS

The experimental program covers one slab. This slab was subjected to loading at the centre, at two edges and two corners. The loading area on the slab was 100×100 mm. Due to the very locale response of a concentrated load, failure at one location in slab has only minor influence on the subsequent failure loads at the other locations. The slab had a square geometry with dimensions 3500×3500 mm. To simulate a larger slab, three points along each edge of the slab were fixed against vertical deformation. The thickness of the slab was 120 mm. A layer of 100 mm of insulation, Jackofoam 400 XPS, represented the supporting soil. The insulation was tested in compression and had a stiffness of approximately 0.15 N/mm³. A plastic sheet between the slab and insulation minimised the friction and moisture transportation

The slab is reinforced with orthogonal longitudinal reinforcement at both top and bottom with 10 mm bars with distance 155mm. The concrete cover was 20 mm. In order to control the mechanical properties, cylinders were casted to evaluate the compressive strength. The mean values obtained after 28-day of curing was 32.1 N/mm² for the compressive strength and 26727 N/mm² for the modulus of elasticity. To capture the structural response of the slab the deformation and strains must was measured. To apply the static loading, a hydraulic jack was used together with a control computer. To transfer the load from the hydraulic jack, a steel prism was used as the loading area. Between the jack and prism specimen, a ball-and-socket joint was placed to avoid bending moments in case of inclined loading. During testing the load was incremented with steps of 20 kN to allow for inspection and marking of cracks.

The failure loads, P_{fail} , in the experiment together with the observed load level at cracking at the top surface and at the cross section edges of the slab are given in Table 1. To verify and validate the failure loads, comparison is made in the table with the yield lines solutions and the punching resistance according to Eurocode 2 (Standards Norway 2008).

Table 1 – Test results and calculated failure loads

| Load [kN] | Centre load | Edge load 1 | Edge load 2 | Corner load 1 | Corner load 2 |
|-------------------|----------------|----------------------|----------------------|-----------------------|------------------------|
| Crack top surface | 325 | 80 | 85 | 33 | 30 |
| Crack edge | - | 35 | 40 | 40 | 40 |
| P_{fail} | 390 | 153 | 140 | 70 | 52 |
| Failure type | punching | bending/ punching | bending/ punching | anchoring/ bending | anchoring/ punching |
| P_{yield} | 348 | 161 | 161 | 48 | 48 |
| $P_{punching}$ | 302 | 227 | 227 | 151 | 151 |

The main goal in this study was to study the bending behaviour of the slab. However, the ultimate capacity of the slab was governed by other failure mechanisms, like punching and anchoring or a combination of mechanisms, as seen in Table 1. In the slabs governed by punching a distinct cone was visible. An indication of anchoring problems was the observed horizontal cracks along the longitudinal reinforcement. The calculated yield line and punching capacities indicates a punching failure for the centre load and bending failure for edge and corner loads, which to a certain extent is confirmed in the tests.

Figure 1 shows the observed cracking at the top surface and the failure mechanism for the different loading. The failure mechanism for the centre load was a punching compression failure. The steel loading prism was pushed straight through the slab without any cracking close to the loading at the top surface. Only minor cracking was observed at the top surface during loading.

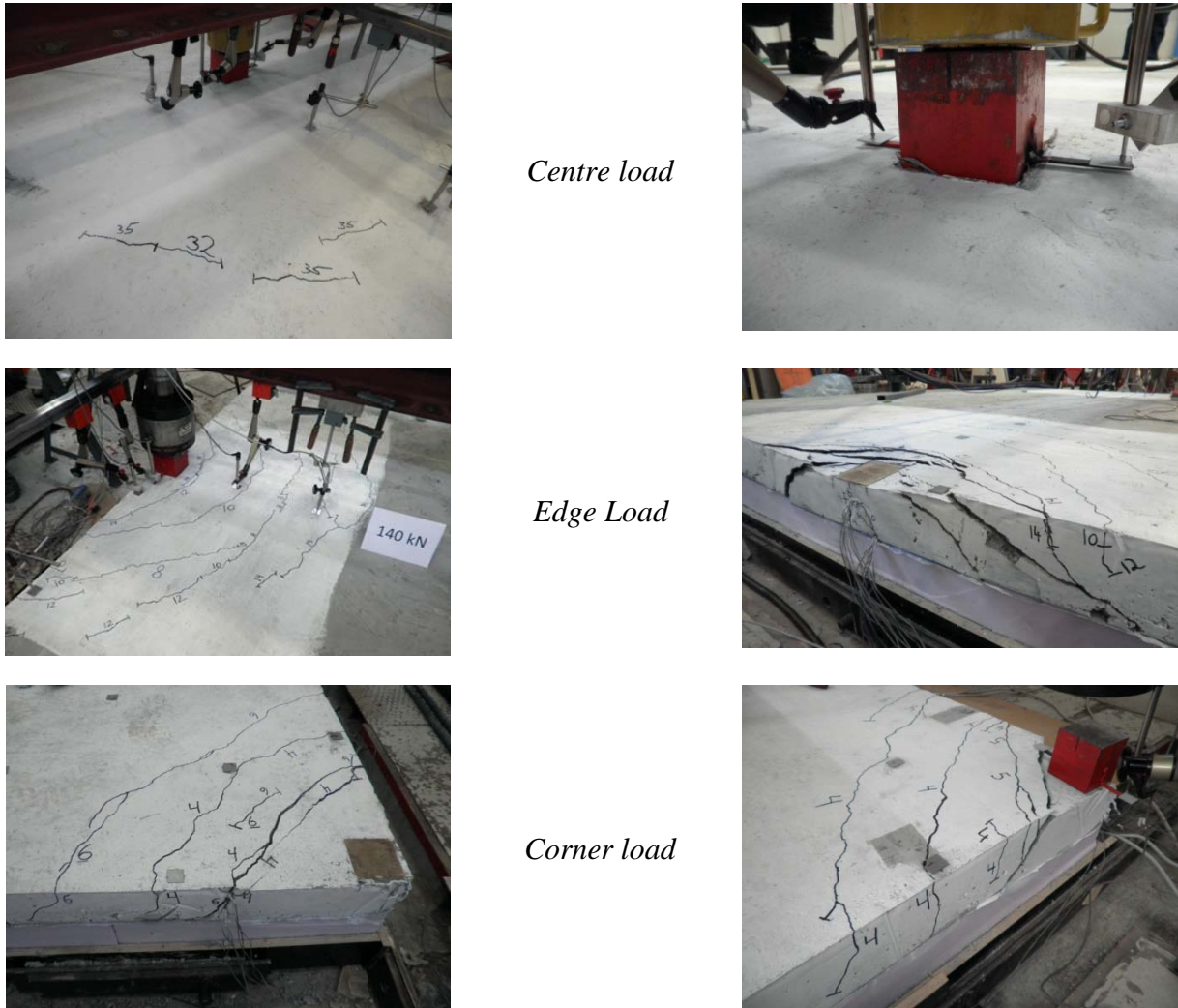


Figure 1 – Crack patterns and failure for centre, edge and corner load.

For the edge load circular cracks formed at the top surface as expected. The first crack occurred approximately 500 mm from the edge towards the centre of the slab. With increasing loading, new cracks formed closer to the loading area. This is in accordance with redistribution of forces closer to the loaded area, as the slab starts to crack. The failure mechanism looked like a combination of a bending and a punching failure. For the corner loads the top surface cracking started along the diagonal from the corner, before being extended to the corner edges. For corner load 1 while corner load 2 was a combined punching/anchoring failure much closer to the loaded area than load 1, as seen in Figure 1. The observed response of the slabs was confirmed by the measured displacements and strains.

3. CONCLUSIONS

In this study a concrete slab on grade was subjected to concentrated centre, edge and corner

loads. The main goal was to study the formation of cracks on the top surface which often is of concern in this type of structure. The response of the concrete slab was as expected; in fact, circular cracks formed at the top surface some distance away from the loading area, which is in agreement with linear elastic theory for slabs on elastic foundation. The failure mode was governed by punching for the centre load, a combined bending/punching for the edge load and anchoring/punching for the corner loads. The capacities were in agreement with requirements for punching in design codes and traditional yield line solutions for bending failures.

ACKNOWLEDGEMENT

The author would like to gratefully acknowledge The Norwegian Concrete Association (Norsk Betongforening) for financial support to the experimental program and M.Sc Runar Heggem and M.Sc Frode Seglem for carrying out the experimental work as part of their master thesis.

REFERENCES

- Al-Nasra, M. & L. R. L. Wang (1994) Parametric study of slab-on-grade problems due to initial warping and point loads. *ACI Structural Journal*, 91, 198-210.
- Beckett, D. (1990) Comparative tests on plain, fabric reinforced and steel reinforced concrete ground slabs. *Concrete*, 24, 43-45.
- Falkner, H., Z. Huang & M. Teutsch (1995) Comparative study of plain and steel fiber reinforced concrete ground slabs. *Concrete International*, 17, 45-51.
- Heggen, R. & F. Seglem. 2010. *Ground bearing slabs subjected to concentrated loads*. Trondheim, Norway: Norwegian University of Science and Technology.
- Losberg, A. (1978) Pavements and slabs on grade with structurally active reinforcement. *ACI Journal Proceedings*, 75, 647-657.
- Meyerhof, G. G. (1962) Load-carrying capacity of concrete pavements. *Journal of the Soil Mechanics and Foundations Division*, 88, 89-116.
- Rao, K. & S. Singh (1986) Concentrated Load-Carrying Capacity of Concrete Slabs on Ground. *Journal of Structural Engineering*, 112, 2628-2645.
- Shentu, D. Jiang & Hsu (1997) Load-Carrying Capacity for Concrete Slabs on Grade. *Journal of Structural Engineering*, 123, 95-103.
- Standards Norway. 2008. *NS-EN 1992-1-1:2004+NA:2008. Eurocode 2: Design of concrete structures - General rules and rules for buildings*. Norway: Standards Norway.
- Westergaard, H. M. (1948) New formulas for stresses in concrete pavement of airfield. *Transactions of ASCE*, 113, 425-444.

Effect of the Boundary Conditions on the Crack Distribution in Early Age Concrete



Majid Al-Gburi ^{a, b}

M. Sc. Ph.D. Student

^a Luleå University of Technology

Division of Structural and Construction Engineering

^b Lecturer in University of Mosul- Iraq

E-mail: Majid.Al-Gburi@ltu.se



Jan-Erik Jonasson

Tech. Dr., Professor

Luleå University of Technology

Division of Structural and Construction Engineering

E-mail: Jan-Erik.Jonasson@ltu.se



Martin Nilsson

Tech. Dr., Lecturer

Luleå University of Technology

Division of Structural and Construction Engineering

E-mail: Martin.Nilsson@ltu.se

ABSTRACT

Restrained movement in early age concrete may cause cracking. The boundary conditions – restraint – influence the possible crack distribution. This study aims at highlighting the effect of such restraint on the crack distribution. This is done by using the “Cracking Model for Concrete” in ABAQUS/Explicit simulating the non-linear behaviour under and after cracking. In the study the typical case wall-on-slab was in focus using a structure previously been tested in laboratory with both fixed and free bottom slab. The result of the modelling shows fairly good agreement with the cracks observed in the tests.

KEY WORDS – Restraint, through cracking, early age concrete, wall-on-slab.

1. INTRODUCTION

Cracking in concrete due to volume changes at early age during the hydration process is one of the major causes of initial defects and structural performance weakening during the service life of concrete structures. Thermal stresses are the result of temperature and moisture strains that are restrained during the hardening process. Cracking originates either from different expansions (due to temperature gradients inside the young concrete) during expansion phase or by restraint from the adjacent structure during the contraction phase. Prevention and limitation of early age cracking is of big importance /Al Gburi et al. 2012/.

To control and limit undesirable effects on the durability and performance of concrete structures, possible cracking due to thermal stress have to be evaluated accurately in the design stage. The analysis helps engineers modify the constructional procedures, arrange construction joints and change the concrete mix design, which can decrease the thermal movement (peak and different temperature), autogenous shrinkage and the restraint; increase the tensile strain capacity, to ensure proper confinement of concrete structures under the environmental conditions at a particular site /Emborg and Bernander, 1994/.

The purpose of the present work is to evaluate the crack distribution at early age and give ideas to designers and the engineers about the concrete behaviour and cracks that might appear in early age concrete due to changes of the boundary conditions. This can then be considered as a relevant help in the process of choosing appropriate concrete and construction techniques in addition to site measures like cooling pipes and reinforcement distribution to prevent or limit cracking. The work includes the effect of temperature variation and restraint from the ground by studying the typical case wall-on slab. The results are compared with previous experimental works, which showed huge influence of boundary conditions on the development of early age cracks /Nilsson, 2000/.

2. STRESS DEVELOPMENT AT EARLY AGE

The development of early-age thermal stresses can be described by studying the concrete element in Figure 1a), which is fully restrained in a uniaxial stress state and with heat development similar to the temperature profile shown. During the temperature raise, the stiffness of the concrete increases coupled with increasing compressive stresses. When the maximum temperature is reached, the hydrating concrete paste is still developing, and the strength of the concrete is relatively low /Nilsson 2003/.

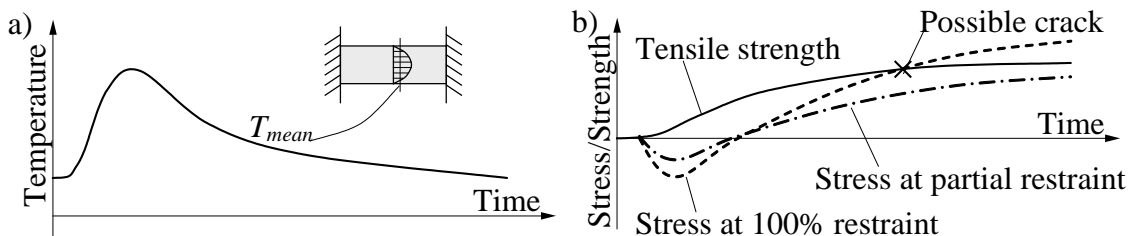


Figure 1 – Illustration of average temperature in young concrete and possible through cracking for different restraint conditions /Nilsson 2003/.

Figure 1-b shows, that during the cooling phase tensile stresses are generated if the movement of the concrete is restrained. These stresses may cause cracking if they exceed the tensile strength of the concrete. The magnitude of the thermal stresses depends on the temperature development and the ambient temperature, the restraint conditions, the moisture content as well as the

concrete properties such as the coefficient of thermal expansion, the shrinkage, and the creep-adjusted modulus of elasticity.

3. METHOD OF CALCULATION

The computer program ABAQUS/6.12, which is an FE based program, is used in this study. This software offers an option to model concrete called “Cracking Model for Concrete” (CMC), which is only available in ABAQUS/Explicit. This is a special purpose analysis technique that uses an explicit dynamic FE formulation. Although developed for dynamic problems, the explicit version is very effective in highly non-linear problems under static loading /Kianousha et al. 2008/. In this study, CMC is used to simulate the non-linear behaviour of concrete under and after cracking. The model assumes that the primary forces in the structure are tensile and that the compressive forces are relatively small. For this reason, the non-linearity of concrete in compression is ignored. Since volumetric induced strains in concrete are mostly tensile and the tensile strength is low, it is very likely that cracking occurs in the concrete. The model includes the temperature variations, tension stiffening and shear retention in the concrete. The weak point in this model is that it assumes that the cracks start when the principle stress reaches the tensile capacity.

4. RESULTS AND DISCUSSION

In /Nilsson 2000/ a laboratory study was reported of walls on slabs under different boundary conditions. On a pre-cast slab (8 m long, 1.4 m wide and 0.2 m high) a concrete wall was cast (5.8 m long, 0.15 m thick and 1.15 m high). In the wall, steel pipes \varnothing 25 mm were cast horizontally in where hot and cool water later were used to simulate the hydration of the concrete. After the concrete wall was cast and its hydration was finished the formwork was removed. Then the steel pipes were used and the temperature was risen to 43 °C and then lowered to 15 °C. By removing the formwork and using hot and cool water to simulate the hydration in the concrete it was possible to see when cracks appeared in the wall.

Two boundary conditions were used; in the first case the slab was fixed to the floor by bolts, in the second the slab was free. In the first wall being tested /Nilsson 2000/ five through cracks were found in the wall and two in the joint between the wall and the footing, see Figure 2. The similar cracking was observed by the modelling. Two of the cracks went all the way from near the joint at the bottom to the top of the wall. Two cracks were visible at the base of the wall reaching half height of the wall. The second through crack was found after the end of the test.

In the second wall being tested /Nilsson 2000/ one through crack was found in the wall, see Figure 3. No cracks were found in the prediction model. The stress level was changed compared to the first case it was close to the tensile strength of the concrete.

Cracking during the contraction phase of a young concrete member cast on an older one very much depends on the boundary conditions; see Figures 2 and 3, but also the joint between the members. If the joint is very strong and contains a lot of through reinforcement, it is capable to transfer the counteraction (restraint) of the free movements from older members to younger ones. On the other hand, if there is a slip in the joint, the restraint stresses are reduced as well as the risk of cracking /Nilsson 2000/. One possible measure to decrease the boundary restraint is to use a bitumen or thin (10 mm) sand layer under the slab to allow movements and reduce the crack risk.

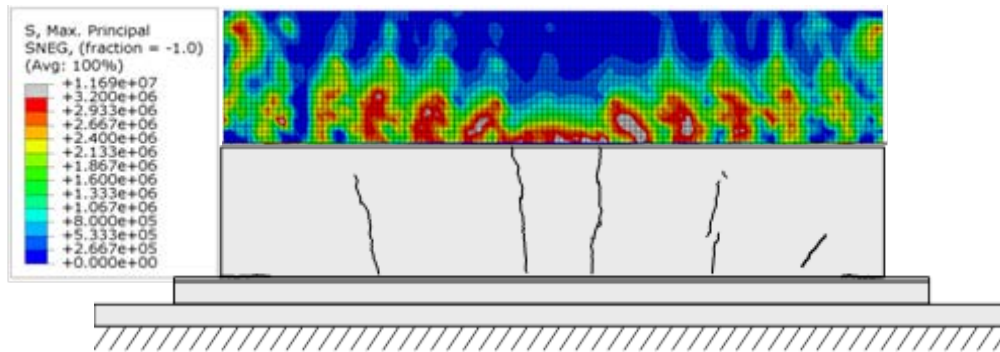


Figure 2 – Results from tests and modeling of cracking in joint and wall at fixed boundary below the slab.

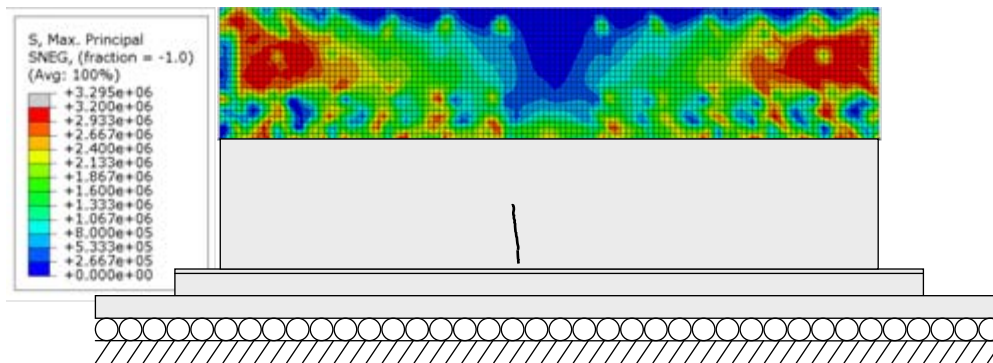


Figure 3 – Results from tests and modelling of cracking in joint and wall at free boundary below the slab.

5. CONCLUSIONS

This study shows that the prediction of cracking in the typical case wall-on-slab subjected to volumetric deformation can be predicted numerically with a reasonable accuracy. The effect of different boundary conditions on the crack development is investigated using the proposed modelling. The main objective of this study was to evaluate the crack distribution at early age and discuss how to avoid these cracks.

REFERENCES

- Al-Gburi, M., Jonasson, J-E., Nilsson, M., Hedlund, H., Hösthagen, A., 2012, “Simplified methods for crack risk analyses of early age concrete part 1: development of equivalent restraint method”, Nordic Concrete Research publication, No.46, 2/2012, 17-38.
- Emborg, M., and Bernander, S., 1994, “Assessment of the risk of thermal cracking in hardening concrete”, Journal of Structural Engineering (ASCE), Vol.120, No 10, October 1994, 2893-2912.
- Kianousha, M.R., Acarcanb, M, Ziari, A., 2008, “Behavior of base restrained reinforced concrete walls under volumetric change”, Engineering Structures, 30, 2008, 1526–1534.
- Nilsson, M., 2003 “Restraint Factors and Partial Coefficients for Crack Risk Analyses of Early Age Concrete Structures”, Luleå, Sweden, Division of Structural Engineering, Luleå University of Technology. Doctoral Thesis 2003, 170 pp.
- Nilsson, M., 2000, “Thermal Cracking of Young Concrete- Partial Coefficients, Restraint Effects and Influence of Casting Joints”, Division of Structural Engineering, Luleå University of Technology, Licentiate Thesis 2000:27, pp. 267.

Plastic Shrinkage Cracking in Concrete: Research in Scandinavia



Faez Sayahi
Ph.D. Student
Div. of Structural Engineering
Luleå University of Technology, LTU
971 87 Luleå, Sweden.
faez.sayahi@ltu.se



Mats Emborg
Professor LTU/Head R&D Betongindustri AB
971 87 Luleå, Sweden. / Betongindustri AB, 100 74 Stockholm, Sweden
mats.emborg@betongindustri.se
mats.emborg@ltu.se



Hans Hedlund
Professor LTU/Skanska Teknik AB
971 87 Luleå, Sweden/Skanska AB, 405 18 Göteborg, Sweden
hans.hedlund@ltu.se
hans.hedlund@skanska.se

ABSTRACT

As plastic shrinkage cracking still causes considerable repair costs annually, an understanding of the phenomenon is essential to prevent these damages in the future. In the paper, the status of present technology to avoid cracking is briefly reported through referring to research conducted in Scandinavia. In addition, on-going activities at LTU are described and future plan is demonstrated. Thus, experiments are performed on concrete slabs cast in rectangular moulds and cured at some variations of environmental conditions. The results will be used to find critical evaporation rate at very early age.

Keywords: Plastic Shrinkage, Cracking, Concrete, Evaporation.

1. INTRODUCTION

Crack-free concrete structures are needed, in order to ensure high level of durability and functionality, since cracks accelerate the ingress of harmful materials that might cause damage in future (i.e. corrosion of the reinforcement). Plastic shrinkage cracking is the first type of cracks occurring directly after placing the concrete, sometimes even before the final setting /Schmidt & Slowik 2013/. This type of cracking mainly occurs on horizontal concrete surfaces such as slabs, pavements, beams, etc. exposed to hot and/or windy conditions. Many factors affect the likelihood of plastic shrinkage cracking such as water-cement ratio, admixture, member size, fines content, concrete surface temperature and ambient conditions (i.e. relative humidity, air temperature and wind velocity) /Uno 1998/. All these factors influence the water evaporation rate from the freshly placed concrete surface which is considered as an indication of the possible beginning of the plastic shrinkage cracking /Uno 1998/.

2. PREVIOUS RESEARCH IN SCANDINAVIA

In order to obtain a better comprehension of the plastic shrinkage cracking phenomenon, various research have been performed world-wide and Scandinavia is not an exception. Researchers such as Hedin /1985/, Johansen and Dahl /1993/, Lund et al. /1997/, Hammer /1999/ and Esping and Löfgren /2006/ studied different aspects of plastic shrinkage cracking and prepared a strong launch platform for further investigations.

For example, ten laboratory experiments and two field trials conducted by Hedin in 1985 to investigate what type of curing best prevents plastic shrinkage in the newly cast concrete. It was stated that covering the concrete with plastic wrap and membrane, decreases the evaporation rate and consequently leads to a crack-free concrete.

Using the same setup, Lund et al. argued that lower water-cement ratio causes less bleeding water and thus, logically, increases the risk of cracking /Lund et al. 1997/. Also the evaporation rate was documented in the study.

In 1993, Johansen and Dahl performed series of experiments in order to develop a method for determination of the cracking tendency of concrete at early ages. During the tests, fresh concrete was cast between two concentric steel rings. The specimen was then placed under an air funnel, to create an air stream with the required velocity over the fresh concrete surface /Johansen and Dahl 1993/. The crack tendency was then judged quantitatively at the end of the test (20 to 24 hours after casting) /NORDTEST NT BUILD 433, 1995/.

Hammer performed a set of experiments to study the relations between autogenous volumetric and linear shrinkage before and during the setting of paste-mortar-concrete, chemical shrinkage bleeding and concrete settlement. The objective was to obtain a reliable and meaningful method to measure the linear autogenous shrinkage of concrete /Hammer 1999/. Among other things it was observed that reabsorption of bleeding water which occurs around the setting is helpful from crack risk point of view /Hammer 1999/.

Esping and Löfgren studied the early age (less than 24 hours) autogenous deformation and pore-pressure development of Self-Compacting Concrete (SCC) and evaluated its crack tendency due to plastic shrinkage. This was done by exposing concrete specimens to early drying conditions (a modified NT BUILD 433). The experiments consisted of different SCC constituents and mix compositions e.g. water-cement ratio from 0.38 to 0.67, silica fume, and different admixtures /Esping & Löfgren 2006/. In addition, the experiments were repeated with standard concrete for comparison. According to the results, Esping and Löfgren argued that a high crack tendency occurs when there is a) a large amount of autogenous shrinkage (low w/c, silica addition, high fineness) b) retardation (retarder or high super plasticizer dosage) c) high water evaporation (low fineness or high w/c) d) low content of coarse aggregate /Esping & Löfgren 2006/.

3. EXPERIMENTS AT LTU

In order to practically study the phenomenon of plastic shrinkage cracking, laboratory tests have been conducted in the laboratory of Complab, Luleå University of Technology (LTU). The experiments were designed in order to monitor and understand the water evaporation rate in concrete slab under varying environmental conditions. Furthermore, how capillary pressure in the concrete develops and its relationship with plastic shrinkage cracking is a part of the project. Various concrete mixtures at different conditions will be tested to understand how the water evaporation rate and capillary pressure develops and influences the plastic shrinkage cracking.

For these experiments, a test rig (1200x400x90 mm) has been designed based on the experimental setups used by Hedin /1985/ and Lund /1997/, (see Figure 1). The frame is made of UPE80-beams placed on a 1 mm thick steel plate. It is possible to disassemble and reuse the frame after each test. Latex is used to seal the beam-plate and beam-beam interfaces. Rebars, 8 mm diameter, are installed inside the mould to create external constraint in the concrete. The rebars are fixed against 18 rods in total around the mould (6 rods along the long- and 3 rods along the short-side). Each rod penetrates the concrete by 60 mm.

The rig is placed on four load cells for continuous weight measurement. A 50 cm wide fan is used to produce wind with constant velocity on the slab surface varying from 0 to 7 m/s in different trials. A wind tunnel is placed on the slab to conduct the wind over the surface. At the moment, two parallel rigs are used to be able to vary curing conditions etc. on exactly the same concrete mix.



Figure 1 – Test setup for plastic shrinkage crack experiments at LTU.

So far tests have been performed with CEM II Portland-limestone cement (Byggcement, Cementa) which is vastly used in standard concrete work such as house building nowadays. Water-cement ratio is 0.38 to reach a 28 days strength of 60 MPa alongside with a S4 slump (160-210 mm) / Lundström 2013/. It should be noted that the mentioned values represent the first tested mixture which may differ by the experiments progress in future.

The aggregates and cement are mixed together for 1 minute in a mixer with 50 litre capacity. Then, water and the super plasticizer are added to the mixture simultaneously. The concrete should be left to mix for 5 minutes. The final fresh concrete would be cast in the above described mould and compacted using a vibrator. At this stage the concrete slab surface should be treated and finished carefully in order to have a smooth surface.

Having prepared the surface, the wind tunnel is placed on the slab and the fan is set on the required speed. Documentation is performed on water evaporation, air temperature, concrete temperature (at 7 points), wind speed and relative humidity. Each specimen is exposed to the wind for at least 4 hours while the surface of the slab is carefully monitored to record the occurrence of possible plastic shrinkage crack initiation.

4. FINAL COMMENTS

In these experiments the total weight lost is considered to be the total water evaporation. By plotting the evaporation rate against time, effect of different factors on the evaporation rate can be understood. The plan is to perform this test for different concretes to achieve a clear picture

regarding the critical water evaporation rate for cracking at different conditions. Furthermore, it is planned to include the capillary pressure measurement in future. Results of the above mentioned tests, can prepare a useful database for further investigations regarding plastic shrinkage cracking in concrete. Outcomes of these experiments, will be compared with full scale tests and the currently used method such as nomograph presented by Uno /1998/. Based on such a comparison, further investigation opportunities may emerge.

ACKNOWLEDGMENT

The authors would like to appreciate the support they received from the Development Fund of the Swedish Construction Industry, SBUF, as well as the personnel of Complab at LTU.

REFERENCES

- Esping, O., & Löfgren, I., 2006
 ”Investigation of Early Age Deformation in Self-Compacting Concrete”, Proceeding, 2nd International Symposium on Advances in Concrete through Science and Engineering, Quebec City, Canada, 11-13 September 2006.
- Hammer, T. A., 1999
 ”Test Methods for Linear Measurement of Autogenous Shrinkage before Setting”, Autogenous Shrinkage of Concrete, Edited by Ei-ichi Tazawa, E & FN Spon, London, United Kingdom, pp. 143-154.
- Hedin, C., 1985
 ”Plastiska Krympsprickor – Motåtgärder”, (in Swedish), Internal technical report 85-3. Central laboratory of Betongindustri AB.
- Johansen, R. & Dahl, P.A., 1993
 ”Control of plastic shrinkage of cement”, Paper presented at the 18th Conference on Our World in Concrete and Structures, Singapore, 1993.
- Lund, A., Skoog, M., Thorstensson, R., 1997
 ”Plastiska Krympsprickor i Betong”, (in Swedish), Dept. of Structural Mechanics and Engineering, Royal Institute of Technology, Stockholm, Sweden, 1997.
- Lundström, J., 2013
 ”Uppkomst av plastiska krympsprickor: Ny försöksuppställning och inverkan av cementtyp och vindhastighet”, Master thesis (in Swedish), Luleå University of Technology, Luleå, Sweden, 2013, 98 pp.
- NORDTEST NT BUILD 433, 1995
 ”Concrete: Cracking Tendency – Exposure to Drying During the First 24 Hours”, NORDTEST, Espoo, Finland, 1995.
- Schmidt, M., & Slowik, V., 2013
 ”Instrumentation for Optimizing Concrete Curing”, Concrete International, Vol. 35 , No. 8, August 2013, pp 60-64.
- Uno, P.J., 1998
 ”Plastic Shrinkage Cracking and Evaporation Formulas”, ACI Material Journal, Vol. 95, No. 4, July-August 1998, pp. 365-375.

Shrinkage cracking of thin concrete overlays



Dr Jonas Carlswård
 Betongindustri AB
 Box 47312
 SE-100 74 Stockholm
 E-mail: jonas.carlsward@betongindustri.se



Prof, Dr. Mats Emborg
 Div. Structural and Construction Engineering,
 Luleå University of Technology
 SE-971 87 Luleå
 Betongindustri AB
 Box 47312
 SE-100 74 Stockholm
 E-mail: mats.emborg@ltu.se / mats.emborg@betongindustri.se

ABSTRACT

Due to a high degree of damages and undesirable end results of bonded overlays, research is conducted to develop recommendations on design and execution. Laboratory and full scale tests as well as theoretical analyses have been carried out including e. g. base and end restraint tests on overlays with various reinforcement, concrete qualities, substrate preparing and curing. Moreover, analytical and numerical calculations have been performed. Results reveal that the e. g. bond between overlay and substrate is a critical parameter for a successful end result. Another key parameter is sufficient curing, while reinforcement generally proved to be less significant. Theoretical models works well on this structural situation and will be further developed.

Keywords: Overlay, Shrinkage, Cracks, Curing, Bond, Steel fibres, Restraint stresses

1. INTRODUCTION

Bonded overlays on concrete substrates are applied in a wide range of applications such as for bridge deck overlays on structural concrete, finishing layers on prefabricated elements or as repairs or strengthening of deteriorated bridge and parking decks, damaged industrial floors etc. In order to ensure that the overlaid system maintains durable and fully functioning during the intended service life it is essential to limit crack widths and to prevent delamination.

However, despite the fact that concrete is utilised on a regular basis for this application area, established practice regarding design and execution is lacking. A consequence is that misapplied execution methods and wrong design are common, resulting in a far too high degree of undesirable end results. Cracking, debonding and edge lifting are among the most frequent

problems, resulting from the differential shrinkage and thermal strain between the newly placed layer and the old sub-base material, see Figure 1.

To develop relevant guidance on how to design and execute overlays avoiding the problems research projects have been and are carried out in cooperation between Betongindustri AB, Strängbetong AB, Betongteknik AB and Ramböll with funding from Trafikverket, SBUF and LTU, /Carlswärd, 2006/, /Carlswärd & Emborg 2010/, /SBUF, 2011/.

2. THEORETICAL MODELS

An analytical model to determine the risk of cracking and the crack width of concrete overlays exposed to shrinkage has been proposed where the analysis is divided into two stages; (1) an analysis in the uncracked stage, and (2) crack width analysis (Fig. 2) /Carlswärd, 2006/. In the uncracked stage tensile stresses are calculated based on composite beam theory. The analysis, see also /Silfwerbrand, 1997/, includes the rate of shrinkage and creep, the development of stiffness and tensile strength and the restraint situation. Two situations are distinguished in the cracked stage, reached when the tensile stress exceeds the overlay strength: a) an internal debonded area developed and b) a still bonded overlay. In case of debonding, one single crack occurs in the unbonded region while a distributed crack pattern is the case for a bonded overlay.

In an ongoing work, the situation is modelled by FEM instead, in this case the ConTest Pro program, including models for moisture, shrinkage, temperature and thermal strain, /ConTestPro, 2007/. The program offers 1D and 2D calculations of thermal and moisture induced stresses and cracking risks of various restraint situations, one of them the actual concrete overlay.

3. OVERLAY TESTS

Various types of tests may be utilized for the calibration of the models above; end-restrained test (1), base restraint tests (2) and ring tests (3), see Figure 2. Category (2) tests are clearly the most suitable from the viewpoint that the restraint condition represents the real overlay conditions. A drawback is that it is difficult to control the bond conditions, which means that the cracking response will rely on the particular restraint situation (bond quality) obtained in each test.

The ring test is certainly the most popular test method. Favourable features are the simplicity of the setup and that the degree of restraint is well defined. However, a review of results reported indicates that the ring test may overestimate influence of crack distribution /Carlswärd, 2006/. Multiple cracking is regularly obtained already at low steel fibre dosages and in fact also for plain concrete. As crack distribution would clearly not take place in unreinforced concrete this leads to speculations regarding the validity of the method assessing the effect of reinforcement.

Instead, end-restrained tests have been used in present studies to assess the effect of steel fibres on cracking potential of SCC. Base restrained tests were also conducted in order to study the effects of restrained shrinkage more realistically in regard to real overlays.

4. RESULTS

Figures 4 and 5 show example of test results and calculations of end restrained and base restrained members. Plain and steel fibre self compacting concrete (SCC, SFRSCC) was examined as well as shrinkage reducing concrete (SRA). In Figure 4 the positive effect of fibre addition could be observed and in Figure 5 the sudden change of upper face strain at cracking can be seen as well as the interesting good correlation between measured and computed strain.

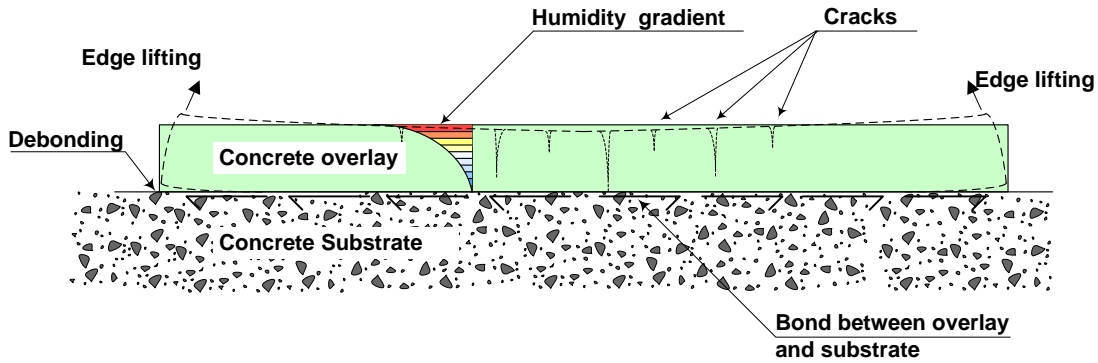
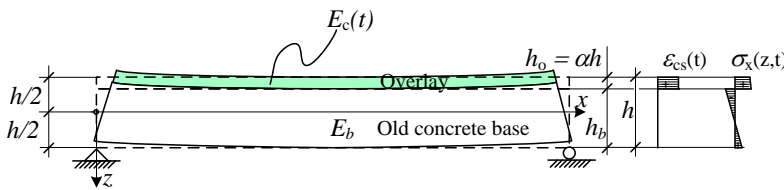


Figure 1. Cracking and edge lifting of overlay due to differential shrinkage, /Carlswärd, 2006/.

1) Uncracked stage



2) Calculation of crack widths

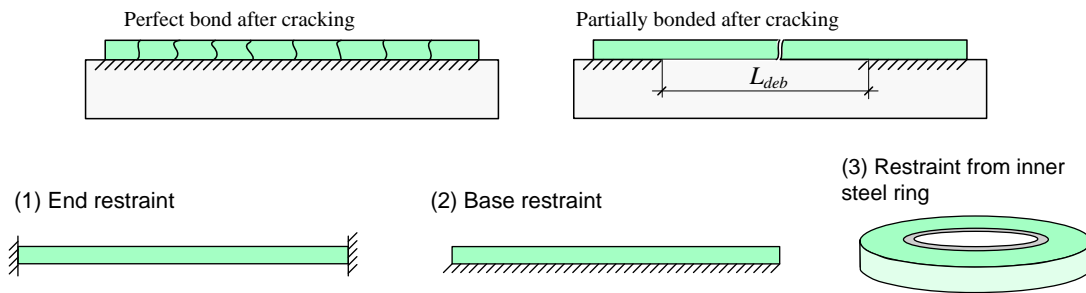


Figure 2. Proposed analytical model divided into two stages: (1) initial stress analysis in the uncracked stage based on composite beam theory and (2) crack width analysis (upper and middle). Common types of test methods used to study the effect of restrained shrinkage (below).

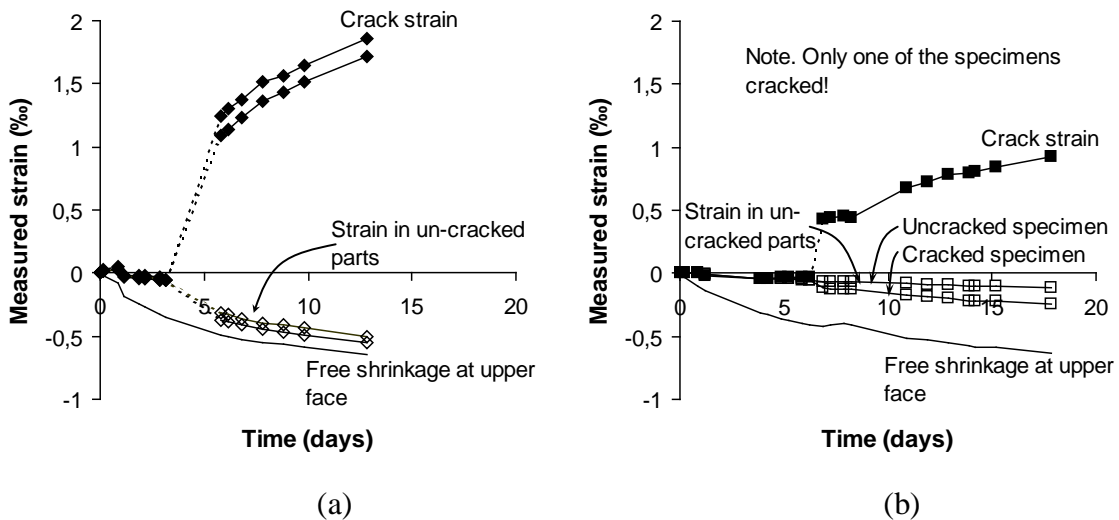


Figure 4. End restrained tests; Strain development measured in the cracked zone (crack strain) and in uncracked parts compared to free shrinkage results. (a) Plain SCC. (b) SFRSCC 40 (0,5 vol% steel fibres), two tests per variation /Carlswärd, 2006, Carlswärd & Emborg 2010/

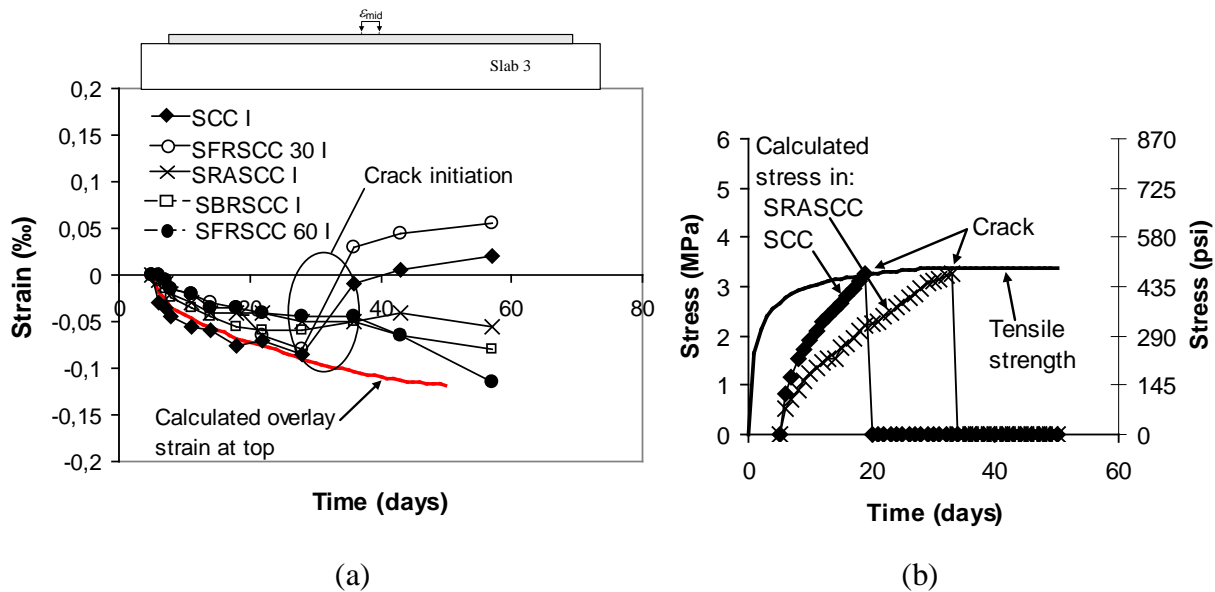


Figure 5. Base restraint tests; (a) Example of measured strain development at upper face of overlay strips (mid-section) compared to calculations using proposed theoretical model. (b) Calculated stress development in overlays of two concrete types /Carlswärd, 2006/.

5. CONCLUSIONS

Results from the overlay test series described above revealed that the choice of preparation of the substrate prior to overlaying is an extremely important parameter. Another parameter that was shown to influence the bond strength was the selection of curing method. It was e.g. indicated that curing is particularly important if the substrate is dry at the time of overlaying.

It can be concluded that reinforcement, mesh or steel fibres, most certainly contributes in case the bond strength between overlay and substrate is poor. However, in areas where the bond strength is high it is more difficult to conclude that reinforcement has a significant influence on crack widths. It is e.g. shown that reinforcement is not required to distribute cracks in thin overlays (~50 mm).

Comparisons of the analytical model with results from the base restrained test series showed a good correlation. For the situation that the overlay is not sufficiently bonded to the substrate it is however difficult to predict potential crack widths of SFRSCC as the extent of debonding will be quite influential.

REFERENCES

- SBUF project nr 12001. "Steel fibre reinforced self compacting concrete overlays", Development Fund of the Swedish Construction Industry) SBUF, www.sbuf.se
- Carlswärd, J. "Shrinkage cracking of steel fibre reinforced self compacting concrete overlays – Test methods and theoretical analysis," Doctoral thesis 2006:55, Div of Struct. Eng, Luleå Univ of Techn, 2006, <http://epubl.luth.se/1402-1544/2006/55/index.html>.
- Carlswärd J, Emborg M "Predicting of stress development and cracking in steel fibre-reinforced self-compacting concrete overlays due to restrained shrinkage", ACI SP-274, proceedings Fiber-reinforced Self-consolidating concrete: Research and application, 2010
- Silfwerbrand, J. "Stresses and strains in composite beams subjected to differential shrinkage" ACI Structural Journal, Vol. 94, No. 4, 1997, pp. 347-353.
- ConTestPro "User manual", JEJMS Concrete, LTU, Cementa, PeabAB, 2007, 200 pages

CHLORIDES.

Estimation of chloride threshold values after 20 years' field exposure in Swedish marine environment



Dimitrios Boubitsas
CBI Betonginstitutet
c/o SP
SE-501 15, Borås
dimitrios.boubitsas@cbi.se

* Corresponding author



Peter Utgenannt
Ph.D.
CBI Betonginstitutet
c/o SP
SE-501 15, Borås
peter.utgenannt@cbi.se



Tang Luping*
Ph.D., Prof
Chalmers Univ. of Techn.
Div. of Building Technology
SE-412 96, Gothenburg
tang.luping@chalmers.se

ABSTRACT

This paper presents the results from two research projects dealing with reinforcement corrosion measurements in concrete exposed to Swedish marine environment after exposure up to over 20 years. In the beginning of the 1990s, some 40 types of concrete slabs were exposed to seawater at the Träslövsläge field site on the west coast of Sweden. In this study the corrosion conditions of the rebars embedded in the concrete slabs were measured after 13 and 20 years' field exposure using a non-destructive method. A destructive visual examination was also carried out to confirm the results from the non-destructive method. The results make it reasonable to assume a chloride threshold value of at least 1% by weight of binder for initiation of corrosion of reinforcement steel embedded in the marine concrete structures.

Key words: Corrosion, chlorides, concrete, durability, field exposure.

1. INTRODUCTION

Chloride-induced reinforcement corrosion is one of the most important degradation processes in reinforced concrete structures exposed to a marine environment and road environment where de-icing salt is used. Steel in concrete is normally protected by the high alkaline nature of the pore solution in concrete which leads to the formation of a passive protective film on the steel surface. However, when chloride ions ingress into concrete and reach a certain critical concentration (chloride threshold value) at the depth of the reinforcement the passive film is broken down and the steel starts to corrode. A lot of research has been devoted to try to determine the chloride threshold value and several parameters have been identified to affect the threshold level. In the recent years comprehensive literature reviews on the subject have been published by Angst et al. (2009); Alonso and Sanchez (2009), in these reviews a large scatter in the reported values was found. One of the decisive parameters for the chloride threshold value has been identified to be pH of the pore solution which mainly depends on the binder type. This paper presents some results from two research projects dealing with reinforcement corrosion

measurements in concretes with different binder types and water-binder ratios exposed to Swedish marine environment after exposure up to over 20 years.

2 EXPERIMENTAL

More than 40 types of concrete slabs were exposed to seawater at the field site, details on specimen design, the field test site and all tested mixture proportions can be found in Boubitsas et al. (2014).

Corrosion rate measurements were performed after 13 and 20 years of exposure, and chloride content measurements were performed after 10-13 and 20 years of exposure. The commercially available RapiCor instrument based on galvanostatic pulse technique was used to measure the corrosion state of the rebars. RapiCor provide an indication of the instantaneous corrosion conditions of rebars. Because the corrosion conditions were not monitored during the exposure, it is unknown when the corrosion was initiated. Therefore, it is difficult to estimate the chloride threshold values from the instantaneous corrosion measurements and chloride profiles. However, it might be possible to roughly estimate the threshold from analysis of corrosion conditions (after 13 and 20 years) and chloride contents at the cover depth under the similar exposure duration. The following methodology was used in this project for evaluating the chloride threshold values in concrete exposed in the Träslövsläge field exposure site:

- Mapping the instantaneous corrosion conditions of rebar using the non-destructive test method RapiCor.
- Verifying the above non-destructive test by destructively releasing some rebars under different corrosion conditions for visual examination.
- Evaluating the chloride contents at the cover depth of the rebars showing the instantaneous corrosion rate $> 5 \mu\text{m/yr}$ as possible ongoing corrosion. The lowest value of chloride content would be taken as the threshold value for ongoing corrosion, to be verified by destructively visual examination.
- Verifying the estimated threshold value by destructively releasing some more rebars for visual examination and measurement of chloride content at the cover depth.

3 RESULTS AND DISCUSSION

Table 1 summaries some data of corrosion rate and chloride content at the cover depth (based on the chloride profiles) after 20 years of exposure together with the chloride content after 10 years and the corrosion rate after 13 years. It can be seen in Table 2 that the chloride content at the cover depth is in the most cases larger than 1% by weight of binder to cause a corrosion rate $> 10 \mu\text{m/yr}$. The lowest value 0.9% by weight of binder was found in concrete 6-35 rebar 1, but the value was measured 3 years earlier before the corrosion measurement. Therefore, it is reasonable to state that, to maintain corrosion at a certain rate, at least 1% chloride by weight of binder is needed. From Table 1 it can be seen that this threshold value of 1% chloride by weight of binder seems valid for various unitary and binary binder with different water-binder ratios (in a range of 0.3 to 0.5), including SRPC (as 7-35 rebar 1), OPC (as 2-50 rebar 2; 8-40 rebar 1) and SRPC+5% silica fume (as 5-40 rebar 2; 6-35 rebars 1 and 2; H1 (w/b 0.30) rebar 1). It seems that the chloride threshold value for the ternary binder as 12-35 rebars 1 and 2 (with 5% silica fume and 10% fly ash with water binder ratio 0.35) is higher than the unitary or binary binder. The chloride content at the cover depth of concrete 12-35 has already reached 2-3% after 10 years' exposure, but no severe corrosion was observed after over 20 years' exposure. No corrosion of rebars has been detected in concretes H2 and H5 owing to their low chloride content at the cover depth.

Table 1. Chloride contents near the rebars corroding at a certain rate after 20 years exposure.

| Concrete | Binder:w/b:air%/ Rebar | Cover [mm] | Diameter [mm] | Corrosion rate [$\mu\text{m}/\text{yr}$] | Cl% wt of binder ^a |
|----------|---------------------------|------------|---------------|--|-------------------------------|
| 1-35 | SRPC:0.35:6/b1 | 10 | 12 | ~50 (~20 ^b) | 2.4 (3 ^b) |
| 1-402 | SRPC:0.40:6/b1 | 15 | 20 | >500 (~20 ^b) | 3 (3.3 ^c) |
| 1-402 | SRPC:0.40:6/b2 | 20 | 20 | >500 (~20 ^b) | 3 (2.7 ^c) |
| 2-35 | OPC:0.35:6/b2 | 25 | 20 | ~40 (~30 ^b) | 2 (1.7 ^c) |
| 2-50 | OPC:0.5:6/b1 | 10 | 12 | ~20 (~70 ^b) | 2.4 (3 ^c) |
| | OPC:0.5:6/b2 | 15 | 12 | ~15 (~10 ^b) | 2 (1.1 ^c) |
| 3-351 | SRPC+5%SF:0.35:6/b1 | 20 | 20 | ~70 (~40 ^b) | 2 (1.8 ^c) |
| 3-351 | SRPC+5%SF:0.35:6/b2 | 15 | 20 | >500 (~150 ^b) | 2.4 (2.3 ^c) |
| 3-352 | SRPC+5%SF:0.35:6/b1 | 10 | 12 | >500 (~10 ^b) | 2.8 (2.9 ^c) |
| 5-40 | SRPC+5%SF:0.4:3/b1 | 15 | 20 | >500 (~70 ^b) | 3 (1.6 ^c) |
| 5-40 | SRPC+5%SF:0.4:6/b2 | 20 | 20 | >500 (~100 ^b) | 2.7 (1.2 ^c) |
| 6-35 | SRPC+5%SF:0.35:2/b1 | 25 | 20 | ~15 (~10 ^b) | 1.2 (0.9 ^c) |
| 6-35 | SRPC+5%SF:0.35:2/b2 | 20 | 20 | ~80 (~70 ^b) | 1.4 (1.2 ^c) |
| 6-40 | SRPC+5%SF:0.4:2/b1 | 15 | 20 | >500 (~70 ^b) | 2.6 (1.7 ^c) |
| 7-35 | SRPC+5%SF:0.35:2/b1 | 20 | 20 | ~30 (~100 ^b) | 2.2 (1.1 ^c) |
| 7-35 | SRPC:0.35:2/b2 | 15 | 20 | ~45 (~40 ^b) | 2.4 (1.5 ^c) |
| 8-40 | OPC:0.4:2/b1 | 20 | 20 | ~10 (~5 ^b) | 2.3 (1 ^c) |
| 12-35 | SRPC+5%SF+10%FA:0.35:6/b1 | 10 | 12 | ~15 (~5 ^b) | 3.2 (3 ^c) |
| 12-35 | SRPC+5%SF+10%FA:0.35:6/b2 | 15 | 12 | ~10 (<5 ^b) | 2.7 (2 ^c) |
| H1 | SRPC+5%SF:0.3:2/b1 | 20 | 12 | ~20 (<5 ^b) | 1.1 (0.5 ^c) |
| H2(II) | SRPC+10%SF:0.3:2/b1 | 30 | 12 | <5 (<5 ^b) | 0.1 (<0.1 ^c) |
| H2(II) | SRPC+10%SF:0.3:2/b2 | 30 | 12 | <5 (<5 ^b) | 0.1 (<0.1 ^c) |
| H5(II) | SRPC+5%SF:0.25:3/b1 | 35 | 12 | <5 (<5 ^b) | <0.1 (<0.1 ^c) |
| H5(II) | SRPC+5%SF:0.25:3/b2 | 35 | 12 | <5 (<5 ^b) | <0.1 (<0.1 ^c) |

^a based on the chloride profiles in the submerged zone.

^b data after 13 years' exposure (Tang et al. 2005).

^c data after 10 years' exposure (Tang 2003b).

4 CONCLUSIONS

- It is reasonable to assume a chloride threshold value of at least 1% by weight of binder for initiation of corrosion of reinforcement steel embedded in the marine concrete structures considering the actual thickness of cover. This threshold value of 1% by weight of binder seems valid for various unitary and binary binders including ordinary Portland cement, sulphate resistance Portland cement and blended cement with 5% silica fume, and also with different water-binder ratios in a range of 0.3 to 0.5.

- For the ternary binder blended with 5% silica fume and 10% fly ash with water binder ratio 0.35, the chloride threshold value can be as high as 2% by weight of binder content.

REFERENCES

Alonso, M.C., Sanchez, M., 2009

“Analysis of the variability of chloride threshold values in the literature”, *Mater. Corros.* 60, 2009 pp. 631-637

Angst, U., Elsener, B., Larsen, C.K., Vennesland, Ø., 2009

“Critical chloride content in reinforced concrete – A review”, *Cem. and Concr. Res.* 39, 2009 pp. 1122-1138.

Boubitsas, D., Tang, L., Utgenannt, P., 2014

“Chloride ingress in concrete exposed to marine environment - Field data up to 20 years’ exposure”, Final Report to SBUF (to be published).

Tang L., 2003b

“Chloride Ingress in Concrete Exposed to Marine Environment – Field Data Up to 10 Years Exposure”, SP Report 2003:16, Borås.

Tang L., Utgenannt P., Fidjestøl, P., 2005

“Evaluation of Chloride-Induced Corrosion of Steel in Concrete after Long-Time Exposure in a Marine Environment”, SP Report 2005:54, Borås.

Experimental determination of chloride threshold values for reinforcement corrosion in concrete: Experiences from the lab



Søren L. Poulsen
MSc, PhD
Danish Technological Institute
Gregersensvej,
DK – 2630 Taastrup
Denmark
E-mail: slp@dti.dk



Henrik E. Sørensen
MSc, PhD
Danish Technological Institute
Gregersensvej,
DK – 2630 Taastrup
Denmark
E-mail: hks@dti.dk

ABSTRACT

The reliability of all commonly used service life models for chloride exposed concrete structures is highly dependent on the applied input parameters of the models, e.g. the chloride threshold value for initiation of reinforcement corrosion. Since 2011, a number of different experiments have been conducted at Danish Technological Institute with the main purpose of developing an accelerated in-lab test method for determination of chloride threshold values. In this paper we report on our experiences from the experimental work.

Key words: Chloride ingress, corrosion, chloride threshold values, testing.

1. INTRODUCTION

The chloride threshold value is the minimum concentration of chloride at reinforcement depth that is able to initiate corrosion of the steel, e.g. in a concrete structure. When attempting to model the expected service life of a reinforced concrete structure, a relatively small change in the chloride threshold value will generally have a marked effect on the calculated service life. Therefore, a commonly accepted test method for a reliable and precise determination of chloride threshold values is greatly needed, but such a method is currently not available. A series of tests have been carried out at Danish Technological Institute with the aim of developing such a method. This work has served as useful input for the RILEM Technical Committee 235-CTC, which was formed in 2009 with the purpose of addressing the problem with the lack of a generally accepted test method of determination of chloride threshold values.

2. EXPERIMENTAL SETUP

A series of experiments was initiated in 2011 at Danish Technological Institute with the purpose of testing an in-lab method for determination of chloride threshold values in reinforced concrete. Part of the test design is based on work by /Nygaard & Geiker 2005/. The basic idea of the experiments is to expose a number of concrete specimens with cast-in rebars to a 6 wt% NaCl solution and subsequently detect the onset of reinforcement corrosion in one of two ways: (1) by observation of a significant drop in the electrochemical potential of the rebar measured against a reference electrode (open circuit approach) or (2) by observation of a significant increase in the

current required to maintain a specific potential of the rebar measured against a reference electrode (potentiostatic approach). Two different potentials is used in the potentiostatic setup, one typical for submerged conditions (-125 mV vs. CSE) and one representing splash-zone conditions (+125 mV vs. CSE). In both setups the chloride concentration is measured at the depth of the rebars when corrosion onset is observed, thus giving the chloride threshold value.

2.1 Preparation of concrete specimens

Eight cubic concrete specimens (P1 to P8), each containing four rebars, were cast from the same batch of concrete with an equivalent water/cement ratio of 0.45 (activity factor 0.5 for fly ash) and a binder composed of 75 wt% of CEM I 52,5 N Portland cement (RAPID[®] cement from Aalborg Portland, Denmark) and 25 wt% of pulverized fly ash (type B4 from *Emineral A/S*). After casting each specimen was cut with a diamond saw to produce the shape displayed in Figure 1(a-c). This was done to reduce the cover thickness to 5 mm (four specimens for potentiostatic approach and two specimens for open circuit approach) or 15 mm (two specimens for open circuit approach) and the purpose of the epoxy coating was to ensure a unidirectional chloride ingress during exposure.

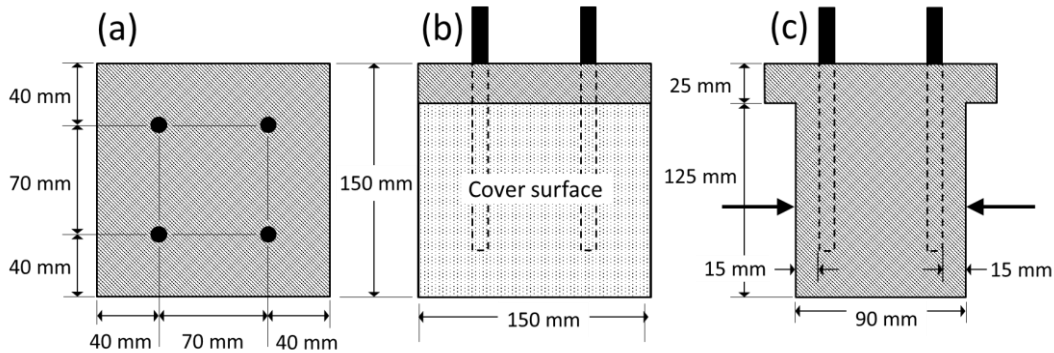


Figure 1 - Top view (a), front view (b) and side view (c) of concrete specimens from specimen series P. Each specimen of the series contains four rebars and all surfaces are sealed with an epoxy coating, except the 'cover surfaces', i.e. the surfaces to be exposed to the chloride solution. The dashed lines indicate the position of the rebars below the concrete surface and the two arrows in part (c) indicate the position of the 'cover surfaces'.

The rebars were prepared from ribbed steel (\varnothing 10 mm) and two of the rebars to be cast in each concrete specimen were cleaned using citric acid ($C_6H_8O_7$) and subsequently repassivated in a solution saturated with $Ca(OH)_2$, whereas the remaining rebars were used as delivered, with some surface rust on them. After 28 days of curing the eight concrete specimens were exposed to an external chloride source by placing two specimens in each of four identical plastic tanks (23 x 27 x 15 cm) containing 7 liters of a 6.0 wt% NaCl solution, thus immersing the specimens to a depth of 10 cm. The chloride solutions were made using water from the tap.

3. RESULTS

In the open circuit setup corrosion onset has been observed for one rebar (after ~940 days of exposure) at the time of writing (March 2014). This was identified by a sudden and significant drop in the measured potential of about 150 mV. After having observed that the potential remained at this new and lower level for at least seven days, the chloride concentration was measured at the depth of the rebar by profile grinding, thus giving a chloride threshold value of 0.73 wt% of binder. It is noted, that the corrosion onset was observed for one of the rebars,

which were cast into the concrete specimen in “as-received condition”. The free potentials of the non-corroding rebars are in the range between approximately -150 and -50 mV vs. CSE.

In the fixed potential setup with +125 mV vs. CSE corrosion onset was observed for two rebars in the same specimen after 835 and 853 days of chloride exposure, respectively. About two weeks after corrosion onset, the rebars were disconnected from the setup and the chloride concentrations were determined at the rebar depths by profiles grinding. The chloride content was very high when measured directly on the corroding specimens after two weeks of high current flowing between the corroding rebars and the potentiostat. Therefore, the chloride content was also measured after a few more weeks in the same concrete specimen at a third rebar where corrosion onset had not been observed. At this rebar a much lower concentration (0.41 wt% of binder) was measured. A number of additional chloride ingress profiles were also determined at earlier exposure times with the purpose of following the general progress of the chloride ingress in the specimens. All the measured profiles are displayed in Figure 2. Two of the specimens used for the profile grinding were also utilized to prepare thin section for optical microscope investigations, which revealed the presence of a thin (~10 μm) and quite dense layer of calcite on the exposed surface of both investigated specimens.

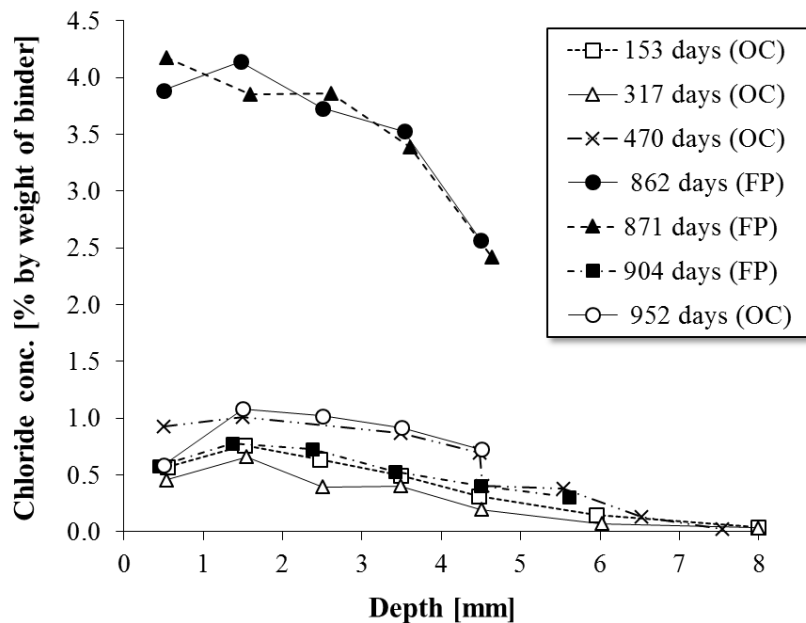


Figure 2 – Chloride profiles measured on concrete specimens that have been exposed to a 6.0 wt% NaCl solution. The chloride contents were determined according to the procedure given in /NT BUILD 208 1984/. The exposure time is indicated for each profile in the legends along with information on the type of experimental setup: OC = Open Circuit setup and FP = Fixed Potential setup. The elevated chloride contents in the two profiles measured after 862 and 871 days are believed to be a result of chloride migration after corrosion onset in the potentiostatic setup (see text for explanation).

4. DISCUSSION

Despite concrete cover thicknesses of only 5 mm for most of the specimens and a prolonged exposure time of more than 900 days, corrosion onset has only been detected for one out of 8 rebars with 5 mm cover in the open circuit setup and for two out of 16 rebars with 5 mm cover in the fixed potential setup. This result was quite unexpected, since the test method was

designed in such a way, that corrosion onset was expected to occur within a few months after the first chloride exposure. Nevertheless, it seems reasonable that active corrosion has not been widely observed during the first 900 days, since the measured chloride profiles have demonstrated a slow ingress of chlorides into the specimens. This might be partly due to (1) the presence of a thin and dense calcite crust on the exposed specimen surfaces, which may have introduced some blocking effect on the ingress of chloride ions, and (2) the high proportion of fly ash in the binder of the concrete, a material which has previously been reported to result in a refinement of the pore structure of the cement paste, as well as enhancement of the chloride binding capacity, thus leading to a higher resistance of the concrete against ingress of chloride ions /Dhir & Jones 1999/. We have encountered similar problems with prolonged exposure times without corrosion onset and slow ingress of chloride in concrete specimens in connection with our participation in the RILEM TC 235-CTC group, which involves a Round Robin test of a newly proposed method for determination of chloride threshold values /Sørensen *et al.* 2012/.

The high chloride contents measured after corrosion onset in the potentiostatic setup is believed to be a result of chloride migration into the sample in the period between corrosion onset and disconnection from the potentiostat, because a high electrical current was required to maintain the fixed potential during this two week period. This notion was supported by the fact that a much lower chloride concentration was measured subsequently in the same specimen at a third rebar for which corrosion had not been detected. Consequently, it is important that the rebar is disconnected from the potentiostat straight after registration of corrosion onset if the chloride threshold value should be determined by measurement directly on the corroding specimen.

5. CONCLUSIONS

Two experimental setups for measuring chloride threshold values in chloride exposed concrete specimens with cast-in rebars have been tested in the lab: One involving an open circuit approach and another with a potentiostatic approach. The tested concrete had an equivalent water/cement ratio of 0.45 (water/powder ratio approx. 0.40) and a binder consisting of ordinary Portland cement blended with 25% fly ash. In the open circuit setup a chloride threshold value of 0.73% (by weight of binder) has been measured at a free potential of approx. -50 mV vs. CSE. In the potentiostatic setup a chloride threshold value of 0.41% (by weight of binder) has been measured at a fixed potential of +125 mV vs. CSE. These results are initial results from an ongoing experiment.

REFERENCES

- Dhir, R.K. & Jones, M.R., 1999
 "Development of chloride-resisting concrete using fly ash", *Fuel*, Vol. 78(2), pp. 137-142.
- NT BUILD 208, 1984
 "Concrete, hardened: Chloride content", 2nd ed., 1984
- Nygaard, P.V. & Geiker, M.R. 2005
 "A method for measuring the chloride threshold level required to initiate reinforcement corrosion in concrete", *Materials and Structures*, Vol. 38, 2005, pp. 489-494.
- Sørensen, H.E., Poulsen, S.L. & Nielsen, E.P., 2012
 "Testing of the chloride threshold values for reinforced concrete structures", *Proc. 3rd Int. Conf. on Concrete Repair, Rehabilitation and Retrofitting, ICCRRR-3*, 3-5 September 2012, Cape Town, South Africa, pp. 187-188.

On the impact of phase changes on chloride profiles in concrete



Dr. Klaartje De Weerd
 Department of Structural Engineering, NTNU
 Richard Birkelands vei 1a, NO-7491 Trondheim
 E-mail: klaartje.d.weerd@ntnu.no



M.Sc. Silje Gystad Ytterdal
 Department of Structural Engineering, NTNU
 Richard Birkelands vei 1a, NO-7491 Trondheim



Prof. Dr. Mette R. Geiker
 Department of Structural Engineering, NTNU
 Richard Birkelands vei 1a, NO-7491 Trondheim

ABSTRACT

The time dependency of the diffusion coefficient and the surface concentration have a large impact on the predicted chloride ingress in the concrete cover. A selection of results obtained within a project of the COIN Focus Area 3.2 are presented. The project focuses on how phase changes due to exposure to NaCl and sea water affect the chloride profiles over time. One of the findings is that concrete is able to bind the major part of the chlorides present and that the binding isotherm determined with CaCl_2 seems to give a more realistic estimate of the chloride binding compared to NaCl. It was also observed that phase changes at the concrete surface e.g. leaching and enrichment in Mg and S lower the actual surface chloride concentration and move the maximum concentration deeper into the sample.

Key words: Binders, Aging, Chlorides, Leaching.

1. FINDINGS

When studying chloride ingress in concrete, generally chloride profiles giving the total chloride content as function of the depth into the concrete are determined. This is done by profile grinding concrete cores and determining the total (acid soluble) chloride content in the resulting concrete powder. Figure 1 shows the total chloride profiles for mortars prepared with ordinary Portland cement (OPC) and a w/c ratio 0.4 exposed to sea water for 28, 90 and 180 days after 1 week of curing. The movement of chlorides through the concrete is generally assumed to be caused by diffusion, even though other mechanisms like capillary suction might also play a role in the outer millimeters. The mortar samples used to obtain Figure 1 were saturated prior to exposure to the sea water to limit the effect of capillary suction, and cut surfaces were used to limit variations in paste content. In the total chloride profiles given in Figure 1 the bound and free chlorides are not distinguished. The free chlorides are the chlorides present in the pore solution and the bound are either chemically bound or physically bound. The bound chlorides

can be looked upon as the stationary chlorides, even though they can be released upon changes in the environment, and the free chlorides are the ones which can “move” through the concrete. In order to study transport of chlorides by diffusion in the pure sense, one has to consider the free chlorides.

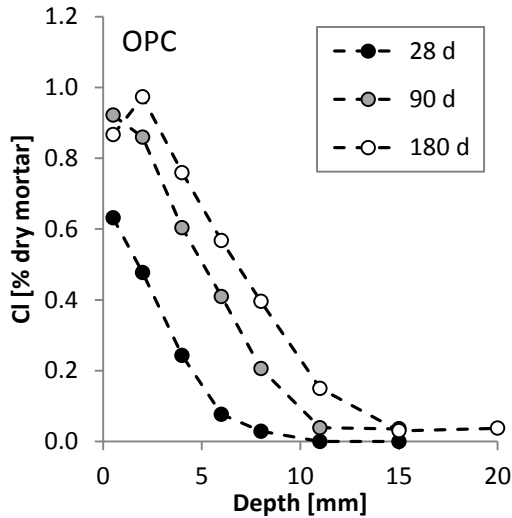


Figure 1 - Total chloride profiles for mortar prepared with OPC exposed to sea water for 28, 90 and 180 days in laboratory conditions (De Weerd et al. 2014b).

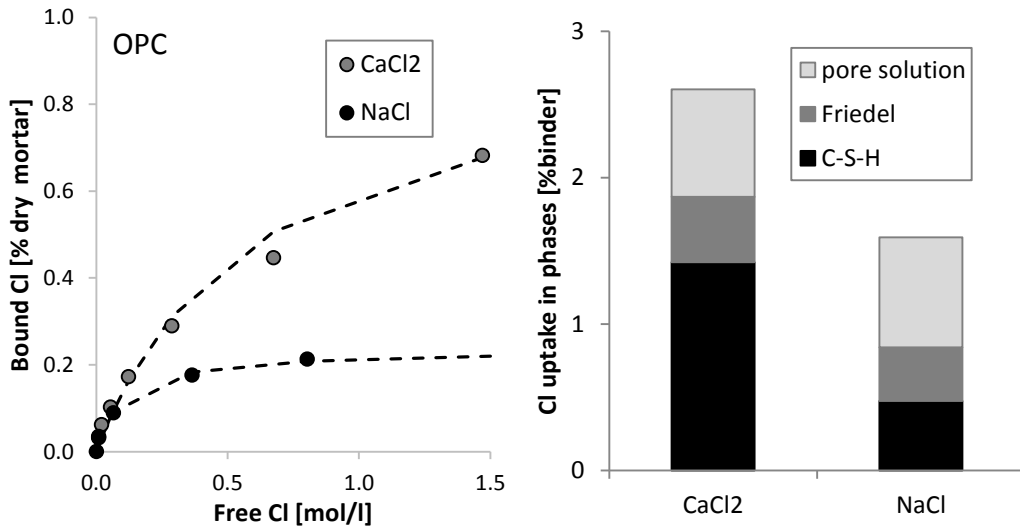


Figure 2 - Left: Binding isotherms and fitted Langmuir curves for mortar prepared with OPC exposed to CaCl_2 and NaCl solutions according to the procedure described in [5]. Right: A schematic representation of the location of chlorides in a cement paste prepared with OPC and w/c 0.5 exposed to 3 M Cl based on the findings from (De Weerd et al. 2013a).

Chloride binding isotherms were determined using a variant of the equilibrium method as described in (De Weerd et al. 2013a). Figure 2 shows the binding isotherms for exposure to NaCl and CaCl_2 solutions at 20°C for the same mortar as the one used for Figure 1. It can be seen that exposure of the mortar to CaCl_2 leads to considerably higher binding than for exposure to NaCl for free Cl concentrations higher than 0.2 M. This was attributed in the previous study (De Weerd et al. 2013a) to a higher binding capacity of the C-S-H when the cement paste is exposed to CaCl_2 compared to NaCl . This is also demonstrated in Figure 2 (Right). The higher

binding capacity of the C-S-H as obtained with CaCl_2 exposure was also observed in a field study conducted in 2012 (De Weerd et al. 2014a).

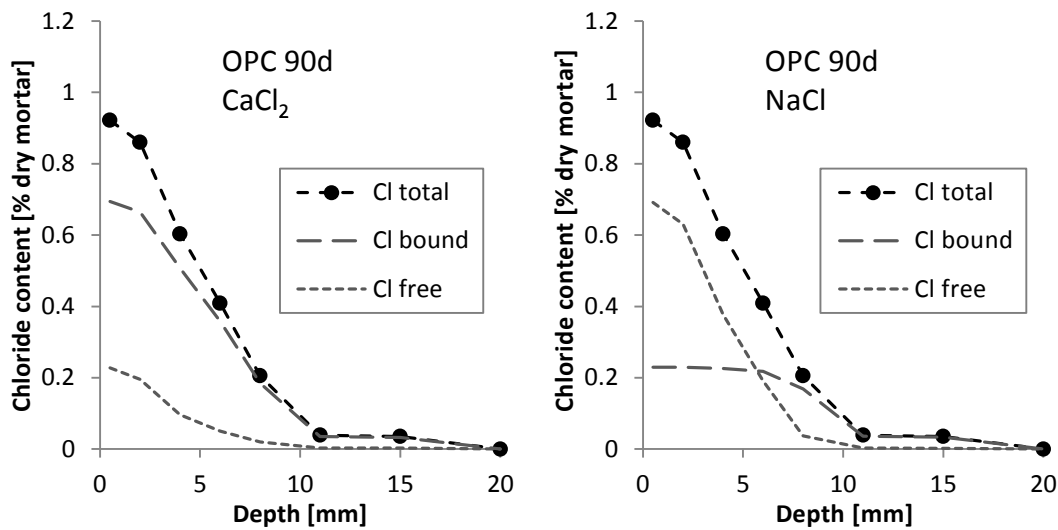


Figure 3 - The measured total chloride profile and calculated bound and free chloride profiles for CaCl_2 (Left) and NaCl (Right) exposure.

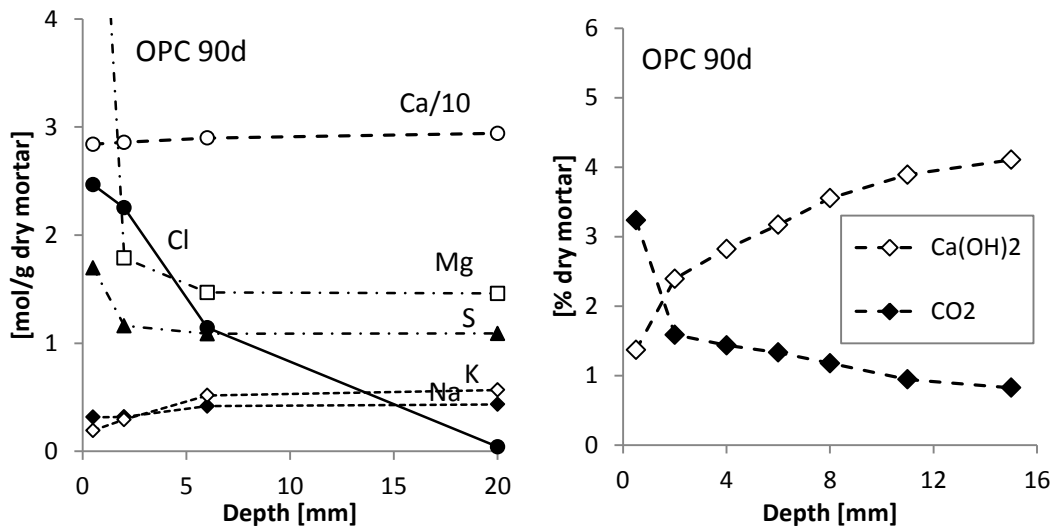


Figure 4 - Left: Elemental changes determined by ICP-MS on acid solubilized ground mortar powder of sections 0-1, 1-3 and 5-7 mm as well as unaffected concrete (De Weerd et al. 2014b). Right: Amount of calcium hydroxide ($\text{Ca}(\text{OH})_2$) and carbonation (mass loss due to CO_2) as function of the depth determined on ground mortar powder sections by thermogravimetric analysis (TGA) (De Weerd et al. 2014b).

The determined binding isotherms can be used to calculate the bound and free chloride profiles as shown in Figure 3. The calculations were performed both for CaCl_2 and NaCl . In the case of NaCl free chloride concentrations up to 5 M chloride are obtained near the surface which is in contact with sea water solution with a concentration of 0.5 M chloride. This indicates that the NaCl binding isotherms obtained with the equilibrium method underestimates the binding behavior of the mortar. The calculations using the CaCl_2 binding isotherms on the other hand show a much higher share of bound chlorides in the first 10 mm from the exposure surface and therefore also a more realistic free chloride concentration near the surface.

Sea water contains other ions besides chlorides, e.g. sodium, sulphate, magnesium, calcium, and carbonates. These ions have been observed to change the chemistry of the outer millimeters of concrete in contact with sea water (De Weerd et al. 2014a), (De Weerd et al. 2013b). Figure 4 (Left) shows the elemental composition of different powder sections of the OPC mortar exposed to sea water for 90 days. At the surface enrichment in magnesium can be observed and the outer millimeters are enriched in sulphates and carbonates. The latter two are known to reduce chloride binding. Worth noticing is that neither sodium nor calcium follow the chloride into the concrete. This indicates that binding isotherms determined by the equilibrium method both with NaCl and CaCl₂ exposure solutions do not fully reflect the binding of chlorides in concrete. Besides ingress of ions, there is also considerable leaching when concrete is exposed to sea water. This is demonstrated in Figure 4 by the decrease in the potassium content (determined by ICP-MS) and calcium hydroxides content (determined by TGA) towards the surface. Leaching will lead to a reduction in the pH and this can be associated with increased binding (De Weerd et al. 2014a). The effect of the changes in chemistry on the phase assemblage in the concrete was discussed in (De Weerd et al. 2014a).

2. PERSPECTIVES

These findings contribute to a better understanding of chloride ingress through the following:

The physical meaning of the apparent diffusion coefficient determined by fitting a total chloride profile with the solution of Fick's 2nd law can be questioned as the free chlorides which are the ones which might actually move by diffusion are not a linear function of the bound chloride and are only a small share of the total chloride content. CaCl₂ binding isotherms seem reflect the binding behavior better than the NaCl isotherms.

The surface concentration obtained by fitting the total chloride profile is only a fitting parameter. The actual surface concentration is strongly influenced by the phase changes in the outer millimeters including leaching. Electron microscopy investigations of marine exposed field samples have shown that the chloride concentration at the surface can very low and that the highest chloride concentration is found inwards from the exposed surface (De Weerd et al. 2013b).

The diffusion of chlorides through concrete is, besides chemical changes, also strongly influenced by the porosity and the moisture conditions in the concrete. The impact of these factors is being studied in a field study in cooperation with the Norwegian Public Roads Administration. The results are planned to be published within 2014.

ACKNOWLEDGEMENTS

The CONcrete INnovation centre (www.coinweb.no) is gratefully acknowledged for facilitating this research project.

REFERENCES

- De Weerd, K., A. Colombo and M. R. Geiker (2013a). "On the impact of the associated cation on the chloride binding of Portland cement paste, experimental and modelling study." *Cement and Concrete Research* **Submitted**.
- De Weerd, K., M. R. Geiker and H. Justnes (2013b). 10 year old concrete wall in tidal zone examined by SEM-EDS. *14th Euroseminar on microscopy applied ot building materials*. U. Hjorth Jakobsen. Helsingør, Denmark.
- De Weerd, K., H. Justnes and M. R. Geiker (2014a). "Changes in the phase assemblage of concrete exposed to sea water." *Cement and Concrete Composites* **47(0)**: 53-63.
- De Weerd, K., D. Orsakova and M. R. Geiker (2014b). Paper under preparation.

The effect of freeze-thaw loading on chloride ingress



Miguel Ferreira
Senior Scientist
VTT Technical Research
Centre of Finland
Kemistintie 3, Espoo
FI-02044, Finland
miguel.ferreira@vtt.fi



Markku Leivo
Principal Scientist
VTT Technical Research
Centre of Finland
Kemistintie 3, Espoo
FI-02044, Finland
markku.leivo@vtt.fi



Hannele Kuosa
Research Scientist
VTT Technical Research
Centre of Finland
Kemistintie 3, Espoo
FI-02044, Finland
hannele.kuosa@vtt.fi



Lasse Makkonen
Principal Scientist
VTT Technical Research
Centre of Finland
Kemistintie 3, Espoo
FI-02044, Finland
markku.leivo@vtt.fi



David Lange
Professor
University of Illinois,
USA
dlange@ilinois.edu

ABSTRACT

The freezing and thawing of water on the surface and in the pore structure of concrete can induce deterioration resulting in changes in the physical, chemical and mechanical characteristics of concrete, and influences the transport properties of moisture in concrete. Recent research has shown a synergetic effect between freeze-thaw action and the penetration of chlorides, but no steps have been taken to characterize and comprehend the mechanisms involved. This paper presents the preliminary findings of an ongoing research project studying the influence of freeze-thaw cycles on chloride ingress into concrete.

Key words: freeze-thaw, chlorides, concrete, durability, frost attack, degradation, performance

1. INTRODUCTION

Despite the many advances in research on freeze-thaw deterioration of concrete, little attention has been given to its effect on chloride ingress. Freeze-thaw reduces the concrete cover due to scaling (in the presence of salts), and by changing the characteristics of both surface and internal concrete due to cracking. Recent research has shown there to be a synergetic effect between freeze-thaw and chloride penetration (Leivo *et al.* 2011; Kuosa, *et al.* 2014; Li 2009; Ferreira *et al.* 2013), but no steps have been taken to characterise and comprehend the mechanisms involved and understand the consequence for durability and the service life of concrete infrastructure. For this reason, a research project was undertaken to ascertain what influence of freeze-thaw cycles have on chloride penetration into concrete. For this purpose, two distinct concretes were subject to four different freeze-thaw test cycles and two ponding conditions. This

paper presents the preliminary findings of the research project.

2. EXPERIMENTAL PROGRAMME

The main task consists of subjecting concrete, with varying quality, to various freeze-thaw tests in which the lowest temperature reached differs (-5, -10 and -20°C). In addition, the concrete was subject to chloride ponding at two constant temperatures (+5 and +20°C). Two concrete mixes, with 0.42 and 0.55 w/b ratios (B42 and B55, respectively), were prepared using a CEM I 42.5 N-SR3 to minimise the possibility of chloride binding. A plasticizer was used in the B42 mix, and an air entrainment agent for both mixes. Basic details of the concrete mixture, workability, and the characteristics of the air entrainment measured in hardened concrete are given in Table 1. Details can be found in Ferreira *et al.* (2014a).

Table 1 – Concrete composition, workability, and air pore characteristics of hardened concrete.

| Series | w/b | Water (l/m ³) | Binder (kg/m ³) | Aggregate (kg/m ³) | Slump (mm) | Spacing factor (mm) | Specific surface (mm ² /mm ³) | Total air (%) | Protective air (%) |
|--------|------|------------------------------|--------------------------------|-----------------------------------|---------------|---------------------------|--|---------------------|-----------------------|
| B42 | 0.42 | 175 | 420 | 1695 | 100 | 0.21 | 33 | 4.1 | 2.9 |
| B55 | 0.55 | 195 | 355 | 1716 | 180 | 0.24 | 21 | 5.9 | 5.1 |

Cubic specimens (150mm) were cast in moulds and compacted using a vibrating table. 24 hours later, the specimens were removed from the moulds and permanently stored in a climate chamber at RH=95 % at 20 ± 2°C until testing. A good air entrainment was achieved in both concretes mixes, as shown by the low spacing factor and the specific surface (Table 1). The specimens were kept in the climate chamber for approximately 8 months to minimise the influence of microstructure changes on the test results due to continuous hydration. After this period, the specimens were moved to a climate chamber at RH=65% for an additional month. Ten days prior to testing, the concrete specimens were prepared for freeze-thaw testing according to the procedure defined in CEN/TS 12390-9. Three days prior to testing, the specimens were ponded with a 3mm layer of deionised water. At the start of testing, this water was replaced with a 3% by weight of NaCl solution.

Three different freeze-thaw testing cycles were used, following the reference test temperature curve for freeze-thaw scaling (CEN/TS 12390-9), but varying in the minimum temperature reached (-5, -10 and -20°C). In total, the concrete specimens were subject to 112 freeze-thaw cycles. The choice of a lower limit temperature in the freeze-thaw cycles was to promote different freezing-thawing behaviour of the brine solution in the pore structure of the concrete. As the temperature decreases, and the longer a certain low temperature is maintained, a greater volume of the pore structure is frozen (Ferreira *et al.* 2013). For reference, ponding tests were carried out at a constant +5°C and +20°C. During testing, scaled material mass, specimen mass variation and fundamental frequency were measured periodically measured. In addition, at certain intervals specimens were removed and the chloride profiles determined. Details of the test setup and the results can be found in Ferreira *et al.* (2014b).

3. RESULTS AND DISCUSSION

Figures 1 and 2 present the average chloride profiles for B42 and B55 concretes, for 112 day surface ponding and 112 freeze-thaw cycles, respectively. Detailed results for several measurements can be found in Ferreira *et al.* (2014b).

The main transport mechanisms contributing to the ingress of water and chlorides during the course of the tests are capillary action (first few days), diffusion (water vapour; chlorides in solution) and micro ice lens pumping (as a result of freeze-thaw loading).

The relative dynamic modulus (RDM) measured using fundamental frequency, after 112 freeze-

thaw cycles for all freeze-thaw tests specimens was greater than 99.5%., indicating that there was practically no internal damage occurring in the concrete. This was expected given the quality of the air entrainment achieved.

Samples subject to freeze-thaw cycles show a larger uptake of water when compared to the samples subject only to ponding. This suggests that during freezing, the formation of micro ice lenses might be assisting water uptake. Concretes subject to freeze-thaw cycles had a water uptake three times greater (by weight) in average than concrete subject only to ponding at 20 °C. Furthermore, no clear difference is noticed in the uptake of water between the freeze-thaw tests at different temperatures, suggesting that the intensity (i.e. minimum negative temperature) of the freeze-thaw cycle does not have a significant influence on the uptake of water, for the duration and intensity of cycles used.

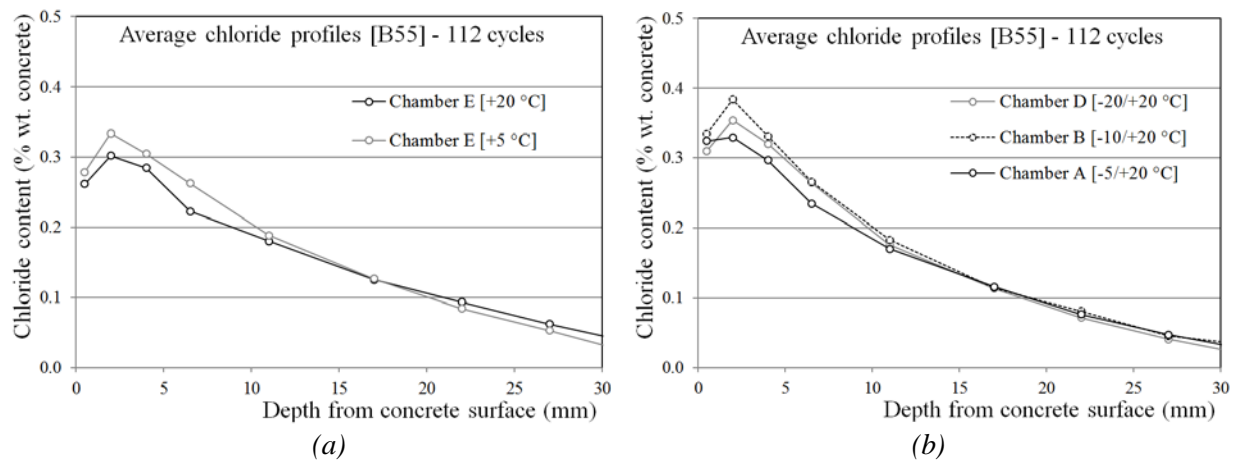


Figure 1: Average chloride profiles after 112 days ponding for (a) B55 and (b) B42 concrete.

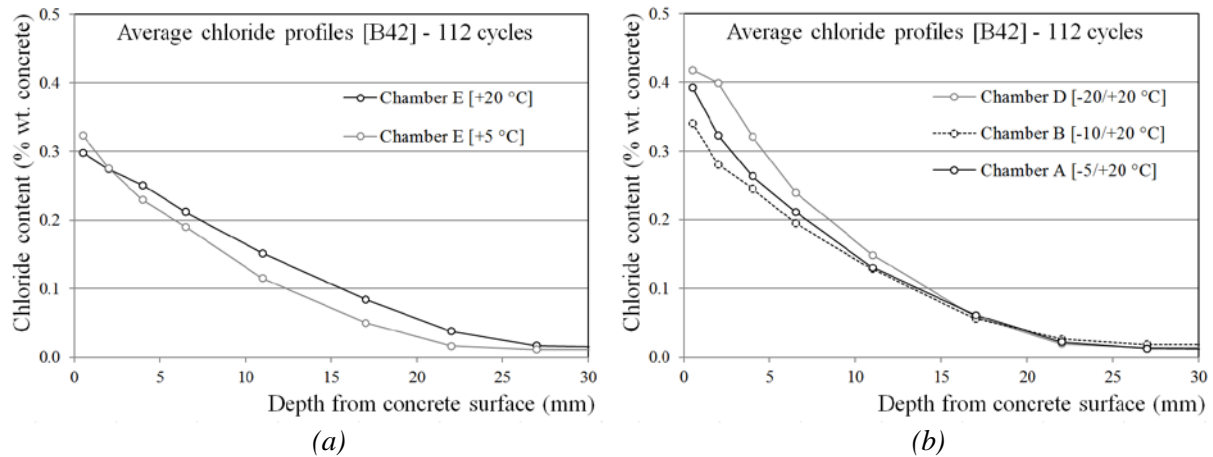


Figure 2: Average chloride profiles after 112 F/T cycles for (a) B55 and (b) B42 concrete.

The ponding chloride profiles results reveal the expected differences between the concrete qualities – higher chloride content at greater depths for B55 compared to B42. Furthermore, the B42 concrete, due to its refined pore structure, distinguishes better between ponding at +5°C and +20 °C.

The profiles from the different freeze-thaw tests show that the influence of the minimum negative temperature reached during the test is small or negligible. In addition, these profiles show small differences when compared to the ponding profiles. This is an unexpected finding as the water uptake is larger for the concretes with freeze-thaw cycles than with just ponding. It is thought that this water uptake is mainly salt free as it occurs due to the ice lens pumping effect,

possibly diluting the concentration of the chloride ions solution. However, the profiles show no such reduction in chloride concentration. This could suggest that diffusion is occurring in saturated microstructure unaffected by the action of freeze-thaw, i.e. diffusion dominates, or, that the interaction between competing transport mechanism is complex that no unique mechanism consistently explains the findings, but their current interaction results in profiles identical to those of pure ponding.

4. CONCLUSIONS

The testing was designed to allow for interaction of multiple transport mechanism. They are complex experiments because they combine capillary water uptake with diffusion at the same time, and overlaying these with the action of freeze-thaw. The results provide an insight into possible interaction, therefore it is important to observe the outcome of the verified behaviour. It can be difficult to extract a full explanation without additional experiments; however, based on the limited tests and samples tested, the following conclusions can be drawn:

- - Concrete samples subject to freeze-thaw cycles have a greater uptake of water than subject to pure ponding, suggesting that micro ice lens pumping is active. The water uptake for B52 is greater than B42, as would be expected due to the pore structure of these concretes;
- No clear difference is noticed in the uptake of water by the intensity of the freeze-thaw cycle (low negative temperature);
- The depth and volume of B55 profiles is greater than B42 profiles, as would be expected due to the pore structure of these concretes;
- The effect of the freeze-thaw cycles on the chloride profile is small or negligible, which is surprising considering the increased water uptake that the same concrete presents. This could suggest that diffusion is occurring in saturated microstructure unaffected by the action of freeze-thaw, i.e. diffusion dominates, or, that the interaction between competing transport mechanisms is complex, with no unique mechanism explaining consistently the findings. Their current interaction may result in profiles identical to those of pure ponding.

ACKNOWLEDGMENTS

This research was supported by a TEKES FiDiPro Program grant for the project CSLA – Concrete Service Life Assessment: modelling frost attack degradation in the presence of chlorides (TEKES-40083/12).

REFERENCES

- Ferreira, R.M., Kuosa, H., Makkonen, L., ‘Performance & Durability of Concrete in Extreme Cold Environment. CSLA Project – Task 1. Literature Review’. VTT Research Report. VTT-R-073643-12. (2012). 108p.
- Ferreira, R.M., Kuosa, H., Leivo, M., ‘Characterization of testing concrete. CSLA Project – Task 5. Testing’. VTT Research Report. VTT-R-01620-14 (2014a)
- Ferreira, R.M., Kuosa, H., Leivo, M., ‘Study of the effect of freeze-thaw on chloride ingress. CSLA Project – Task 6. Test setup and results’. VTT Research Report. VTT-R-01621-14 (2014b)
- Kuosa, H., Ferreira, R.M., Holt, E., Leivo, M., Vesikari, E., ‘Effect of coupled deterioration by freeze-thaw, carbonation and chlorides on concrete service life.’ *Cement.& Concrete Composites*. 47 (2014) 32–40
- Leivo, M., Sistonen, E., Al-Neshawy, F., Piironen, J., Kuosa, H., Holt, E., Koskinen, R., Nordqvist, C., ‘Effect of interacted deterioration parameters on service life of concrete structures in cold environments. Laboratory results 2009 -2010’. VTT Research Report. VTT-R-04799-11, 2011. 57 p.
- Li, B., ‘Chloride transport in concrete under frost action – An experimental study’. Master Thesis. TCH. Göteborg. 2009, 156p.

Chloride ingress in concrete – Results from over 20 years’ field exposure in Swedish marine environment



Tang Luping*
Ph.D., Prof
Chalmers Univ. of Techn.
Div. of Building Technology
SE-412 96, Gothenburg
tang.luping@chalmers.se

* Corresponding author



Peter Utgenannt
Ph.D.
CBI Betonginstitutet
c/o SP
SE-501 15, Borås
peter.utgenannt@cbi.se



Dimitrios Boubitsas
CBI Betonginstitutet
c/o SP
SE-501 15, Borås
dimitrios.boubitsas@cbi.se

ABSTRACT

This paper presents the results from a number of research projects dealing with chloride ingress in concrete exposed to Swedish marine environment after exposure up to over 20 years. In the beginning of the 1990s, some 40 types of concrete slabs were exposed to seawater at the Träslövsläge field site on the west coast of Sweden. The concrete slabs were periodically sampled for chloride ingress profiles after exposure for 0.5-2, 5, 10 and 20 years. These chloride profiles were used for validation of prediction models for chloride ingress. The results show that the chloride ingress is in general more severe in the submerged zone than in the other zones. Multi-pozzolanic additions such as fly ash and silica fume can effectively reduce chloride ingress.

Key words: Chloride, concrete, durability, field exposure, modelling.

1. INTRODUCTION

In the beginning of the 1990s, a Swedish national project called “BMB” – Durability of Marine Concrete Structures – was initiated /Sandberg 1996/. As a part of work in the BMB project, some 40 types of concrete specimens were exposed to seawater at the Träslövsläge field site on the west coast of Sweden. The specimens were periodically sampled for chloride penetration profiles, which served to provide “first-hand” information about chloride ingress into concrete and are believed valuable for the examination of modelling for chloride penetration. The chloride ingress profiles for samples exposed for up to five years to seawater at the field site have been measured during the lifetime of the BMB project.

After the BMB project, many concrete slabs were left at the field site for continuous long-term exposure. To collect the field data after 10 years’ exposure, SP Technical Research Institute of Sweden (the parent company of CBI Betonginstitutet AB) together with Chalmers University of Technology (Chalmers) carried out a project under the financial support of Swedish National

Road Administration (SP Report 2003:16). Further, to collect the field data after 20 years' exposure CBI together with SBUF (The Development Fund of the Swedish Construction Industry), Cementa and Elkem carried out this project.

The Träslövsläge field site is perhaps the first field exposure site in the world for systematic collection of chloride ingress profiles in various types of concrete. Nanukuttan et al. /2010/ reported some chloride ingress data from one type of concrete (CEM I, w/c 0.4) after exposure under the North Sea tidal zone near the Dornoch bridge, Scotland, for 18 years. Baroghel-Bouny et al. /2013/ reported some chloride ingress profiles from 15 different types of concrete after exposure under the Atlantic tidal zone in La Rochelle, France, for 10 years. It can be noticed that these published field data were taken from tidal zone which make the modelling and validation more complicated. On the other hand, the data from the Träslövsläge field site were taken mainly from the submerged zone, which supplies unique opportunity for validating chloride ingress models under clearer boundary conditions with the longest exposure time (over 20 years).

2 CONCRETE SPECIMENS AND EXPOSURE CONDITIONS

The original mixture proportions of concrete cast 20 years ago are published elsewhere in /Sandberg 1994/, /Tang 2003a/ and /Boubitsas et al. 2014/. The main variations included water-binder ratio (0.25, 0.3, 0.35, 0.4, 0.5, 0.6 to 0.75), binder type (four types of cement with different additions of silica fume and fly ash), and air content (6% entrained air and non-AEA). Concrete slabs of 1000×700×100 mm were cast at the SP Swedish Technical Research Institute. After moisture curing for about two weeks, the slabs were transported to the Träslövsläge field site and mounted on the sides of pontoons for exposure with the bottom side of the slab facing the seawater in which the chloride concentration varies from 10 to 18 g Cl per litre, with an average value of about 14 g Cl per litre and the typical water temperature +11°C as an annual average. A parallel set of slabs was transported to the laboratory at Chalmers for measurement of accelerated chloride transport as it is described in /Tang 2003b/.

3 MEASUREMENT OF CHLORIDE INGRESS PROFILES

The concrete slabs were sampled after 0.5, 1, 2, 5, 10 and 20 years of exposure for measurement of chloride ingress profiles. The cores of 80-100 mm diameter were taken from the slabs at three exposure zones namely atmospheric (upper 30 cm), splash (30-60 cm from the upper side) and submerged (lower 40 cm). After coring the cores were sealed in the plastic bags and stored in the laboratory not longer than two weeks prior to sampling for profiles. Powder samples were then taken from each core by means of dry-grinding on a lathe with a diamond tool, successively from the exposed surface to a certain depth. The depth of each sample was measured from the lathe with an accuracy of 0.5 mm. After the grinding, the powder samples were immediately dried at 105 °C and then stored in a desiccator for later chloride and calcium analysis. The calcium analysis is for an estimation of binder content in the same sample for chloride content so as to be able to more precisely express the chloride content by mass % of binder.

The acid soluble chloride content in each sample was determined principally in accordance with AASHTO T260 using potentiometric titration on an automatic titrator with chloride selective electrode and Ag/AgCl reference electrode. A sample size of 1-1.5 gram was used to facilitate the parallel calcium analysis, that is, after the chloride titration the solution was alkalized and titrated again with calcium selective electrode and 0.1 EDTA as titrant. The detailed description of the titration method for determination of soluble calcium content parallel to the determination of chloride content can be found in /Tang 2003c/. Since similar techniques were employed in the

precious investigations even though by different operators, the data from various investigations should be reliable and comparable.

4 MODELLING CHLORIDE INGRESS

Many models have been proposed in the past decades for predicting chloride ingress in concrete. As reported by Tang et al. /2012/, DuraCrete model /2000/ has been widely recognized in the world owing to its EU-project characteristics. This model has also been introduced by Betongföreningen /2007/. On the other hand, a mechanism-based model the so called ClinConc model was developed by /Tang 2008/. These two models were used for modelling of chloride ingress in the concretes exposed under the seawater (sub-zone) at the Träslövsläge exposure site. The detailed description of these two models and input parameters used in the prediction can be found in /Boubitsas et al. 2014/.

5 RESULTS AND CONCLUSIONS

The measured chloride ingress profiles are summarized in /Tang 2003b/ (for the 0.5-10 years' exposure) and /Boubitsas et al. 2014/ (for the 20 years' exposure), in the latter the modelled results can also be found. The measured results show that the chloride ingress is in general more severe in the submerged zone than in the other zones. Multi-pozzolanic additions such as fly ash and silica fume can effectively reduce chloride ingress. From the modelled results it can be concluded that the ClinConc model fits fairly well to the measured values from one year up to 20 years' field exposure for most types of concrete. Therefore, it is reasonable to use this model to predict chloride ingress in concrete exposed in Swedish west coast seawater. The predicted profiles are shown in Figure 1.

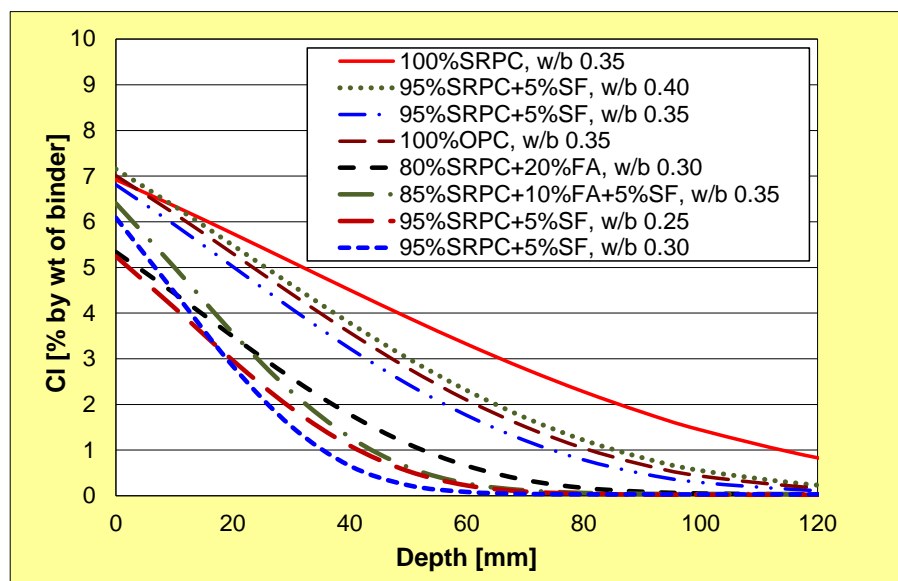


Figure 1 – Predicted chloride profiles in concrete after 100 years' exposure in Swedish west coast seawater.

It can be seen from the prediction that, if the chloride threshold value of 1% by weight of binder is assumed, the concrete with plain sulphate resistant Portland cement (SRPC) with water-binder ratio of 0.35 needs a cover thickness of >110 mm to protect the reinforcement for a service life of 100 years. With addition of 5% silica fume and w/b 0.35, it is possible to achieve 100 years' service life with 80 mm cover. The best measure to obtain 100 years' service life with a cover thickness of for example 60 mm is to use either 5% silica fume or 20% fly ash with reduced

water-binder ratio ≤ 0.30 , or to use a combination of both fly ash and silica fume (w/b 0.35). It seems that a water-binder ratio lower than 0.30 does not further reduce chloride ingress. However, the uncertainty in the prediction should be further investigated before this promising model can be applied to the service life design and redesign of reinforced concrete structures exposed to a marine environment.

REFERENCES

- Baroghel-Bounya, V., Dierkensb, M., Wanga, X., Soivec, A., Saillioad, M., et al., 2013, "Ageing and durability of concrete in lab and in field conditions: investigation of chloride penetration", *Journal of Sustainable Cement-Based Materials*, 2 (2) 67-110.
- Betongföreningen, 2007, "Guidelines for durability design of concrete structures" (in Swedish), Swedish Concrete Association, Report No. 12, Stockholm, Sweden.
- Boubitsas, D., Tang, L. and Utgenannt, P., 2014, "Chloride ingress in concrete exposed to marine environment - Field data up to 20 years' exposure", Final Report to SBUF, to be published.
- Duracrete, 2000, "General Guidelines for Durability Design and Redesign", Report R15, in 'EU Brite-EuRam III project DuraCrete (BE95-1347): Probabilistic Performance Based Durability Design of Concrete Structures', TNO Netherlands Organisation for Applied Scientific Research, Delft, Netherlands.
- Nanukuttan, S., Basheer, P.A.M., Holmes, N., Tang, L. and McCarter, J., 2010, "Use of performance specification and predictive model for concretes exposed to a marine environment", in *Structural Faults and Repair Conference 2010*, 15-17 June 2010, Edinburgh, Scotland, 12 pages, CDROM.
- Sandberg, P., 1996, "Systematic collection of field data for service life prediction of concrete structures", in *Durability of Concrete in Saline Environment*, Cementa AB, Stockholm.
- Tang, L., 2003a, "Estimation of cement/binder profile parallel to the determination of chloride profile in concrete- Nordtest project No. 1581-02", SP Report 2003:7, SP Swedish National Testing and Research Institute, Borås, Sweden.
- Tang L., 2003b, "Chloride Ingress in Concrete Exposed to Marine Environment – Field Data Up to 10 Years Exposure", SP Report 2003:16.
- Tang L., 2003c, "A Collection of Chloride and Moisture Profiles from the Träslövsläge Field Site – From 0.5 up to 10 years investigations", Chalmers Publication P-03:3.
- Tang, L., 2008, "Engineering expression of the ClinConc model for prediction of free and total chloride ingress in submerged marine concrete", *Cement and Concrete Research*, 38(8-9), pp. 1092-1097.
- Tang, L., Utgenannt, P., Lindvall, A. and Boubitsas, D. (2012), "Validation of models and test methods for assessment of durability of concrete structures in the road environment", CBI Report 2:2012, Swedish Cement and Concrete Research Institute, Stockholm, Sweden, 2012.

SELF-COMPACTING CONCRETE (SCC).

Analytical and Empirical Equations to Predict Pressure during Pumping of Self-Consolidating Concrete



Dimitri Feys
Missouri University of
Science and Technology,
Department of Civil,
Architectural, and
Environmental Engineering,
1401 N. Pine St., Rolla, MO
65409, USA
Feysd@mst.edu



Kamal H. Khayat
Missouri University of
Science and Technology,
Department of Civil,
Architectural, and
Environmental Engineering,
500 W. 16th St., Rolla, MO
65409, USA
Khayatk@mst.edu

ABSTRACT

Several practical guidelines are available in literature for proportioning pumpable concrete and to estimate the pumping pressure. For more workable concrete mixtures, including SCC, the practical guidelines are not always applicable. This paper validates, by means of full-scale pumping tests, the analytical prediction model developed by Kaplan et al., for concrete mixtures with enhanced workability. Furthermore, based on the experimental results, empirical equations to predict pumping pressure for SCC are developed, based on pipe diameter, flow rate and rheology, tribology or workability.

Keywords: SCC, rheology, pumping, tribology, pressure

1. INTRODUCTION

Concrete pumping is a widespread placement method and significant amounts of information on proportioning concrete and estimating pressure can be found in practical guidelines (ACI 304, 1998, V. Eckhardstein, 1983). Despite the increasing research on pumping of highly-workable and self-consolidating concretes (HWC/SCC), the practical guidelines are not yet adjusted for these new concrete types. The empirical relationship between slump (yield stress) and pumping pressure for conventional vibrated concrete (CVC) is no longer valid for HWC and SCC, due to their low yield stresses. Instead, the pressure loss shows a good correlation with concrete viscosity (Feys et al, 2013).

In this paper, the analytical equations developed by Kaplan (2001) to predict pumping pressures in straight pipes are evaluated for HWC and SCC by means of full-scale pumping tests. For these equations, the properties of the lubrication layer, which is a layer depleted of (coarse) aggregates formed near the pipe wall, need to be determined. Also in this paper, empirical equations to predict pumping pressures based on rheology, tribology and workability are presented. Bends, reducers and vertical pumping are not included.

2. ANALYTICAL APPROACH

2.1. Prediction equations

Kaplan (2001) developed two theoretical equations predicting the pressure during pumping of concrete in straight pipes (eqs. 1 and 2):

$$\Delta p = \frac{2}{R} \left(\frac{Q}{\pi R^2} \eta_{LL} + \tau_{0,LL} \right) \quad (1)$$

$$\Delta p = \frac{2}{R} \left(\frac{\frac{Q}{\pi R^2} - \frac{R}{4\mu_p} \tau_{0,LL} + \frac{R}{3\mu_p} \tau_0}{1 + \frac{R}{4\mu_p} \eta_{LL}} \eta_{LL} + \tau_{0,LL} \right) \quad (2)$$

Where: Δp = pressure loss per unit of length (Pa/m), R = pipe radius (m), Q = flow rate (l/s), $\tau_{0,LL}$ = yield stress of lubrication layer (Pa), η_{LL} = viscous constant of the lubrication layer (Pa s/m), τ_0 = concrete yield stress (Pa), μ_p = concrete plastic viscosity (Pa s).

The difference between eq. 1 and eq. 2 is that in the former, the rheological properties of the concrete are not included. Eq. 1 is only valid when the bulk concrete is not sheared ($\Delta p R/2 < \tau_0$), while eq. 2 is valid when shearing occurs in both the lubrication layer and the concrete.

2.2 Tribology to measure lubrication layer properties

Tribology for concrete has been defined as the science of concrete flowing near a smooth surface. The measurements are performed with tribometers (Kaplan, 2001), which are similar to coaxial cylinders rheometers for concrete. In concrete rheometers, protruding ribs, blades or vanes are installed to prevent particle migration during the measurement. In a tribometer, the surfaces are smooth to enhance the formation of the lubrication layer. As a consequence, the concrete is no longer homogeneous, as a layer depleted of (coarse) aggregates is formed near the inner cylinder. The torque measured at different rotational velocities is thus significantly lower than in concrete rheometers. If the bulk concrete is not sheared (due to its relatively high yield stress), the properties of the lubrication layer (yield stress and viscous constant) can be directly determined for the shear stress – linear velocity relationship (Kaplan, 2001). If the bulk concrete is sheared (which is mostly the case for SCC), an additional calculation step must be performed, as described in (Feys et al, 2014). This additional calculation requires measuring the concrete rheological properties in parallel. It should also be noted that the viscous constant combines the lubrication layer viscosity and its unknown thickness.

2.3 Validation by means of full-scale pumping tests.

The analytical equations developed by Kaplan were validated by means of full-scale pumping tests at the Universite de Sherbrooke. In total, three CVC, four HWC (slump flow between 350 and 600 mm) and 18 SCC mixtures were pumped through a 30 m loop circuit. Each concrete was pumped four to six times at six to eight different flow rates, varying between 2 and 18 l/s (Khatib, 2013). The loop circuit was equipped with pipes having two different diameters (100 and 125 mm) in the pressure loss was measured in two horizontal 10 m long sections. After each time the concrete was pumped through the circuit, the workability, rheological and tribological properties were determined. The rheological properties were measured with the ICAR rheometer. However, the ICAR rheometer delivers significantly lower viscosity values than the ConTec Viscometer 5, which can lead to problems interpreting the tribometer data (Feys et al, 2014). As a result, the ICAR results were transformed to their equivalent ConTec values based on a comparative study. The tribometer used was the device developed at the Universite de Sherbrooke, described in (Feys et al, 2014).

These full-scale pumping tests lead to more than 1300 data points, on which eq. 1 or 2 was applied, depending on whether the bulk concrete was sheared in the pipes. The predicted pressure losses, based on rheology, tribology, pipe diameter and flow rate are compared to the experimentally measured pressure losses in Figure 1. In average, the analytical equations provide an 8% larger estimation of the pressure loss, with an excellent correlation factor. Furthermore, the results were validated for CVC, HWC and SCC, proving the general applicability of the analytical equations.

3. EMPIRICAL MODELS

The application of equations 1 or 2 requires the use of a rheometer and a tribometer at the same time. The following empirical models, based on the pumping results, were developed, relating the pressure losses to concrete rheology, total flow resistance in the tribometer and the V-Funnel flow time.

Pressure loss predicted by Kaplan's equations (kPa/m)

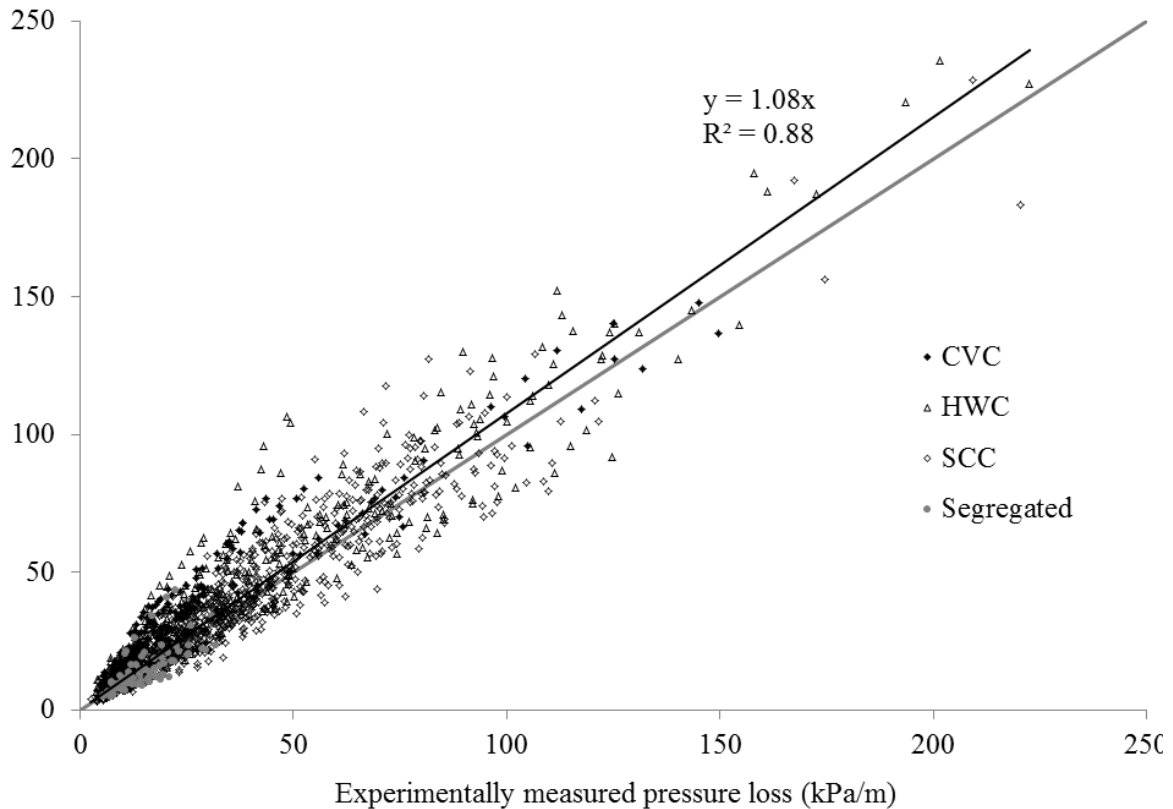


Figure 1: The pressure loss predicted by means of equations 1 or 2 is similar to the pressure loss measured during the experiments.

3.1. Pressure loss based on concrete plastic viscosity

It has been proven in literature that pressures occurring during pumping of SCC relate well with the plastic viscosity of the concrete (Feys et al, 2013). The same conclusion was obtained during the full-scale pumping tests for SCC and HWC (flowable concrete that is not yet SCC). Even for the CVC, the viscosity has an influence on the pumping pressure, but a sole $\Delta p - \mu_p$ relationship could not be obtained due to the influence of the yield stress. The pressure loss Δp , in kPa/m, can be estimated based on eqs. 3 and 4. Note that Q is expressed in l/s and μ_p has Pa s as unit and is measured (or transformed) with the ConTec Viscometer 5.

$$\Delta p = 0.94 - 1.14 Q + 0.050 \mu_p + 0.13 Q \mu_p \text{ (for 100 mm pipes)} \quad (3)$$

$$\Delta p = 3.58 - 0.70 Q - 0.062 \mu_p + 0.067 Q \mu_p \text{ (for 125 mm pipes)} \quad (4)$$

3.2. Pressure loss based on total flow resistance in the tribometer

Similar to eqs. 3 and 4, empirical equations were developed relating the pressure loss to the total flow resistance in the tribometer. For HWC and SCC, the rheological properties of the concrete are needed to calculate the tribological parameters $\tau_{0,LL}$ and η_{LL} . To avoid this complexity, the parameter I_{trib} is introduced. I_{trib} denotes the total flow resistance of the concrete in the tribometer and is the slope of the torque – rotational velocity relationship, similar to “H” for a concrete rheometer. I_{trib} has Nms as unit, but its value depends on the geometry of the tribometer. The following equations are valid for the tribometer described in Feys et al, 2014. It should be noted that eqs. 5 and 6 do not include the influence of concrete yield stress, similar to eqs. 3 and 4, providing thus a less precise estimate of pumping pressures for CVC.

$$\Delta p = 0.20 + 0.53 Q + 1.78 I_{trib} + 2.54 Q I_{trib} \text{ (for 100 mm pipes)} \quad (5)$$

$$\Delta p = 2.29 + 0.35 Q - 1.45 I_{trib} + 1.24 Q I_{trib} \text{ (for 125 mm pipes)} \quad (6)$$

3.3. Pressure loss based on the V-Funnel flow time

It is known from literature that the V-Funnel flow time is related to the plastic viscosity for SCC. As a consequence, a relationship between the pressure loss and the V-Funnel flow time has been established. It should be noted that eqs. 7 and 8 are only valid for concrete mixtures with slump flows larger than 600 mm, as the V-Funnel flow time is also influenced by the yield stress of the concrete.

$$\Delta p = 0.40 + 0.46 Q + 0.41 VF + 0.85 Q VF \quad (\text{for } 100 \text{ mm pipes}) \quad (7)$$

$$\Delta p = 2.93 + 0.16 Q - 0.60 VF + 0.44 Q VF \quad (\text{for } 125 \text{ mm pipes}) \quad (8)$$

4. CONCLUSIONS

A series of full-scale pumping tests was conducted to evaluate analytical equations predicting pressure during pumping of concrete, as well as to develop empirical relationships relating the pressure loss of highly-workable concrete, including self-consolidating concrete, to rheology, tribology and workability.

The analytical equations developed by Kaplan for conventional vibrated concrete, deliver in average an 8% larger estimation of the pumping pressure, relative to the experiments. This result proves the validity of the equations for a wide range of concrete types, as the workability of the concrete mixtures varied between relatively stiff to self-levelling concrete. On the other hand, for highly-workable concrete mixtures, the low yield stress causes the concrete to be sheared in the pipes and in the tribometer. As a result, the rheological properties need to be determined to measure the tribological properties of the lubrication layer.

Based on the experiments executed with two different pipe diameters, empirical equations were developed for highly-workable concrete mixtures, including self-consolidating concrete, relating the pressure loss to the viscosity of the concrete and the flow rate in the pipes.

A similar set of equations was developed to relate the pressure loss to the total flow resistance in the tribometer (I_{trib}). This latter parameter is the slope of the torque – rotational velocity line resulting of concrete measured in the tribometer. However, I_{trib} is not a fundamental unit and depends on the geometry of the tribometer.

A last set of two prediction equations was derived for the prediction of the pressure loss based on the V-Funnel flow time. A good correlation exists between the V-Funnel flow time and the plastic viscosity of SCC, justifying these relationships. However, for concrete mixtures with slump flows lower than 600 mm, the V-Funnel flow time is also influenced by the yield stress, reducing the accuracy of the prediction for non-self-consolidating concrete.

REFERENCES

- ACI-Committee 304 (1998), *Placing Concrete by Pumping Methods*, American Concrete Institute, Farmington Hills.
- Feys D., De Schutter G., Verhoeven R. (2013), Parameters influencing pressure during pumping of self-compacting concrete, *Mat. Struct.* 46:4, 533-555
- Feys D., Khayat K.H., Perez-Schell A., Khatib R. (2014a), Development of a Tribometer to Characterize Lubrication Layer Properties of Self-Consolidating Concrete, accepted for publication in *Cement and Concrete Composites*.
- Kaplan D. (2001), *Pumping of Concrete*, Ph-D thesis (in French), Laboratoire Central des Ponts et Chaussées.
- Khatib R. (2013), *Insights into Pumping High-Strength Self-Consolidating Concrete*, Ph-D thesis, Université de Sherbrooke.
- Von Eckardstein K.E. (1983), *Pumping, Concrete and Concrete Pumps – A Concrete Placing Manual*, Schwing.

Stability of Entrained Air in Self-Consolidating Concrete Under Vibration



David A. Lange, Ph. D.
 Professor, Civil and Environmental Engineering
 University of Illinois at Urbana-Champaign
 205 N Mathews Ave, Urbana, IL 61801
 dlange@illinois.edu



Daniel I. Castaneda, M. S. C. E.
 Research Assistant, Civil and Environmental Engineering
 University of Illinois at Urbana-Champaign
 205 N Mathews Ave, Urbana, IL 61801
 castane6@illinois.edu



Jeremy A. Koch, M. S. E.
 Research Assistant, Civil and Environmental Engineering
 University of Illinois at Urbana-Champaign
 205 N Mathews Ave, Urbana, IL 61801
 jakoch2@illinois.edu



Randy H. Ewoldt, Ph. D.
 Assistant Professor, Mechanical Science and Engineering
 University of Illinois at Urbana-Champaign
 1206 W Green St, Urbana, IL 61801
 ewoldt@illinois.edu



Kyle A. Riding, Ph. D.
 Associate Professor, Civil Engineering
 Kansas State University
 2118 Fiedler Hall, Manhattan, KS 66506
 riding@ksu.edu

ABSTRACT

Fresh concrete is routinely vibrated to achieve consolidation in formwork, but over-vibration poses a risk to the entrained air system that provides freeze-thaw durability. The mechanics of vibration, rheology, and air bubble movement are examined in this study. The experimental work considers cementitious materials and model materials under vibration using an immersion probe. The magnitude of vibration is measured by an immersed accelerometer sensor. Initial findings show aggregate volume fraction playing a strong role in determining the radius of vibrational influence. Video imagery of transparent model materials shows the movement of entrapped air at further distances from the immersion probe as the particle volume fraction increases. A better understanding of vibration of yield stress fluids and bubble buoyancy will lead to improvements in best practices for vibration of concrete.

Key words – vibration, aggregate, rheology, modelling

1. INTRODUCTION

Concrete is vibrated in order to drive out entrapped air and to minimize honeycombing around the reinforcement and form walls. ACI Committee 309 reports (309.1 and 309.8) provide guidance for concrete practitioners. However, relatively little information is known about the effects of time of vibration, mould geometries, material proportions, and entrained air bubble size distribution. As such, control of entrained air can be challenging for concrete products that undergo vibration during placement. In this study, mortars and polymer gels were used to investigate the extent of vibrational influence with respect to maximum peak acceleration and observable movement of entrapped and entrained air within a transparent fluid.

2. MATERIALS AND EXPERIMENTAL METHOD

2.1 Vibration of fresh materials using immersion probe (pencil vibrator)

A 15.24 cm by 15.24 cm by 122 cm Plexiglas mold was constructed to hold fresh mortar with water-to-cement ratio of 0.30 using ASTM C150 Type I Portland cement, Sika Viscocrete 2100 as a high-range water reducer, MasterSet DELVO as a set-retardant, and increasing volume fractions of river sand. Carbopol 980 Polymer was also produced at a weight fraction of 0.24% and mixed with increasing volume fractions of ASTM C778 standard sand. A 220 Hz 2.67 cm diameter DeWalt pencil vibrator was positioned at one end of the mould approximately 7.6 cm away from the three form walls to a depth of 14 cm. A tri-axial accelerometer was positioned using an adjustable lever arm at increasing distances from the immersion probe at a constant depth of 7.62 cm.

Carbopol 980 Polymer is a crosslinked polyacrylate polymer that is mixed with water to form a clear gel which is stable at neutral pH. The gel features design-controllable yield stress and viscosities that can suspend particles and air while maintaining a high amount of clarity through the material. The gel has been utilized in other rheological studies as a surrogate material for fibre reinforced concrete [Boulekbache *et al*, 2010].

2.2 Measuring rheology

Both the cementitious and polymer fluids were treated as Bingham plastics, which are characterized by a dynamic yield stress (tangent intercept) and plastic viscosity (slope at large shear strain rate). The static yield stress was also measured, but is not considered in the determination of the Bingham fit parameters. Both fluids were firstly measured for their rheology and thereafter immediately placed into the Plexiglas beam mould to be tested. The rheological properties were measured using an ICAR Rheometer or an AR-G2 Rheometer, both with rotating vane geometries.

2.2 Image capture of model materials

In a 10 cm by 30 cm by 20 cm Plexiglas mould was constructed and vibrated using a custom-built pencil vibrator with 0.5 inch diameter probe. The position and movement of and the probe and entrapped air were monitored through both the top surface and side walls.

3. RESULTS AND DISCUSSION

3.1 Changing rheology as a function of increasing aggregate volume fraction

Table 1 shows the measured rheological properties for the polymer gel and cementitious materials mixtures as the volume of fine aggregate is increased. The advantage of the polymer gel material is that it does not undergo hydration meaning that its rheological properties are

unchanging with respect to time. As such, the contribution of the increasing aggregate volume fraction is notable at 60% where the rheological properties markedly increase. This is most attributable to the increasing shearing interaction between particles directly whereas their interaction is less in a dilute (0-40%) volume fraction. The cementitious mixtures also show a similar increase in rheological properties at 60% volume fraction while the dilute volume fractions have comparable rheological properties.

Table 1 Rheological properties of cementitious and model materials

| | Mean Static Yield Stress (Pa) and COV | | Mean Dynamic Yield Stress (Pa) and COV | | Mean Plastic Viscosity (Pa.s) and COV | |
|-------------------|---------------------------------------|-----|--|-----|---------------------------------------|-----|
| Carbopol + 00% FA | 35.3 | 0% | 39.7 | 2% | 0.7 | 7% |
| Carbopol + 20% FA | 20.4 | 15% | 22.0 | 10% | 1.6 | 22% |
| Carbopol + 40% FA | 45.3 | 7% | 55.8 | 1% | 2.8 | 2% |
| Carbopol + 60% FA | 1669.1 | 46% | 1345.7 | 11% | 32.1 | 84% |
| Mortar + 00% FA | 244.8 | 15% | 175.7 | 5% | 27.6 | 13% |
| Mortar + 20% FA | 203.7 | 17% | 127.4 | 6% | 37.9 | 20% |
| Mortar + 40% FA | 294.1 | 34% | 85.6 | 4% | 58.1 | 14% |
| Mortar + 60% FA | 1178.4 | 92% | 145.5 | 65% | 339.7 | 20% |

3.2 Radius of action

Figure 1 shows the average peak resultant acceleration within the Plexiglas beam. In the polymer gel material, there is a general trend for the peak acceleration to increase to higher magnitudes. Also, the curve shifts rightward meaning more volume of the material is being engaged by the vibration. There is a slight hump at Carbopol + 60% FA at 45 cm which is explained by reflective and constructive waves associated with the small geometry of the beam mould. In the hydrating cementitious materials, a similar trend is observed where increasing volume fractions leads to an increase in the peak acceleration and a shift toward the right meaning that there is an increase in the radius of action.

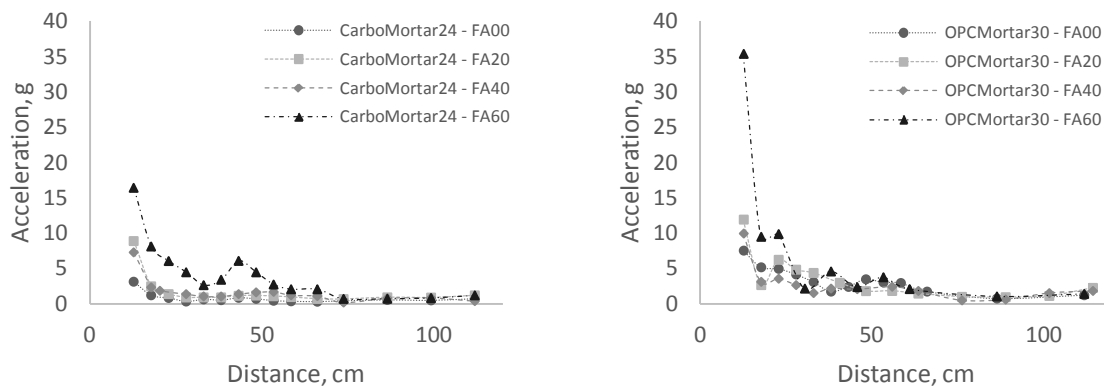


Figure 1 Average peak resultant acceleration as a function of distance

3.3 Model material image capture

Images taken of the polymer gel with bubbles, before and after three minutes of vibration, are seen in Figure 2. Most notably, the bubbles that are initially away from the probe by more than a centimetre are undisturbed by the vibration. Meanwhile, bubbles within a few millimetres of the probe have risen and left the system. This is evidence that the radius of action is quite small when there is no aggregate system to spread the vibration outwards.

The entrained air bubbles behave as predicted by viscous theory – namely, that larger bubbles rise more rapidly.. The most notable consequence of such behaviour is demonstrated by Figure 3, which displays the results of a simple simulation of vibration in a yield stress fluid. The histogram denotes a decreasing count of larger diameter bubbles, while small bubbles, with their slower rise speed, remain within the domain.

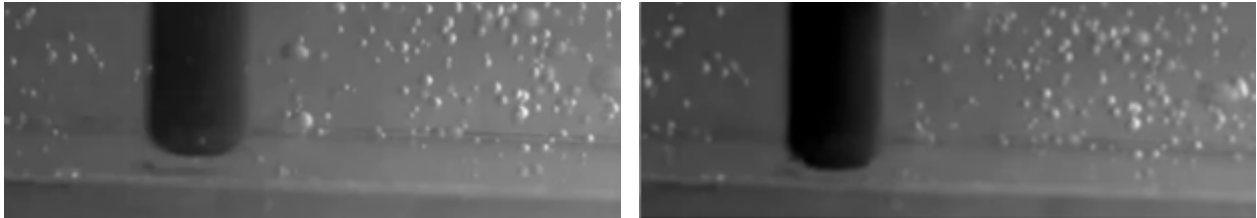


Figure 2 Bubble distribution in polymer gel before (left) and after (right) 3 minutes of vibration

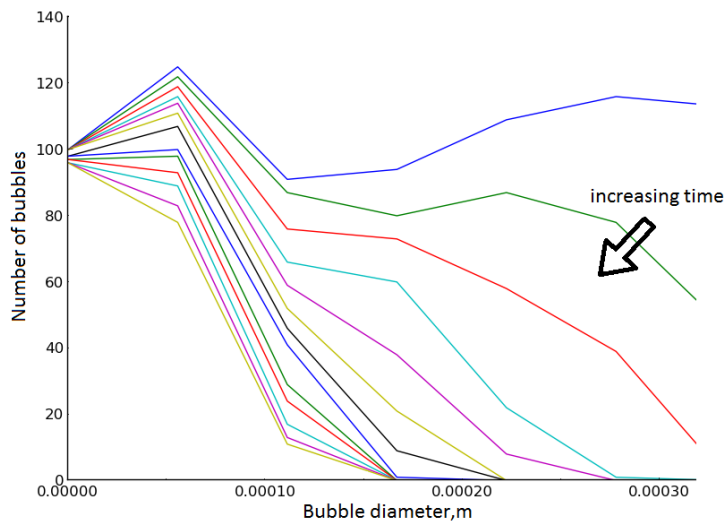


Figure 3 Histogram of bubble diameter for increasing time

4. CONCLUSION

This study is leading to a new model for vibration of concrete leading to better understanding of fluid properties, propagation of vibration energy, volume fraction of aggregate plays a role in extending the range of peak acceleration in fluid materials. This effect is confirmed by images of transparent model fluids, where notably the lack of an aggregate systems leads to very limited spatial influence of the vibration source.

REFERENCES

Boulekbatche, B., Hamrat, M., Chemrouk, M., and Amziane, S. “Flowability of fibre-reinforced concrete and its effect on the mechanical properties of the material.” *Construction and Building Materials* 24 (2010): 1664 – 1671.

Frost Resistance of Non Air Entrained Self-Compacting Concrete



Thordur I. Kristjansson
 B.Sc., M.Sc.
 ICI Rheocenter, Reykjavik University & Innovation Center Iceland
 Arleynir 2-8
 IS-112 Reykjavik
 E-mail: thordur.k@nmi.is



Olafur H. Wallevik
 Dr.Ing., Prof.
 ICI Rheocenter, Reykjavik University & Innovation Center Iceland
 Arleynir 2-8
 IS-112 Reykjavik
 E-mail: wallevik@ru.is

ABSTRACT

Self-compacting concrete (SCC) mixes were cast which contained different w/b ratio changing stepwise from 0.42 down to 0.29, and also different silica fume content, 0%; 6% and 12% (by weight) on a cement replacement basis. SCC turned out to be frost resistant at w/b ratio around 0.34 but increasing silica content did not improve the frost resistance and therefore the w/b ratio 0.30 has to be established for silica fume content of 12%. Rheological measurements on fresh concrete as well as compressive strength on hardened concrete were also carried out.

Key words: Frost resistance, Freeze-thaw durability, Self compacting concrete, Silica fume, Rheology.

1. INTRODUCTION

In Iceland freeze-thaw resistance is one of the major properties that have to be considered in a concrete mix design regarding durability. When evaluating the durability of a concrete mix with regard to freezing and thawing a lot of fundamental variables should be considered, for instance type of aggregates, w/b ratio, minimum cement or binder content and so on. The repeated cycles of freezing and thawing represent a severe environmental condition that may cause deterioration and or spalling of the concrete. Use of de-icing chemicals accentuates this problem /Malhotra 1983/.

Adding silica fume to a concrete mix may improve the freezing and thawing resistance, and is based on existing experience and knowledge. Studies have though also shown that use of silica fume in a concrete mix may accelerate the deterioration at a later stage, and thus it has been recommended that the test specimens should be subjected to more cycles of freezing and thawing than normally prescribed /Sabir 1997/. This might though be an artefact of the test method as it pumps in water and silica fume addition reduces the water permeability immensely.

There is still a controversy about whether or not non air entrained High Performance Concrete is durable when subjected to freeze-thaw distress. Some researchers have reported good results of non-air entrained concrete with w/c ratio ranging from 0.25-0.35, while others have doubts and conclude that it is necessary to air entrain these concretes to make them frost resistant, the main concern being that the concrete may turn out as durable for the first 50 to 100 freeze-thaw cycles but then start to accelerate in deterioration, and thus suggesting that stricter rules have to be applied to non-air entrained concrete. Many highlight also on necessitate of air entrainment in HPC /Aitcin 2003//Gjorv 2009//Hale 2009//Pigeon 1996/.

2. MATERIALS AND METHODS

The research program consisted of 13 SCC mix designs. The total binder content (cement + silica fume) ranged from 406 kg/m^3 to 553 kg/m^3 . The amount of water was constant around 150 kg/m^3 except when the w/b ratio was about 0.41, then the amount of water was increased to 160 kg/m^3 . The freeze-thaw test was used to evaluate the efficiency of the concrete mix regarding freeze-thaw durability. The different mix designs were also evaluated with a coaxial cylinder viscometer and the slump and slump flow was measured as well as the 28 day compressive strength.

Danish rapid hardening Portland cement type CEM I 52.5 N was used in this project, the silica fume used came from Elkem, Iceland, and the superplasticizer Omnicon SPC-25 is a type of carboxylic ether polymer with lateral chains. The aggregates used in this project came from Björgun, which are widely used for concrete in Reykjavik and surrounding districts. The sand and gravel is excavated from the sea-bed and crushed, sifted and washed on land. The water content in saturated surface dry condition was measured to 4.6% for the sand fraction and 3.0% for the gravel fraction.

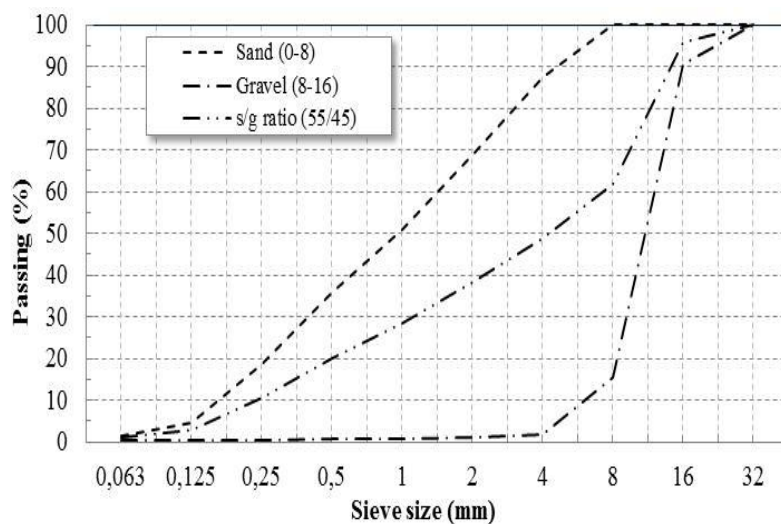


Figure 1 – Cumulative particle size distribution of aggregates.

Figure 1 displays the particle size distribution of the sand and gravel from Björgun as well the combined grading with the sand to gravel ratio 55/45.

3. RESULTS AND DISCUSSION

Table 1 displays the fresh properties of the mix designs such as slump and rheological measurements as well as the compressive strength. Generally when w/b ratio is lowered, both the yield value and the plastic viscosity increase. The superplasticizer dosage was varied in

order to aim for certain workability, this did not always prove successful. But one can see a tendency; for instance when the binder contains 0%, 6% and 12% silica fume on replacement basis the yield value and plastic viscosity increase when the w/c ratio drops from 0.42 to 0.29. Further, when introducing silica fume to the system, the plastic viscosity decreases significantly. As expected the compressive strength increases when reducing the w/c ratio and increases with added silica fume content.

Table 1 – Mix designs, slump, rheological characteristics and compressive strength

| | Silica fume (%) of binder | w/b ratio | Slump/Slump flow (mm) | Yield value (Pa) | Plastic viscosity (Pa·s) | Compressive strength (MPa) |
|-------|------------------------------|-----------|-----------------------------|------------------------|--------------------------------|----------------------------------|
| MIX1 | 0 | 0.30 | 255/680 | 189 | 192 | 84.2 |
| MIX2 | 0 | 0.34 | 270/565 | 59 | 92 | 73.3 |
| MIX3 | 0 | 0.39 | 270/600 | 74 | 118 | 63.4 |
| MIX4 | 0 | 0.39 | 270/625 | 87 | 127 | 67.4 |
| MIX5 | 0 | 0.42 | 270/560 | 60 | 89 | 60.9 |
| MIX6 | 6 | 0.29 | 265/695 | 136 | 143 | 92.0 |
| MIX7 | 6 | 0.34 | 270/570 | 109 | 122 | 73.9 |
| MIX8 | 6 | 0.38 | 270/590 | 98 | 99 | 74.5 |
| MIX9 | 6 | 0.42 | 270/575 | 64 | 72 | 71.4 |
| MIX10 | 12 | 0.29 | 265/660 | 52 | 108 | 91.9 |
| MIX11 | 12 | 0.33 | 270/480 | 93 | 92 | 79.3 |
| MIX12 | 12 | 0.38 | 270/620 | 55 | 77 | 76.4 |
| MIX13 | 12 | 0.42 | 270/570 | 60 | 72 | 70.6 |

In Iceland the limit for scaling after 56 freeze-thaw cycles test is set to less than 1 kg/m². Additionally, the ratio between scaling after 56 freeze-thaw cycles and 28 freeze-thaw cycles should not exceed 2.

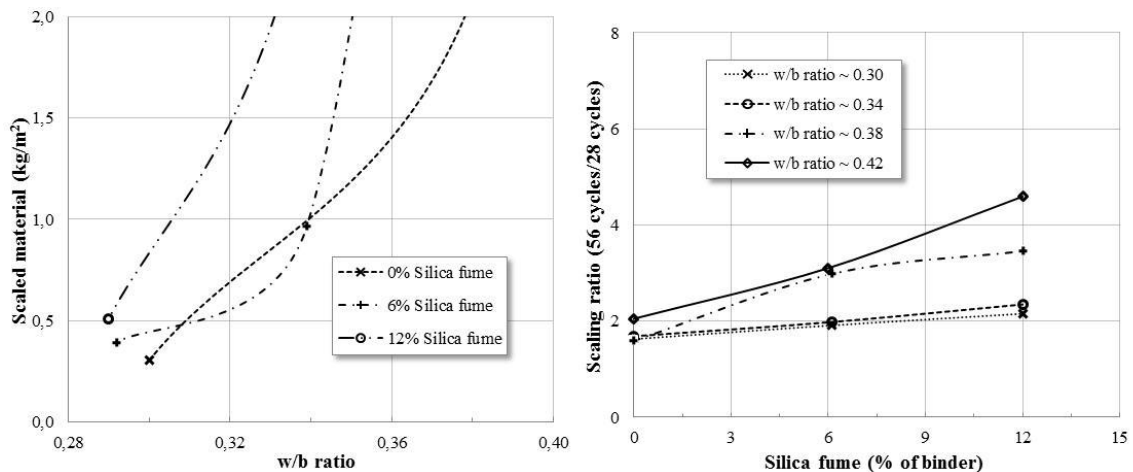


Figure 2 – Scaling after 56 cycles as a function of w/b ratio (left) and ratio between 56 freeze-thaw cycles and 28 freeze-thaw cycles (right).

Figure 2 to the left indicates that for a mix without silica fume the w/b ratio should not exceed 0.34 to be frost resistant. That seems also to be valid for mixes containing 6% silica fume on replacement basis. But when adding 12% of silica fume to the system, the w/b ratio drops here to 0.30, so this extra 6% silica fume does not contribute to the frost resistance. But looking at

figure 2 to the right, one can see that 5 mixes out of 13 pass the limit (the same that had scaling less than 1 kg/m^2), three with no addition of silica fume and two with 6% silica fume of binder. All these mixes have a w/b ratio of 0.34 or lower except for one without addition of silica fume and a w/b ratio of 0.38.

4. CONCLUSIONS

Within the limitation of the work here conducted, one can likely achieve a frost resistant SCC mix by using w/b ratio of 0.34 or lower. The addition of silica fume does not contribute to the frost resistance. The scaling ratio of 56 cycles and 28 cycles increases with increased silica fume content as none of the mixes pass the criteria when with 12% silica fume is used. The mix containing 6% silica fume revealed 0.95 kg/m^2 scaling (or just below the limit of 1 kg/m^2) having w/b ~ 0.34 (w/c about 0.36). This mix design is very workable although it requires much more additives than the one without silica fume. It should however be noted that aggregates are relatively low grade and the tests should be repeated with high grade aggregates.

REFERENCES

- Aitcin, P. C. (2003), *The Durability Characteristics of High Performance Concrete: A Review*, Cement and Concrete Composites, volume 25, Issue 4-5, p. 409-420.
- Cordon, W. A. (1966), *Freezing and Thawing of Concrete – Mechanisms and Control*, Published jointly by American Concrete Institute, Detroit, Michigan, USA and The Iowa State University Press, Ames, Iowa, USA, p. 70.
- Gjorv, O. E. (2009), *Durability Design of Concrete Structures in Severe Environments*, Taylor & Francis, 270 Madison Ave, New York, NY, USA.
- Hale, W. M; Freyne, S. F. and Russell, B. W. (2009), *Examining the Frost Resistance of High Performance Concrete*, Construction and Building Materials, volume 23, Issue 2, p. 878-888.
- Malhotra, V. M. (1983), *Fly Ash, Silica Fume, Slag & Other Mineral By-Products in Concrete*, vol II, Publication SP-79 American Concrete Institute, Detroit, USA, p. 709-713.
- Pigeon, M; Marchand, J. and Pleau, R (1996), *Frost Resistant Concrete*, Construction and Building Materials, volume 10, Issue 5, p. 339-348.
- Sabir, B. B. (1997), *Mechanical Properties and Frost Resistance of Silica Fume Concrete*, Cement and Concrete Composites, volume 19, Issue 4, p. 285.

Nonlinear Modelling of Rheology of Self-Compacting Concrete with two Rapid Cements



Abhay Bulsari
Nonlinear Solutions Oy, Turku, Finland,
Tel. +358 2 2154721
abulsari@abo.fi



Klaus Juvas
Consolis Oy, Rusko, Finland,
Tel. +358 40 5160316
klaus.juvas@consolis.com

ABSTRACT

To be able to control the rheological properties, it is necessary to have a good knowledge of the effects of the composition variables on yield strength and plastic viscosity in quantitative form. These relations are fairly complicated and have strong cross term effects. It is not possible to use physical modelling for this purpose. New techniques of nonlinear modelling use free form nonlinearities and have much superior capabilities for approximating unknown nonlinearities than conventional linear statistical techniques. In this work, self-compacting concrete with two rapid cements, superplasticiser and limestone filler was studied. Nonlinear models were developed for yield stress and plastic viscosity from experimental data.

Key words: self-compacting concrete, rheology, nonlinear modelling, yield stress

1. INTRODUCTION

Rheological properties are critical for self-compacting concretes. They have low yield stresses and moderate plastic viscosities, which are just enough for the concrete to flow under its own weight without segregation or bleeding. These concretes are used where compaction is not feasible. For example, large building elements are often cast with self-compacting concrete. This concrete tends to be somewhat more expensive, which makes its mix proportioning an important issue.

The concrete has to have the right rheological properties, early strength as well as 28 day strength. In addition, it should not be very expensive. Rheological properties are characterised by yield stress and plastic viscosity, which are calculated from flow table tests (see Figure 1). The flow table tests give two main results: flow table diameter and time to 500 mm diameter. Yield stress and plastic viscosity are calculated from these two results of the flow table tests.

Parma, a subsidiary of Consolis, has a precast concrete plant in Nummela in Finland, where self-compacting concrete is used for residential building construction elements. Two rapid cements along with a fine limestone filler, a superplasticiser, water and three aggregates are used for the

concrete. This work has focused on developing better and cheaper recipes with the same raw materials in different proportions.

2. NONLINEAR MODELLING

There is hardly any material behaviour which is absolutely linear. It is therefore wise to treat the nonlinearities rather than ignore them. To treat the nonlinearities, one can use new techniques of nonlinear modelling, like feed-forward neural networks. The proponents of linear techniques draw on their simplicity and the possibility of adding nonlinear terms in linear regression. Often this is not done, and is not efficient even if it is done. Nature does not follow the simplicities that we try to fit it in, using common linear techniques.

Feed-forward neural networks have the so-called universal approximation capability [1] which make them particularly suitable for most function approximation tasks we come across in engineering and in process industries. The user does not need to know the type and severity of nonlinearities while developing the models.

There are many different types of neural networks, and some of them have practical uses in process industries [2]. Neural networks have been in use in process industries for about twenty years [3]. The multilayer perceptron, a kind of a feed-forward neural network, is the most common one. Most neural network applications in industries are based on them, including our earlier work on concrete and aggregates [4 - 9].

3. EXPERIMENTATION

Concretes of different compositions were prepared and tested on a flow table for their rheological properties. There was a large variation in the yield stress as well as plastic viscosity in the experimental data. Although this work should have needed hardly about 20 experiments, 34 experiments were carried out, of which a couple of them were repetitions. There was moderately good repeatability of the experiments. In a couple of cases, there was bleeding, but no segregation was observed.

About 12 kg of the ingredients were mixed in each experiment for a fixed amount of time. The temperature of the concrete at the end of mixing was measured and recorded. Then a part of the fresh concrete was used in a flow table test, and the average diameter and the time taken by the concrete to flow to 500 mm were recorded. The automated equipment calculated yield stress and plastic viscosity from these measurements.

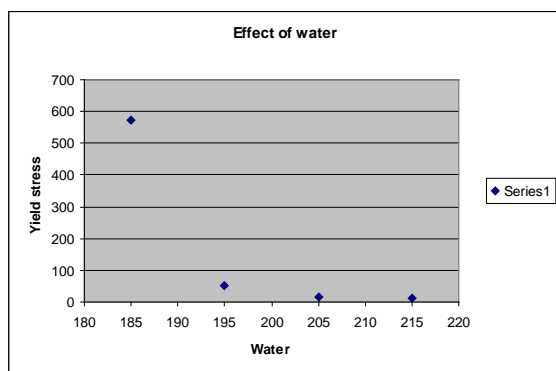


Figure 1. Effect of water on yield stress as seen from the experimental data

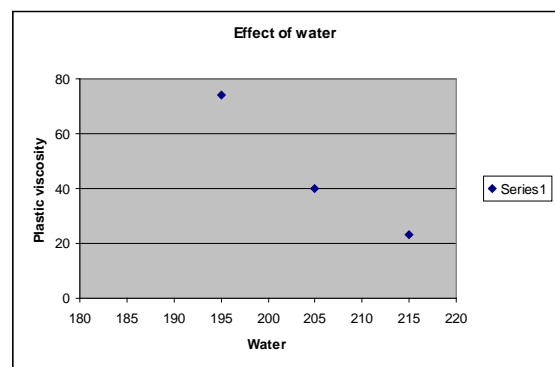


Figure 2. Effect of water on plastic viscosity as seen from the experimental data

It was possible to see some clear effects from the raw experimental data. For example, the effects of water on yield stress as well as plastic viscosity are clearly negative. That can be seen from Figures 1 and 2. Increasing the amount of one of the cements generally reduced the yield strength first until a minimum after which the yield strength increased. This kind of effects were not clearly visible from the experimental data but were visible clearly from the nonlinear model.

4. NONLINEAR MODEL OF YIELD STRESS

Nonlinear models were attempted for yield stress and plastic viscosity using NLS 020 software. For yield stress, a total of 33 observations were available from the experimental data. Most of the good models resulted in a very high correlation coefficient, above 99.8%. The characteristics of the selected model are as follows.

rms err of output variable 1: 1.6139
 mean |err| of output variable 1: 1.1544
 max |err| of output variable 1: 3.8946
 Correlation of output variable 1:
 0.9997

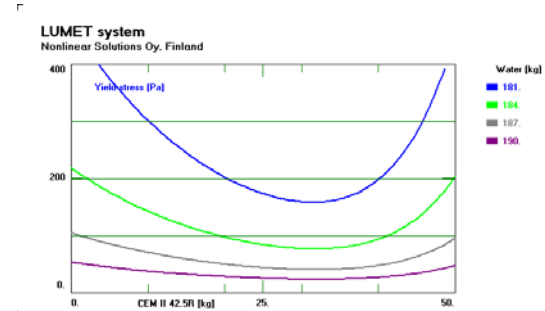


Figure 3. Effect of one cement on yield stress for different amounts of water as predicted by the model

The models of yield stress and plastic viscosity were implemented in a LUMET system, a set of software components for easy use of nonlinear models. This allowed us to study the models and use them for various calculations including optimisation of the cost in presence of constraints. Figure 3 shows plots of yield stress against one cement for different amounts of water. Other independent variables are kept constant. As expected, there is a minimum in each curve. The location of the minimum varies a little bit with the amount of water.

5. NONLINEAR MODEL OF PLASTIC VISCOSITY

Nonlinear models in the form of feed-forward neural networks were attempted with different configurations for plastic viscosity also. For plastic viscosity, a total of 19 observations were available from the experimental data. Most of the good models resulted in high correlation coefficients, typically above 94%. The statistical characteristics of the selected model are as follows.

rms err of output variable 2: 8.9421
 mean |err| of output variable 2: 7.0367
 max |err| of output variable 2:
 20.4814
 Correlation of output variable 2:
 0.9432

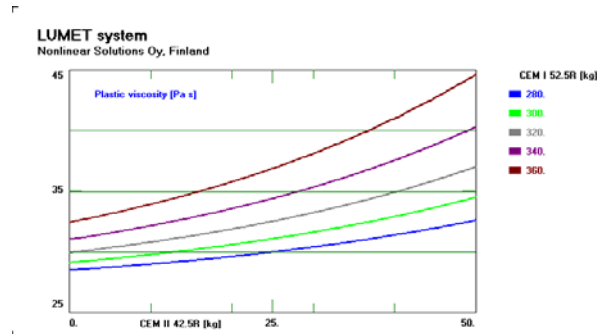


Figure 4. Effect of one cement on plastic viscosity for different amounts of the second cement

Figure 4 shows plots of plastic viscosity against one cement for different amounts of the other cement. Other composition variables are kept constant. As expected, the plastic viscosity increases when either of the two cements is increased, since the amount of water and superplasticiser are constant.

6. CONCLUSIONS

To be able to control the properties of self-compacting concrete well, it is necessary to have a good understanding of the quantitative effects of composition variables.

Effects of composition variables of self-compacting concrete were studied experimentally and modelled mathematically. The effects are complicated, and there are also strong cross term effects of several pairs of variables. For example, the effect of one cement on yield stress showed a minimum, which depended on amounts of other ingredients. Similarly, the effect of limestone filler also showed a minimum which seemed to be independent of the amount of water.

This work demonstrated how from a modest series of experiments, it was possible to develop fairly good nonlinear models of yield stress and plastic viscosity. The nonlinear models can be used to determine cost efficient recipes which have desired levels of yield stress and plastic viscosity.

REFERENCES

- [1] Hornik, K., Stinchcombe, M. and White, H., "Multilayer feedforward networks are universal approximators," *Neural Networks*, Vol. 2, (1989) 359-366
- [2] A. Bulsari (ed.), *Neural Networks for Chemical Engineers*, Elsevier, Amsterdam, 1995
- [3] A. Bulsari, "Quality of nonlinear modelling in process industries", Internal Report NLS/1998/2
- [4] A. Bulsari, E. Nordenswan and A. Käppi, "Nonlinear models help reduce cement consumption by better packing of aggregates", *Concrete Plant International*, No. 2 (April 2008) 32-36
- [5] A. Bulsari and K. Juvas, "An efficient way to determine the optimal packing of four aggregates with nonlinear modelling", *Concrete Plant International*, No. 3 (June 2009) 38-43
- [6] A. Bulsari, H. Kylmämetsä and K. Juvas, "Nonlinear models of workability and compressive strength help minimise costs", *Concrete Plant International*, No. 6 (December 2009) 36-42
- [7] A. Bulsari, H. Kylmämetsä and K. Juvas, "Nonlinear models get the rheology of self-compacting concrete right", *Concrete Plant International*, No. 3 (June 2010) 82-87
- [8] A. Bulsari and K. Juvas, "Nonlinear models help determine optimal rapid cement dosing", *Concrete Plant International*, No. 6 (December 2012) 56-60
- [9] A. Bulsari and K. Juvas, "Better control of early strength with nonlinear dynamic models - hardening of concrete with two cements", *Concrete Plant International*, No. 3 (June 2013) 28-31

Influence of Addition Sequence of Materials on Rheological Properties of Self-Compacting Concrete



Farid Van Der Vurst
Ghent University, Department
of Structural Engineering,
Magnet Laboratory for
Concrete Research,
Technologiepark-Zwijnaarde
904, 9052 Ghent, Belgium
Farid.VanDerVurst@ugent.be



Ehsan Ghafari
Missouri University of Science
and Technology, Department
of Civil, Architectural, and
Environmental Engineering,
1401 N. Pine St., Rolla, MO
65409, USA
Ehsan.Ghafari@mail.mst.edu



Dimitri Feys
Missouri University of
Science and Technology,
Department of Civil,
Architectural, and
Environmental Engineering,
1401 N. Pine St., Rolla, MO
65409, USA
Feysd@mst.edu



Geert De Schutter
Ghent University, Department
of Structural Engineering,
Magnet Laboratory for
Concrete Research,
Technologiepark-Zwijnaarde
904, 9052 Ghent, Belgium
Geert.DeSchutter@ugent.be

ABSTRACT

In order to determine how the mixing process influences the fresh properties of self-compacting concrete (SCC), a SCC mix composition was produced using six different mixing procedures, varying the addition sequence of the materials and the initial moisture content of the sand. When pre-mixing the aggregates with water, or soaking them for 12 hours, part of the water is absorbed by the aggregates, resulting in a lower slump flow and higher dynamic yield stress, compared to the case when aggregates were added to the cement paste. The measured values for the V-funnel flow time and plastic viscosity were slightly higher.

Keywords: SCC, rheology, mixing sequence, mixing process, workability

1. INTRODUCTION

Self-compacting concrete (SCC) is a highly fluid type of concrete which does not need any type of external consolidation, and is able to fill a formwork entirely under its own weight (De Schutter et al., 2008). To combine high fluidity with a sufficiently high segregation resistance, a well-balanced proportioning of the amount of sand, coarse aggregates, cement and other fine materials is needed, including superplasticizers and sometimes viscosity-modifying admixtures. Fresh SCC is more sensitive to small variations in material properties, mixture proportions, and variations in the method of mixing (Lowke and Schiessl, 2005, Bonen et al., 2007, Naji et al., 2011). In order to investigate the influence of the addition sequence of the aggregates, cement, and water in the rheology of SCC, several mixtures were produced varying in the order of addition of these components, but applying the same total mixing time.

2. MATERIALS AND METHODS

2.1. Concrete mix designs

Six SCC mixtures of 85 l were produced in an intensive mixing Eirich mixer. Table 1 summarizes the mix composition used for all mixtures. The mixtures were made with air dry river sand and river gravel with maximum aggregate size of 9.5 mm, cement Type I/II, limestone filler, tap water, and a PCE superplasticizer. The grading curve of the sand and gravel are given in Figure 1, the different mixing procedures are given in Table 2.

Table 1: Mix composition

| Component | Amount [kg/m ³] |
|----------------------|-----------------------------|
| River sand | 1064 |
| River gravel | 510 |
| Cement type I/II | 300 |
| Limestone powder | 300 |
| Water | 165 |
| PCE superplasticizer | 4.15 |

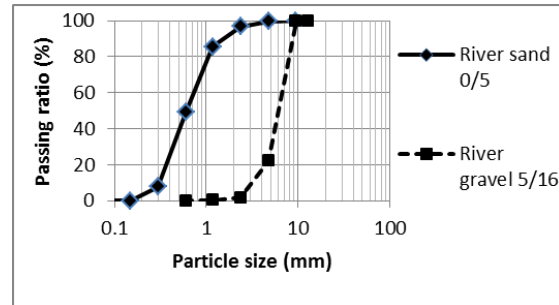


Figure 1: Grading curve of sand and gravel

Table 2: Mixing procedure of each mixture

| SCC1 | SCC2 | SCC3 | SCC4 | SCC5 | SCC6 |
|---|---|--|--|--|--|
| Aggregates 1 min | Aggregates 30 sec Half of water 30 sec | Cement 1 min | Cement 1 min | Aggregates soaked with all water 30 sec | Dry aggregates and all water 30 sec |
| Cement and filler 1 min All water 1 min SP 2.5 min | Cement and filler 1 min Half of water 1 min SP 2 min | All water 1 min SP 1 min Aggregates 2.5 min | All water 1 min Aggregates 1 min SP 2.5 min | Cement 1 min SP 2.5 min | Cement 1 min SP 2.5 min |

2.2 Testing procedure and equipment

In order to evaluate the influence of the mixing procedure on the fresh properties of the concrete mixtures, several tests were performed at specific times, time starting at first contact of cement and water:

- The slump flow and V-funnel time were measured at 20 minutes, after remixing the concrete for 30 seconds.
- The Sieve Segregation Index (S.S.I.) was measured at 25 minutes.
- The dynamic yield stress and plastic viscosity were measured at 10 minutes with a Contec viscometer 5.

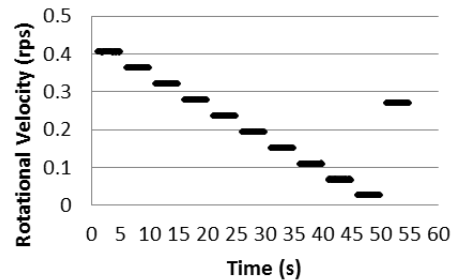


Figure 2: The applied rotational velocity profile in the Contec rheometer

The Contec viscometer 5 is a wide gap concentric cylinder rheometer with an inner cylinder radius of 100 mm and an outer cylinder radius of 145 mm. A preshear at a rotational velocity of 0.40 rps during 25 seconds was applied, followed by the stepwise decreasing rotational velocity profile as given in Figure 2. The dynamic yield stress and plastic viscosity were calculated assuming the Bingham fluid model (Eq. 1) in which τ is the shear stress, $\dot{\gamma}$ is the shear rate, $\tau_{0,p}$ is the dynamic yield stress, and μ_p is the plastic viscosity. When plug flow occurred (Wallevik, 2003), a plug flow correction was performed. Such a correction was only needed for mixture SCC4. When the torque measurement during a constant rotational velocity step was not in equilibrium, it was not considered in the analysis. For all mixtures, the torque – rotational velocity diagram was linear and thus the Bingham model was applicable.

$$\tau = \tau_{0,p} + \mu_p \cdot \dot{\gamma} \quad (1)$$

3. RESULTS AND DISCUSSION

3.1. Influence of the mixing sequence

Based on the Sieve Segregation Index chart in Figure 3, the slump flow – V-funnel time diagram in Figure 4, and the rheograph in Figure 5, one can distinguish three cases:

- SCC3 and SCC4 have a higher slump flow, a slightly lower V-funnel time, and the lowest dynamic yield stresses and thus can be considered as the more fluid mixtures. Both mixtures also have a slightly higher Sieve Segregation Index. In these mixtures, the cement and water were first mixed together, before the aggregates and superplasticizer were added.
- SCC2 has a lower slump flow, a slightly higher V-funnel time, the lowest Sieve Segregation Index, the highest dynamic yield stress and plastic viscosity, and thus has a lower fluidity and higher segregation resistance. The aggregates were premixed with part of the water, before the cement and filler were added in the mixer.
- SCC1 is an intermediate mix, with a slump flow, V-funnel time, Sieve Segregation Index, and Bingham parameters in between the two other cases. In this mixture, the cement and aggregates were mixed together, before the water was added to the mixture.

A possible explanation for these observations could be the adsorption of part of the water by the aggregates in mixture SCC2, as the aggregates were air-dry. When the water and cement are first mixed together in mixtures SCC3 and SCC4, a paste is formed before any contact with the aggregates. Because the adsorption of water by the aggregates is prevented, more water is available in the paste, creating thus a more fluid paste for SCC3 and SCC4, compared to SCC2. When the cement and aggregates are mixed together before the water is added to the mixer, as in SCC1, the adsorption effect will be smaller, resulting in a concrete with an intermediate fluidity.

Table 3: Fresh properties of SCC1 to SCC4

| | SCC1 | SCC2 | SCC3 | SCC4 |
|-----------------------------|------|------|------|------|
| Sieve Segregation Index [%] | 6.0 | 4.6 | 6.6 | 7.9 |
| Slump flow (mm) | 705 | 715 | 775 | 760 |
| V-funnel time (s) | 3.9 | 4.5 | 3.8 | 3.8 |
| Dynamic yield stress [Pa] | 14 | 24* | 8 | 13 |
| Plastic viscosity [Pa] | 27 | 32* | 29 | 26 |

* Corrected value for plug flow

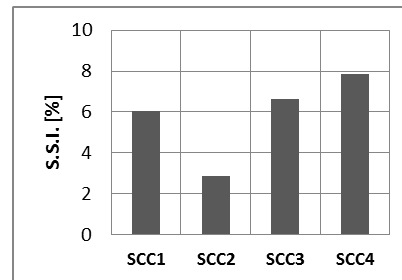


Figure 3: Influence of the mixing sequence on the Sieve Segregation Index

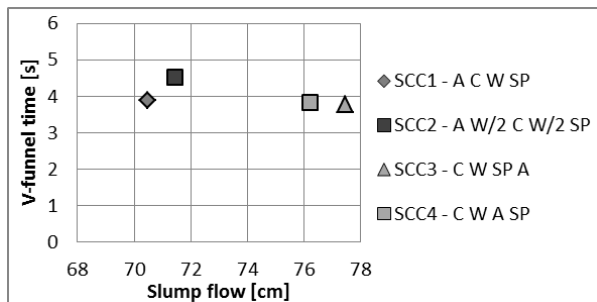


Figure 4: Influence of the mixing sequence on the slump flow and V-funnel time

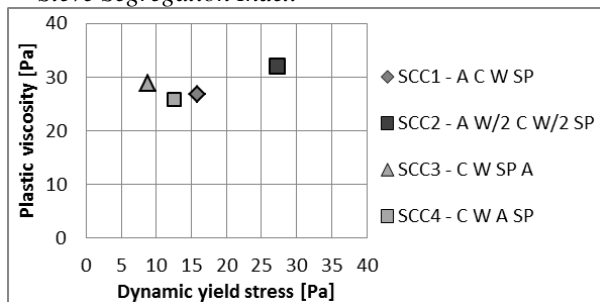


Figure 5: Influence of the mixing sequence on the Bingham parameters

3.2. Influence of the moisture content of the aggregates

Because the adsorption of water by the aggregates seemed to play a major role on the rheological behaviour of SCC, another test was performed in order to check if the moisture content of the aggregates could also influence the rheological behaviour. In mixtures SCC5 and SCC6, the same mixing sequence was used (Table 4), but instead of adding the water and air-dry aggregates together in the mixing pan in mixture SCC6, the water of mixture SCC5 had been poured over the sand and soaked for one night to assure full adsorption by the aggregates. Any evaporation of water from the buckets with sand was prevented by closing them with a plastic cover. In a similar experiment in which the influence of the moisture content on the slump flow evolution was examined, described in the doctoral thesis of Billberg (Billberg, 2006), large differences in the slump flow evolution were observed when

sand with a moisture content of 3% instead of 0.2% was used in SCC, keeping the total amount of water in the mixture constant.

Table 4: The mixing sequence of SCC5 and SCC6

| Mixing time | Added in mixer: |
|-------------|----------------------|
| 30 sec | Aggregates and water |
| 1 min | Cement and filler |
| 2.5 min | Superplasticizer |

Table 5: Fresh properties of SCC5 and SCC6

| | SCC5 | SCC6 |
|-----------------------------|------|------|
| Sieve Segregation Index [%] | 4.6 | 3.1 |
| Slump flow (mm) | 690 | 760 |
| V-funnel time (s) | 4.5 | 5.1 |
| Dynamic yield stress [Pa] | 14 | 9 |
| Plastic viscosity [Pa] | 34 | 37 |

The Sieve Segregation Index, the slump flow, V-funnel time, and Bingham parameters are summarized in Table 5, Figure 6, and Figure 7. The V-funnel time and plastic viscosity of both mixtures are rather similar, but the slump flow and dynamic yield stress differs a lot. Mixture SCC5, with the soaked sand, has a much lower slump flow and a yield stress of about 5 Pa higher. Based on the experiments, the differences in water adsorption can be assumed to be the origin of a change in dynamic yield stress and slump flow.

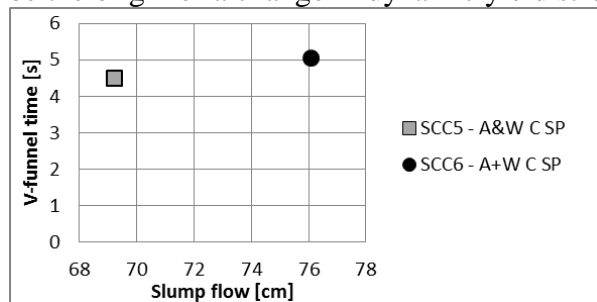


Figure 6: Influence of the moisture content of the aggregates on the slump flow and V-funnel time

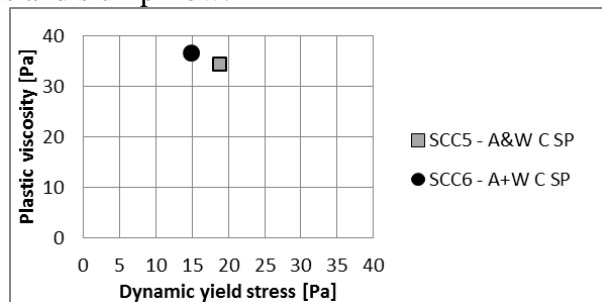


Figure 7: Influence of the moisture content of the aggregates on the Bingham parameters

4. CONCLUSIONS

This study shows the addition sequence of the aggregates has a major impact on the fresh properties of self-compacting concrete. When the aggregates are premixed together with the water, part of the water is absorbed by the aggregates, reducing the water content in the paste: the dynamic yield stress increases, the slump flow decreases, the Sieve Segregation Index decreases, and the plastic viscosity and V-funnel time increase slightly. On the contrary, if the adsorption of water by the aggregates is prevented, by adding aggregates in cement paste, the workability of the mixtures improves and the rheological properties decrease. Based on the experiments, the differences in water adsorption can be assumed to be the origin of a change in dynamic yield stress and slump flow. More experiments are being conducted in order to obtain an estimation of the amount of adsorbed water on the aggregates surface, and to evaluate the timeframe needed for the water adsorption.

REFERENCES

- BILLBERG, P. 2006. *Form pressure generated by self-compacting concrete - Influence of thixotropy and structural behaviour at rest*. Doctoral thesis, Royal Institute of Technology.
- BONEN, D., DESHPANDE, Y., OLEK, J., SHEN, L., STRUBLE, L., LANGE, D. A. & KHAYAT, K. H. 2007. Robustness of SCC. In: LANGE, D. A. (ed.) *Self-consolidating concrete*. Urbana, IL, U.S.A.: The Center for Advanced Cement Based Materials (ACBM).
- DE SCHUTTER, G., BARTOS, P. J. M., DOMONE, P. & GIBBS, J. 2008. *Self-compacting concrete*, Dunbeath, Scotland, UK, Whittles Publishing.
- LOWKE, D. & SCHIESSL, P. 2005. Effect of mixing energy on fresh properties of SCC. In: SHAH, S. P. (ed.) *Second North American Conference on the Design and Use of Self-consolidating Concrete / 4th International RILEM Symposium on Self-Compacting Concrete*. Chicago, IL, USA: Hanley Wood, LLC.
- NAJI, S., HWANG, S.-D. & KHAYAT, K. H. 2011. Robustness of self-consolidating concrete incorporating different viscosity-enhancing admixtures. *ACI Materials Journal*, 108, 432-438.
- WALLEVIK, J. E. 2003. *Rheology of particle suspensions - Fresh concrete, mortar and cement paste with various types of lignosulfonates*. Doctoral thesis, The Norwegian University of Science and Technology (NTNU).

CRACKING, CREEP AND REPAIR

Cont.

Experimental Investigation of Concrete Fatigue Resistance



Eng. Sara Korte¹
Scientific researcher
Sara.Korte@
UGent.be



Veerle Boel¹
Prof. Dr. Eng.
Veerle.Boel@
UGent.be



Wouter De Corte¹
Prof. Dr. Eng.
Wouter.DeCorte@
UGent.be



Geert De Schutter²
Prof. Dr. Eng.
Geert.DeSchutter@
UGent.be

¹Ghent University
Faculty of Engineering and Architecture
Dept. of Industrial Technology & Construction
Valentin Vaerwyckweg 1, B-9000 Ghent

²Ghent University
Faculty of Engineering and Architecture
Dept. of Structural Engineering
Technologiepark 904, B-9052 Zwijnaarde

ABSTRACT

A lack of knowledge on the fatigue resistance of self-compacting concrete (SCC) structures has led to the research presented in this paper. Several reinforced concrete beams were subjected to both static and cyclic four-point bending tests in order to determine the failure mechanism, the static ultimate load, the fatigue performance, the deformation, and crack width evolution. For comparison purpose, different mixtures were considered, including a vibrated concrete (VC) type and two SCCs (one with similar strength and one with equal w/c ratio, compared to VC). The mutual relationship is strongly depending on the stress level caused by the repeated loading.

Keywords: Vibrated Concrete, Self-compacting Concrete, Reinforcement, Fatigue, Cracking

1. INTRODUCTION

The different composition of SCC, compared to VC, influences various material characteristics, such as the microstructure, the interfacial transition zone, the compressive and tensile strength, the stiffness, and also the fracture behaviour. Therefore, it is assumed that the fatigue resistance of both concrete types might be different, since it is governed by a damage process, related to micro-crack initiation, material damage, and fracture behaviour in general.

2. EXPERIMENTAL PROGRAM

2.1 Mixtures

Three concrete batches were used: one vibrated concrete (VC) and two self-compacting concretes (SCC1 with similar strength and SCC2 with equal w/c ratio of 0.45). Table 1 and 2 provide the composition quantities of the mixtures, and their main properties.

2.2 Specimens

Aiming for concrete crushing at ultimate load with the steel rebar deformation remaining fully elastic, the 2.40m long beams were over-reinforced by using three longitudinal bars Ø20mm at

the bottom, two longitudinal bars $\text{Ø}6\text{mm}$ at the top, and vertical stirrups $\text{Ø}6\text{mm}$ every 55mm (Fig. 1). In addition, the upper part of the geometrical section is narrowed, thus generating larger concrete compressive bending stresses than there would occur in case of a rectangular section.

Table 1 – Concrete compositions

| Composition | VC | SCC1 | SCC2 |
|--------------------------|----------------------|----------------------|----------------------|
| | [kg/m ³] | [kg/m ³] | [kg/m ³] |
| CEM III/A 42.5 LA | 360 | 293 | 360 |
| Water | 161 | 161 | 161 |
| Sand 0/4 | 759 | 651 | 651 |
| Crushed limestone 2/6.3 | 433 | 523 | 523 |
| Crushed limestone 6.3/14 | 610 | 321 | 321 |
| Limestone filler | - | 377 | 317 |
| Superplasticizer (PCE) | 2.7 | 9 | 9.5 |

Table 2 – Concrete hardened properties

| Properties | VC | SCC1 | SCC2 |
|---------------------------------------|--------|--------|--------|
| | [MPa] | [MPa] | [MPa] |
| f_{cm} | 53.4 | 51.3 | 60.0 |
| $f_{c,cub,m}$ | 54.3 | 53.9 | 63.8 |
| $f_{ck} = f_{cm} - 1.64s^*$ | 45.4 | 43.3 | 52.0 |
| $f_{c,cub,k} = f_{c,cub,m} - 1.64s^*$ | 46.3 | 45.9 | 55.8 |
| $f_{ctm} = 0.3 f_{ck}^{2/3}$ | 3.8 | 3.7 | 4.2 |
| E_{cm} | 38,423 | 38,093 | 35,290 |

* s = standard deviation

2.3 Test procedure

Fig. 2 depicts the four-point bending test setup, applied for both static and fatigue tests. During all the experiments, the structural behaviour of the beams was registered by means of three strain gauges (n°1 in the middle of the top surface, n°2 along the side of the beam at 5cm from the top, n°3 at the lower side of the middle rebar) and three deflection gauges (at midspan and below the point loads). The crack width evolution was measured using a crack width microscope with an accuracy of 20 μm . Three reference beams per concrete type were tested statically, with increments of 5kN up until failure, in order to determine the failure mechanism and the ultimate load P_{ult} . The cyclic tests then were conducted by applying a sinusoidal load function with a frequency of 1Hz and a lower limit of 10% P_{ult} and upper limits of 60%, 70%, 80%, and 85% P_{ult} .

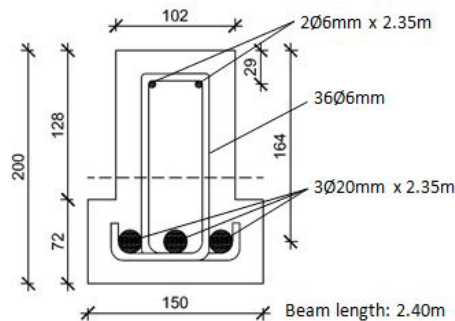


Fig. 1 – Concrete beam cross section

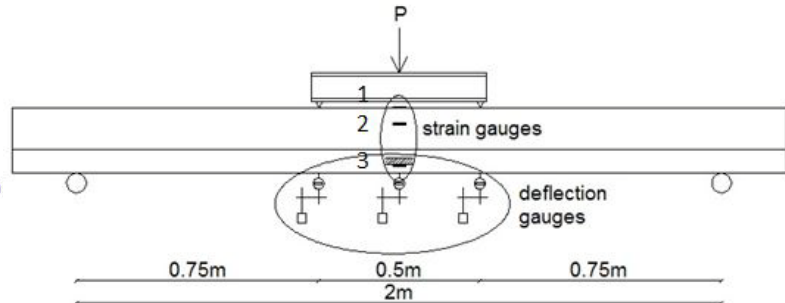


Fig. 2 – Test setup

3. RESULTS AND DISCUSSION

3.1 Static tests

All nine reference beams failed by pure concrete crushing. The average ultimate load was 132kN for VC, 162kN for SCC1, and 158kN for SCC2. The higher value for SCC2 is not surprising, given its higher compressive strength, but SCC1, which has a compressive strength similar to VC, can also resist a substantially higher load. As regards the average experimental midspan deflection, the measurements reveal smaller values for the SCC types. The difference with VC is minimal at the beginning of the static test, but increases towards failure. At a common load of 120kN the deviation with respect to VC is 17% in case of SCC1 and 14% in case of SCC2. Since VC has the smallest failure load, its larger deflection could be expected. Despite this, the crack width progression demonstrates a larger amount of cracks and consequently a more dense crack pattern for SCC (especially SCC1), compared to VC. The crack widths of SCC1 are up to 16% smaller than those of VC and up to 33% smaller than in case of SCC2. When considering the concrete strain evolution, corresponding values are noticed

for both SCCs, which are exceeded by the concrete strain in VC with approximately 28% (near the point of collapse). The ultimate strain values confirm the concrete crushing failure mode, for the strain failure limit of 3.5‰ is (practically) reached for all concrete types. From the results of the strain measurements on the reinforcement steel, the linear evolution ascertains that no plastic rebar deformation occurred during the loading process.

3.2 Fatigue tests

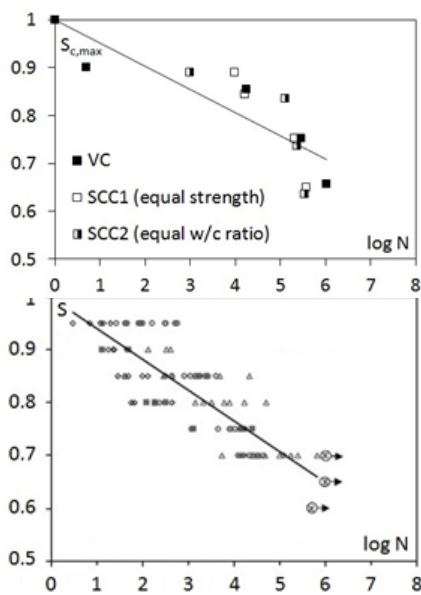
Table 3 lists the number of cycles to failure and the failure mode of the cyclic tests. It can be seen that the beams, subjected to the loading intervals 10-80 and 10-85 fail by crushing of the concrete in the compression zone, whereas for the lower upper limits the larger number of cycles causes rebar fatigue damage, developing more quickly than the deterioration process in the compressed concrete takes place. Specimen SCC1(10-70) is an exception, but examination of the reinforcement steel after collapse visibly demonstrated fatigue crack initiation. Despite some scatter, it is clear that the fatigue life depends on the applied load level: the higher the upper load limit, the least cycles the beams can sustain. When comparing SCC to VC, it could be stated that VC performs best in the fatigue tests with lower load levels (10-70, 10-60), which corresponds with the lower fatigue resistance of SCC, mentioned in Model Code 2010, due to the higher paste content and the different pore structure. The higher loading ranges, however, yield an opposite relationship: the longest fatigue life occurs for SCC1 (10-85) or SCC2 (10-80).

Table 3 – Number of cycles to failure

| Load level | VC | | SCC1 | | SCC2 | |
|------------------|-----------|--------------|----------|--------------|----------|--------------|
| | # cycles | Failure mode | # cycles | Failure mode | # cycles | Failure mode |
| 10-85% P_{ult} | 5 | CC | 9,837 | CC | 992 | CC |
| 10-80% P_{ult} | 17,812 | CC | 16,402 | CC | 126,443 | CC |
| 10-70% P_{ult} | 290,598 | RF | 206,989 | CC | 234,500 | RF |
| 10-60% P_{ult} | 1,050,056 | RF | 378,618 | RF | 339,551 | RF |

When considering the deformation evolution during the fatigue experiments, similar curves are found for the vertical displacement and strain measurements. First, a long period of slightly increasing deformation is present, followed by a rapid growth up to failure. Again, the loading range is crucial: the initial (and ultimate) value increases as the upper load limit increases. The relationship between the three concrete types is not unique, but also depends on the loading interval. In case of the lowest levels (10-70, 10-60), where most of the specimens failed by rebar fatigue and where VC showed the longest fatigue life, the deflection of VC is consistently smaller than that of the SCC mixtures. The other load levels (10-85, 10-80) indicate a larger deviation. The highest value occurs for SCC1, followed by VC and SCC2, respectively. However, there is no link with the number of cycles to failure. In contrast to these findings, the concrete strain data do not reveal an explicit relationship between VC and SCC regarding the magnitude of the strain values, even though a faster strain increase is noticed in case of SCC. Furthermore, it is observed that none of the specimens – not even those which collapsed by crushing of the concrete – achieves the 3.5‰ strain limit, which can be attributed to the redistribution process of the compressive stresses from the most degraded top fibres towards the lower and less damaged fibres in the compression zone (Zanuy et al. 2007). The rebar strain development shows nearly horizontal curves for all specimens far below the threshold value for yielding, pointing out merely elastic cross-sectional deformations. As regards the crack patterns, drawn during the cyclic tests, no substantial differences appear between the initial crack lengths (at the beginning of the experiment) and the ultimate crack lengths (at the end of the fatigue life). The crack widths do increase significantly as a function of the number of cycles. Depending on the loading range, the curves have an initial crack width between 0.1mm and 0.2mm. The gradual increase is quite similar for all concrete types, but the crack growth takes

place at an accelerated level for the SCC mixtures, especially in case of the highest loading intervals. This may be explained by the better bond properties of SCC, which induce significantly larger rebar stresses at the cracks, opposed to at the bar lengths between the cracks (Zanuy et al. 2011). Minimal differences in crack width values occur for the load levels 10-60 and 10-80, whereas in case of the other load limits SCC1 shows the largest crack widths, followed by VC and SCC2, respectively. Strangely, no correspondence is present with the rebar strain evolution. Observing the number of cracks, SCC1 and particularly SCC2 seems to produce more cracks, compared to VC. This phenomenon might be ascribed to the development of negative tension stiffening (negative bond stresses at the steel-concrete interface between cracks) during unloading stages, as it is observed by Zanuy et al. (Zanuy et al. 2011).



Based on the experimental fatigue data, the S-N curves in Fig. 3a represent the relationship between the maximum applied fatigue stress $\sigma_{c,max}$ (determined by using a nonlinear calculation method) and the number of load cycles N which cause fatigue failure. Relating $\sigma_{c,max}$ to the ultimate static concrete crushing stress f_{cc} yields the dimensionless term S , thus partly eliminating influences such as w/c ratio, moisture content, age at loading, etc. (Lee & Barr, 2004). A gently descending curve with similar slopes can be noticed for the three concrete types, which means that, when a certain fatigue stress level is applied, VC, SCC1 and SCC2 are able to endure an equal number of loading cycles before failing. Comparison of the outcome with Fig. 3b for plain concrete under repeated compressive loading (Lee & Barr, 2004), reveals good agreement.

Fig. 3 – S-N curve – a) experiments – b) Lee & Barr, 2004

4. CONCLUSIONS

During the cyclic tests, VC and SCC demonstrate a similar deformation evolution, but the values are larger for SCC in case of the highest applied load levels (10-80% and 10-80% of the static failure load). Furthermore, SCC (especially SCC2 with equal w/c ratio, with respect to VC) generates, on average, a larger amount of cracks in these loading intervals, and the fatigue crack propagation also takes place at an accelerated level. Strangely, SCC1 (with similar strength, compared to VC) shows the best fatigue resistance at the 10-85 range and SCC2 at the 10-80 interval, whereas VC shows the best fatigue resistance in case of the lower loading levels. No consistent relationship, covering the full loading scope, can be observed. The S-N curves point out that the studied concrete types do not have a remarkably different fatigue behaviour, since almost identical slopes are found.

REFERENCES

Lee, M.K., Barr, B.I.G., 2004

“An overview of the fatigue behaviour of plain and fibre reinforced concrete”, *Cement & Concrete Composites*, Vol. 26, 2004, pp. 299-305.

Zanuy, C., de la Fuente, P., Albajar, L., 2007

“Effect of fatigue degradation in the compression zone of concrete in reinforced concrete sections”, *Engineering Structures*, Vol. 29, 2007, pp. 2908-2920.

Zanuy, C., Maya, L.F., Albajar, L., de la Fuente, P., 2011

“Transverse fatigue behaviour of lightly reinforced concrete bridge decks”, *Engineering Structures*, Vol. 33, 2011, pp. 2839-2849.

Moisture and Mechanical Properties Aimed for Crack Risk Analyses of Early Age Concrete



Dr. Jan-Erik Jonasson
Professor
Luleå University of Technology
Dept. of Structural Engineering
jan-erik.jonasson@ltu.se



Dr. Lars-Olof Nilsson
Professor
Lund University, Faculty of
Engineering
Div. of Building Materials
lars-olof.nilsson@byggtek.lth.se



Dr. Mats Emborg
Head of R&D,
Betongindustri AB
Professor
Luleå University of Technology
Dept. of Structural Engineering
mats.emborg@ltu.se



Dr. Hans Hedlund
Adj. Professor
Skanska Sverige AB
Technology
Bridge and Civil Engineering
hans.hedlund@skanska.se

ABSTRACT

Within the project “Crack-Free-Con – Nordic coordination for sustainable construction by novel shrinkage modelling and user friendly Expert System”, a collaborative project between the research area of Building Materials at Lund University (LTU) and the area of Structural Engineering at Luleå University of Technology (LTU), a comprehensive test program has been performed.

The tests at LTH are concentrated on moisture related properties like relative humidity at drying and at sealed conditions as well as shrinkage determination, while the tests at LTU cover mechanical properties as total deformation (momentaneous and creep behaviour) at drying and at sealed conditions and stress development in a temperature-stress-testing-machine (TSTM). At present the interesting work to combine the tests results from the two laboratories are in progress.

Key words: Testing, Drying, Creep, Shrinkage, Self-desiccation, Drying Creep, Cracking, Modelling

1. INTRODUCTION

In concrete structures cracks cannot be tolerated. Besides impairing the durability or function, cracking may also be aesthetically unacceptable. Costly repairs of cracked concrete are common and, in some cases, it is even necessary to demolish severely cracked structures at an age much lower than lifetime. Hence, it is a significant task developing methods to control cracking.

However, it is well known that shrinkage due to moisture changes also is one of the main mechanisms causing concrete cracking. Therefore, it is surprising that no reliable theoretical model or computer program exists that considers the effect of shrinkage on cracking.

This paper is focusing on

- Presentation of experimental results from LTH and LTU for the same types of concrete, and

- Discussion how they will be used in a comprehensive model concerning shrinkage and shrinkage induced stresses

2. TYPE OF TESTS

2.1 Shrinkage and moisture related tests at LTH

All tested concrete mixes at LTH, see specimen size in Figure 1, comprise the following base measurements

- Shrinkage deformations at sealing and at drying
- Relative humidity inside the concrete sample
- Weight loss of the concrete specimen
- The environmental relative humidity and temperature

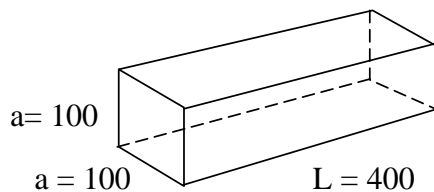


Figure 1 -. Dimension and shape of the concrete specimen at moist related tests

One example of RH (Relative Humidity) measurements at different drying conditions is presented in Figure 2. The environmental humidity is about 33 %.

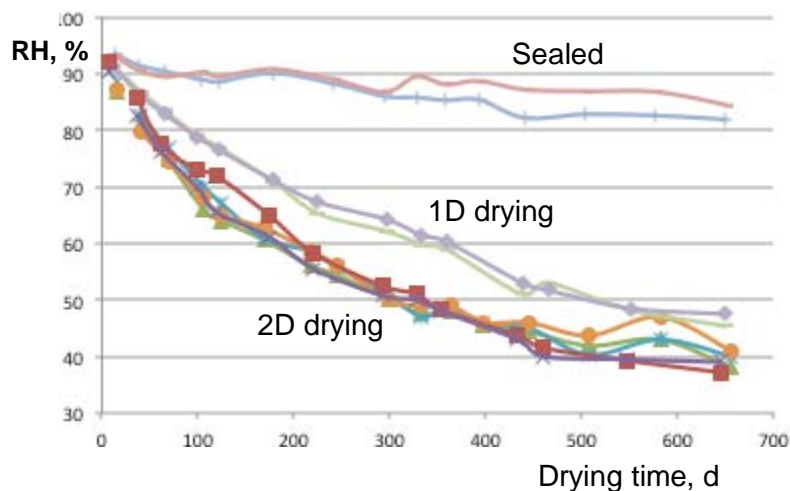


Figure 2 – Example of measured RH development for different conditions for the test specimen size presented in Figure 1. From Nilsson and Johansson (2013)

Similar tests as shown in Figure 2 has been performed also for larger ($a = 150$ mm) and smaller ($a = 60$ mm) test specimens, see further Nilsson and Johansson (2013).

In addition to the direct shrinkage related measurements, some general moist property tests were performed at LTH with respect to

- Capillary degree of saturation
- Degree of hydration
- Evaporable water content

- Desorption isotherm
- Moisture transport properties

2.2 Mechanical and stress related tests at LTU

At LTU “the full test program for stress analyses”, see for instance Hedlund (2001), was applied to the same concrete mixes as studied at LTH. The full test program is designed to give necessary properties to estimate temperature and stress calculations for sealed conditions, which is the “normal” situation for most civil engineering structures, and the testing comprises the following property areas

- Heat of hydration
- Strength growth at variable temperatures
- Creep tests at sealed conditions for at least two loading ages
- Free movements for almost constant temperature and for a real temperature-time development
- Stress at full restraint for a real temperature-time development

In addition to these tests aimed for analyses of “larger” civil engineering structures, the creep behaviour is also performed for a non-sealed specimen, which can be denoted

- Drying creep tests for the same loading ages as for the creep test at sealed conditions

Drying creep tests are needed to get relevant information about the increase of creep when moisture flow is present, see part b) in Figure 3, compared with creep at moisture sealed conditions, see part a) in Figure 3.

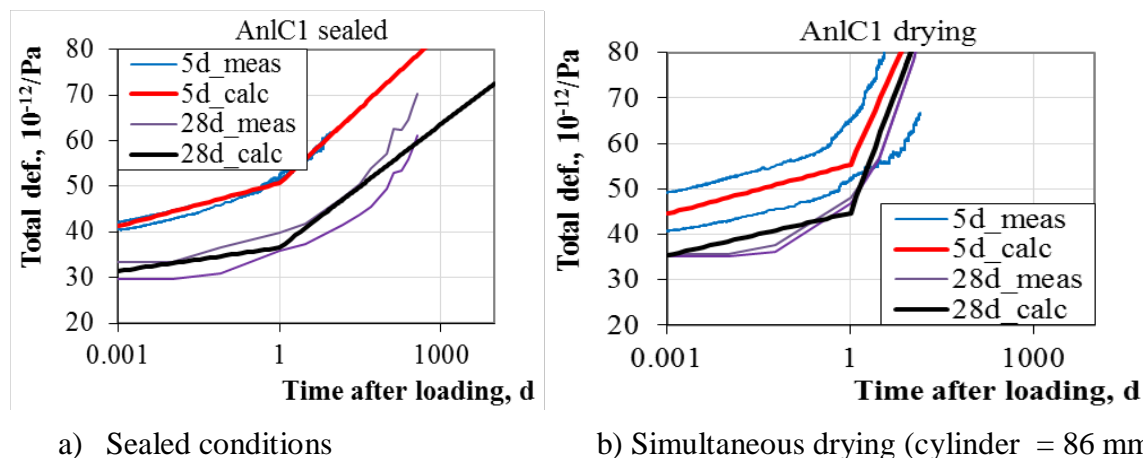


Figure 3 – Creep tests for young concrete (loading ages 5 d and 28d, respectively) both at sealed conditions (part a) and at simultaneous moisture flow (part b). (Evaluation in progress, LTH 2014)

3. MODELLING OF THE COMBINED MOISTURE AND MECHANICAL TESTS

3.1 Satisfactory existing models

The existing models and computer programs can in a unified and satisfactory way model

- Self-desiccation and basic shrinkage at temperatures about 20°C
- Temperature development in structures at sealed conditions
- Compressive and tensile strength growth at sealed conditions
- Thermal induced stresses due to restraint in structures at sealed conditions

In the denotation “thermal induced stresses” above includes also an approximate estimation of moist induces stresses at sealed conditions.

3.2 Areas with non-satisfactory models

With respect to estimation of shrinkage and shrinkage induced stresses, there are two obvious areas that do not have well established unified descriptions (models) for young concrete at present. These areas can be formulated as

- Effects of *variable temperature* on self-desiccation and basic shrinkage, see for instance Johansson (2012) and Bjøntegaard (1999)
- Effects of *simultaneous moisture* flow on concrete *creep*, se Figure 3 above.

The consequence for the present project with respect to the ambition to combine moisture and stress calculations to get “novel” information on shrinkage cannot be full-filled at present.

However, there are a lot of data for young concrete produced in the project, and some interesting preliminary results from the on-going evaluation are

- The free (unrestrained) shrinkage of young concrete seems to be able to model depending on the change of evaporable water content (using the moisture model from Norling Mjörnell, 1997 and Jonasson et al, 2005)
- The translation from 2D to 1D drying, see Figure 2, can be performed according to the model presented in Jonasson (1992)
- The temperature effect on self-desiccation might be able to model by a shift in the isotherms depending on the rate of hardening
- One possible way to model drying creep might be to use more than two splines, which is technically possible, see further Larson and Jonasson (2003)

4. CONCLUDING REMARKS

Although the ambition to combine moisture and stress calculations to get “novel” information on shrinkage cannot be full-filled at present, there exist a lot of useful and interesting data concerning both moisture and mechanical properties for young concrete. Besides, the new knowledge has started a fruitful discussion of how to proceed and refine/adjust some of the existing models.

REFERENCES

- Bjøntegaard Ø, 1999,
 “Thermal Dilation and Autogenous Deformation as Driving Forces in High Performance Concrete”,
 Doctoral Thesis, Norwegian University of Science and Technology, Trondheim
- Johansson P, 2012
 “Drying of Concrete - Laboratory Tests behind TorKaS3”, Report TVBM 3165, Div. of Building
 Materials, Lund Institute of Technology (in Swedish)
- Jonasson J-E, Carlsson C, and Mjörnell M, 2005,
 “Model for Calculation of Moisture in Modern Concretes at Variable Temperature”, Journal Bygg&
 Betong, No. 7/2005 (in Swedish)
- Jonasson J-E, 1992,
 “Shrinkage of Hardened Concrete”, Ch. 15 in Concrete Handbook – Materials (in Swedish)
- Larson M and Jonasson J-E, 2003,
 “Linear Logarithmic Model for Concrete Creep”, Journal of Advanced Concrete Technology, Vol. 1,
 No. 2/2003
- Nilsson L-O and Johansson B, 2013,
 “Crack Free Con. – Data from Shrinkage Experiments”, Report TVBM 3171, Div. of Building
 Materials, Lund Institute of Technology (in Swedish)
- Norling Mjörnell K, 1997,
 “Moisture Conditions in High Performance Concrete – Mathematical Modelling and Measurements”,
 Doctoral thesis, Chalmers University of Technology, Göteborg

Self-Healing Concrete HEALCON



Markku Leivo
 D.Sc.(Tech), Principal Scientist
 VTT Technical Research Centre of Finland
 Kemistintie 3, Espoo
 P.O Box 1000
 FI-02044 VTT, Finland
 markku.leivo@vtt.fi

ABSTRACT

The project HEALCON, which deals with self-healing concrete to create durable and sustainable concrete structures, is funded by EU-FP7 and started in January 2013. The coordinator is Prof. De Belie and the partners are UGent, Avecom, TU Delft, Acciona, TUM, TTI, VTT, COWI, DTI, CEINNMAT, Devan and Fescon.

Thanks to the existing expertise of the consortium in the field of self-healing concrete at a lab-scale, a thoughtful selection of promising techniques is possible. Different healing agents and encapsulation techniques are developed and scaled up. Finally the efficiency is validated in a large scale lab test and implemented in an actual concrete structure.

Key words: Cracking, admixtures, repair, self-healing, concrete, durability, water tightness

1. INTRODUCTION

Adequate perpetuation of the road, tunnel and bridge network, is crucial to preserve European cohesion and business operations; and around 70% of this infrastructure is made of concrete. In order to guarantee liquid tightness of concrete structures, and enhance durability of elements prone to bending cracks, smart concrete with self-healing properties will be designed.

Reinforced concrete is designed to crack, but crack widths are limited to 0.2 to 0.4 mm depending on exposure class and type of concrete (reinforced or prestressed). Although these cracks do not impair structural stability, through-going cracks drastically affect liquid tightness. This is a major problem in tunnels and large underground structures, where cement hydration reactions and temperature/shrinkage effects in large concrete segments might result in the formation of early age cracks. Since liquid-tightness is necessary, expensive preventive measures are taken or repair works are needed right after construction. Furthermore, even if not through-going, cracks will allow faster penetration of aggressive liquids and gases. Certainly in case of chloride containing liquids or in case of high CO₂ concentrations (e.g. in urban environments), there will be a higher risk of reinforcement corrosion, which compromises the long-term durability of the structure. Current practice requires regular inspection, maintenance and repair, to ensure structural safety over the service life of the structure. These practices involve large direct and indirect costs, such as economic losses from traffic jams. Additionally, not all structures are easy to access for inspection and repair.

In their search to overcome these problems, researchers have been inspired by nature. Biological systems such as bones, skin or plants have the capacity to detect damage very quickly and have

moreover the unique feature to repair the damage efficiently. It would be an enormous advantage if this concept could be translated to our engineering materials, such as concrete. The application of so-called “self-healing” concrete, which will in an autonomous way repair cracks, could reduce the maintenance costs drastically. Additionally, indirect costs such as due to traffic congestion can be avoided.

HEALCON aims to further develop some initial concepts that have been explored earlier by the different partners, in order to ensure practical application in concrete structures.

2. CONTENT

Depending on the type of damage, another self-healing concept is envisioned in the project (Figure 1). Early age cracks are filled with a non-elastic material, while bending cracks in e.g. bridge beams are filled with an elastic healing material to cope with the opening and closing movement of cracks under a dynamic load. This means that biogenic healing agents as well as polymeric healing agents (hydrogels and elastic healing agents) are considered. Besides, suitable encapsulation techniques for each of the healing agents are being developed and the effect of the capsules on the fresh concrete properties are investigated.

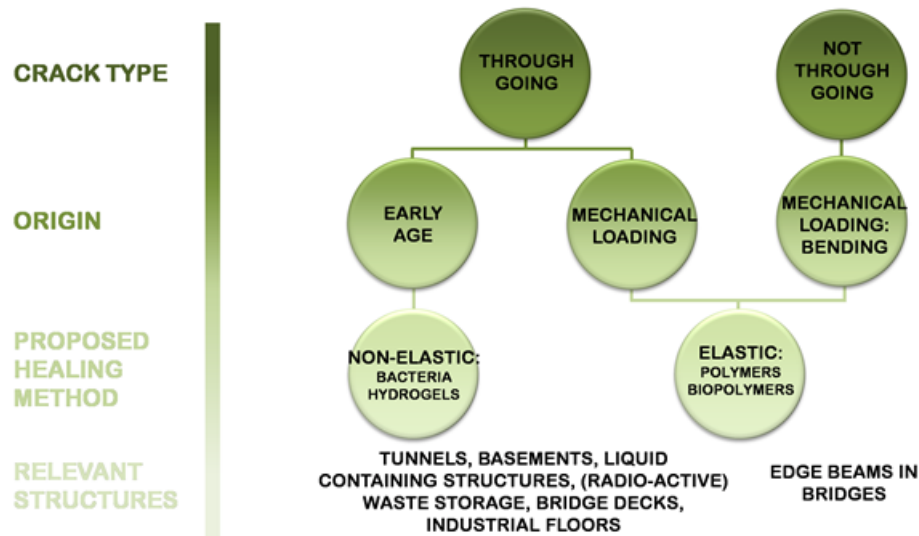


Figure 1 - Overview of the self-healing applications considered in HEALCON /De Belie 2013/.

The efficiency of the different self-healing mechanisms with regard to mechanical behaviour, liquid-tightness and durability are first quantified at lab-scale. Based on the outcome of these tests and the outcome of the developed computer models, which will simulate the fracturing and self-healing mechanisms, the mechanisms are scaled to an industrial level. The production of self-healing agents is up-scaled and the developed self-healing methodologies are experimentally validated in large-scale elements, under conditions close to reality. In the last stage, the new technologies will be demonstrated by their implementation in an actual concrete structure. Furthermore, a life cycle cost (LCC) analysis is being performed for the same structural element as used for the field test / demonstration and the LCC analysis is supplemented by a life cycle assessment (LCA).

During the laboratory tests as well as during the field tests, non-destructive monitoring techniques are used to characterize healing.

3. METHODS AND RESULTS

In this section some of the research methods used and some examples of results are presented. Different healing strategies are being investigated in the project. The bacteria-based (biogenic healing) approach is a very interesting solution. In this approach bacteria that precipitate CaCO_3 are introduced in concrete. This approach is developed especially by UGent and TU Delft. Example of precipitation in cracks can be seen in Figure 2. Also polymer-based healing agents are being investigated. Example of these healing results are presented in Figure 3.

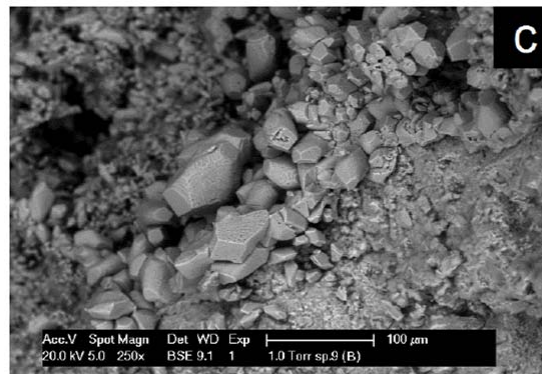


Figure 2 - Precipitation of CaCO_3 due to bacteria / Tziviloglouet.al. 2014/.

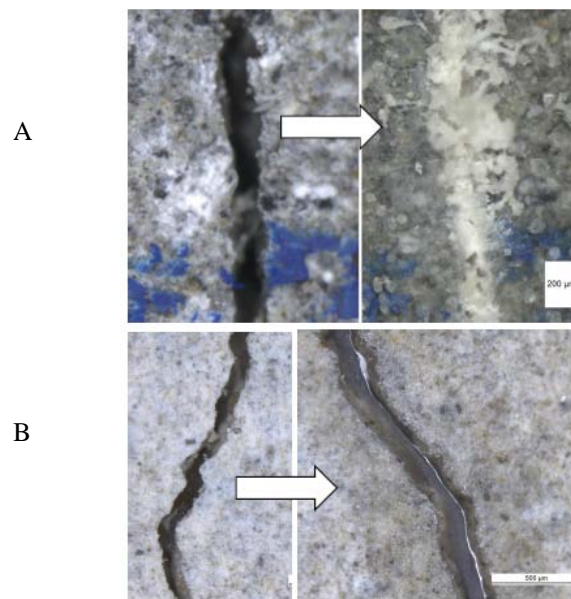


Figure 3 – A. Stimulating CaCO_3 precipitation and cement hydration by incorporating hydrogels, B. Crack healing with elastic PU. /HEALCON project-poster/

One part of the research is to develop suitable non-destructive testing (NDT) methods to evaluate the healing of cracks. During the first part of the research, laboratory methods are used but later these methods will be demonstrated in full-size structures to assure the healing actions. An example of a used acoustic emission result is presented in Figure 4.

Encapsulation of healing agents is one of the important subjects to solve for self-healing concrete. Capsules have to withstand high forces during concrete mixing and casting. On the other hand they must break when needed. Also encapsulation should provide protection of

healing agents to ensure long service life. Different encapsulation methods are investigated, for example fluid bed coating, hollow fibres, porous particles, spray drying and others. An example of coated SAP samples is presented in Figure 5.

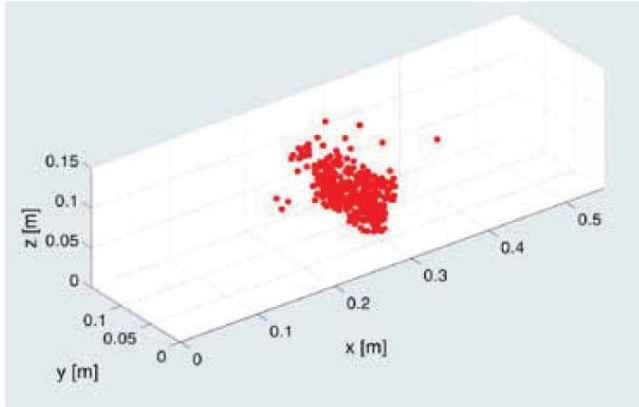


Figure 4 - Acoustic emission results in bending after healing. /Grosse & Malm 2014/

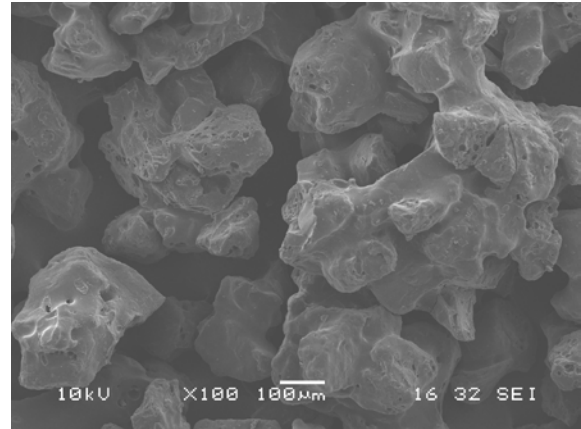


Figure 5 - Coated SAP particles.

The project work is underway and it is expected that the outcomes of the project will result in new material techniques to extend the service life of structures. More information on the project is available from the HEALCON project web page <http://www.healcon.eu>.

ACKNOWLEDGEMENTS

The research has received funding from the European Union Seventh Framework Programme (FP7/2007-2013) under grant agreement n° 309451 (HEALCON).

REFERENCES

- De Belie, N. 2013. HEALCON – Self-Healing Concrete to Create Durable and Sustainable Concrete Structures. ICSHM 2013. 16-20. June 2013.
- Grosse, C.U. & Malm, F. 2014. Concrete with properties to repair itself, Development and Testing. 58. Beton Tage, 18 - 20 February 2014.
- Tziviloglou, E., Jonkers, H.M., Schlangen, E. 2014. Bacteria-based self-healing concrete to increase liquid tightness of cracks. Proceedings of the Intern. Conference of Materials & Structures, Delft 26-28 May 2014. The Netherlands.

Evaluation of the Linear Logarithmic Creep Model



Katalin Orosz
Tec. Licentiate, Ph.D student
Luleå University of Technology
katalin.orosz@ltu.se



Peter Fjellström
Tec. Licentiate
Luleå University of Technology
peter.fjellstrom@ltu.se



Dr. Jan-Erik Jonasson
Professor
Luleå University of Technology
jan-erik.jonasson@ltu.se



Dr. Mats Emborg
Professor
Luleå University of Technology
Head R&D Betongindustri Ltd.
mats.emborg@ltu.se
mats.emborg@betongindustri.se



Dr. Hans Hedlund
Adj. Professor
Luleå University of Technology
Skanska Sweden Ltd., Göteborg
hans.hedlund@skanska.se

ABSTRACT

In order to make reliable predictions of thermal cracking risks in young concrete, modelling of the creep behaviour is important. The linear logarithmic creep model (LLM) has only been used to describe the creep behaviour of moisture-sealed concrete samples (basic creep). The aim of the present research is to check whether LLM could be also applied to drying creep. The results indicate that the LLM delivers good results for sealed but not for drying samples. Thus, refinement of the existing model (e.g., tri-linear instead of bi-linear in logarithmic time scale), or a new model is needed to account for the increase of creep due to on-going drying.

Key words: Concrete, Basic Creep, Drying Creep, Linear Logarithmic Creep Model

1. INTRODUCTION

Concrete creep is traditionally divided into basic (at moisture-sealed conditions) and drying (at a simultaneous drying out process creep. Drying will increase the creep (known as the Pickett effect).

For simulations of basic creep, a model denoted Linear Logarithmic Model (LLM) was developed at LTU (Luleå University of Technology). The relatively easy to use model was based on basic creep measurements evaluations presented in /Larson and Jonasson 2003a, Larson and Jonasson 2003b/.

There is thus a need to evaluate whether the LLM can describe *both* basic and drying creep. For this purpose, eight common concrete recipes have been tested /Fjellström 2013/. Two of the recipes use Anläggningcement (Anl), which is a commonly used Swedish cement intended for

civil engineering constructions. Six recipes are made with BAS cement, which is a new cement for application primarily to housing structures.

2. TESTING

Tested recipes and test outline are listed in Tables 1-2. The hydraulic laboratory setup aimed for creep testing at early ages is described in detail in /Westman 1999, Hedlund 2000/. Here it is used for measurements at the age of loading of 5 days. Creep measurements for the samples with loading age of 28 days are conducted using mechanical rigs where the load is adjusted with a hydraulic pump. Three pairs of measuring points are placed symmetrically around the test sample at 200 mm distance. The gauge measurement device type is STAEGER.

Table 1 – Tested concrete recipes. BAS is of type CEM II/A-V 52,5 N containing about 4% LL and 16% fly ash, and, AnlC is of type CEM I 42,5 N SR3 MH/LA

| Recipe No. | Notation | Concrete type | Cement content [kg/m ³] | w/C [-] |
|------------|----------|---------------|--|------------|
| 1 | AnlC2 | Traditional | 455 | 0,40 |
| 2 | AnlC1 | Traditional | 340 | 0,55 |
| 3 | BAS1 | Traditional | 470 | 0,38 |
| 4 | BAS2 | Traditional | 360 | 0,55 |
| 5 | BAS3 | Traditional | 285 | 0,70 |
| 6 | BAS4 | SCC | 480 | 0,38 |
| 7 | BAS5 | SCC | 370 | 0,55 |
| 8 | BAS6 | SCC | 320 | 0,60 |

Table 2 – Test outline. For each test, a loaded and unloaded sample is used.

| Recipe No. | Notation | Sealed [d] | | Drying [d] | |
|------------|----------|------------|----|------------|----|
| | | 5 | 28 | 5 | 28 |
| 1 | AnlC2 | x | x | X | x |
| 2 | AnlC1 | x | x | X | x |
| 3 | BAS1 | x | x | | |
| 4 | BAS2 | x | x | X | x |
| 5 | BAS3 | x | x | | |
| 6 | BAS4 | x | x | | |
| 7 | BAS5 | x | x | X | x |
| 8 | BAS6 | x | x | | |

3. EVALUATION OF CREEP WITH THE LINEAR LOGARITHMIC MODEL

The LLM uses two or more linear lines (in logarithmic scale) to describe the creep development. In this paper two lines are used, see Eqs. 1-5 from /Larson and Jonasson 2003a/.

$$J(\Delta t_{load}, t_0) = E(t_0)^{-1} + \Delta J(\Delta t_{load}, t_0 + \Delta t_0) \quad (1)$$

$$\Delta J(\Delta t_{load}, t_0 + \Delta t_0) = a_1(t_0) \cdot \log(\Delta t_{load} / \Delta t_0) \quad \text{for } \Delta t_0 \leq \Delta t_{load} < \Delta t_1 \quad (2)$$

$$\Delta J(\Delta t_{load}, t_0 + \Delta t_0) = a_1(t_0) \cdot \log(\Delta t_1 / \Delta t_0) + a_2(t_0) \cdot \log(\Delta t_{load} / \Delta t_1) \quad \text{for } \Delta t_{load} \geq \Delta t_1 \quad (3)$$

$$E(t_0) = E_{ref} \cdot \beta_E(t_0) = E_{ref} \cdot \left\{ \exp \left[s \cdot \left(1 - \sqrt{(28 - t_s) / (t_0 - t_s)} \right) \right] \right\}^{0,5} \quad (4)$$

$$a_i(t_0) = a_i^{\min} + (a_i^{\max} - a_i^{\min}) \cdot \exp \left(- \left[(t_0 - t_s) / t_{ai} \right]^{n_{ai}} \right) \quad \text{for } i = 1, 2 \quad (5)$$

where $J(\Delta t_{load}, t_0)$ [Pa⁻¹] = total creep compliance; $\Delta J(\Delta t_{load}, t_0 + \Delta t_0)$ [Pa⁻¹] = creep compliance associated with the elastic modulus; Δt_{load} [d] = $t - t_0$ = load duration; t [d] = time after mixing; t_0 [d] = time of loading specified as time after mixing; Δt_0 [d] = “elastic” load duration = 0,001d /Westman 1999/; Δt_i [d] = load duration at end of line No. i for $i \geq 1$; $E(t_0)$ [Pa] = $J(\Delta t_0, t_0)^{-1}$ = elastic modulus for load duration = Δt_0 ; $\beta_E(t_0)$ [-] = relative time development of elastic modulus; E_{ref} [Pa] and s [-] are fitting parameters; t_s [d] = apparent setting time; $a_i(t_0) \left[Pa^{-12} / \log(\Delta t_{load}) \right]$ = logarithmic creep rate; $a_i^{\min} \left[Pa^{-12} / \log(\Delta t_{load}) \right]$, $a_i^{\max} \left[Pa^{-12} / \log(\Delta t_{load}) \right]$, t_{ai} [d] and n_{ai} [-] are fitting parameters.

4. RESULTS

The fitted parameters for each individual recipe describing the general elastic modulus (Eq. 4) and creep rate (Eq. 5) are presented in Tables 3 and 4. A calculated example of total creep compliance is given in Figure 1 for both moisture-sealed and drying out samples of recipe 4 (BAS2). As can be seen from Figure 1, LLM in the present formulation works well for basic creep (moisture sealed conditions), but not for drying creep. The same holds for all tested concretes in this paper. For more details, see /Fjellström 2013/.

Table 3 – Evaluated fitting parameters with Eq. 4. * Refers to drying out conditions.

| Parameter | Recipe | | | | | | | | | | | |
|-----------|--------|-------|-------|-------|-------|-------|-------|-------|-------|-------|-------|-------|
| | 1 | 1* | 2 | 2* | 3 | 4 | 4* | 5 | 6 | 7 | 7* | 8 |
| E_{ref} | 34,34 | 29,50 | 31,82 | 28,29 | 38,69 | 30,83 | 30,46 | 28,46 | 38,94 | 30,69 | 29,54 | 30,43 |
| [GPa] | | | | | | | | | | | | |
| s [-] | 0,331 | 0,262 | 0,379 | 0,320 | 0,372 | 0,243 | 0,209 | 0,190 | 0,496 | 0,293 | 0,404 | 0,252 |
| t_s [d] | 0,208 | 0,208 | 0,208 | 0,208 | 0,250 | 0,271 | 0,271 | 0,333 | 0,271 | 0,292 | 0,292 | 0,313 |

Table 4 – Evaluated fitting parameters with Eq. 5. * Refers to drying out conditions. The units used in Table 4 are in accordance with the denotation list in connection to Eqs. 1-5.

| Parameter | Recipe | | | | | | | | | | | |
|--------------|--------|------|------|------|------|------|------|------|------|------|------|------|
| | 1 | 1* | 2 | 2* | 3 | 4 | 4* | 5 | 6 | 7 | 7* | 8 |
| a_1^{\min} | 1,0 | 4,0 | 1,7 | 3,4 | 1,7 | 1,3 | 3,0 | 2,5 | 2,9 | 1,5 | 3,5 | 1,5 |
| a_1^{\max} | 100 | 100 | 95 | 100 | 95 | 100 | 80 | 90 | 95 | 90 | 100 | 95 |
| t_{a1} | 0,18 | 0,20 | 0,18 | 0,20 | 0,18 | 0,20 | 0,18 | 0,17 | 0,18 | 0,15 | 0,18 | 0,17 |
| n_{a1} | 0,16 | 0,20 | 0,16 | 0,20 | 0,16 | 0,15 | 0,15 | 0,17 | 0,16 | 0,12 | 0,15 | 0,16 |
| a_2^{\min} | 5,8 | 29,0 | 9,0 | 33,0 | 8,0 | 10,5 | 27,0 | 10,5 | 7,0 | 10,0 | 16,0 | 10,5 |
| a_2^{\max} | 30 | 40 | 25 | 45 | 25 | 35 | 40 | 28 | 30 | 40 | 50 | 30 |
| t_{a2} | 6,00 | 4,00 | 6,00 | 2,00 | 6,00 | 4,00 | 7,00 | 4,00 | 6,00 | 5,00 | 2,10 | 2,00 |
| n_{a2} | 2,70 | 4,00 | 2,70 | 2,00 | 1,70 | 1,90 | 5,00 | 1,80 | 1,50 | 2,80 | 0,17 | 0,70 |

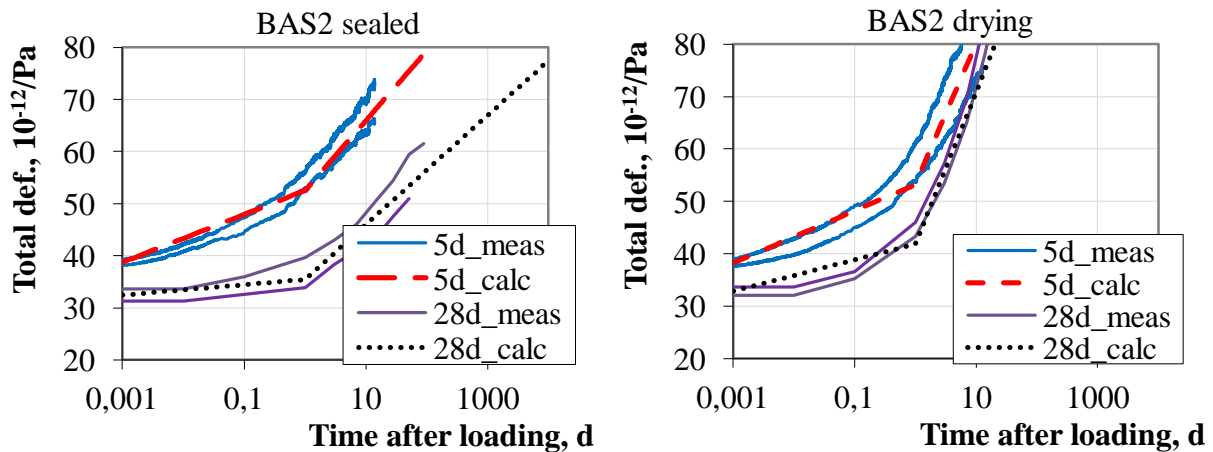


Figure 1 – Calculated total creep compliance compared with measured results (BAS2).

5. CONCLUDING REMARKS

Creep at constant temperature is evaluated from tests with eight Swedish concrete mixes and two kinds of cement. The results show that the LLM is suitable to describe basic creep for the tested concretes, i.e., creep at moisture-sealed conditions. However, there is a need to either refine the existing model or develop a new model to account for the increase of creep due to on-going drying. The LLM can describe the creep progress more accurately by adding more than two lines in logarithmic scale, which is straightforward in the LLM technique. This might be one possibility to refine the LLM for drying creep.

REFERENCES

Fjellström, P., 2013

"Measurement and Modelling of Young Concrete Properties". Licentiate Thesis, Luleå University of Technology, Luleå, Sweden

Hedlund, H., 2000

"Hardening Concrete: Measurements and Evaluation of Non-Elastic Deformation and Associated Restraint Stresses". Doctoral Thesis, Luleå University of Technology, Luleå, Sweden

Larson, M. and J.-E. Jonasson, 2003a

"Linear Logarithmic Model for Concrete Creep I. Formulation and Evaluation." *Journal of Advanced Concrete Technology* Vol. 1, No. 2, pp. 172-187.

Larson, M. and J.-E. Jonasson, 2003b

"Linear Logarithmic Model for Concrete Creep II. Prediction Formulas for Description of Creep Behaviour." *Journal of Advanced Concrete Technology* Vol. 1, No. 2, pp. 172.

Westman, G., 1999

"Concrete Creep and Thermal Stresses: New Creep Models and Their Effects on Stress Development". Doctoral Thesis, Luleå University of Technology, Luleå, Sweden

Analytical model for predicting time to concrete cover cracking due to corrosion of reinforcement



Edgar Bohner
Dr.-Ing., Senior Scientist
VTT Technical Research Centre of Finland
P.O. Box 1000, FI-02044 VTT, Finland
edgar.bohner@vtt.fi



Harald S. Müller
Prof. Dr.-Ing., Full Professor
Karlsruhe Institute of Technology (KIT)
Institute of Concrete Structures and Building Materials
Kaiserstr. 12, D-76131 Karlsruhe, Germany
sekretariat-bt@imb.kit.edu

ABSTRACT

Cracking due to reinforcement corrosion defines an important limit state of durability and structural stability of concrete structures. By means of a comprehensive research work the influence of concrete porosity on the corrosion morphology and the mechanical behaviour of the concrete cover affected by the corrosion process could be investigated. The investigations allowed for the detailed analysis of the stresses, strains and the crack formation within the concrete cover. An analytical prediction model for concrete cover cracking was derived. This model enables the prediction of the time dependent damage process under conditions of practical relevance.

Key words: corrosion, cracking, reinforcement, constitutive modelling, prediction model, durability, carbonation, chlorides

1. INTRODUCTION

The service life design of reinforced concrete structures requires material models capable of reliably describing both mechanisms of damage and the general progression of damage over time. However, the most advanced models that are currently available only capture the processes of carbonation and chloride penetration into the uncracked concrete that is at the very beginning of the damaging process and leads to depassivation of the reinforcing steel (initiation period) /fib 2006/. These models thus disregard the actual damaging phase (propagation period), i.e. the corrosion of the reinforcement. As a result, the service life design established to date only considers the end of the initiation period of the damaging process, or, in other words, the onset of damage (time of depassivation and onset of corrosion) as a critical limit state. The ongoing corrosion of the reinforcement and its consequences, i.e. the damage to the concrete caused by crack formation and spalling, are not considered, which may lead to substantially incorrect conclusions.

In the case of reinforcement corrosion, months or even decades may pass from the time of depassivation to crack formation and spalling. In the latter case (several decades), repair and upgrading works carried out, for instance, at the end of the initiation period would have been unnecessary if the damage had occurred after the end of the intended service life. Being aware of the time period to the occurrence of damage, which results in a restricted serviceability, is thus of considerable economic significance.

Against this background, a comprehensive research project was carried out for seven years at the Institute of Concrete Structures and Building Materials of the Karlsruhe Institute of Technology (KIT) and funded by the German Research Foundation (DFG). The project focused on processes of crack formation in concrete that occur during damage progression in the surface zones of structural components.

The mechanism of fracture and the magnitude of stresses and strains causing cracking of the concrete cover were studied in detail. The influence of the concrete porosity on the corrosion morphology and the behaviour of the concrete cover affected by splitting stresses could be investigated on the basis of miscellaneous experiments. By combining further novel experimental and numerical investigations it was possible to determine the modulus of elasticity of the corrosion products /Müller & Bohner 2012/. The knowledge of the mechanical behaviour of rust is essential for a reliable simulation of the time dependent damage process, which was performed by means of an especially developed numerical model. This modelling approach, involving sophisticated material laws, allowed for the detailed analysis of the stresses, strains and the crack formation within the concrete cover as well as for a realistic prediction of the time development of cover cracking caused by the corrosion of the reinforcement /Bohner 2013/.

Based on parameter studies, which are subjected to different corrosive conditions, an analytical prediction model for concrete cover cracking was derived. This model – which is presented in the subsequent chapter – enables the prediction of the time dependent damage process under conditions of practical relevance and serves as a part of a full probabilistic design approach for durability of reinforced concrete structures.

Detailed information about the comprehensive experimental investigations, the derivation of the modulus of elasticity for rust based on an inverse analysis and the development of the complex numerical model are given in /Bohner 2013/.

2. ANALYTICAL PREDICTION MODEL

2.1 Preliminary remark

The research project aimed to develop an analytical prediction model for corrosion-induced crack formation in the cover zone of concrete structures. The model shall serve as a tool to perform a probabilistic durability design based on the limit state of concrete cover cracking. The general principle of a durability design, using the damage progression law presented in the following, is shown in Fig. 1 schematically. The failure probability for cover cracking can be calculated by the overlap of the distributions for action S (defined as increase of reinforcement bar radius due to corrosion Δr_{corr}) and resistance R (defined as the critical reinforcement bar radius at the time of cracking Δr_{crack}).

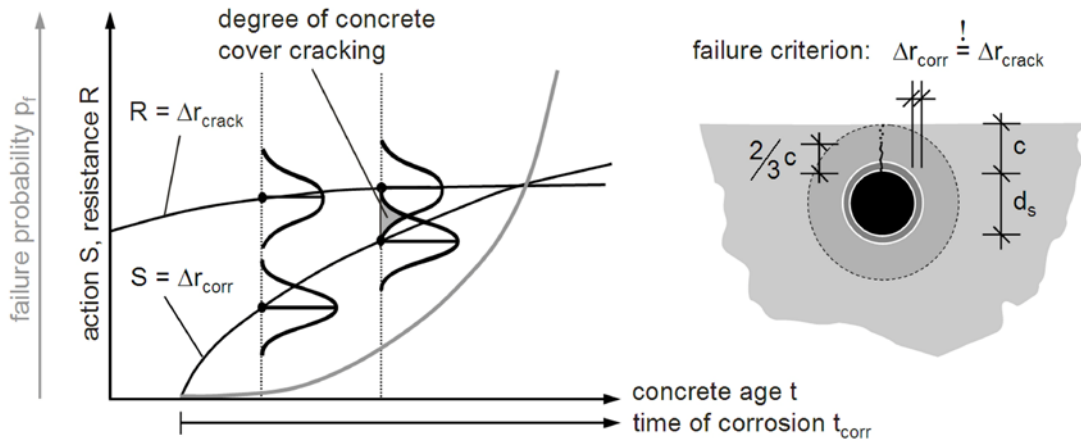


Figure 1 – Schematic representation of the time dependent increase of reinforcement bar radius due to corrosion Δr_{corr} (action S), the critical reinforcement bar radius at the time of cracking Δr_{crack} (resistance R) and the resulting failure probability (left) as well as the schematic sketch of concrete cover cracking above a reinforcement bar (right).

2.2 Development of the model

In order to describe the action S, which represents the propagation of corrosion, the increase of reinforcement bar (rebar) radius Δr_{corr} has to be defined. This increase is dependent on the time of corrosion and results from the reduction of the rebar radius due to corrosion in combination with the expansion of the occurred corrosion products (see Eq. 1). The reduction of the rebar radius is based on the corrosion rate \dot{x}_{corr} . In case of laboratory experiments the corrosion rate can be either determined experimentally or it can be calculated by means of the model for reinforcement corrosion established by the Research Unit 537 of the German Research Foundation (DFG) /Osterminski & Schießl 2011/. The expansion factor, as well known as volume ratio λ , is calculated by the quotient of the volume of rust and the volume of steel.

$$\Delta r_{\text{corr}}(t_{\text{corr}}) = \dot{x}_{\text{corr}}(t_{\text{corr}}) \cdot [\lambda - 1] \cdot t_{\text{corr}} - d_{\text{por}}(t_{\text{corr}}) \quad (1)$$

where Δr_{corr} = increase of rebar radius due to corrosion [mm]; t_{corr} = time of corrosion [a]; \dot{x}_{corr} = corrosion rate [mm/a]; λ = volume ratio [-]; d_{por} = function to take account of rust migration into concrete pores [mm].

The experimental investigations had shown that the initial radius increase of the corroding rebar is weakened by the migration of corrosion products into voids and pores of the concrete. This results in a time delay during the development of corrosion-induced stresses. Stress levels that are able to cause concrete cracking occur not until a certain saturation of the pores in the transition zone around the steel surface has taken place. By means of a continuous function (see Eq. 2), which could be derived based on physical considerations, the migration of rust into the concrete pores can be considered:

$$d_{\text{por}}(t_{\text{corr}}) = p \cdot d_{\text{tz}} \cdot \tanh\left(\frac{\dot{x}_{\text{corr}}(t_{\text{corr}}) \cdot (\lambda - 1)}{p \cdot d_{\text{tz}}} \cdot t_{\text{corr}}\right) \quad (2)$$

where p = porosity of the transition zone accessible for corrosion products [-], valid $0 \leq p < 1,0$; d_{tz} = thickness of the transition zone accessible for corrosion products [mm].

The resistance R (see Fig. 1) that is faced with the action S is caused by the concrete surrounding the rebar. It can be defined as the critical increase of rebar radius due to corrosion at the time of cracking (see Eq. 3). This threshold value is among others depended on concrete age, concrete properties, size and shape of rebar and concrete cover. It was derived based on the linear elastic theory assuming linear viscoelastic behaviour of the concrete (for further information see /Bohner 2013/):

$$\Delta r_{\text{crack}}(t) = \frac{f_{\text{ct}}(t)}{E_{\text{c,eff,D}}} \cdot \left[\frac{d_s + 2c \cdot \left(1 + \frac{c}{d_s}\right) \cdot (1 + \nu)}{1 + \left(\frac{3d_s + 6c}{3d_s + 4c}\right)^2} \right] \cdot k_{\text{nonlin}} \cdot k_{\text{local}} \cdot k_{\mu} \quad (3)$$

where Δr_{crack} = critical increase of rebar radius due to corrosion at time of cracking [mm]; t = concrete age [a]; f_{ct} = tensile strength of concrete [MPa]; $E_{\text{c,eff,D}}$ = effective modulus of elasticity of concrete (influence of creep, relaxation and degradation, see /Müller & Kvitsel 2002/) [MPa]; ν = Poisson's ratio of concrete [-]; d_s = rebar diameter [mm]; c = concrete cover [mm]; k_{nonlin} = factor for consideration of plasticity and cracking of concrete [-]; k_{local} = factor for consideration of a localisation of corrosion (pitting corrosion) [-]; k_{μ} = factor for consideration of percentage of reinforcement [-].

For a detailed discussion of Eq. (1) to (3) and further information on the factors k_{nonlin} , k_{local} and k_{μ} including the verification of the model based on experiments see /Bohner 2013/.

5. CONCLUSIONS

The presented model serves as a tool that enables an accurate analysis or forecast of the future condition of a structural component as early as at the planning and design stage. Targeted measures can be derived (such as providing an appropriate combination of components and material parameters pertaining to structural design and concrete technology) that allow for an onset of damage only at a very late point in time or prevent damage altogether during the intended service life of the structure. The findings and new models established in this research lay the groundwork for a probabilistic durability design of concrete structures starting from the limit state of actual concrete damage.

REFERENCES

- Fédération International du Béton (fib): “Model Code for Service Life Design”, Bulletin 34, Lausanne, Schweiz, Feb. 2006.
- Bohner, E.: “Rissbildung in Beton infolge Bewehrungskorrosion”, Dissertation, Karlsruhe Institute of Technology (KIT), Institute of Concrete Structures and Building Materials, 2013.
- Müller, H. S., Bohner, E.: “Rissbildung infolge Bewehrungskorrosion”, In: Beton- und Stahlbetonbau, Vol. 107, No. 2, 2012.
- Müller, H. S., Kvitsel, V.: “Kriechen und Schwinden von Beton. Grundlagen der neuen DIN 1045 und Ansätze für die Praxis”, In: Beton- und Stahlbetonbau, Vol. 97, No. 1, 2002, pp. 9-19.
- Osterminski, K., Schießl, P.: “Voll-probabilistische Modellierung von Bewehrungskorrosion: Ein Beitrag zur Dauerhaftigkeitsbemessung”, Schlussbericht zum Teilprojekt D der DFG-Forschergruppe 537 „Modellierung von Bewehrungskorrosion“, Centrum Baustoffe und Materialprüfung, Technische Universität München, 2011.

Upgrading the Haparanda Bridge – Unbonded Posttensioning



Jonny Nilimaa
Luleå University of Technology
Department of Civil, Environmental and
Natural Resources Engineering
SE – 971 87 Luleå
E-mail: jonny.nilimaa@ltu.se

ABSTRACT

The Haparanda Railway Bridge was upgraded for a higher load resistance in the summer of 2012. The slab of the 50 year old bridge was subjected to horizontal posttensioning and the railway administrators could thereby permit higher axle loads, 300 kN instead of the original 250 kN. The strengthening procedure was first examined in a laboratory pilot study and since the results were good, the method was applied on a real bridge. The posttensioning of the Haparanda Bridge reduced the strain in the tensile reinforcement substantially; all strains from a 215 kN/axle train were in fact counteracted.

Key Words: Posttensioning, Renovation, Repair, Strengthening, Testing, Upgrading

1. INTRODUCTION

The Swedish government has proposed to increase the funding for infrastructural projects and Prop. 2012/13:25 accounts for a 522 billion SEK budget, for the period 2014-2025, for developing the transportation system to meet current and future demands on sustainability and structural resistance. Refurbishing and upgrading existing structures are by many considered as activities of socioeconomic- and environmental friendly nature and should therefore be prioritized before replacing a structure. A life cycle cost analysis might be a good support for finding the most cost effective alternative for an existing bridge in need of attention. The incorporation of a life cycle cost decision perspective in the Swedish bridge management system was for example discussed by Safi et al (2013).

There are a great number of different methods and techniques for strengthening of existing structures. One method that was recently developed is unbonded internal posttensioning of bridge slabs (Nilimaa 2013). The method was examined through laboratory testing of two small scale concrete trough specimen.

Trafikverket wanted to increase the maximum axle loads on the Haparanda railway line from 250 to 300 kN. The load capacity of the Haparanda Bridge was however examined as unsatisfactory for the higher loads and strengthening was prescribed for the slab. Internal posttensioning was chosen for this purpose and further details are given in Nilimaa (2014).

2. METHOD

A concrete double-trough bridge was strengthened by posttensioning. The slab of the 50 year old Haparanda Railway Bridge was first prepared with eight horizontal holes for installation of prestressing bars with lateral spacing of 1500 mm, as seen in Figure 1. Plastic PE ducts provided

a combination of mechanical- and corrosion protection for the steel bars and a heat shrinking sleeve surrounding the bars provided further corrosion protection.

Core drilling was the method applied for drilling the holes at mid-height of the 400 mm thick slab, see Figure 2. The nominal diameter of the threaded steel bars, Dywidag 26WR, was 26.5 mm and hydraulic jacks provided a posttensioning of 430 kN/bar. The bars were embedded to the structure by anchor plates and –nuts, and the strengthening system was finally sealed by galvanized retention caps. The characteristic tensile strength and modulus of elasticity of the prestressing bars were 1.05 and 205 GPa, respectively.

The strains of the bridge, during loading with a reference train of 215 kN/axle, were monitored before and after strengthening. Linear variable differential transformers (LVDT) measured the deflections of the bridge, while strain gauges were welded onto the tensile reinforcement to monitor the strain. The monitoring layout is shown in Figure 2 and all results are regarding the midspan of the bridge.

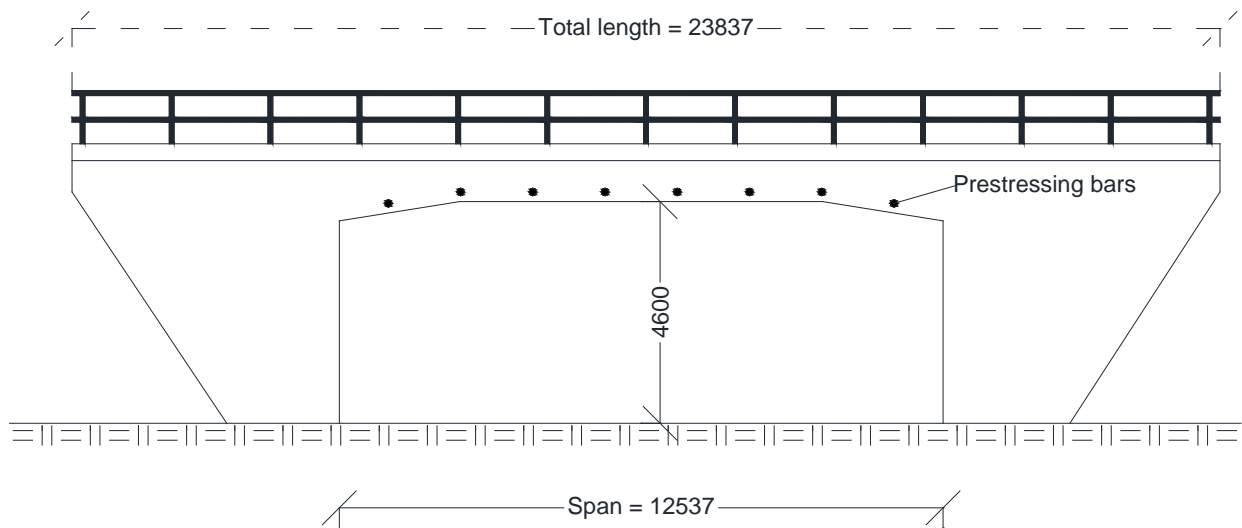


Figure 1 – The Haparanda Railway Bridge.

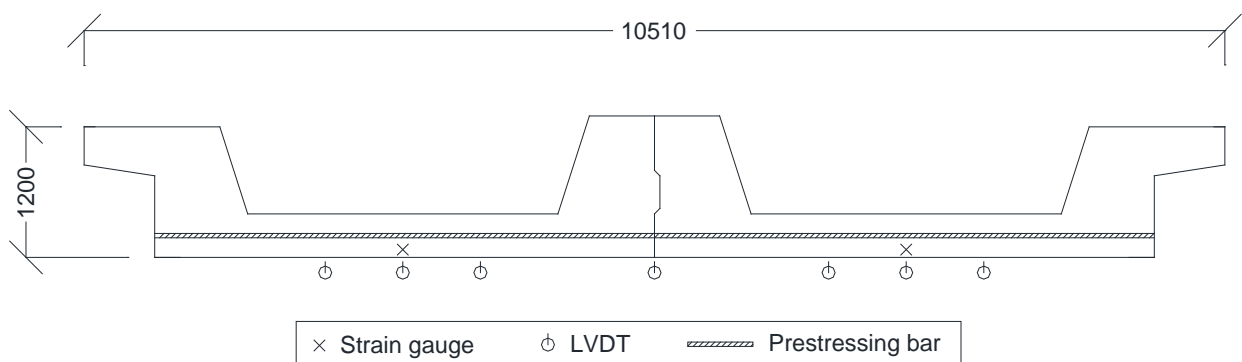


Figure 2 – Cross section of the double-trough with strain gauges, LVDTs and prestressing bars.

Load tests were performed both for moving- and static trains. The static tests were conducted in the following procedure; the train approached and entered the bridge at a low speed before the engine was shut down and the train was arranged with the axles symmetrically about midspan.

The engine was off for about 4-5 minutes before it was started and the train left the bridge at a low speed. Only one of the two troughs was loaded at any point of testing.

3. RESULTS

The strain in the tensile reinforcement for one static test before and one after strengthening are presented in Figure 3. A relative tensile strain of $22 \mu\text{m/m}$ was produced by the reference train loading before strengthening (solid line) and the corresponding relative strain for the posttensioned bridge was about 20 (dashed line). The posttensioning compressed the tensile reinforcement by $23 \mu\text{m/m}$ and the stress from the train was thereby completely counteracted by the strengthening.

Figure 4 illustrates the deflection curve of the Haparanda Railway Bridge during static loading of the unstrengthened bridge. Only the left trough in Figure 2 was loaded, i.e. the trough that is situated between the distance 0 and 4605 mm in Figure 4. The strengthening had small effect on the deflections and the corresponding curve for the strengthened bridge had a similar shape and magnitudes as the one in Figure 4.

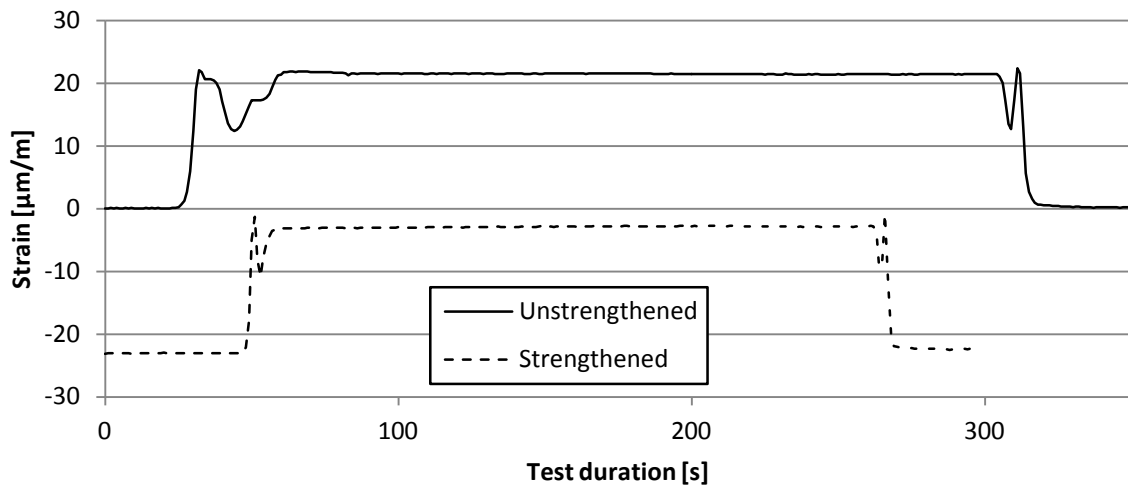


Figure 3 – Maximum tensile strain for loading by a reference train with axle loads of 215 kN, before and after strengthening.

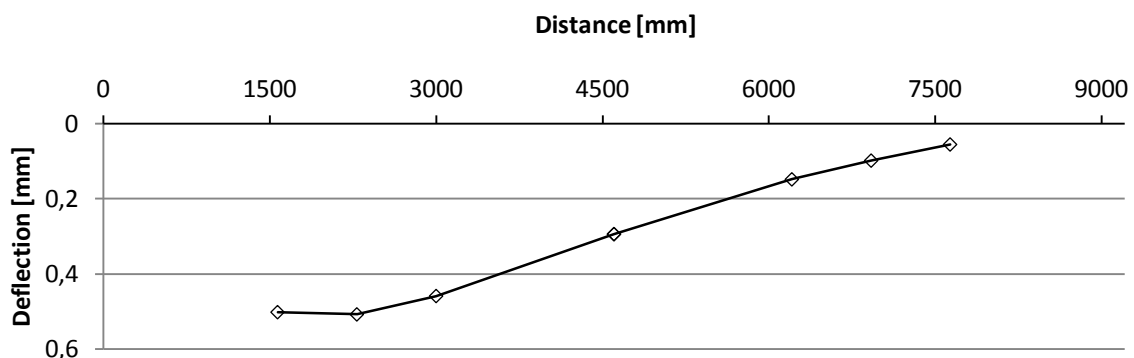


Figure 4 – Deflection for loading by a reference train with axle loads of 215 kN, before and after strengthening.

3. ANALYSIS AND DISCUSSION

Posttensioning can be considered as an active strengthening method and in difference to traditional passive methods it is not only the service load, but also the permanent load, that is undermined. This was shown by the initial compression of the tensile reinforcement in the strengthened bridge in Figure 3. The load increased the strain in the tensile reinforcement with 22 $\mu\text{m/m}$ in the unstrengthened bridge, while the corresponding strain increase for the strengthened bridge was 20 $\mu\text{m/m}$. That implies that the same load caused a smaller relative strain increase in the strengthened bridge, i.e. it had a higher stiffness. The largest effect of the posttensioning was however the reduced overall strains.

The reason for the posttensioning's small effect on the deflections might be explained by the placement of the prestressing bars. The bars were installed at mid depth of the slab and should therefore be located relatively close to the neutral layer, especially if the slab is uncracked. Since the strains are zero in the neutral layer, the prestressing bars have no possibility to reduce the deflection. The prestressing bars could however have a higher effect on the deflection for loads closer to the ultimate limit state.

Internal posttensioning was proven to be an effective method to strengthen existing concrete slabs. The drilling of horizontal holes through the slab was one of the most critical parts of the strengthening procedure and high precaution must be given to avoid cutting the internal reinforcement. Mid depth is therefore recommended for most slabs with reinforcement concentrated at the top- and bottom sections.

4. CONCLUSION

The results of the Haparanda Railway Bridge test indicate that posttensioning is an effective method to strengthen the slab of existing concrete bridges.

5. FUTURE RESEARCH

Further tests are needed to study the effects of changing the lateral spacing between prestressing bars and optimize the design from an economic and performance based perspective.

ACKNOWLEDGEMENTS

Trafikverket and Mainline are acknowledged for funding the research project. Complab assisted in strengthening and testing the bridge and Green Cargo provided trains for the tests.

REFERENCES

- Nilimaa, J., Blanksvärd, T., Täljsten, B. and Elfgren, L., 2014
 "Unbonded Transverse Posttensioning of a Railway Bridge in Haparanda, Sweden",
 Journal of Bridge Engineering, Vol. 19, No. 3, March 2014.
- Nilimaa, J., 2013
 "Upgrading Concrete Bridges – post-tensioning for higher loads", Luleå University of
 Technology, Licentiate Thesis, February 2013.
- Prop. 2012/13:25
 "Regeringens proposition: Investeringar för ett starkt och hållbart transportsystem",
 Stockholm, October 2012, pp. 219.
- Safi, M., Sundquist, H., Karoumi, R. and Racutanu, G., 2013
 "Development of the Swedish bridge management system by upgrading and expanding the
 use of LCC", Structure and Infrastructure Engineering, Vol. 9, No. 12, December 2013,
 pp. 1240-1250.

CARBONATION AND CORROSION

Effect of mesh alignment on simulated interference of localised corrosion on adjacent reinforcement rebars



Mahdi Kioumars
 B.Sc. Eng., M.Sc. Eng, PhD Candidate
 NTNU, Department of Structural Engineering
 Rich. Birkelandsvei 1A,
 NO-7491 Trondheim
 E-mail: mohammad.kioumars@ntnu.no



Max A.N. Hendriks
 Professor
 NTNU, Department of Structural Engineering
 Rich. Birkelandsvei 1A,
 NO-7491 Trondheim
 TU Delft, Department of Structural Engineering
 Stevinweg 1,
 NL-2628CN, Delft, the Netherlands
 E-mail: max.hendriks@ntnu.no



Mette Geiker
 Professor
 NTNU, Department of Structural Engineering
 Rich. Birkelandsvei 1A,
 NO-7491 Trondheim
 E-mail: mette.geiker@ntnu.no

ABSTRACT

The interference of corrosion pits on adjacent reinforcement bars in an under-reinforced concrete beam in bending and its effect on the ultimate limit state (ULS) is quantified using full 3D finite element (FE) modelling. This paper focusses on the influence of the mesh alignment of the FE model. Simulations reveal a limited influence of the mesh configuration on the simulated crack patterns and the ULS.

Key words: Concrete structure, localised corrosion, pitting, bending ultimate limit state, finite element modelling, mesh alignment.

1. INTRODUCTION

Experimental investigations on the effect of corrosion on the structural behaviour of reinforced concrete beams have been summarized by Kioumars et al. (2014a). Figure 1 illustrates the importance of taking into account the maximum cross section area loss, including local corrosion effects or pits, to predict the bending ultimate limit state (ULS) (Figure 1b) as opposed to taking only the average cross section loss into account (Figure 1a). In current guidelines (Du et al. 2005) the impact of corrosion is modelled via empirical relations for stiffness, strength and ductility of the corroded reinforcement bars. Localised corrosion is usually treated as uniform corrosion with larger impact coefficients (Hanjari et al. 2011). The mechanisms resulting from

localised corrosion have received limited attention. Recently, the impact of localised corrosion on the ULS and the possible interference of corrosion pits on adjacent rebars were quantified (Kioumarsis et al. 2014a, 2014b). These studies were based on full 3D finite element modelling. Interference of corrosion pits is explained by coalescing crack planes which eventually might bridge pits on adjacent bars. This paper provides a further verification of the finite element modelling used by studying the effect of mesh alignment.

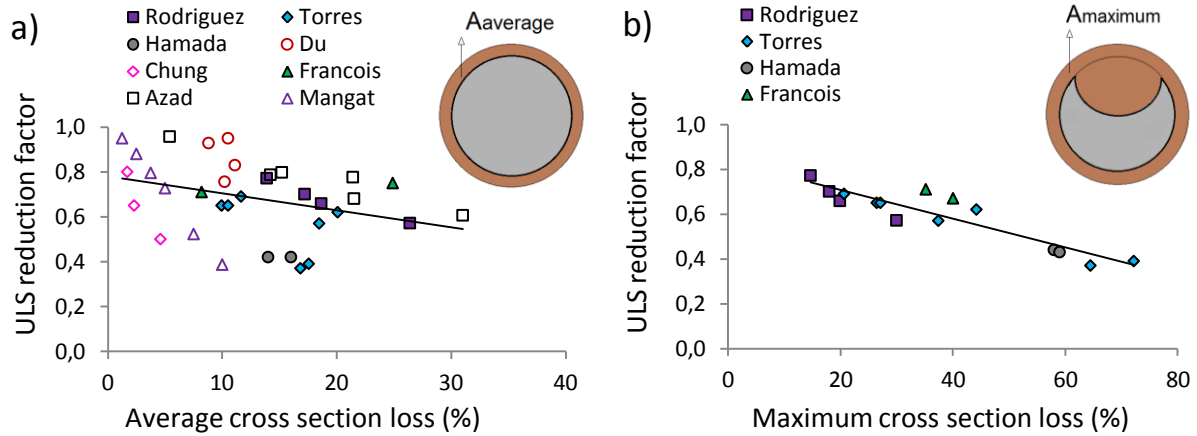


Figure 1 – Reduction factor of the ultimate limit state as a function of a) average rebar cross section loss and b) maximum rebar cross section loss (Kioumarsis et al. 2014a).

2. INTERFERENCE OF LOCALISED CORROSION ON ADJACENT REBARS

In Kioumarsis et al. (2014a, 2014b) an idealized case was selected to quantify the possible interference of localised corrosion on adjacent rebars in an under-reinforced beam subjected to bending. In the idealized case two adjacent rebars each have one corrosion pit. In a series of FE models the combined influence of two variables on the ULS was quantified: the pit distance to bar distance ratio l_p/l_r and the pit cross section ratio A_{pit}/A_0 (see insert in Figure 2). From the numerical simulations it was found that pits only interfere within a critical distance. Interference of pits reduces gradually for increasing distances between the pits along the rebars. For the investigated beam with 80 mm (l_r) between tensile bars the critical distance was 100 mm; i.e. for higher ratios of $l_p/l_r > 100/80 = 1.25$ no interference was observed, see Figure 2.

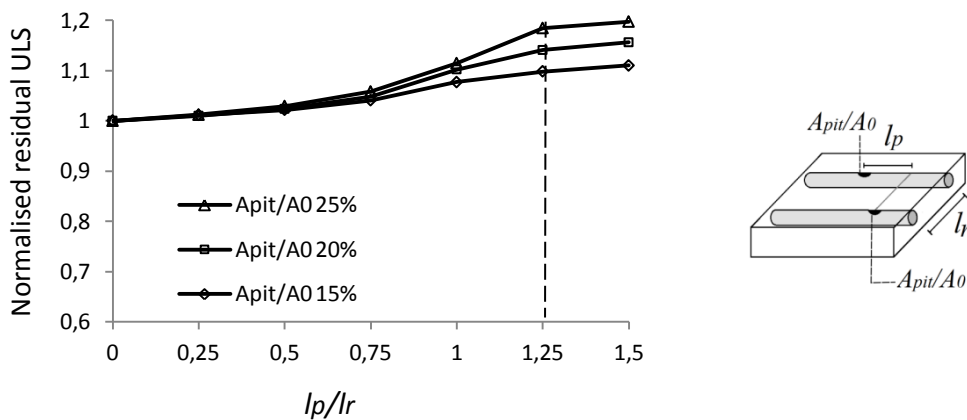


Figure 2 – Effect on ultimate limit state of varying ratio of pit distance in longitudinal direction on adjacent bars to rebar distance (l_p/l_r) (Kioumarsis et al. 2014a).

The main reason of interference of pits is the orientation and number of bending cracks. Figure 3 shows the crack pattern in terms of maximum principle strain for three different pit distances ($l_p = 0, 40$ and 120 mm) on adjacent bars ($l_r = 80$ mm). For $l_p = 0$ there is only one main bending crack bridging the pits (Figure 3a). For $l_p = 40$ mm a skew crack between the pits developed (see Figure 3b). In contrast, for $l_p = 120$ mm ($l_p/l_r > 1.25$) the two pits initiated separate cracks (see Figure 3c).

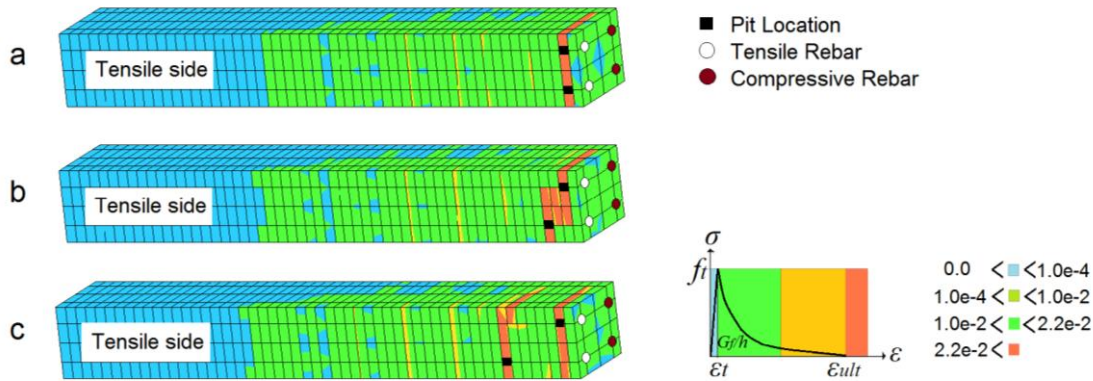


Figure 3 – Crack patterns in terms of maximum principle tensile strains from 3D numerical analyses, pit distance in longitudinal direction on adjacent bars (l_p); a) 0 mm, b) 40 mm and c) 120 mm (Kioumarsis et al. 2014b).

3. EFFECT OF MESH ALIGNMENT

When using classical smeared crack concepts, mesh alignment sensitivity might influence crack propagation and cause cracks to propagate along mesh lines (Rots et al. 1984). In the other words, the possible crack paths may depend on the mesh chosen lines of the model. In order to study the effect of the mesh alignment on crack formation and propagation, alternative models with different mesh alignments in the critical bending zone were used. The finite element models b-1, b-2 and c-1, shown in Figure 4, are alternative models for the corresponding model b and c, shown in Figure 3. Due to meshing restrictions, the respective pit distances l_p are now 37 mm and 125 mm and thus slightly different than in the reference models. It is indeed observed that the cracks, visualized by maximum tensile strains, tend to follow the direction of the mesh lines; but for $l_p/l_r < 1.25$ the obtained crack patterns still bridge the pits in the adjacent bars, regardless of mesh configuration.

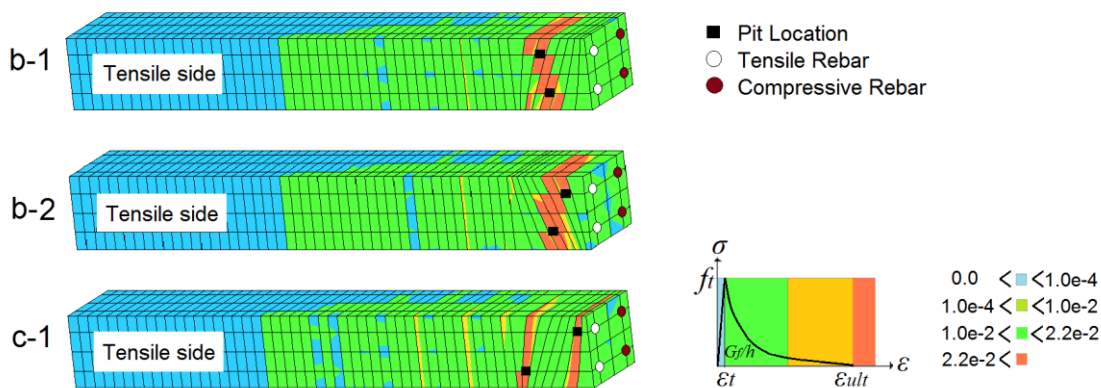


Figure 4 – Crack patterns in terms of maximum principle tensile strains from 3D numerical analyses for alternative mesh alignments.

Figure 5 compares the load deflection curves for the models with rectangular and skew mesh lines. The load-deflection curves of the corresponding l_p distances are comparable. The small local differences in the crack patterns, visible when comparing Figure 4 with Figure 3, hardly lead to changes in the ULS. This can be explained by the similar global crack patterns: for $l_p = 40$ (37) mm the pits are bridged by the cracks, for $l_p = 120$ (125) mm they are not.

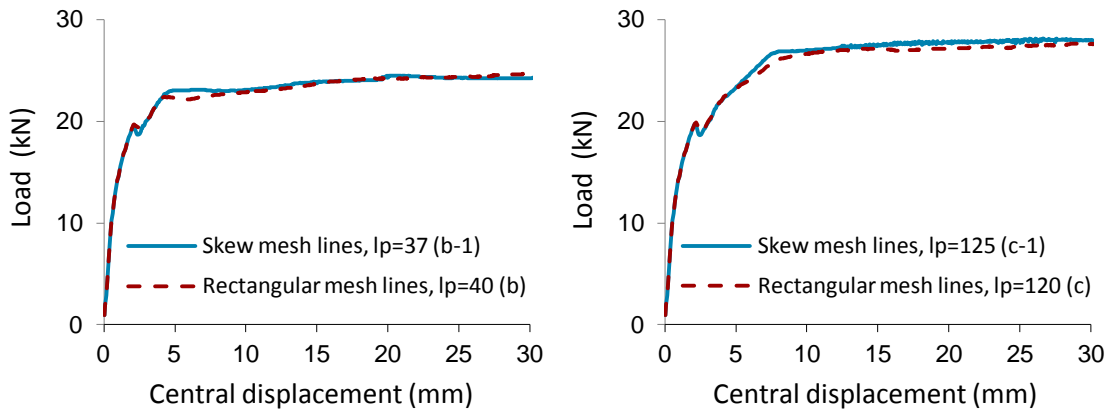


Figure 5- Load deflection curve for models with rectangular (Figure 3) and skew (Figure 4) mesh lines in the bending zone

4. CONCLUSION

The effect of mesh alignment in the numerical simulation of crack formation due to bending of an under-reinforced beam with localised corrosion was quantified. The impact of localised corrosion was illustrated using an idealised case with one corrosion pit in each of two adjacent rebars. Alternative finite element models with different mesh alignment in the bending zone were used.

The simulations indicate that for ratios of pit distance in longitudinal direction on adjacent bars to rebar distance less than a critical value ($l_p/l_r < 1.25$) the crack pattern follows the path between the corrosion pits regardless of mesh configuration. The mesh alignment did not have a significant influence on the load deflection curve.

REFERENCES

- Du, Y.G., & Clark, L.A., & Chan, A.H.C., 2005
 “Residual capacity of corroded reinforcing bars. Magazine of Concrete Research, 57, 135-147.
- Hanjari, K.Z., & Kettil, P., & Lundgren, K., 2011
 “Analysis of mechanical behavior of corroded reinforced concrete structures”. ACI Structural Journal, 108, 532-541.
- Kioumars, M.M., & Hendriks, M.A.N., & Geiker, M.R., 2014a
 “Quantification of the interference of localised corrosion on adjacent reinforcement bars of a beam in bending”. Sub. to Nordic Con Res.
- Kioumars, M.M., & Hendriks, M.A.N., & Geiker, M.R., 2014b
 “Interference of localised corrosion in adjacent reinforcement bar of a beam in bending”, Concrete innovation conference, CIC, Oslo, Norway.
- Rots, J.G., & Nauta, P., & Kusters, G.M.A., 1984
 Blaauwendraad, J., “Smeared crack approach and fracture localization in concrete”, HERON, 30(1) (1984) 1-48.

A Novel Anode Material for Cathodic Prevention of Steel Reinforced Concrete Structures with Hybrid Functions



Emma Qingnan Zhang
PhD candidate
Division of Building Technology
Chalmers University of Technology
SE-412 96, Gothenburg
emma.zhang@chalmers.se



Tang Luping
Ph.D., Prof
Division of Building Technology
Chalmers University of Technology
SE-412 96, Gothenburg
tang.luping@chalmers.se

ABSTRACT

Carbon fiber mesh anode is used as an alternative of traditional anode material for cathodic protection system. Theoretical analysis of feasibility and preliminary experimental work of the new material is presented in this paper. Long-term exposure in marine environment has been simulated using an electrochemical acceleration method to shorten the experimental time. Treated specimens are examined by scanning electron microscope (SEM) and laser-ablation inductive-coupled-plasma mass spectroscopy (LA-ICP-MS) for microstructure study and chemical analysis. Preliminary results show a ring-pattern zone at anode adjacent area but no sign of damage at anode and anode adjacent area.

Key words: cathodic prevention, cathodic protection, corrosion, concrete, carbon fiber mesh anode, SEM, LA-ICP-MS, electrochemical acceleration, durability.

1. INTRODUCTION

The conventional means to protect the steel reinforcement from corrosion is to increase the thickness of concrete cover and/or to use low water/cement (w/c) ratio concrete. It will obviously consume more cement and other raw materials which it is at the sacrifice of more CO₂ emission and natural resources. Therefore, new and more sustainable approaches are needed for corrosion prevention or protection of reinforcement steel in concrete. Cathodic protection (CP) technique has been proved to be a successful application in providing long-term corrosion control for steel in concrete (ISO). This paper presents a novel approach for cathodic protection by utilizing the principle of electrochemical migration in order to lower the cost of the system. The innovation from the traditional system and preliminary results are presented.

2. DIFFERENCE FROM CONVENTIONAL CATHODIC PROTECTION

2.1 Intermittent power supply

Conventional cathodic protection needs a careful regulation of current density with continuous power supply and a complex monitoring system for maintenance, which are energy consuming, financially costly and high level of technical difficulties. Glass et al. has proved the laboratory evidence that intermittent current can still provide protection effect on reinforcement (Glass et

al., 2001). This provides possibility of using natural solar, wind, or wave energy instead of traditional power supply. Because of the rate of ionic diffusion under the current intermittent period is much lower than the rate of ionic migration under the external electrical field, it is possible to prolong the service life of the system and reduce the intensiveness of maintenance compared with conventional CP system.

2.2 Anode material

Activated titanium electrodes are most commonly used anode materials nowadays which are commercially available in several forms. The most widely used form is expanded mesh. Service life of this type of anode is predicted in a range of 20 years to in excess of 100 years from laboratory tests as well as practice (Pedefferri, 1996). However the main service life of CP system applied in Europe is about 25 years (Polder et al., 2013). One of the reasons that can cause system failure is due to anode degradation caused by acid formation at anode zone which the cell resistance will increase and may lead to bond loss (Mietz et al., 2001). If low intermittent current is applied, the current intensity will be much lowered (average current density $\leq 5\text{mA/m}^2$ through proper design). Therefore, anode materials with lower conductivity than titanium can be alternatives for CPre system, such as carbon fiber and glass fiber with conductive coatings which is relatively affordable price. In addition, carbon fiber and glass fiber have approved history as reinforcement material for concrete such strength reinforcement and preventing cracks.

3. PRELIMINARY RESULTS

According to the theoretical feasibility analysis (Tang et al., 2012) of this approach, an electrochemical acceleration method can be used to investigate the effect of applied electrical field on cement matrix and anode material. The specimen was partially emerged in 10% NaCl solution and connected to continuous power supply. The accumulated power applied is equivalent to 130-year intermittent power supply. The specimen was prepared using the form shown in Figure 1 and the dimension is $40\text{mm} \times 40\text{mm} \times 250\text{mm}$. the mould contained a plain steel reinforcement bar and a strip of carbon fiber mesh (SIGRATEX Grid 300 supplied by SGL Group) at certain distance.



Figure 1 Image of the casting mould (left), the carbon fiber mesh anode (middle) and the dimension of specimen (right).

After one-month period of connecting to external electrical field, the specimen was taken out, sawed into slice and the dimension of the ring-pattern around carbon fibre anode was investigated by SEM shown in Figure 2. The back-scattered SEM image also confirmed that the ring-pattern area has different phases as it is layered, as shown in Figure 3. LA-ICP-MS provided a semi-quantified analysis of chemical changes around the anode area as shown in Figure 4. Due to the nature of C-S-H gel, the distribution of silicon (Si) in the cement paste matrix is assumed unchanged because the Si-O bonding is very stable and hardly to be broken or reformed even under strong electrical currents (Ryu et al., 2002). Therefore the changes of Ca/Si ratio can be considered the changes of calcium in the cement paste matrix. On the other hand, positive ions sodium and potassium did not show the same movement as calcium. The signal intensity ratio shows that at the junction of ring 1 and ring 2, the signal intensities of sodium and potassium reached a peak and then gradually decreased to a base level.

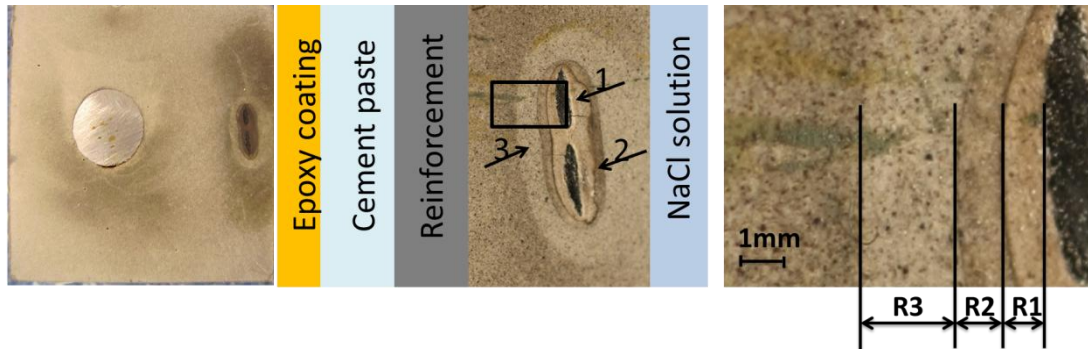


Figure 2 Sawed samples (left), ring-pattern (middle) and the dimension of the ring-pattern (right).

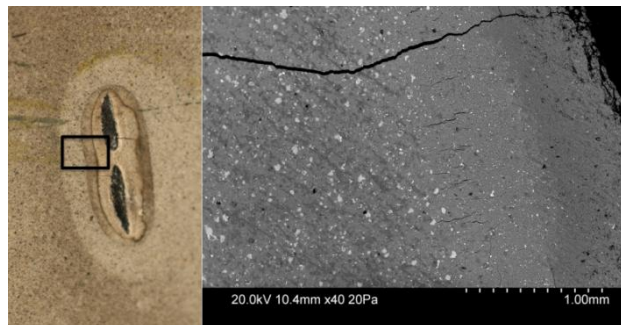


Figure 3 Back-scattered SEM image of the ring-pattern area. The crack through the ring area was formed after experiment possibly caused by drying.

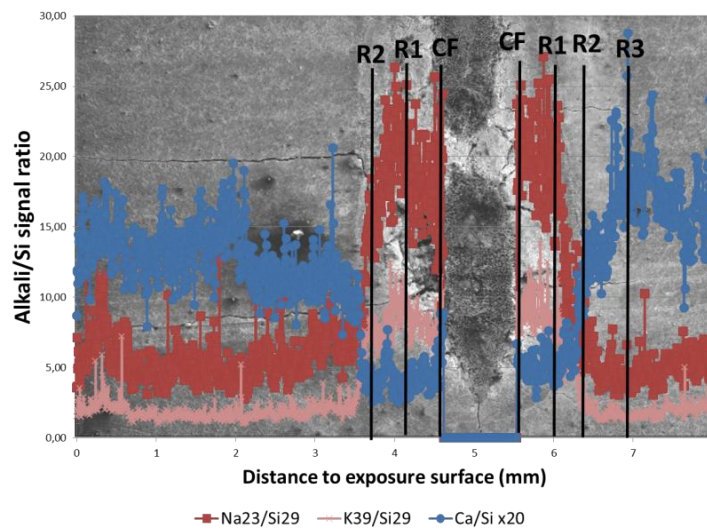


Figure 4 ICP-LA-MS analysis on the ring-pattern area. The exposure surface is on the left side. Signal intensities are normalized to Si and are proportional to the concentration of elements. However, there is no intensity-concentration correlation between different elements. CF, R1, R2 and R3 stand for carbon fiber, ring 1, ring 2 and ring 3 respectively.

The carbon fiber anode showed a sign of loss of matrix material at the area of anode-paste interface, as shown in Figure 5. This can be caused by acidification that the polymer matrix degrades or decomposes, or by the process of sawing, polishing during the preparation stage which cannot be ruled out. Except for a certain loss of matrix material at the area of anode-paste interface, there is no obvious crack or delamination around the carbon fiber mesh, implying that it is suitable to be used as anode for corrosion prevention at a low current density for over 100 years.

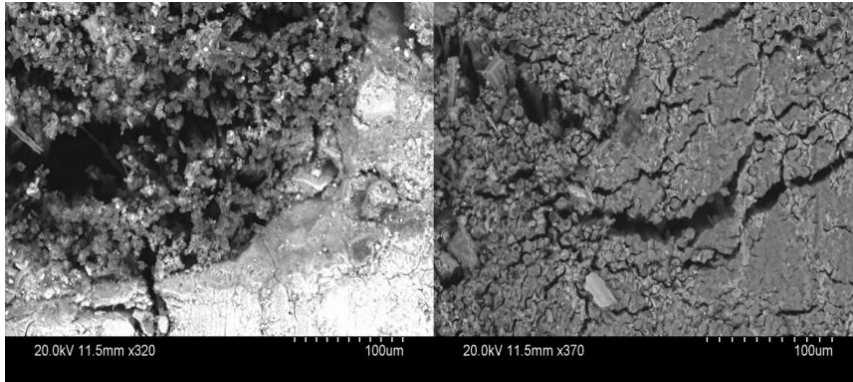


Figure 5 Back-scattered SEM images of carbon fiber anodes at the anode-paste interface (left) and in the middle of the grid (right).

4. CONCLUDING REMARKS

With the development of solar cells and conductive fiber meshes, this novel approach of anode material with hybrid functions can be built up to cathodically prevent reinforcement steel in concrete from corrosion and mechanically prevent concrete surface from cracking. With this low current density the service life of the cathodic prevention system should be significantly longer than the conventional cathodic protection system. Thus the troubles due to the imposed current can be reduced or even eliminated. With this new type of anode material and intermittent power supply, the properties of concrete with high w/c can be better utilized and the cover thickness can be reduced. As a consequence, cement and raw materials will be less consumed in the reinforced concrete structures.

REFERENCES

- GLASS, G., HASSANEIN, A. & BUENFELD, N. 2001. Cathodic protection afforded by an intermittent current applied to reinforced concrete. *Corrosion Science*, 43, 1111-1131.
- ISO, B. 12696 (2012). *Cathodic Protection of Steel in Concrete*.
- MIETZ, J., FISCHER, J. & ISECKE, B. 2001. Cathodic protection of steel-reinforced concrete: structures-results from 15 years' experience. *Materials performance*, 40, 22-26.
- PEDEFERRI, P. 1996. Cathodic protection and cathodic prevention. *Construction and Building Materials*, 10, 391-402.
- POLDER, R. B., LEEGWATER, G., WORM, D. & COURAGE, W. 2013. Service life and life cycle cost modelling of cathodic protection systems for concrete structures. *Cement and Concrete Composites*.
- RYU, J.-S., OTSUKI, N. & MINAGAWA, H. 2002. Long-term forecast of Ca leaching from mortar and associated degeneration. *Cement and concrete research*, 32, 1539-1544.
- TANG, L., ZHANG, E. Q., FU, Y., SCHOUENBORG, B. & LINDQVIST, J. E. 2012. Covercrete with hybrid functions—A novel approach to durable reinforced concrete structures. *Materials and Corrosion*, 63, 1119-1126.

Experimental Investigation on Rebar Corrosion in Combination with Fibres



Carlos Gil Berrocal
PhD-student
Chalmers University of
Technology
412 96 Göteborg, Sweden
carlos.gil@chalmers.se



Karin Lundgren
Professor
Chalmers University of
Technology
412 96 Göteborg, Sweden
karin.lundgren@chalmers.se



Ingemar Löfgren
PhD,
Thomas Concrete Group AB
412 54 Göteborg, Sweden
ingemar.lofgren@tcg.nu

ABSTRACT

In this paper, early results from an on-going project aimed at investigating the influence of fibre reinforcement on corrosion of rebar are presented. Resistivity of mixes containing fibres was reduced when compared with plain concrete while chloride migration seemed to remain unaffected. On the mechanical properties, results showed that while the flexural behaviour was greatly enhanced by addition of fibres up to 0.5% vol., the variation in compressive strength was negligible regardless of the fibre type. Early results from the main experiments indicated a tendency of earlier corrosion initiation with increasing crack width, and that the initiation time was somewhat delayed for the fibre reinforced specimens.

Key words: cracking, chlorides, corrosion, fibres

1. INTRODUCTION

Civil engineering structures like bridges and harbour piers require the use of a dense concrete (low w/c ratio), thick concrete covers and strict crack width limitations due to the risk for chlorides to cause reinforcement corrosion. In practice, this leads to large reinforcement amounts which often cause complications in production, but still with difficulties in controlling the surface crack width due to the large concrete cover. Fibre reinforcement has been extensively used in applications such as buildings, floors or slabs on grade for crack control (Bentur and Mindess 2007). Therefore, it would be beneficial to use fibres, in complement to the traditional reinforcement, also in civil engineering structures where their crack limiting effects are of interest.

However, the use of fibres in combination with conventional reinforcement in chloride environments raises questions due to the limited research available in this field. Some of these questions are related to the influence fibres may have with respect to chloride ingress and moisture transport. The main issues that have yet to be dealt with are the potential risk of galvanic corrosion due to the different steel types used in the fibres and in the traditional reinforcement, and the risk of higher corrosion rates due to lower resistivity of steel-fibre reinforced concrete. In an on-going Ph.D. project at Chalmers University of Technology, the

authors investigate the durability of concrete structures with regard to chloride induce corrosion when fibre reinforcement is combined with conventional reinforcement.

2. EXPERIMENTAL PROGRAMME

The main task in the project consists of a long-term experimental campaign specifically conceived to answer the aforementioned questions. The experiments include a total of 56 beam specimens with dimensions 100×180×1100 mm and reinforced with 3 Ø10 mm diameter rebar as illustrated in Figure 1. The reinforcement was placed to get a clear concrete cover of 30 mm and the separation between bars was kept to 45 mm to allow the fibres to easily flow through them and ensure a more homogenous material.

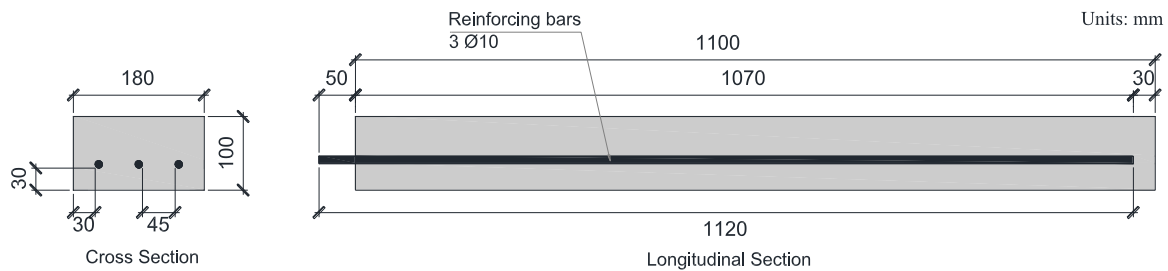


Figure 1. Geometry of the test specimens

A single concrete mix and three types of fibres were used to cast four different types of concrete, hereafter referred as to: *plain*, for ordinary concrete; *steel*, for steel-fibre reinforced concrete; *hybrid*, for a combination of steel and micro polyvinyl-alcohol fibre reinforced concrete; and *synthetic*, for macro polyvinyl-alcohol fibre reinforced concrete. Table 1 shows the mixture proportion and fibre dosages used in each mix. Further parameters varied are the loading conditions, including sound specimens (never cracked) and specimens cracked and subjected to cyclic loading (bond degradation), sustained loading, or no loading. Also the influence of surface crack width is studied with openings ranging from 0.1 to 0.4 mm. Six specimens are kept immersed in potable water as a reference while the rest are exposed to an accelerated process of natural corrosion by partial immersion in 10% Cl⁻ solution and cycles of 14-day wetting and 14-day drying. Moreover, companion specimens to study chloride ingress, chloride migration and resistivity of concrete, as well as compressive strength and flexural behaviour of fibre concrete were cast.

Table 1. Mixture proportions, kg/m³

| Component | | | | |
|--------------------------------------|-------|-------|--------|-----------|
| Cement (CEM I 42,5N SR 3 MH/LA) | | | | 360 |
| Limestone filler (Limus 40) | | | | 165 |
| Fine aggregate (Sand 0/4) | | | | 770 |
| Coarse aggregate (crushed 5/16) | | | | 833 |
| Effective water | | | | 169 |
| Superplasticizer – Glenium 51/18 | | | | 5.76 |
| Air entrainer – MicroAir 105 | | | | 0.72 |
| Fibre (Volume, %) | Plain | Steel | Hybrid | Synthetic |
| Steel – Dramix [®] 65/35-BN | - | 0.5 | 0.35 | - |
| PVA – Kuralon [™] RFS400 | - | - | 0.15 | - |
| PVA – Kuralon [™] RF4000 | - | - | - | 0.75 |

3. RESULTS AND DISCUSSION

Some results are shown in Figure 2, as can be seen, the addition of fibres in low dosages had a marginal effect on the compressive strength of concrete. Similarly, no significant variation was observed in the chloride migration coefficient for the different mixes. These results are in agreement with those from (Sanchez, Alonso, and Barragán 2009) or (Teruzzi et al. 2004) who concluded that the interfacial zone between fibres and the cement paste does not act as a preferential path for the ingress of detrimental agents. Resistivity tests, on the other hand, revealed a clear influence of fibres on this property. Resistivity of series containing steel fibres is invariably reduced with lower values for higher fibre contents. Moreover, synthetic series, with PVA fibres, also show a decrease in resistivity with respect to their ordinary concrete counterpart. Similar results are reported in (Roque et al. 2009), indicating that PVA fibres, despite their high resistivity ($\sim 3.5 \cdot 10^5 \Omega\text{m}$) and unlike other fibres such as polypropylene, may reduce the resistivity of concrete.

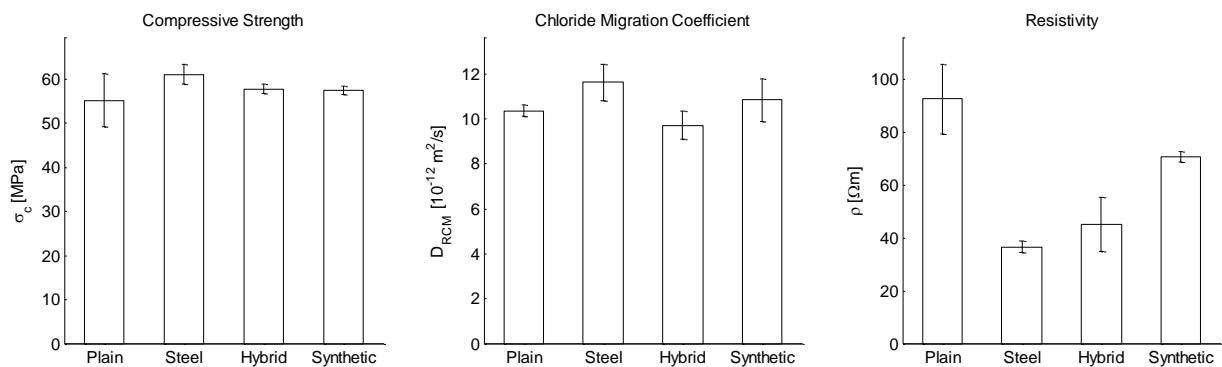


Figure 2. Results on material tests for compressive strength, chloride migration coefficient and resistivity of concrete (mean values and standard deviation for 3 specimens)

The flexural behaviour of fibre reinforced concrete was studied by means of three-point bending tests according to (RILEM TC 162-TDF 2002). Figure 3 evidences the enhanced flexural behaviour of fibres in terms of toughness while the increase in tensile strength is negligible.

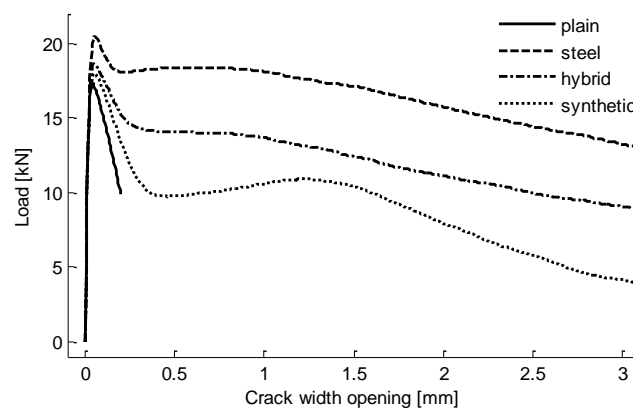


Figure 3. Load versus crack mouth opening displacement for three-point bending beam tests (Averaged curves for 6 specimens each)

In the long-term experiments, half-cell potential (HCP) are continuously monitored using an embeddable reference electrode. HCP describes the thermodynamic state of a metal's surface and, alone, does not provide information about the corrosion rate. However, it can indicate whether the reinforcement is actively corroding or in a passive state and it may suggest a range of corrosion rates. A proposed range to determine the probability of corrosion can be found in

(ASTM C876-91 1999). Based on that, the corrosion initiation times of each mix are shown in Figure 4 for varying crack width and for 3 different loading conditions. Note the difference in scales for loaded and unloaded series; the shorter initiation times for the loaded specimens are due to the cracks being kept open, while the values of the crack width in the other two series was the measured ones *before* unloading. A clear tendency is observed where larger crack widths led to earlier corrosion, except for the loaded specimens, where corrosion generally started soon after the first exposure to chlorides regardless of the crack opening. Additionally, a slight delay in the corrosion initiation time is observed for the fibre-reinforced mixes.

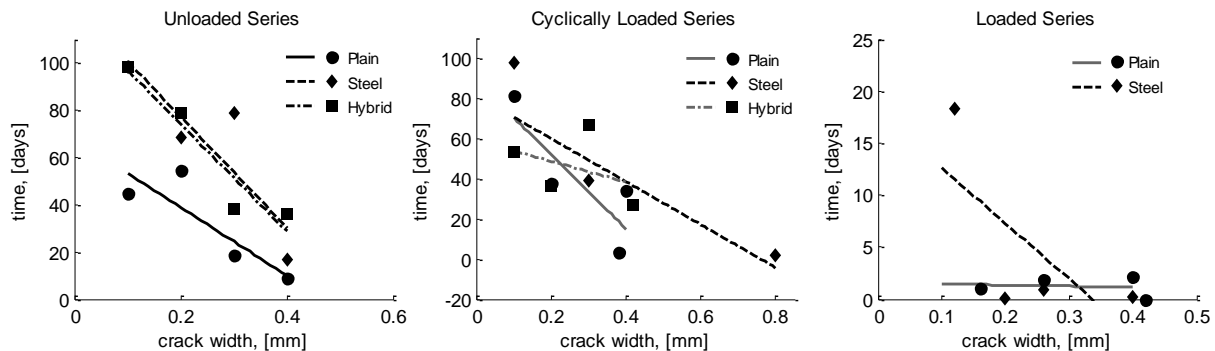


Figure 4. Corrosion initiation times for different loading conditions

4. CONCLUSIONS

The results from this investigation indicate that controlling the crack width is crucial in order to delay the initiation of corrosion in reinforced concrete structures. Fibre reinforcement can effectively control the crack width and provides a considerable improvement of the tensile properties of concrete in terms of toughness. Besides, given the same surface crack width, results show that corrosion initiation was somewhat delayed for fibre-reinforced mixes. On the physical properties, no adverse effect is detected regarding the chloride migration coefficient for FRC. Conversely, electrical resistivity is greatly decreased by the presence of steel fibres, and even in the case of PVA fibres, results show a reduction. Today, this fact represents the major impediment to use fibre reinforcement in combination with conventional rebar in chloride environments, as there are concerns that a reduced resistivity will increase the corrosion rates. Therefore, further investigations are required to address this issue.

REFERENCES

- ASTM C876-91. 1999. "Standard Test Method for Half-Cell Potentials of Uncoated Reinforcing Steel in Concrete." 91(Reapproved).
- Bentur, Arnon, and Sidney Mindess. 2007. *Fibre Reinforced Cementitious Composites*. 2nd ed. Abingdon, United Kingdom: Taylor & Francis.
- RILEM TC 162-TDF. 2002. "Test and Design Methods for Steel Fibre Reinforced Concrete - Bending Test." 35(November): 579–82.
- Roque, Reynaldo, N Kim, Byoungil Kim, and George Lopp. 2009. *Durability of Fiber-Reinforced Concrete in Florida Environments*. Tallahassee, FL.
- Sanchez, M., M.C. Alonso, and B. Barragán. 2009. "Durability Performance of Plain and Fiber Reinforced Self-Compacting Concrete." *CPI- Concrete Plant International-2*: 62–64.
- Teruzzi, T., E. Cadoni, G. Frigeri, S. Cangiano, and G. A. Plizzari. 2004. "Durability Aspects of Steel Fibre Reinforced Concrete." In *6th RILEM Symposium on Fibre-Reinforced Concretes*, 625–34.

A model to calculate the CO₂-uptake in a country's concrete structures during service life and after



Katja Fridh, Assistant Professor, PhD
 Division of Building Materials
 Faculty of Engineering, LTH, Lund University
 P O Box 188, SE-221 00 Lund, Sweden
 Phone +46 46 222 3323
 E-mail: katja.fridh@byggtek.lth.se



Ronny Andersson, PhD
 Division of Structural Engineering
 Faculty of Engineering, LTH, Lund University
 P O Box 188, SE-221 00 Lund, Sweden
 Phone +46 46 222 3112
 E-mail: ronny.andersson@kstr.lth.se



Håkan Stripple, PhD
 IVL Swedish Environmental Research Institute
 Box 5302, 400 14 Göteborg, Sweden
 Phone +46 31 725 62 42
 E-mail: hakan.strippl@ivl.se



Martin Häglund, PhD
 Bryggaregatan 3, 241 30 Eslöv, Sweden
 E-mail: martin@haeglunds.se



Lars-Olof Nilsson, Professor
 Division of Building Materials
 Faculty of Engineering, LTH, Lund University
 P O Box 188, SE-221 00 Lund, Sweden
 Phone +46 46 222 7408
 E-mail: Lars-Olof.Nilsson@byggtek.lth.se



Björn Lagerblad, Associate Professor
 Division of Concrete Structures
 KTH, Royal Institute of Technology
 P O Box, SE-100 44 Stockholm, Sweden
 Phone +46 10 516 68 18
 E-mail: bjorn.lagerblad@cbi.se

ABSTRACT

During the project 'The CO₂-cycle in cement and concrete' an analytical model to quantify the CO₂-uptake in a country a specified year was developed. That was accomplished by deriving a new model for the carbonation process and as input to that, measurements of carbonation in

concrete indoors and studies of carbonation in crushed concrete were made. Through knowledge of the cement production each year, the distribution of the cement into different products and estimations of what concrete quality each product has, the total uptake for Sweden was calculated. For the year 2011 was the CO₂-uptake calculated to 300 000 tons.

1. INTRODUCTION

To produce cement to be able to produce concrete a large amount of limestone has to be burnt at about 1450 °C. When 1000 kg limestone is burnt (calcinated) about 500 kg carbon dioxide (CO₂) is emitted. To heat the kiln to 1450°C a significant amount of fuel is needed and this leads to emission of CO₂. These two emission sources lead to that the global production of cement accounts for 5% of the global emissions of CO₂. Large efforts to reduce these emissions by using alternative fuels and additives have been done for some time now and the numbers are improving. To be able to get the net CO₂ emission numbers for cement and/or concrete it is also important to investigate the uptake of CO₂ during the service life of a concrete structure and also after its service life, then often as a filling material (most common use of concrete after demolition today), /Stripple 2013/. The overall objective of the project ‘The CO₂-cycle in cement and concrete’ was to present a model which could estimate the uptake of CO₂ in a country’s concrete structures for a specified year. The methodology and complementary studies involved in the work of deriving this model is presented below.

2. MODELLING CARBONATION

A model for calculating depth of carbonation was derived, /Nilsson 2011/. The carbonation was assumed to progress as a front and all the CO₂ is consumed at the front. The depth of carbonation is then described as, x_{CO_2}

$$x_{CO_2} = \sqrt{\frac{2 \cdot D_{CO_2} \cdot c}{a}} \cdot \sqrt{t} \quad (1)$$

and found to be dependent of the diffusion coefficient of CO₂ in carbonated concrete (D_{CO_2} , m²/s), the concentration of CO₂ in the air, (c , kg/m³), the time (t , s) and the amount of CO₂ that is needed to move the carbonation front dx (a , kg/m³). The diffusion coefficient is assumed constant in the section since the CO₂-binding capacity is assumed to be zero in the carbonated layer. The variable a is dependant of the amount of cement, the amount of CaO in the cement and how much of the CaO that carbonates (the degree of carbonation).

The degree of carbonation has been estimated theoretically to 75-100% for fully hydrated outdoor concrete, /Lagerblad 2005/. For the degree of carbonation of indoor concrete new measurements were done and the degree was found to be 30-50%, /Fridh and Lagerblad 2013/.

3. THE EXISTING CONCRETE

After trying several different approaches it became evident that an estimation of existing concrete for a country could be based on amounts of sold cement, /Andersson et al. 2013/. These figures are also reasonable easy to find for most countries. It was then assumed that a standard concrete contains 15% cement.

The cement is then used in different applications that use different kinds of concrete. To be able to estimate how much cement that was used to different applications, statistics on investments in the building sector was used. These investments were then condensed into seven applications

(relative distribution between applications): Bridge (0.15), Residential (0.2), Offices (0.37), Roof tiles (0.03), Concrete pavement (0.11), Shotcrete (0.07) and Sleepers (0.07).

Each application was given w/c-ratios and their surfaces-to-volume-ratios were estimated. Each surface was then given one of eleven different environments:

- Outdoors: with or without shelter giving different relative humidity (RH) and degrees of hydration of the concrete and with and without paint giving a diffusion coefficient for the paint.
- Slab on ground with four different foundations (mineral wool or polystyrene or without insulation but with coarse gravel or without insulation but with sand/gravel giving different RH and degrees of hydration for the concrete).
- Indoors: with and without paint and other surface materials giving different RH and degrees of hydration for the concrete and different diffusion coefficients for the surface materials.

With these estimations it is now possible to calculate the uptake in the Swedish concrete structures.

4. CALCULATING THE CO₂-UPTAKE

The depth of carbonation of all surfaces can now be calculated by the model since all the variables has been estimated; w/c-ratio, CaO content, degree of carbonation, cement content, surface coating, CO₂ content and RH.

The different depths of carbonation of each surface (obtained after a specified amount of time), degrees of carbonation and areas are used to calculate the ratio carbonated-volume-to-uncarbonated-volume (k_v) of each application. That ratio includes all CO₂-uptake until the specified year. If an uptake a specified year is wanted then the k_v for the year before is subtracted.

The potential uptake for a specified year $P(t)$ for all products is calculated by using a calcination of 0.494 kton CO₂/kton cement, the amount of sold cement that year and the relative distribution of the present application.

The uptake for one application AU is obtained by

$$AU = P(t) \cdot k_v$$

In the same way can all applications be added for the same year.

5. ESTIMATING UPTAKE IN DEMOLISHED CONCRETE

When concrete is demolished a lot of new surfaces are created. This will facilitate the uptake but the size of the concrete is still large so the effect will probably be minor. To be able to use the concrete as e.g. landfill the material will be crushed to smaller fractions and then stored in piles. During the present work, the carbonation in piles of crushed concrete was studied, /Fridh 2014/ and it was found that unreacted cement that was exposed to the rain reacted and the surface of the piles became very dense and the ingress of CO₂ was very small. The conclusion was therefore that the handling of demolished concrete today does not contribute to the uptake to any large extent.

6. CONCLUSIONS

With the methodology described above it was possible to calculate the CO₂-uptake in concrete structures and demolished concrete in Sweden 2011 to 300 000 tonnes. The gain in CO₂-uptake with an improved system for demolished concrete was evident.

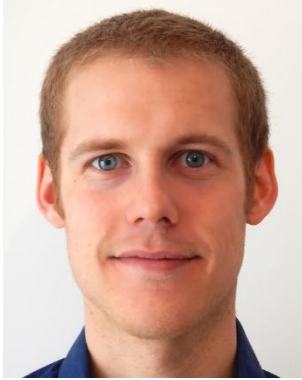
ACKNOWLEDGEMENTS

The authors would like to express their sincere gratitude towards all towards (i) the Swedish Consortium for Financing Basic Research in the Concrete Field, (ii) the Swedish Environmental Research Institute (IVL) and (iii) Cementa AB/Heidelberg Cement Group for their financial support. In addition, Christer Ljungkrantz (researcher at Cementa AB, Sweden) have critically reviewed and continuously made important insights that have improved the progress and quality of the work.

REFERENCES

- Andersson, R, Fridh, K, Stripple, H and Häglund M., 2013
 “Calculating CO₂ Uptake for Existing Concrete Structures during and after Service Life”, *Environ. Sci. Technol.*, 2013, 47 (20), pp 11625–11633.
- Fridh, K., 2014
 “Carbonation of crushed concrete”, Report TVBM-7216, Division of Building Materials, Lund University.
- Fridh, K and Lagerblad, B., 2013
 “Carbonation of Indoor Concrete”, report, TVBM-3169; Division of Building Materials Lund University.
- Lagerblad, B., 2005
 “Carbon dioxide uptake during concrete life cycle”, State of the art, CBI Report 2(2005).
- Nilsson, L. O., 2011
 “A new model for CO₂-absorption of concrete structures”, report, TVBM-3158, Division of Building Materials, Lund University.
- Stripple, H., 2013
 “Greenhouse gas strategies for cement containing products”, IVL Report B2024, www.IVL.se

Representativeness of accelerated carbonation testing of cement pastes



M. Auroy¹, S. Poyet¹, P. Le Bescop¹, J-M. Torrenti², T. Charpentier³, M. Moskura³, X. Bourbon⁴

¹ CEA, DEN, DPC, SECR, Laboratoire d'Etude du Comportement des Bétons et des Argiles, F-91191 Gif-sur-Yvette, France.

² Université Paris-Est, IFSTTAR, Département Matériaux & Structures, 14-52 Boulevard Newton, F-77447 Marne la Vallée Cedex 2, France.

³ CEA, DSM, IRAMIS, NIMBE, Laboratoire Structure et Dynamique par Résonance Magnétique, F-91191 Gif-sur-Yvette, France.

⁴ Andra, Parc de la Croix Blanche, 1-7 rue Jean Monnet, 92298 Chatenay-Malabry Cedex, France.

Corresponding author's email: martin.auroy@cea.fr

ABSTRACT

Carbonation is one of the main factors involved in corrosion of reinforced concrete structures. The impact of carbonation on the durability of cementitious-based materials is of major importance. However, carbonation is a very slow process (around 0.04% CO₂ in the atmosphere). Accelerated test are then commonly used in the laboratory. The representativeness of accelerated test compared to natural carbonation is then an important issue. In this context, this study focuses on the mineralogical characterisation of ancient and recent cement pastes, respectively submitted to natural (in air) and accelerated carbonation (3% CO₂). As a major conclusion, the mineralogical changes assessed using complementary techniques have highlighted a good agreement between natural and accelerated carbonation.

Key words: Natural and Accelerated Carbonation, Representativeness, Cement, Mineralogy.

1. INTRODUCTION

Carbonation involves the reaction between the CO₂ and the cement hydrates, resulting in the fall of the concrete pH at a value below 9. This causes the depassivation of the protective oxide layer and promotes rebar corrosion. Carbonation also induces significant mineralogical changes (hydrates dissolution and calcium carbonates precipitation) and, subsequently microstructural alterations (reduction of total porosity and alteration of the pore size distribution). Furthermore, natural carbonation is a very slow process (due to the low content of CO₂ in the atmosphere, around 0.04% volume). It takes years to observe significant structural changes on dense concrete structures. Accelerated carbonation tests are therefore commonly used in the laboratory using higher CO₂ concentrations. Using Transmission Electron Microscopy and Nuclear Magnetic Resonance (²⁹Si NMR) (Groves et al. 1991) highlighted that accelerated carbonation of C₃S pastes (in pure CO₂) leads to a less polymerized C-S-H with the formation of silica gel, which is not observed in air. More recently, (Castellote et al. 2009) observed that low CO₂ concentrations (below 3%) do not impact significantly the microstructure compared to natural carbonation. While, at high CO₂ concentrations (10% and 100%), the C-S-H has completely disappeared (contributing to the formation of silica gel). They conclude that accelerated carbonation tests up to a 3% of CO₂ are representative of natural carbonation. It is also reported that CO₂ concentration directly affects the nature of the CaCO₃ polymorphs (Anstice et al. 2005). For instance, calcite, vaterite and aragonite are detected in natural carbonation, while in pure CO₂, only calcite is present.

The mineralogy and the pore structure of the solid phases appear to be greatly influenced by the CO₂ content. The representativeness of accelerated carbonation compared to natural one is then an important issue. Because literature data are limited, this study aims at complementing the current data by comparing the mineralogical evolution of a blended cement paste after natural (P_{CO₂}≈0.04%) and accelerated (P_{CO₂}≈3%) carbonation.

2. EXPERIMENTAL

The experimental programme was carried out using hardened cement pastes. Two similar commercial ternary blends (European CEM V/A, water to binder ratio of 0.4) were used:

- (i) The first one (“AV” in this study) is a product from Origny Cements (Lumbres, France), made of 55% clinker, 22% slag and 23% fly ash. Specimens were kept in air during 18 years, making them a reference for natural carbonation.
- (ii) The second one (“RV” in this study) is a product from Calcia (Airvault, France), made of 50% clinker, 25% slag and 25% fly ash. Specimens were carbonated using the device developed by (Drouet et al. 2010) at a CO₂ content of $3 \pm 0.1\%$ ($25 \pm 0.1^\circ\text{C}$ and $55 \pm 1\%$ RH) during 315 days. The use of X-ray Diffraction (XRD¹) and Thermogravimetric Analysis (TGA²) confirmed that the carbonation state was uniform within the specimens after this period.

The resulting specimens (AV and RV) were characterised using XRD, TGA and ²⁹Si NMR³. The obtained mineralogical signatures of AV and RV are then compared.

3. RESULTS AND DISCUSSION

The XRD patterns of the AV and RV specimens (sound and carbonated) are provided on Figure 1. The contents of portlandite (Ca(OH)₂) and calcium carbonates (CaCO₃) were evaluated using TGA and reported in Table 1. The X-ray diffractograms highlight that Ca(OH)₂ remains after carbonation regardless of the concentration of CO₂, which is confirmed from the TGA results (Table 1). This is generally attributed to the formation of a CaCO₃ layer at the surface of Ca(OH)₂ crystals, which therefore reduces their dissolution rate. The ettringite (AFt) peaks have completely disappeared at 3% CO₂ but remain at 0.04% CO₂, which was also observed using ²⁷Al NMR (not shown here) and frequently described in the literature. Calcite, aragonite and vaterite are identified both in natural and accelerated carbonation (Figure 1), which is consistent with the literature (Anstice et al. 2005). In each case, the amounts of CaCO₃ formed are similar (Table 1). Only the X-ray intensities of vaterite and aragonite peaks differ from natural to accelerated carbonation (Figure 1). This can be attributed to the specific environmental conditions (RH and CO₂ concentration). For instance, some research has found that vaterite formation is inversely related to RH. More recently, (Drouet et al. 2010) have shown that vaterite and aragonite are more abundant for low RH rather than for high RH. These results suggest that polymorphic transformation (aragonite and vaterite to calcite) is inhibited at low RH.

¹ PANalytical X'Pert diffractometer, with a Cu K α ($\lambda = 1.54 \text{ \AA}$) radiation

² NETZSCH STA 409 PC LUXX, with alumina crucibles, at a 10 K min^{-1} heating rate, under N₂ constant flow rate, from ambient temperature to 1150°C

³ Bruker Avance 300 WB (7 Tesla), with zirconia rotors (4 mm diameter), at rotational frequencies of 10 to 12.5 kHz

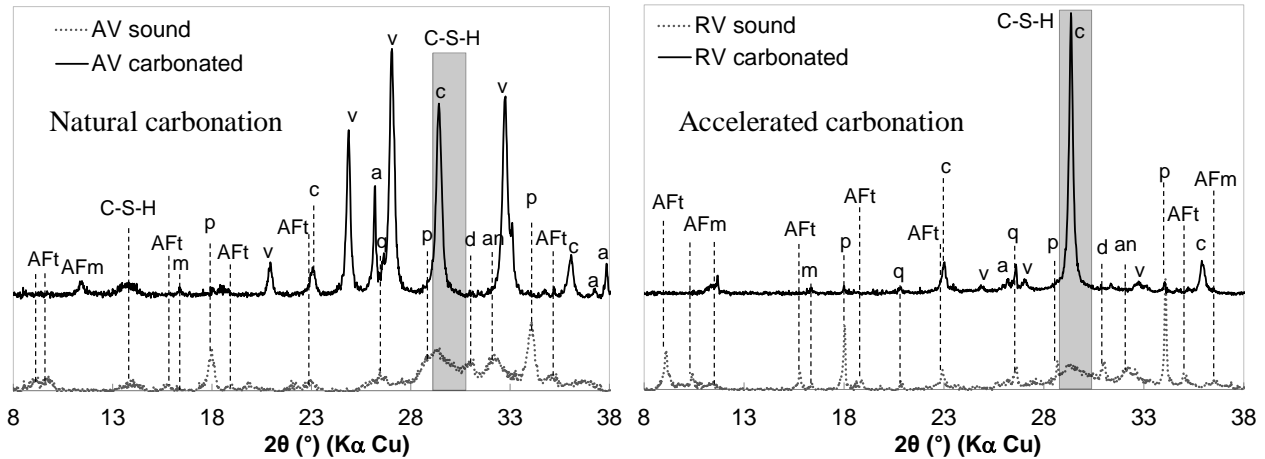


Figure 1 – X-ray diffractograms of AV (left) and RV (right) (AFt: ettringite, AFm: monosulfate, m: mullite, p: portlandite, q: quartz, c: calcite, v: vaterite, a: aragonite, d: dolomite, an: anhydrous phases C_2S and C_3S)

Table 1 – Percentages of portlandite and calcium carbonates estimated using TGA (based on the initial weight of the sample dried at $1150^{\circ}C$)

| Mineralogical phases | $Ca(OH)_2$ | | $CaCO_3$ | |
|------------------------------|------------|------------|----------|------------|
| | Sound | Carbonated | Sound | Carbonated |
| Accelerated carbonation (RV) | 12.9% | 4.0% | 2.6% | 60% |
| Natural carbonation (AV) | 10.8% | 5.6% | 0.9% | 72.0% |

^{29}Si NMR spectra of the AV and RV sound specimens (Figure 2) show the characteristic peaks of the cement paste with the resonance of Q^0 (anhydrous phases C_2S and C_3S , -71.4 ppm), Q^1 , Q^2_p and Q^2 (C-S-H, -78.6, -80.5 ppm and -84.0 ppm). Structural characterisation of C-S-H is of major importance, as it is the main constituent of the paste. Thus, after both natural and accelerated carbonation the anhydrous phases (Q^0) drastically decrease, which is in agreement with the XRD results (Figure 1). It is also observed that almost all the C-S-H decomposes to a phase (Q^3_{gel} and Q^4_{gel}) close to silica gel. The NMR spectra show that the chain end groups and bridging groups (Q^1 and Q^2_p) silicon tetrahedra (SiO_4) are more available with regard to carbonation than the SiO_4 middle groups (Q^2) which are strongly linked to the C-S-H structure. Therefore, carbonation induces, simultaneously both loss of calcium (decalcification) and polymerisation of the C-S-H, which lead to the formation of a silica gel structure (Ca-enriched silica gel) (Groves et al. 1991) (Castellote et al. 2009). Using the NMR results, the degree of polymerization of the C-S-H can be quantified (i.e. the calcium to silicon ratio of the C-S-H: C/S), which is an efficient mean to evaluate the accelerated carbonation representativeness in regard to natural carbonation. The initial C/S is assumed to be equal to 1.7. The deconvolution of NMR spectra allows estimate the relative proportion of silicate species (% Q^n) present in the specimens (surface under each peak). The “quantification” of Q^3_{gel} and Q^4_{gel} species then leads to the direct evaluation of the C/S of the Ca-enriched silica gel (Table 2). Therefore, both in natural and accelerated carbonation, the C/S values are very close (around 0.50).

Table 2 – ^{29}Si NMR spectra deconvolution results

| Silicate species (% Q^n) | Q^3_{gel} (%) | | Q^4_{gel} (%) | | C/S | |
|------------------------------|-----------------|-----------|-----------------|-----------|-------|------------|
| | Sound | Carbonate | Sound | Carbonate | Sound | Carbonated |
| | d | d | d | d | | |
| Accelerated carbonation (RV) | 18 | 50 | 0 | 39 | 1.70 | 0.49 |
| Natural carbonation (AV) | 8 | 38 | 0 | 42 | 1.70 | 0.48 |

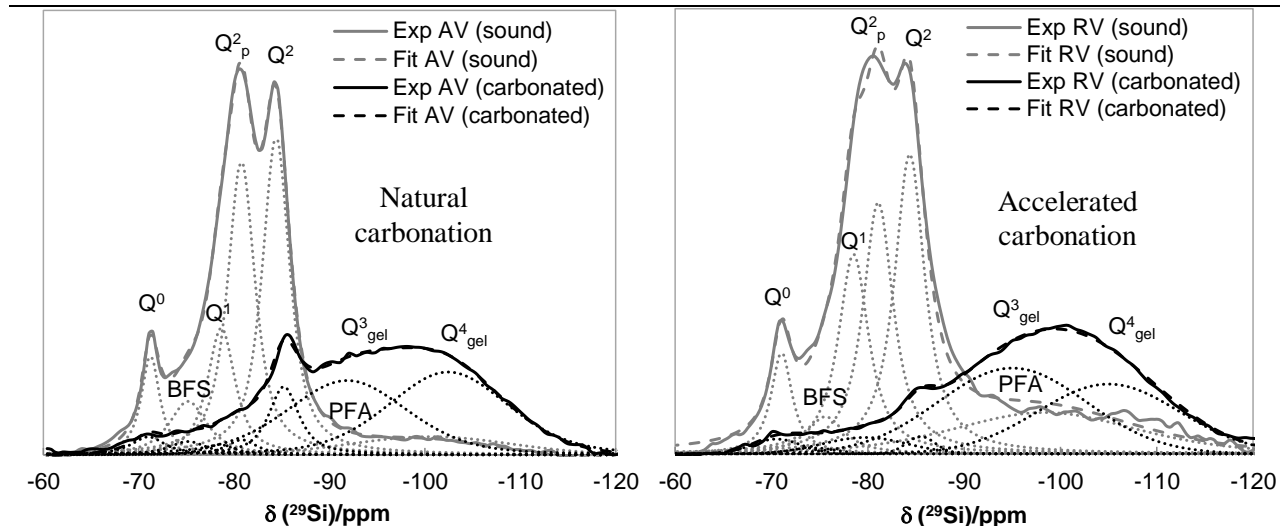


Figure 2 – ^{29}Si M.A.S.-N.M.R. experimental (solid lines) and simulated (dashed lines) spectra of AV and RV

4. CONCLUSION

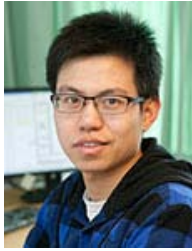
This paper aims to compare the effect of both natural ($P_{\text{CO}_2} \approx 0.04\%$) and accelerated carbonation ($P_{\text{CO}_2} \approx 3\%$) on the mineralogy of blended cement pastes (European CEM V/A, $w/c=0.4$). For this purpose, ancient specimens (18 years natural carbonation) and recent ones (315 days accelerated carbonation) are characterised using complementary techniques (XRD, TGA and ^{29}Si NMR). From the results obtained, either in natural or accelerated carbonation, the following conclusions can be drawn: (i) the phases identified are basically the same; (ii) the portlandite and calcium carbonates contents evolutions are very close; (iii) portlandite remains in the carbonated zone; (iv) the C–S–H decomposes to a Ca-enriched silica gel structure, (v) the C/S of the Ca-enriched silica gel (eq. indicator of their degree of polymerization) are similar (close to 0.5). Given the positive results achieved, accelerated carbonation test, at a CO_2 content of 3%, can be considered representative of natural carbonation. Future experimental work should involve more different types of cement (Portland and blended) and microstructural investigations (water retention curves, mercury intrusion porosimetry) to extend the current data.

REFERENCES

- Anstice, D.J., Page, C.L., Page, M.M., 2005,
 “The pore solution phase of carbonated cement pastes”, *Cement and Concrete Research*,
 Vol.35, No. 2, 2005 pp. 377–383
- Auroy, M., Poyet, S., Le Bescop, P., Torrenti, J-M., 2013,
 “Impact of carbonation on the durability of cementitious materials: water transport
 properties characterization”, *EPJ Web of Conferences*, Vol. 56, 2013, pp. 01008
- Castellote, M., Fernandez, L., Andrade, C., and Alonso, C., 2009,
 “Chemical changes and phase analysis of OPC pastes carbonated at different CO_2
 concentrations”, *Materials and Structures*, Vol. 42, 2009 pp. 515–525
- Drouet, E., Poyet, S., Le Bescop, P., Torrenti, J-M., 2010,
 « Chemical changes and carbonation profiles of carbonated cement pastes at 80°C for
 different relative humidities”, *Concrete Under Severe Conditions – Castro-Borges et al.*
 (eds) CRC Press 2010 321-328
- Groves, G.W., Brough, A., Richardson, I.G., Dobson, C.M., 1991,
 “Progressive changes in the structure of hardened C_3S cement pastes due to carbonation”,
Journal of the American Ceramic Society, Vol. 74, No. 11, 1991 pp. 2891–2896

MODELLING, ANALYSING AND TESTING

Structural assessment of bridge deck slabs



Jiangpeng Shu, M.Sc., Ph.D.
Student

E-mail:
jiangpeng.shu@chalmers.se



Karin Lundgren, Ph.D.,
Professor

E-mail:
karin.lundgren@chalmers.se



Mario Plos, Ph.D., Associate
Professor

E-mail:
mario.plos@chalmers.se



Kamyab Zandi, Ph.D.,
Researcher

E-mail:
Kamyab.Zandi@chalmers.se

Department of Civil and Environmental Engineering, Chalmers University of Technology
SE-412 96 Göteborg, Sweden

ABSTRACT

The overall aim of this project is to develop improved methods for assessment of the load carrying capacity and response of bridge deck slabs. This research project was carried out by laboratory experiments, analytical computational analysis, linear and non-linear finite element analyses. The on-going non-linear analyses of tested slabs show possibility to accurately predict the load carrying capacity and to realistically simulate the crack pattern and load distribution.

Key words: bridge deck slabs, assessment, modelling, capacity

1. INTRODUCTION

Existing infrastructure represents a substantial part of the societal assets and existing bridges represent a huge capital that need to be well administrated. Bridge deck slabs are one of the most exposed bridge parts and are often critical for the load carrying capacity. Consequently, it is important to examine if the current analysis and design methods are appropriate. In a pre-study, the need for research and development to achieve more robust bridge deck slabs (Sundquist 2011) was identified. The overall aim of this project is to develop improved methods for assessment of the load carrying capacity and response of bridge deck slabs.

2. EXPERIMENTAL STUDY

Initially, a literature survey and laboratory experiments were carried out. Three two-way slabs were tested to failure and loads, deformations, and distribution of support reactions along the supporting edges were measured (Fall et al. 2014). The specimens were two-way octagonal slabs (80 mm in thickness) supported on four edges and subjected to a point-load at the centre, see Fig. 1. Moreover, the loading jack was coupled to a load cell which was placed over a steel plate (280 × 280 × 30 mm). Even load distribution was ensured by placing a wood fibre board ($t = 12$ mm) between the steel plate and the slab.

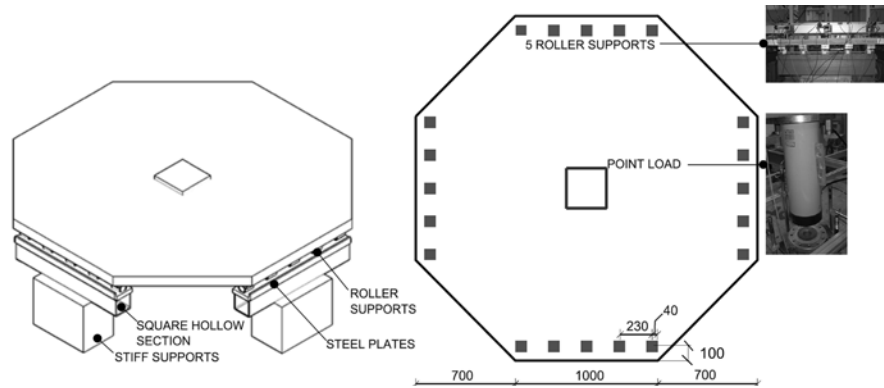


Fig. 1 Test set-up of two-way slabs; all dimensions in mm (Fall et al. 2014).

Regarding the material, the compressive strength ($f_c = 50.9$ MPa) and tensile strength ($f_t = 2.7$ MPa) of the concrete, together with the tensile strength of steel reinforcement ($f_y = 621$ MPa, $E_s = 210$ GPa) were tested. The reinforcement had a bar diameter of 6 mm, placed with a clear cover of 20 mm from the bottom of the slab to the most dense layer. There were totally 25 reinforcement bars with 96 mm spacing in strong direction and 13 bars with 196 mm spacing in weak direction.

3. ANALYTICAL AND FINITE ELEMENT ANALYSIS

Analyses of the slabs on different levels of detail were carried out. First, analytical equations were used to calculate the load carrying capacity of the slabs using yield line method (Johansen 1972). Thereafter linear FE analysis was used to check the capacity according to a FE guideline (Pacoste, Plos, and Johansson 2012).

In order to increase the understanding of the response of the slabs, non-linear FE analysis was used to simulate the behaviour of slabs, and the results were compared to the tests. Parametric studies with non-linear FE analyses were carried out as a basis for further development of existing methods of calculation and design methodology.

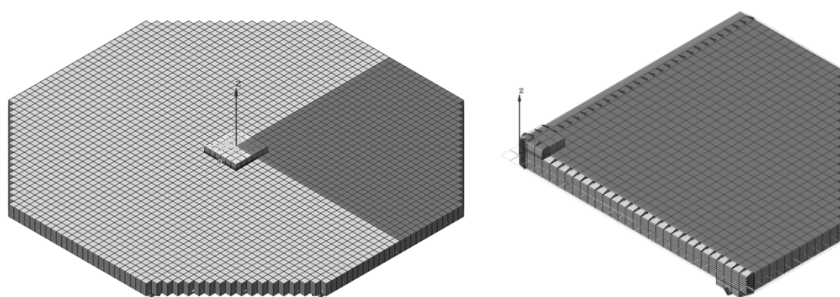


Fig. 2 FE model of the tested slabs

The finite element software DIANA 9.4.4 was used to model the slabs, using a 3D model. Due to symmetry, only a quarter of the slab was included in the model, to reduce the computation time, see Fig. 2. In the test, steel plates and roller bearings were used at the supports. In the FE model, the steel plates were modeled and interface elements were used between the concrete and the steel plates to account for friction. Under the steel plates at the supports, the nodes were supported both in vertical direction and along the roller supports. All nodes at the symmetry faces were fixed in the perpendicular direction. The material properties were taken from material test. Both geometrical and physical nonlinearity were included in the FE analysis.

To investigate the influence of varying modeling choices, several models with different element types, mesh density and ways to model the interaction between concrete and reinforcement were analyzed. The properties of the models are shown in Table 1. An analysis (B40F) with $40 \times 40 \times 10$ mm brick elements and full interaction to the reinforcement was selected as reference. In analysis W40F, wedge elements were chosen to investigate the influence of element types. In analyses B30F and B20F, element sizes of 30 and 20 mm in plane were chosen, respectively, to study the influence of mesh density. In analysis B40B, a bond-slip relation was assumed for the interaction between reinforcement and concrete.

Table 1 Five analyses with varying modeling choices

| Analysis | Element type | Element size (mm) | Bond model |
|------------------|---------------|--------------------------|------------------|
| B40F (reference) | Brick element | $40 \times 40 \times 10$ | Full interaction |
| W40F | Wedge element | $40 \times 40 \times 10$ | Full interaction |
| B30F | Brick element | $30 \times 30 \times 9$ | Full interaction |
| B20F | Brick element | $20 \times 20 \times 8$ | Full interaction |
| B40B | Brick element | $40 \times 40 \times 10$ | Bond-slip |

4. RESULTS AND CONCLUSIONS

The capacity calculated both from yield line method and FE linear analysis were 40.5 kN. Since the three tested specimens had the same dimensions and reinforcement arrangements, the results in the three tests were very similar. Here, the one with intermediate values (CR2) was taken as a reference to be compared with the analysis results, see Fig. 3; as can be seen, the agreement is good with nonlinear analysis but higher than the capacity obtained with yield line and linear FE analysis.

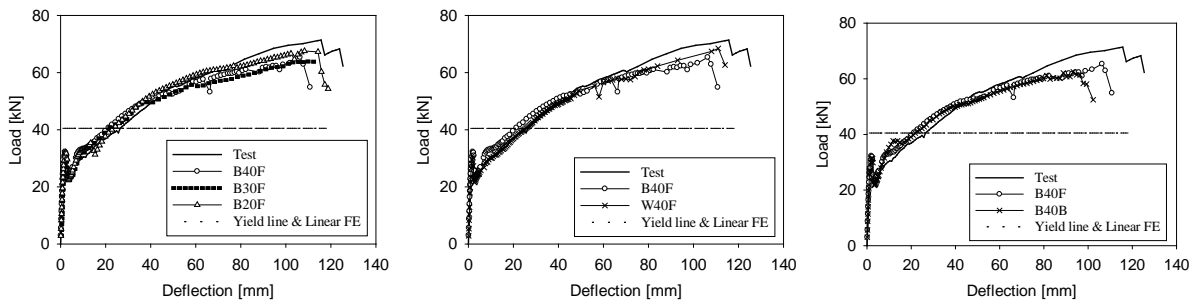


Fig. 3 Load-deflection curve with different mesh densities (left), element types (middle) and bond models (right)

Comparing the models with different modelling choices (Fig. 3), the models in B40F and B30F showed similar results, while the model in analysis B20F had a response closer to test because of the denser mesh. The analysis with wedge elements (W40F) gave better estimation of the load-deflection curve, but it was more difficult to achieve convergence than with brick elements. The analysis with bond-slip interaction (B40B) gave similar results but slightly less capacity and deflection at failure compared to fully bonded reinforcement.

Comparing the crack pattern of the FE analysis and experiment, see Fig. 4, crack localization became more visible for decreasing element size (Column C). Concerning element shape, the cracks tended to propagate along the mesh direction (Column D); as wedge elements gave more freedom in this sense, the crack pattern in the analysis with wedge elements therefore agreed best with the experimental response. The analysis including bond-slip showed more localized cracks, while the models with full interaction showed distributed cracks (Column E).

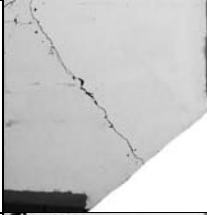
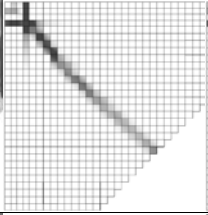
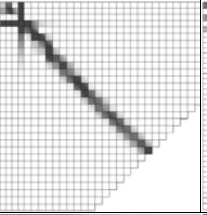
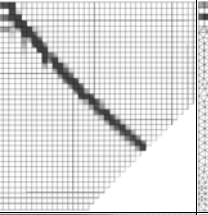
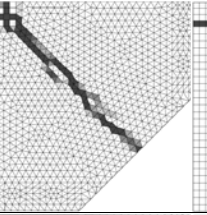
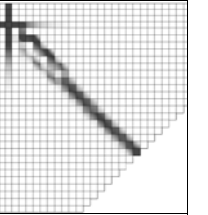
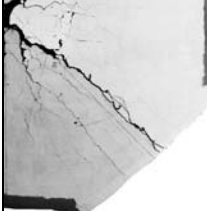
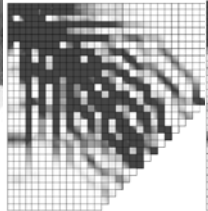
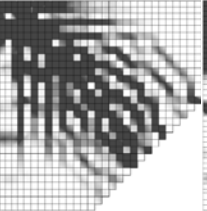

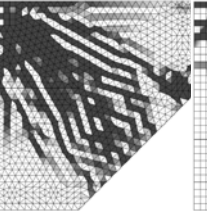
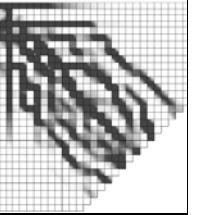
| | Column A | Column B | Column C | | | Column D | Column E |
|---------|---|---|---|--|---|---|---------------------|
| | Experimental | Reference | Element size | | | Element Type | Reinforcement Model |
| | | B40F | B30F | B20F | W40F | B40B | |
| @ 31 kN |  |  |  |  |  |  | |
| @ 63 kN |  |  |  |  |  |  | |

Fig. 4 Crack Pattern from experiment (column A); reference model (column B), and model with different element size (Column C), with different element types (Column D) and with different concrete-reinforcement interaction model (Column E) at initial crack state and ultimate state.

In the future, existing methodologies for the design and evaluation of bridge deck slabs are to be further developed, especially for structural assessment of existing bridge deck slabs using linear FE analysis and enhanced evaluation with nonlinear FE analysis. Recommendations for such analyses will be established and parameters for evaluation of safety will be developed.

ACKNOWLEDGMENT

The presented research was funded by the Swedish Transport Administration (Trafikverket) and the European Community's Seventh Framework Programme under grant agreement NMP2-LA-2009-228663 (TailorCrete). More information about the research project TailorCrete can be found at www.tailorcrete.com.

REFERENCES

- Fall, D., J. Shu, R. Rempling, K. Lundgren, and K. Zandi. 2014. "Two-Way Slabs: Experimental Investigation of Plastic Redistributions in Steel Fibre Reinforced Concrete." *Engineering Structures* (Submitted).
- Johansen, K.W. 1972. *Yield-Line Formulae for Slabs*. ISBN 0-721. London: Cement and Concrete Association.
- Pacoste, Costin, Mario Plos, and Morgan Johansson. 2012. *Recommendations for Finite Element Analysis for the Design of Reinforced Concrete Slabs*. ISSN 1103-. Stockholm: TRITA-BKN Rapport 114.
- Sundquist, H. 2011. "Robustare Brobanplatta - State-of-the-Art Och Förslag till FUD Program. Preliminär Rapport Utarbetad Av Konstruktionsgruppen Inom Sveriges Bygguniversitet På Uppdrag Av Trafikverket." Stockholm.

Statistical Investigation on the Ultimate Load Behaviour of RC Beams Subjected to Multiple Failure Modes



Mr. F. Sangiorgio
Division of Structural Engineering and Bridges
KTH Royal Institute of Technology
Brinellvägen 23,
SE - 10044 Stockholm
E-mail: filippo.sangiorgio@byv.kth.se



Prof. Dr. J. Silfwerbrand
Division of Structural Engineering and Bridges
KTH Royal Institute of Technology
Brinellvägen 23,
SE - 10044 Stockholm
E-mail: jsilfwer@kth.se



Prof. Dr. G. Mancini
Department of Structural, Geotechnical and Building
Engineering
Politecnico di Torino
Corso Duca degli Abruzzi, 24
IT - 10129 Torino
E-mail: giuseppe.mancini@polito.it

ABSTRACT

Geometric and mechanical properties influence the whole behaviour of RC structures and may increase the risk of a shear failure.

This paper presents a statistical investigation on the ultimate load behaviour of RC beams subjected to multiple failure modes. A full probabilistic resistance model based on both the Eurocode 2 and the JCSS Probabilistic Model Code is derived. Different beams are studied through nonlinear analysis via Monte Carlo simulations. A statistical evaluation of outcomes is performed.

Results show the prevalent failure modes relating to the different structural schemes and highlight the important role played by shear in structural safety evaluations.

Key words: Structural Design · Modelling · Reinforcements · Monte Carlo Simulations · Shear Failure

1. INTRODUCTION

Normal practice in engineering design is to use a linear elastic analysis for calculating the bending moment and shear force distributions in a structure. However, for RC structures this assumption is only reasonable at low levels of loading while it becomes increasingly invalid at higher loads due to cracking and the development of plastic deformations.

RC structures are brittle compared to steel structures, therefore it becomes important to deeply know their behaviour under design load conditions so as to prevent the formation of non-ductile failure mechanisms. The objective of this paper was to statistically investigate the ultimate load behaviour of RC beams having different geometrical configurations and subjected to diverse combinations of load actions resulting in flexural failure, shear failure, or combined flexural and shear failure. Results give information on the prevalent failure modes relating to the different structural schemes and show up the important role played by shear in structural safety evaluations, highlighting for which cases the stirrups yield before the flexural capacity of the structure is fully exhausted.

2. THE METHODOLOGY

Four sets of RC beams were properly designed on the basis of linear elastic analysis for serviceability and ultimate limit states according to the Eurocodes 2 and 8 for various ductility classes (Low DCL, Medium DCM, and High DCH). Concrete C25, steel S500, and exposure class X0 were assumed. The cross-section is constant over the length and has a rectangular shape with a width $b=0.30\text{m}$ (fixed for all beams) and a depth h defined depending on the specific needs. Beams were supposed to carry a typical domestic floor of 4m width total. Samples are consisted as follow: (A) a simply supported beam, $h=0.45\text{m}$, 5m in length, DCL; (B) a two equal spans continuous beam, $h=0.45\text{m}$, 5-5m in length, DCL/M/H; (C) a two unequal spans continuous beam, $h=0.60\text{m}$, 7.5-5m in length, DCL/M/H; and (D) a two unequal spans continuous beam, $h=0.75\text{m}$, 10-5m in length, DCL/M/H.

A full probabilistic model based on the JCSS Probabilistic Model Code, able to describe the mechanical properties of concrete and reinforcement steel, the reinforcement area, the geometrical properties of the cross-section, and the model uncertainty, was defined. Details are given in Table 1. For each simulation setting (designed beam), 10,000 samples were generated via the Monte Carlo method covering a wide range of mechanical and geometrical properties. The statistical population included a total of 250,000 numerical experiments.

The different beams were then analyzed up to complete loading and mechanical behaviour through material nonlinear analysis using the incremental-iterative approach and considering both bending and shear failure. A MATLAB routine based on the modified stiffness method was implemented (see, for instance, Valipour et al. 2010) and tested with ADINA. The Bernoulli-Navier beam theory was adopted. Bond slip between steel and concrete was neglected. Spurious sensitivity of results due to both load step and convergence criteria was reduced. The resistance model for both bending and shear is based on the Eurocode 2 assumptions. Tension stiffening effects were considered (Massicotte et al. 1990). The estimates were projected at 50 years from design. The statistical evaluation of the outcomes was finally performed.

Table 1 – Probabilistic model

| Basic Variable | Symbol | Distr. | Dim. | μ | σ | C.o.V. | Corr. coeff. ρ_{ij} | | |
|--|---------------------|--------|-----------------|------------------------|---------------------------|--------|--------------------------|------|------|
| In situ concrete compressive strength (50 years) | f_{c25} | LGN | MPa | 47.82 | 8.20 | 0.17 | | | |
| Concrete tensile strength | f_{ct} | LGN | MPa | 3.94 | 1.30 | 0.33 | | | |
| Bar area | A_s, A_s', A_{sw} | N | mm ² | nom. area | - | 0.02 | 1.00 | 0.50 | 0.35 |
| Steel yield stress | f_y, f_{yw} | N | MPa | 560.00 | 30.00 | - | 0.50 | 1.00 | 0.85 |
| Steel ultimate strength | f_u | N | MPa | $1.15 \cdot f_{y,nom}$ | 40.00 | - | 0.35 | 0.85 | 1.00 |
| Dimensions of cross-section | h, b | N | mm | $0.003 \cdot X_{nom}$ | $4 + 0.006 \cdot X_{nom}$ | - | | | |
| Concrete cover to top steel | c_s | LGN | mm | $X_{nom} + 10$ | 10.00 | - | | | |
| Effective depth of cross-section | d | N | mm | $X_{nom} + 10$ | 10.00 | - | | | |
| Uncertainty of resistance for bending moment | $\theta_{R,B}$ | LGN | - | 1.20 | - | 0.15 | | | |
| Uncertainty of resistance for shear | $\theta_{R,S}$ | LGN | - | 1.00 | - | 0.10 | | | |

3. RESULTS AND DISCUSSION

The results of the statistical investigations are shown in Table 2. For each sets of RC beams, the following data are given: (1) the structural scheme, the load configurations, the ductility class, and the design notation; (2) the statistical percentage of the different failure mode occurrences; (3) the design load values; and (4) the statistical properties of the structural resistance factor, λ , expressed as the ratio between the ultimate load and the design load.

From the numerical experiments, we notice that the ultimate load behaviour of a RC structure designed according to the Eurocodes 2 and 8 is not all the same for different structural schemes, load configurations and ductility class, some of which lead to a preferential failure mode, and it demonstrates the importance of the properly inclusion of the shear resistance in the design process. As one can easily ascertain from the chart, the prevalent failure mode of a simply supported beam is bending (the flexural capacity is fully exhausted in more than 95% of cases) while it is enough to just consider a two equal span continuous beam to see a sudden change in the structural behaviour marked by (i) an abrupt passage to a shear prevalent failure mode (non-ductile failure), almost regardless of the ductility class for which the structure was designed, (ii) a significant decrease of the λ mean value followed by (iii) a slight increase of its scatter. The shift becomes more pronounced for more unsymmetric structures.

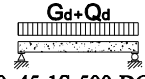
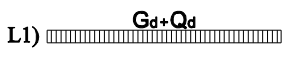


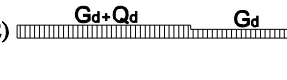
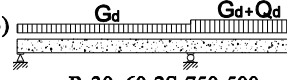
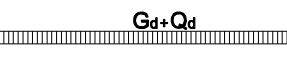


4. CONCLUDING REMARKS

In summary, the ultimate load behaviour of RC beams designed according to the Eurocodes 2 and 8, and subjected to the combination of bending moment and shear force failure mode, has been shown to vary significantly depending upon a variety of factors (design requirements, geometrical configuration, mechanical properties of materials, and load combination). Results highlight that the European design specifications are not always successful in preventing the formation of non-ductile failure mechanisms before the flexural capacity of a structure is fully exhausted.

More details about the probabilistic model and the nonlinear analysis as well as more case studies will be published in forthcoming publications.

Finally, it is pointed out that the designs of the test beams are provided to interested researchers by contacting the first author of the paper.

Table 2 – Results

| Exp. Set | Structural Scheme and Description | Failure Mode | | Design Load [kN] | | λ [-] | | | | | | | | | |
|--|--|------------------|-------|------------------|----------------|---------------|----------|------|----|----|----|-----|------|------|------|
| | | Bending | Shear | G _d | Q _d | μ | σ | | | | | | | | |
| | | Total Percentage | | | | | | | | | | | | | |
| | | 0 | 10 | 20 | 30 | 40 | 50 | 60 | 70 | 80 | 90 | 100 | | | |
| A |  R-30x45-1S-500-DCL-L1 | | | | 31.4 | 12.0 | 1.74 | 0.17 | | | | | | | |
| B |  L1) R-30x45-2S-500-500 | -DCL | | | | | | | | | | | 1.49 | 0.19 | |
| | | -DCM | | | | | | | | | | | | 1.56 | 0.21 |
| | | -DCH | | | | | | | | | | | | 1.72 | 0.23 |
| |  L2) R-30x45-2S-500-500 | -DCL | | | | | | | | | | | | 1.54 | 0.19 |
| | | -DCM | | | | | | | | | | | | 1.61 | 0.20 |
| | | -DCH | | | | | | | | | | | | 1.77 | 0.21 |
| C |  L1) R-30x60-2S-750-500 | -DCL | | | | | | | | | | | 1.34 | 0.17 | |
| | | -DCM | | | | | | | | | | | | 1.37 | 0.17 |
| | | -DCH | | | | | | | | | | | | 1.50 | 0.19 |
| |  L2) R-30x60-2S-750-500 | -DCL | | | | | | | | | | | | 1.43 | 0.17 |
| | | -DCM | | | | | | | | | | | | 1.44 | 0.18 |
| | | -DCH | | | | | | | | | | | | 1.54 | 0.18 |
|  L3) R-30x60-2S-750-500 | -DCL | | | | | | | | | | | | 1.45 | 0.18 | |
| | -DCM | | | | | | | | | | | | 1.51 | 0.19 | |
| | -DCH | | | | | | | | | | | | 1.65 | 0.21 | |
| D |  L1) R-30x75-2S-1000-500 | -DCL | | | | | | | | | | | 1.37 | 0.17 | |
| | | -DCM | | | | | | | | | | | | 1.33 | 0.16 |
| | | -DCH | | | | | | | | | | | | 1.41 | 0.17 |
| |  L2) R-30x75-2S-1000-500 | -DCL | | | | | | | | | | | | 1.38 | 0.17 |
| | | -DCM | | | | | | | | | | | | 1.34 | 0.16 |
| | | -DCH | | | | | | | | | | | | 1.42 | 0.17 |
|  L3) R-30x75-2S-1000-500 | -DCL | | | | | | | | | | | | 1.64 | 0.20 | |
| | -DCM | | | | | | | | | | | | 1.68 | 0.21 | |
| | -DCH | | | | | | | | | | | | 1.89 | 0.23 | |

REFERENCES

EN 1992-1-1 (Eurocode 2)

“Design of concrete structures. Part 1-1: general rules and rules for buildings” European Standard, december 2004

EN 1998-1 (Eurocode 8)

“Design of structures for earthquake resistance” European Standard, 1998

Joint Committee on Structural Safety, 2000

“Probabilistic Model Code”, JCSS-OSTL/DIA/VROU-10-11-2000

Massicotte, B., Elwi, A.E., MacGregor, J.G., 1990

“Tension-Stiffening Model for Planar Reinforced Concrete Members”, ASCE J. Struct. Eng., Vol. 116, No. 11, 1990, pp. 3039-3058

Valipour, H.R., Foster, S.J., 2010

“A total secant flexibility-based formulation for frame elements with physical and geometrical nonlinearities”, Finite Elem Anal Des, Vol. 46, 2010, pp. 288-297

Analysis of buried reinforced concrete pipelines subjected to seismic waves



Doctoral student. MSc. Roghayeh Abbasiverki
KTH Royal Institute of Technology, Concrete Structures,
SE - 100 44 Stockholm
E-mail: roghayeh.abbasiverki@byv.kth.se



Prof. Dr. Anders Ansell
KTH Royal Institute of Technology, Concrete Structures,
SE - 100 44 Stockholm
E-mail: anders.ansell@byv.kth.se

ABSTRACT

Buried reinforced concrete pipelines are widely used in e.g. water and wastewater systems. Failure of these infrastructures can result in drastic effects and recently they have been put in focus as vital components in safety systems for nuclear power installations. The high level of safety has here lead to a demand for reliable earthquake risk analyses. In this paper, methods are compared and the use of seismic design loads demonstrated. FE analysis in 2D of soil-pipe interaction under seismic wave propagation is performed. The performance of concrete pipes subjected to seismic waves with different frequency content is evaluated with respect to burial depth.

Key words: Modelling, Nuclear, Reinforcement, Structural Design.

1. INTRODUCTION

Buried pipelines are linear structures often used to transport essential liquid materials and gas in order to support human life. The importance of this type of infrastructure systems have been set in focus during the last years as they are vital components in the safety system for nuclear power installations. The high level of safety has led to a demand for reliable seismic analyses, also of structures built in areas that traditionally have not been considered as highly seismically active. During propagation of seismic waves in soil the components that propagate along the pipeline axis induce alternate axial compression and tension which cause axial deformations and the components of the waves that propagate in a direction perpendicular to the longitudinal axis cause bending deformations (Owen and Scholl, 1981). The induced damages largely depend on material and joints of the pipelines (Lanzano et al., 2012). Therefore, they divide into two categories in terms of damage patterns; continuous (ductile) pipes and segmented (brittle) pipes. Empirical data from earthquake loads on pipelines indicates that the damage induced by wave propagation for brittle pipelines is more severe than for ductile pipelines which only show 30% of the vulnerability compared to the latter (FEMA, 1999). Continuous and segmented pipelines have different failure modes. Continuous pipelines often fail due to tensile rupture, local buckling (wrinkling) of the pipe wall due to axial compression and flexural failure and beam buckling (global buckling). The failure modes of segmented pipelines, especially of those with

large diameters and thick walls, are tensile failure (axial pull-out), compression failure (crushing of joints), and circumferential flexure and joint rotation (O'Rourke and Liu, 1999). Reinforced concrete pipes (bell and spigot joints) and steel pipes (arc-welded joints) are widely used in buried water pipeline networks. The former is considered as segmented (brittle) pipes and the latter are classified as continuous (ductile) pipes. Reinforced concrete is when compared to steel an economical and durable material, widely used in water and wastewater networks. On the other hand, as abovementioned, their vulnerability during ground shaking is higher than for steel pipes. Therefore, in a first part of this project a 2D plain strain finite element model is implemented to study the behaviour of transverse sections of reinforced concrete pipes subjected to seismic waves with different frequency content.

2. EARTHQUAKE LOADS

The input ground motions employed in the following time-history analysis are artificial accelerograms corresponding to the Swedish hard rock response spectra (SKI), the Eurocode 8 response spectrum for ground type A (extracted by Seismomatch software) and accelerograms recorded at Pacoima Dam station (average shear wave velocity equal to 2016.10 m/s) during the 1994 Northridge earthquake and at LAMONT 1060 station (average shear wave velocity equal to 782 m/s) from the 1999 Duzce earthquake (PEER database). Vertical and horizontal ground acceleration time histories are applied at the base of the soil-pipe models by assuming that the soil rests on the bedrock. Figure 1 illustrates an example of applied acceleration-time history.

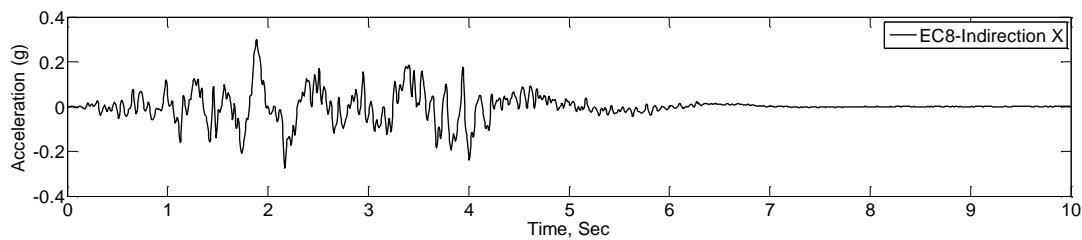


Figure 1- Acceleration-time history corresponding to Eurocode 8 response spectrum

Spectrum intensity is the area under the pseudo velocity response spectrum (S_v) within the period range 0.1- 2.5 sec and can be computed for any structural damping ratio (ξ). It indicates the earthquake severity and captures amplitude and frequency content in the range of interest for structures (Housner, 1952). This parameter is in displacement dimension, if divided by 2.4 sec as in Eq. (1) it takes a value similar to the maximum velocity of ground motion which is suitable for illustration of the induced damage on buried pipelines during wave propagation. In Japan, a device called SI sensor for gas supply network has been designed. To avoid secondary disasters caused by gas leaks, monitored SI values that exceed 30 to 40 cm/sec stops the gas supply automatically (Nakayama et.al, 2004). Table 1 shows the used ground motion parameters.

$$SI = \frac{1}{2.4} \int_{0.1}^{2.5} S_v(T, \xi) dT \quad (1)$$

Table 1 – Ground motion parameters.

| Location | Peak ground acceleration (g) | | Velocity spectrum intensity ($\xi = 5\%$) (cm/sec) |
|------------|------------------------------|----------|---|
| | Transverse | Vertical | |
| Sweden | 0.1462 | 0.0929 | 2.42 |
| Eurocode8 | 0.3 | 0.35 | 38.987 |
| Duzce | 0.05 | 0.022 | 6.76 |
| Northridge | 1.58 | 1.23 | 73.14 |

3. BURIED PIPE SYSTEMS

Typical reinforced concrete pipe (bell and spigot joint) with 1200 mm nominal diameter and 135 mm thickness which commonly is used in water and wastewater networks of Sweden is selected for the study. Material qualities C45/55 and B500B are assigned for concrete and steel reinforcement, respectively. The pipe is surrounded by frictional soil with 250 m/s shear wave velocity, 1800 kg/m³ density and a friction angle equal to 38 degrees.

4. NUMERICAL EXAMPLES

Seismic finite element modelling of buried concrete pipes has been performed using the ABAQUS/Standard finite element program. The simulation is done in a two dimensional plane strain system. The simulated soil volume was considered to be rectangular with 150 m width and 25 m depth. To investigate the effect of burial depth, i.e. the distance between ground surface and center of pipe, two different depths are considered; shallow and deep pipes with 1 m and 9 m burial depth, respectively. The finite element meshes consist of 4-node bilinear plane strain quadrilateral (CPE4R) and 3-node quadratic 2D truss (T2D3) elements. In order to prevent reflection of seismic waves at lateral boundaries of the model through the soil medium, and to represent elastic continuity of the lateral soil, infinite elements (CINPE4) are implemented. A surface to surface discretization method (master-slave contact) is assigned to represent tangential and normal contact behavior of the soil-pipe interaction. Material damping is another important parameter attenuating the internal energy generated from seismic loading, introduced in the model for two frequencies corresponding to when 5% and 80% of the cumulative effective mass is active. From frequency analysis the lower frequency was 2.3429 Hz and 4.9977 Hz for the higher frequency. The Rayleigh damping coefficients for modal damping ratio equal to 5% was calculated ($\alpha = 0.86064$ and $\beta = 0.0018618$). The analyses have been performed in two steps; with static analysis under gravity load and then a time history analysis. Figure 2 shows an example of induced stress in a RC pipe section. Since seismic response of structures is dependent on interaction between structure and input ground motion characteristics, the seismic spectrum intensity is selected to describe the effect of seismic waves on maximum response of RC pipelines, see Figure 3.

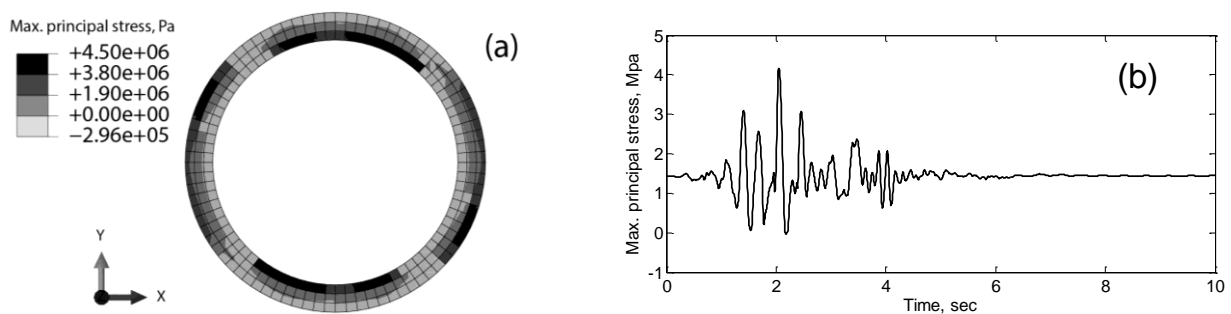


Figure 2: Seismic response of deep buried RC pipe subjected to EC8 artificial synthetic time histories. Maximum stress induced in pipe section (a), Time history response for element at crown of pipe (b).

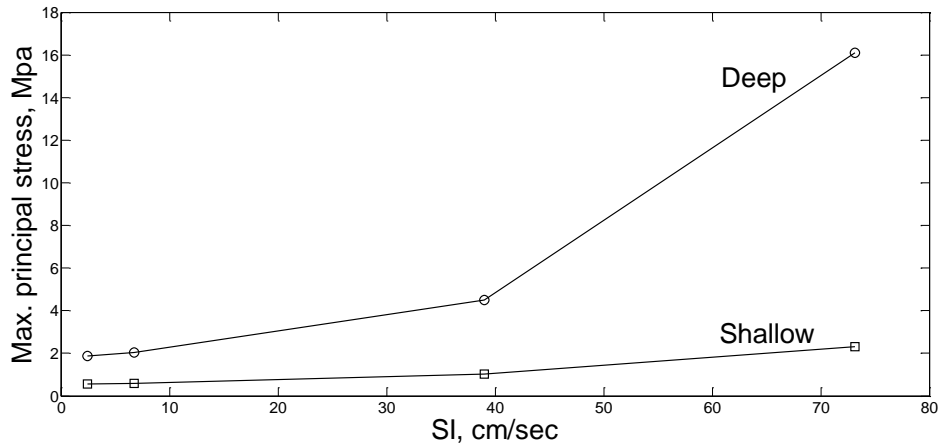


Figure 3: Maximum response of RC pipes subjected to different seismic wave intensity.

5. CONCLUSION

Seismic response intensity (SI) is a relevant ground motion parameter to illustrate the severity of earthquake on buried pipelines systems. With increased earthquake intensity the RC pipe will experience higher stress. This becomes significant when the seismic spectrum intensity exceeds 40 cm/sec. As shown in Figure 3 deep buried pipes will experience higher stress than shallow pipes. The distribution of maximum stress along the thickness of the pipes indicates an oval deformation of transverse cross section. The further work of this research will focus on the effects from wave propagation on longitudinal cross sections of RC pipes and the joints.

REFERENCES

- Owen, G.N. and Scholl, R.E., 1981,
 “Earthquake engineering of large underground structures”, Report no. FHWA/RD-80/195, Federal Highway Administration and National Science Foundation, Washington, D.C, USA.
- Lanzano, G., Salzano, E., Santucci De Magistris, F., Fabbrocino, G., 2012,
 “An observational analysis of seismic vulnerability of industrial pipelines”, Chemical Engineering Transaction, 26, 567-572.
- FEMA: HAZUS-MH MR4, 2003,
 “Multi-hazard loss estimation methodology, earthquake model”, Technical Manual, National Institute of Building Science, Washington, D.C.
- O’Rourke M.J., and Liu X., 1999,
 “Response of buried pipelines subjected to earthquake effects”, MCEER Monograph No.3, University of New York, Buffalo, USA.
- Swedish Nuclear Power Inspectorate (SKI), 1992,
 Seismic safety – Characterization of seismic ground motions for probabilistic safety analyses of nuclear facilities in Sweden.
- Seismosoft, 2014,
<http://www.seismosoft.com/en/SeismoMatch.aspx>
- Pacific Earthquake Engineering Research Center (PEER), 2014,
<http://peer.berkeley.edu/>
- Housner, G.W., 1952,
 “Intensity of ground motion during strong earthquakes”, ONR Report, 1-60.
- Nakayama, W., Shimizu, Y., Koganemaru, K., 2004,
 “Development of super dense real-time disaster mitigation system for urban gas supply network”, Journal of Japan Association for Earthquake Engineering, Special Issue, 124-127.

Finite element analyses of an arch dam subjected to seismic loads and hydrodynamic forces



Researcher, Dr. Richard Malm
KTH Royal Institute of Technology, Concrete Structures
SE - 100 44 Stockholm
E-mail: richard.malm@byv.kth.se



Doctoral student, M.Sc. Tobias Gasch
KTH Royal Institute of Technology, Concrete Structures
SE - 100 44 Stockholm
E-mail: tobias.gasch@byv.kth.se

ABSTRACT

A concrete arch dam subjected to seismic ground accelerations has been analysed using the finite element method. The response of the concrete structure is calculated through dynamic implicit analyses using two different modelling approaches, the Westergaard added mass approach with hydrodynamic inertia forces from a finite water volume and a model based on acoustic elements. The models show high tensile stresses near the base of the dam which indicate a risk for cracking. The study demonstrate that the choice of damping, the type of seismic excitation and use of quiet boundaries have a significant influence on the result.

Key words: Modelling, Structural Design

1. INTRODUCTION

Nowadays, the most common method for performing seismic evaluation of large concrete dam structures is to use the finite element method (FEM). When performing such an evaluation, one of the most important aspects of the analysis is how to account for the dynamic properties of the water reservoir. Other important properties, as in all seismic analyses, are how to define the boundaries of the unbounded computational domain and how to define the material damping. To increase the knowledge of such properties related to seismic evaluation of dams, the International Commission of Large Dams (ICOLD) arranged a benchmark workshop on the subject, see (ICOLD, 2013). The ICOLD benchmark workshops are devoted to bridge the gap between numerical analyses, the interpretation of results and their theoretical as well as practical relevance. In this study, two methods with different levels of complexity are used to account for the dynamic properties of the water reservoir. Furthermore, the influence from reflecting versus non-reflecting boundaries of the computational domain on the response of the dam is evaluated.

2. FINITE ELEMENT MODELS

A concrete arch dam, 220 m high and 430 m wide at the crest and 80 m at the base, has been analysed using the finite element software Abaqus. The dam is subjected to seismic ground accelerations applied to the surrounding rock mass and also hydrodynamic forces from the water

reservoir. The geometry of the dam as well as the material properties and loading conditions are given in the definition of the benchmark (ICOLD, 2013). The finite element model used in this study is shown in Figure 1a) and time histories of the seismic ground acceleration are shown in Figure 1b). For a complete description of the model used, see (Malm et. al., 2013).

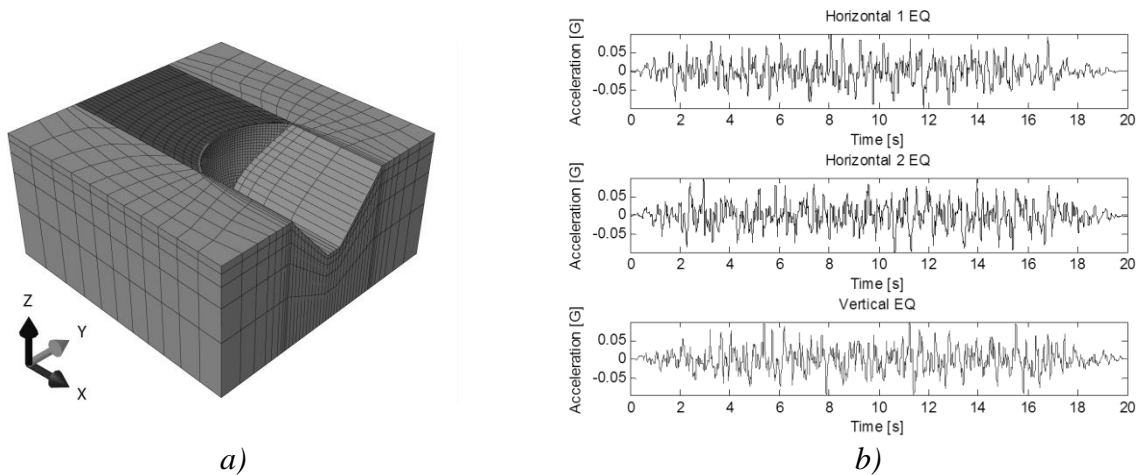


Figure 1 –Finite element model (a) and seismic ground accelerations (b).

The response of the concrete arch dam is analysed in the time domain through dynamic implicit analyses, including a comparison between two different modelling approaches and as a reference a model without water. The first is based on the Westergaard added mass approach (Westergaard, 1933). This simplified model assumes that hydrodynamic forces on the upstream face of the dam are equivalent to the inertia forces from a finite volume of water attached to the dam during the vibration. It thus uses discrete masses attached to the upstream face of the dam to describe the water reservoir in a finite element context. The second approach uses acoustic theory to describe wave propagation in the water reservoir, see e.g. Reynolds (1981). In the context of finite elements, the water reservoir is described as a continuum and discretized with continuum elements with the fluid velocity as the independent variable. The second model also includes quiet boundaries based on the theories of Lysmer and Kuhlemeyer (1969) to account for non-reflecting boundaries, both at the end of the water reservoir and at the boundaries of the rock mass. All models in this study use a Rayleigh material damping. The damping ratio for the concrete dam has been taken equal to 4 % according to US NRC Regulatory Guide 1.61. The damping of the water is usually assumed to be 0.5 %, but has been judged to be negligible and is not included in the analyses. The average Rayleigh damping in the frequency interval 1.27 – 9.76 Hz is 3.6 %, i.e. slightly lower than the target value of 4 % and thereby conservative. The frequency interval has been defined to cover the range between 5 % - 80% of the cumulative effective mass.

3. RESULTS

A selection of the results from this study is presented in the following, additional results are given in Malm et. al. (2013). The acoustic model gives frequencies that are in-between the case without water and the case with Westergaard added mass. These two models can be seen as conservative limits for the maximum and minimum frequencies for each mode and the frequencies obtained with the acoustic elements are the most accurate. The first frequency mode of the acoustic model at 1.51 Hz is shown in Figure 2a). It should be noted that the added mass model and model without water has a first frequency of 1.37 Hz and 2.0 Hz, respectively. A comparison of the response of the arch dam, where the variation of hoop stresses over the height of the mid-section of the dam, is shown in Figure 2b) for the two models that account for the

water reservoir. The stresses are shown on the downstream face of the dam and as the max and min envelope over the time history. As seen in the figure there are quite similar results from the simplified Westergaard added mass method and the more advanced method with acoustic and quiet boundaries. Summarising the additional results from Malm et. al. (2013) it can be noticed that the min principal and hoop stresses generally shows better resemblance between the two models than the max principal and vertical stresses.

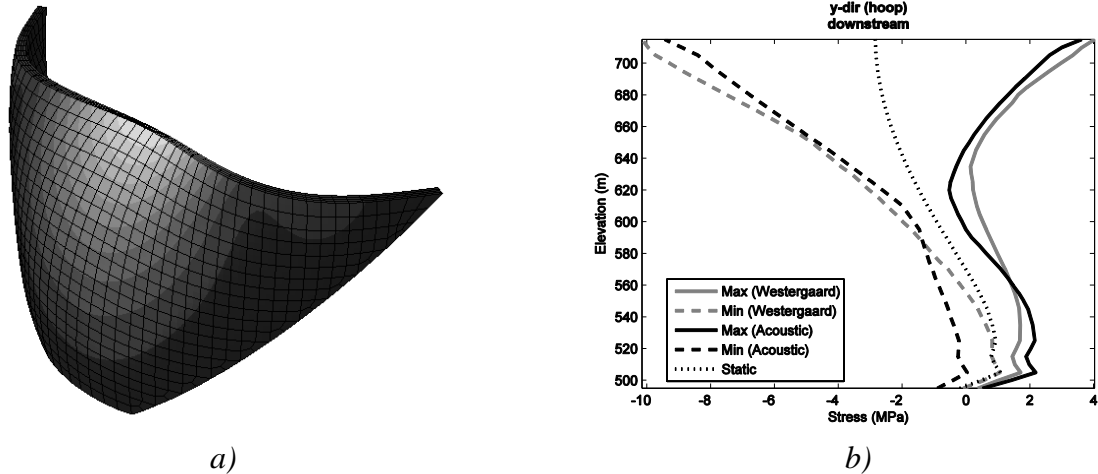


Figure 2 –First frequency of the concrete dam (a) and envelope of hoop stresses at the mid-section of the dam (b).

In order to further illustrate the difference between the more advanced model with acoustic elements and quiet boundaries and the simplified model based on Westergaard added mass approach, the relative displacement in the radial direction for the centre section is shown in Figure 3a). It can be observed that significantly higher deflections are obtained for the model with acoustic elements compared to the simplified model based on the Westergaard added mass approach.

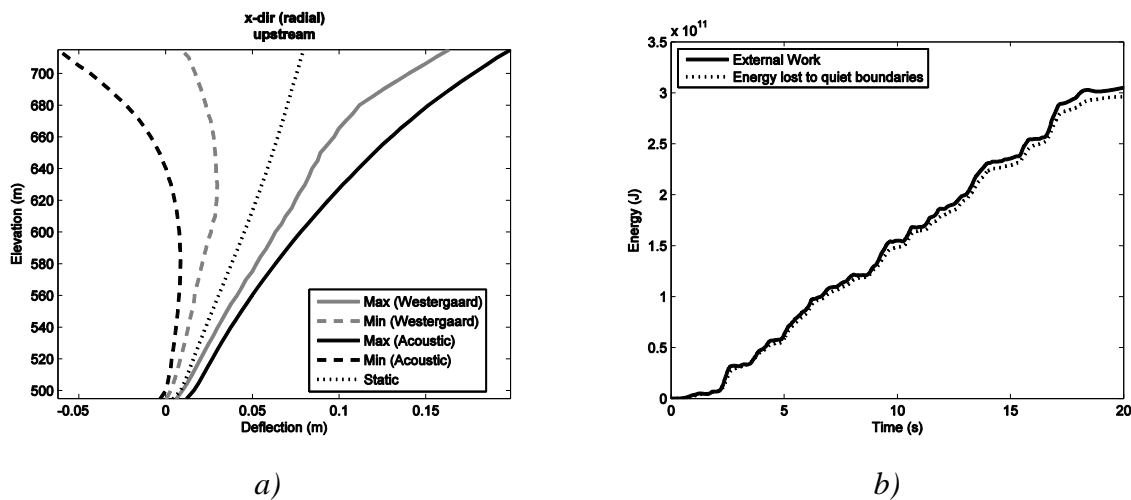


Figure 3 –Radial displacement of the centre section (a) and energy dissipated at quiet boundaries compared to the external work (b).

To emphasise the importance of using quiet boundaries in this type of analysis the total external work for the whole model compared to the energy that is lost to the quiet boundaries is shown in Figure 3b). As seen, almost all energy is lost to the quiet boundaries.

4. CONCLUSIONS

A concrete arch dam have been analysed during seismic loading with a model based on acoustic elements to describe the water and quiet boundaries to prevent wave reflection. The results from this model have also been compared to a simplified model based on Westergaards added mass approach. For global response of the concrete dam the two modelling approaches give similar results. Both models show high tensile stresses near the base of the arch dam that would indicate a risk for cracks. Generally, the Westergaard added mass gives higher tensile stresses than the acoustic model, while it often underestimates the compressive stresses. However, any general conclusions cannot be drawn from this study, whether the simplified Westergaard added mass approach is more or less conservative than the more advanced method.

Apart from the effects of the water reservoir, the performed analyses in this study, and also from other participants in the ICOLD benchmark workshop, have shown that there are several factors which are usually assumed that have a significant influence on the results, these include

- Rayleigh damping – the choice of damping ratio for the different materials and especially the choice of corresponding frequencies when defining Rayleigh damping has a large influence on the results.
- Seismic excitation – in these analyses, only the bottom of the foundation is subjected to the prescribed seismic excitation. Effects such as seismic wave incoherence have not been considered.
- Non-reflecting boundaries – in the analyses quiet boundaries have been defined for both the rock mass and the reservoir.

ACKNOWLEDGEMENT

The research presented was carried out as a part of "Swedish Hydropower Centre - SVC". SVC has been established by the Swedish Energy Agency, Elforsk and Svenska Kraftnät together with Luleå University of Technology, KTH Royal Institute of Technology, Chalmers University of Technology and Uppsala University. www.svc.nu.

REFERENCES

- ICOLD, 2013,
 “12th International benchmark workshop on numerical analysis of dams. Theme A – Fluid structure interaction. Arch dam – reservoir at seismic loading”, Graz University of Technology, Austria.
- Lysmer, J., Kuhlemeyer, R. L., 1969,
 “Finite dynamic model for infinite media,” *Journal of the Engineering Mechanics, Division of the ASCE*, 95, 859–877.
- Malm, R., Pi Rito, C., Hassanzadeh, M., Rydell, C., Gasch, T., 2013,
 “Concrete arch dam at seismic loading with fluid structure interaction”, *Proceedings, ICOLD 12th International benchmark workshop on numerical analysis of dams*, Graz, Austria.
- Reynolds, D. D., 1981,
 “Engineering principles of acoustics: noise and vibration Control”, Allyn and Bacon.
- US NRC Regulatory Guide 1.61,
 “Damping values for seismic design of nuclear power plants”, U.S. Nuclear Regulatory Commission, 2007.
- Westergaard, H. M., 1933,
 “Water pressures on dams During Earthquakes”. *Transactions, American Society of Civil Engineers*, 98.

Water Absorption in Concrete – Experiments and Modelling



Tekn Lic, Niklas Johansson
 PhD-student
 Cementa AB
 P.O. Box 104, S-624 22 Slite
 Div. Structural and Construction Engineering
 Luleå University of Technology
 S-971 87 Luleå
 E-mail: niklas.johansson@cementa.se / niklas.johansson@ltu.se



Dr. Peter Johansson
 Div. Building Materials, Lund Institute of Technology
 PO Box 118
 SE 221 00 Lund
 E-mail: peter.johansson@byggtek.lth.se

ABSTRACT

Water absorption in concrete can delay the drying process implying costly actions for faster drying like heating the concrete. Sources of the water are normally precipitation during construction and water leakages in the finished building. In tests, fresh and matured concrete with different w/c ratios have been exposed to water loads with different durations up to 7 days. A theoretical absorption model has been compared with experimental data and it is shown that the water load has a little impact on the RH for concretes with w/c ratio $< 0,45$.

Key words: Drying, concrete, water absorption, moisture

1. INTRODUCTION

High moisture levels in concrete floors may cause degradation of organic materials in contact with the concrete. One example is chemical decomposition of adhesive underneath PVC-flooring leading to chemical emissions of the indoor air. High moisture level may be caused by water absorption due to precipitation during construction and water leakages in the finished building. It is clear that this water absorption delays the drying process at hardening i. e. the normal drying process is restarted.

Drying of concrete is a combination of self-desiccation and moisture transport. Moisture transport, i. e. the only way to get rid of the late absorbed water, is however a very slow process. It can be accelerated by increasing the concrete temperature or by decreasing the water vapour content in the air. Evidently, both these actions consume a lot of energy i. e. they are costly and have a negative effect on the environment.

It is known that the available tools to calculate concrete drying process do not treat water absorption properly. It is thus important to find relevant model to incorporate the water absorption. The research presented in the paper is one attempt to establish a base for development of such a model.

2. EXPERIMENTS

2.1 Water absorption in fresh concrete

Concrete with five water cement ratios between 0,35 and 0,70 were tested at four water load durations (1, 2, 4 and 7 days). The concrete specimens were 120 mm high and the relative humidity was measured with Vaisala probes at 15 mm and 48 mm depth from the concrete surface. The water was added on the concrete surface approximately 3 hours after casting and after that, specimens were stored at +5°C and 80% RH for 28 days and thereafter at +20°C and 60% RH. For each w/c ratio, a specimen without water load was tested as a reference.

2.2 Water absorption in matured concrete

After 6 months, the same specimens above were placed under water with four water load durations (3, 7, 14, 28 days). Water absorption was monitored by weight documentations and RH was measured similarly to above.

3. MODELLING

3.1 General

Water absorption in porous materials is often described by a capillary suction model where a water front reaches a certain depth in the material. This approach is not valid for concrete according to the experiments presented by Johansson /2005/, whose results showed that the water load leads to a RH increase but not often up to 100 % RH i. e. the water absorption will be calculated as a moisture transport process i. e. not a moving water front.

3.2 Calculations

The moisture flow calculations were performed by the simulation tool, JAM, which is based on the fundamental flow potential, ψ [kg/m•s] /Arfvidsson 1989/. Calculations of the moisture levels were performed as transient water absorption simulations using the one-dimensional version of the simulation tool.

The input options in terms of material data comprised five alternatives, only one of which used a combination of moisture diffusivities and sorption isotherms. Since both the sorption isotherms and moisture diffusivities were known for the materials studied, this alternative was chosen. For the simulations, the specimens were divided into fourteen cells and the results were provided as the mean value of the moisture content for each cell.

3.3 Input data

When calculating moisture transport due to water absorption, the following input parameters should be taken into account:

- **Duration of water:** the time period of water absorption
- **Initial moisture conditions:** RH profile in the concrete when water absorption starts
- **Concrete properties:** water cement ratio, cement type and cement content
- **Degree of hydration:** cement hydration as a function of time and w/c
- **Chemically bound water:** a function of hydration degree and cement content
- **Moisture transport coefficient:** a function of w/c, hydration degree and RH
- **Sorption isotherms:** desorption- and scanning curves as a function of degree of hydration and w/c

4. RESULTS

The experiments show that exposure to water on fresh concrete with a water cement ratio $\leq 0,40$ does not have any significant influence on the drying time, see Figure 1, see also /Johansson

2005/. However, for concrete with $w/c \geq 0,45$, early water exposure has a negative effect on the drying, an effect that increases with increased w/c -ratio and duration of the water exposure. Furthermore, it is observed in the tests that the water absorption in mature concrete decrease with a lower w/c ratio, see Figure 2. The duration of the water has small influence the total amount of absorbed water.

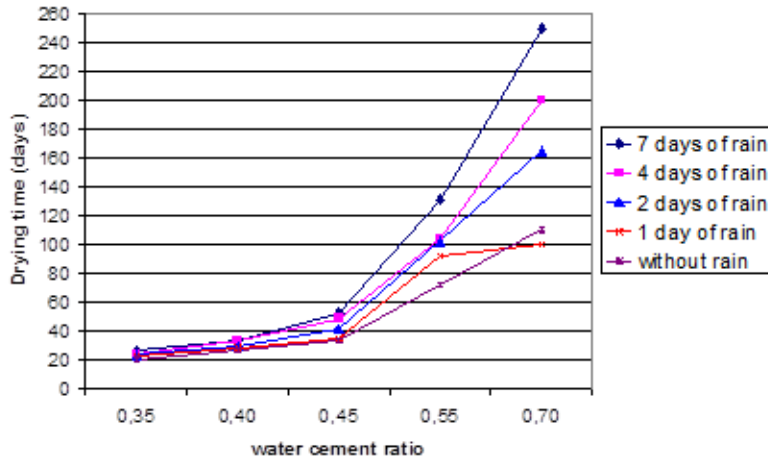


Figure 1 - Drying times to reach 85% RH and the influence of different rain exposure /Johansson 2005/.

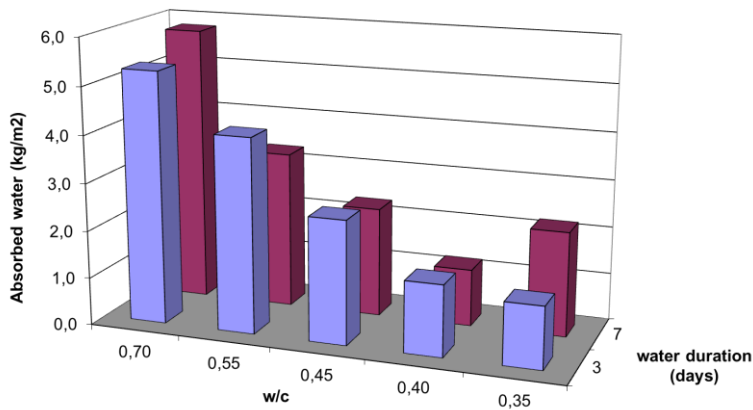


Figure 2 - Water absorption in mature concrete /Johansson 2005/.

The calculations show that it's possible to use moisture transport models to describe the water absorption in mature concrete, see Figure 3.

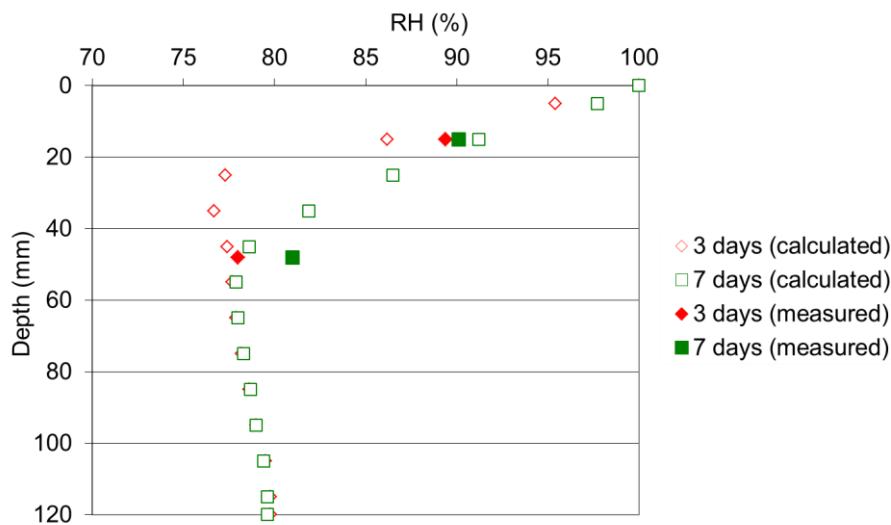


Figure 3 - Calculated and measured RH in mature concrete at w/c 0,40 /Johansson & Nilsson 2006/.

Water absorption calculations have also been performed on fresh concrete. The comparisons with measured data shows that the correlation is not as good as for mature concrete. A reason is that it is more complicated to determine the absorption since self desiccation is present and the degree of hydration is increasing rapidly. Comparisons with measured results show that the moisture transport coefficient must be multiplied by 2,5-10 at high RH for w/c > 0,50. Concrete

5. CONCLUSIONS

Water absorption in mature concrete can be calculated as a moisture transport process. For fresh concrete more input data regarding rate of hydration and sorption isotherms must be determined to make reliable calculations.

REFERENCES

Arfvidsson, J., 1989

”Moisture transport in porous media: Modelling based on Kirchhoff potentials”, Report TVBH-1010, Division of Building Physics, Lund Institute of Technology.

Johansson, N., 2005

”Drying of concrete – Effect of cement type, concrete quality and outer moisture conditions”, Div. of Building Materials, Lund Inst. of Technology. Report TVBM-3124, 164 pp. (In Swedish)

Johansson, P., & Nilsson, L-O., 2006

”Vatteninsugning i betong – Laboratorieundersökningar, fältmätningar, beräkningar och modeller”, Div. of Building Materials, Lund Inst. of Technology. Report TVBM-3134, 106 pp. (In Swedish)

NUCLEAR, HYDRAULICS & AGGRESSIVE ENVIRONMENTS

Modelling of the chemo-mechanical behaviour of a composite made of ion exchange resins incorporated into a cement-based matrix



M. Neji
CEA, DEN, DPC, SECR,
Laboratoire d'Etude du
Comportement des Bétons et des
Argiles, F-91191 Gif-sur-Yvette,
France.
mejdi.neji@cea.fr

B. Bary
CEA, DEN, DPC, SECR,
Laboratoire d'Etude du
Comportement des Bétons et des
Argiles,
F-91191 Gif-sur-Yvette,
France

N. Burlion
Polytech Lille –
LML UMR 8107 Villeneuve
d'Ascq, France

P. Le Bescop
CEA, DEN, DPC, SECR,
Laboratoire d'Etude du
Comportement des Bétons et des
Argiles,
F-91191 Gif-sur-Yvette,
France

ABSTRACT

This study focuses on the analysis of a composite material made up of ion exchange resins (IER) used in nuclear applications solidified into a cement paste matrix. Because of ion exchange processes, the volume change of the IER may cause internal pressures leading to a degradation of the waste packages. A predictive multi-scale modelling has been developed to determine the chemo-mechanical behaviour of such material. It is based on thermodynamic equilibriums to determine the IER internal pressures, and on analytical homogenization techniques to estimate both mechanical and coupling parameters. The model and the experimental data obtained during the project allow understanding the swelling mechanisms and predicting the macroscopic behaviour of the material.

Key Words: Cement paste, Ion exchange resins, Modelling, Chemo-mechanical coupling, Homogenization, Nuclear applications

1. INTRODUCTION

The ion exchange resin is one of the existing ways to depollute a fluid from an undesirable ionic species. This material realizes an ion exchange with the effluent to trap the polluted ionic part of the fluid into its structure. During this ionic exchange process, the IER tends to swell or shrink due to the thermodynamic equilibrium between the IER and the surrounding environment. Once the IER are solidified into the cement matrix, the same process would occur with the cement interstitial solution. Because of the confinement of the resins, their volume change may result in a mechanical degradation of the package (Matsuda et al 1992). In this paper, we present some experimental research about the several phenomena which may impact IER/cement composite paste and the related numerical modelling.

The following section summarizes the main experimental results which are important to understand with this kind of material, and how the chemical processes might have an impact on its mechanical performances.

Next, from the concept developed previously, a second part describes each step of the modelling from the pressure determination at the microscopic scale (IER/cement paste) to the macroscopic

stress and strain (composite).

The last part presents the results from numerical simulation in comparison with those obtained in the experiments.

2. PHENOMENOLOGICAL STUDY

2.1 Materials

The ion exchange resins used in this paper is the Amberlite IR-120, a cation exchanger. To clearly understand the phenomena responsible for the degradation of the composite, the cement paste has been chosen to be as simple as possible. Indeed it's more complicated to split reactions which own to cement paste than those from IER when the number of ionic species into the interstitial solution is important. We then employed tri-calcium silicate (C3S), since there is no alkaline ionic species into its pore solution; it is easier to characterize the evolution of ions exchange process.

2.2 Experiments

According to the previous studies quoted above, the aim was to start with a sound sample (C3S/IER-Ca) and disturb enough the system to obtain the destructive formulation C3S/IER-Na. To achieve this goal, we insert a sample into a solution of NaOH and another into a solution of NaCl both at 1 mol/L. We then work on qualitative study of the cracking state to classify which formulation presents some mechanical issues. And finally, the sample has been analyzed by Elemental mapping with scanning electron microscopy (SEM).

2.3 Results

As we expected, even the sample inserted into NaOH has been destroyed in few days, however we have not anticipated the non-destructive behaviour of the sample which has been inserted into NaCl (Table 1).

Table 1 - Qualitative study about the mechanical state of sample C3S/IER-Ca after experiment

| Initial System | Perturbing Solution (1mol/L) | Final System | Mechanical State |
|----------------|------------------------------|--------------|------------------------|
| | ∅ | C3S/IER-Ca | Sound after 2 weeks |
| C3S/IER-Ca | NaOH | C3S/IER-Na | destroyed after 5 days |
| | NaCl | | Sound after 2 weeks |

First for each sample, according to previous study (Lafond 2013), IER may swell until 6% of volume strain when the ion exchange process is realize between the calcium from IER and a solution of sodium.

But, thanks to the use of SEM Elemental mapping, we found on the degraded sample where the system has been disturbed with a solution of NaOH, another phenomenon: a shell of Portlandite around each IER. This shell is the second key point, to understand the degradation of this kind of composite. Basically the Portlandite would reduce the initial volume of IER which would have to increase its swelling pressure to respect the thermodynamic equilibrium

3. MICRO/MACRO MODELLING

From the results of the phenomenon study, we have set up a predictive model able to estimate the macroscopic mechanical behaviour of a composite IER/C3S subject to a disturbance, like diffusion of NaOH as we have presented above. This section takes up the main points of the modelling.

3.1 Modelling

The first phase is to handle the ion exchange process. In case detailed in the previous chapter for instance, to respect the thermodynamic equilibrium, the exchange process between calcium and sodium ionic species has to be ruled by the following expression (NEJI 2013):

$$\left([Na]_r + \frac{T_{S_{IER}}}{V_r}\right)^2 \cdot \left([Ca]_s + \frac{T_{S_{IER}}}{2 \cdot V_s}\right) = K_{Na/Ca} \left([Na]_s - \frac{T_{S_{IER}}}{V_s}\right)^2 \cdot \left([Ca]_r - \frac{T_{S_{IER}}}{2 \cdot V_r}\right) \quad (1)$$

Where:

| | |
|-----------------|--|
| $[Na]_r/[Ca]_r$ | Concentration of sodium and calcium into the IER (mol/L) |
| $[Na]_s/[Ca]_s$ | Concentration of sodium and calcium into the pore solution (mol/L) |
| V_r | Volume of the internal solution of the IER (L) |
| V_s | Volume of pore solution (L) |
| $K_{Na/Ca}$ | Thermodynamic exchange equilibrium constant |
| $T_{S_{IER}}$ | Quantity to reach the thermodynamic equilibrium (mol) |

Then $T_{S_{REI}}$ is added into a second Fick conservation equation to follow the evolution of the diffusion of the disturbing ionic species into the sample:

$$\frac{\partial [Na]_s}{\partial t} + \frac{D_{Na}}{\phi_{C_3S}} \cdot \frac{\partial^2 [Na]_s}{\partial x^2} + T_{S_{IER}} = 0 \quad (2)$$

Where:

| | |
|---------------|---|
| D_{Na} | Diffusivity coefficient (m ² /s) |
| ϕ_{C_3S} | Porosity |

At the same time, depending on disturbing ionic species choice, the calcium release into the pore solution would precipitate, or not, in a shell of portlandite around each IER. Finally a microscopic swelling pressure can be obtained via a calculation based on experimental data (Lafond 2013) to determine the deformation of IER ϵ_{IER} (3).

$$\pi_{IER} = 3 \cdot k_{C_{IER}} \cdot \epsilon_{IER} \quad (3)$$

Where:

| | |
|------------------|--------------------------------------|
| π_{IER} | Microscopic swelling pressure of IER |
| ϵ_{IER} | Microscopic strain of IER |
| $k_{C_{IER}}$ | Bulk modulus of IER |

The mechanical properties of the composite and the interaction tensor has been estimated with homogenization method derived from Eshelby theory. This microscopic stress π_{IER} might be applied to the macroscopic scale via the following behaviour law (Bary 2008) (4):

$$\Sigma = C_H \cdot E - \pi_{IER} \cdot B_{IER} \quad (4)$$

Where:

| | |
|-----------|-------------------------------------|
| Σ | Macroscopic strain of the sample |
| E | Macroscopic strain of the sample |
| C_H | Homogenized stiffness of the sample |
| B_{IER} | Interaction coefficient |

3.2 Results

The case in which we subject a sample IER-Ca/C3S with a solution of NaCl is still in progress. The mechanical behaviour of a composite IER-Ca/C3S into a solution of NaOH provides good results. The figure 1a represents the distribution of the microscopic pressure into the composite. We can notice that the higher value is obtained close to the NaOH exposed surface. The most important ionic exchange process would occur in this part of the sample because to the closeness to the external solution. In the same time, because of the release of calcium from IER, a shell of Portlandite would appear around the IER which would compress each IER and

increase the internal pressure. When moving away from this area, the pressure decreases depending on the quantity of NaOH which have penetrated (Figure 1b).

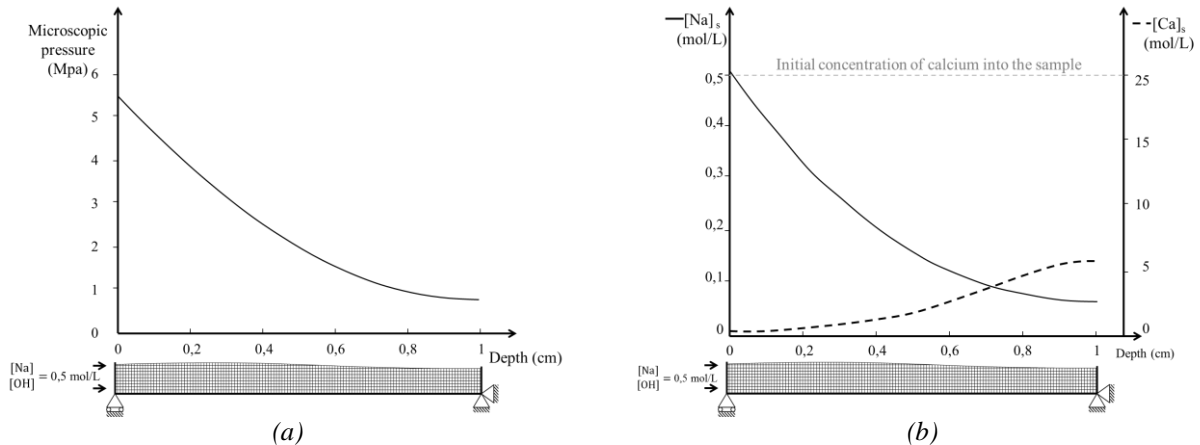


Figure 1 : Numerical results representing the mechanical behavior of a composite IER-Ca/C3S disturbed, during 15 days, by a solution of NaOH. (a) Distribution of the microscopic pressure into the sample (b) Evolution of sodium and calcium in the interstitial solution of the sample.

4. CONCLUSION

The mechanical behaviour characterization of a composite made up with IER embedded into a cement paste matrix, is a complex problem. After an experimental campaign we got an initial explanation of its potential mechanical damages with two chemical phenomena which, in a row, would lead to damage the IER-Ca/C3S formulation. When this composite is disturbed with a solution containing sodium ionic species, because of the ion exchange process, IER would tend to swell into the cement paste matrix. Depending on the co-ion of the disturbing solution, the release of calcium during the ion exchange process may lead to the precipitation of portlandite in the form of shell surrounding the IER. This phenomenon is expected to increase the pressure from the IER. A model has been developed to be close to the experimental results. The case of IER-Ca/C3S disturb with NaOH has been successfully simulated, however the model has to be consolidate with new configurations like the case of IER-Ca/C3S disturbed with a solution of NaCl.

ACKNOWLEDGEMENTS

The authors are deeply grateful to AREVA for its financial support and L. Stefan from AREVA for her support of the project.

REFERENCES

- Lafond, E. 2013. « Etude chimique et dimensionnelle de résines échangeuses d'ions cationiques en milieu cimentaire ». *Thèse, Université Bourgogne*.
- Bary, B. 2008. « Simplified Coupled Chemo-Mechanical Modeling of Cement Pastes Behavior Subjected to Combined Leaching and External Sulfate Attack ». *International Journal for Numerical and Analytical Methods in Geomechanics* 32 (14): 1791 - 1816.
- Neji, M., Bary, B., Burlion, N., Le Bescop, P. 2013 «Modelling of the interaction between chemical and mechanical behaviour of ion exchange resins incorporated into a cement-based matrix». *EPJ Web of Conferences* 56, 02004.
- Matsuda, M., Nishi, T., CHINO, K., et Kikuchi, M. 1992. « Solidification of spent ion exchange resin using new cementitious material,(I) ». *Journal of Nuclear Science and Technology* 29 (9): 883 - 89.

Moisture Profiles in Concrete Walls of a Nuclear Reactor Containment after 30 Years of Operation.



Tech. Lic. Mikael Oxfall
 PhD Student
 Vattenfall R&D AB / Lund University, LTH
 Älvkarleby Laboratory
 SE - 814 26 Älvkarleby
 Mikael.Oxfall@vattenfall.com



Dr. Peter Johansson
 Assistant Professor
 Lund University, LTH
 John Ericssons väg 1
 SE - 223 63 Lund
 Peter.Johansson@byggtek.lth.se



Dr. Manouchehr Hassanzadeh
 Adjunct Professor, Technical Specialist
 Vattenfall AB / Lund University, LTH
 Vattenfall AB
 SE - 169 92 Stockholm
 Manouchehr.Hassanzadeh@vattenfall.com

ABSTRACT

The fourth, and last, main barrier for preventing radioactive leakage from a nuclear power plant is the containment wall. Due to the importance of the structure it is of great advantage to understand the nature of the structures and how it changes over time. One important area is the moisture distribution in the concrete, since e.g. the moisture contents affect the shrinkage and creep of the concrete. Results from long term measurements of RH distribution and degree of capillary saturation measurements of a containment wall are presented. These results show that the structure is still drying, even after 30 years of exposure to a significant temperature gradient and a low relative humidity within the containment. The results also show that the affects of the temperature gradient should be considered when modelling the concrete drying in these conditions.

Key words: Nuclear, Hygrothermal transport, Aging, Monitoring campaign

1. INTRODUCTION

The containment wall of a nuclear reactor containment is the last barrier for preventing radioactive leakage from the nuclear power plant in case of an accident. The containment walls of the Swedish nuclear power plants consists of three parts; two concrete walls and an intermediate steel liner. The steel liner ensures the leak tightness and the concrete walls acts as protection of the liner and as load bearing structures. During operation the temperature inside the containments results in a temperature gradient over the wall that in some cases can be up to 50 °C. This in combination to the dry environment inside the containment gives a harsh environment regarding drying of the concrete of the inner wall. Due to the function of the structure it is important to understand and to be able to predict the moisture distribution inside the concrete. The moisture content is of interest regarding e.g. the durability of the structures and shrinkage of the concrete.

2. METHODS

The moisture distribution in the containment wall presented in this paper was measured with two methods, equilibrium relative humidity (RH) and degree of capillary saturation (S_{cap}). The RH profile was measured using a RH/temperature measurement setup as presented in /Oxfall 2013, Oxfall et.al 2013/. The measurements were conducted during one operational year and the measurement setup was installed on four different depths in the wall. In /Oxfall 2013/ the results from measurements on three different nuclear power plants are presented with RH profiles from several zones in each of the containments.

The S_{cap} is a measured value that describes how much of the capillary pores that is water filled at a certain point. The method is suitable to use as an alternative to moisture ratio if the specimen's does not have a representative size, 3-4 times the biggest aggregate. The S_{cap} is determined by comparing the mass of the water in the specimen with the mass of the specimen's water when capillary saturated, eq 1 /Hedenblad Nilsson 1985/.

$$S_{cap} = \frac{m_w - m_0}{m_{cap} - m_0} \quad (1)$$

where m_w is the mass of the specimen, m_{cap} is the mass of the specimen when capillary saturated and m_0 is the mass after drying to equilibrium in 105 °C.

Fagerlund defines the capillary saturated point as the point between the two stages of the water uptake /Fagerlund 1977/. The first stage is seen as a more rapid mass increase, due to the filling of capillary pores, and the second as much slower, due to the filling of bigger pores. In ideal measurement these two stages changes in a distinguished point "the nick point" /Fagerlund 1977/. The nick point defines the mass when the specimen is capillary saturated.

In the study S_{cap} was measured at Ringhals 4 as a supplementary measurement to RH and which also included the outer cylinder wall. The specimens were collected from a total of six concrete cores with a diameter of 300 mm. The cores were collected from a concrete block extracted from the containment at Ringhals 4 in connection with the steam generator change in 2011. Two of the cores were 800 mm long and gathered from the outer cylinder wall (S1 and S2) and four were 300 mm long from the inner cylinder wall (P1-4). To avoid influence of the water from the cooling of the core-drill the concrete specimens were collected from the centre of the cores. A total of eight samples were used on the 800 mm cores and four from the 300 mm cores.

The specimens were placed on soaked super absorbent cloths on the bottom of a lidded plastic box. One specimen was weighed at a time and the remaining was left in the box with the lid on. This was done to minimize drying of the specimens. The measurements were conducted during 93 hours. A more exhaustive description of the procedure for the measurements are presented in appendix 3 in /Oxfall 2013/. When capillary saturated the specimens were dried in 105 °C.

3. RESULTS AND DISCUSSION

Figure 1 shows the results from the S_{cap} measurements and figure 2 the measured RH distribution in the inner containment wall 72 days after the reactor was put into operation. The RH profile is presented as the average RH during that day. The variation of the RH and temperature during one operational year can be found in /Oxfall 2013/.

The S_{cap} measurements on five of the specimens were prematurely stopped before they reach equilibrium in the second stage. For these five specimens the nick points were assumed to be the last measured value. This assumption was quite rough but with the accessible data it gave a plausible value. In addition an uncertainty on ± 20 %-points was assessed on the mass increase which gave a ± 4 %-points error on S_{cap} , which can be seen as a conservative estimation.

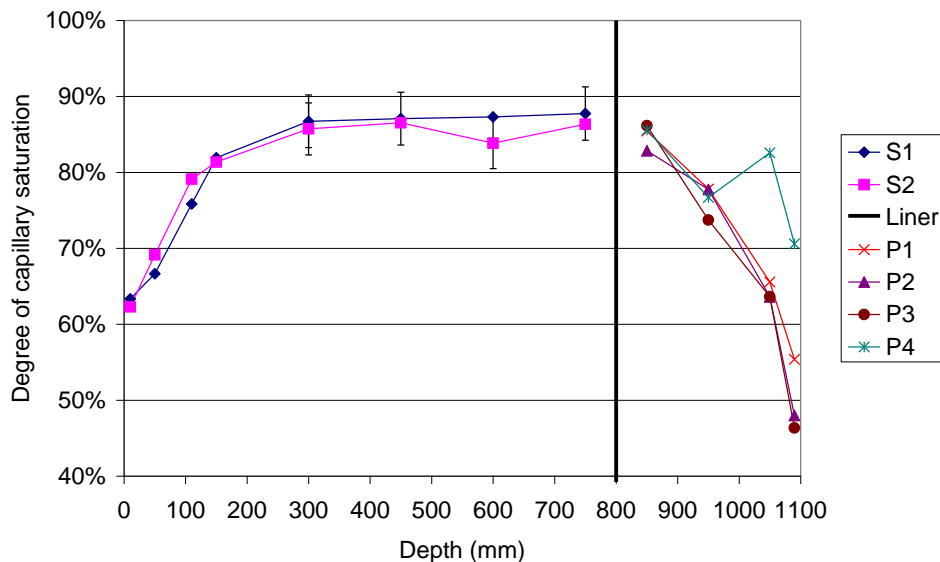


Figure 1 - Measured S_{cap} on concrete from the outer (0-800 mm) and inner (800-1100 mm) cylinder wall at Ringhals 4.

The S_{cap} profile shows a clear moisture gradient on both sides of the liner. The S_{cap} close to the liner is equivalent on either sides which indicates that the concrete on great depth has not, or only marginal, dried even after 30 years of exposure. The results from the outer wall also show some additional important results. The profile shows that when modelling the moisture transport in a nonisothermal condition the vapour content can not be used as the only transport potential /Nilsson 2013/. A better result is established if moisture content or RH is used but to establish an even better value of the moisture transport the temperature gradient has to be included in the moisture transport model /Nilsson 2013/. This was already stated in the 50th /Philips DE Vries 1957/ but no other studies of the impact of hygrothermal transport on long term exposures with large temperature gradients have been found by the authors.

The RH profile from the inner containment wall, figure 2, shows clear similarities to the S_{cap} measurements. During operation the RH varies some %-points due to temperature variations which results in moisture transport variations.

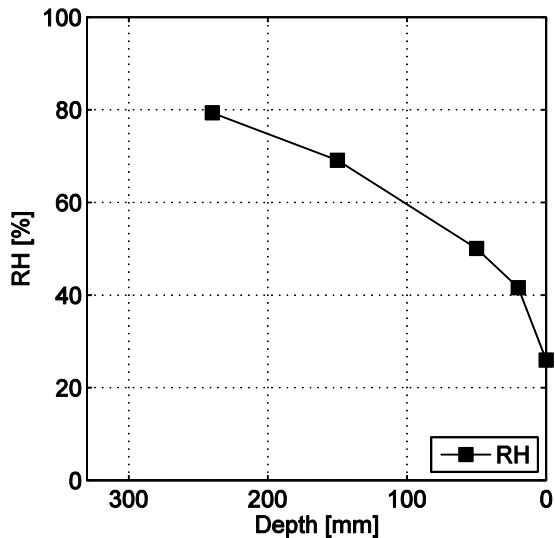


Figure 2 - Measured RH profile from the 4/12 2012 in the inner containment wall at Ringhals 4. 0 mm depth corresponds to the boundary conditions.

4. CONCLUSION

The concrete in the containment walls at nuclear power plants are still drying after 30 years of exposure to a significant temperature gradient and drying potential. The results also give evidence that a model for hygrothermal transport has to be accounted for when predicting future moisture distribution in the containment walls due to the temperature gradient.

ACKNOWLEDGMENTS

The authors would like to thank Ringhals AB for making the measurements possible and the financier for the doctoral project, Elforsk Nuclear Concrete program and its board members.

REFERENCES

- Fagerlund, G., 1977,
 “The critical degree of saturation method of assessing the freeze/thaw resistance of concrete”, *Matériaux et Constructions*, Vol. 10, no. 4, July 1977, pp. 217-229.
- Hedenblad, G. and Nilsson, L.-O., 1985,
 “Degree of Capillary Saturation - A tool for better evaluation of the moisture content in concrete”, TVBM 7005 Lund University, Division of Building Materials. Lund, Sweden, 1985, 15 pp.
- Nilsson, L.-O., 2013,
 “Moisture transport under a temperature gradient - Some old and new studies”, *Proceedings, Understanding the fundamental properties of concrete*, Trondheim, Norway, April 2013, 14 pp.
- Oxfall, M., 2013,
 “Climatic condition inside nuclear reactor containments - Monitoring campaigns”, *Licentiate Dissertation*, TVBM 3172, Lund University, Lund, Sweden, 2013, 103 pp
- Oxfall, M., Hassanzadeh, M., et al., 2013,
 “Moisture levels and drying potential of the concrete in Swedish reactor containments”, *EPJ Web of Conferences*. Vol. 56, no. 03002, July 2013, 8 pp
- Philips, J. R. and DE Vries, D. A., 1957,
 “Moisture movement in porous materials under temperature gradients”, *Transactions, American Geophysical Union*, Vol. 38, no. 2, April 1957, pp. 222-232.

Deterioration of Concrete in Hydraulic Structures due to Frost Action



Martin Rosenqvist
Lic. Eng., Ph.D. Student
Vattenfall Research and Development AB / Lund University
Älvkarlebylaboratoriet,
SE-814 26 Älvkarleby
martin.rosenqvist@vattenfall.com



Katja Fridh
Ph.D., Assistant Professor
Division of Building Materials
Lund University,
Box 118, SE-221 00 Lund
katja.fridh@byggtek.lth.se



Manouchehr Hassanzadeh
Ph.D., Adjunct Professor
Vattenfall AB / Lund University,
SE-169-92 Stockholm
manouchehr.hassanzadeh@vattenfall.com

ABSTRACT

Climatic conditions during the winter in countries situated in the north can be considered severe. This is especially true for hydraulic structures, such as hydro power structures, dams, harbours, canals and some bridge foundations. Freezing of concrete in contact with unfrozen fresh water may have a considerable impact on the deterioration process of concrete. This paper presents results obtained in experimental investigations based on observations of superficial and internal damage to concrete in hydraulic structures in Sweden. It was shown that superficial damage at the waterline is caused by interactions between leaching, frost action and abrasion. Further, the results indicate that internal damage to some thin concrete dams has been due to formation of macroscopic ice lenses causing spalling of concrete. Knowledge about degradation mechanisms and how they interact is crucial in order to be able to perform durable repairs.

Key words: Frost Action, Scaling, Ice Segregation, Moisture Conditions, Hydraulic Structures

1. INTRODUCTION

Owing to the winter conditions in countries situated in the north, the effects of frost action may have a considerable impact on the deterioration process of concrete in hydraulic structures. A hydraulic structure is defined as a structure built in any body of water with the purpose to control or change the natural flow of water. Hydro power structures, dams, harbours, canals and some bridge foundations are all examples of hydraulic structures.

Both superficial and internal damage, which are suspected to have been caused by frost action, have been found in concrete in hydraulic structures. These observations have raised questions about the long-term behaviour of hydraulic structures in fresh water bodies in cold regions:

- Which degradation mechanisms cause gradual deterioration of the concrete surface at the waterline of hydraulic structures?
- What are the conditions for spalling of concrete in thin concrete dams subjected to long periods of freezing temperatures?

In order to answer these questions, Rosenqvist (2011) presented a research program as part of a PhD study. The aims of the study are to determine moisture conditions in hydraulic structures and to investigate effects of frost action on the deterioration process of concrete. Observations of concrete damage in Swedish hydro power structures have formed the basis for the PhD study.

In the first of two parts of this PhD study, the exposure conditions and degradation mechanisms causing superficial and internal damage have been investigated experimentally. Laboratory test methods have been developed in order to, as far as possible, reproduce exposure conditions similar to those at existing structures. The work is described by Rosenqvist (2013).

2. SUPERFICIAL DAMAGE

Superficial damage, similar in appearance to salt scaling, can be observed at the waterline of most hydraulic structures. Gradual deterioration of the concrete surface leads to exposure of coarse aggregate in a short-term perspective and reinforcing steel in a long-term perspective, see Figure 1. The greatest amount of damage is found at the waterline, which normally corresponds to the maximum water level. The amount of damage decreases with increasing water depth.



Figure 1 – Exposure of coarse aggregate and reinforcing steel at the waterline.

The effects of freezing due to alternating temperatures were investigated by subjecting concrete specimens to climatic conditions similar to those at the waterline. A test method was developed by Persson & Rosenqvist (2009). Specimens with water to cement-ratio (w/c-ratio) 0.62 sustained only minor superficial damage at the waterline after 112 freeze-thaw cycles, whereas specimens with w/c-ratio 0.54 and air entrainment sustained no damage. The lack of damage to the specimens with w/c-ratio 0.54 did not agree with observations at existing structures.

Hence, deterioration of concrete at the waterline involves several degradation mechanisms. The effects of interactions between leaching, frost action and abrasion were investigated by Pham & Terzic (2013). Also in this investigation, concrete mixes with w/c-ratio 0.62 and 0.54 were used. The specimens were subjected to leaching in deionised water titrated to pH 7 with nitric acid (HNO₃). After the leaching process, the specimens were subjected to seven freeze-thaw cycles according to the procedure described in the test method SS 13 72 44:2005.

It was shown that the scaling resistance of concrete decreases with increasing time of leaching. The reduction in scaling resistance was greater for specimens subjected to leaching in deionised water titrated to pH 4. Hence, a possible deterioration process may start with calcium leaching during the snowmelt runoff period. The concrete surface thus becomes frost susceptible. During the following winter, the surface layer is damaged by frost action and removed by ice abrasion. The process starts all over again during the next snowmelt runoff period.

3. ICE SEGREGATION

Spalling of concrete has been observed far below the water level on the upstream face of some thin concrete dams. During inspections, divers have been able to remove pieces of concrete with their hands, see Figure 2. None of the dams had been provided with heat insulating walls on the downstream side during the construction time. A hypothesis is that poor quality concrete or the effects of aging have made the concrete susceptible to formation of macroscopic ice lenses when subjected to long periods of freezing temperatures. Formation of macroscopic ice lenses, also termed ice segregation, is a well known phenomenon in soil since it causes frost heave in winter. However, little is known about formation of macroscopic ice lenses in hardened concrete.

Three types of specimens with w/c-ratio between 0.5 and 1.4 were produced; (1) specimens of undamaged concrete, (2) specimens with internal damage due to frost action and (3) specimens with sheets of paper cast into the concrete to represent cavities or other imperfections. The top surface of the specimens was subjected to freezing, whereas the bottom surface was in contact with unfrozen water. The test method is described by Rosenqvist et al. (2012).

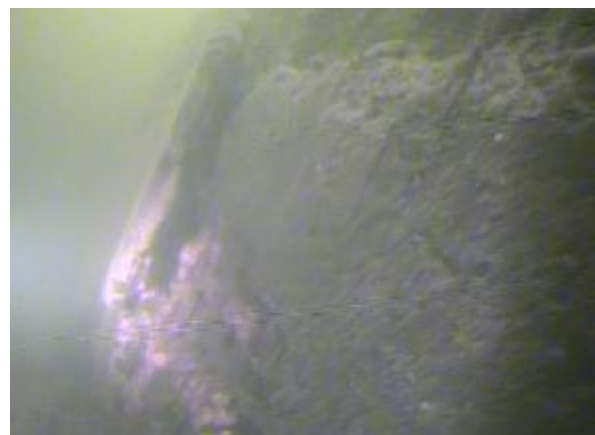


Figure 2 – Loose pieces of concrete on the upstream face of a thin concrete arch dam.

In rather stable thermal conditions, ice segregation occurred in undamaged concrete with w/c-ratio 0.9 or higher. In frost-damaged concrete, macroscopic ice lenses formed within a few days regardless of the w/c-ratio. Also in concrete with cavities or other imperfections, ice segregation occurred. However, the period of freezing required to facilitate ice segregation increased with decreasing w/c-ratio. Nevertheless, the risk of concrete spalling in thin concrete dams cannot be overlooked since unfavourable temperature and moisture conditions may exist in winter.

4. CONCLUDING REMARKS

According to the results obtained so far in the PhD study, superficial damage at the waterline is due to interaction of multiple degradation mechanisms. Whether the concrete is air entrained or not, especially leaching reduces the scaling resistance. Fortunately, the general experience so far is that the deterioration rate is low. The need for rehabilitation becomes, however, obvious when structural reinforcement bars are exposed. The risk of concrete spalling in thin concrete dams is insidious since ice segregation can be ongoing for a long time without notice. Damage to the upstream face is neither visible from the dam crest nor the inspection gallery.

Repairs of concrete in hydraulic structures are normally complicated and expensive due to limited accessibility and, if necessary, underwater work. Hence, the expected service life of repairs should be in line with the expected service life of the whole structure. Knowledge about degradation mechanisms and how they interact is therefore crucial in order to be able to perform durable repairs. The overall purpose of gathering knowledge about degradation mechanisms and deterioration processes is to secure and to safely extend the service life of hydraulic structures.

ACKNOWLEDGEMENTS

The authors express their gratitude to Elforsk AB (Swedish Electrical Utilities' R&D Company), SBUF (The Development Fund of the Swedish Construction Industry), SVC (Swedish Hydro Power Centre) and Vattenfall Research and Development AB for funding the PhD study.

REFERENCES

- Pham, L.W., Terzic, A., 2013,
 “Effects of Leaching and Abrasion on the Scaling Resistance of Concrete”, Report TVBM-5093, Div. of Building Materials, Lund University, Lund, 2013, 119 pp. (Swedish)
- Persson, M., Rosenqvist, M., 2009,
 “Frost Damage in Concrete Dams”, Report TVBM-5074, Division of Building Materials, Lund University, Lund, 2009, 88 pp. (Swedish)
- Rosenqvist, M., 2011,
 “Moisture Transport in Concrete Structures in Swedish Hydro Power Plants”, Proceedings, XXI Nordic Concrete Research Symposium, Hämeenlinna, Finland, May-June 2011, pp. 159-162.
- Rosenqvist, M., Fridh, K., Hassanzadeh, M., 2012,
 “Macroscopic Ice Lens Growth: Observations on Swedish Concrete Dams”, Proceedings, 3rd International Conference on Concrete Repair, Rehabilitation and Retrofitting, Cape Town, South Africa, September 2012, pp. 658-664.
- Rosenqvist, M., 2013
 “Moisture Conditions and Frost Resistance of Concrete in Hydraulic Structures”, Report TVBM-3173, Division of Building Materials, Lund University, Lund, 2013, 78 pp.
- SS 13 72 44:2005,
 “Concrete Testing – Hardened Concrete – Scaling at Freezing”, Swedish Standards Institute, 2005

Chloride Penetration Resistance of Calcium Depleted Concrete Specimens



Arezou Babaahmadi
PhD candidate
Division of Building Technology (Building Materials)
Chalmers University of Technology
S-412 96 Gothenburg, Sweden
arezou.babaahmadi@chalmers.se



Luping Tang
Professor
Division of Building Technology (Building Materials)
Chalmers University of Technology
S-412 96 Gothenburg, Sweden
Tang.luping@chalmers.se



Zareen Abbas
Associate Professor
Department of Chemistry
University of Gothenburg
Kemivägen 4, SE-412 96, Gothenburg, Sweden
Zareen@chem.gu.se

ABSTRACT

To facilitate the service life predictions regarding durability of nuclear waste repositories acceleration methods enhancing the decalcification process are used. However, in order to reach an efficient leaching rate small sample sizes have been used which limits further testing. In this study an electro-chemical migration method to accelerate leaching of calcium from concrete specimens of size $50 \times 100 \text{Ø}$ is presented. Rapid chloride migration test is utilized to account for the changes in chloride diffusion coefficient of concrete specimens due to calcium depletion. The results indicate up to at least 70% of increase of chloride diffusion coefficient as a result of decalcification.

Key words: Aging, Chlorides, Nuclear, Sustainable, Testing.

1. INTRODUCTION

It is known that the long-term contact between the concrete barriers in nuclear waste repositories and the surrounding groundwater /Berner 1992, Reardon 1992/ is one of the main reasons of causing degradation. To account for the long term effect of degradation on properties of cementitious materials used in nuclear waste repositories several studies are reported in the literature regarding leaching of calcium from cementitious materials based on immersion of the solid cementitious specimens in water or enhancement of the decalcification process with acceleration methods /Adenot 1992, Faucon 1998, Haga 2005, Faucon 1996, Mainguy 2000, Maltais 2004, Ryu 2002, Saito 1992, Wittmann 1997, Carde 1997, Heukamp 2001, Revertegat 1992/ However, although several conclusions can be drawn from these studies regarding the properties of aged cementitious materials these types of experiments are either very time consuming due to the slow kinetics of the decalcification process or small sample sizes should be implemented which limits further examination of the mechanical properties of the samples or their diffusivity. In addition it should be noted that previous

studies reported in the literature often used paste specimens or even powder samples and there is limited information about calcium depleted concrete specimens with sufficient large size for testing mechanical and physical properties.

Recently a newly developed acceleration method simulating the leaching of calcium from concrete specimens was developed by Babaahmadi et al. /Babaahmadi 2014/. In this study the changes in transport properties (chloride diffusion coefficient) of solid concrete specimens of proper size after decalcification by the use of the newly developed method /Babaahmadi 2014/ are presented. Rapid chloride migration test method was utilized to account for the change in chloride penetration resistance of decalcified concrete specimens.

2. MATERIAL AND METHODS

2.1 Specimen preparation

The Concrete specimens used in this study were cast using Swedish structural Portland cement for civil engineering (CEM I 42.5N BV/SR/LA). The specimens were casted in cylinders in two different sizes of Ø100×200 mm and Ø50×250 mm with two different water cement ratios (according to the properties of the concrete used in SFR) / Höglund 2001, Tang 1996/, Table 1. The observations from the slump test prior to casting was 25 mm slump for the concrete with W/C=0.48 and 35 mm for W/C=0.62. The specimens were cured in saturated lime water for more than 3 month. Then cut to cylinders with the size of Ø50×75 and Ø100×50mm to be used in electrochemical migration method.

Table 1. Properties of concrete used in SFR repository located in Forsmark

| Properties | Silo ¹⁾ |
|---|---------------------------|
| Cement type | Swedish structural cement |
| W/C | 0.48 |
| Cement content kg/m ³⁾ | 350 |
| Aggregate volume fraction ²⁾ | 0.7 |

1) Based on Emborg et al. / Emborg 2007/ but with symmetrical deviation of 48±5 MPa in compressive strength instead of 43-58 MPa with mean 48 MPa.

2) Estimated base on general mix design of concrete mix proportion, which is in agreement with Höglund,/ Höglund 2001/ for the concrete in silo

2.2 Electrochemical migration method

Concrete specimens decalcified by the use of the newly developed method for accelerated calcium leaching of large solid specimens /Babaahmadi 2014/. The experimental set-up of the electrochemical migration method was inspired by the rapid chloride migration test developed by Tang /Tang 1996/. Concrete specimens of size Ø100×50 were used in this study. 0.3 M ammonium nitrate solution was used as catholyte solution in order to increase the dissolution rate of calcium hydrates /Carde 1997/ and 2 M Lithium hydroxide solutions was used as anolyte solution to maintain conductivity of the system. The cells were connected to an external potential supplier with adjustable current and potential. A constant current of 250 mA was applied to the specimens for a duration of 6 weeks to reach to complete leaching of Portlandite content as demonstrated by Babaahmadi et al. Babaahmadi 2014/ In order to maintain the pH level in the catholyte and anolyte solutions as well as to compensate for the consumed ions (OH⁻ ions in the anolyte solution and H⁺ ions in the catholyte solution), the solutions were frequently recharged.

2.3 Rapid chloride migration test

The chloride diffusion coefficient plays an important role in long term durability predictions. To account for the chloride diffusion coefficient of concrete samples rapid chloride migration test was performed according to NT BUILD 492 and as described by Tang / Tang 1996, NT BUILD 492 1999/. It should be noted that in the case of the calcium depleted specimens owing to a reduced ionic concentration in pore solution compared to normal concrete specimens, adjusted shorter experimental duration was applied to these specimens. Moreover, due to a considerable increase in porosity of the calcium depleted concrete it is not easy to predict the proper test duration. In this study the test duration was set to 15 hours instead of 24 hours. However, chloride ions penetrated through the whole thickness of the specimens in this time duration. As a result the minimum chloride diffusion coefficient was calculated for the calcium depleted concrete specimens.

3. CONCLUDED RESULTS

The changes in chloride diffusion coefficient of the concrete samples due to calcium depletion are presented in Figure 1. As illustrated up to at least 70% increase in chloride diffusion coefficient is expected after calcium depletion. It should be noted that the presented results regarding the calcium depleted specimens are the minimum chloride diffusion coefficient owing to the full penetration through the specimen thickness as it was pointed out previously. the results are in good agreement with the presented results by Choi / Choi 2013/.

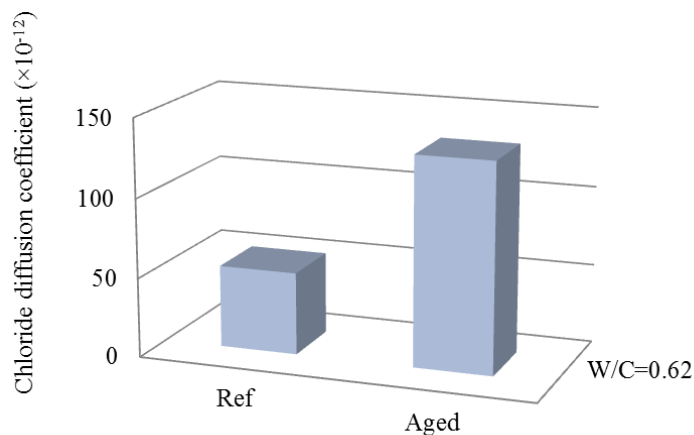


Figure 1. Chloride diffusion coefficient (minimum diffusion coefficient in the case of aged samples)

REFERENCES

- F. Adenot, M. Buil, 1992
Modelling of the corrosion of the cement paste by deionized water, *Cement and Concrete Research*, 22 (1992) 489-496.
- A. Babaahmadi, L. Tang, Z. Abbas, T. Zack, P. Mårtensson, 2014
Characterization of Cement Paste Subjected to Accelerated Decalcification by an Electro-Chemical Method, Submitted to *Cement and Concrete Research*, (2014).
- U.R. Berner, 1992
Evolution of pore water chemistry during degradation of cement in a radioactive waste repository environment, *Waste Management*, 12 (1992) 201-219.
- C. Carde, R. François, 1997
Effect of the leaching of calcium hydroxide from cement paste on mechanical and physical properties, *Cement and Concrete Research*, 27 (1997) 539-550.

- Y.S. Choi, E.I. Yang, 2013
Effect of calcium leaching on the pore structure, strength, and chloride penetration resistance in concrete specimens, *Nuclear Engineering and Design*, 259 (2013) 126-136.
- M. Emborg, J.-E. Johansson, S. Knutsson, 2007
Långtidsstabilitet till följd av frysning och tining av betong och bentonit vid förvaring av låg- och medelaktivt kärnavfall i SFR 1, SKB Report, Svensk Kärnbränslehantering AB, 2007.
- P. Faucon, P. Le Bescop, F. Adenot, P. Bonville, J.F. Jacquinet, F. Pineau, B. Felix, 1996
Leaching of cement: Study of the surface layer, *Cement and Concrete Research*, 26(1996) 1707-1715.
- P. Faucon, F. Adenot, J.F. Jacquinet, J.C. Petit, R. Cabrillac, M. Jorda, 1998
Long-term behaviour of cement pastes used for nuclear waste disposal: review of physico-chemical mechanisms of water degradation, *Cement and Concrete Research*, 28 (1998) 847-857.
- K. Haga, S. Sutou, M. Hironaga, S. Tanaka, S. Nagasaki, 2005
Effects of porosity on leaching of Ca from hardened ordinary Portland cement paste, *Cement and Concrete Research*, 35 (2005) 1764-1775
- F.H. Heukamp, F.J. Ulm, J.T. Germaine, 2001
Mechanical properties of calcium-leached cement pastes: Triaxial stress states and the influence of the pore pressures, *Cement and Concrete Research*, 31 (2001) 767-774.
- M. Hinsenveld, A Shrinkage 1992
Core Model as a Fundamental Representation of Leaching Mechanism in Cement Stabilized Waste, Doctoral Thesis, in, Department of Civil and Environmental Engineering, University of Cincinnati, Cincinnati, OH, 1992.
- L.-O. Höglund, 2001
Project SAFE: Modeling of long-term concrete degradation processes in the Swedish SFR repository, SKB Report, Svensk Kärnbränslehantering AB, 2001.
- M. Mainguy, C. Tognazzi, J.-M. Torrenti, F. Adenot, 2000
Modelling of leaching in pure cement paste and mortar, *Cement and Concrete Research*, 30 (2000) 83-90.
- Y. Maltais, E. Samson, J. Marchand, 2004
Predicting the durability of Portland cement systems in aggressive environments— Laboratory validation, *Cement and Concrete Research*, 34 (2004) 1579-1589.
- NT BUILD 492, 1999
Concrete, Mortar and Cement-based Repair Materials: Chloride Migration Coefficient from Non-steady-state Migration Experiments, 1999.
- E.J. Reardon, 1992
Problems and approaches to the prediction of the chemical composition in cement/water systems, *Waste Management*, 12 (1992) 221-239.
- E. Revertegat, C. Richet, P. Gégout, 1992
Effect of pH on the durability of cement pastes, *Cement and Concrete Research*, 22 (1992) 259-272.
- J.-S. Ryu, N. Otsuki, H. Minagawa, 2002
Long-term forecast of Ca leaching from mortar and associated degeneration, *Cement and Concrete Research*, 32 (2002) 1539-1544.
- H. Saito, S. Nakane, S. Ikari, A. Fujiwara, 1992
Preliminary experimental study on the deterioration of cementitious materials by an acceleration method, *Nuclear Engineering and Design*, 138 (1992) 151-155.
- L. Tang, 1996
Electrically accelerated methods for determining chloride diffusivity in concrete - Current development, *Magazine of Concrete Research*, 48 (1996) 173-179
- F.H. Wittmann, 1997
Corrosion of Cement-Based Materials under the Influence of an Electric Field, *Materials Science Forum*, 247 (1997) 107-126.

Developing Low pH concrete for tunnel plugging structures in nuclear waste containment



Markku Leivo
Dr. (Tech.), Principal Scientist
VTT Technical Research Centre of Finland
P.O. BOX 1000
FI-02044 VTT, Finland
E-mail: markku.leivo@vtt.fi



Tapio Vehmas
M.Sc. (Tech.), Research Scientist
VTT Technical Research Centre of Finland
P.O. BOX 1000
FI-02044 VTT, Finland
E-mail: tapio.vehmas@vtt.fi



Erika Holt
Ph.D., Research Team Leader
VTT Technical Research Centre of Finland
P.O. BOX 1000
FI-02044 VTT, Finland
E-mail: erika.holt@vtt.fi

ABSTRACT

This presentation describes research done within an EU FP7 Euratom project, to develop and validate the performance of low-pH concretes used in high level radioactive nuclear waste containment structures. The unique type of concrete is used for deposition tunnel end plugs that are approximately 400 metres underground within repository conditions. The research has focused on producing highly workability mixtures with local materials, where rheology and heat of hydration have been optimized simultaneously with long-term durability and watertightness targets. The results are being implemented with full-scale construction of the 6 metre long tunnel plug in the 15 m² tunnel cross section.

Key words: nuclear, durability, binders, silica fume, fly ash, rheology, SCC, performance, permeability, structural design, testing

1 INTRODUCTION

Innovative research has been done to develop and validate the performance of low-pH concrete used in high level radioactive nuclear waste containment structures. The unique type of concrete is used for deposition tunnel end plugs acting as hydraulic and mechanical barriers in Finland's deep underground repository. Due to long-term material safety requirements, the concrete pH leachate must be lower than normal, thus the concrete mixtures have been made with very low amounts of cement while utilizing 40% or more of alternative binders such as silica fume and fly ash. The mixtures must also have high workability, thus the research has focused on both rheology and high durability performance to ensure the long service life in the challenging environmental conditions. It was possible to achieve two different mixtures, having compressive strengths over 50 MPa, adiabatic temperature rise under 10°C, minimal shrinkage, extremely

low permeability and a pH under 11 in groundwater leachate. These excellent performance results provide two new potential concrete alternatives, either as binary or ternary blends of binder, to be used in nuclear repository conditions very long-service life structures. The results are being utilized in the design specifications and construction of the Finnish nuclear waste repository facility in Olkiluoto, Finland, operated by Posiva Oy.

The tunnel end plug is a reinforced concrete structure having dimensions of 4.35 to 6.35 metres in diameter and 6 metres in length (Figure 1). The plug contains approximately 150 m³ of concrete and 20 tons of steel reinforcement and it will be cast in two sections. A permeable filter layer made from customized low-pH blocks is placed behind the plug to handle water during construction and operation, also during the accelerated pressurization test. The service life of the concrete plug is 100 years, yet the plug is one component of the Engineering Barrier System (EBS) that should protect the environment for hundreds of thousands of years during the storage of spent fuel. The original structural designs and calculations for Posiva's plug are described within their Backfill Production Line report /Posiva 2012/, which is based on earlier experiences in Sweden's similar repository design and demonstrations.

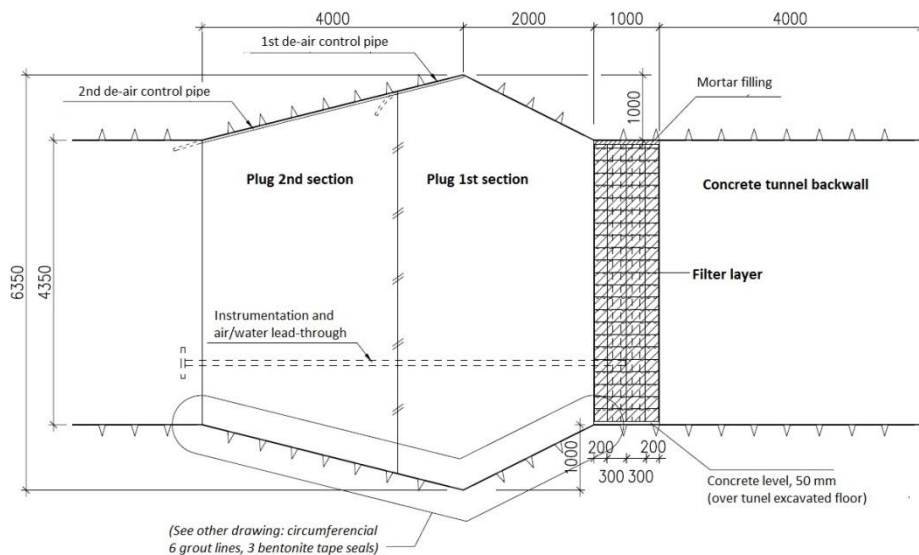


Figure 1 - Posiva's design for the deposition tunnel end plug (POPLU), units in mm.

2 MIXTURE DESIGNS & TEST METHODS

The initial basis for the Finnish plug concrete recipe was the experience gained by other waste management organizations, especially in Sweden and Canada. The new innovations with the Finnish recipe have been to account for local materials, stricter requirements for repository in-situ foreign material safety regarding chemical admixtures, and the higher durability demands. The plug concrete needs to be highly workable, with potentially slight vibration being used within the mould at the time of placement. The cement used was sulphate resistance CEM I 42,5 MH/SR/LA (Cementa, Annlägningscement). The silica fume incorporated to the mixture was in granular form (Finnsementti, Parmix-Silika). Aggregates were local materials available on-site at ONKALO, with the addition of quartz filler having $d_{50} = 35 \mu\text{m}$ (Sibelco Nordic, Nilsiä). VTT laboratory Finnish aggregates were used to replicate the aggregate gradation of the Swedish B200 –concrete. For the new POPLU mixtures, a naphthalene-based superplasticizer was used (HaBe, Pantarhit LK (FM)), while in the Swedish plug concrete (recipe labelled B200), a polycarboxylate-based superplasticizer (Glenium C151) was used.

The recipes were evaluated for early age performances, assessing workability by slump, flow, and rheology (SFS-EN 12350 and Contec5-viscometer), air content (SFS-EN 12350), setting time (SFS 5289), segregation and heat of hydration using semi-adiabatic conditions (RILEM TC119-TCE1). The hardened properties evaluated included compressive and split tensile strengths and density (EN 12390), elastic modulus (SFS 5450), watertightness (EN 12390), autogenous and drying shrinkage, non-steady state chloride migration (NT Build 492), sulphate resistance, and pH leachate. In the analysis, the Swedish “B200” mixture was used as reference comparisons in addition to traditional high performance normal concrete.

Two applicable mix designs and a reference mix were developed. The first mix design (Binary mix) had a binder composition equal to the Swedish plug concrete. In the modified version, the plasticizer was changed to naphthalene-based superplasticizer, limestone filler was replaced with quartz and the water content was lowered from 157 l/m³ to 125 l/m³ by modifying the aggregate grading curve. All of these mixtures required a high dosage of superplasticizer to achieve the workability, with dosages in the order of 4.5-7.5% by binder content. These new modifications, compared to the reference Swedish mixture, were expected to increase the durability of the concrete while not cause drastic changes in other qualities.

The second mix design was labelled as the Ternary mix design, in which a high quality fly ash was used in addition to the silica fume. Again a workable concrete was obtained with an effective water content of 126 l/m³. For reference purposes, the Swedish B200 mix design was also re-cast using Finnish laboratory materials.

Table 1 - Final mix designs of Posiva’s low-pH concretes

| | Final Ternary mix design | Final Binary mix design | B200 SKB mix, with Finnish laboratory materials |
|---------------------------|--------------------------|-------------------------|---|
| CEM I 42,5 MH/SR/LA | 105 kg/m ³ | 120 kg/m ³ | 120 kg/m ³ |
| Silica fume | 91 kg/m ³ | 80 kg/m ³ | 80 kg/m ³ |
| Fly ash | 84 kg/m ³ | - | - |
| Quartz filler | 114 kg/m ³ | 256 kg/m ³ | - |
| Limestone filler | - | - | 370 kg/m ³ |
| Local aggregate | 1840 kg/m ³ | 1805 kg/m ³ | - |
| VTT laboratory aggregates | | | 1600 kg/m ³ |
| Effective water content | 126 kg/m ³ | 125 kg/m ³ | 157 kg/m ³ |
| Water/binder –ratio | 0,45 | 0,60 | 0,79 |

3 RESULTS AND CONCLUSIONS

The workability of all of these developed mixes was quite high. The Binary mix had a slump of 260 mm and the Ternary mix 190 mm. The Binary mix was almost self-compacting concrete, having slump flow 650 mm. The heat development is a concern for using concretes in this type of massive concrete tunnel plug structure, and thus lowering it was one of the key design targets. The temperature rise was low in all of these concretes due to low cement content. The compressive strength target was only 50 MPa and all of these concretes exceed that target quite remarkably. Table 2 provides a summary of the achieved results for the two new Finnish plug mixtures are given. The target values, Swedish B200 reference concrete as well as normal concrete values are also presented for comparison purposes.

Table 2 - Summary of Finnish low-pH concrete (POPLU) performance results, compared to traditional high performance concrete and the target values.

| | POPLU Target | POPLU Binary | POPLU Ternary | Reference Swedish "B200" ^a | "Normal concrete" |
|--|-----------------|-----------------------|-----------------------|---|-------------------------|
| Compressive strength, MPa | > 50 | 91.5 | 79.5 | 67.5 | 50 |
| Split tensile strength, MPa | 3.2 | 5.6 | 4.5 | - | 3.2 |
| Modulus of elasticity, GPa | 34 | 37.4 | 34.2 | - | 34 |
| Autogenous shrinkage, mm/m | (min) | 0.22 | 0.15 | 0.03 | 0.1 |
| Drying shrinkage, mm/m | (min) | 0.17 | 0.22 | - | 0.6 |
| Water tightness, mm | max 50 | 4.0 | 5.0 | 5.3 | 25 |
| Chloride diffusivity, m ² /s | (min) | 2.1*10 ⁻¹² | 2.8*10 ⁻¹² | | 10-20*10 ⁻¹² |
| Sulphate damage | (min) | None at 180d | None at 180d | | |
| pH of leachate at 90 days (reference/Groundwater) | < 11 | 11.4 / 10.3 | 11.4 / 10.3 | 11.4 / 10.3 | >12,5 |

^a Results are based on re-production of mix in Finland

The POPLU demonstration tunnel end plug will be built during 2014. Prior to emplacement, a mock-up is being constructed above ground by the concrete supply contractor, to demonstrate feasibility of the mixture, placement techniques and performance via quality control testing. The actual in-situ full-scale plug performance will be evaluated using an accelerated pressurization up to 7.5 MPa, simulating the swelling pressure and groundwater pressure experience over the plug's operational lifetime. The pressurization will be done in gradual steps over a one year period, to assess the mechanical behaviour and hydraulic watertightness. The plug will be instrumented with approximately 65 sensors, including temperature, relative humidity, pore and total pressure, strain and displacement. The results will be used to update the performance models and design, including the concrete recipe and construction specifications. In the future repository operation scheduled to begin in 2022 in Finland, there will be one plug constructed per year for 100 years of operation. These types of low-pH concretes and grouts are needed worldwide in the containment of nuclear waste, where concrete and bentonite compatibility are essential for an extremely long service life of thousands of years.

ACKNOWLEDGEMENT

The research leading to these results has received funding from the European Union's European Atomic Energy Community's (Euratom) Seventh Framework Programme FP7/2007-2013 under Grant agreement no 323273, the DOPAS project.

REFERENCES

- Hansen J., Holt E. and Palmu M. DOPAS 2012. Full scale Demonstrations of Plugs and Seals in Proceedings of the Euradwaste '13 conference by European Commission held in Vilnius, Lithuania 14-16 October, 2013 (to be published).
- Posiva. 2012. Backfill Production Line 2012. Design, production and initial state of the deposition tunnel backfill and plug. Posiva 2012-18, Eurajoki, Finland: Posiva Oy, 182 p.

Development of resistant concrete pipes to be exposed in aggressive environments



Lise Juel-Hansen
Consultant, M.Sc.
Danish Technological
Institute
Gregersensvej,
DK-2630 Taastrup
E-mail: ljh@dti.dk



Martin Kaasgaard
Consultant, M.Sc.
Danish Technological
Institute
Gregersensvej,
DK-2630 Taastrup
E-mail: mkaa@dti.dk



Jack Anderson
Senior Consultant, M.Sc.
Danish Technological
Institute
Gregersensvej,
DK-2630 Taastrup
E-mail: jaa@dti.dk



Claus Pade
Team Manager, M.Sc.
Danish Technological
Institute
Gregersensvej,
DK-2630 Taastrup
E-mail: cpa@dti.dk

ABSTRACT

Development of concrete sewer pipe more resistant to the sulphuric acid attack has been performed. Performance of a reference earth-moist concrete composition was compared to four candidate technologies by exposure to a sulphuric acid solution. The investigated candidate acid resistant technologies were limestone aggregate, geopolymer binder, calcium aluminate cement and slag cement. All the tested technologies appeared to perform better than the reference composition. The most promising technology was to use limestone as aggregate material.

Key words: Concrete pipes, service life, sulphuric acid deterioration, earth-moist concrete

1. INTRODUCTION

The chemically aggressive environment within the concrete sewer pipe structures exposes the inside surface of the structures to sulphuric acid attack. The cost of maintenance and repair of concrete sewer pipe is substantial. In Denmark alone the yearly costs of maintenance, repair and expansion is estimated to 1 billion DDK [Miljøministeriet, 2006]. Furthermore, leakage from concrete sewer pipe structures can induce risks of unwanted pollution of the groundwater [Vollertsen et.al., 2002]. The study described in this paper is part of a Danish Research & Development project aiming to develop concrete sewer pipe structures which are more resistant to acid in order to achieve a prolonged service life of minimum 75 years. Four potential technologies, limestone aggregate, geopolymer binder, calcium aluminate cement and slag cement were investigated and selected results obtained so far are presented below.

2. TECHNOLOGIES

The investigated acid resistant technologies were selected based on the following hypotheses:

- 1) Limestone aggregate: Limestone is used as a sacrificial material in concrete neutralising the sulphuric acid, so that the rate of attack on the cement paste is reduced [Chang et.al. 2005].
- 2) Geopolymer binder: The fly ash based alkali activated binder results in an aluminium silicate polymer network that is known to have a good resistance to acids [Thokchom et. al. 2009].

- 3) Calcium aluminate cement: Calcium alumina hydrate is stable down to a pH around 3 or 4 and the dissolution of the calcium component of the other hydrates leads to the formation of additional quantities of this phase, which again fills in the pores, protecting the concrete from further attack and generally giving a smoother attacked surface with less aggregate loss [Scrivener et.al., 1999].
- 4) Slag cement: Blast furnace slag cement based concretes has a different pore distribution which leads to a substantially lower diffusivity and permeability compared to Portland cement based concretes. The microstructure of slag cement concretes makes the concrete less susceptible to sulphuric acid attack [Bijen, 1996].

3. EXPERIMENTAL

Concrete sewer pipe is most commonly produced from earth-moist concrete (zero slump concrete) using a combination of compression and vibration to compact the concrete. Samples ($\text{\O}100 \times 80$ mm) of a reference mix design currently used for production of $\text{\O}600$ mm sewer pipe and of selected mix designs representing the candidate technologies for improved acid resistance were prepared in a compactor. In the compactor specimens were prepared between two angled eccentrically rotating cylindrical piston heads, using a compaction pressure of 4 bars. Subsequently, the properties of the candidate mix designs were compared to the reference mix.

The following changes to the reference mix design were studied, see Table 1:

- Coarse and fine aggregate replaced by limestone aggregate on a volumetric basis
- Cement paste replaced by geopolymer-paste on a volumetric basis
- Portland cement and fly ash replaced by calcium aluminate cement, while maintaining w/c ratio and on a volumetric basis paste content
- Portland cement and fly ash replaced by slag cement (CEM III/B), while maintaining w/c ratio and on a volumetric basis paste content

Table 1 – Mix designs used for the experiments, all values having the unit kg/m^3

| Concrete type | Reference | Limestone aggregate | Geopolymer binder | Calcium aluminate cement | Slag cement |
|--------------------------|-----------|---------------------|-------------------|--------------------------|-------------|
| Portland cement | 332 | 332 | | | |
| Calcium aluminate cement | | | | 400 | |
| Slag cement | | | | | 385 |
| Fly ash | 74 | 74 | 380 | | |
| 0/4 sand | 709 | | 709 | 709 | 709 |
| 2/4 gravel | 250 | | 250 | 250 | 250 |
| 2/8 stone | 750 | | 750 | 750 | 750 |
| 0/2 limestone | | 700 | | | |
| 2/12 limestone | | 1020 | | | |
| Water | 127 | 127 | | 137 | 132 |
| Sodium silicate | | | 96 | | |
| Sodium hydroxide | | | 44 | | |
| Total | 2242 | 2253 | 2229 | 2246 | 2226 |

The alkaline activators used for the geopolymer were a 35 wt-% sodium hydroxide solution and a 40 weight-% sodium silicate solution with a $\text{SiO}_2/\text{Na}_2\text{O}$ molar ratio of 2.

After 28 days of storage immersed in water at 20 °C the samples were exposed to a 1 wt-%

sulphuric acid solution in order to investigate their sulphuric acid resistance based on a modified version of ASTM C267. At selected time steps up to 126 days of exposure, the samples were removed from the solution, rinsed under running water and weighed. Furthermore, the visual appearance was recorded and photo documented. At all the selected time steps the 1 wt-% sulphuric acid solution was replaced by fresh solution.

4. RESULTS AND DISCUSSION

The recorded relative mass change with time is shown in Figure 1. The reference samples had the largest weight loss and the samples containing limestone aggregate had the least weight loss – actually a slight weight gain was observed.

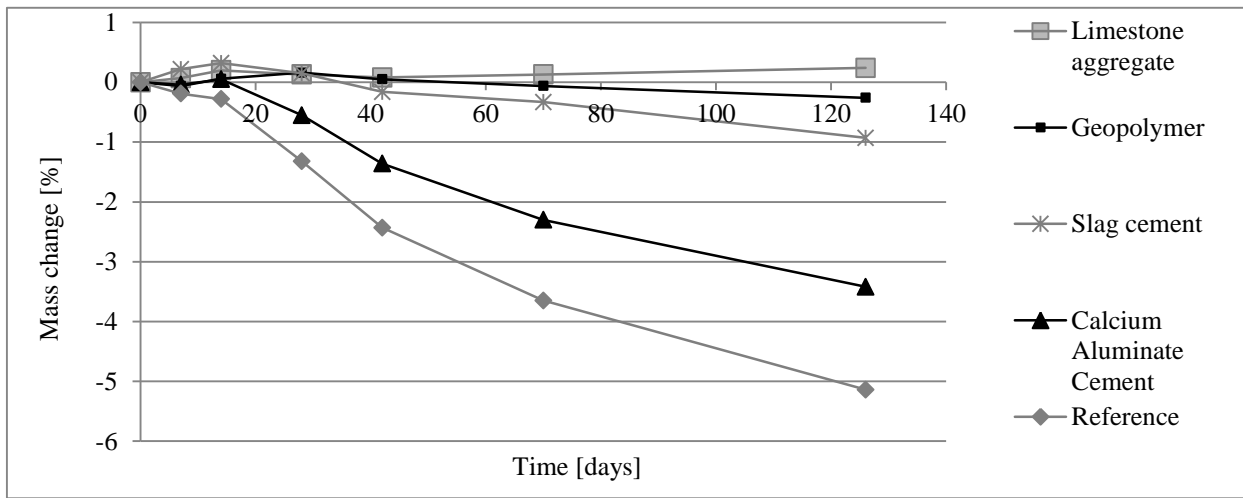


Figure 1 – Mass change of samples exposed to 1 wt-% sulphuric acid solution in relation to the start weight before exposure

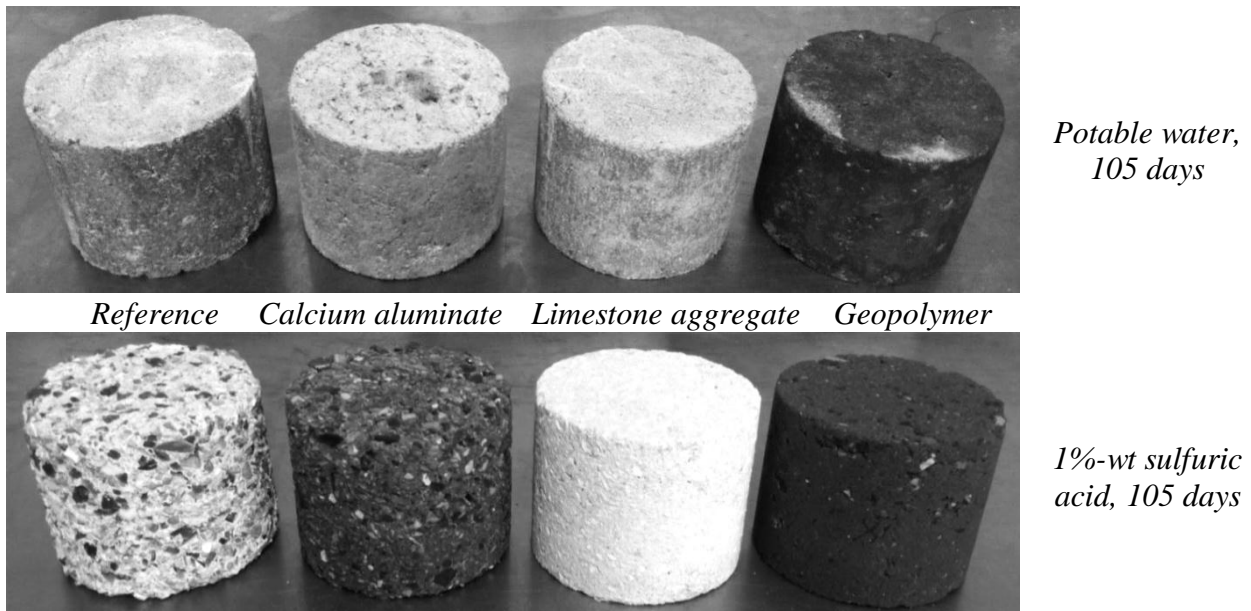


Figure 2 – Effect of storage solution

In Figure 2 the visual appearance of samples after 105 days of exposure is compared to reference samples stored in water. The surfaces of the reference samples and the samples with calcium aluminate cement appear very rough as a consequence of the cement paste being

attacked. When comparing the weight changes of the two mix designs, the samples with calcium aluminate cement have a lesser weight loss than the reference samples.

There is a tendency that the samples with limestone aggregate are gaining weight with time. The bright white coloured sample in Figure 2 indicates that a gypsum formation on the surface of the sample has occurred, which can explain the weight increase with time. The samples cast with geopolymer seem to have little change of surface appearance from the storage in the acid solution; however, a slightly rougher surface is observed which corresponds with the slight weight loss.

5. CONCLUSION

Laboratory experiments were conducted testing four different technologies to obtain more acid resistant concrete sewer pipe structures. All the tested technologies appear to perform better than the reference concrete composition currently used for concrete pipe production as evidenced by a smaller weight loss when exposed to a sulphuric acid solution. The most promising technology is to use limestone aggregate. Further studies are undergoing to investigate the different technologies in relation to resistance in aggressive environments and cost effectiveness versus service life. This includes exposure to actual sewer environment, full scale production of sewer pipe and implementing new technology for the construction of 500m trial sewer pipeline.

ACKNOWLEDGEMENT

The authors would like to thank all the involved project partners in particular the Environmental Protection Agency of the Danish Ministry of the Environment for their funding of the project.

REFERENCES

- Bijen, J., 1996
 “Blast Furnace Slag Cement for Durable Marine Structures”, Stichting BetonPrisma
- Chang, Z.T., Song, X.J, Munn, R., Marosszeky, M., 2005
 “Using limestone aggregates and different cements for enhancing resistance of concrete to sulphuric acid attack”, Cement and Concrete Research 35, 1486-1494.
- Miljøministeriet, Miljøstyrelsen, 2006
 ”Afløbssystemets levetid og renovering” Section 1.1 ”Baggrund”.
- Scrivener, K. L., Cabiron, J.L., Letourneux, R., 1999
 “High-performance concretes from calcium aluminate cements”, Cement and Concrete Research 29, 1215-1223
- Thokchom, S., Ghosh, P., Ghosh, S., 2009
 “Acid Resistance of Fly ash based Geopolymer mortars”, International Journal of Recent Trends in Engineering, Vol. 1, No. 6, May 2009. 4.
- Vollertsen, J., Vorkamp K., Hvitved-Jacobsen, T., 2002
 ”Udsivning af spildevand fra afløbssystemer”, Miljøstyrelsen, Miljøministeriet, Miljøprojekt nr. 685

MODELLING, ANALYSING AND TESTING
Cont.

Measurement and Modelling of Strength and Heat of Hydration for Young Concrete



Dr. Jan-Erik Jonasson
Professor
Luleå University of Technology
Dept. of Structural Engineering
jan-erik.jonasson@ltu.se



Dr. Mats Emborg
Head of R&D, Betongindustri AB
Professor
Luleå University of Technology
Dept. of Structural Engineering
mats.emborg@ltu.se



Dr. Hans Hedlund
Adj. Professor
Skanska Sverige AB and
Luleå University of Technology
Dept. of Structural Engineering
hans.hedlund@skanska.se

ABSTRACT

Strength development and heat evolution at hydration are two of the most important properties when analysing concrete structures concerning young age concrete, both for prediction of strength for different purposes and as a base when estimating crack risks.

The presented model for strength development is shown to properly predict the strength development at high early concrete temperatures during the hardening stage for different types of concrete.

The determination of the heat of hydration based on semi-adiabatic tests (insulated concrete samples without regulation of the concrete temperature) has been refined with respect to the warming up of the test equipment. The correct description of the total energy is given for two types of semi-adiabatic test equipments.

Key words: *Modelling, Testing, Strength, Heat of hydration, Adiabatic tests*

1. INTRODUCTION

For estimation of temperature and associated hardening of the young concrete, models of heat of hydration and strength development are needed. Important predictions of strength might be protection against harmful early freezing (usually 5 MPa), estimation of form removal time, and estimation of curing hardening times based on strength demands. Besides, heat of hydration and strength growth are essential properties as the base when estimating crack risks at early ages.

This paper focuses on two material related properties:

- The effect on temperature on strength development in concrete
- Estimation of heat of hydration using semi-adiabatic tests

1.1 Strength development

It is known since long, see for instance Davis et al (1933), that the influence of temperature on

strength development is twofold; 1) Partly a direct influence on the rate of hardening, known as the “maturity function”, see first part of Figure 1, where all curves coincide as function of equivalent time, and 2) Partly lower final strength values at higher curing temperatures, usually denoted as “cross over effect”, see left part of Figure 1a, or “strength reduction”, see right part of Figure 1.

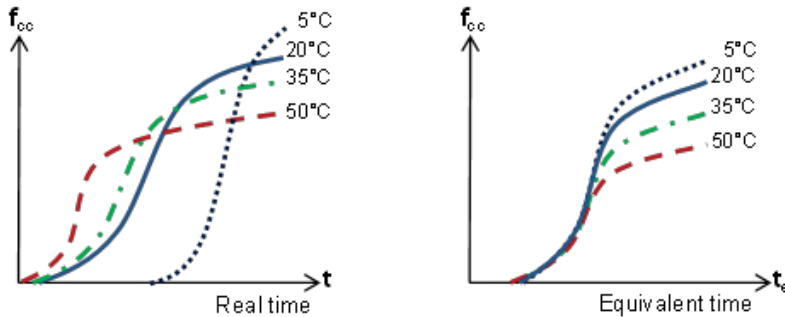


Figure 1 – Typically strength results for specimens cured between 5°C and 50°C, at left plotted in real time and to the right in equivalent time (Fjellström, 2013).

The main interest in this paper is modelling of strength growth for arbitrary curing temperatures, which includes both the maturity function and the cross over or strength reduction effect.

1.1 Heat of hydration

The heat of hydration of concrete can be based on different kinds of tests, and here the focus is on the evaluation of tests using the semi-adiabatic technique. The main interest is to examine the influence of the energy stored in the materials surrounding the concrete specimen in the test setup. This energy is traditionally ignored in relation to the energy stored in the concrete.

2 STRENGTH REDUCTION AT ELEVATED TEMPERATURES

The strength reduction at elevated temperatures is most probably an effect of the formation of different capillary pore distributions at different curing temperatures, which is supported by observations in Sellevold and Hauck (1997).

The model is based on the following assumptions:

1. The amount of gel formed at different temperature is controlled by a temperature dependent rate function (usually denoted maturity function or, more correct, temperature dependent maturity function)
2. The formation of the shape of capillary pores is dependent on the rate of hardening.

Usually the strength drop is defined as the strength reduction at elevated temperatures compared with curing at 20°C, which means that the potential strength gain at prolonged hardening at curing temperatures below 20°C, see typical behaviour for curing at 5°C in Figure 1, is ignored. For detailed information concerning the material related modelling of strength drop, see further Fjellström (2013).

Two examples of the modelling for tests with Swedish cements are presented in Figure 2 from Fjellström (2013). As can be seen in the figure, strength drop might be quite different for different types of cement, and at present no unified model for different binders exists. So, in general all important mixes, where high temperatures are expected, should be tested with respect to strength drop at elevated temperatures.

The model of strength drop has also been shown to work for British concretes with different amounts of PFA (Pulverised Fly Ash) and GGBS (Ground Granulated Blast-furnace Slag) added to OPC (CEM I) at the ready mix factory, see Figure 3. Figures 2 and 3 show that the evaluated

model for strength drop can be adapted for different compositions of cements and different types of SCM (Supplementary Cementitious Materials).

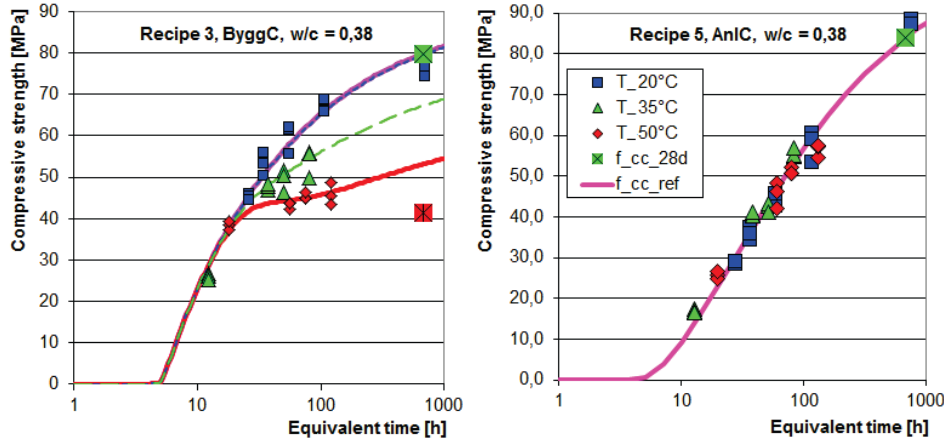


Figure 2 – Modelling of strength growth including strength drop at elevated temperatures for two concretes with the water-to-cement ratio = 0.38. The cement in Recipe 3 is of type CEM II/A-LL with about 13 % Limestone content, and Recipe 5 is made of cement type CEM I aimed for use in civil engineering structures. From Fjellström (2013).

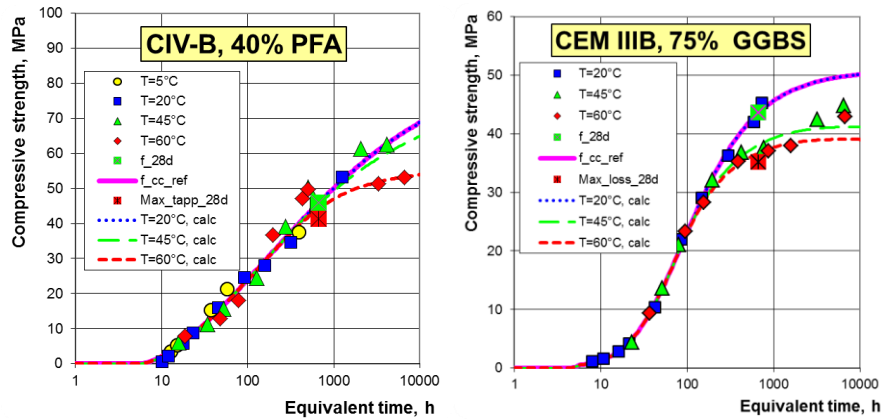


Figure 3 – Modelling of strength drop for British concretes with addition of fly ash (PFA) or slag (GGBS). From Jonasson (2014).

2. HEAT OF HYDRATION AND EFFECTS OF ENERGY IN THE TEST SETUP

Traditional evaluation of semi-adiabatic tests with concrete do not take into account the effect of energy stored in the materials of the test setup except the energy stored in the concrete specimen, which can be formulated by $\eta = 1$ in Eq. 1. The traditional evaluation is based on the assumption that the effect of heat energy in the test setup materials is assumed to be neglected. Besides, the refined model with $\eta > 1$ in Eq. 1 only influences the shape of the hydration curve, not the total evolution of heat in the concrete. The heat of hydration evaluated from semi-adiabatic tests is expressed, see further details in Fjellström (2013), as

$$q_{cem} = \frac{\rho_c \cdot c_c}{C} \cdot \left[\eta \cdot (T_c(t) - T_{air}) + a \cdot \int_0^t (T_c(t) - T_{air}) \cdot dt \right] \quad (1)$$

The analytical evaluation of the correction factor $\eta > 1$ is presented in Fjellström (2013) for an associated sphere for the temperature profile for a stationary heat flow. Two different semi-adiabatic test situations, a cylindrical and a square shaped equipment, see Figure 4, have been analysed.

The resulting correction factors, η , for the test equipments in Figure 4 are given in Figure 5. For the analysed semi-adiabatic cylindrical test setups the correction factor is in the size of order of 1.07 and 1.14, respectively, and for the used square shaped test setup the correction factor is

approximately 1.1. The effect of these corrections is that the calculated maximum temperature at application for structures is increased, see further Fjellström (2013).

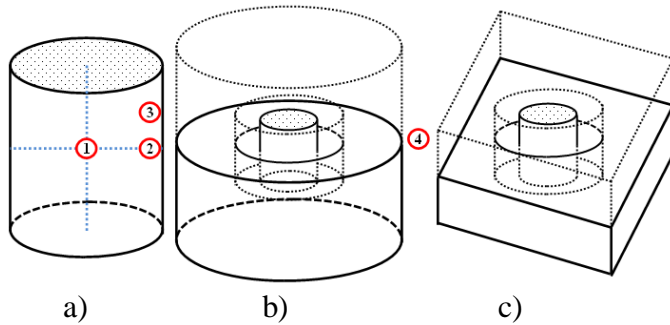


Figure 4 – Analysed semi-adiabatic equipments b) and c) with cellular plastic as insulation material. In addition, test equipment c) has an outer layer of plywood. a) = concrete test specimen; b) = cylindrical shaped; and c) = square shaped test equipment. From Fjellström (2013).

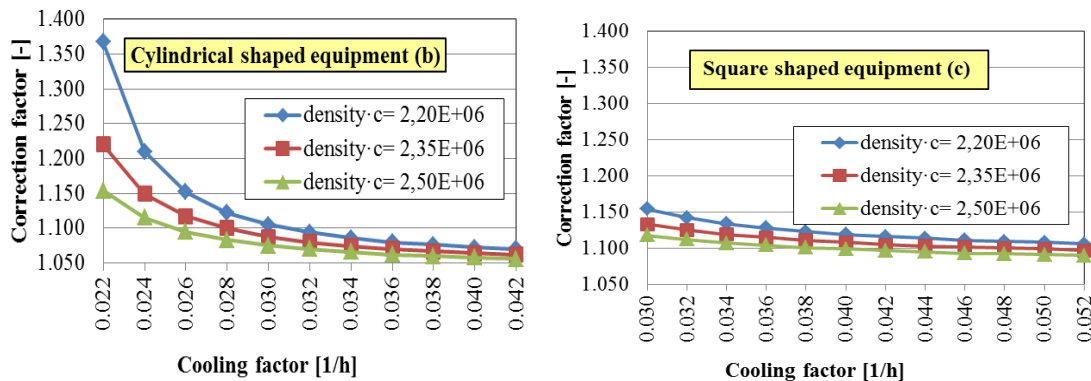


Figure 5 – Resulting correction factor, η , for a cylindrical and a square shaped semi-adiabatic test setup. From Fjellström (2013).

3. CONCLUDING REMARKS

Within the areas of evaluation of tests on strength growth and on heat of hydration the following concluding remarks are stated:

- The model for concrete strength growth at arbitrary curing temperatures including strength reduction at elevated temperatures is robust, which is demonstrated for different types of cements and different types of supplementary cementitious materials.
- The refined model for evaluation of heat of hydration including the effects of energy stored in the semi-adiabatic test setup is presented for both a cylindrical shaped and a square shaped semi-adiabatic equipment. The energy stored in the analysed test setups materials are approximately ten per cent of the energy stored in the concrete test specimen.

REFERENCES

- Davis R E, Carlson R W, Troxell G E, and Kelly J W, 1933,
 “Cement Investigations for the Hoover Dam”, Journal of the American Concrete Institute - Proceedings at the 29th annual Convention, Chicago, February 21-23 1933, pp. 413-431.
- Fjellström P, 2013,
 “Measurement and Modelling of Young Concrete Properties”, Licentiate thesis, Luleå University of Technology.
- Jonasson J-E, 2014,
 “Evaluation of Recent Tests with Respect to Modelling the In Situ Strength of Concrete”. Part of the ICE Research Project 1004 (in progress April 2014).
- Sellevold E J and Hauck C J, 1997,
 “Effect on Curing Temperature and Silica Fume on the Pore Structure of Hardened Cement Paste”, Contribution in Report TVBM 3078, Lund Institute of Technology, pp164-169.

Thermal Crack Risk Estimations - Equivalent Restraint Method Correlated to Empirical Observations.



Anders Hösthagen
M.Sc. Ph.D. Student
Projektengagemang AB &
Lulea University of
Technology
Dept. of Structural
Engineering
Email: anders.hosthagen@
projektengagemang.



Dr. Jan –Erik Jonasson
Professor
Lulea University of
Technology
Dept. of Structural
Engineering
Email: jej@ltu.se



Dr. Mats Emborg
Professor
Lulea University of
Technology
Dept. of Structural
Engineering
Email: Mats.Emborg@ltu.se



Dr. Hans Hedlund
Adjunct professor
Skanska Sverige AB
And Lulea University of
Technology
Dept. of Structural
Engineering
Email:
hans.hedlund@skanska.se



Kjell Wallin
Consulting Engineer
Projektengagemang AB
Email:
kjell.wallin@projektengage
mang.se

ABSTRACT

The present study deals with the correlation between numerical models and empirical observations in newly cast concrete structures. The model used is the equivalent restraint method, ERM, which is established from several local restraint method calculations, LRM. The casting of walls in a tunnel construction is investigated. Correlation between models and empirical measurements is established in three steps: 1) the restraint situation is analyzed; 2) the calculated temperature developments are compared to empirical temperature measurements to calibrate the models; and 3) calculated strain ratios are compared with observed crack patterns, and in general a good correlation is achieved.

Key words: Local restraint method, equivalent restraint method, cracking, modelling, early age concrete.

1. INTRODUCTION

The movements within newly cast concrete are heritage from temperature and moisture states and may cause cracking during the construction. For complex structures, such as bridges, tunnels, foundations and piers, comprehensive pre-calculations need to be performed in order to analyze the risk of through and surface cracking. If high strains/stresses are predicted for some part of the construction, measures are needed to avoid cracking. Examples of measures are

cooling of the young concrete, preheating of the adjoining construction and/or optimized concrete mix (alternative binders, lower cement content etc.). In the case of casting section against an adjoining structure or a restraining entity (such as rock, subgrade), the restraint influencing on the newly cast concrete increases, and with high restraint the risk of cracking becomes higher. It is understood that to design the measures in a cost-effective fashion reliable calculations are needed. It is known that the restraint is usually difficult to estimate correctly and therefore is an uncertain factor. Different models to estimate the risk of cracking have benefits and withdrawals. Here the model called equivalent restraint method, ERM /Al-Gburi 2012/, is used. The benefits of this method are the possibility to extract the restraint analyzed by elastic 3D calculations and implement it into a compensated plane method for young concrete. These calculations are efficient from a time saving point of view compared with the use of a 3D viscoelastic- viscoplastic simulation for young concrete. Furthermore, the ERM makes it possible to analyze arbitrary measures on site, cooling and/or heating.

2. AIMS AND OBJECTIVES

Aims and purposes of the present research are to:

- Investigate different casting order when pouring walls on a base slab, and specially analyze the influence on restraint when casting a segmented wall in series (Case 1) or casting a wall in between two completed walls (Case 2).
- Correlate the estimated crack risk to empirical observations of the resulting crack pattern using the numerical model ERM (Equivalent Restraint Method, /Al-Gburi 2012/).

3. CALCULATIONS AND RESULTS

3.1 Restraint conditions

The studied situation is shown in Figure 1. A wall segment (thickness = 1.2 m, height = 8.35 m and length = 17.5 m) is cast on a base slab (width = 3.5 m, height = 1.2 m and length = 17.5 m). In the figure Case 1 means that one of the end walls is cast as the last wall, and for Case 2 the intermediate (second wall) is cast between two existing walls.

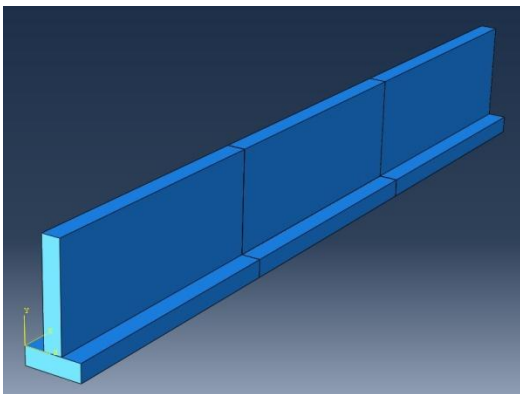


Figure 1 – Illustration of three casting sequences for typical case wall-on-slab. In Case 1, one of the end walls is the last casting, and in Case 2 the intermediate wall is the last casting.

For the walls the direction of interest is along the X-axis (longitudinal direction), and the corresponding restraint is shown in Figures 2 and 3. The restraint calculations are performed using the program Abaqus. Stresses/strains in the longitudinal direction cause the typical crack pattern where cracks appear perpendicular to the joint between the base slab and the wall, see Figure 4. The geometry in the figure is described by Case 1.

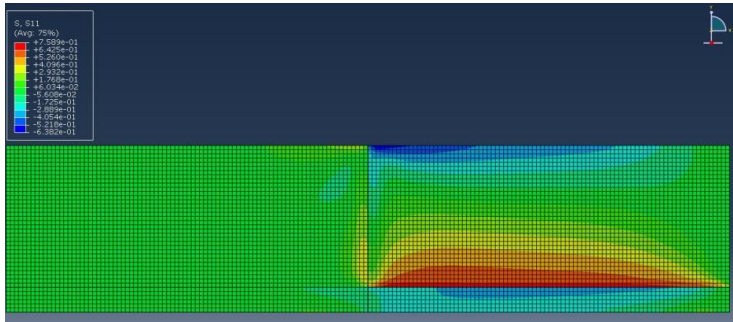


Figure 2 – The restraint profile for Case 1. Elastic calculations using the program Abaqus, where the newly cast concrete is contracting homogeneously.

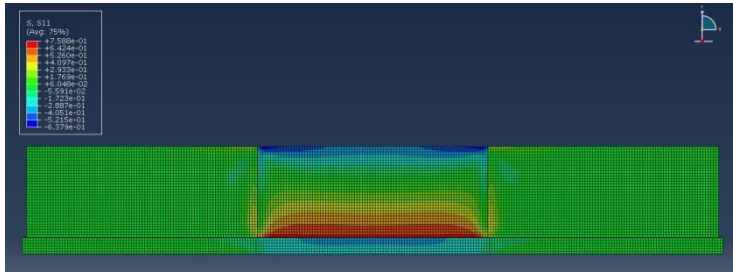


Figure 3 – The restraint profile for Case 2. Elastic calculations using the program Abaqus, where the newly cast concrete is contracting homogeneously.

From the restraint analysis presented in Figures 2 and 3, it is seen that the maximum restraint in the two cases are similar, 0.76 for both cases. The main difference is that the distribution of the restraint in the latter case shows a more extensive distribution of high restraint. This is probably the explanation why more cracks were observed in Case 2 than in Case 1 for the studied tunnel construction.

3.2 Observed crack pattern and post-calculation for Case 1

With the aim of meeting the requirements of a crack free situation cooling pipes in the walls were used. However, despite the cooling, during a period with the daily mean temperature of about 5° C cracks occurred in the walls and the observed crack pattern for Case 1 is shown in Figure 4.

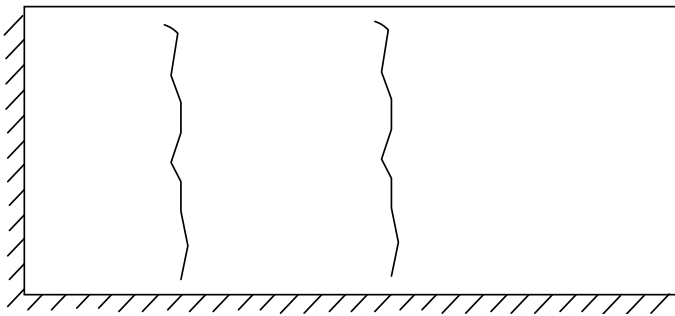


Figure 4 – Observed cracks at a 1.2 m thick, 8.35 m high and 17.5 m long wall of Case 1.

The situation for the observed crack situation is now estimated in a post-calculation using the ERM with the existing cooling pipes and the registered environmental temperatures.

The procedure starts with the restraint conditions presented in Figure 2 described by corresponding LRM (Local Restraint Method, see /Al-Gburi 2012/) strain ratios for the actual situation. The result from the subsequent regression analysis using ERM to resemble the LRM strain ratio values is presented in Figure 5 for the base situation without any measures on site.

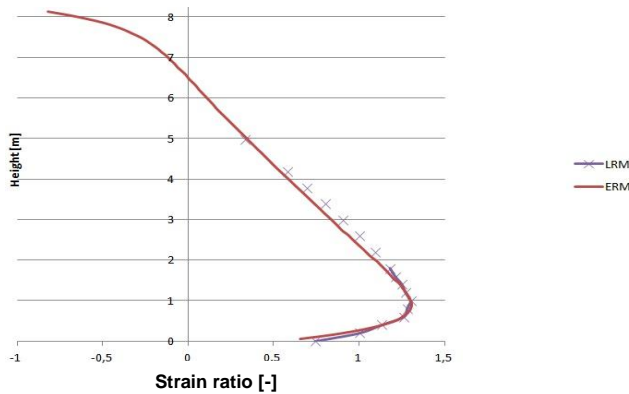


Figure 5 – Resulting ERM to resemble the LRM strain ratios without measures.

The same cooling pipes as in the observed situation are now introduced in the ERM, and the resulting strain ratio at the position of the maximum strain ratio as a function of time is shown in Figure 6. From the figure it is seen that the calculated strain ratio about 10 days (240 h) after time of casting reaches the maximum level of about 0.94, and that the high strain ratio remains for a rather long period of time. From follow up calculations of cracked situations it is stated in / Larson 2000/ that cracks were observed for estimated strain ratios of about 0.80 to 1.05. So, the conclusion here is that the numerical modelling gives a clear indication that the wall is in danger of cracking during the current parameter set. The observed status of the construction part shows a moderate crack pattern suggesting that the strain within the construction is just enough to create cracks.

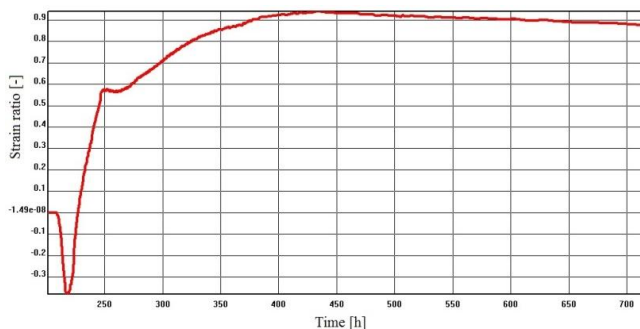


Figure 6 – Strain ratio versus time in the ERM model for the design position about 1 m above the joint in the wall showed in Figure 5.

4. CONCLUDING REMARKS

The calculation of restraints most likely explains why more cracks were observed casting intermediate walls than casting end walls.

For the study of a cast end wall a good correlation between the ERM and empirical observations was shown.

REFERENCES

- Al-Gburi M., Jonasson J-E., Nilsson M., Hedlund H. & Hösthagen A., 2012, "Simplified Methods for Crack Risk Analyses of Early Age Concrete - Part 1: Development of Equivalent Restraint Method", Nordic Concrete Research No. 46, 2012/2.
- Larson M., 2000, "Estimation of Crack Risks in Early Age Concrete – Simplified Methods for Practical Use", Licentiate Thesis 2000:10, Luleå University of Technology, Luleå. 2000.

Bridge deck concrete overlays – full scale studies and theoretical analysis



Martin Persson
M.Sc., Ph.D. Student
Div. Structural and Construction Engineering/Ramböll Sverige AB
Luleå University of Technology/Ramböll Sverige AB
S-971 87 Luleå/SE-104 62 Stockholm
E-mail: martin.persson@ltu.se/martin.persson@ramboll.se



Ulf Ohlsson
Ph.D.
Div. Structural and Construction Engineering,
Luleå University of Technology
S-971 87 Luleå
E-mail: ulf.ohlsson@ltu.se



Mats Emborg
Prof. /Head R&D
Div. Structural and Construction Engineering/Betongindustri AB,
Luleå University of Technology/ Betongindustri AB,
S-971 87 Luleå/100 74 Stockholm
mats.emborg@ltu.se/mats.emborg@betongindustri.se

ABSTRACT

Concrete overlays on bridge decks are thought to be more durable when comparing with the more common solution with asphalt. Of interest is to evaluate the concrete overlay regarding traffic and shrinkage/temperature induced stresses. In a pilot study nondestructive test systems were evaluated with focus on detecting hidden defects, (e.g. debonding), that may have induced identified surface cracks. Furthermore, calibration of material parameters for a similar composite slab was done using finite element technique and compared with experimental studies in laboratory. Good agreement was found between numerical and experimental results. This will serve as an input for future bridge FE-models.

Keywords: Concrete, Bridge overlay, Cracking, Modelling, Nondestructive testing.

1. INTRODUCTION

Bridge decks are important elements of the infrastructure. A critical detail on bridge decks is the top layer which protects the structural concrete of the deck against environmental loads such as rain, snow, de-icing salt etc. The most common solution is to apply an impermeable layer on the structural concrete with a wearing course of asphalt, Figure 1a. However, frequently this solution suffers from damages e.g. formation of bubbles in the impermeable layer early at service stage, causing leakage of water and chloride ion entrainment, leading to costly repair. At construction, the system is complex, includes many moments and is time consuming.

An alternative to the one above is an overlay by a high performance concrete cast directly onto the structural concrete, Figure 1b. A relatively large amount of bridges managed by the Swedish transport administration have already been accomplished with overlays of concrete, more than 500, even though the share of total concrete bridges is low - about 5% /Sundquist, 2011/.

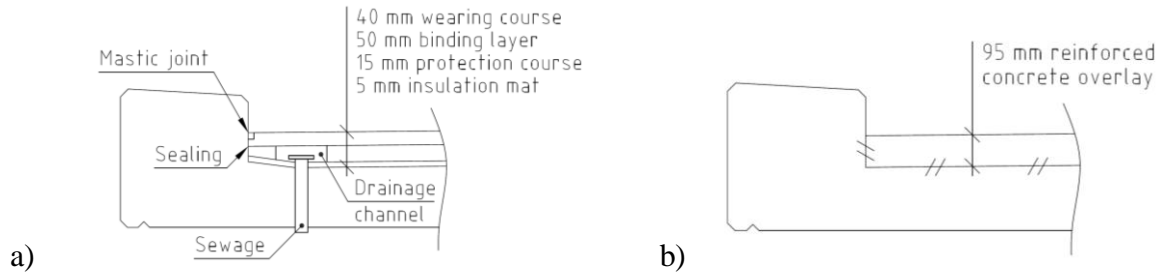


Figure 1 – Typical and common solutions for protection of structural bridge decks by insulation mat, etc. (a) and directly cast concrete overlay (b).

The system with directly cast overlays of concrete, is environmental friendly; no epoxy primers, durable, has lower noise levels from traffic, is cost effective; long life-time, low maintenance, robust structure, has no drainage channels (avoidance of performance problems at construction and no expensive maintenance costs), gives light pavement, i.e. optical advantage and includes few moments at construction.

Important issues for concrete overlays are general performance with respect to external loads as well as cracking due to shrinkage and/or temperature strain and bond to substrate. The effects of these phenomena are however not fully understood and there is a lack of knowledge regarding performance, design, analysis, construction etc., especially when new types of concrete are used. Thus, the objectives of the newly started Ph.D. project (with support from the Swedish transport administration) is to secure the performance of concrete overlays for a sustainable structure, i.e. concrete overlays with high durability, low maintenance cost and optimization regarding material usage and global environmental loads. The project includes laboratory tests, full scale observations and theoretical analysis. Below some examples are given.

2. THEORETICAL STUDIES IN COMPARISON WITH LABORATORY STUDIES

To evaluate the behaviour of a bridge deck with a concrete overlay FE analysis is performed by means of the program ATENA /Červenka et al, 2013/. Initially comparisons are performed with laboratory tests /Silfwerbrand, 1987/ on simply supported slabs featuring an overlay concrete (Figure 2) aiming at calibrating material and structural models. The shrinkage of the concrete is modelled in a simplified way. Result components (e. g. shear- and normal stresses along composite interface due to shrinkage and vertical point load are shown in Figures 6 and 7.

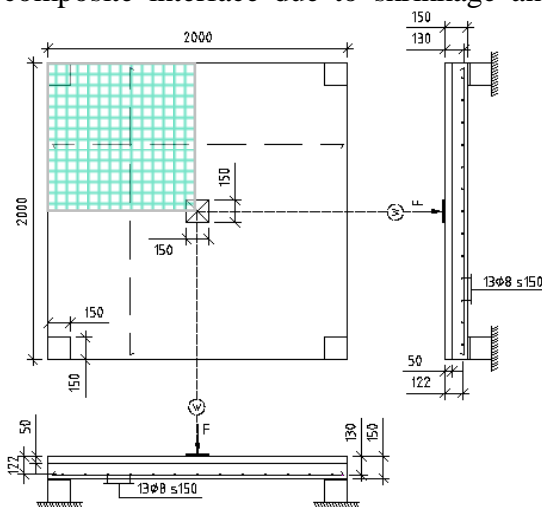


Figure 2 – Lab-test /Silfwerbrand, 1987/.

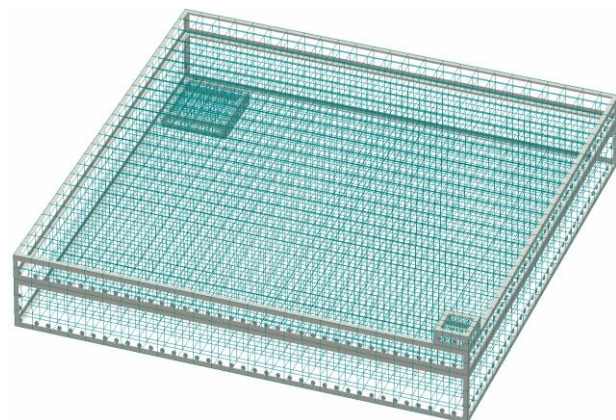


Figure 3 – FE mesh in ATENA (1/4 of the slab)

Figure 3 shows the ATENA model of the simply supported slab. Only $\frac{1}{4}$ of the slab is modelled due to the symmetry. A comparison with load-deflection curves from the test (Figure 4) show that agreements are good up to first cracking between registered and calculated loads. For higher loads however a rather large scatter occurs, whose reasons will be further analysed in the project. In next step a more accurate modelling of shrinkage and creep will be made to be able to analyse the global bridge behaviour with different types of overlays, types of external loading and shrinkage and thermal situations.

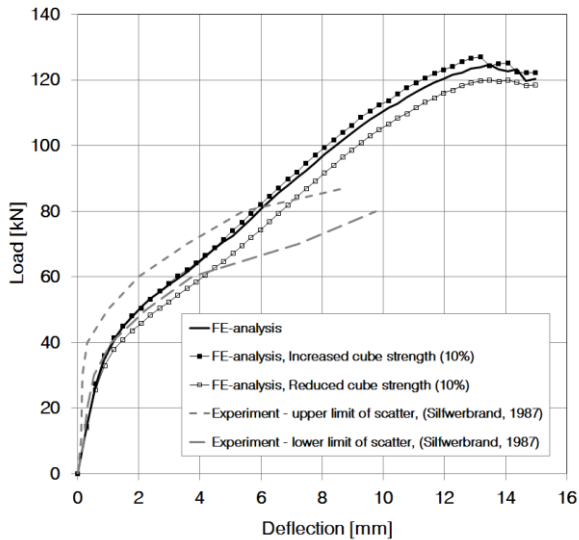


Figure 4 – Load-deflection curve for a point load F , at $(x,y) = (1,1)$.

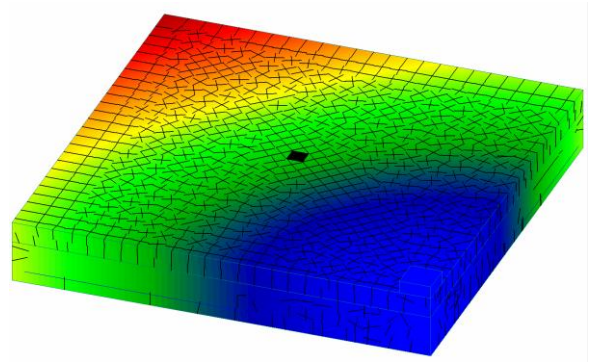


Figure 5 – Shrinkage and bending cracks at deflection $\delta_{zz} = 6$ mm.

Figure 5-7 show shrinkage and bending cracks and stresses in the interfacial zone concrete overlay and structural concrete. The highest shear stresses occur near the point load and along the edges. Tensile normal stresses occur near the edges.

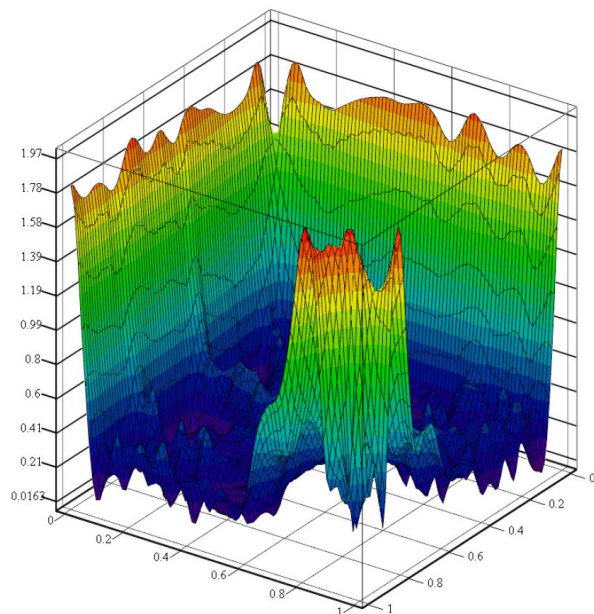


Figure 6 – Effective shear stress, τ_{eff} at deflection $\delta_{zz} = 6$ mm.

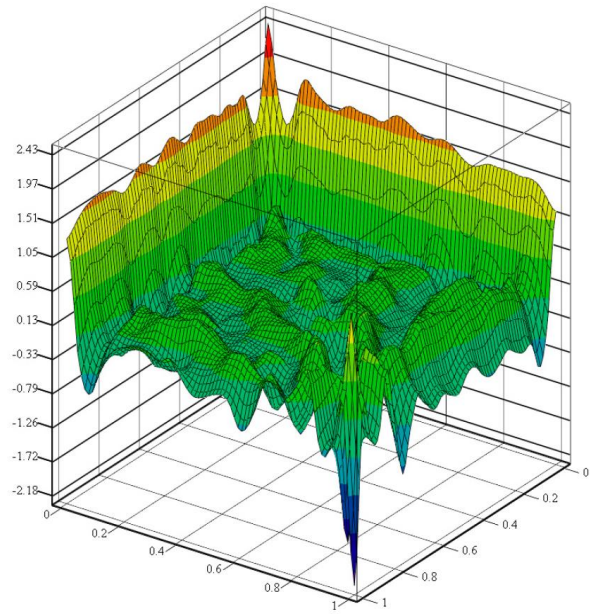


Figure 7 – Normal stress, σ_{zz} at deflection $\delta_{zz} = 6$ mm.

3. FULL SCALE OBSREVATIONS

To gain an initial overview of the overall behaviour of directly cast overlays in the bridge system, two bridges have been studied in full scale observations. Nondestructive test methods were used (*s'MASH* detecting voids, deboned areas etc., *Surfer* detecting crack depths and widths) as well as infra-red camera mapping, visual inspection, surface crack width detections and drill core samples. Figure 8 shows example of observed cracking (probably plastic shrinkage cracking) of overlay and Figure 9 shows grid of *s'MASH* and *Surfer* cracking and delamination detection.



Figure 8 – Diagonal plastic shrinkage cracks in full scale observations

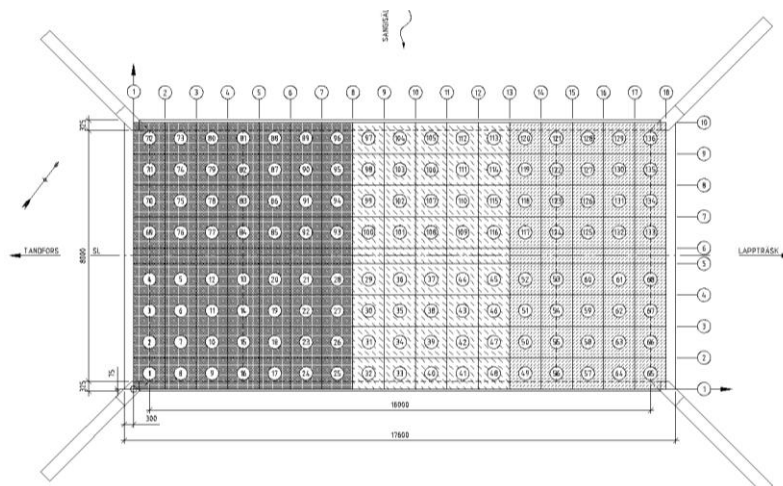


Figure 9 – Mapping-grid for Surfer and *s'MASH*

4. CONCLUSION

It is concluded that it seems possible to use the ATENA program to model the behaviour of external loads properly for small scale concrete slabs. However, regarding estimations of effects of shrinkage and thermal effects as well as global behaviour of bridge decks with concrete overlay, deeper studies are needed to have a base for conclusions. Full scale observations (health monitoring) are important to obtain a picture of the status of bridges constructed in similar way to be able to estimate needs for possible renovation. This is also important for knowledge gain as an input for future design and construction.

REFERENCES

- Červenka, V., Jendele, L., Červenka, J., ATENA Program Documentation, Part 1, Theory. Prague, 2013, 268 pages.
- Silfwerbrand, J., "Effects of differential shrinkage, creep and properties of the contact surface on the strength of composite concrete slabs of old and new concrete". Stockholm, Sweden: Structural Engineering, Royal Institute of Technology, Rapport nr 147, 1987, 131 pages. (In Swedish)
- Sundquist, H. (editor), "Robust brobanepatta. State-of-the-art och förslag till FUD program", Sveriges Bygg universitet, 2011, 123 pages. (In Swedish)

Nonlinear modelling of the dynamics of accelerated hardening of concrete



Abhay Bulsari
Ab Nonlinear Solutions Oy
Turku/Åbo
Finland
E-mail: abulsari@abo.fi



Erik Nordenswan
Nordkalk Oy Ab
Pargas
Finland
E-mail: Erik.Nordenswan@nordkalk.com

ABSTRACT

Achieving a certain desired release strength in a certain period of time is essential in production of precast concrete products like hollow core slabs. To determine cost optimal recipes which will attain a desired strength in a specified time, it is necessary to have quantitative information on the effects of the composition variables on the hardening curves, which show the strength as a function of time. It is not feasible to use physical modelling to relate the composition variables with the strength of concrete as a function of time. Conventional methods of empirical modelling are linear statistical techniques which are not very suitable for describing complicated nonlinear effects which are present in the dynamics of hardening. New techniques of nonlinear modelling, however, are very suitable, as has been demonstrated by many examples on concrete earlier, and this work also illustrates the same.

Key words: Concrete, admixtures, accelerators, precast concrete, modelling

1. INTRODUCTION

Pre-stressed hollow core slabs are produced on long pallets with extruders which are able to compact no-slump concrete so that the product needs no supporting moulds. The pre-stressing strands are tensioned before extruding and the pre-stressing forces are transferred to the hardened concrete by cutting the slabs with a diamond saw. A certain strength level is required for the transfer to secure a good bond between the strands and the concrete, and to avoid loss of pre-stress because of creep and elastic deformation of the young concrete. It is therefore essential to control the strength before the transfer of pre-stress forces.

The hardening of concrete strongly depends on the temperature, and heating can be used in order to reduce the hardening time. For this reason, testing of the concrete at a constant temperature is not sufficient. When evaluating the performance of concrete mixes containing accelerators it is necessary to obtain data for accurate prediction of the reaction heat liberation, relation between reaction rate and temperature and the development of strength. This can be done by combining calorimetric methods and strength testing.

Figure 1. The production facility for the accelerator

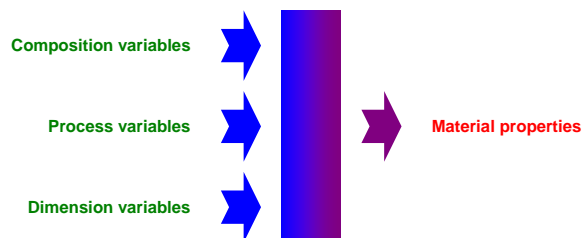


Recent research shows that the early reactions of cement are controlled by nucleation and growth. New accelerators have been developed in order to facilitate those processes. Calcium carbonate is a very favourable substrate for growth of the reaction products of cement and water. In this test series the performance of a modified limestone filler has been tested.

2. NONLINEAR MODELLING

For materials development work, we are usually interested in achieving certain combinations of material properties. In case of concrete, these are typically mechanical properties and flow properties, and sometimes thermal properties. All kinds of material properties depend on composition variables, process variables of the process by which they are produced or prepared, and sometimes we also need dimension variables. That is summarised in Figure 2.

Figure 2. A schematic diagram for nonlinear modelling of material properties



There is hardly any material behaviour which is absolutely linear. To treat the nonlinearities, one can use various techniques of nonlinear modelling. The newer methods include feed-forward neural networks, kernel regression, multivariate splines, etc. which do not require *a priori* knowledge of the nonlinearities in the relations. Feed-forward neural networks have the so-called universal approximation capability /Hornik 1989/ which make them particularly suitable for most function approximation tasks we come across in engineering and in process industries.

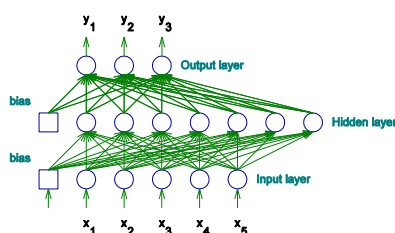


Figure 3. A typical feed-forward neural network

Feed-forward neural networks consist of neurons in layers directionally connected to others in the adjacent layers (see Figure 3). There are many different types of neural networks, and some of them have practical uses in process industries /Bulsari 1995/. Neural networks have been in use in process industries for about twenty years /Bulsari 1998/. The multilayer perceptron, a kind of a feed-forward neural network, is the most common one. Most neural network applications in industries are based on them, including our earlier work on concrete and aggregates /Bulsari 2008/

3. EXPERIMENTATION

Concretes with different compositions (one cement, water, one admixture, one accelerator, fly ash and three aggregates) were prepared in a laboratory scale mixer and compacted in an IC-tester to a fixed degree of compaction. The number of cycles was recorded as the workability.

4. NONLINEAR MODEL OF HARDENING DYNAMICS

Hardening of concrete takes place because of several phenomena. Thus, phenomenological modelling is not very feasible, but from a moderately small number of experiments, empirical or semi-empirical nonlinear models can be developed, which can then be used to determine good recipes. The dynamics of hardening of concrete can be written as follows:

$$\frac{dY}{dt} = f(C_{cement}, C_{water}, C_{superplasticizer}, C_{accelerator}, \dots, T)$$

where Y is the compressive strength, C_k are the concentrations of k , and T is the temperature. The hardening rate goes through a maximum a few hours after water has been added. Then the hardening rate drops and then reduces slowly. It is clear that linear statistical methods are not very suitable for approximating this function.

The rms (root mean square) error of the selected model was 1.06 MPa over a range of 8 to 40 MPa. This amounts to a correlation coefficient of about 98%.

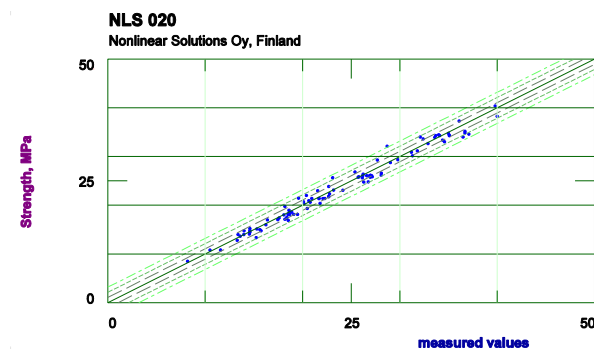


Figure 5. A comparison of measured values of compressive strength with the values predicted by the nonlinear model

Figure 5 shows a comparison of the measured values of compressive strength with the values predicted by the nonlinear model. Most observations have been predicted very well by the nonlinear model. This is possible because the experimental data has been consistent.

The accelerator affects the hardening dynamics positively such that a given strength, typically the release strength, is achieved earlier. Figure 6 (a) shows the effect of the accelerator on the

strength development as a function of time. Increasing the amount of accelerator increases the strength at any given time and the rise is slightly earlier. That is visible from Figure 6 (b) in terms of hardening rate.

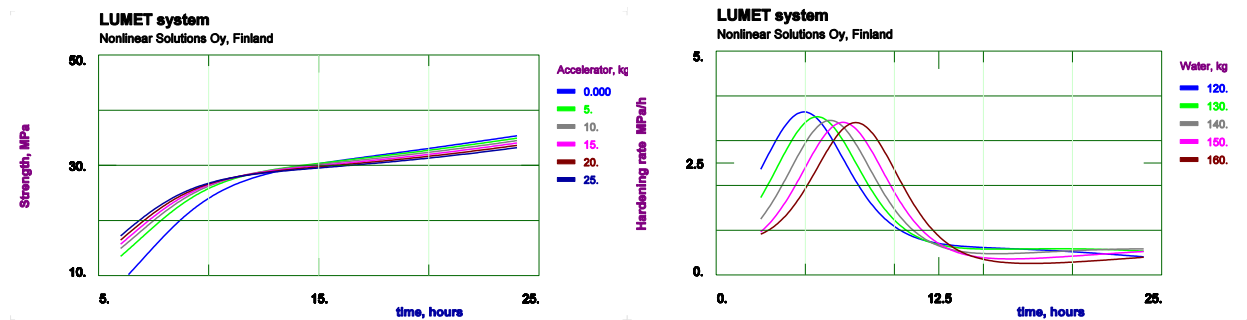


Figure 6. (a) Effect of the accelerator on hardening curves as predicted by the nonlinear model
(b). Effect of the accelerator on hardening rate curves as predicted by the nonlinear model

This work demonstrated how from a moderately small experiment series, it was possible to develop nonlinear models of hardening dynamics. This kind of nonlinear models can be used for optimisation of recipes for given release strength and time. Small amounts of accelerator can lead to significant savings in cement.

5. CONCLUSIONS

Nonlinear modelling turned out to be a very effective tool for describing the hardening dynamics of concrete for hollow core slabs. The effects of cement, water, admixture and accelerator on the hardening rates of concrete are fairly complicated and highly nonlinear.

REFERENCES

- Bulsari, A., 1995
(ed.), *Neural Networks for Chemical Engineers*, Elsevier, Amsterdam, 1995
- Bulsari, A., 1998
"Quality of nonlinear modelling in process industries", Internal Report NLS/1998/2
- Bulsari, A., Nordenswan, E. & Käppi, A. 2008
"Nonlinear models help reduce cement consumption by better packing of aggregates", *Concrete Plant International*, No. 2 (April 2008) 32-36
- Hornik, K., Stinchcombe, M. & White, H. 1989
"Multilayer feedforward networks are universal approximators," *Neural Networks*, Vol. 2, (1989) 359-366

Using Isothermal Calorimetry to predict early Mortar Strengths



Lasse Frølich Engsig
M.Sc., Civil Engineer
Aalborg Portland A/S
Rørdalsvej 44, DK-9100 Aalborg
E-mail: lasse.f.engsig@aalborgportland.com

ABSTRACT

This study investigates whether isothermal calorimetry measurements on cement paste are sufficiently accurate and precise to replace standardised strengths measurements on mortar. The test series is designed to provide information on the mechanisms that will affect the relationship between heat of hydration and early strengths – not to establish an empirical relationship. Results show a repeatability of strengths and calorimetry measurements in the same magnitude. Isothermal calorimetry could therefore be a viable alternative to early age strength measurement.

Key words: Heat development, Isothermal calorimetry, Cement, Testing

1. INTRODUCTION

Measuring the heat of hydration (HoH) in concrete can be useful for several applications. For massive constructions such measurements are often used to predict the heat development over time and the risk of thermal cracking. Concrete HoH is often measured by adiabatic or semi-adiabatic calorimetry.

For cement investigations isothermal calorimetric measurements with higher precision is more suitable. This type of measurements on paste will provide a signature like a fingerprint for the particular cement. Special attention has to be taken to the sulphate/alumina balance as described in /Sandberg 2005/. Procedures for measuring hydration kinetics by isothermal calorimetry are described in /ASTM C 1679 2008/. The principles from this publication have been applied to a great extent in this study.

For Portland cement the chemical composition and the fineness are of special importance for the HoH. In figure 1 the heat production rate from cement paste is shown schematically.

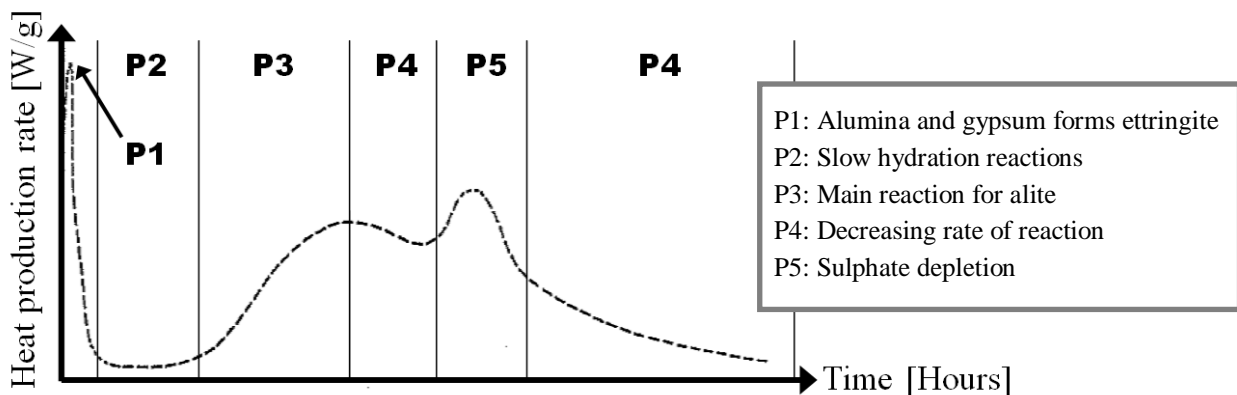


Figure 1 – Heat production rate at 20 °C illustration of periods. From /Hansen 1978/.

The purpose of this study is to test whether isothermal calorimeter is a viable alternative to standardised 1 day mortar strength measurements. Calorimeter measurements have the

advantage of being less labour intensive to perform and do furthermore provide information on hydration kinetics.

It is assumed that parameters affecting the rate of reaction of alite (C_3S) will give the same relative response to the HoH and strengths. Factors which give a different response are assumed to include alumina (C_3A) content, C_3A reactivity and the SO_3/C_3A ratio. I cases where the C_3A reaction is not sufficiently balanced by SO_3 , higher HoH will generally be expected to correspond to lower strengths.

This study includes investigation of a number of parameters affecting HoH and strengths. As an example 1.0 % extra alkali has been added to the reference cement to measure whether the response to HoH and early strengths is the same. The level of extra alkali (and other modifications) does not correspond to typical cement variations; i.e. significantly higher levels have been chosen. This is because it is a general study of parameters more than an empirical study.

2. EXPERIMENTAL

2.1 Materials

A low alkali sulphate resistant Portland cement CEM I 42.5 N - SR 5 (EA) has been used as reference cement. Properties of the cement are given in table 1.

Table 1 – Properties of reference cement

| Property | Result |
|--|------------------|
| Strengths - EN 196 {1, 2, 7, 28 days} (MPa) | {10, 17, 29, 57} |
| Initial setting time - EN 196 (min) | 100 |
| Fineness – EN 196 Blaine (m^2/kg) | 360 |
| Bogue clinker { C_3S , C_2S , C_3A , C_4AF } (%) | {47, 29, 5, 12} |
| Eq. total alkali (%) | 0.32 |
| SO_3 (%) | 2.7 |

2.2 Mix designs

The reference cement has been modified in a number of ways – see table 2. Details on modifications are given in the following:

- C_3S content has been boosted by replacing some of the cement by a white cement CEM I 52.5 R - SR 5 (EA) with a particularly high C_3S content (Bogue app. 77 %).
- Fineness has been increased by further grinding in a laboratory scale mill
- Limestone filler with high fineness (Blaine app. 1200 m^2/kg) has been added
- C_3A content has been increased by adding synthetic C_3A . XRD analysis have proved this C_3A to be 94% cubic and 6 % orthorhombic
- Alkali content has been increased by adding Sodium Hydroxide
- Chloride content has been increased by adding Calcium Chloride
- Sulphate content has been increased by adding hemihydrate

Extra added C_3A and sulphate are expected to give a different relative response between strengths and HoH. Other modifications are expected to give same relative respons.

Table 2 – Composition of mixes

| Mix nr. | Composition |
|---------|--|
| 1 | 100 % reference cement |
| 2 | 75 % ref. cement + 25 % high C ₃ S cement |
| 3 | 50 % ref. cement + 50 % high C ₃ S cement |
| 4 | 25 % ref. cement + 75 % high C ₃ S cement |
| 5 | 100 % high C ₃ S cement |
| 6 | Ref. cement +1000 cm ² /g in Blaine |
| 7 | Ref. cement +1500 cm ² /g in Blaine |
| 8 | Ref. cement + 5 % Filler |
| 9 | Ref. cement + 10 % Filler |
| 10 | Ref. cement + 25 % Filler |
| 13 | Ref. cement + 2 % C ₃ A (cubic) |
| 14 | Ref. cement + 4 % C ₃ A (cubic) |
| 15 | Ref. cement + 0.5 % Na ₂ O eq. |
| 16 | Ref. cement + 1.0 % Na ₂ O eq. |
| 17 | Ref. cement + 0.5 % Cl |
| 18 | Ref. cement + 1.0 % Cl |
| 19 | Ref. cement + 0.7 % SO ₃ |
| 20 | Ref. cement + 1.4 % SO ₃ |

2.3 Isothermal calorimetry and mortar strengths

For each mix a cement paste and a standard mortar with the same w/c was prepared.

For isothermal calorimetry cement paste has been placed directly into the calorimeter after mixing. The cement pastes were prepared by mixing 50 g cement and 25 g water for 20 sec. A Calmetrix ICal 2000 HPC isothermal conduction calorimeter was used to measure the HoH at 20 °C.

Standard mortars were prepared according to /DS/EN 196-1: 2005/ and cured at 20 °C. At 1 day the compressive strength was measured.

3. RESULTS AND CONCLUSIONS

Test results are given in figure 2 and 3 (figure 2 only selected results). In the analysis of the results the first 90 min HoH from the initial ettringite peak have been excluded.

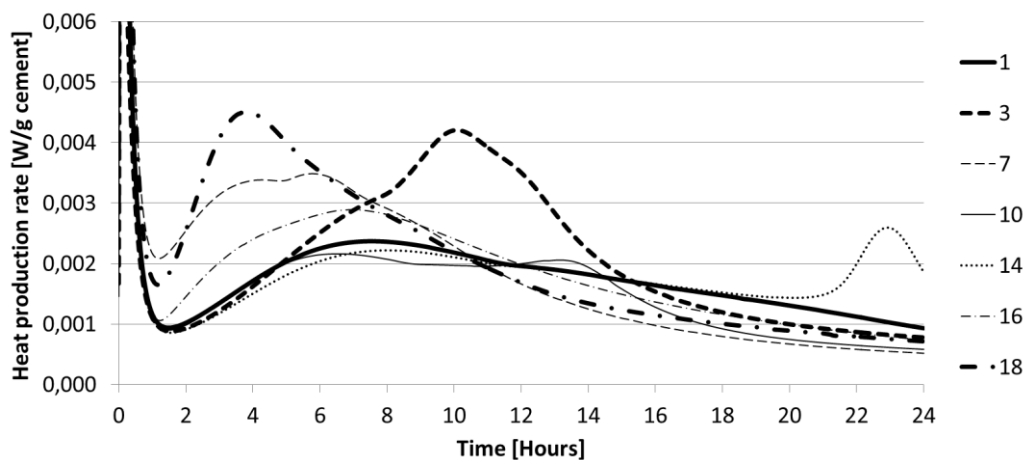


Figure 2 – Selected heat production rate plots

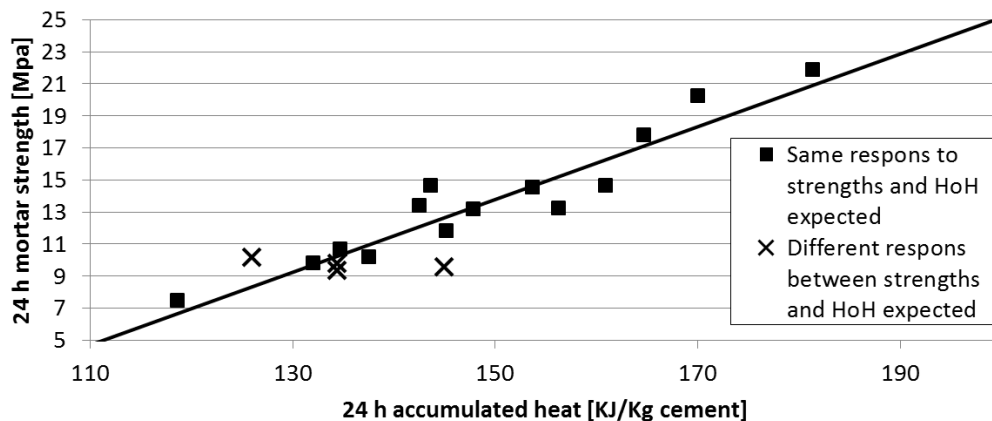


Figure 3 – Accumulated heat versus strengths after 24 hours excluding first 90 min heat. $R^2=0.90$ for mixes with same expected response to strengths and HoH

Figure 2 illustrates how the course of heat production rate is altered by different modifications to the cement. The reference cement is a low fineness low C_3S cement. Therefor the C_3S peak is not very steep (mix 1). By increasing the C_3S content the C_3S peak become more distinct (mix 3) and by grinding the cement finer the reactions proceed faster (mix 7). These modifications also produce more significant ettringite to mono sulphate conversion peaks (sulphate depletion). Adding 4% extra C_3A (mix 14) do not change the C_3S peak significantly, but produces an unexpected late peak after 22 hours. This is properly caused by a slower reacting synthetic C_3A compared to the C_3A in the clinker.

Extra alkali and chloride accelerate the main hydration in a similar way to grinding finer (mix 16 and 18).

Figure 3 illustrates the correlation between accumulated heat and strengths at the age of 24 hours. Measurements with extra added C_3A and SO_3 do not fit the regression line. These measurements are excluded in the correlation analysis.

The laboratory that carried out the mortar strengths measurements has typical early strengths repeatability/coefficient of variability (CV) of 3.5 %. Assuming the same repeatability of the HoH measurements one would expect a CV of the residuals from the regression line of 5.0 %. The actual value from the measurements is 5.3 %. This means that the uncertainty from the strength and HoH measurement is in the same magnitude. At the same time the HoH method provides information that can be used to locate unconformities due to undesired reactions. The conclusion from this study is that measuring HoH by isothermal calorimetry provides a viable alternative to measuring early strengths according to EN 196 on standardized mortar.

REFERENCES

Hansen, P.F., 1978

”Hærdetnologi-1 (Hardening Technology)”, BKF-centralen, February 1978

DS/EN 196-1:2005

”Methods of testing cement - Part 1: Determination of strength”, February 2005

Sandberg, P., Roberts, L, 2005.

”Cement-Admixture Interactions Related to Aluminate Control”, Journal of ASTM International, June 2005, Vol. 2, No. 6

ASTM C 1679 – 08, 2008

”Standard Practice for Measuring Hydration Kinetics of Hydraulic Cementitious Mixtures Using Isothermal Calorimetry”, ASTM, 2008

Concrete Café.

Teaching Concrete Structures: Development and new experiences



Dr. Per Goltermann
 Technical University of Denmark, Building 118,
 DK – 2800 Lyngby
 E-mail: pg@byg.dtu.dk

ABSTRACT

The teaching of concrete structures has been revised and a number of new approaches have been developed, implemented and evaluated. Inductive teaching, E-learning and “patches” have been found to be improvements and may be an inspiration and help for others development of the teaching and learning

Key words: Knowledge and Teaching, Structural Design, Testing.

1. INTRODUCTION

The Technical University of Denmark offers 61 different engineering educations (17 BEng, 16 BSc and 28 MSc educations). The faculty members responsible for the development and execution of the courses and projects should ideally use 50 % of their time on research and 50 % on teaching and supervision. This shows that teaching is as important for the university as the research, since the engineering candidates must be seen as one of the university’s main products. This makes it very important to evaluate, rationalize and improve the teaching and learning activities for the faculty and the students.

The department of Civil Engineering employs app. 60 faculty members, is responsible for 130 courses (some offered bi-annually) and supports significantly 9 educations. The author has for the last 8 years been the main responsible for the courses in basic concrete structures on the educations BEng Architectural Engineering, BEng Arctic Technology, BEng Civil Engineering, BSc Building Technology and BSc Architectural Engineering. The author has in his professor (MSO) assignment experimented with changes in the teaching and grading, use of inductive approaches and E-learning, in order to record, review, develop and test new approaches to rationalize and improve the teaching and learning.

2. DEVELOPING AND TESTING NEW TEACHING

2.1 The intentions – what we really want

We teachers probably all wish our teaching and our students learning to be better and more effective. In order to achieve this, some main actions has been taken:

- Base lectures an inductive approach, which links reality and theory together from the beginning of the session.
- Increase student motivation through illustration of the lectures relevance.
- Improve the possibilities for the students to study independently.
- Record student performance and activities and link these to the exam results.
- Reduce time consumption and the amount of boring work for the teacher.

In order to check the results of these actions the students attending exercises are counted or later even registered individually, the frequency of Youtube hits recorded, course evaluations collected, additional questionnaires issued about students work habits and use of the teaching materials.

2.2 What has been tried so far

During the last years the changes and new activities introduced in the courses have been:

- Introduce the inductive approach, where the lecturer show the phenomena first and develop the theory based on the observations from the observations. This is either based on videos from student final project work or based on a demonstration in the auditorium. Requirement: Students who do testing and videorecord their tests (now standard activity in final projects) plus a Webcam for demonstrations in the auditorium.
- Cancel the mandatory assignments, which formed a part of the grading in the courses.
- Develop a “Patch” for the students who had not understood or perhaps forgotten their basic building mechanics (prerequisite course), dealing with estimations of cross-sectional constants
- Introduce consistent and detailed examples and solutions, following the rules from the patch.
- Introduce detailed solutions to exercises, in the first semester to be handed out after the exercises and in the following semesters to be handed from the beginning of the semester.
- Introduce multiple choice questions as a part (35 %) of the exam.
- Change the course from being offered biannually to being offered only once a year (spring semester) and instead offer a “Concrete Café” in the autumn semester to support failed students in their independent study for the re-exam.
- Develop the course homepage www.concretestructures.byg.dtu.dk, where the course plan and all the teaching materials are publicly available. This contains also 8-10 old exams for download with solutions, following the consistent approach.
- Develop an App “DTU Beton” for iPhone and iPad’s to provide easy access to the course materials.
- Videorecord lectures. The videos are placed on Youtube, account ConStruct2800Lyngby. Requirement: DTU’s LearningLab recorded and edited the lectures in real time for streaming and storing.
- Produce E-presentations from the Powerpoint show by recording the presentation and the accompanying speech, exporting them as wmv-files and placed these on the Youtube account. Requirement: A Skype Headset and Office 2010.
- Generate E-examples as dynamic pdf-files, placed on the homepage. The text can be seen and printed and the student can listen to the explanations. Requirement: A SmartPen and paper with a special print, where the lecturer writes on the paper and talks exactly as he would do with a student sitting next to him. The students will need Adobe Reader and Adobe Flash Player.

2.3 Overview of the main results

The main results are that

- The student performance at the exam has been improved by a) cancelling the mandatory assignments and b) producing consistent examples and solutions. The performance has not been changed by c) making detailed solutions available prior to the exercises or d) introducing E-learning materials in the spring semesters as shown in Table 1, but it did have a significant improvement at the re-exams as shown in Table 2.
- Productivity has also gone up as the number of students, who pass the courses annually have been increased with app. 50 %, the percentage of re-examined students passing their second attempt has increased app. 50 % and the course is now only offered once a year, reducing the number of lectures with 50 %.

- The students do not have a fixed preference for a specific type of E-learning materials as seen in Table 3, but they do use the materials, especially in the autumn semester.
- There is a clear correlation between how often the students show up for the exercises and how well they do at the exam as seen in Table 4. This can also be correlated to their past performance during the studies and represents essentially their ambition and study habits, (but it did also enable the teacher to identify the 5 % of the students, who worked independently, rarely showed up and still received top grades).

Table 1 - Student performance in spring semester.

| Semester Spring | Signed up for courses | Attending exercises (average) | Signed up for exam | Passed Course | Correct answers at exam among passed at exam |
|--------------------|--------------------------|----------------------------------|-----------------------|-------------------------------|---|
| S2007 | 138 ¹ | Not counted | 136 | 104/85 (76%/62%) ² | 67%/73% ² |
| S2008 | 177 ¹ | Not counted | 167 | 114 (68%) | 65% |
| S2009 | 193 ¹ | Not counted | 178 | 120 (67%) | 66% |
| S2010 | 222 | 142 (64%) | 213 | 173 (81%) ³ | 74% |
| S2011 | 231 | 136 (59%) | 220 | 151 (69%) ⁴ | 73% |
| S2012 | 230 | 151 (66%) | 227 | 159 (70%) ⁵ | 75% |
| S2013 | 236 | 131 (56%) ⁶ | 218 | 156 (72%) ⁵ | 72% |
| S2014 | 256 | 156 (61%) ^{6,7} | (-) ⁷ | (-) ⁷ | (-) ⁷ |

*Table 2 - Student performance in autumn semester
(among those failed in the spring attend the re-exam in next semester).*

| Semester Autumn | Signed up for concrete café | Attending exercises (average) | Passed Course | Correct answers at exam among passed at exam |
|--------------------|--------------------------------|----------------------------------|-------------------------|---|
| A2007 | (9) ¹ | (-) ¹ | 3 (33%) ¹ | 68% |
| A2008 | (20) ¹ | (-) ¹ | 11 (55%) ¹ | 58% |
| A2009 | (25) ¹ | (-) ¹ | 13 (52%) ¹ | 59% |
| A2010 | 12 | 8 | 5 (42%) ⁸ | 59% |
| A2011 | 24 | 10 | 12 (50%) ⁸ | 60% |
| A2012 | 25 | 4 | 17 (68%) ^{8,9} | 65% |
| A2013 | 33 | 6 | 23 (72%) ^{8,9} | 71% |

Notes for Tables 1 and 2

1. Courses are offered biannual until end of 2009, after this only in spring semester.
2. Grade and passing of the course (76% pass) is based on a combination of written exam (62% pass) and assignments (90% pass). The first values in Table 1 are based on those who pass the course and the second are based on those who actually pass the exam. This approach was abandoned after spring 2007, after which the grades are based entirely on the exams. The exams in the spring are 35% based on MultipleChoice and 65 % on traditional questions, whereas autumn examinations are normally entirely based on traditional questions.
3. Detailed solutions are now developed for all problems and made available after excises. A "Patch" has been developed in the shape of a cookbook with examples for the determination of cross-sectional properties. The cookbooks approach is implemented in all examples and solutions.
4. Detailed solutions are made available from beginning of semester and a homepage is developed.
5. Lectures are being recorded in S2012 and S2013 and placed on Youtube (user ConStruct2800Lyngby) along with E-presentations. The remaining course materials

including the E-examples are placed on the course homepage (www.concretestructures.byg.dtu.dk).

6. Individual registration of attendance three times during the semester (student signatures).
7. Exam in spring 2014 will be in May after this paper is handed in, so data for this semester are either missing or incomplete at the moment. Lectures are not recorded this semester.
8. After 2010 the courses are only taught in the spring semester and a “concrete cafe” is offered for those students, who sign up for a re-exam in the autumn semester.
9. E-learning materials from spring semester are available in the autumn.

*Table 3 - Questionnaires 2012 and 2013 on use of E-material.
Question: “How much did you use the following E-material ?”.*

| Answer | Videos of lectures | | E-presentations | | E-examples | | At least one of the types | |
|------------|--------------------|-------|-----------------|-------|------------|-------|---------------------------|-------|
| | S2012 | A2012 | S2012 | A2012 | S2012 | A2012 | S2012 | A2012 |
| Very much | 14% | 20% | 10% | 0% | 16% | 6% | 28% | 25% |
| Much | 15% | 33% | 18% | 44% | 25% | 31% | 32% | 63% |
| A little | 35% | 40% | 35% | 38% | 36% | 63% | 27% | 13% |
| Not at all | 36% | 6% | 37% | 19% | 23% | 0% | 13% | 0% |

Table 4 – Students performance versus attendance at exercises (individual registration 3 times in spring 2013). Note 1: Grades are A=12,B=10,C=7,D=4,E=2,Fx=0,F=-03.

| Parameter | Registered 0/3 | Registered 1/3 | Registered 2/3 | Registered 3/3 |
|---|----------------|----------------|----------------|----------------|
| Number of students in S2013 | 33 % | 25 % | 21 % | 21 % |
| Correct answers at exam | 42 % | 55 % | 64 % | 71 % |
| Percentage passed exam | 44% | 62% | 80% | 88% |
| ECTS/semester | 23,2 | 25,5 | 27,5 | 28,5 |
| Average grade during their studies ¹ | 6,3 | 6,9 | 7,0 | 7,8 |
| Building mechanics, grade ¹ | 4,2 | 5,3 | 6,8 | 8,1 |
| Mathematics, grade ¹ | 6,1 | 6,9 | 7,1 | 7,8 |
| Failure percentage in their studies | 23,3% | 13,2% | 9,5% | 5,7% |

Student motivations has also gone up in these years, registered by the course evaluations and students comments, resulting in the author receiving the students associations price as “Teacher of the Year” at DTU in spring 2013 for the teaching in the courses.

3. CONCLUSIONS

The main conclusions are that

- The new approaches have worked quite well, but study habits (amount of work and work methods) still dominate the student performance. Consistent teaching approaches and substantial possibilities for selfstudy help the students significantly.
- The teachers’ workload can be reduced while achieving the same or better performance from the students. The E-learning can often be established with a minimum of investment and training, but should probably always be combined with the traditional interaction between the students and the teacher. The E-learning opens new possibilities.
- Using an inductive approach helps motivating the students, but will not alone improve the student performance.
- Changes in the teaching or learning should preferably always be dealt with as a scientific experiment, where the outcome is measured and compared to a reference (as e.g. how well the students normally perform and how many resources are used).

Authors list - XXII Nordic Concrete Research Symposium

| Name | Page |
|--------------------------------|---------------|
| A | |
| Abbas, Zareen | 487 |
| Abbasiverki, Roghayeh | 461 |
| Abebe, Yared Assefa | 333 |
| Agustdottir, Eva L. | 307 |
| Alaskar, Abdulaziz | 311 |
| Albahtiti, Mohammed | 197 |
| Al-Gburi, Majid | 347 |
| Andersen, Thomas Juul | 149 |
| Anderson, Jack | 495 |
| Andersson, Ronny | 443 |
| Ansell, Anders | 131, 295, 461 |
| Auroy, M. | 447 |
| B | |
| Babaahmadi, Arezou | 487 |
| Bach, Holger | 171 |
| Bagge, Niklas | 83 |
| Barbosa, Ricardo Antonio | 65, 69 |
| Bary, B. | 475 |
| Bernspång, Lars | 25, 83 |
| Berrocal, Carlos Gil | 223, 439 |
| Billberg, Peter | 163 |
| Birgisson, S. R. | 91 |
| Bjøntegaard, Øyvind | 127 |
| Björnsdóttir, Þórdís | 145 |
| Blanksvärd, Thomas | 25, 83, 289 |
| Boel, Veerle | 405 |
| Bohner, Edgar | 25, 83, 289 |
| Boubitsas, Dimitrios | 361, 377 |
| Bourbon, X. | 447 |
| Bryne, Lars Elof | 131, 263, 295 |
| Bulsari, Abhay | 395, 513 |
| Burlion, N. | 475 |
| C | |
| Carlswärd, Jonas | 355 |
| Carolin, Anders | 25, 83 |
| Castaneda, Daniel I. | 387 |

| | |
|--------------------------|----------|
| Cepuritis, Rolands | 175 |
| Charpentier, T. | 447 |
| Colombo, Alessia | 251, 267 |
| Coussot, Philippe..... | 329 |
| Cwirzen, Andrzej | 281 |

D

| | |
|--------------------------------|---------------|
| Danner, Tobias Alexander | 251, 267 |
| de Corte, Wouter | 405 |
| de Schutter, Gert | 399, 405 |
| de Weerd, Klaartje | 193, 267, 369 |

E

| | |
|---------------------------------|--|
| Einarsson, Guðbjartur Jón | 145 |
| Ekström, Daniel | 79 |
| Ekström, Jonas | 157 |
| Elfgren, Lennart | 25, 57, 83 |
| Emborg, Mats..... | 113, 201, 299, 351, 355, 409, 417, 501, 505, 509 |
| Engen, Morten..... | 47 |
| Engsig, Lasse Frølich | 517 |
| Eren, Özgür..... | 167 |
| Ewoldt, Randy H..... | 387 |

F

| | |
|--------------------------|-------------------|
| Faure, Pamela..... | 329 |
| Ferreira, Miguel | 373 |
| Feys, Dimitri | 383, 399 |
| Fjellström, Peter | 417, 435, 501 |
| Flansbjer, Mathias. | 61 |
| Flosason, Valgeir O..... | 307 |
| Fourmentin, Marine..... | 329 |
| Fridh, Katja | 53, 163, 443, 483 |

G

| | |
|------------------------------|------------------------------|
| Gasch, Tobias..... | 237, 465 |
| Geiker, Mette Rica | 141, 251, 267, 281, 369, 431 |
| Ghadban, Ahmad | 197 |
| Ghafari, Ehsan..... | 399 |
| Ghasemi, Yahya | 109 |
| Goltermann, Per | 87, 223, 523 |
| Gram, Hans-Erik | 105, 113 |
| Guettala, Abd El Hamid | 241 |
| Gunnarsson, Andri | 153 |

H

| | |
|-------------------------------|------------------------------|
| Hakola, Ilkka..... | 123 |
| Hallgren, Mikael | 339 |
| Hansen, Kurt Kielsgaard | 65, 69, 303 |
| Hardarson, Johann A. | 179 |
| Hasholt, Marianne Tange | 21 |
| Hassanzadeh, Manouchehr | 479, 483 |
| Hedlund, Hans..... | 299, 351, 409, 417, 501, 505 |
| Helgason, Thorgeir S..... | 171 |
| Hendriks, Max A.N | 47, 141, 431 |
| Hjartarson, Bjorn..... | 13 |
| Hoang, Linh Cao | 65, 69 |
| Hofer, Vera | 171 |
| Holt, Erika..... | 321, 491 |
| Hooton, R. Doug | 9, 311 |
| Häggström, Jens | 25 |
| Häglund, Martin | 443 |
| Häkli, Janne | 135 |
| Hösthagen, Anders | 505 |

J

| | |
|------------------------------|--------------------------------------|
| Jacobsen, Stefan | 175, 119, 193 |
| Jansson, Helén..... | 255 |
| Jensen Pernille Erland | 233 |
| Johansson, Morgan..... | 39 |
| Johansson, Niklas | 109, 201, 469 |
| Johansson, Peter | 469, 479 |
| Jonasson, Jan-Erik..... | 31, 57, 299, 347, 409, 417, 501, 505 |
| Jönsson, Ulf | 17 |
| Juel-Hansen, Lise | 495 |
| Justnes, Harald | 189, 251, 259, 267, 317 |
| Juvas, Klaus | 395 |

K

| | |
|-------------------------------|-----------------------------|
| Kaasgaard, Martin..... | 17, 495 |
| Kanstad, Terje | 43, 127, 141, 211, 215, 281 |
| Khayat, Kamal, H..... | 383 |
| Kioumars, Mahdi | 431 |
| Kirkelund, Gunvor Marie | 233 |
| Kjellmark, Gunrid | 127, 215 |
| Klausen, Anja..... | 127 |
| Koch, Jeremy A..... | 387 |
| Kompen, Reidar | 101 |

| | |
|------------------------------|----------|
| Korte, Sara | 405 |
| Kuosa, Hannele | 321, 373 |
| Kristjansson, Thordur I..... | 179, 391 |

L

| | |
|------------------------------|-------------------------|
| Lagerblad, Björn | 105, 263, 443 |
| Lange, David A. | 197, 373, 387 |
| Larsen, Erik Stoklund..... | 65 |
| Le Bescop, P. | 447, 475 |
| Lehikoinen, Timo | 135 |
| Leivo, Markku..... | 373, 413, 491 |
| Lesueur, Didier..... | 239 |
| Löfgren, Ingemar | 223, 439 |
| Lohaus, Ludger | 333 |
| Loimula, Kalle | 325 |
| Lund, Mia Schou Møller | 303 |
| Lundgren, Karin | 223, 439, 453 |
| Luping, Tang..... | 255, 361, 377, 435, 487 |

M

| | |
|-------------------------------------|----------|
| Maag, Iben | 69 |
| Makkonen, Lasse | 373 |
| Malaga, Katarina..... | 61 |
| Malm, Richard | 237, 465 |
| Mancini, Giuseppe | 457 |
| Martius-Hammer, Tor Arne..... | 3, 215 |
| Mohaghegh, Ali Mohammadi..... | 219 |
| Mørtsell, Ernst..... | 175 |
| Moskura, M..... | 447 |
| Müller, Harald S..... | 421 |
| Munch-Petersen, Christian | 17, 245 |
| Munch-Petersen, Gitte Normann | 245 |

N

| | |
|-----------------------------|----------|
| Nedrelid, Håvard..... | 43 |
| Neji, M..... | 475 |
| Nes, Linn Grepstad | 35 |
| Ng, Serina | 189 |
| Nielsson, Indriði..... | 13 |
| Nikolakopoulos, George..... | 31 |
| Nilimaa, Jonny | 25, 425 |
| Nilsson, Lars-Olof..... | 409, 443 |
| Nilsson, Martin | 229, 347 |

Nordenswan, Erik..... 513

O

Ohlsson, Ulf 25, 509

Olawuni, Kayode Bamikole..... 167

Orosz, Katalin207, 299, 417

Ottosen, Lisbeth 233

Oxfall, Mikael 479

P

Pacoste, Costin 39

Pade, Claus 17, 273, 495

Paulsson, Björn 25

Pedersen, Bård 101, 193

Peng, Ya..... 193

Persson, Martin 509

Peter, Ulrike 329

Plos, Mario..... 39, 79, 157, 453

Popescu, Cosmin 285

Portal, Natalie Williams 61

Poulsen, Søren Lundsted 365

R

Rempling, Rasmus 79, 157

Riding, Kyle A. 197, 387

Riu, Jaume Cirera..... 105

Rogers, Patrick 167

Ronin, Vladimir 57

Rosenqvist, Martin 483

S

Saaed, Tarek Edrees 31

Sangiorgio, Filippo..... 457

Sarmiento, Elena Vidal..... 141

Sas, Gabriel..... 25, 285, 289

Sayahi, Faez 351

Shu, Jiangpeng 453

Silfwerbrand, Johan..... 75, 219, 457

Smepllass, Sverre 175

Snaebjornsson, Jonas Thor 153

Sørensen, Henrik E..... 365

Strand, Martin 53

Stripple, Håkon 443

| | |
|----------------------------------|----------|
| Švec, Oldřich | 273, 281 |
| Sveinbjörnsson, Sveinbjörn | 145 |

T

| | |
|--------------------------------|--------------|
| Tabet, Mohamed | 241 |
| Tammo, Kristian | 61 |
| Tamužs, V | 277 |
| Thorhallsson, Eythor Rafn..... | 91, 145, 153 |
| Thun, Håkan..... | 25 |
| Torrenti, J-M. | 447 |
| Trygstad, Steinar | 211 |
| Täljsten, Björn..... | 83, 285, 289 |

U

| | |
|-----------------------|----------|
| Utgenannt, Peter..... | 361, 377 |
|-----------------------|----------|

V

| | |
|----------------------------|-----|
| Van Der Vurst, Farid | 399 |
| Vehmas, Tapio | 491 |
| Vepsä, Ari | 123 |

W

| | |
|----------------------------|------------------------|
| Wallevik, Jon E. | 185 |
| Wallevik, Olafur H..... | 13, 179, 185, 307, 391 |
| Westerholm, Mikael | 113 |
| Wigum, Børge Johannes..... | 97, 175 |

Y

| | |
|------------------------------|-----|
| Ytterdal, Silje Gystad | 369 |
|------------------------------|-----|

Z

| | |
|--------------------------|-----|
| Zandi, Kamyab..... | 453 |
| Zhang, Emma Qingnan..... | 435 |
| Žirgulis, Giedrius | 281 |

Ø

| | |
|------------------------|-------------|
| Østnor, Tone A..... | 317 |
| Øverli, Jan Arve | 35, 47, 343 |

Å

| | |
|----------------------|-----|
| Åldstedt, Erik | 47 |
| Årskog, Vemund | 219 |